SPIRE Beam Steering Mirror Design Description

v 5.0

Distribution List:

SPIRE-Project	Ken J. King	
	Bruce M. Swinyard	
	Matt Griffin	
	Eric Sawyer	
	Doug Griffin	**x**
UK ATC	Colin Cunningham	**x**
	Gillian Wright	**x**
	Phil Parr-Burman	**x**
	David Lee	
	Brian Stobie	
	Tom Paul	
	Brenda Graham	
	Tom Baillie	
LAM	Didier Ferrand	
	Dominique Pouliquen	
	Patrick Levacher	
MPIA	Ralph Hofferbert	

Update:

Date	Index	Remarks
5 Jun 2000	1	Creation of the document
28 Aug 2000	2	Revision of the document, internal to ATC
	3.1, 3.2.	Revision of the document, internal to ATC
12 Oct 2000	3.3	Revision – adding significant mechanical, electronics & controls content. Produced summary description for verbatim release in SPIRE-ATC-PRJ-001 and -003
02 Feb 01	3.4	Updated update table to include unreleased versions. Amended images to latest mechanical design state. Included flex pivot call out.
20.Jul.01	4.0	Updated substantially for DDR
22.Feb.02	4.1	Revised and reformatted. Updated substantially
02 Jul 04	5.0	Updated following completion of design and PFM test

1. Table of Contents

1. Table of Contents 3
1.1 Tables 5
1.2 Table of figures 5
2. Scope of the Document 7
3. Document List 8
3.1 Applicable Documents 8
3.2 Reference Documents 9
4. Glossary 10
5. Outline Description of the Beam Steering Mirror mechanism subsystem. 11
5.1 Overview 11
5.2 Mission profile 12
6. BSM Block Diagram 13
7. Detailed Description - Mechanical 15
7.1 Load environment 15
7.2 The Cryogenic Mechanism BSMm 16
7.2.1 General 16
7.2.2 Finite Element Analysis 18
7.2.3 Flex Pivots 18
7.2.4 Flex Pivot Protection 19
7.3 Structural Interface 21
7.3.1 The Support Structure BSMs Design 21
7.3.2 BSMs Finite Element Analysis 23
7.3.3 Outputs 25
7.4 Components & Declared Lists 25
7.4.1 Declared Components List (DCL) 25
7.4.2 Motor coils 25
7.4.3 Magnets 26
7.4.4 Fasteners 27
7.4.5 Materials 27
7.4.6 Declared Processes 27
8. Thermal Control 28
8.1 Thermal Path 28
8.1.1 Strap Connection 28
8.1.2 Heat Path to Mirror 29
8.1.3 Heat Path to Motors 30
8.1.4 Flex Pivot Thermal Stresses 31
8.1.5 Magnetic shielding 32
8.2 Thermometers 33
8.3 Coatings 35
8.4 Surface Finish 35
8.5 Mass budget 35

9. Optics 36

9.1 General 36

9.2 Mirror 36

9.3 Baffle 37

9.4 Light Tight Enclosure 38

9.5 Harness Feed-Through 38

9.6 Alignment 38

9.7 OGSE 39

10. BSM Electronics & Controls 40

10.1 Control System Design 40

10.2 Parameters 40

10.3 Dynamic Analysis 40

10.4 Simulink Model 41

10.5 Performance 42

10.5.1 Power Dissipation 42

10.5.2 Rise Time 45

10.5.3 Positional Stability 45

10.5.4 Gain and Phase Margins 45

10.6 BSMe Electronics 45

10.6.1 Block Diagram 46

10.6.2 Position Sensors (Current Source) 47

10.6.3 Position Sensor Read-Out Circuit 47

10.6.4 Thermometry 49

10.6.5 Power Supply 49

10.6.6 Grounding Scheme 49

10.6.7 Harness/Cables 49

10.6.8 Interface to Digital Controller 50

10.6.9 Motor Function & Wiring 50

10.7 Components & Declared Lists 52

10.7.1 Component List 52

10.7.2 Processes Soldering 52

10.7.3 Processes Crimping 52

10.8 Electronics Systems Interfaces 53

10.8.1 MCU 53

10.8.2 Command List 53

10.8.3 EGSE 53

11. Reliability & Redundancy 54

11.1 Reliability Block Diagram 55

11.2 Single Point Failures 55

11.3 FMECA 55

11.3.2 Electronics : 56

11.3.3 Mechanical : 56

11.4 Critical Components Identification 56

12. Interface Control Documents 57

13. Assembly, Integration & Verification 58

13.1 General 58

13.2 Assembly 58

13.2.1 Flex pivot protection sleeves: 59

13.2.2 Mirror handling 59

13.2.3 Chop Stage (drawing SPIRE-BSM-020-004) 60

13.2.4 Motor Assemblies (drawing SPIRE-BSM-020-005) 60

13.2.5 Jiggle assembly (drawing SPIRE-BSM-020-003) 61

13.2.6 Jiggle frame to structure assembly 62

13.2.7 Harness routeing 62

13.3 Integration 62

13.4 Verification 62

13.5 Transport & Storage 62

13.6 Handling 62

13.7 Test Programme & Test Matrix 63

14. Appendices 64

14.1 Appendix 1 : Not used 64

14.2 Appendix 2 : Not used 64

14.3 Appendix 3 : Structural Analysis : 64

14.4 Appendix 4 : Not used 64

14.5 Appendix 5 : Not used 64

14.6 Appendix 6 : Thermal Calculations 64

14.7 Appendix 7 : Control Analysis 64

14.8 Appendix 8 : Not used 64

14.9 Appendix 9 : Single axis prototype test results 64

1.1 Tables

Table 1: Rated static loads and margins. 19
Table 2: BSMs + BSMm vibration modes 24
Table 3: BSM Reaction Loads 25

1.2 Table of figures

Figure: 1 Photometer Layout, BSM in green, highlighted with green dashed oval 11
Figure 2: SPIRE Block Diagram 14
Figure 3 BSM launch load random vibration requirements 15
Figure 5: top side of jiggle frame and mirror. All fasteners are M2.5. 17
Figure 6 BSMm and BSMs with baffle ommitted. 18
Figure 7 : Flex pivot protection sleeves, à la Goddard 20
Figure 8 : Flex pivot and sleeve 20
Figure 9: BSMm and BSMs, with baffle. 3D view from Pro/E model looking from the rear. 22
Figure 10 BSM showing the baffle. This view shows that much of the mechanism is visible (non-conformal baffle) 23

Figure 11 Zeiss/PACS coils, courtesy MPIA 26
Figure 12 BSM thermal block diagram 28
Figure 13: predicted mirror temperature at varying background radiation loads. The Sky or Motor coil temperature is varied (x-axis) and the predicted mirror temperature shown (y-axis). The local radiation from motor copils is shown to be a small effect 30
Figure 14: Cooling of motors : heat flow balanced along thermal path at 0.5mW. 31
Figure 15 : Actual cooldown data (2 axis prototype) 32
Figure 16 Assembly of a shielded motor assembly (SPIRE-BSM-020-005) with heat shielding 33
Figure 17 Cernox 1030 sensor (SD package) 34
Figure 18 Cernox 1030-CU package 34
Figure 19: BSM with optical beam (20% oversized)space envelopes provided by RAL 36
Figure 20: BSM baffle. The end 'tabs' provide debris closure of the flex-pivot apertures. 38
Figure 21 Simulink model 41
Figure 22 Filtered Difference 42
Figure 23 Predicted power (chop stage) 44
Figure 24 : Predicted chop stage risetime 45
Figure 25 : Warm electronics overview 46
Figure 26 sensor supply 47
Figure 27 Chop sensor conditioner 48
Figure 28 Chop Power Amp 49
Figure 29 BSM on-board harness run showing prime and redundant harness runs 50
Figure 30 Motor Function Schematic 51
Figure 31 Wiring schematic for BSM motor 52
Figure 32: The model includes the mechanism with its inertia, flex joint spring and damping, and the motors, power amplifiers and position sensors. 53
Figure 33 : BSM electronics architecture showing parallel redundancy 54
Figure 34 flex pivot mounted in protection sleeve (note holes for adhesive- this allows glue to be added after assembly and reduces risk of adhesive being placed on moving parts) 59
Figure 35 underside of mirror showing light-weighting and 4-off tapped holes for process mounting 59
Figure 36 Chop stage assembly showing sensor cores (pink), magnets (purple) and flex-pivots (green) 60
Figure 37 Jiggle stage assembly showing jiggle frame (green), sensor cores (pink), Infineon sensors (red) 61

2. Scope of the Document

This document describes the design of the Herschel-SPIRE Beam Steering Mirror mechanism subsystem at the time of manufacture and delivery of the Proto Flight Model and Flight Spare Model.

3. Document List

3.1 Applicable Documents

	Title	Author	Reference	Date
AD1	SPIRE Beam Steering Mirror Mechanism Subsystem Specification	P. Parr-Burman	SPIRE-BSM-PRJ-000460 v 3.7	11 Sep 03
AD2	SPIRE Project Development plan	K.J.King	SPIRE-RAL-PRJ-000035 issue 1.1 Draft	12 Apr 01
AD3	Herschel-SPIRE BSM PA Plan	B. Graham	SPIRE-ATC-PRJ-000711 v1.5	09 Jun 03
AD4	Optical System Design Description	K.Dohlen, B.Swinyard	SPIRE-LAM-PRJ-000447 Issue 1	18.Dec.00
AD5	Spire Harness Definitions	D.K.Griffin	SPIRE-RAL-PRJ-000608 iss 1.1	05 Mar 03
AD6	ICD Structure - Mechanical I/F	B.Winter	MSSL/SPIRE/SP004.11 (formerly SPIRE-MSS-PRJ-00617) Issue 3	14 Feb 03
AD7	SPIRE BSM FMECA	I. Pain	SPIRE-ATC-PRJ-01118	Jan 2002
AD8	SPIRE BSM Interface Control Documents	P. Parr-Burman	SPI-BSM-PRJ-0713 iss 3.1	Mar 2004
AD9	SPIRE BSM Declared Process List	B. Graham	SPI-BSM-PRJ-0708 iss 1.6	15/06/04
AD10	SPIRE BSM Declared Parts List	B. Graham	SPI-BSM-PRJ-0709 v1.3	15/06/04
AD11	SPIRE BSM Declared Materials List	B. Graham	SPI-BSM-PRJ-0710 v1.5	15/06/04
AD12	SPIRE BSM Electronics Parts List	B. Graham	SPI-BSM-PRJ-0704 v1.4	15/06/04

3.2 Reference Documents

	Title	Author	Reference	Date
RD1	Instrument Requirements Document	B.M.Swinyard	SPIRE-RAL-PRJ-000034 v1.1	02.Jan.02
RD2	Instrument Development Plan	K.King	SPIRE WE Review viewgraphs	6 Dec 1999
RD3	Proposal for Beam Steering Mirror	R.Sidey	ATC contract no. 017693	undated
RD4	Assessment of System Level Failure Effects for SPIRE	B.M.Swinyard	SPIRE-RAL-NOT-000319 v 4	4-APR-2001
RD5	BSM Development Plan	I.Pain	SPIRE-ATC-PRJ-000466 v 5.1	30/01/02
RD6	Space Engineering, Mechanical Part 3 - Mechanism Design	ESA	ECSS-E30(a)-part3	25 Apr 00
RD7	Optical design. Diffraction analysis & design.	M.Caldwell	SPIRE-RAL-DOC-000441 ISSUE: 1.0	14 Jun 00
RD8	Mirror Thermal Cycling Procedure	I.Pain	SPIRE-ATC-Internal-NOT-003 V 1.3	17/06/04
RD9	CM4 Hole Size Considerations and stray light control	T.Richards	SPIRE-RAL-NOT-000576 ISS 1.0	23 Jan 01
RD10	Spectrometer and photometer pupil imagery and CM4 SIZE CONSIDERATIONS	T.Richards	BSMSIZE_MEMO.DOC	21.Sep.00
RD11	SPIRE Optical Alignment Verification plan	A.Origne, K.Dohlen	SPIRE-LAM-PRJ-000445	10.Apr.01
RD12	SPIRE AIV plan	B.Swinyard	SPIRE-RAL-DOC-000410 issue 2.0	23.Feb.01
RD13	A cold Focal Plane Chopper for Herschel-PACS - Critical Components and Reliability	R.Hofferbert, D.Lemke et al	paper	undated
RD14	Thermal contraction sizing note.	T.Paul	SPI-BSM-NOT-0010	25.Jan.02
RD15	Spire BSM Vibration Analysis	DC Reed, Frazer Nash	FNC 5505/24072R	May 2002

4. Glossary

Abbr.	Meaning	Abbr.	Meaning
AD	Applicable Document	LAT	Lot Acceptance Tests
ADP	Acceptance Data Package	MAC	Multi Axis Controller
ATC	United Kingdom Astronomy Technology Centre	MAPTIS	Materials and Processes Technical Information Service
BSM	Beam Steering Mirror	MSFC	Marshall Space Flight Centre
BSM	Beam Steering Mirror dummy	MCU	Mechanism Control Unit
BSMe	Beam Steering Mirror electronics	MIP	Mandatory Inspection Point
BSMm	Beam Steering Mirror mechanism	MGSE	Mechanical Ground Support Equipment
BSMs	Beam Steering Mirror structure	MPIA	Max Planck Institute for Astronomy
CAE	Computer Aided Engineering	MSSL	Mullard Space Science Laboratory
CDR	Critical Design Review	NASA	National Aeronautical Space Agency
CoG	Centre of Gravity	NA	Not Applicable
CIL	Critical Items List	NCR	Non Conformance Report
CQM	Cryogenic Qualification Model	NCRP	Non Conformance Review Panel
CTD	Change to Drawing/Document	OGSE	Optical Ground Support Equipment
DCL	Declared Components List	PA	Product Assurance
DDR	Detailed Design Review	PAD	Part Approval Document
DM	Development Model	PFM	Proto Flight Model
DML	Declared Materials List	PPARC	Particle Physics and Astronomy Research Council
DPA	Destructive Physical Analysis	PI	Principal Investigator
DSP	Digital Signal Processor	PID	Proportional – Integral - Derivative
ECSS	European Co-operation for Space Standardisation	QA	Quality Assurance
EGSE	Electrical Ground Support Equipment	RAL	Rutherford Appleton Laboratory
ESA	European Space Agency	RAL SSD	RAL Space Science Department
FMEA	Failure Modes and Effects Analysis	RD	Reference Document
FMECA	Failure Modes, Effects and Criticality Analysis	rms	Root mean square
FPGA	Field Programmable Gate Array	SDOF	Single Degree of Freedom
FPU	Focal Plane Unit	SMEC	Spectrometer Mechanism
FS	Flight Spare	SPIRE	Spectral and Photometric Imaging Receiver
FSM	Flight Spare model	TBC	To Be Confirmed
GSFC	Goddard Space Flight Center	TBD	To Be Defined
GSE	Ground Support Equipment	TBW	To Be Written
HoS	Head of Specialism	UK ATC	United Kingdom Astronomy Technology Centre
Herschel	ESA Mission name (formerly FIRST)	UK SPO	UK SPIRE Project Office
ICD	Interface Control Document	WE	Warm Electronics
IBDR	Instrument Baseline Design Review		
KIP	Key Inspection Point		
LAM	Laboratoire d'Astrophysique de Marseilles		

5. Outline Description of the Beam Steering Mirror mechanism subsystem.

5.1 Overview

The Beam Steering Mirror mechanism subsystem (BSM) is a critical part of the SPIRE Instrument. It is used to steer the beam of the telescope on the photometer and spectrometer arrays in 2 orthogonal directions, for purposes of fully sampling the image, fine pointing and signal modulation.

The position of the BSMm & BSMs on the Spire Optical Bench are indicated in Figure: 1

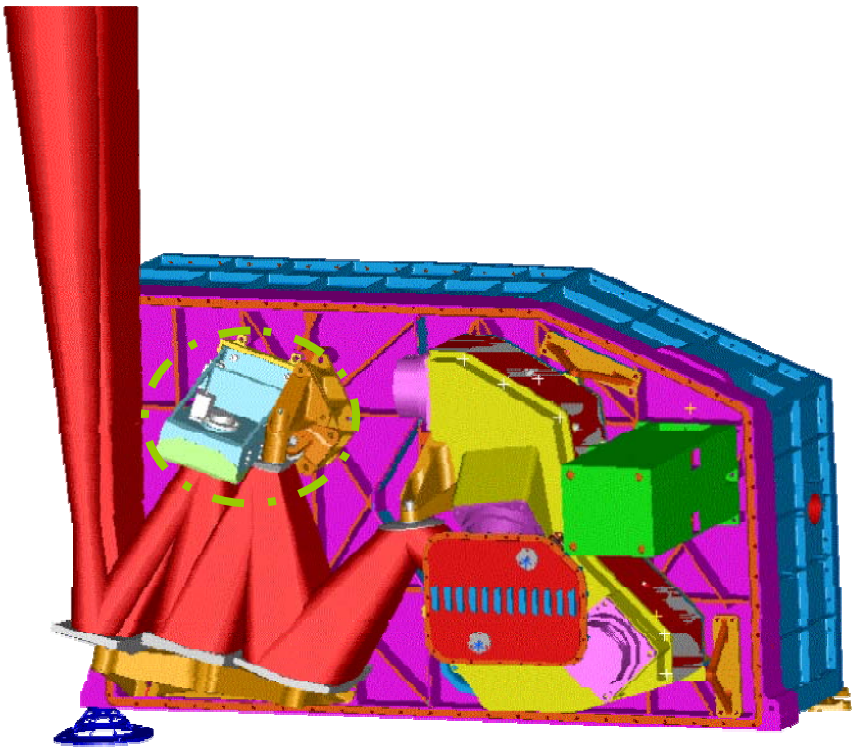

Figure: 1 Photometer Layout, BSM in green, highlighted with green dashed oval

The BSMm consists of an aluminium alloy mirror, nominal diameter 32mm, machined as part of the chop axis. This is mounted within a gimbal frame which provides for jiggle axis motion. The axes are suspended by flex-pivot mounts. The BSMm is a cryogenic device with nominal operating temperature 4-6K. Nominally, the chop axis provides 2.53° of mirror motion at 2 Hz and the jiggle axis provides 0.57° of motion at 1 Hz. The mirror also provides an aperture through which the Photometer Calibration Source is directed towards the detector arrays

The BSMs provides location of the BSMm on the SPIRE optical bench, and will also provide for a light tight enclosure and structural support for harnessing and thermometry. The BSMs also supports the SPIRE Photometer Calibration Source (PCAL), supplied by the University of Cardiff, a baffle (supplied by ATC) and the SPIRE optical bench (MSSL). The BSMs is a cryogenic structure with nominal temperature 4-6K.

The BSMe provides electrical actuators which are used to provide motion of the mirror. Electrical transducers are used to measure the mirror position to allow control of the mirror position. The BSMe baseline design makes use of cryogenic motors used in PACS and magneto-resistive sensors used in

ISOPhot. Each axis houses a rare-earth (NdFeB) permanent magnet moving pole piece and is driven by a motor coil fixed to the mechanism housing/structure.

The cryogenic electronics are connected to the analogue power and amplifier electronics on the Warm Electronics (WE) by a cryogenic harness which will also feed out signal cables from thermocouples on the BSMs. The BSM operates under control of the Detector Readout and Control (HSDRC) sub-system's Mechanism Control Unit (MCU) supplied by LAM. The BSMe will be specified and designed by the UK ATC, then manufactured by LAM in conjunction with the SMEC electronics. Integration and test will be at LAM, with support from ATC.

The BSMd may comprise several actual dummies, with at least (1) an optical dummy for initial alignment work and (2) a mass-representative model for structural vibration tests. Designs for mass and optical alignment dummies will not be specified in detail until the BSMs/BSMm design is complete.

5.2 Mission profile

The BSM is developed as a sub-system and then integrated to the SPIRE FPU. The SPIRE instrument is subsequently integrated to Herschel. The instrument is to be cryogenically cooled, and will be cold during launch. The mission duration is a minimum of 4.25 years.

Per RD1, in normal operations the satellite is expected to have a 24-hour operational cycle with data being collected autonomously for 21 hours and a 3 hour ground contact period – the Data Transfer and Commanding Period (DTCP). During the DTCP the data will be telemetered to the ground and the commands for the next 24-hour period will be uplinked.

6. BSM Block Diagram

The block diagram below is adopted from “Spire Block Diagram rev 5.8, J. Delderfield” and shows the relationships between the sub-systems of the SPIRE instrument.

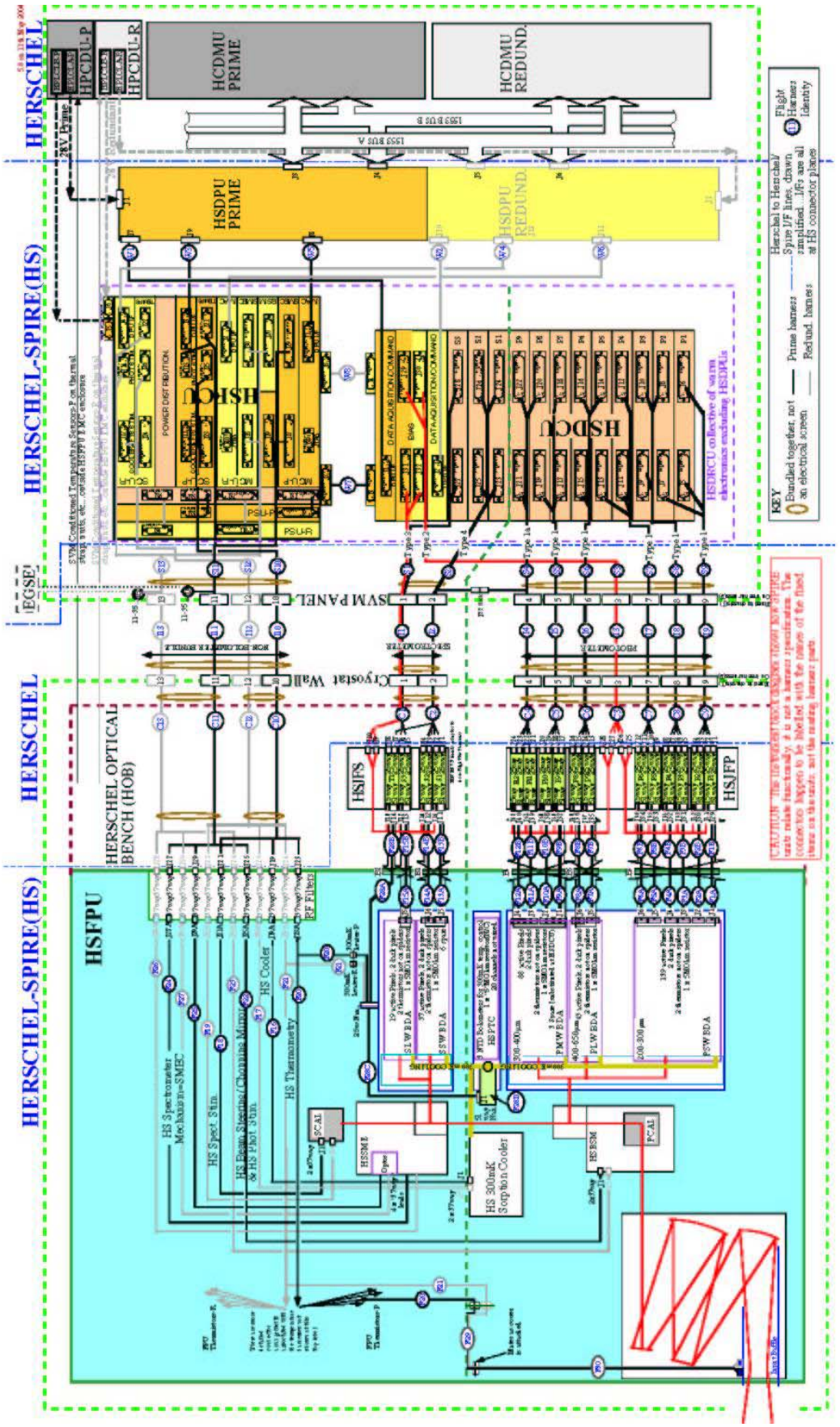

Figure 2: SPIRE Block Diagram

7. Detailed Description - Mechanical

7.1 Load environment

The BSM is a cryogenic mechanism, attached to the SPIRE Level 1 thermal straps to give a temperature in orbit at 3.5-6K. It is cooled down prior to launch and experiences a vibration load from the spacecraft, potentially amplified by the SPIRE optical bench structure. On orbit, the mechanism operates in a micro-gravity environment where the principal loads are self-induced fatigue loads during chop and jiggle motion.

During manufacture, qualification and integration the design must survive warm vibration tests (room temperature), bake-out to 80°C, thermal cooldown at a rate of at least 20K/hr (space-craft), life tests of many million cycles at 20K and cold vibrations (at 4K).

The load environment is specified in AD1, as derived from AD6. In summary the maximum quasi-static loads are 25g, sine vibration 40g and random vibration 11g $_{rms}$. The random vibration environment is summarised graphically as:

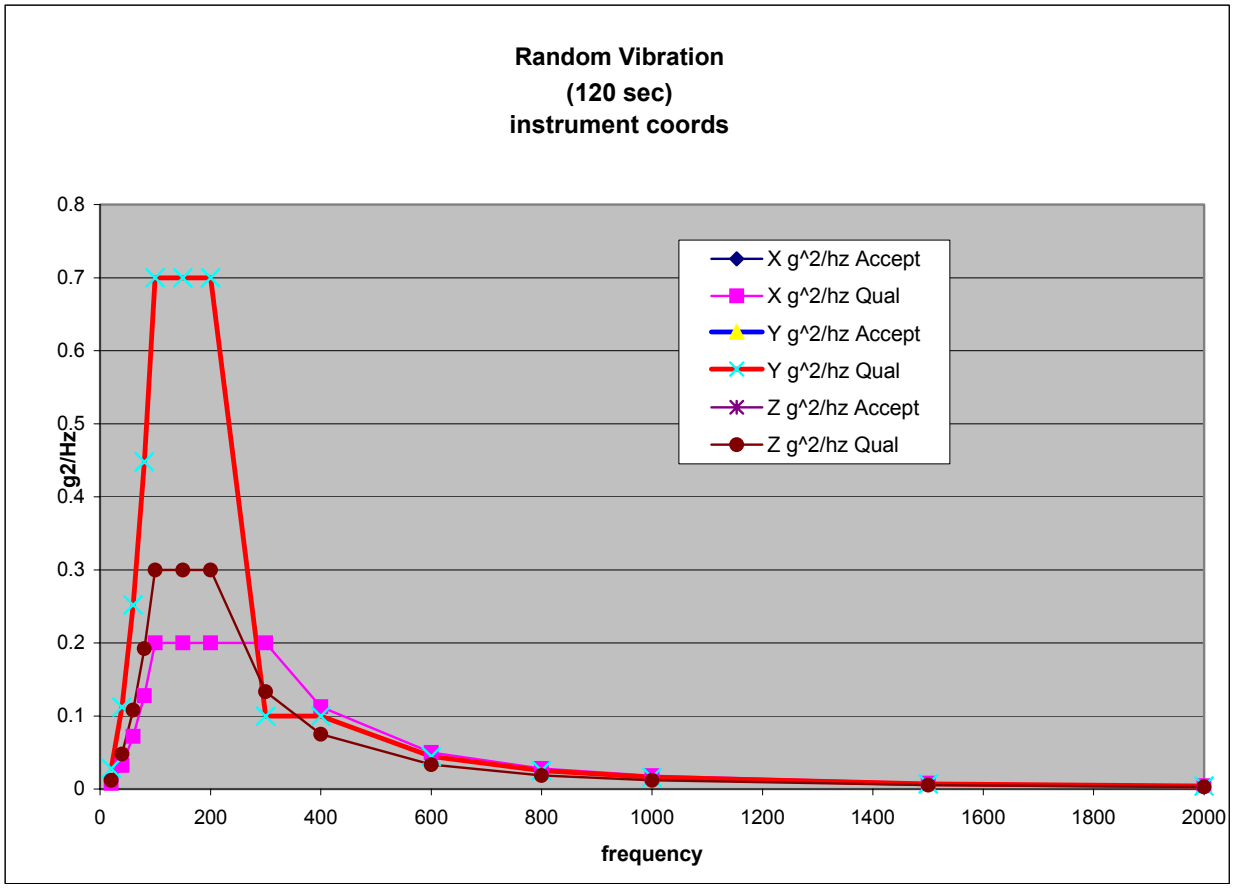

Figure 3 BSM launch load random vibration requirements

7.2 The Cryogenic Mechanism BSMm

7.2.1 General

The BSMm comprises a mirror of diameter 32.5mm, mounted so as to pivot on two axes to provide chop and jiggle motion.

The jiggle axis lies directly coincident with the mirror surface. The chop axis is recessed by 2.25mm from the mirror surface.

Each axis houses a rare-earth magnet moving pole piece and is driven by a motor coil fixed to the mechanism housing/structure. Lucas TRW (jiggle) and C-Flex (chop) flex-pivots provide low friction motion and a small restoring torque.

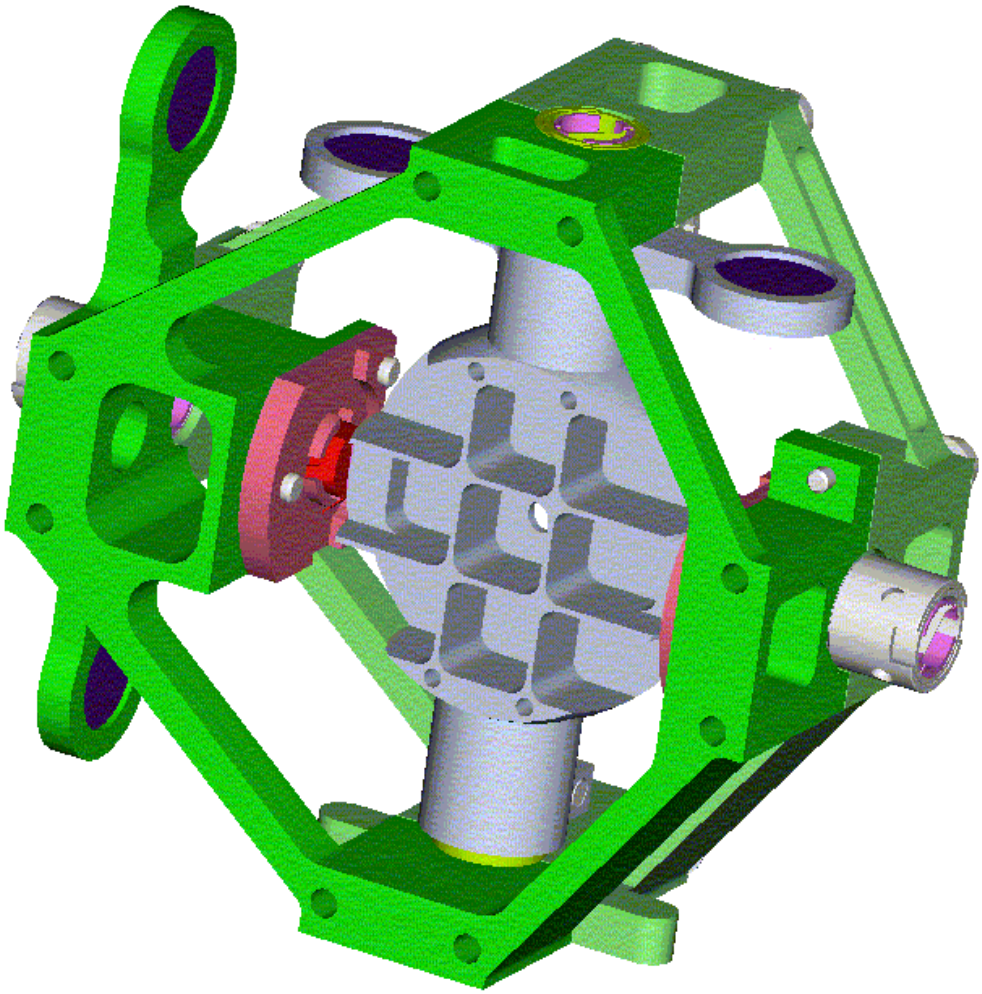

Figure 4: View on underside of mirror - Chop stage grey, jiggle stage green, motor magnets purple and sensor mounts (shown without adhesive) red.

The chop and jiggle stages are shown above. The chop stage is monolithic with the mirror machined integrally. The underside of the mirror is light-weighted and has pockets for the iron plates for the magneto-resistive position sensors. The chop direction is along the long axis of the array (the spacecraft y-axis). A 2.8mm diameter hole in the centre provides an optical path for the calibrator mounted behind the BSMm.

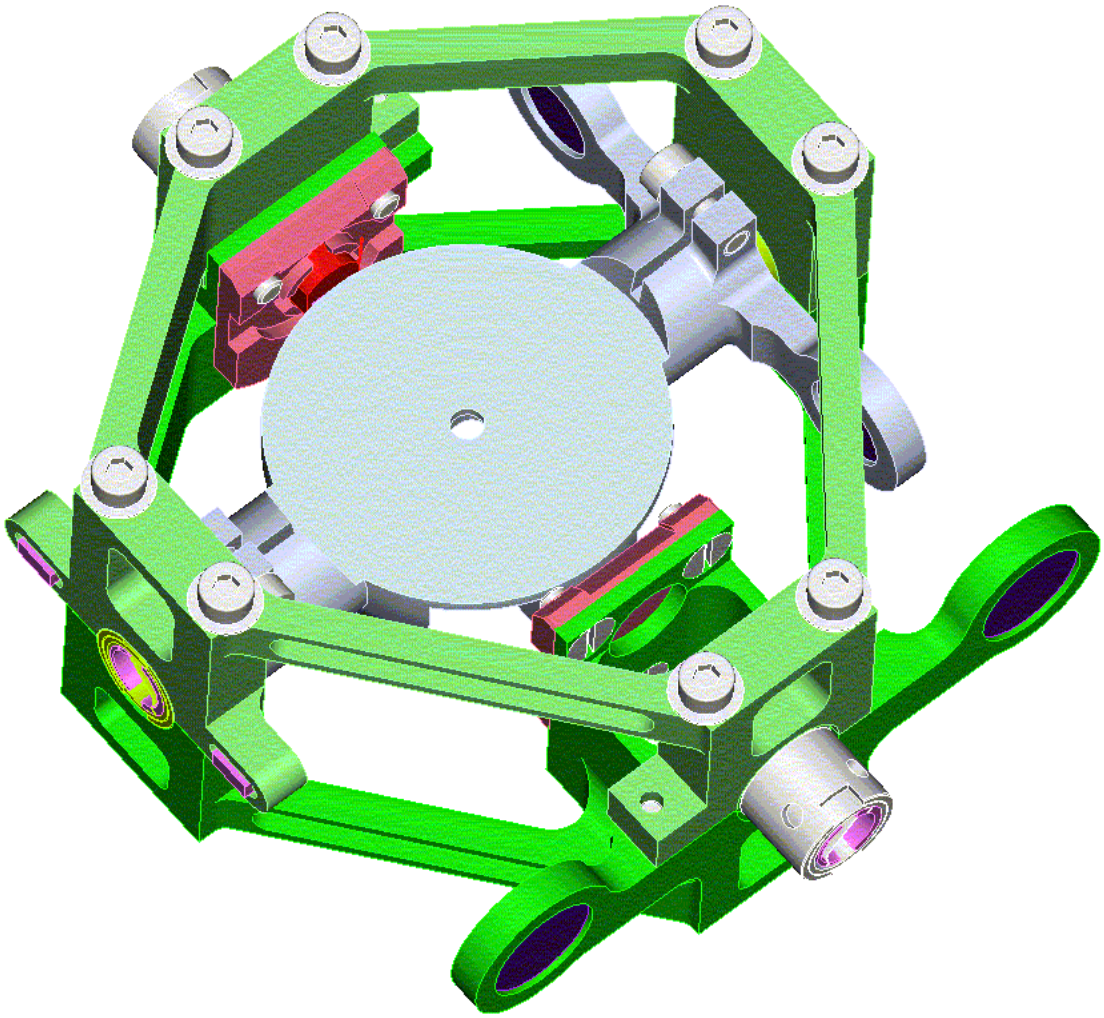

Figure 5: top side of jiggle frame and mirror. All fasteners are M2.5.

The moment of inertia of the chop stage has been minimised to reduce power consumption during chop transitions. At 2.68 kg.mm^2, it is little more than the ISOPhot rotor which was 1.57 Kg.mm^2. Rotating mass, at 21 gm is also minimised to keep loads on the flex pivots down during qualification and launch.

The jiggle stage is in the form of a split frame which clamps together around the flex pivots. Stainless steel fasteners (M2.5) are used in self locking inserts, with a stainless steel disc-spring to retain clamping forces during cooldown. [RD14 refers]

To balance the jiggle stage the framework in the opposite corner to the coils has been made solid. This also increases the stiffness of the structure. This structure carries the chop stage, and is inevitably heavier. The moment of inertia is estimated at 47.9 kg.mm^2 and mass at 96gm. Fortunately, the requirements call for lower amplitude and frequency in this axis, so we can use stiffer flexures.

Both stages are designed to be stiff, so that the first resonant frequencies are high enough (> 700 Hz that the system modelling can regard them as rigid bodies. [RD15 refers]

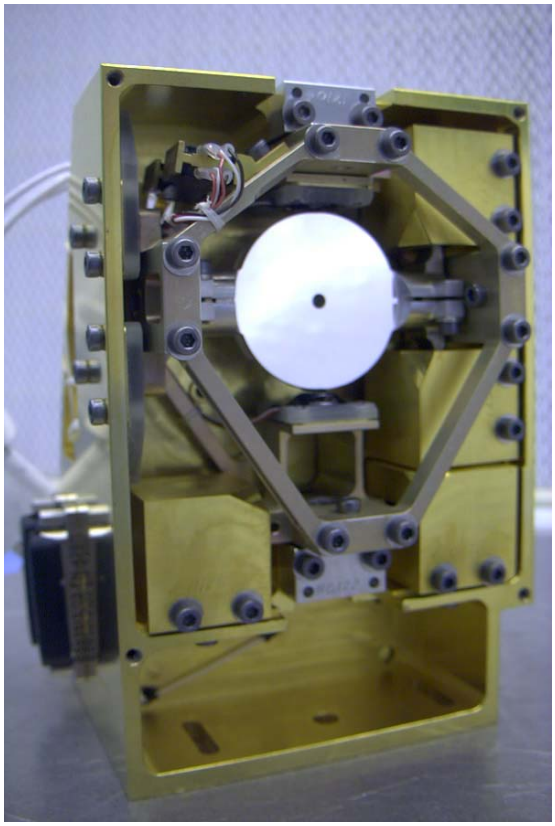

Figure 6 BSMm and BSMs with baffle ommitted.

The coils and sensors are located as shown in Figure 6. There will be a 'primary' and 'cold redundant' motor for each axis.

The coils are adopted directly from the PACS chopper design, RD 13, as it has been determined to be more cost effective to buy into a well tested coil meeting the SPIRE requirements than to design our own.

All the motor coils mount directly to the BSMs, i.e. the chop stage air gaps must be slightly over-size to accommodate chopping whilst in various jiggle modes. The magnetic circuit has not been modelled.

Position sensors for the chop axis are mounted on the jiggle stage, which means flexible pcb connections are required, unlike the jiggle stage position sensors, which mount directly on the non-moving housing.

7.2.2 Finite Element Analysis

See section 7.3.2

7.2.3 Flex Pivots

Two flex pivot types are envisaged, a light pivot for the Chop axis, and a heavier one for the Jiggle.

The jiggle axis pivots are supplied by Lucas Aerospace TRW (formerly Bendix) type 5010-600. This unit is standard commercial off-the-shelf and uses AISI grade 420 and 429 stainless steel components, assembled by brazing. The off-the-shelf grade material can suffer from cryogenic embrittlement and this high risk approach is being taken due to budgetary constraints (inconel pivots were investigated up to DDR, but with costs for a minimum quantity >$100,000 were not obtainable within the BSM budget).

The chop axis uses CuBe type pivot (sizes E-10 and E-20) is being investigated, supplied by C-Flex.

7.2.4 Flex Pivot Protection

The flex pivots are the most critical element of the BSM design, and the most vulnerable. Much design effort is thus directed towards their protection. In general flex pivots are observed to fail under shear load, by buckling of the pivot flexures or 'blades'. This failure mode is more likely if the pivots are prevented from rotating - hence any form of launch locking is undesirable.

7.2.4.1 Load control & Margin

As a first approach, the loads on the pivots are controlled as far as possible.

- Mass of the structures carried by the flex pivots (the chop axis and jiggle frame) is kept as low as practical, as this minimises loading during launch. Additional margin could be obtained by further light-weighting of the jiggle frame components, but is currently not required on technical grounds.
- The BSM mounting structure, jiggle frame and chop stage are kept stiff so that the risk of amplification of the loads transmitted during launch is minimised.

Initial FEA work of the flex pivots has been performed to calculate stresses in flex pivots upon launch.

In addition, a static analysis is presented in Appendix 3C. The safety factor for 3-sigma peak response during vibration testing is:

BSM margin - flex pivots								
Temp	Component	mass (incl contingency)	load limit of component (N)	required FoS	survival load (in g) for 2 pivots	margin on rms response	margin on 50% peak response	margin on 3-sigma peak response
WARM 290K	C-Flex Chop axis flex pivot	21.0	25.4	1.0	246.6	8.70	1.84	1.45
	LUCAS jiggle axis flex pivot	96.0	245.0	1.0	520.3	18.35	3.87	3.05
COLD 4K	C-Flex Chop axis flex pivot	21.0	28.1	1.0	273.1	9.63	2.03	1.60
	LUCAS jiggle axis flex pivot	96.0	259.2	1.0	550.4	19.42	4.10	3.23

Table 1: Rated static loads and margins.

The 'required 'FoS' is set to 1.0 as the Qualification load factor incorporates the ESA mechanism FoS.

The C-Flex CuBe grade pivots are manufactured in a higher grade material and have additional margin. The manufacturer's quoted rated load should be treated with caution, but is nominally as shown.

The rated life for these flexures, is in the 'infinite life' range of the spectrum, assuming 1g loadings. The flight hardware will receive the bulk cycling in zero-g.

7.2.4.2 Protection Sleeves

To prevent damage by shear of the mechanism on launch a flex pivot capture sleeve, similar to that used by Goddard on COBE, will be utilised, as sketched below.

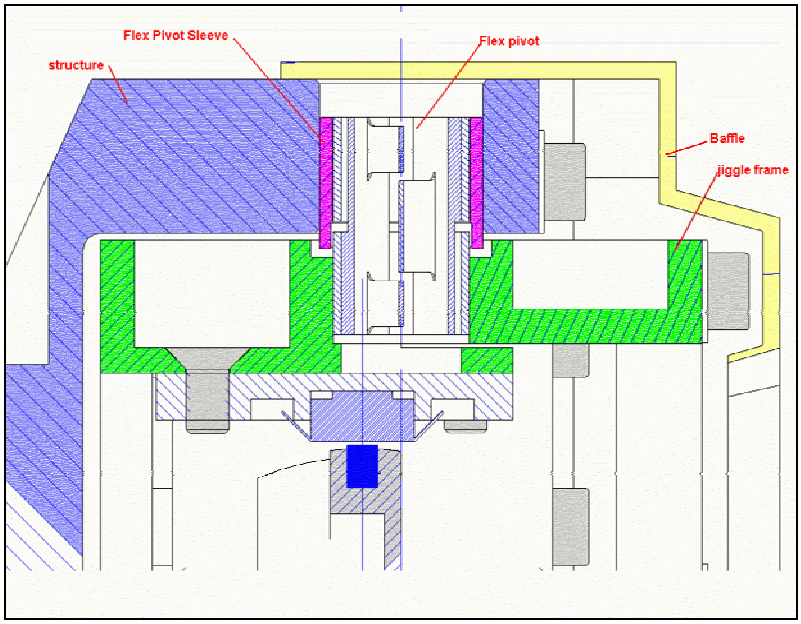

Figure 7 : Flex pivot protection sleeves, à la Goddard

Based on holding the +/-0.18° requirement on the nominal (0,0) position, in the BSM specification a ~ 125 micron diametral clearance would be required on the pivot sleeves given the ~80mm distance between pivots. This would prevent slop in the jiggle pivots producing an apparent chop motion, or vice versa. Without constraint, the standard flex-pivots would produce about +/-200um of slop (though they would fail before this was reached).

A working flex pivot produces some de-centring motion as it twists anyway: about +/-20um of linear motion in our case. We would arrange for this to be in the plane of the mirror (careful of course to install flex pivots in handed pairs, to prevent twist).

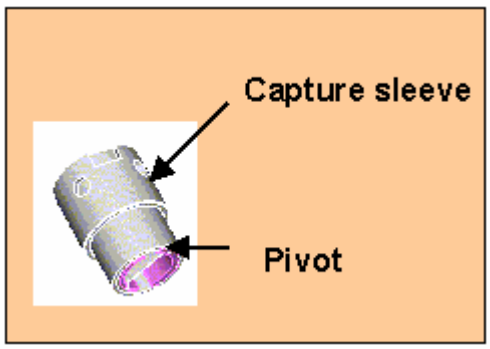

Figure 8 : Flex pivot and sleeve

The ATC pivot sleeve design provides for 50-75um of clearance, which is sufficient to

- allow normal rotation (and associated de-centre),
- prevent buckling failure of the pivot by shear loading (TBC by load tests)
- provide for capture of any broken pivot with 0.111 degrees of slop, sufficient to meet the fail-safe regime

Assembly of the sleeve to the pivot is by a light push fit, which becomes a close fit on cooldown. As this would be inadequate to survive warm vibration, an adhesive will be used to ensure the flex pivot is secured ? The adhesive is supplied via radial holes drilled in the sleeve. The sleeve also contains an alignment slot to aid assembly.

7.2.4.3 Flex-pivot failure modes:

Launch loads are a much larger concern than long term fatigue life, which is well characterised and easily tested. Tests performed by LAM suggest that the primary failure mode on launch would be where the flex pivots suffer shear in the radial direction, and the flex pivots fail in a buckling mode.

a) In the event of flex pivot failure, we could control position by motors alone and the random slop of the pivots would remain within spec. Long term chop or jiggle would not be advocated as we presume the capture sleeves would make poor journal bearings and would wear relatively quickly. However, the aim would be to move the mirror to a rest position and then hold it against spacecraft micro vibration.
b) In the event of motor failure (or launch damper failure to disengage), the flex pivots would provide self-centring (note that alignment of the centred position on integration will thus be critical, unless this is adjustable elsewhere in the optical path).
c) If both motors and pivots fail the position would be completely indeterminate, probably an end-stop out of the spectrometer field of view.
d) One other failure mode could occur - the linear de-centre of the flex pivot is produced by a combination of opposing de-centre of each flex spring. If only one of them fails we assume that the de-centre will include an out-of plane component. e.g. if one chop pivot 'half failed' then a chop demand to the end-stop would also produce a 20um lift of that end of the chop axis (a small jiggle and a mirror translation of 10um upwards). This failure mode would probably only exist for a short while until the second flexure also failed, and would be correctable in software if identified.

7.3 Structural Interface

7.3.1 The Support Structure BSMs Design

The BSM Structure – or BSMs is a machined stiff aluminium alloy mount with a mass of ~ 310 gm, and an associated baseplate (or ‘mounting shoe’) of mass ~ 85gm.

The mounting and alignment functions of the baseplate are described in section 9 (optics)

The BSMs provides for mounting of the:

- jiggle stage flex-pivots,
- jiggle stage sensors
- the jiggle and chop stage motors
- thermometry
- Photometer calibration source (PCAL)
- harness and connector mounts
- baffle

Figure 6 Above (page 18) shows the BSM with baffle omitted.

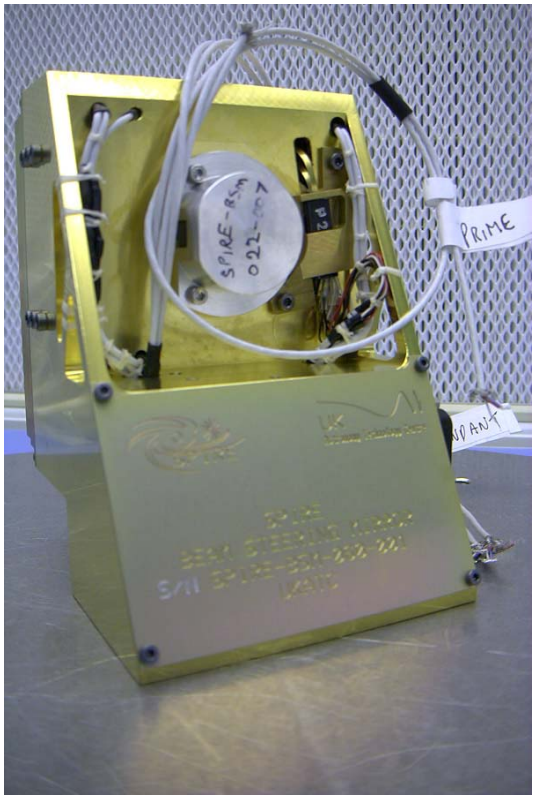

Figure 9: BSMm and BSMs, with baffle. 3D view from Pro/E model looking from the rear.

The PCAL unit (a space model here) is shown mounted to the flat surface to the rear of the jiggle frame and motors.

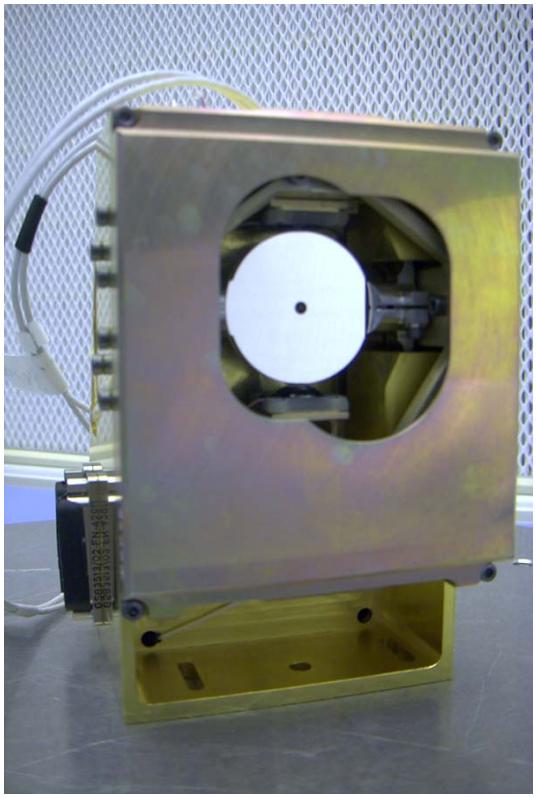

Figure 10 BSM showing the baffle. This view shows that much of the mechanism is visible (non-conformal baffle)

7.3.2 BSMs Finite Element Analysis

7.3.2.1 Vibration Analysis

FEA was performed on the design in early 2002, which was used to inform design modifications. [RD 15 refers]

The principal conclusions were:

- The first structural mode of the main casing and baseplate is calculated to be 392 Hz
- Large rotations of the chop and jiggle stages were identified that would have interacted with the launch latch (which was a feature of the design baseline at the time). Recommendations were made to reduce the amplitude of the response, but in the end the launch latch was removed from the baseline so these measures proved not to be necessary.

The free vibration response was analysed as:

Mode	Frequency	Description
1	13.6	Jiggle stage fundamental
2	21.4	Chop stage fundamental
3	392	Sideways rocking
4	398	Front-back rocking
5	791	Jiggle frame diagonal twist
6	925	Jiggle frame vertical motion and skew
7	1036	Jiggle magnet beam rocking and mirror sideways translation in phase

Mode	Frequency	Description
8	1087	Jiggle magnet beam rocking and mirror sideways translation in antiphase
9	1278	Jiggle magnets move side-side due to rotation of jiggle frame about front-back axis
10	1302	Front baffle bending about horizontal axis
11	1370	Front baffle twist about vertical axis + jiggle frame motion similar to mode 8
12	1510	Front baffle twist about vertical axis + jiggle frame motion vertical motion in antiphase
13	1557	Front baffle twist + jiggle frame rotation about the chop axis
14	1595	Front baffle twist + jiggle frame moves slilghtly side-side in phase
15	1682	Front baffle twist + jiggle frame moves slilghtly side-side in antiphase
16	1781	Jiggle magnet beam bending (magnets in phase) + jiggle frame panting (squeezing)
17	1937	Complex mode of front baffle
18	1960	Complex mode of front baffle
19	2066	Jiggle magnet beam bending (magnets in antiphase) + vertical motion of mirror and top pivot block in antiphase

Table 2: BSMs + BSMm vibration modes

7.3.2.2 Stress Analysis

An earlier analysis examined stresses in the design at that time.

An FEA of the structure has been performed to establish the likely induced stresses on launch, and the vibration modes. The results are detailed in Appendix 3B.

The model was analysed in Pro/Mechanica, based on the Pro/Engineer solid model with some small simplifications. Three runs were performed:

1. A three-axis static gravity load of 50G in each axis was applied to the structure. These were applied to give maximum tensile loads at the rear harness connection points.
2. A second run was performed as (1) but with point loads also applied at the relevant positions to simulate loads from the motors, jiggle and chop stage and attached components.
3. A basic vibration mode search for the first 12 resonant modes was performed.

Reported peak von-Mises and principal stresses peak at 36 MPa, situated around the connector mounting points. Using conservative values of permissible load (per BS8118), allowable stresses would be:

For fatigue
- 67 MPa friction grip bolted zones (not strictly applicable here as loads are not construction level friction grip)
- 96MPa for re-entrant features
- 76MPa small holes (dia < 3t)

For parent plate
- 240 MPa with suggested load factor of 2.5, i.e. a target of 96 MPa in this case

The permissible stresses for space rated components per RD6 are

- Margin of Safety = allowable stress limit / (actual stress x factor of safety)
- Where factor of safety = 1.25 on yield, 1.5 on ultimate, factor of 4 x (cycles) on fatigue.

7.3.3 Outputs

The BSM will output a vibration to the Optical Bench during chopping and jiggling. The primary output will be at the chop and jiggle frequencies : 2 Hz and 0.5 Hz respectively, with harmonics. Local resonances of the BSM (eg of the baffle) may modify the harmonics.

Neglecting harmonics and any structural amplification (which should be small anyway, as the structure is stiff) the output forces take the form of a torque reaction in the structure in response to the acceleration of the mirror and jiggle frame in chop and jiggle.

An approximation to this torque reaction may be made by taking the inertia of the moving masses, and an average acceleration over the specified rise time.

BSM reaction loads summary table	Chop (*)	Jiggle (**)	Units
Torque reaction about chop axis (average)	11.25E-06	0	Nm
Torque reaction about jiggle axis (average)	0	10.03E-06	Nm
reaction force at hole at (242.57, 117.2, 526.863)	10.65-05	1.47E-04	N
reaction force at hole at (351.861, 117.2, 521.426)	-5.32E-05	3.81E-05	N
reaction force at hole at (334.299,117.2, 467.198)	-5.32E-05	3.81E-05	N
** Chop reaction forces in optical bench y-axis* *** Jiggle reaction forces in optical bench z-x plane (normal to BSM jiggle axis)*			

Table 3: BSM Reaction Loads

Strictly, these reaction forces are in matched pairs with no net thrust effect. Thus an equivalent 'micro-g' output cannot be attributed to the BSM, i.e., a 'micro-g' input is only resolved at the interface between the optical bench and another supported system.

As a working figure, at a BSM mass of 0.82kg, the 'g' loading required to provide this type of force input combining the chop and jiggle loads gives a nominal acceleration at the front hole of 3.09E-04 m/s², i.e. an 'equivalent g loading' of 31.5 micro-g. In reality, the relevant mass is that of the whole structure, which is an order of magnitude more massive than the BSM. Thus accelerations attributable to the BSM will be well below 10 micro-g.

7.4 Components & Declared Lists

7.4.1 Declared Components List (DCL)

The Mechanical declared parts list is maintained as a project configured document, AD10. Additional electronic components are declared in AD12

7.4.2 Motor coils

The BSM motor coils are adapted from the PACS design, and will be supplied as space-rated items by Zeiss, via MPIA. Per RD13 the motor construction is:

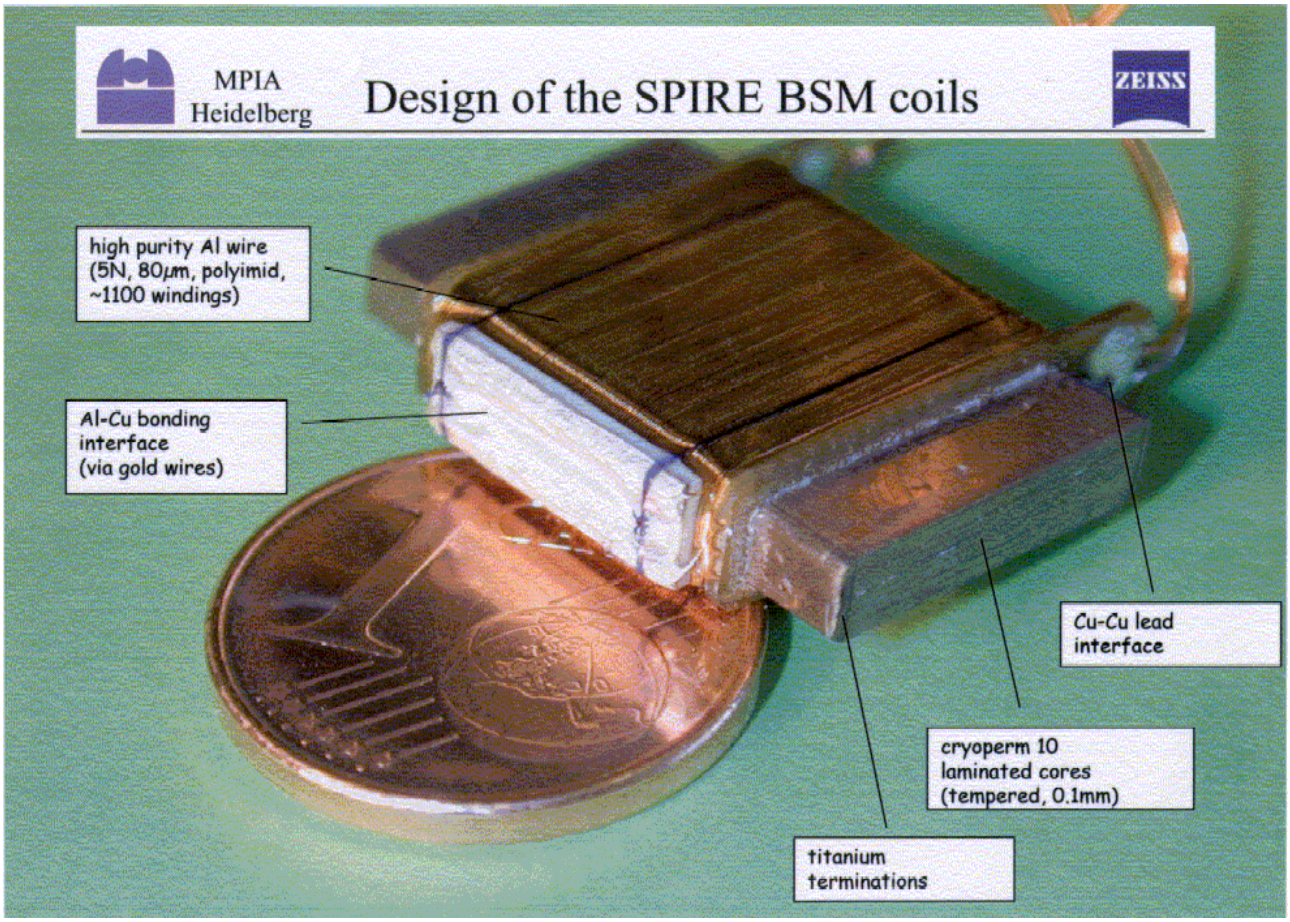

Figure 11 Zeiss/PACS coils, courtesy MPIA

The core material is Cryoperm 10 (Vakuumschmelze) with high permeability ($\mu_r > 10^5$) and high saturation fields ($B_s > 0.9T$), both at temperatures around 4K. This is laminated with ~112 sheets each at 0.1mm, glued and encapsulated with Stycast 1266 in layers of approximately 10μm thick. After vacuum degassing the laminates are milled to size and prepared for windings. A titanium termination provides a rounded winding surface and improved thermal path. The winding comprises 80μm 5N aluminium (1100 windings).

The aluminium wires are terminated via an intermediate gold strip on a ceramic pad, and feed out to copper wires which provides a standard Cu-Cu solder lead tab.

7.4.3 Magnets

The motor function is completed by magnets fitted to the mirror component for chop and to the gimbal frame for jiggle.

In the Proto Flight Model the magnets used NdFeB type N42. This type proved to be susceptible to demagnetising when baked out at 80 degC, causing a reduction in torque from the motor leading to reduced angular travel.

For the Flight Spare Model the type was changed to Vacodym 633, which is rated to 110 degC by the supplier, Vacuumschmelze.

The magnets are fitted in place with adhesive, further restrained by the action of differential thermal contraction.

7.4.4 Fasteners

All fasteners are a cryogenic grade (i.e. austenitic) stainless steel. Fasteners will all be locked to withstand vibration. This is achieved by use of a locking insert in the tapped hole. The smallest locking inserts readily available are M2.5, and this is hence the generally preferred BSM fastener size. the advantage of universal usage of these fasteners is that in general any obviously tight screw will be locked by default. Inspection of the tapped component at manufacture must verify that locking inserts have been assembled in to the component.

The connectors are held in place by screw and nut. In this case the nut is staked in place with Scotchweld 2216.

Torque control is important in ensuring a locked connection, and providing sufficient pre-load to avoid loosening of an Al-SS joint on cooldown. To avoid vacuum welding of cleaned metal-metal components in vacuum conditions, and to reduce variability of preload all screw threads are treated with a lubricant. The lubricant used is tungsten disulphide, applied to the screws by the company WS2 in the UK. This process is used for other assemblies in the Spire Optical Bench.

For M2.5-0.45 threads the recommended preloads are discussed SPI-BSM-NOT-00018, approximately 480Nmm.

The SPIRE optical bench thread sizes are UNC to match an elliptical closure insert favoured by the SPIRE structure supplier, MSSL. MSSL will provide these fasteners.

Fastener torques are important and must be sufficient to ensure adequate lock up of joints, but not over-torqued where damage to the mounted components and the fastener or the thread may occur. Guidelines on fastener torque will be added to assembly drawings, and will be verified during prototype assembly.

Thread lock will not be used in the BSM, mainly as subsequent verification by inspection is difficult.

7.4.5 Materials

The declared materials list is maintained as a project configured document, AD11.

7.4.6 Declared Processes

The declared processes list is maintained as a project configured document, AD9

8. Thermal Control

8.1 Thermal Path

The BSM block diagram is shown in Figure 12 below.

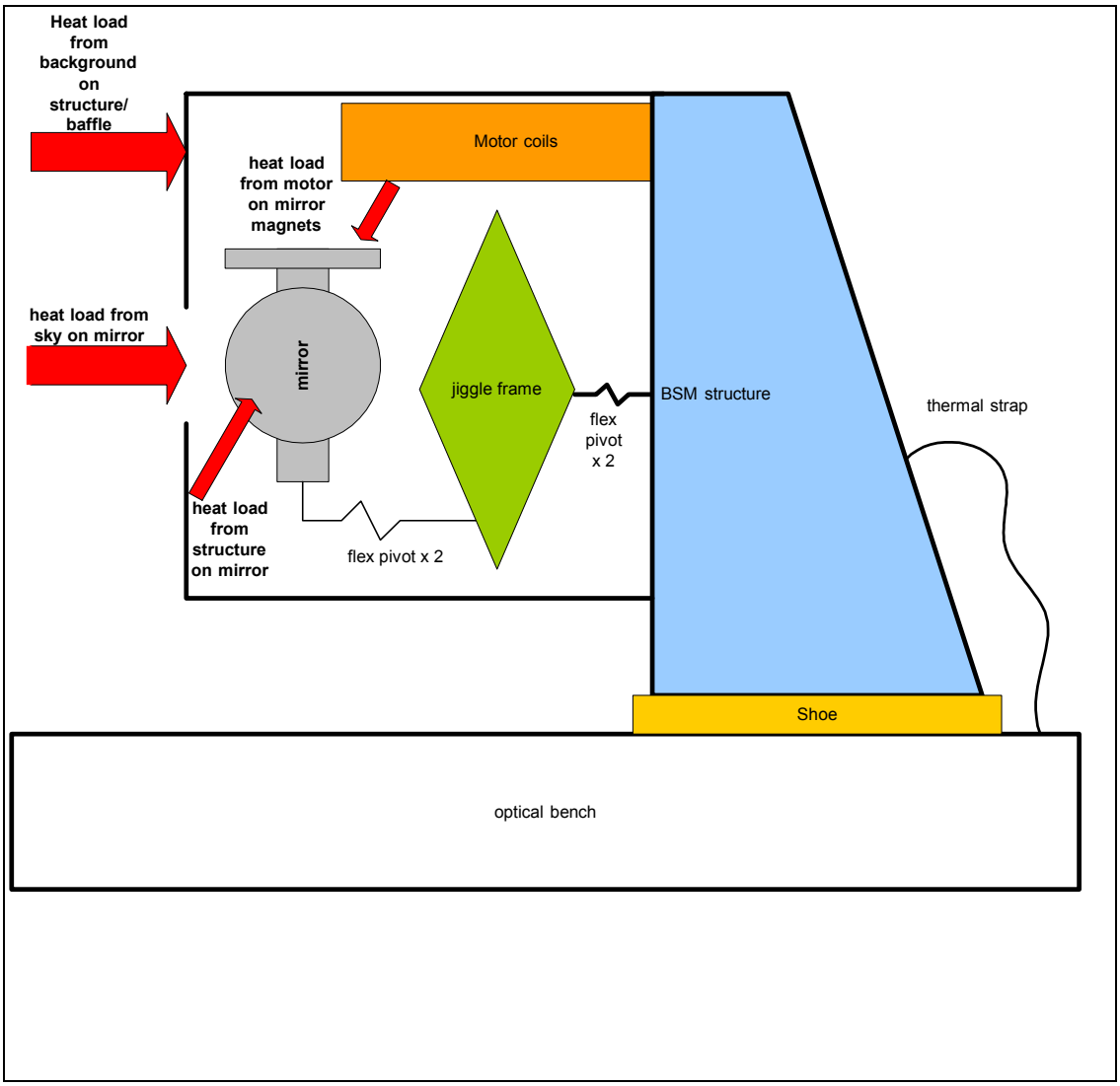

Figure 12 BSM thermal block diagram

8.1.1 Strap Connection

A provision has been made on the BSMs structure for a thermal strap connection against the eventuality that thermal straps are required in addition to bolting to the SPIRE optical bench. These may be required in particular if the interface 'shoe' provides too high a thermal resistance, or if the optical bench sees heat loads from other mechanisms.

A clearance hole for M4 is nominally provided on the side of the BSMs to take a nut and bolt clamping a thermal wick end-tab.

8.1.2 Heat Path to Mirror

One area of concern is the thermal path through to the mirror, which includes two sets of flex pivots, five bolted joints and two adhesive or clamp-fit joints.

Calculations (appendix 6) made with the previous design baseline of all stainless steel flex pivots indicate that the chop axis flex pivots restrict the thermal path (i.e. are significantly less than all bolted joints and/or of material sections downstream).

As the specified instrument cooling rate is to be no more than 20K/hour the thermal shock and differential expansion issues are minimised. However, a remaining issue - more so for ground based tests at ATC than for the integrated instrument, is that thermal load on the mirror from cryostat background radiation is significant compared to the ability to dissipate the load via the pivots.

Results of calculations (appendix 6) are shown in the chart below, and indicate that with cryostat background temperatures of >30K the thermal specification that the mirror 'not exceed the BSMs temperature by >1K' would not be met.

For tests, this may require that a thermal IR filter be fitted to the test cryostat radiation shield, or that the temperature validation tests are performed with the radiation shield aperture closed.

Note that the above applies to stainless steel flex pivots. The design was changed to use CuBe flex pivots which improve the situation but this has not been quantified with a new analysis.

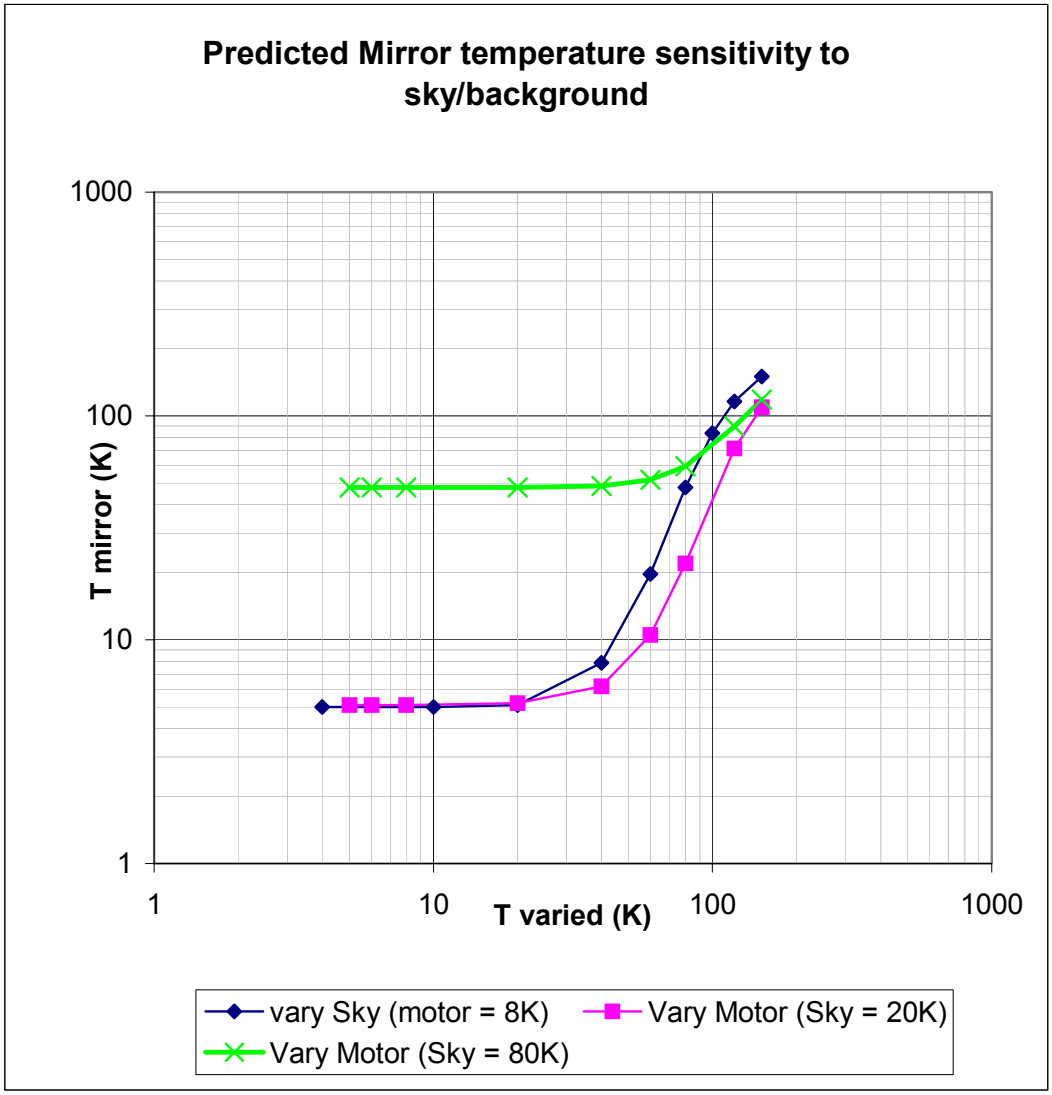

Figure 13: predicted mirror temperature at varying background radiation loads. The Sky or Motor coil temperature is varied (x-axis) and the predicted mirror temperature shown (y-axis). The local radiation from motor copils is shown to be a small effect

The jiggle stage sensor cables will provide some thermal path, though they will not be locally heat sunk.

8.1.3 Heat Path to Motors

A second concern is that the motor coils may overheat, causing either life reduction or a thermal hot spot visible to the detectors. To minimise eddy current losses the motors are housed in an aluminium mounting with a G-10 end cap providing a non-metallic closure.

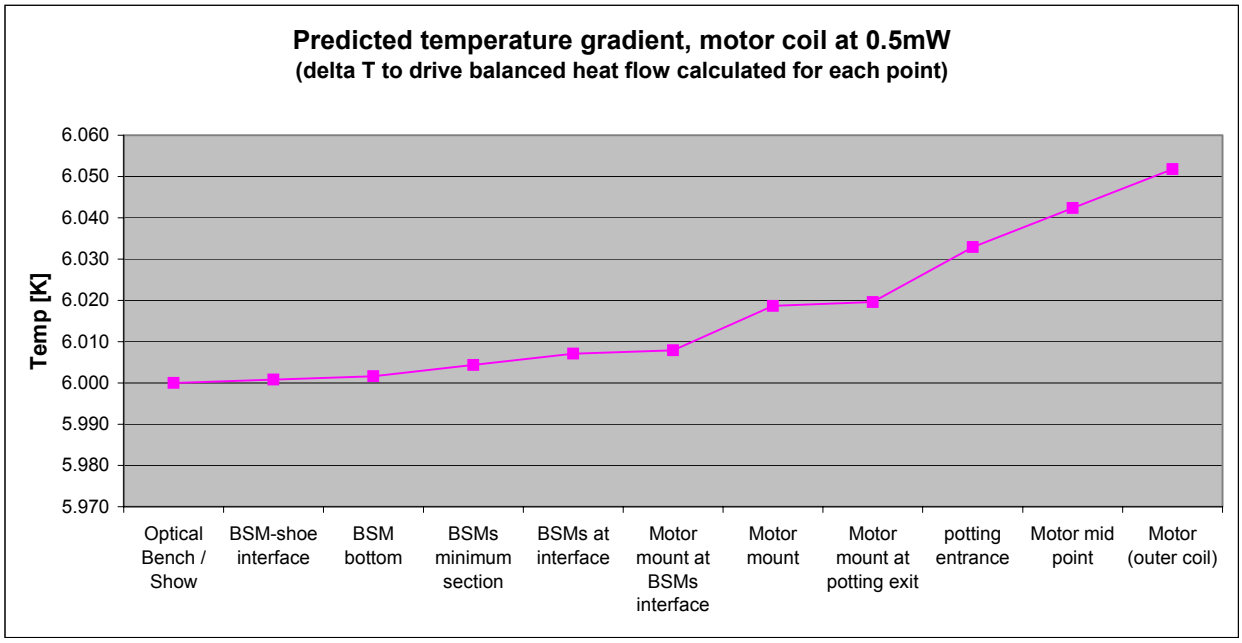

Figure 14: Cooling of motors : heat flow balanced along thermal path at 0.5mW.

The temperature curve indicates the temperature required to drive heat flow of 0.5mW. Radiation from the motors is considered, assuming a 'sky' temperature of 6K, but radiation from the structure is ignored. The main restrictions on thermal path are at the motor-mount to structure bilted joint, and at the potting layer which holds the motor in (thermal properties of Stycast 1266 used). The motor core is assumed to have conductivity similar to mild steel, In practice it is a NiFe/Stycast sandwich with Ti strips down each side. The analysis suggest background temperature would remain in specification (<1K above structure).

The possibility of local hot spots may remain, and is dealt with by a combination of a local baffle around the motors, combined with heat sinking of this local shield to Aluminium parts of the structure.

8.1.4 Flex Pivot Thermal Stresses

Given the restricted thermal path of the pivots, concerns exist for flex pivot stresses induced during cooldown. 2 axis prototype data, using stainless steel flex pivots, indicates worst case differentials of:

chop stage (225K) - jiggle stage (186K) = 39K
jiggle stage (260k) - structure (100K) = 160K

Again, the final design uses CuBe flex pivots which will improve the situation.

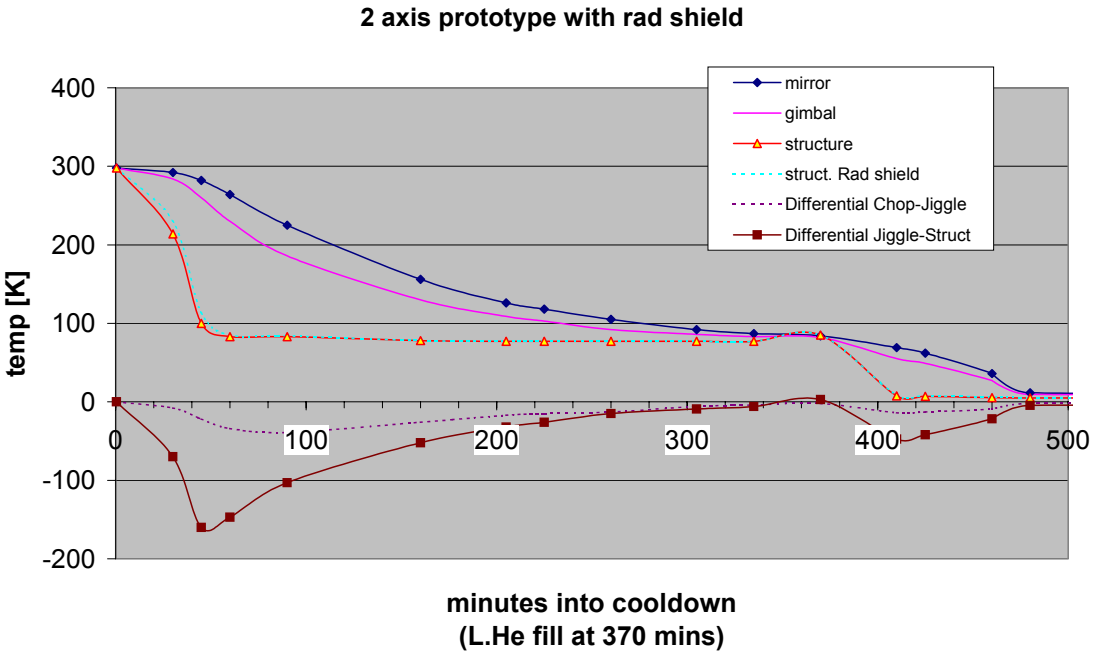

Figure 15 : Actual cooldown data (2 axis prototype)

The worst case differential equates to a compression of the jiggle axis by 0.22mm, however stresses on the flex pivots are minimised by the inherent flexibility of the jiggle frame. The Stiffness of each pivot in compression is ~3100 N/mm, the frame at ~0.9N/mm (based on manual approximation that each jiggle frame arm is a simple beam). This keeps the total axial forces down to ~0.2N.

In the chop axis case, the central axis is stiff but again the jiggle axis flexibility limits the loads. The peak differentials on the chop and jiggle stages occu well spaced in time, which ensures the jiggle axis can provide the required flexibility first in one direction, then the other.

8.1.5 Magnetic shielding

Strong stray magnetic fields around the motor coils would be undesirable if they interfered with the BSM magneto-resistive sensors or the instrument detectors. No EMC requirement has was set by the SPIRE systems team at the time of BSM design, and it is assumed that the local BSM requirement dominates.

The ideal magnetic shield enclosure would be similar to those discussed for local heat shields above. However, magnetic shielding is generally achieved by thin sheets of a magnetically soft material (e.g. mu-metal) built up in layers. This would be difficult to achieve around the BSM motor assemblies within the compact space envelope currently envisaged. In contrast a heat shield may be of monolithic construction, making fabrication and fastening easier.

Basic lab tests (appendix 9) indicate no problems with the magneto-resistive sensors even when deliberately placed close to the operating BSM motors, which has lead the BSM design to de-emphasise full magnetic shields.

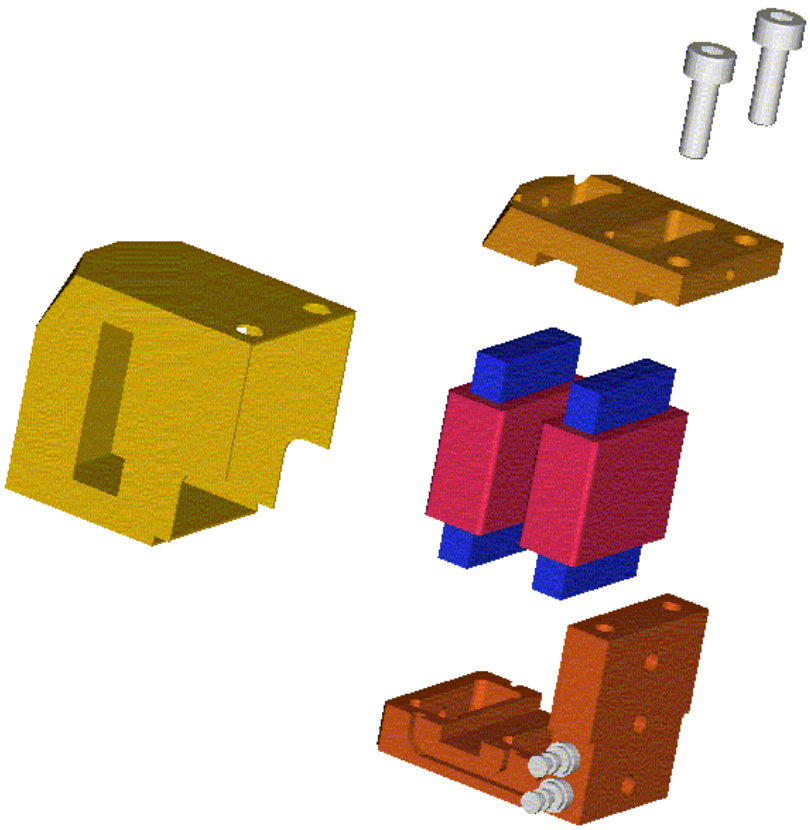

Figure 16 Assembly of a shielded motor assembly (SPIRE-BSM-020-005) with heat shielding

Drawing SPIRE-BSM-020-005, illustrated in Figure 16 above shows the motor block assembly concept.
The motor housing details require re-design in detail to accommodate the revised Zeiss coils, but the concept remains unchanged

8.2 Thermometers

The operating temperature of the BSMm will be 4-6K and the mirror or structure is to rise by no more than 1K from the nominal operating temperature.

The temperature of the BSMm will be monitored using a Lakeshore Cernox 1030 sensor, illustrated in Figure 17 below. This component is in fact more precise, and operates at lower temperatures (to 1.4 mK) than required by the BSM. However, to simplify spacecraft electronics and software architecture a common thermistor – driven by the requirements of the SPIRE cooler – is adopted.

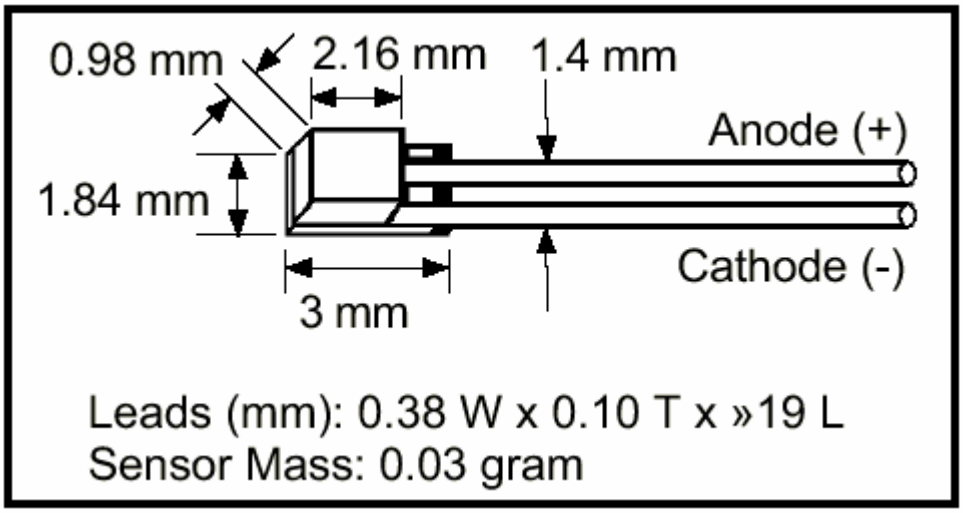

Figure 17 Cernox 1030 sensor (SD package)

CX-1030-CU copper canister , Figure 18 below, incorporates the above sensor, and provides for greater ease of mounting.

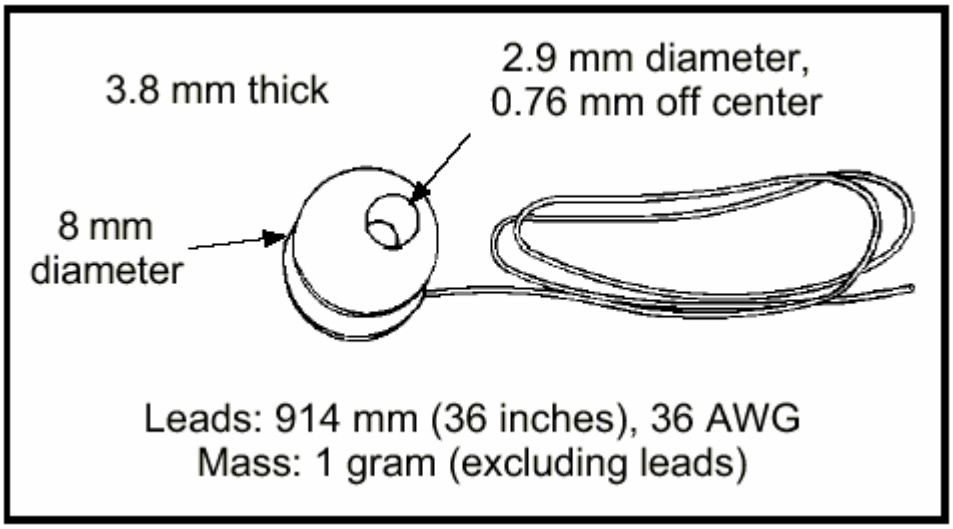

Figure 18 Cernox 1030-CU package

This device is sensitive over the 1.4K to 325K region. For cost reasons, flight rated but uncalibrated sensors will be procured centrally (e.g. by RAL) and calibrated against a calibrated sensor.

The maximum temperature rating is 325K, as shown in the data sheet Appendix 6, but as the specified soldering temperature exceeds this, no particular concerns are identified for bake-out at 353K.

The thermometers will be mounted to the BSMs – and a convenient location is identified as being in the rear “shelf” below the PCAL. This location allows space for mounting and for running the thermometer wires, and will provide a representative temperature of the motor and flex pivot-mounting environment, but could not be used to isolate heating or friction in a particular component.

8.3 Coatings

No coating requirements have been specified by SPIRE.

The BSM is widely gold-coated to control emissivity, and enhance thermal contacts at bolted joints, and in some places finished with alachrom 1200 finished (where no emissions control requirements exist but where corrosion control is required)

Gold plating of aluminium components will be a subcontract operation carried out directly on the machined surface and identified in the Declared Process List.

8.4 Surface Finish

Surface finish will be specified on component drawings as required.

8.5 Mass budget

The overall BSM mass budget, including the prime and redundant cryogenic harness is specified as less than 1100 gm, including harness. A full mass budget breakdown is given in Annex B, and illustrated below. The structural interface is the bulk of the mass, and could be addressed further to find additional light-weighting, though at additional cost.

BSM MASS BREAKDOWN BY FUNCTION (%)

Total 1120gm incl contingency

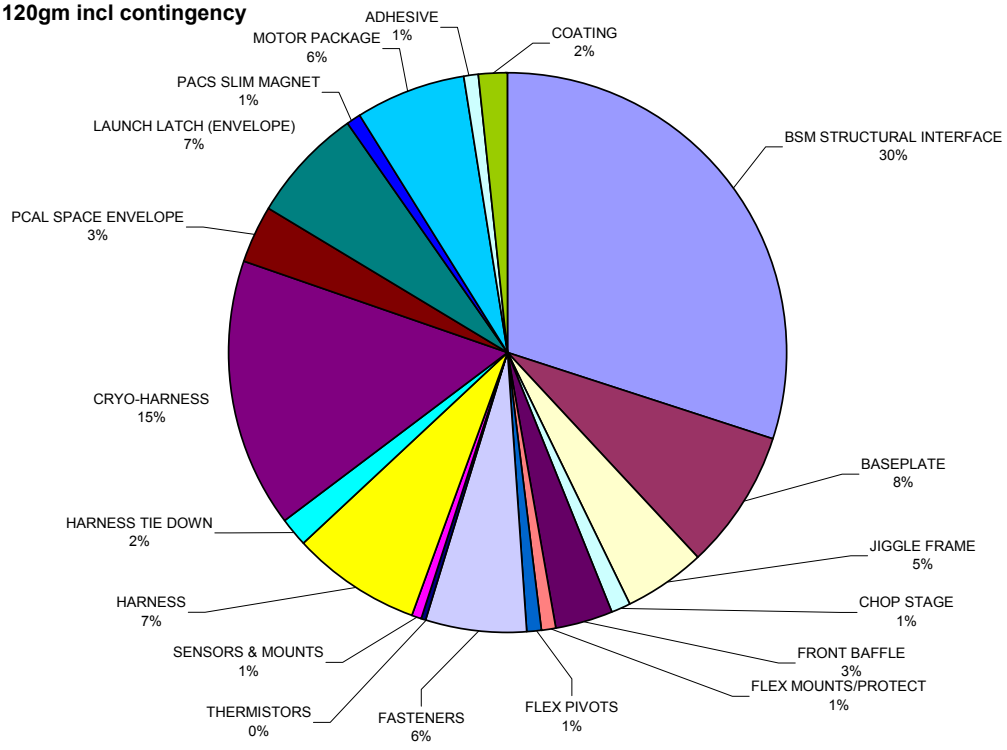

9. Optics

9.1 General

The BSM is a critical part of the overall SPIRE optical design (AD4). The BSM, designated CM4 in the optical scheme, allows for chop and jiggle motion to ensure full sampling of the instrument arrays without the overhead of moving the entire spacecraft. Fine pointing corrections may also be provided.

Requirements of the optical design (LAM) and stray light and baffling control (RAL) drive the BSM mirror design. Optical beam space envelopes, based on 20% oversize photometer and spectrometer beams are presented to ATC by RAL in the form of IGES surfaces and the BSM space envelope based around this.

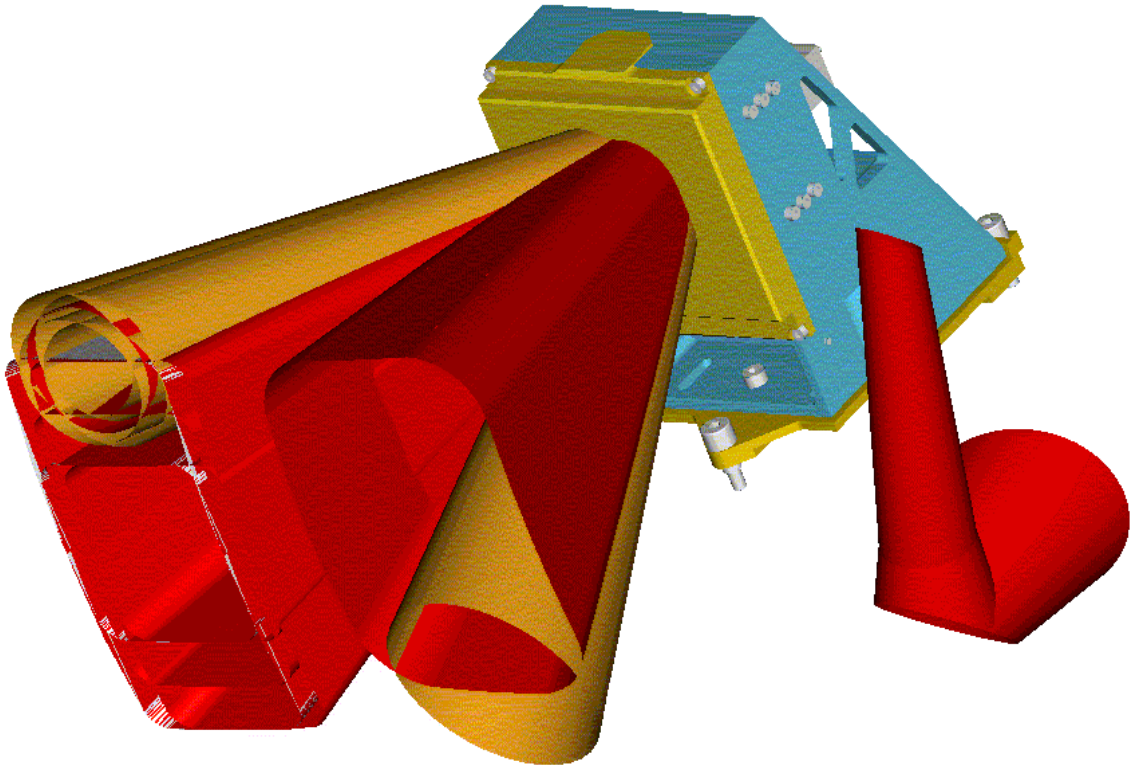

Figure 19: BSM with optical beam (20% oversized)space envelopes provided by RAL

The requirements of the optical design are encapsulated in the BSM specification document and it is to these purely mechanical parameters that the BSM is designed.

9.2 Mirror

The required (AD1) minimum mirror diameter is 32 mm. These requirements are derived from RD7 – Spire optics diffraction description.

The BSM design incorporates a 32.5mm diameter mirror. The monolithic mirror is incorporated into the chop axis and light-weighted from behind. The mirror is produced in aluminium 6061 alloy, thermally stabilised, as per ATC stabilisation procedure (RD8), and diamond machined to an optical finish.

The mirror surface of the BSM is required to

- Be flat to <100nm P-V to allow for optical testing. This is a tighter specification than the 1μm rms. (2μm WFErms.) which is required for functioning of the instrument.
- Have a surface roughness of <10nm (rms).
- The reflectivity of the mirror surface >99% in the wavelength range 200 - 670 μm. This will not be measured; it is assumed that this will be satisfied by machined aluminium 6061. (The emissivity of the mirror surface <1% in the wavelength range 200 - 670μm.)

For the purposes of interferometric testing at 633nm this surfaces specification will be adequate for testing of the surface form. At this wavelength the reflectivity will be approximately 80% which is more than sufficient.

These surface requirements are readily met by standard diamond machining techniques.

No requirement is placed on the BSM for any post-machining mirror surface coating. The mirror will be stored in a dry environment to prevent deterioration.

The BSM is required to have a central aperture, nominally of 2.8mm minimum diameter, to accommodate the PCAL source ‘light pipe’.

9.3 Baffle

The “baffle” is in fact just a pierced plate over the structure with the aperture sized to pass the oversized beams. The aperture size is designed by first cutting the solid model with the beams provided, and then 'tidying up' by applying next-largest size radii to facilitate machining. Precision location of the baffle is not required. Given the comfortable 20% optical oversizing, the requirement on location would be driven by the need to avoid mechanical fouls.

For this to be acceptable no part of the BSM structure must be hotter than 1K above the ambient temperature, and there must be no part of the structure clipping the 20% oversized beams. The motors will be sufficiently well heat sunk and shielded not to be seen as hotter than one degree above ambient.

The baffle or plate mounts to the BSMs front surface via 4 off M2.5 self-locking screws. The flanges at the top and bottom serve primarily to block the jiggle-frame flex pivot apertures, preventing contamination ingress and reducing light leakage paths

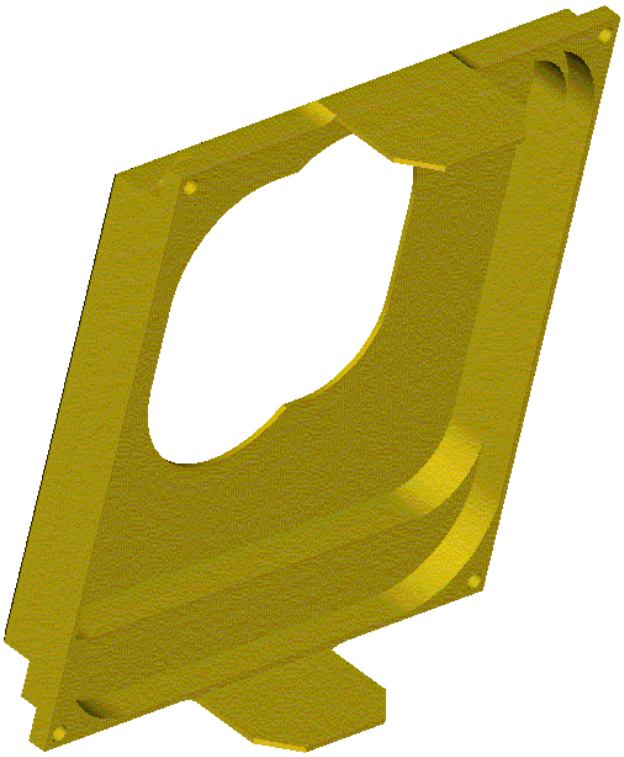

Figure 20: BSM baffle. The end 'tabs' provide debris closure of the flex-pivot apertures.

9.4 Light Tight Enclosure

There is no firm requirement on light tightness placed upon the BSM.

9.5 Harness Feed-Through

The BSM wiring harness to the motors require the mechanism enclosure to be pierced in a number of places for motor wiring feed through. These openings are at the rear of the BSM, which faces away from all optical elements of the SPIRE design.

9.6 Alignment

Alignment tolerances for the optical train are given in RD11, Spire optical alignment verification plan. These require that the BSM be positioned to ±0.1mm in x, y and z, with a total angular precision that would allow for the maximum total angular alignment error of the mirror, in the event of failure, to be ±0.18º.

Although the BSM provides for steering corrections and offsets, it remains desirable to provide precise location on the desired optical path such that a failure of the drive motors would leave the BSM in the failsafe position within ±0.18º of the nominal (0,0) position.

Rough calculations[1] show that direct mounting of the BSM to the optical bench would require that holes were placed with approximately +/- 0.1mm precision, and that the BSM rest position toleranced to +/- 0.14 degrees. The hole position tolerance is achievable, but the BSM rest angle may prove more problematic (as it will be attitude dependent) and an overly tight tolerance will increase assembly costs exponentially.

[1] Maximum mount hole pitch approx. 110mm. Allow BSM assembly to have errors of 0.14 degree, leaving 0.11 degrees for mount holes (RSS calc). Tan(0.11)x110 = 0.21mm, but allocate across 3 holes = sqrt(0.21^2/3) = 0.12mm

To allow additional latitude in the BSM assembly precision shoulder bolts will be used to locate on the optical bench a mounting 'shoe' with three machined pads, as commonly used in ATC cryogenic mechanisms. The BSMs proper will mount to this shoe, with the precise location (and the provision for one-off corrective machining) provided by mounting against the pads.

For alignment, the shoe is placed upon the SPIRE optical bench and actual positions measured via CMM. The as assembled BSM rest position and BSMs dimensions will have been characterised at ATC and the relevant offsets required would then be calculated. The shoe is removed from the bench and machined to provide pitch roll and yaw adjustment, then re-positioned.

The shoe, (drawing SPIRE-BSM-020-001-002) has been drawn to nominal size, but would be produced with +1mm oversized thick pads to allow for machining.

This scheme also allows removal of the BSM from the optical bench for trouble-shooting during AIV without loss of alignment.

9.7 OGSE

For alignment of the SPIRE optical train, a fixed mirror replaces the BSM whilst other systems are aligned (e.g. using a laser). The fixed mirror is 'Optical Ground Support Equipment' – OGSE and is supplied by ATC. The fixed mirror is required because the BSM is susceptible to vibrations when not damped or servoed to the (0,0) position powered. The resulting vibrations would make alignment work difficult, and the BSMe would not be connected/powered up during initial alignment.

The BSM OGSE consists of a mounting structure similar to the BSMs with a fixed, standard commercial optical quality, flat mirror mounted to it. It is designed for room temperature operation lab environment only.

The BSM OGSE will be mounted to the spire mount shoe as described for the BSM alignment.

10. BSM Electronics & Controls

10.1 Control System Design

The control system for the BSM is based on a PI compensator and rate feedback with demand feed-forward. In the case of the Chop axis, an input slew rate limiter is used to limit the mechanism acceleration to improve transient response. In addition, some cross-coupling correction is used from Chop to Jiggle to counteract dynamic magnetic forces.

The rate feedback signal is derived by a filtered differentiation of the position sensor output.
All control functions are implemented in software, allowing considerable flexibility – for example, in the event of some faults, such as a broken flex joint or loss of position signal, some degree of control can still be obtained, though of course performance is not to full specification.

The ‘no-sensor’ degraded mode operation derives a rate signal from the motor control voltage and current and then uses this to stabilise step response action. Amplitude control relies on the linearity of the flex joint spring torques.

It has not been possible to test a ‘broken flex’ scenario, but it is expected that adjustment of the existing parameters will give a useable performance from the system.

Section 10.4 describes the simulation of the software in Matlab-Simulink.

The electronics required to implement the control scheme is fairly simple, and limited to
a) Pre-amplification of the position signal from the magneto-restive sensor
b) Power amplification of the motor drive signal
c) A-D and D-A conversion to and from the software controller

The testing of the development models uses similar Simulink models to those described in this section. The relevant parts of the block diagrams (i.e. the control loops) are compiled into code using the same type of 'dSPACE' prototype development system that is also used by LAM. This code is then run on the Digital Signal Processor (DSP) that operates in the hardware part of the dSPACE system. The dSPACE system allows the necessary connections to the test hardware using A-D and D-A converters. This allows rapid prototype development of the software part of the BSM system. It is possible to alter code parameters while the hardware system is running to immediately evaluate the effects on performance.

10.2 Parameters

Normally, the control parameters are fixed and require no adjustment. However, all parameters used in the control algorithms can be changed if required, for example in the event of a fault. Each axis has up to 12 parameters for servo control.

In addition, there are lookup tables for linearisation of the position sensor outputs.

By use of flags and switches in the software, the structure of the controller can also be changed (in particular to suit fault conditions) by setting appropriate parameters as required.

10.3 Dynamic Analysis

See section 7.3.2(Mechanism mechanical analysis)

10.4 Simulink Model

The Matlab-simulink model used to simulate the software, test performance and establish control parameters is shown below. With regard to the following figure, the main model elements are described. As the

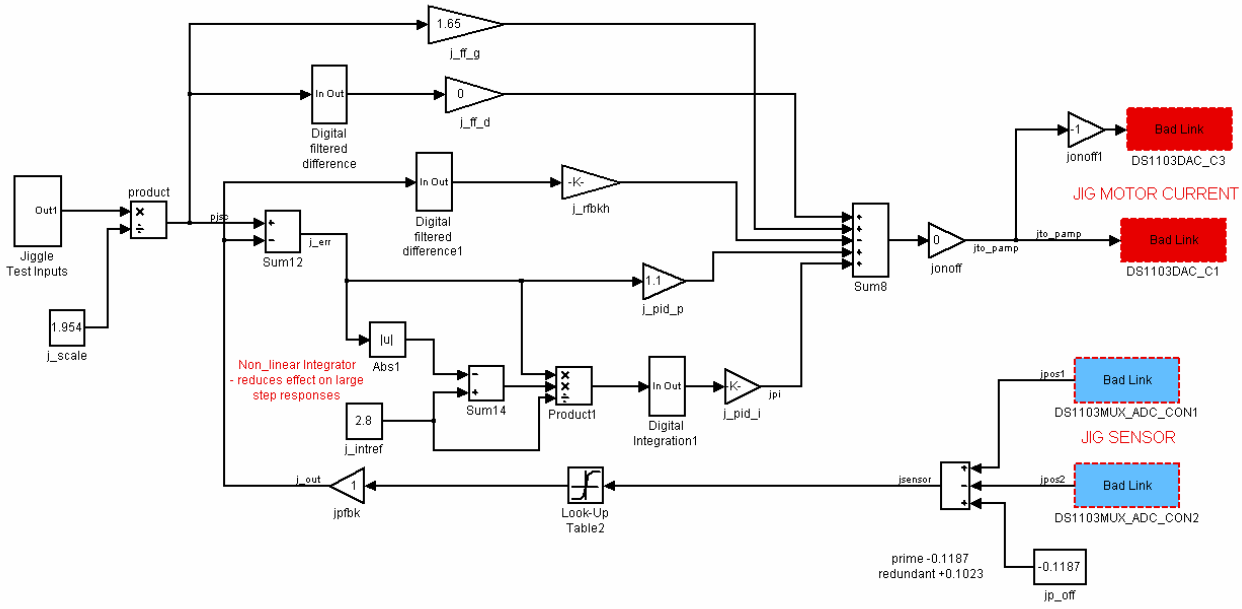

Figure 21 Simulink model

The software model includes gains, integrators, summing junctions and filtered differentiations.

The filtered difference is used to estimate rate from position sensor output, and to improve the feedforward signal from the demand.

The integrator has a voltage limit to prevent ‘wind-up’.

The Lookup Table is used to linearise the position sensor output to produce a linear movement of the BSM angle with respect to the demanded angle. Each sensor (PRIME and REDUNDANT, Chop and Jiggle) has its own table.

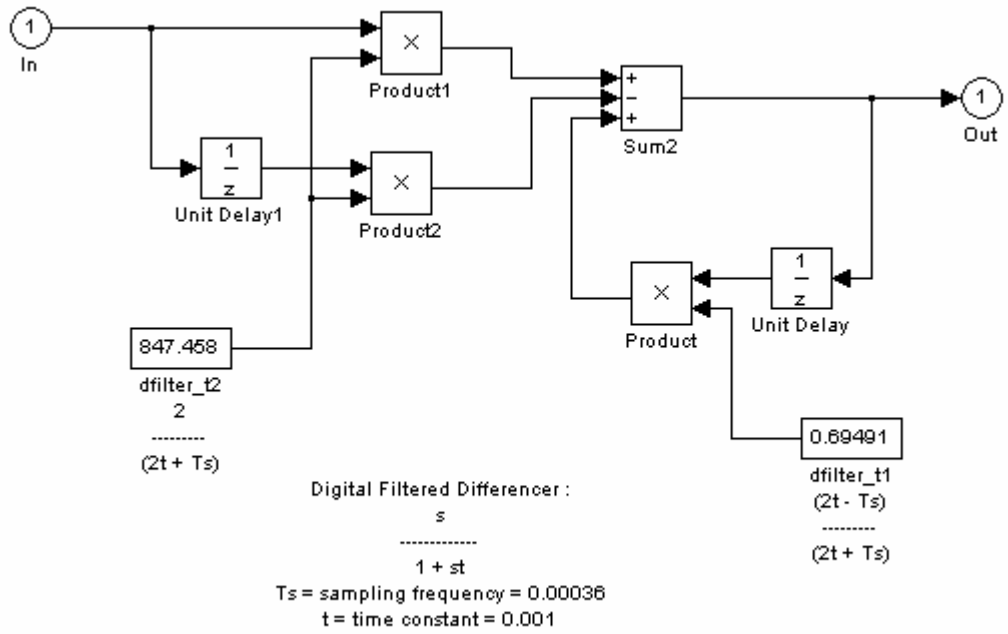

Figure 22 Filtered Difference

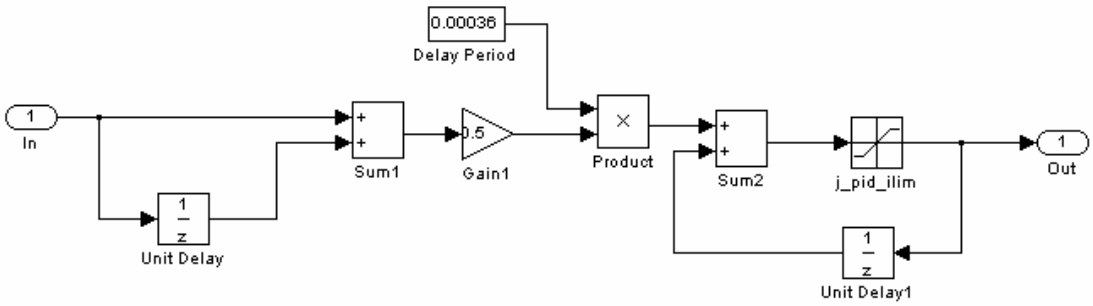

Figure 28 Integrator

10.5 Performance

10.5.1 Power Dissipation

System power calculations have been produced as follows.

The calculations are based on test results from the PFM model, but are generic when the correct parameters are inserted as indicated.

The BSM comprises two motors and two position sensors. The motors are composed of stators wound from either aluminium or copper wire, and rare earth permanent magnets. The position

sensors are regarded as fixed resistors for the purposes of this analysis, though in use this resistance changes by a slight amount.
The BSM mirror is constrained by low friction torsional springs, which require a constant force for a constant angle – this relationship is linear.

In operation, the mirror quickly slews between two fixed points, and stops for a relatively long time period, here called 'stare'. Due to the much longer period spent at the fixed locations, this phase dominates the average power calculations.
The stare power is caused by the constant force required to hold the angle against the support springs.

The motor power dissipation is calculated using the relationship
$P = I^2R$
where
P = power (watts)
I = current (Amps)
R = Resistance (Ohms)

The sensor power dissipation is fixed as a constant current is used.

The power dissipation calculations should include a duty cycle factor to produce an average power from the peak acceleration powers.
However, as the total power over time is dominated by the required spring force in the stare or static mode, the acceleration power has relatively little effect.

Average Power Dissipation = Chop transient power + I*I*R + Sensor Power

From PFM test data, Chop transient power can be estimated at 5mW average for 25mS. Therefore at 2 Hz the average transient power is 5.0*25/250 = 0.5mW.

Current as a function of angle can be obtained from data in spreadsheet "pfm_power.xls" , where (for example) Ichop(deg) = 21 mA/deg

To illustrate the calculation method, if the PRIME Chop axis continuously moves between -1.25 and 1.25 deg., Chop sensor power = 0.46mW and R = 0.822 ohm at 4 deg.K, the average power dissipation is therefore

= 0.0005 + (1.25*0.021)^2*0.822 + 0.00046 W

= 0.0005 + 0.00057 + 0.00046 W

= 1.53mW.

For more complex sets of movements, a spreadsheet can be used to calculate the average dissipation based the time sequence of movements, and assuming a linear relationship between transient power and chopped angle.

The Simulink model has also been used to estimate the BSM dynamic power performance.

The power dissipation of the BSM is dominated by the torque required to keep the axes at fixed non-zero positions against the spring force. Acceleration forces are of comparatively short duration. The figure below illustrates this.

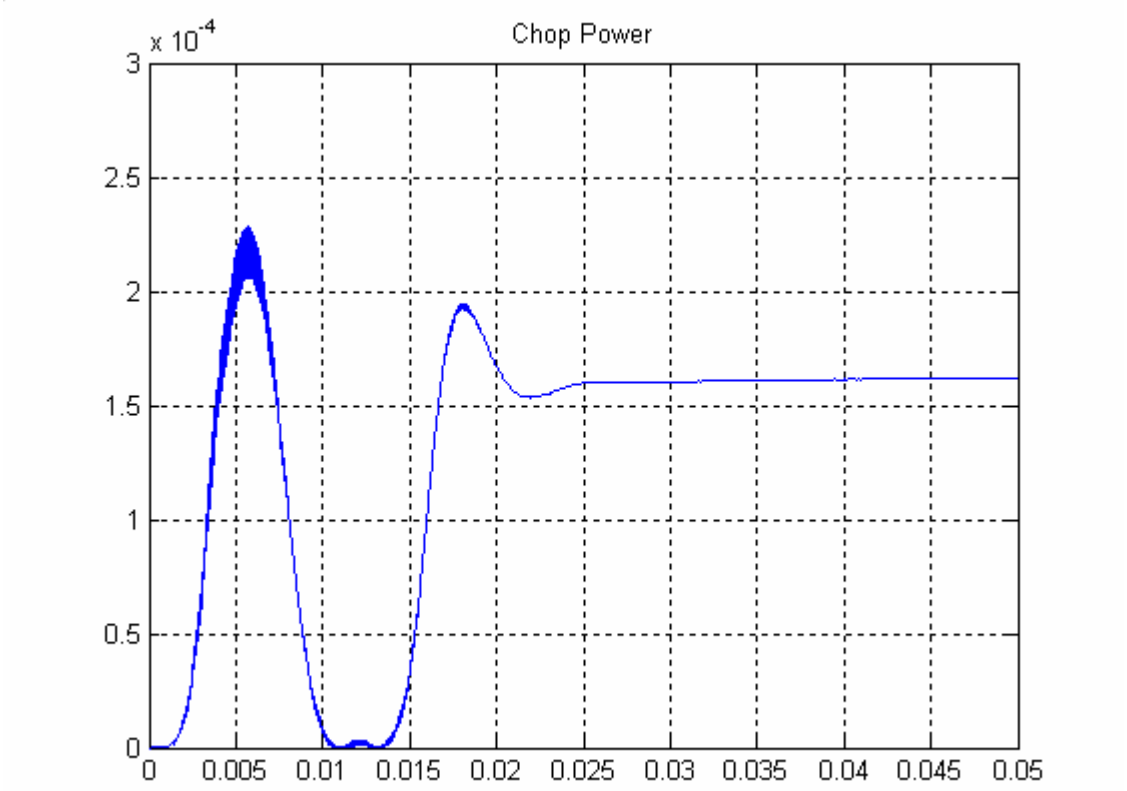

Figure 23 Predicted power (chop stage)

10.5.2 Rise Time

The simulated position rise times are within specifications for both axes (15 mS Chop, 40 mS Jiggle, for specification 20 and 100 mS respectively)

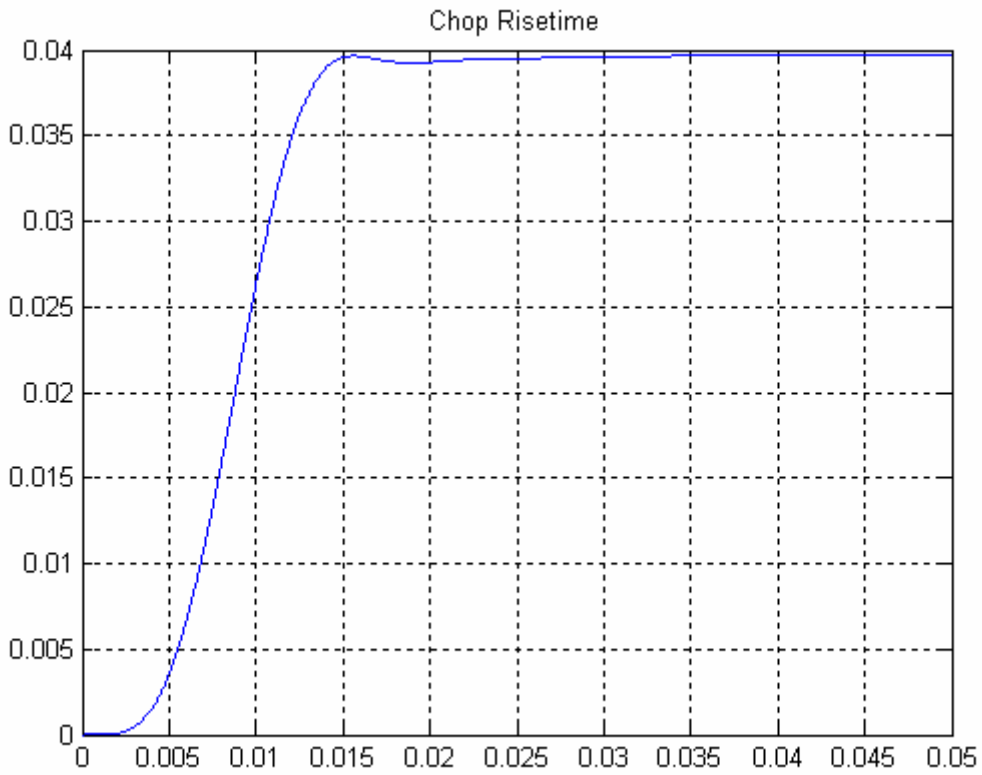

Figure 24 : Predicted chop stage risetime

Actual measured risetimes are the same as simulation for the Jiggle axis and slightly outside specification for the Chop axis at the maximum peak-to-peak throw.

10.5.3 Positional Stability

Both long and short term stability have been verified by optical methods (see End Item Data Pack of PFM), and found to be in specification.

10.5.4 Gain and Phase Margins

System gain and phase margins are described in the document 'BSM Control Systems Analysis', which indicates robust stability margins for the BSM control loops, allowing reasonable parameter variations without significantly affecting BSM performance.
Some resonance search testing on the two axis prototype using a sinewave drive to the power amplifiers and observing the position outputs using a Transfer Function Analyser has shown no significant resonance problems. The main flex joint support resonance is at approximately 15 Hz, consistent with theory, with minor structural modes at 663 and 830 Hz. Higher frequencies are not testable using this simple method.

10.6 BSMe Electronics

The Electronics specified by UKATC and designed by LAM takes the following form.

10.6.1 Block Diagram

In simplified form, this illustrates the interconnects between the BSM and its electronics.
The BSM mechanism motors and launch latch are powered from the Warm Electronics. The BSM position sensors are preamplified by the Warm Electronics.
The A-D and D-A functions, and the controlling code, operate within the LAM MAC board.
Finally, data and commands are exchanged via the MAC board to the SPIRE system.

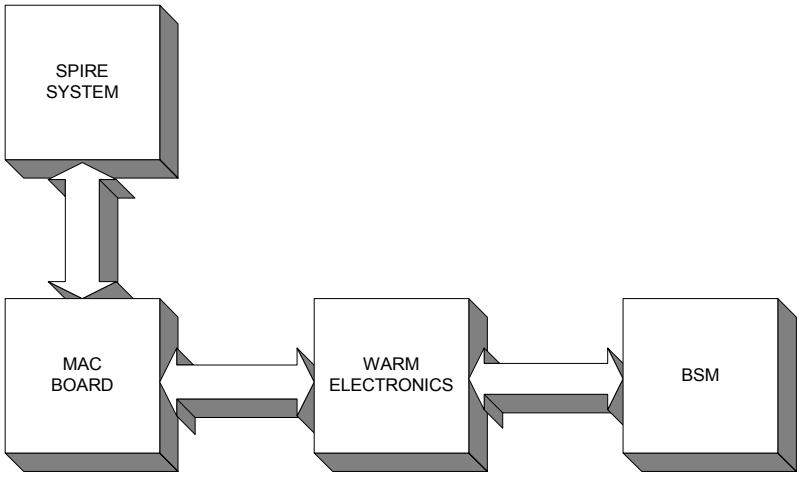

Figure 25 : Warm electronics overview

10.6.2 Position Sensors (Current Source)

The current sources use precision voltage sources (AD584) and voltage-to-current amplifiers.
The drawing below indicates prototype electronics. Refer to LAM data for the latest issue.

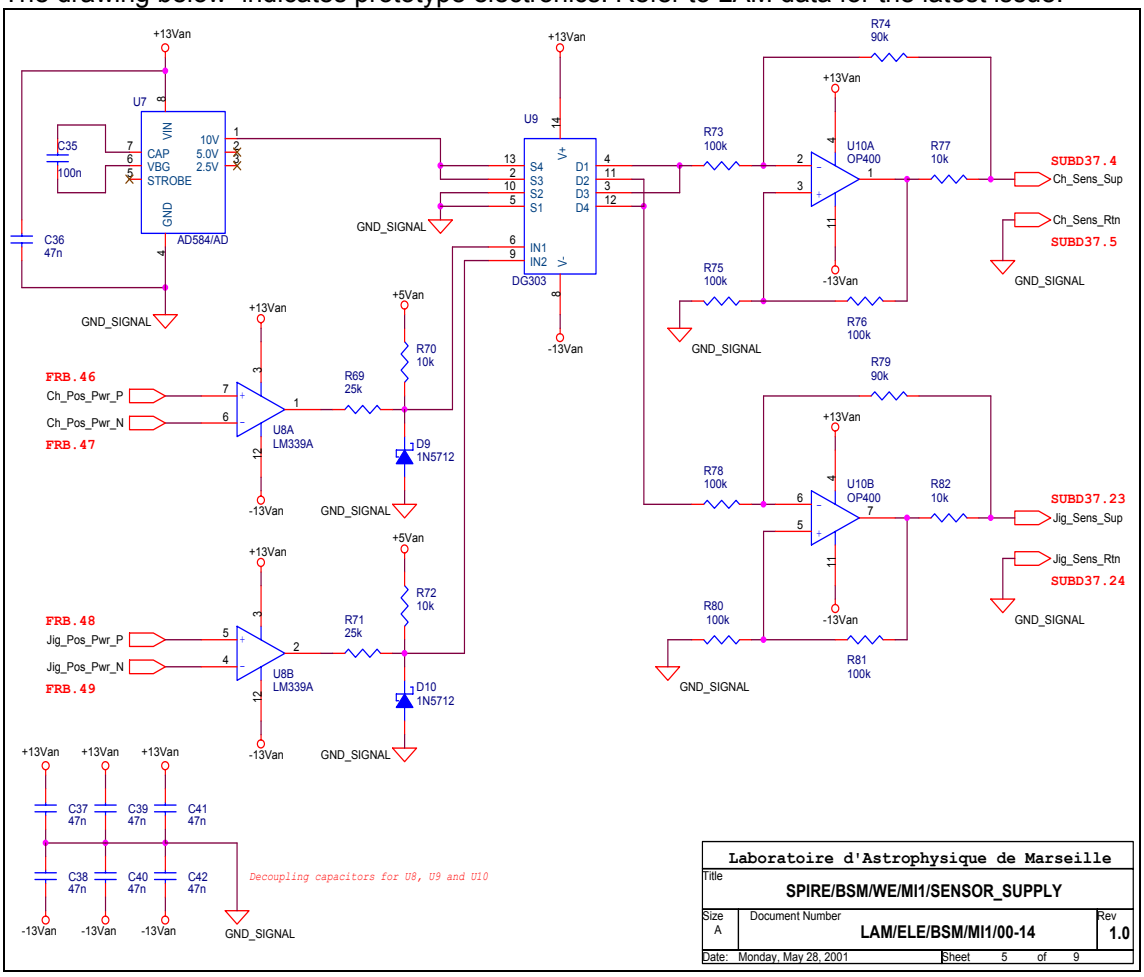

Figure 26 sensor supply

10.6.3 Position Sensor Read-Out Circuit

The position sensor outputs are differentially amplified to reduce noise pickup using monolithic instrumentation amplifiers.
The drawing below indicates prototype electronics. Refer to LAM data for the latest issue.

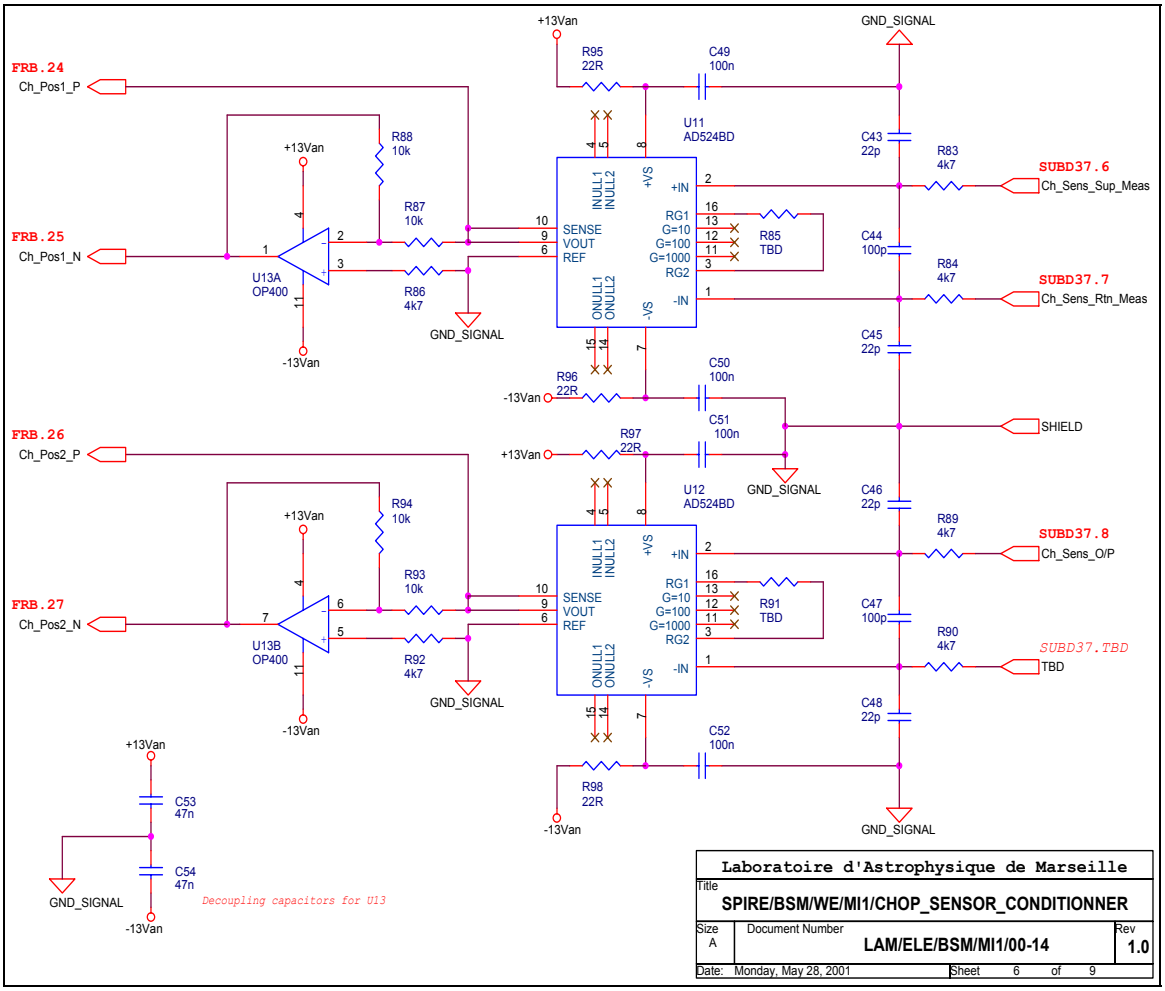

Figure 27 Chop sensor conditioner

10.6.3.1 Motor Power Amplifiers

The motors are driven by voltage-to-current amplifiers, which as well as reducing the effects of motor electrical time constant on the control loop, ensure stable operation with the large changes in motor resistance between cryogenic and ground test temperatures.
The drawing below indicates prototype electronics. Refer to LAM data for the latest issue.

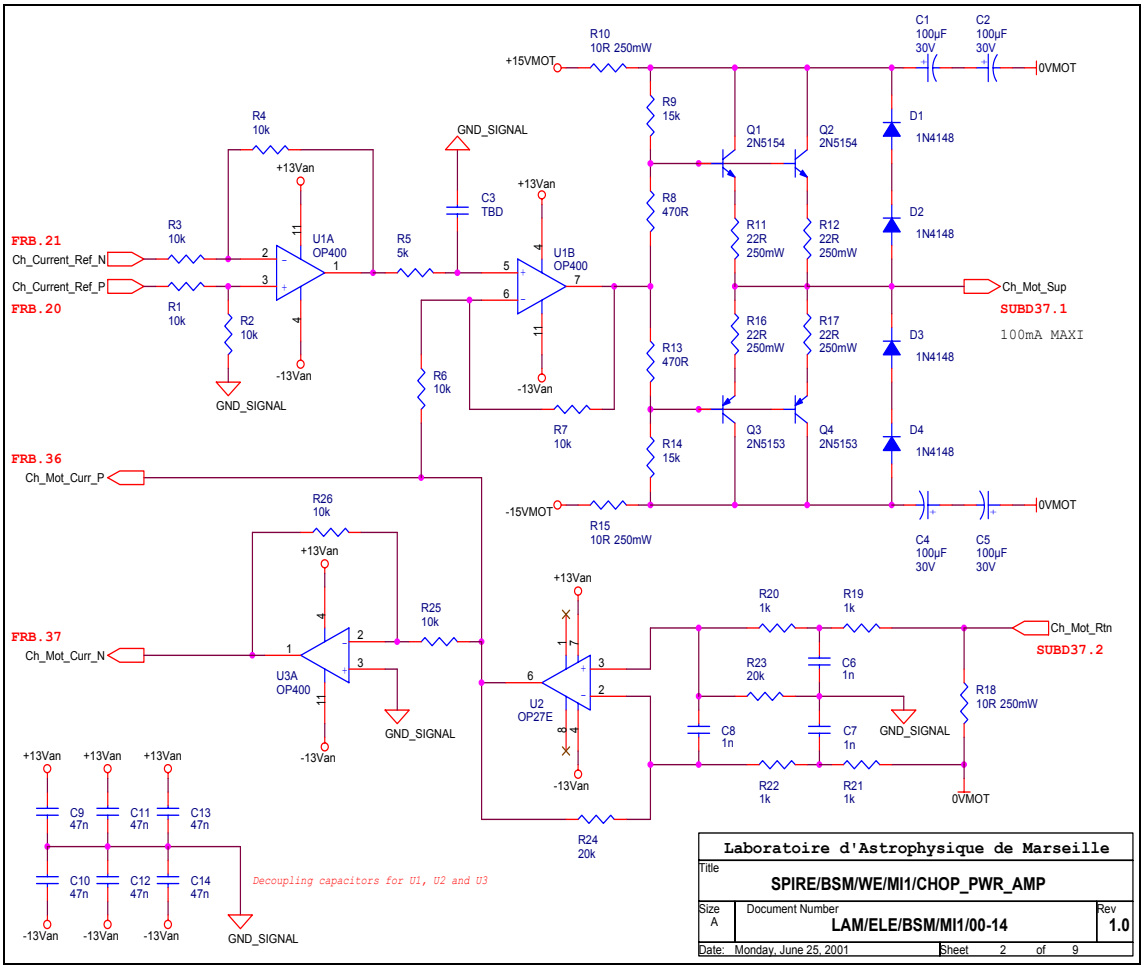

Figure 28 Chop Power Amp

10.6.4 Thermometry

Standard Cernox 1030 thermometers are used to sense local temperature on the BSM.

10.6.5 Power Supply

Power Supplies are standard +/- 15V and +5V supplies suitable for analogue electronics and digital electronics respectively.

10.6.6 Grounding Scheme

The grounding scheme ensures no electrical contact with the BSM structure, with the exception of overall screens on harness wire bundles from connectors, that should connect to chassis. Inner screened wires will terminate at the required component without any connection – however, the end at the warm electronics will be terminated to the local electrical ground for EMC screening. Overall electronics screening and grounding policy is agreed between UKATC, LAM and SPIRE systems.

10.6.7 Harness/Cables

Electronic/Electrical

The BSM wiring harness is designed to minimise EMC and cross-talk by suitable screening, and is described in detail in the UKATC BSM Electronic Interface document, AD 8.

The mechanically critical harness link between the Jiggle axis and the fixed structure uses a custom flexible tape with printed wires and screening, to produce minimum spring torque load.

The EMC effects of the harnesses are difficult to predict theoretically due to the strong dependence of layout on the capacitances between wires. As all wires also have braid screens connected to 0V,

it means crosstalk should be at the practical minimum. It is therefore not considered useful to analyse this further, and no problems have been found during testing.

Mechanical

The BSM prime and redundant harness are separate. Each harness includes the motor, sensor, thermometry and PCAL cables and interfaces via a fully populated 37-way MDM connector, as specified in AD5. The harness is run to the BSM as described in AD6, with a total length of approximately 415 mm.

Figure 29 shows the harness run on the PFM model..

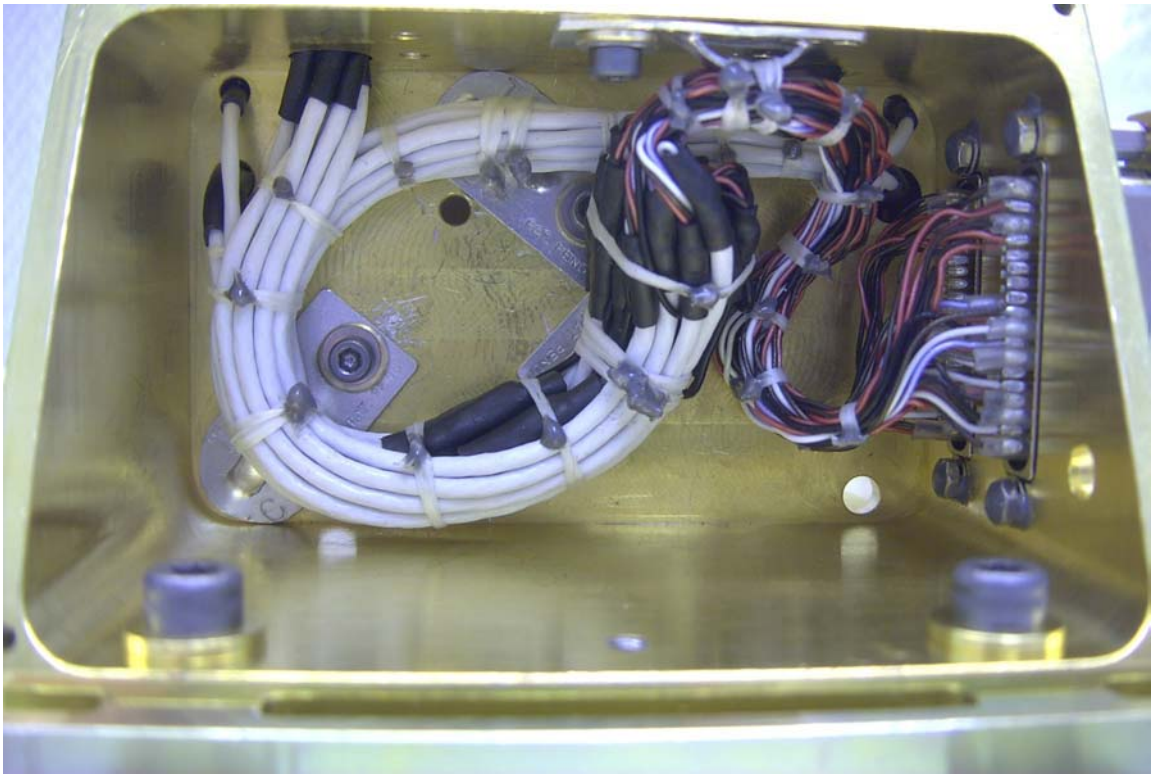

Figure 29 BSM on-board harness run showing prime and redundant harness runs

Key issues incorporated during development of this harness were :

1) provide apertures for the wiring to pierce the structural members.
2) Avoid light leaks as much as possible.
3) Provide for stake out of the harness, via P-clips, lacing and adhesive.

10.6.8 Interface to Digital Controller

The A-D and D-A interfaces, which are within the LAM MAC board, using SEi 78705 ALPRP 16-bit and Sei 7846 RP 16 bit converters respectively, ensure in particular an accurate position signal conversion, which is essential for BSM angle stability and accuracy.

The noise contribution from these devices is negligible. The most sensitive component is the A-D, which only produces a noise of 0.002% of full scale, equivalent to 0.0001 deg.

10.6.9 Motor Function & Wiring

A brief outline of motor wiring is described here. Mechanically, two coils are packaged together on each end of the chop and jiggle lever arms. However, electronically, a 'motor' consists of one coil at each side, as illustrated below.

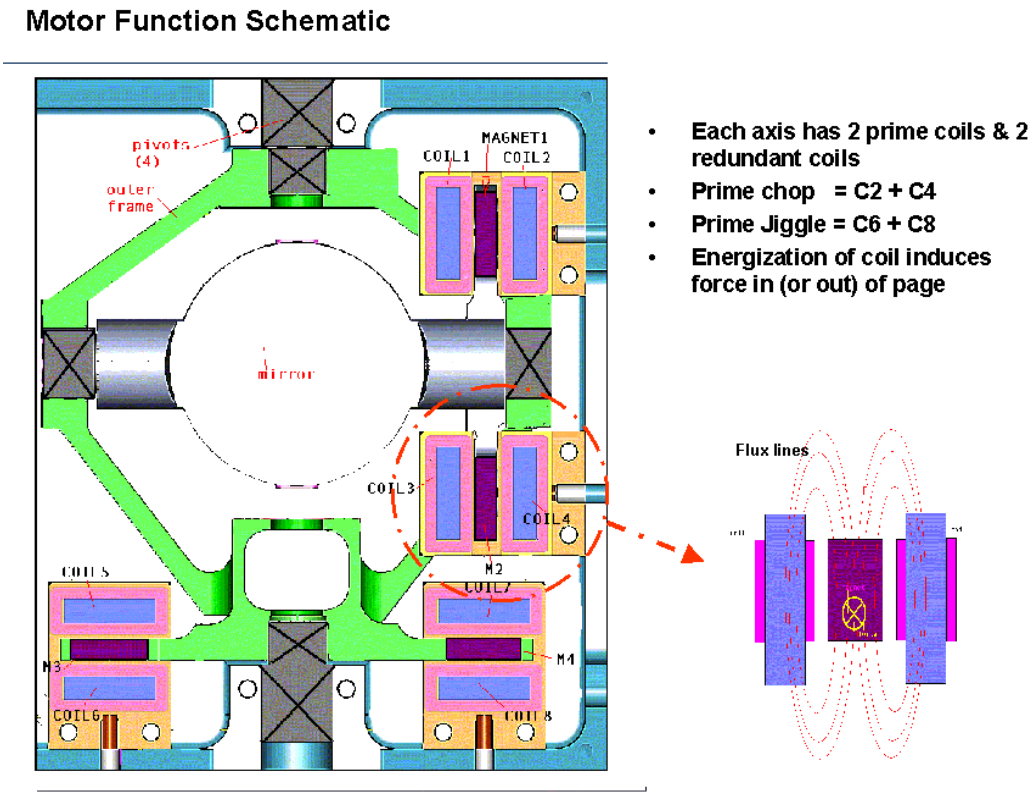

Figure 30 Motor Function Schematic

The wiring to each coil consist of a sense and voltage supply to each coil, and a single bridging wire between the two coils. Mechanically, the sense and voltage wires are run together (within a common screened cable). The bridging wire is run back behind the mechanism cavity, and joined by a solder joint. See the figure below.

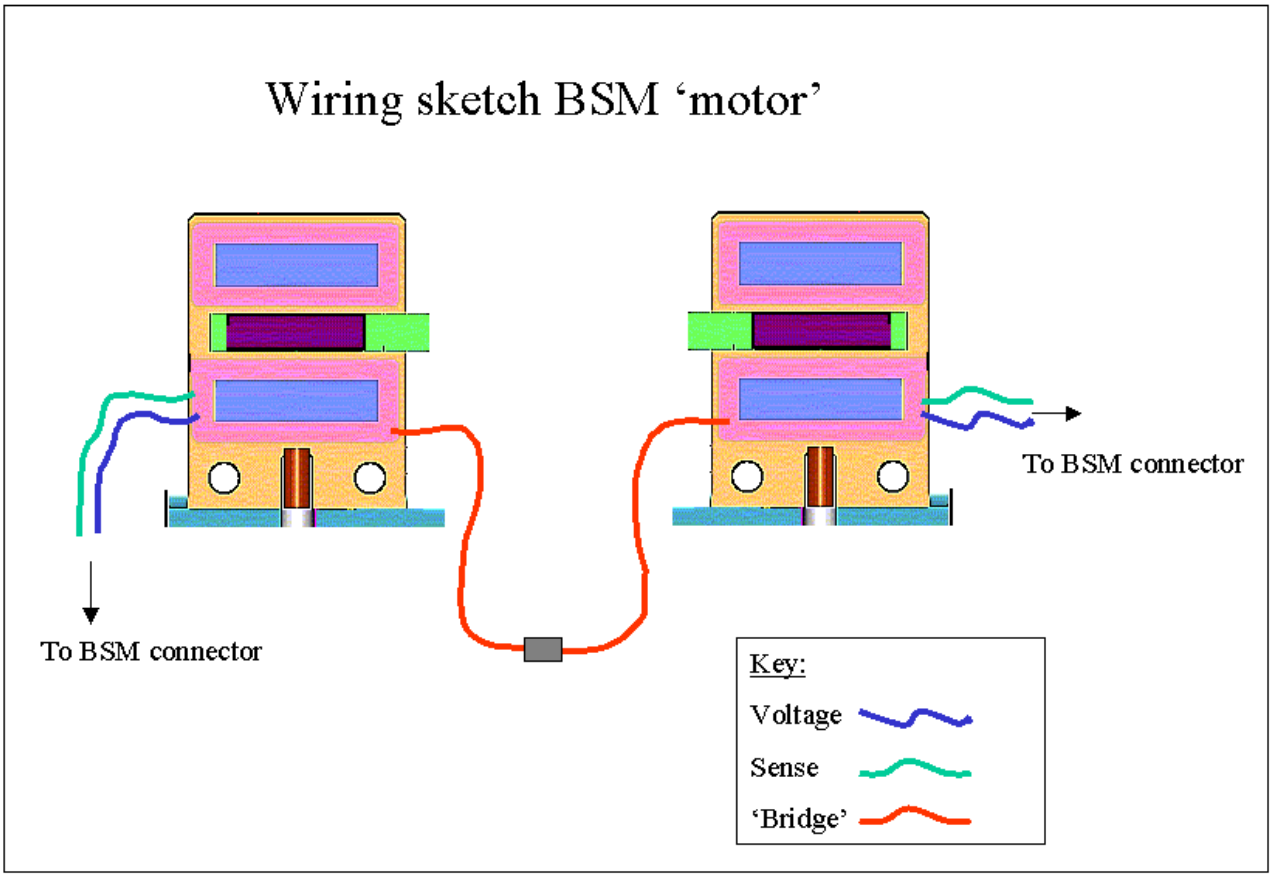

Figure 31 Wiring schematic for BSM motor

10.7 Components & Declared Lists

10.7.1 Component List

The detailed component list for components on the BSMm is provided in AD12, those in the BSMe are provided by LAM as part of the MCU DCL.

Generally, pre-space models use MIL-STD parts, and space-rated models use ESA/SCC parts obtained through the SPIRE common parts procurement system, for all electronics associated with the BSM, that is the BSM mechanism, Warm Electronics and MAC board.

Parts for the Warm Electronics and the MAC board are the responsibility of LAM.

10.7.2 Processes Soldering

UKATC wiring and assembly personnel have been trained at approved agencies in sufficient time for BSM assembly of space-rated parts. Therefore the soldering process conforms to the required ESA standards

10.7.3 Processes Crimping

No crimping is used in the BSM.

10.8 Electronics Systems Interfaces

10.8.1 MCU

The BSM does not interface directly with the MCU, however the DSP controller (MAC board) that runs the BSM control code also communicates with the MCU, so there is an indirect interface.
Refer to the LAM document: 'Mechanism Control Unit Design Description' LAM/ELE/SPI/000619 for a detailed description of the hardware interface.

10.8.2 Command List

Refer to the LAM document: 'MCU/DCU Command List ICD and User Manual' LAM/ELE/SPI/011011
For a detailed description of the software commands available for the pointing and operation of the BSM.

10.8.3 EGSE

The BSM mechanism is tested using the dSPACE system.
The control software can be modelled in real-time, or the BSM mechanism and associated electronics can be emulated for testing the software.
The dSPACE system emulates the following Simulink model of the BSM mechanism (one axis shown).

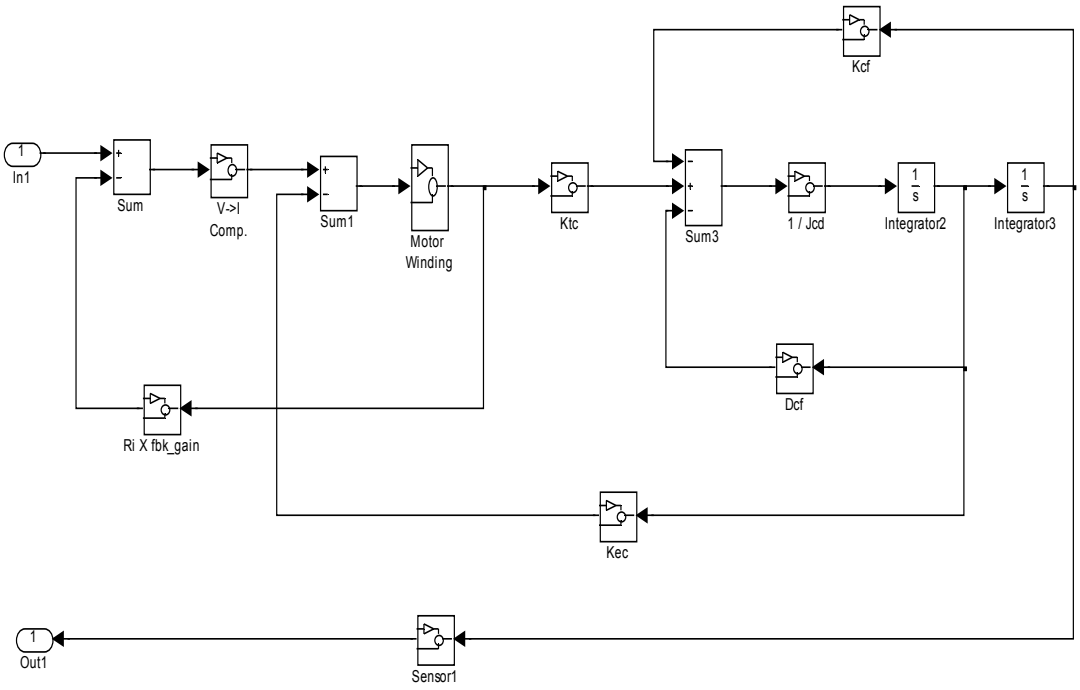

Figure 32: The model includes the mechanism with its inertia, flex joint spring and damping, and the motors, power amplifiers and position sensors.

11. Reliability & Redundancy

In the BSM design redundancy principles have been implemented so as to avoid single point failures, and the propagation of failures to other subsystems, by means of dedicated redundancy and specific protection devices. Where redundancy can not be realised the architecture is designed to limit the effects of a failure.

The BSMe consists of two complete separate circuits (situated on the same double Eurocard, but supplied by separate connectors to the BSMm). This provides complete parallel redundancy, with main and redundant position sensors and motors, driven by separate main and redundant analogue boards, which are in turn supported by separate main and redundant MACs and DPUs as shown in Figure 33 below. A common backplane connector is however advised by LAM for the MCU interface, for packaging reasons. The harnesses, both warm and cryogenic, are also maintained as separate systems.

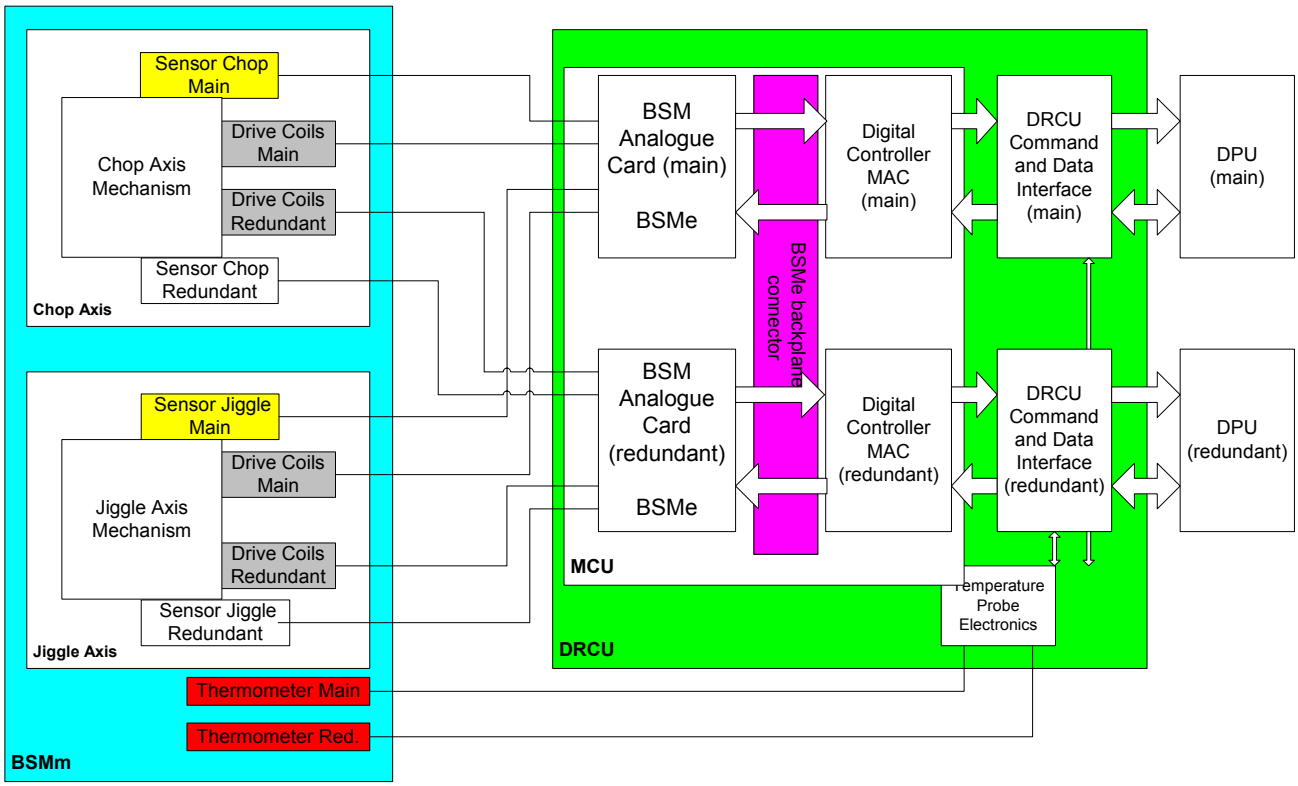

Figure 33 : BSM electronics architecture showing parallel redundancy

The BSMe redundancy scheme will not be able to operate independently of the SMEC mechanism. A failure in the primary system of either mechanism results in both switching to the redundant schemes. Equally, the PCAL and thermometry units carried aboard the BSMs would be required to switch at the same time.

The BSMs and BSMm mechanical design incorporates little redundancy. The structural parts are in general over-designed from a strength viewpoint in order to give adequate stiffness. The structures are maintained at very low stress levels during launch and even lower stresses during orbit. The primary sources of stress will be those induced on assembly and thermal cooldown. The components are manufactured from space-proven materials with good fatigue and stress corrosion cracking properties. The design includes the ability to limit the motion of the BSM during launch, to protect the flexures, and physical limits to the motion in the event of a component failure.

The design of the BSMs and BSMm should be such that the BSM will meet the reliability requirements for SPIRE as set out in the IRD (AD-1). In summary this is that a failure of the BSM should not lead to a total loss of the instruments ability to do science, albeit with loss of efficiency due to the need to use a backup observing mode. If for some reason the BSM were unable to move in either axis at all, then science could be obtained using the scan mapping mode - although there would be a serious loss of efficiency/sensitivity. The jiggle axis would provide some limited ability to modulate signal in event of a catastrophic failure in the chop axis and much worse than expected 1/f noise. In order to ensure that SPIRE can obtain data in the event of a BSMm failure, the mechanism must fail such the field of view of the FTS is still available, and that large or unpredictable offsets of the photometer field are not required.

This is achieved by ensuring *by design* that in the event that there is no drive signal reaching the BSM the mirror will be within +/- 0.18 degrees of the nominal bore-sight, and that in the event of a complete mechanical failure the mirror will be within +/- 1 degree of its nominal position.

11.1 Reliability Block Diagram

A reliability block diagram is presented in AD7. Key results are summarised here.

11.2 Single Point Failures

1. The wiring harness is a potential Single point failure, unless both the BSMe 'half' boards have an individual cable harness with it's own connectors.
2. The BSM structure and jiggle frame are SPF's. No surprise, but it reinforces the requirement for analysis of these structures for survival, and possible additional tests (e.g. to verify the FEA).
3. The analysis was performed assuming a launch damper (shorted motor coils), In the primary operations mode the launch damper 'unlatch' command must unlatch the primary mode motor coil, BUT MUST ALSO unlatch the cold redundant motor coils latching circuit. Vice versa for the redundant mode. This is discussed in the BSME schematic Subsystem Specification Document (Beam Steering Mechanism, Figure 4).
4. The same comment as (1) applies for the cables which send the unlatch command - they should remain separate and parallel.
5. The common connector at the BSMe board is undesirable but is advised by LAM on the grounds of space constraints and the problem that alignment tolerances could lead to an over stress of components if a single board is to be mated via two back-plane connectors simultaneously. Clearly, fully redundant connectors and boards would be preferred, and is being investigated by LAM

11.3 FMECA

A failure modes, effects and criticality analysis (FMECA) has been performed, AD7. This was carried out during the early design work.

The FMECA ‘viewpoint’ is that of normal operation, with the observing mode being assumed to require combined chop and jiggle motion of the BSM.

FMECA for the other states – off, standby, thermal cooldown, launch, have not been performed. For the first two the main implications are understood to be electronic. Cooldown and Launch failures have been folded into the main FMECA, as this is more pragmatic than creating a duplicate analysis.

For each element of the reliability block diagram, a number of failure modes and their implications are considered. The analysis is limited to considering a single component failure at any one time, except for cold redundant components where the operation is exposed only after a prime mode has failed.

The principal recommendations resulting from the FMECA are shown below. Note that these have been edited to remove those that don’t apply to the final design:

11.3.1.1 Software

1. Observation Definition Software needs to be robust handling chop/jiggle requests (i.e. not forgetting them or sending wrong one, or out of range value .....)
2. The bistable deployable end stop relay may have an indeterminate state, in which case the MCU must be robust against it.
3. MCU needs voltage limiter on analogue outputs, and software needs similar check to prevent the system from being driven out of range.
4 need to set invalid sensor range flags in WE (MCU) software

11.3.2 Electronics :

1. Single connector at BSMe backplane undesirable. The trade is between a single but rugged backplane connector and two less rugged single connectors. LAM to advise.
2. The short circuit case for the DRCU should be carefully considered in the MCU FMECA concerning propagation to the DPU.
3. Propagation of shorts between separate boards of the BSMe and the internal protection should also be considered. in the MCU FMECA

11.3.3 Mechanical :

1. Good process control on magnet adhesive is required
2. The flex pivot mounting is critical.

11.4 Critical Components Identification

We assume that items which require declaration here are those which "fail to meet the project requirements" for *failure tolerance*, or undetectable loss of redundancy.

As discussed above for SPIRE the failure tolerance is total loss of science - i.e. a failure of the BSM which would result in (a) large pointing offset for the photometer or/and (b) inability to take data with the FTS due to loss of its field of view. i.e. critical components would be those whose failure would result in the BSM failing to meet the required fail safe positions defined in SPIRE-ATC-PRJ-000460, 4.2.13 and 4.2.14.

No such components were identified, but the design must ensure that the fail-safe positions are met should one or more flex pivots or motors fail.

12. Interface Control Documents

This is a separately controlled project document

13. Assembly, Integration & Verification

13.1 General

AIV requirements are primarily programmatic, and met through the product assurance plan (AD3), the test plan and development plan (RD5). These programmatic issues are not discussed in the design description

However, there are several design implications and features of relevance, which are discussed below.

13.2 Assembly

The BSM design is compatible with assembly in a class 1000 clean room. Volatile materials are avoided, and all components are capable of immersion/cleaning with isopropyl alcohol or in an ultrasonic bath.

The development and product assurance plan requires that parts are fully traceable for build configuration control on deliverable models, and where test data forms part of the qualification process. For all components of adequate size the design drawing identifies a location to permanently mark the component drawing number, revision and serial number. Components of small size will either be marked with the serial number alone (which shall be unique for all components and cross-referenced to drawing number, revision and manufacturing lot). Below a certain size of component (e.g. small fasteners, P-clips) the components will be 'bagged and tagged', with the packaging identifying the part numbers.

The method of marking each component is based on engraving or etching. Where components are subject to high stress levels the design drawing will ensure that marking will not act as a stress raiser.

The BSM design is inevitably comprised of small components within a tightly packed assembly. Consideration has been given to access for fasteners and wiring harness, and additional lessons learnt from prototyping will be incorporated into the design via the change-control process. The BSM comprises several sub-assemblies and the tight alignment tolerance leaves the design vulnerable to tolerance stack up if not correctly approached. The following design features and assembly aids are incorporated into the design:

13.2.1 Flex pivot protection sleeves:

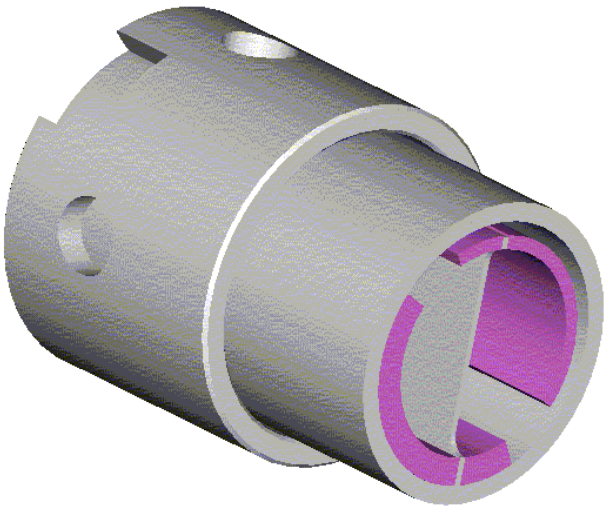

Figure 34 flex pivot mounted in protection sleeve (note holes for adhesive- this allows glue to be added after assembly and reduces risk of adhesive being placed on moving parts)

The flex pivots are sized as a light push fit, avoiding buckling loads on the flexures during installation. To ensure survival of warm vibration and maintain position during build, the pivots are fixed with a cryogenic space rated adhesive - Eccobond 285. The pivots are not marked for identification, but the flex pivot sleeves are identified externally as they are required in handed pairs..

13.2.2 Mirror handling

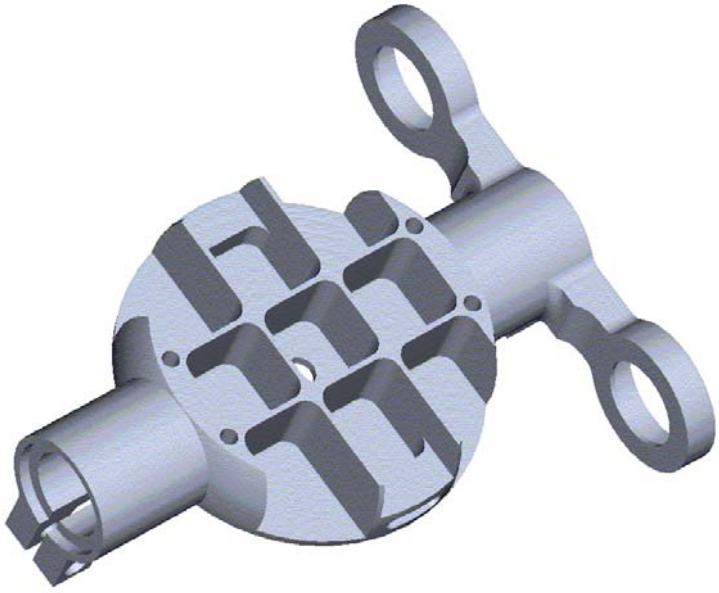

Figure 35 underside of mirror showing light-weighting and 4-off tapped holes for process mounting

The chop stage and mirror have four tapped holes on the mirror backing structure. These provide a clamping facility for optical machining, and are useful in subsequent processes. Inserts are not placed in the threads to avoid print through at cryogenic temperatures.

13.2.3 Chop Stage (drawing SPIRE-BSM-020-004)

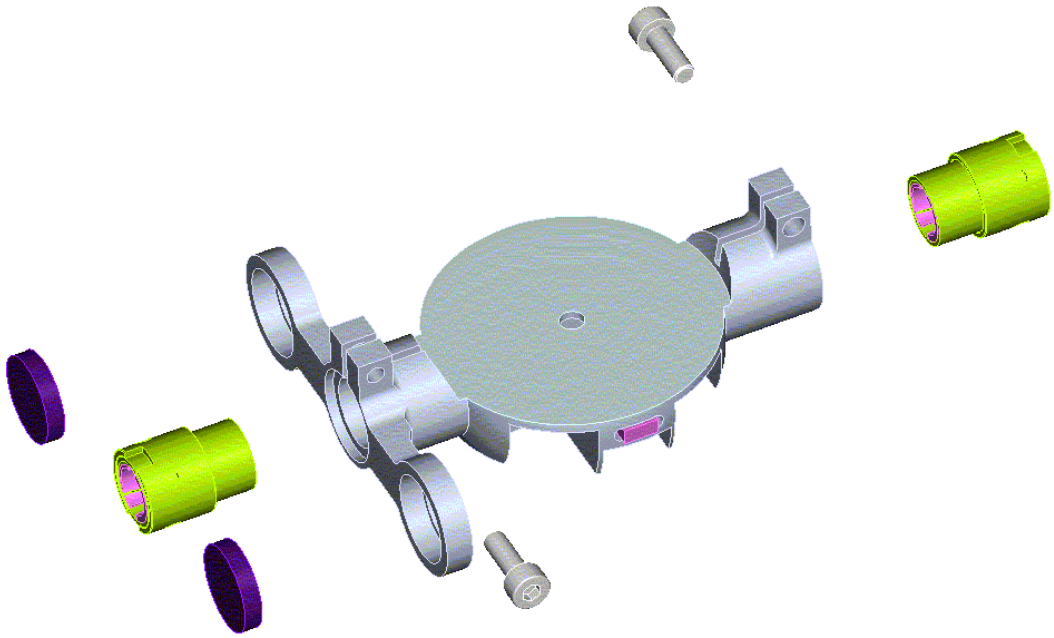

Figure 36 Chop stage assembly showing sensor cores (pink), magnets (purple) and flex-pivots (green)

The insertion of flex pivots into the chop stage is facilitated by an open fit, clamped up by a screw after assembly and alignment.

The sensor cores are pushed into the bottom of their pockets, facilitating positioning, and glued in place.

The magnets are a slight push fit. They are centralized in the mounting pocket by measurement and retained by a fillet of adhesive.

13.2.4 Motor Assemblies (drawing SPIRE-BSM-020-005)

Alignment of the motor air gaps is a critical design parameter - both to optimize torque performance and to avoid the possibility of fouls.

A design aim is to avoid shimming or adjustment of the assemblies, as with 4 off motor assemblies per BSM model there will be strong advantages to interchangeability.

The motor assemblies be bolted together with the coil cores as a loose fit in their pockets (0.25-0.5mm gap). An assembly jig (BSM-022-002) will locate the motor coils with high precision with respect to the coil bracket mounting face and hold them in place whilst the adhesive cures. This will produce an assembly with high precision (25-50 microns) repeatability on mounting.

13.2.5 Jiggle assembly (drawing SPIRE-BSM-020-003)

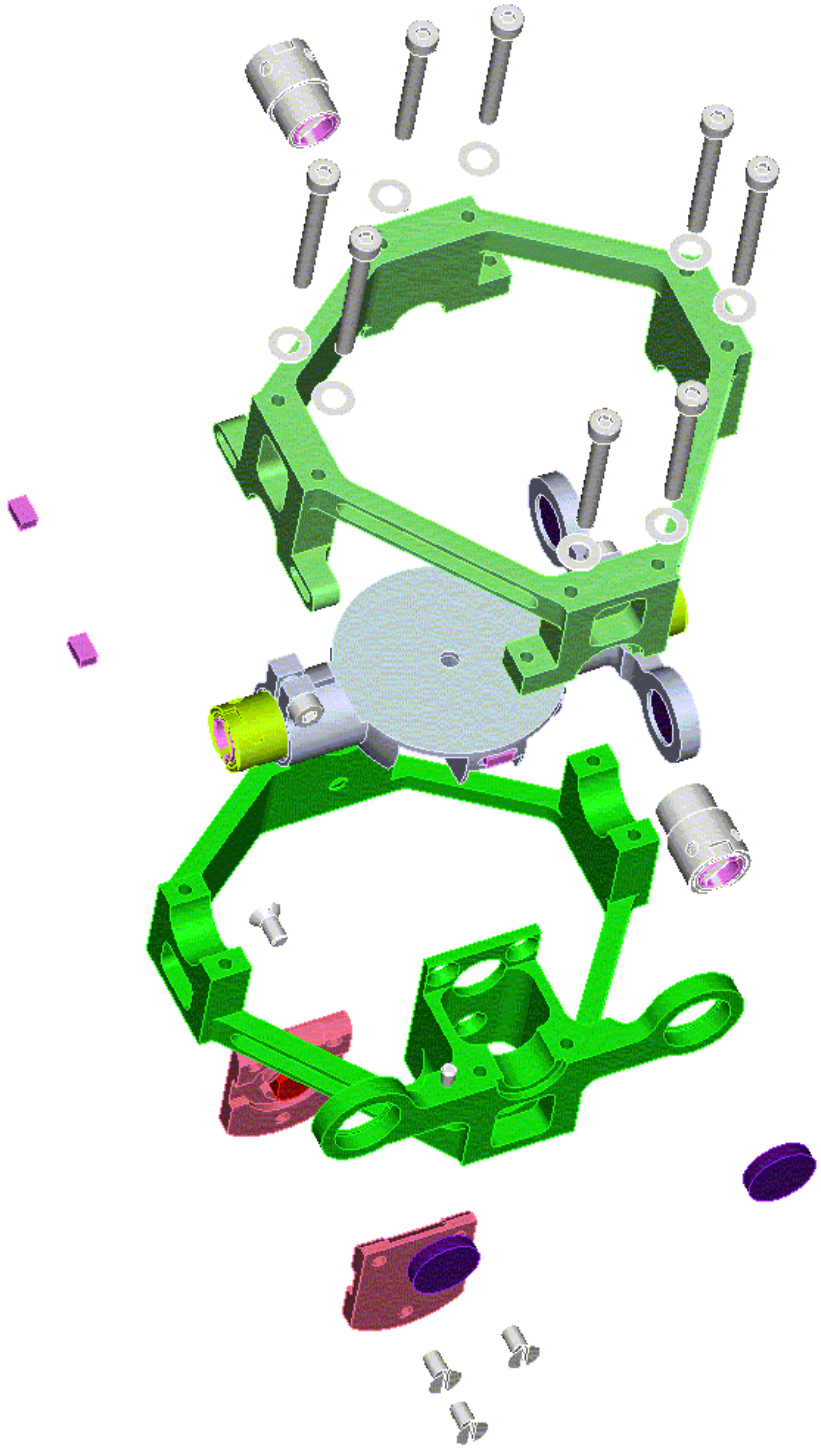

Figure 37 Jiggle stage assembly showing jiggle frame (green), sensor cores (pink), Infineon sensors (red)

Alignment of the mirror at the correct geometric location is important,

- to minimise optical alignment of the BSM on integration to SPIRE
- to ensure that the distance between the chop axis magnet lever-arms and the jiggle axis bores is correct, to prevent fouls between the magnet lever-arms and the drive motor assemblies.

- the mirror must be located flat within the jiggle frame so that it's rest position will be within the fail-safe tolerance.

This task is complicated because

- the flex pivots will easily take a small pre-load during the assembly process, and thus spring back to an undesired position when done.
- The presence of strong magnets attracted to local objects creates offsets or lack of control,
- The need to fit the 'lower' chop axis motor housing during the build of this assembly adds a dead weight to one lever arm.

The rest position of the mirror is checked, by reflection of a laser from the mirror surface compared with the reflection from a mirror fixed to the structure and visible through the central hole. A small re-adjustment of the mirror is then necessary.

13.2.6 Jiggle frame to structure assembly

The complete 2 axis gimbal mount and remaining three motor assemblies are installed at this stage. Due to CNC machining of the structure, and to position of the mirror by measurement, the tolerance stack up is limited. Nevertheless the motor air gap is checked and the motor coils assembly adjusted at this stage.

13.2.7 Harness routeing

The motors and sensors have flying leads soldered to them at the sub-assembly stage. These flying leads are then be routed through apertures in the BSMs bulkheads and staked down as appropriate. The attachment of the flying leads into the on-BSM connectors will require soldering operations on an assembly which will be 'clean' at that point. This operation is carried out in cleanroom conditions.

13.3 Integration

All components are capable of withstanding bake out to 80 deg C.

The PCAL interface is a toleranced hole and mounting face, and no mechanical problems are envisaged.

The alignment issues of integration to the SPIRE optical bench are discussed elsewhere in this document (section 7 Mechanical and section 9, Optical)

13.4 Verification

Verification / test plans for the design are outlined in RD 5 and described in test reports (see End Item Data Pack for PFM).

13.5 Transport & Storage

The BSM will be transported in a sealed container. As postal service vibration loads are well known to be more rigorous than launch loads, the device will be hand carried.

The transport container will provide for storage facilities also. Components and sub-assemblies will be stored in dry Nitrogen environments where required. For corrosion control and protection during handling, components will in general be gold plated, Alochromed or sealed / potted as applicable.

13.6 Handling

No special handling requirements are envisaged, beyond normal clean room care and attention.

13.7 Test Programme & Test Matrix

The Verification / test plans for the design are outlined in RD 5

14. Appendices

14.1 Appendix 1 : Not used

14.2 Appendix 2 : Not used

14.3 Appendix 3 : Structural Analysis :

14.4 Appendix 4 : Not used

14.5 Appendix 5 : Not used

14.6 Appendix 6 : Thermal Calculations

14.7 Appendix 7 : Control Analysis

14.8 Appendix 8 : Not used

14.9 Appendix 9 : Single axis prototype test results

This page left intentionally blank

Document Ends

Appendix 3
v1.0

3A: DYNAMIC ANALYSIS OF THE BSM

1 BSM DESIGN

2 FEA MODEL

2.1 MODELLING
2.2 LOAD CASES

3 RESULTS

3.1 STATIC STRESS ANALYSIS
3.2 DYNAMIC ANALYSIS
3.2.1 Frequency analysis
3.2.2 Damping
3.2.3 Chop axis excitation
3.2.4 Jiggle axis excitation

4 REFERENCES

4.1 MASS PROPERTIES

APPENDIX 3B: STRUCTURAL INTERFACE FEA RESULTS

1 SCOPE

2 MODEL

2.1 DESIGN
2.2 FEA REPRESENTATION
2.3 SOFTWARE

3 RESULTS

3.1 50 G ACCELERATION LOAD CASE
3.1.1 Deflection results
3.1.2 Von Mises Stress results
3.1.3 Analysis report (extracts)
3.1.4 Verification
3.2 MODAL ANALYSIS
3.2.1 Modal Analysis Results
3.2.2 Model report (extracts)
3.2.3 Verification

APPENDIX 3C: STRUCTURAL INTERFACE MANUAL CALCULATIONS

1 SCOPE

2 CALCULATION

3 DISCUSSION

3A: Dynamic Analysis Of The BSM

Document No:	spire-bsm-001-tdn-001.doc.133
Status:	Draft
Version:	10
Modified by:	Richard Bennett
Modified date:	29 June 2004 1:19
Author:	Richard Bennett
Created date:	4 May 2000 5:04 PM
Category:	Technical Design Note
Type:	
Generated with:	Microsoft Word 8.0

1 BSM Design

The SPIRE Beam Steering Mirror has been modelled for finite element analysis as a simplified representation of the Pro/E solid model shown below.

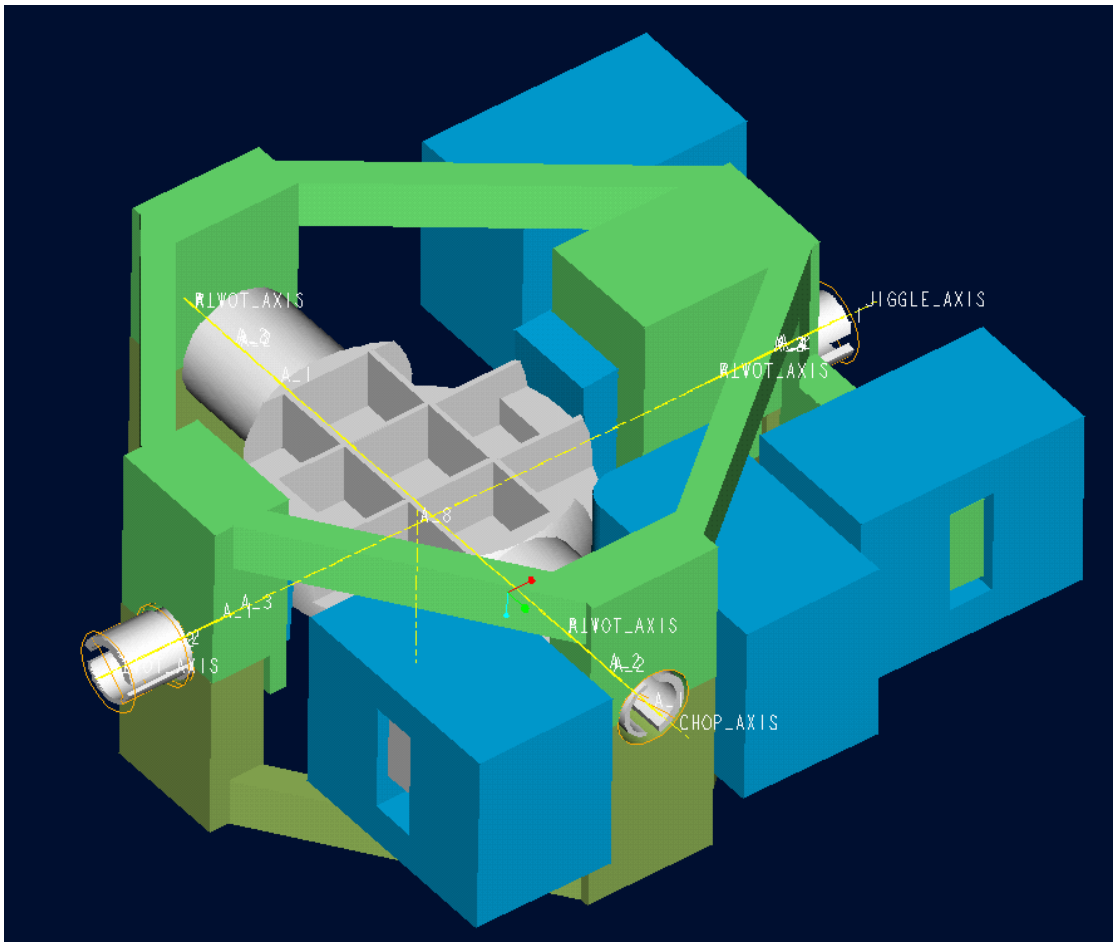

- The chop stage is monolithic. The underside of the mirror is lightweighted and has pockets for the iron plates for the sensors.
- The jiggle stage is split and clamps together around the flex pivots.
- Space envelopes for the coils and sensors (potted) are shown in blue.
- The outer rings of the flex-pivots are not shown for clarity.
- In this revision Lucas 5010-600 pivots have been used for the jiggle axis and 5010-800 for the chop axis. These have torsional stiffnesses of 0.0286 and 0.0036 lb.in/degree respectively.

2 FEA Model

2.1 Modelling

- The jiggle stage structure has been represented by thin shell elements;
- The chop stage has been represented by a tube of solid elements together with lumped masses (shown red in the illustration below) to give the same mass and moments of inertia as the solid model;
- The flex pivots have been modelled using a combination of solid and shell elements.

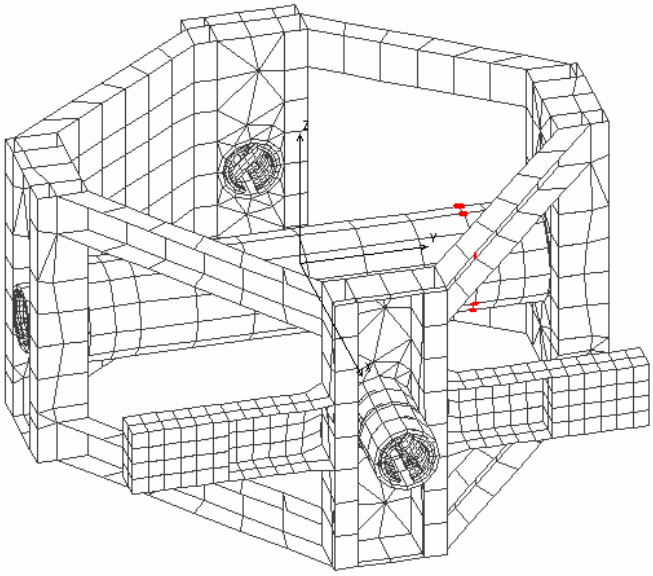

- The jiggle stage framework between the flex-pivot housings has been modelled as 5mm x 5mm x 0.5mm channel section.
- The pivots have been moved as far as reasonably practical towards the mirror to minimise the inertia and maximise the stiffness. To clear the coils this leads to an asymmetric arrangement.
- To balance the jiggle stage the framework in the opposite corner to the coils has been made solid. This also increases the stiffness of the structure. Due to the use of lumped masses which do not give the correct products of inertia and also because the jiggle stage has not been dynamically balanced their will be some inaccuracy in modelling coupling of the stages.

2.2 Load cases

The following analyses have been made:

- 50 g static load in X,Y and Z directions
- Frequency response analysis for excitation of the chop and jiggle stages by couples of 1 Newton forces at the centre of the drive magnets (equivalent forces for the chop stage.)

3 Results

3.1 Static stress analysis

The three load cases (50g in X, Y and Z) lead to stresses in the flexures of similar magnitude.

The highest stress, 265 MPa, occurs in the jiggle axis flex-pivots. The 0.2% proof and ultimate tensile stresses and of 420S29 equivalent to the stainless steel used for these items are 555 MPa and 755 MPa respectively so the design appears relatively safe. It should be noted however that the model is a simplified representation for dynamic analysis and would need refinement for accurate stress calculation.

The load capacity of each of the pivots is 245 N (55 lb) and the weight of the jiggle and chop stages at 50g is 27 N.

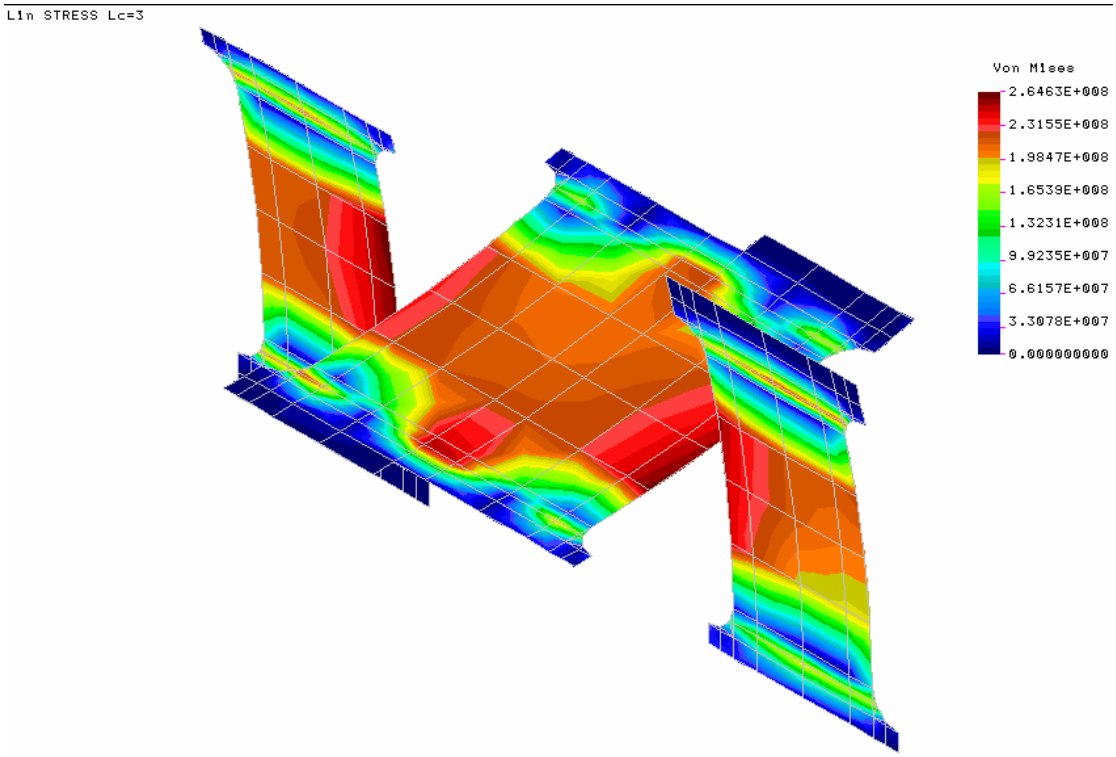

3.2 Dynamic Analysis

3.2.1 Frequency analysis

The model was analysed to obtain the first 50 natural frequencies. The resonant frequencies of the chop and jiggle stages are 23 and 18 Hz respectively.

The first parasitic resonance occurs at 729 Hz.

FREQUENCY NUMBER	FREQUENCY (RAD/SEC)	FREQUENCY (CYCLES/SEC)	PERIOD (SECONDS)
1	.1142200E+03	.1817867E+02	.5500952E-01
2	.1454493E+03	.2314898E+02	.4319844E-01
3	.4577739E+04	.7285698E+03	.1372552E-02
4	.5822649E+04	.9267033E+03	.1079094E-02
5	.7800567E+04	.1241499E+04	.8054781E-03
6	.9250813E+04	.1472313E+04	.6792036E-03
7	.1019618E+05	.1622772E+04	.6162294E-03
8	.1030486E+05	.1640069E+04	.6097305E-03
9	.1129106E+05	.1797028E+04	.5564743E-03
10	.1459196E+05	.2322382E+04	.4305923E-03

3.2.2 Damping

The damping ratio for the near rigid-body modes (chop and jiggle) were set to 0.0004 based on data in the Lucas flex-pivot catalogue. For the higher frequency where the flexure of the jiggle-stage framework is significant the ratio was set to 0.02 which is typical of a well engineered bolted structure.

Set no.	First Mode	Last Mode	Damping Ratio
1	1	2	.4000E-03
2	3	50	.2000E-01

3.2.3 Chop axis excitation

Forces were applied equivalent to a couple of 1Newton forces acting at the chop magnet radius (15mm from the axis).

Below the resonance the response tends to the static case; a rotation of 0.086 radian.

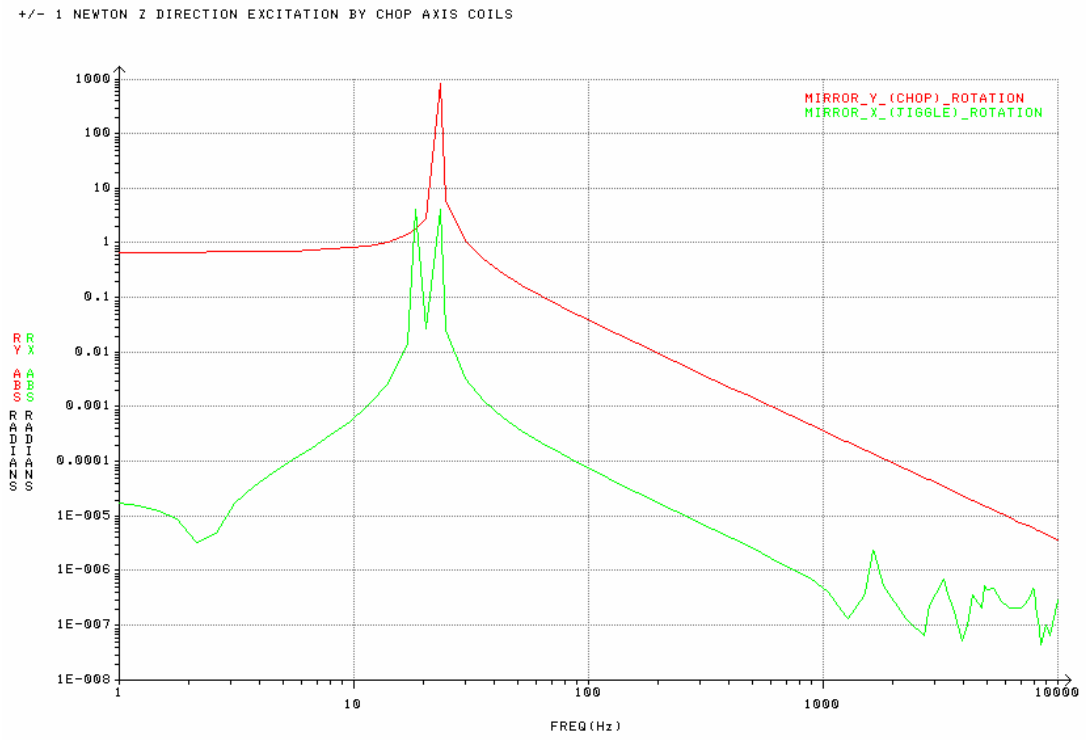

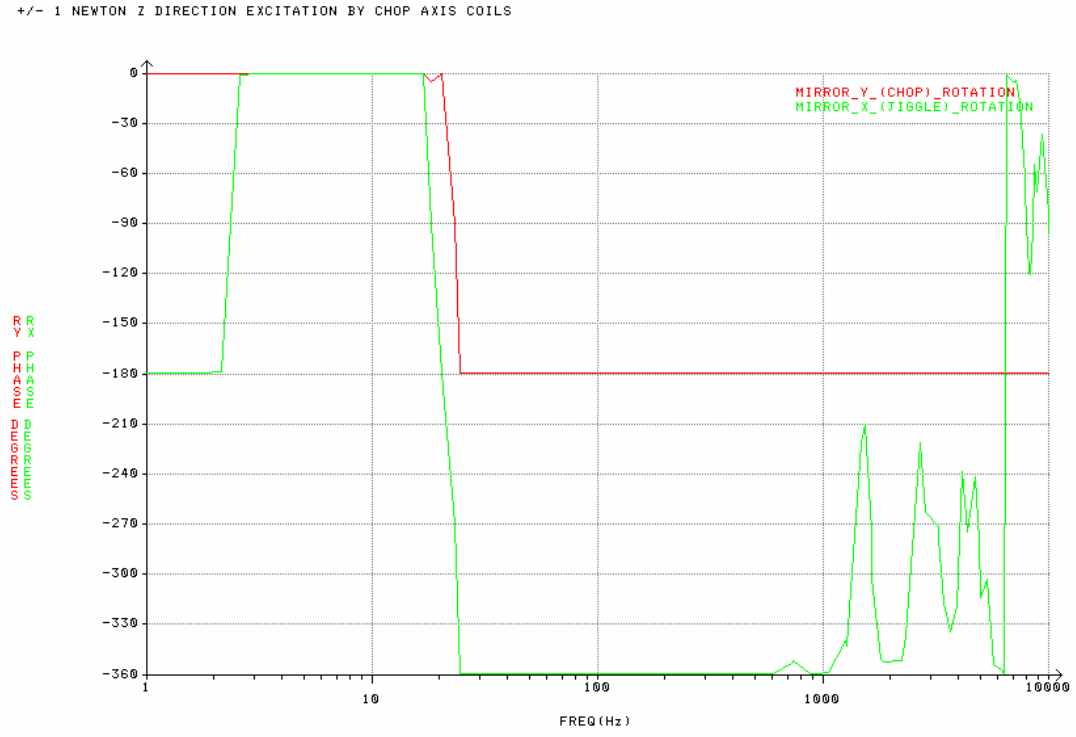

3.2.4 Jiggle axis excitation

A couple of 1Newton forces acting at the centre of the jiggle magnets. Below the resonance the response tends to the static case; a rotation of 0.14 radian.

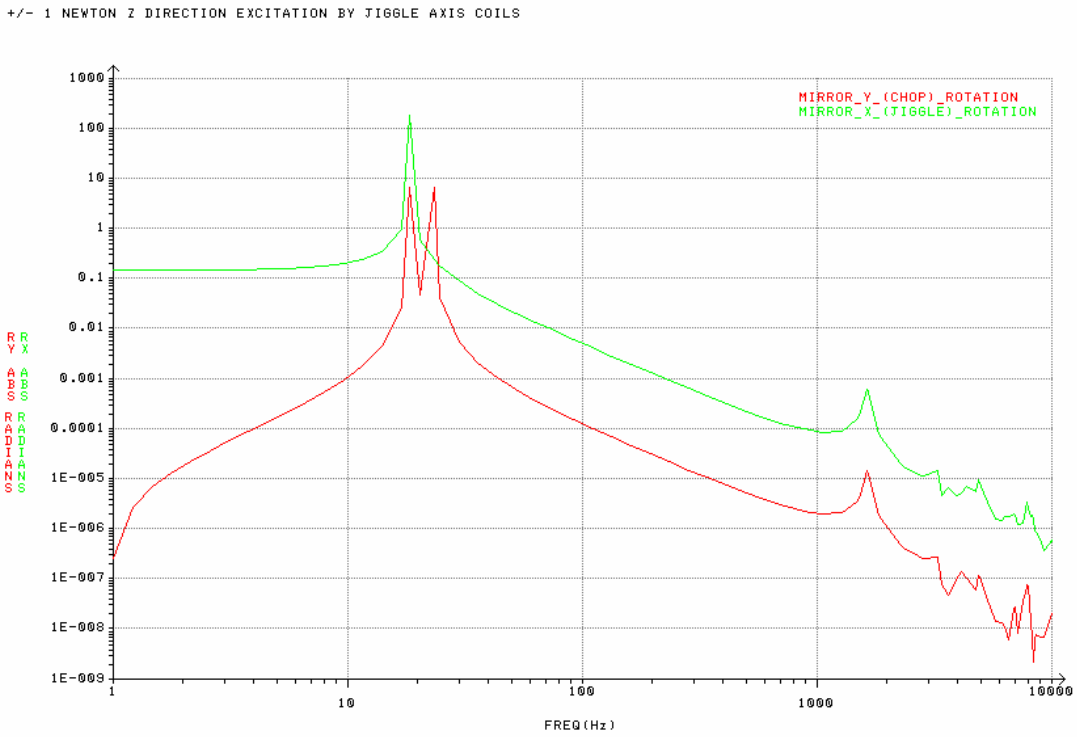

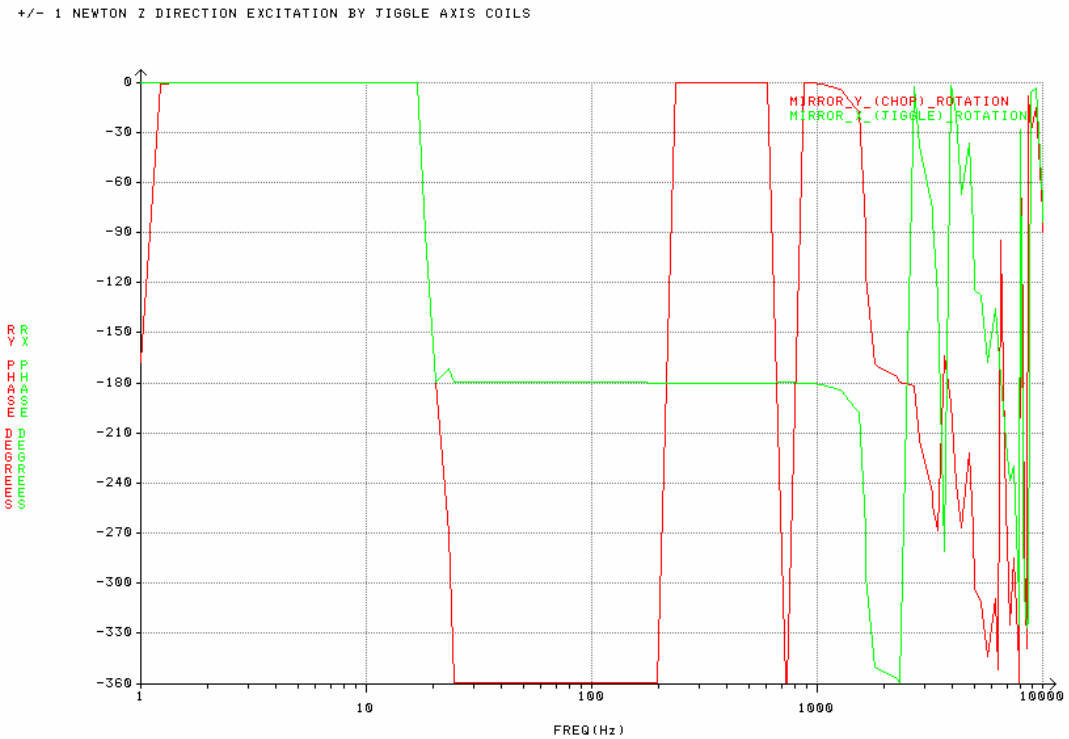

4 References

4.1 Mass properties

The following parameters are derived from the FEA model. The section dimensions used will be fed back into the solid model and more accurate values obtained in due course.

Stage	Parameter	Value
Chop	Mass	0.018 Kg
	Moment of Inertia	2.1 Kg.mm^2
Jiggle	Mass	0.054 Kg
	Moment of Inertia	27 Kg.mm^2

Appendix 3B: Structural Interface FEA Results

1 Scope

This document records a Finite Element Analysis performed on the SPIRE Beam Steering Mirror structure component,

2 Model

2.1 Design

The model is based on Pro/Engineer drawing number BSM-02-001-001 dated Rev 1 (WIP) 29.May.01.

2.2 FEA representation

The FEA was performed as a solid model in integrated Pro/Mechanica. Multi-pass adaptive meshing was used, with convergence set at 10%. Small fillets and holes were generally suppressed, with the exception of connector pin and base mounting features. Material was assigned as Aluminium 6082

2.3 Software

- Pro/Engineer 2000i2
- Pro/MECHANICA STRUCTURE Version 22.3(305) (integrated mode)

3 Results

3.1 50 G acceleration load case

3.1.1 Deflection results

Maximum displacement is predicted at 43 microns under this load case, with prime deflections occurring in a twisting mode (from the side loading) and a pistoning mode around the front mounting hole (from vertical and fore-aft loads).

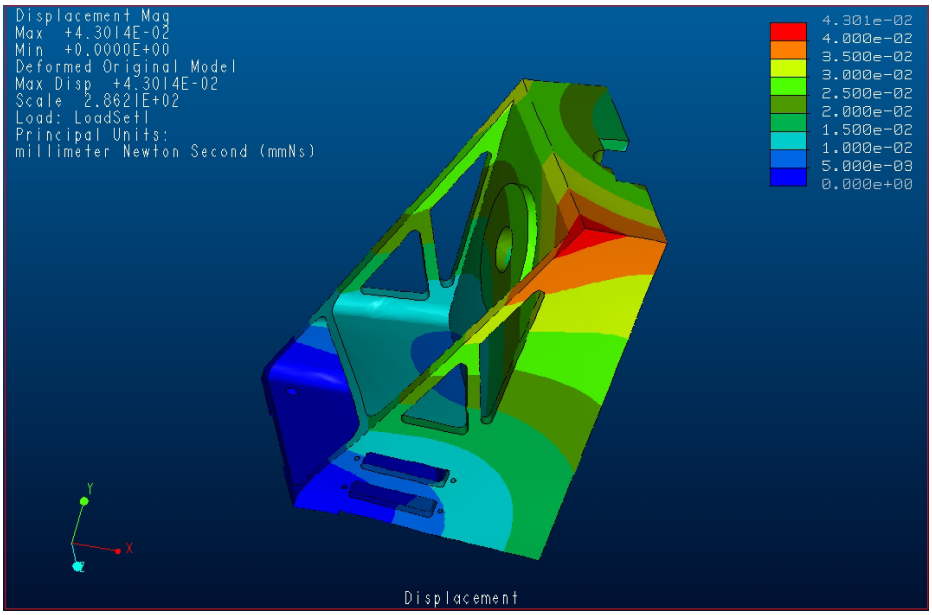

Figure 1 : displacement results (millimetres)

3.1.2 Von Mises Stress results

stresses peak at 36 MPa.

Permissible is per BS8118 (IP's design log no 9, p57)

For fatigue with FoS of 1.0

- 67 MPa friction grip bolted zones (not strictly applicable here as loads are not construction level friction grip)
- 96MPa for re-entrant features
- 76MPa small holes (dia < 3t)

For parent plate
240 MPa with suggested load factor of 2.5, ie a target of 96 MPa in this case

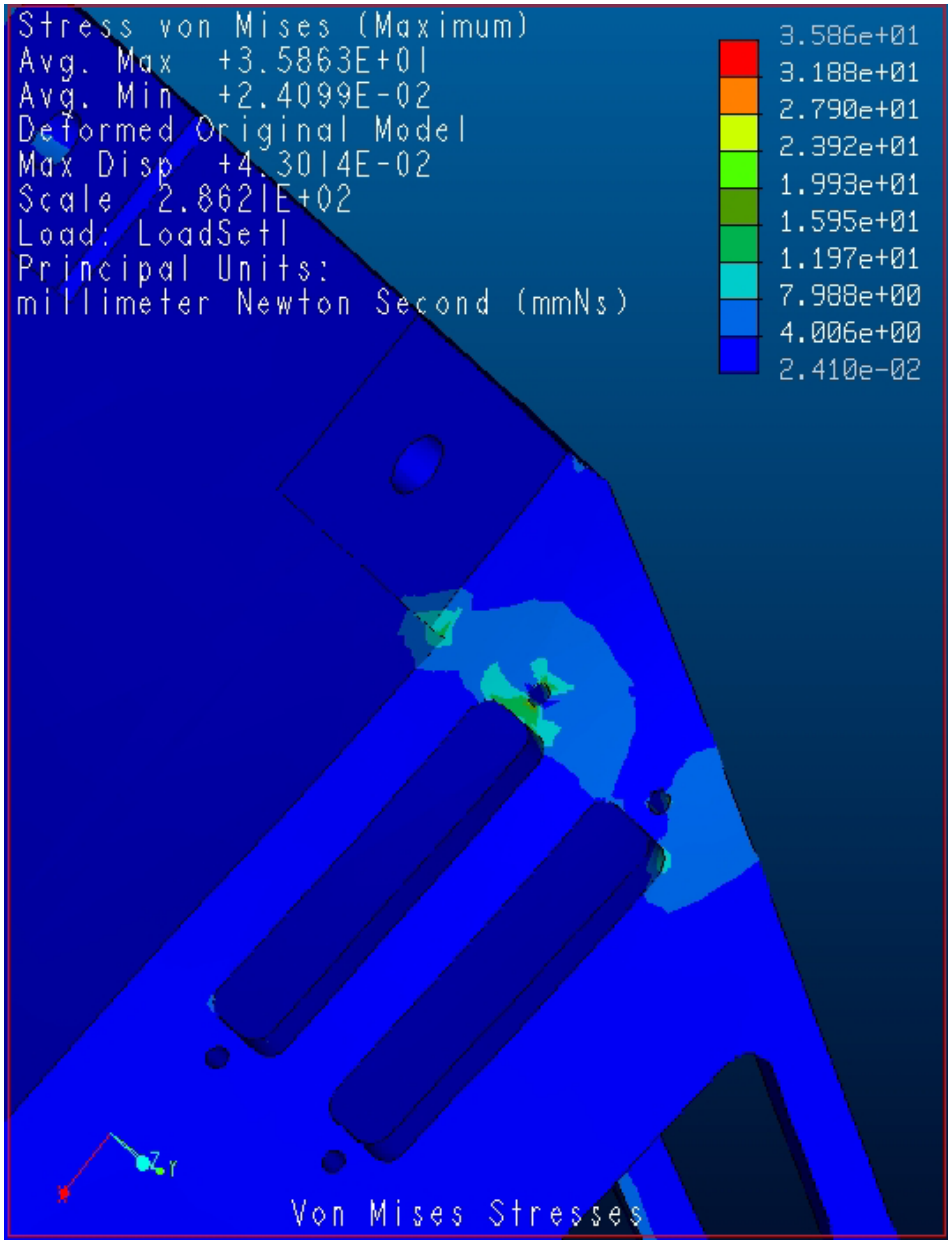

Figure 2 stress distribution around connector cut out and mounting feet

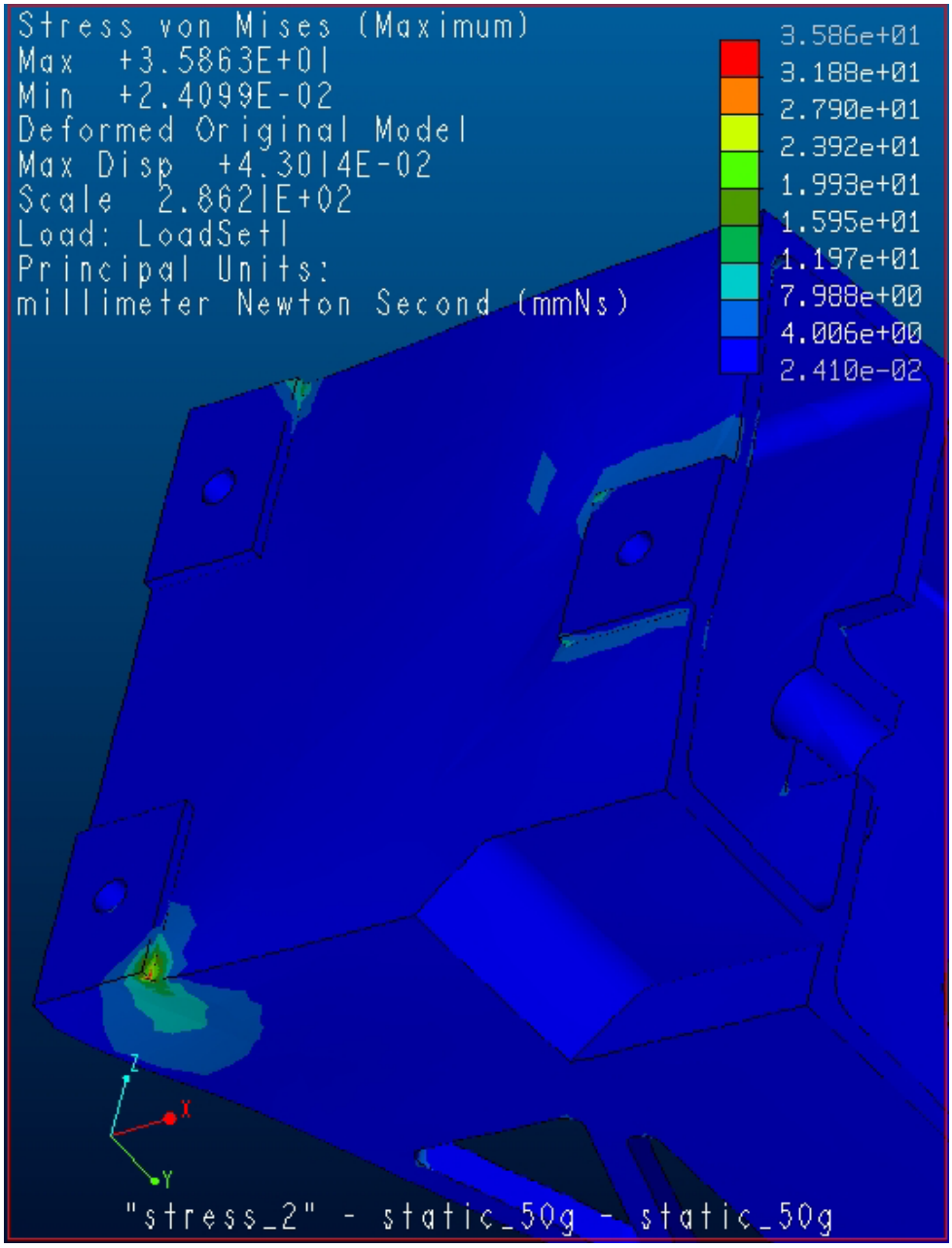

Figure 3 stress distribution around rear mounting foot

3.1.3 Analysis report (extracts)

```
---------------------------------------------------------------
Pro/MECHANICA STRUCTURE Version 22.3(305)
Summary for Design Study "static_50g"
Mon Jun 04, 2001   19:10:01
---------------------------------------------------------------
No errors were found in the model.

Pro/MECHANICA STRUCTURE Model Summary

  Principal System of Units: millimeter Newton Second (mmNs)

  Length:         mm
  Force:          N
  Time:           sec
  Temperature:    C

  Model Type: Three Dimensional

  Points:      1146
  Edges:       5435
  Faces:       7465

  Springs:       0
  Masses:        0
  Beams:         0
  Shells:        0
  Solids:      3189

  Elements:    3189

---------------------------------------------------------------

Standard Design Study

Description:
  50G loads applied in x,y,z

Static Analysis "static_50g":

  Convergence Method: Multiple-Pass Adaptive
  Plotting Grid:     4

  >> Pass  1 <<

        Total Number of Equations:    3330
        Maximum Edge Order:              1

        Elements Not Converged:       3189
        Edges Not Converged:          5435
        Local Disp/Energy Index:     100.0%
        Global RMS Stress Index:     100.0%
>> Pass  2 <<

        Total Number of Equations:   19418
        Maximum Edge Order:              2

Elements Not Converged:       1956
        Edges Not Converged:          4627
        Local Disp/Energy Index:     100.0%
        Global RMS Stress Index:      84.8%
  >> Pass  3 <<
        Total Number of Equations:   63723
        Maximum Edge Order:              4
        Elements Not Converged:       1639
        Edges Not Converged:          2628
        Local Disp/Energy Index:     100.0%
        Global RMS Stress Index:      80.9%

  >> Pass  4 <<
        Total Number of Equations:  117789
        Maximum Edge Order:              5
```

```
        Elements Not Converged:       815
        Edges Not Converged:          207
        Local Disp/Energy Index:    100.0%
        Global RMS Stress Index:     36.4%

  >> Pass  5 <<
        Total Number of Equations:  174100
        Maximum Edge Order:           6
        Elements Not Converged:       146
        Edges Not Converged:          0
        Local Disp/Energy Index:     54.9%
        Global RMS Stress Index:     13.1%

  >> Pass  6 <<
        Total Number of Equations:  199893
        Maximum Edge Order:           6
        Elements Not Converged:       22
        Edges Not Converged:          0
        Local Disp/Energy Index:     30.1%
        Global RMS Stress Index:     12.0%

      RMS Stress Error Estimates:

      Load Set         Stress Error  % of Max Prin Str
      ---------------  ------------  -----------------
      LoadSet1          4.56e-01      1.3% of  3.63e+01

** Warning: Convergence was not obtained because the maximum
        polynomial order of 6 was reached.

  The analysis did not converge to within 10% on
  edge displacement and element strain energy.

  Total Mass of Model:  2.943847e-04

  Mass Moments of Inertia about WCS Origin:

    Ixx:  1.41233e+00
    Ixy: -2.35807e-01  Iyy:  3.84633e-01
    Ixz: -4.52996e-03  Iyz:  1.01220e-03  Izz:  1.29888e+00

  Principal MMOI and Principal Axes Relative to WCS Origin:

        Max Prin          Mid Prin          Min Prin
       1.46399e+00       1.29874e+00       3.33110e-01

  WCS X:  9.76566e-01       2.74581e-02       2.13461e-01
  WCS Y: -2.13377e-01      -5.97632e-03       9.76952e-01
  WCS Z: -2.81010e-02       9.99605e-01      -2.26723e-05

  Center of Mass Location Relative to WCS Origin:
            ( 1.02862e+01,  4.89316e+01, -5.38177e-02)

  Mass Moments of Inertia about the Center of Mass:

    Ixx:  7.07486e-01
    Ixy: -8.76379e-02  Iyy:  3.53484e-01
    Ixz: -4.69293e-03  Iyz:  2.36968e-04  Izz:  5.62882e-01

  Principal MMOI and Principal Axes Relative to COM:

        Max Prin          Mid Prin          Min Prin
       7.28123e-01       5.62755e-01       3.32974e-01

  WCS X:  9.73328e-01       2.64026e-02       2.27892e-01
  WCS Y: -2.27705e-01      -9.92492e-03       9.73680e-01
  WCS Z: -2.79695e-02       9.99602e-01       3.64820e-03

  Constraint Set: ConstraintSet1

  Load Set: LoadSet1

    Resultant Load on Model:
```

in global X direction: 1.451317e+02
in global Y direction: 1.451317e+02
in global Z direction: 1.451317e+02

Measures:

Name	Value	Convergence
max_disp_mag:	4.301418e-02	0.8%
max_disp_x:	3.048651e-02	0.8%
max_disp_y:	-1.805561e-02	0.9%
max_disp_z:	2.839908e-02	0.8%
max_prin_mag:	3.626618e+01	3.8%
max_stress_prin:	3.626618e+01	3.8%
max_stress_vm:	3.586344e+01	0.2%
max_stress_xx:	2.019206e+01	15.5%
max_stress_xy:	1.101872e+01	15.7%
max_stress_xz:	7.227989e+00	0.5%
max_stress_yy:	3.609924e+01	2.9%
max_stress_yz:	-7.932948e+00	0.6%
max_stress_zz:	-1.609714e+01	0.5%
min_stress_prin:	-3.532419e+01	1.2%
strain_energy:	9.345811e-01	0.6%

3.1.4 Verification

Reaction loads

- need checking

Manual verification

- required,

3.2 Modal Analysis

3.2.1 Modal Analysis Results

To limit run time, the maximum number of modes to sweep for was set to 12. The results were:

Mode	Frequency
1	6.881738e+02
2	8.638142e+02
3	1.780816e+03
4	2.715497e+03
5	3.058290e+03
6	3.283797e+03
7	3.344646e+03
8	3.614443e+03
9	3.957047e+03
10	4.096691e+03
11	4.676689e+03
12	5.185199e+03

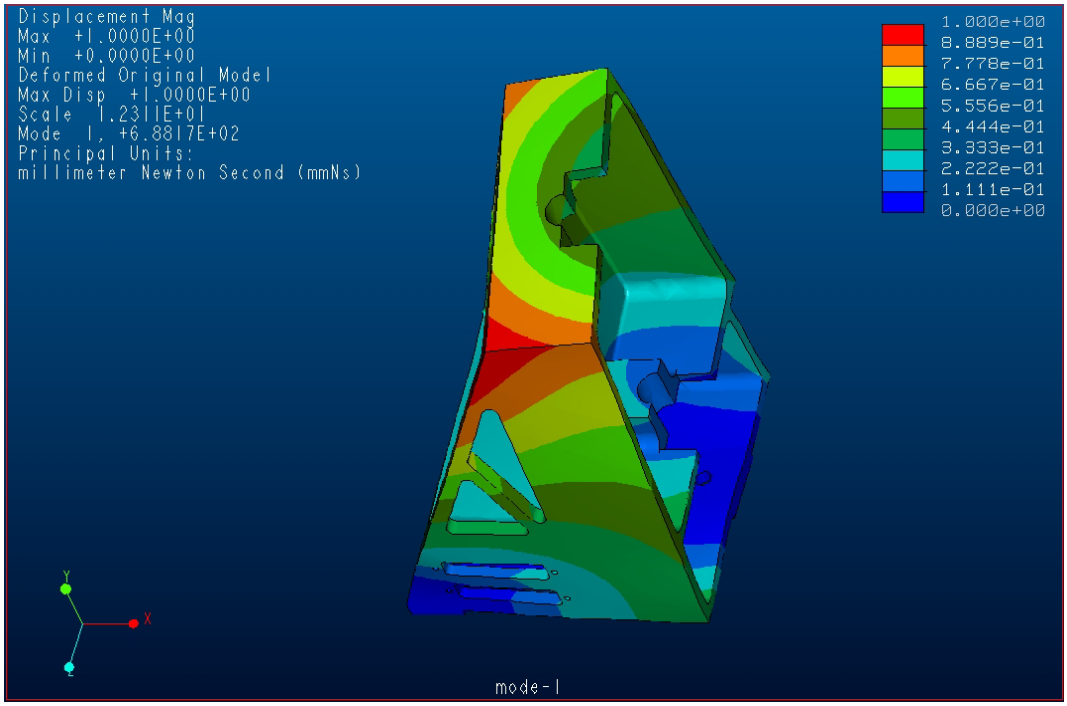

Figure 4 First resonant mode, twisting of entire structure, 688 Hz

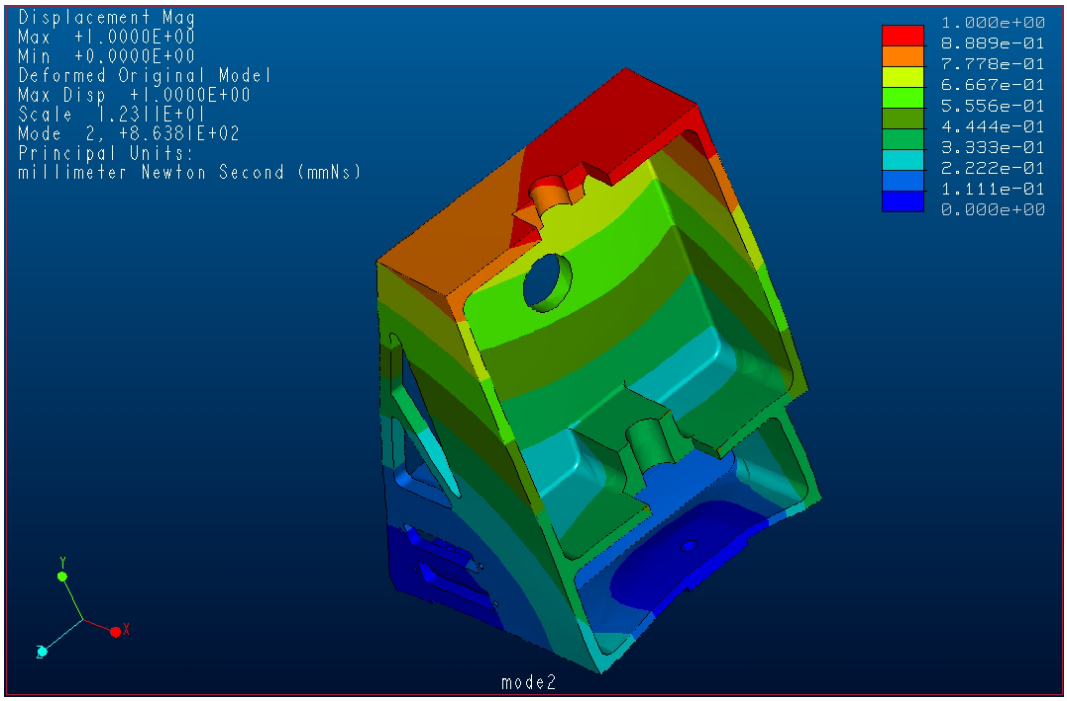

Figure 5 mode 2 , 864Hz. Piston and twist of whole structure

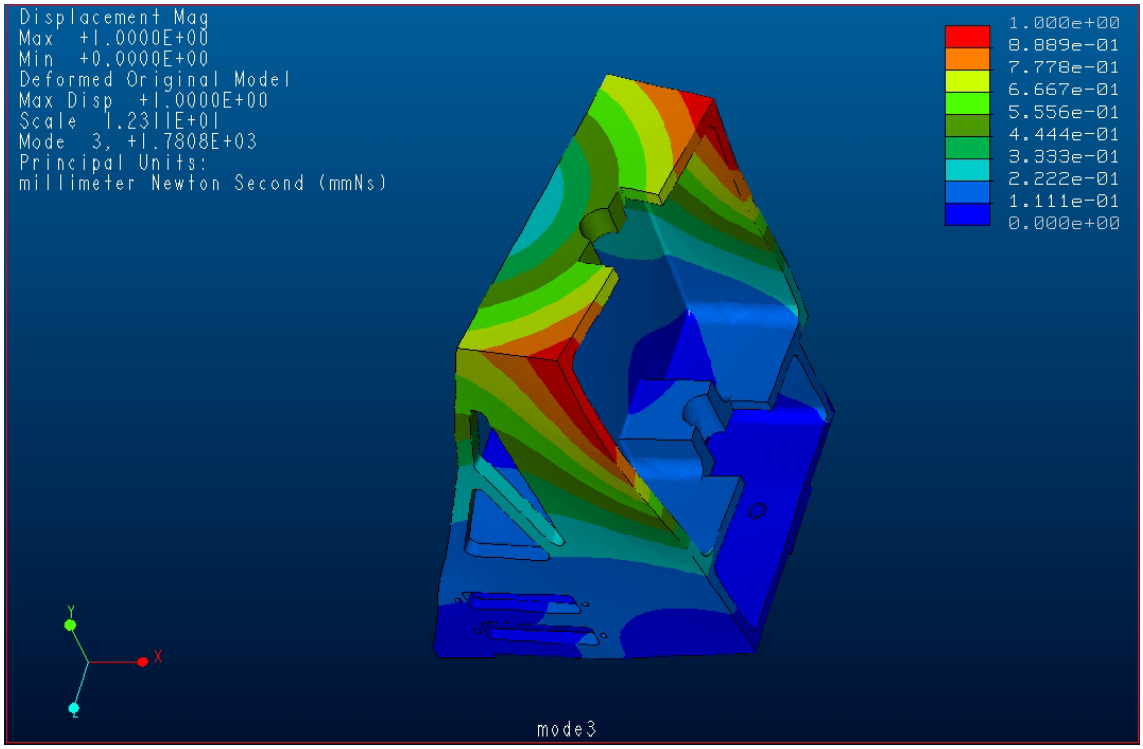

Figure 6 Mode 3 , 1780- Hz, rocking forward of whole structure

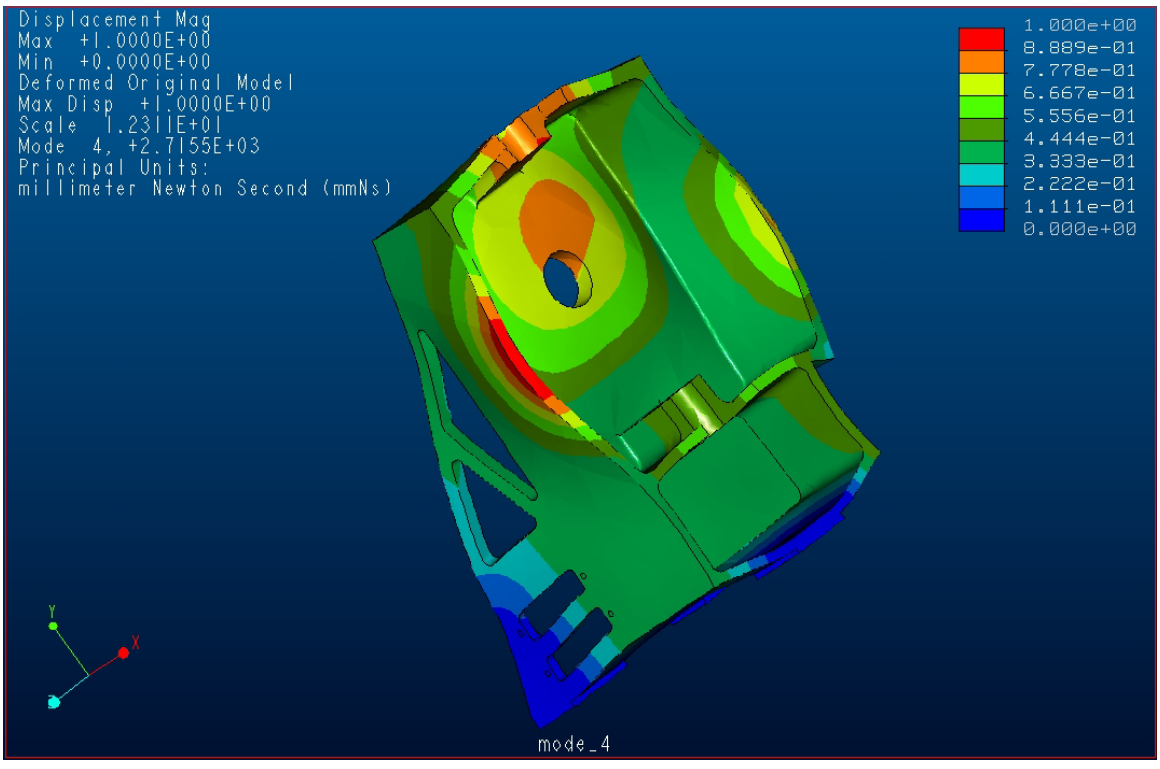

Figure 7 Mode 4, 2716 Hz, local resonance of plates

3.2.2 Model report (extracts)

Pro/MECHANICA STRUCTURE Version 22.3(305)
Summary for Design Study "modal"
Tue Jun 05, 2001 08:32:47

No errors were found in the model.

Pro/MECHANICA STRUCTURE Model Summary

Principal System of Units: millimeter Newton Second (mmNs)

Length: mm
Force: N
Time: sec
Temperature: C

Model Type: Three Dimensional

Points: 1146
Edges: 5435
Faces: 7465

Springs: 0
Masses: 0
Beams: 0
Shells: 0
Solids: 3189

Elements: 3189

Standard Design Study

Description:
basic modal analysis

Modal Analysis "modal":

Convergence Method: Single-Pass Adaptive
Plotting Grid: 4

Convergence Loop Log: (08:33:15)

>> Pass 1 <<
Calculating Element Equations (08:33:15)
Total Number of Equations: 57792
Maximum Edge Order: 3

>> Pass 2 <<
Calculating Element Equations (08:36:33)
Total Number of Equations: 65469
Maximum Edge Order: 5

RMS Stress Error Estimates:

Mode	Stress Error (% of Max Modal Stress)
1	0.8%
2	0.7%
3	2.4%
4	1.3%
5	1.1%

6	0.8%
7	0.9%
8	1.6%
9	4.3%
10	2.4%
11	2.0%
12	1.0%

Total Mass of Model: 2.943847e-04

Mass Moments of Inertia about WCS Origin:

Ixx: 1.41233e+00
Ixy: -2.35807e-01 Iyy: 3.84633e-01
Ixz: -4.52996e-03 Iyz: 1.01220e-03 Izz: 1.29888e+00

Principal MMOI and Principal Axes Relative to WCS Origin:

Max Prin	Mid Prin	Min Prin
1.46399e+00	1.29874e+00	3.33110e-01
WCS X: 9.76566e-01	2.74581e-02	2.13461e-01
WCS Y: -2.13377e-01	-5.97632e-03	9.76952e-01
WCS Z: -2.81010e-02	9.99605e-01	-2.26723e-05

Center of Mass Location Relative to WCS Origin:
(1.02862e+01, 4.89316e+01, -5.38177e-02)

Mass Moments of Inertia about the Center of Mass:

Ixx: 7.07486e-01
Ixy: -8.76379e-02 Iyy: 3.53484e-01
Ixz: -4.69293e-03 Iyz: 2.36968e-04 Izz: 5.62882e-01

Principal MMOI and Principal Axes Relative to COM:

Max Prin	Mid Prin	Min Prin
7.28123e-01	5.62755e-01	3.32974e-01
WCS X: 9.73328e-01	2.64026e-02	2.27892e-01
WCS Y: -2.27705e-01	-9.92492e-03	9.73680e-01
WCS Z: -2.79695e-02	9.99602e-01	3.64820e-03

Constraint Set: ConstraintSet1

Number of Modes: 12

Mode	Frequency
1	6.881738e+02
2	8.638142e+02
3	1.780816e+03
4	2.715497e+03
5	3.058290e+03
6	3.283797e+03
7	3.344646e+03
8	3.614443e+03
9	3.957047e+03
10	4.096691e+03
11	4.676689e+03
12	5.185199e+03

3.2.3 Verification

- need checking manually

Appendix 3C: Structural Interface Manual Calculations

1 Scope

This document records a calculation performed on the SPIRE Beam Steering Mirror flex pivots and structure mounting bolts.

2 Calculation

The Input load is as provided in the table below. A static equivalent acceleration load is applied by assuming a Single Degree of Freedom system and using the Miles approximation:

rms accel = (pi . Fn. Wx(Fn)) / 4L)^0.5

where,
Fn = natural frequency
Wx(Fn) = structure input accel from the PSD at the frequency
L = damping ratio = 1/sqrt(Frequency)

BSM random Specification			Ref. instrument co-ordinate system							
			calc by I.Pain from ramp profile supplied by B.Winters, 01.Oct.01							
X 60 sec	X g^2/hz	X g^2/hz		Y 60 sec	Y g^2/hz	Y g^2/hz		Z 60 sec	Z g^2/hz	Z g^2/hz
f	Accept	Qual		f	Accept	Qual		f	Accept	Qual
20		0.008		20		0.028		20		0.012
40		0.032		40		0.112		40		0.048
60		0.072		60		0.252		60		0.108
80		0.128		80		0.448		80		0.192
100		0.2		100		0.7		100		0.3
150		0.2		150		0.7		150		0.3
200		0.2		200		0.7		200		0.3
300		0.2		300		0.1		300		0.133333
400		0.1125		400		0.1		400		0.075
600		0.05		600		0.044444		600		0.033333
800		0.028125		800		0.025		800		0.01875
1000		0.018		1000		0.016		1000		0.012
1500		0.008		1500		0.007111		1500		0.005333
2000		0.0045		2000		0.004		2000		0.003
g-rms				g-rms				g-rms		

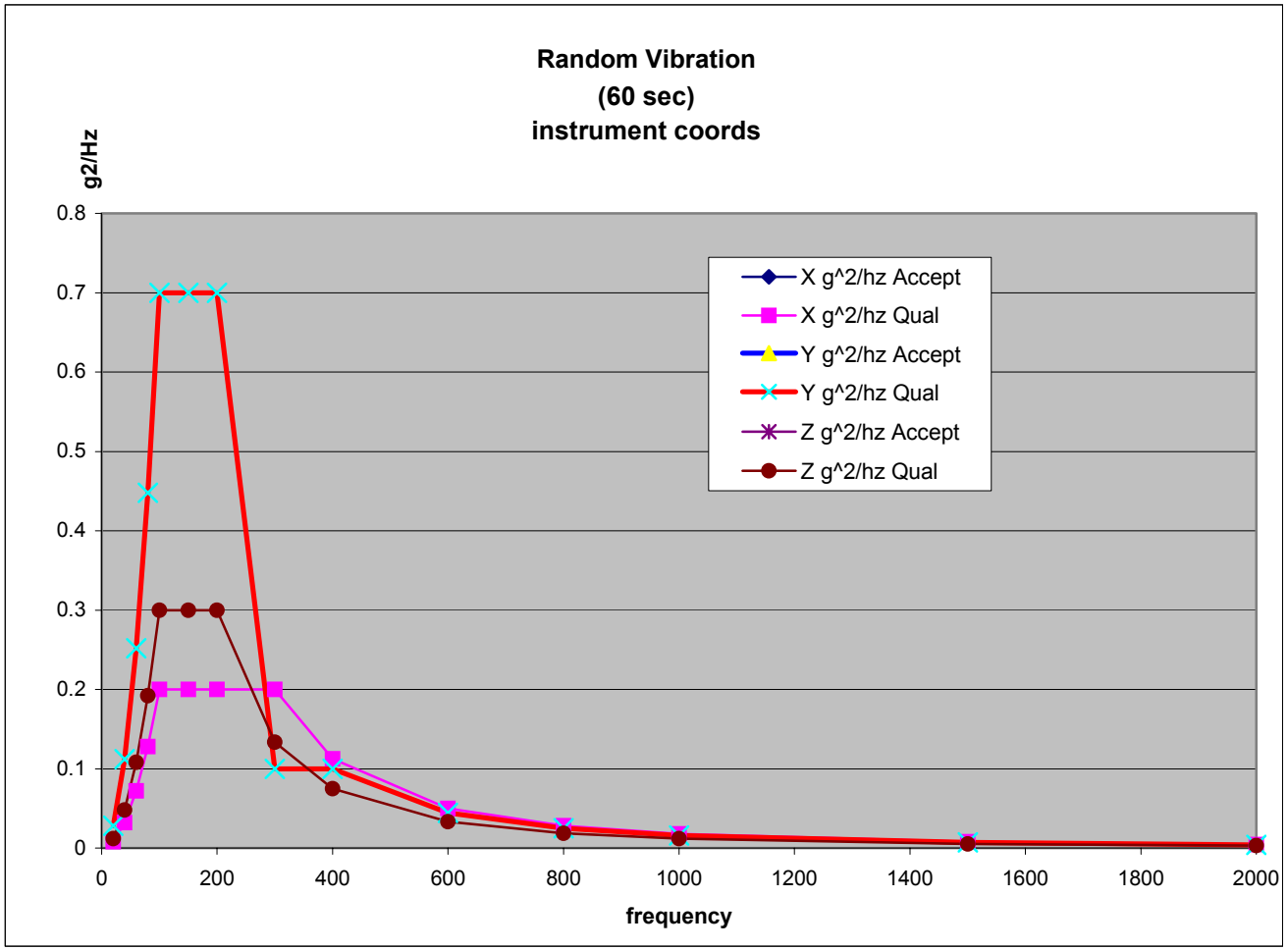
Random Vibration
(60 sec)
instrument coords
g2/Hz
0.8
0.7
0.6
0.5
0.4
0.3
0.2
0.1
0
0
200
400
600
800
1000
1200
1400
1600
1800
2000
frequency
X g^2/hz Accept
X g^2/hz Qual
Y g^2/hz Accept
Y g^2/hz Qual
Z g^2/hz Accept
Z g^2/hz Qual

BSM Response			**calc I.Pain 10.OCT.01**				**version 3.0**
fn	freq	interpolate spec	damping = 1/freq^0.5	rms accel (Miles)	multiplier: probable peak response, 120 sec test	50 % peak response	X qual 3sigma peak response
Hz	Hz	g²/Hz	Hz-1	'g' = x9.81m/s²		'g' = x9.81m/s²	'g' = x9.81m/s²
				X qual rms			
350	350	0.156	0.053452	28.3	4.7	134.3	170.6
400	400	0.113	0.05	26.6	4.8	126.7	161.0
450	450	0.097	0.04714	27.0	4.8	129.1	164.0
500	500	0.081	0.044721	26.7	4.8	128.6	163.3
550	550	0.066	0.04264	25.8	4.8	124.6	158.3
600	600	0.050	0.040825	24.0	4.9	116.6	148.0
650	650	0.045	0.039223	24.1	4.9	117.2	148.8
				Y qual rms			Y qual 3sigma peak response
350	350	0.100	0.053452	22.7	4.7	107.5	136.5
400	400	0.100	0.05	25.1	4.8	119.5	151.8
450	450	0.086	0.04714	25.4	4.8	121.8	154.6
500	500	0.072	0.044721	25.2	4.8	121.2	154.0
550	550	0.058	0.04264	24.3	4.8	117.5	149.2
600	600	0.044	0.040825	22.6	4.9	109.9	139.6
650	650	0.040	0.039223	22.7	4.9	110.5	140.3
				Z qual rms			Z qual 3sigma peak response
350	350	0.104	0.053452	23.1	4.7	109.7	139.3
400	400	0.075	0.05	21.7	4.8	103.5	131.4
450	450	0.065	0.04714	22.0	4.8	105.4	133.9
500	500	0.054	0.044721	21.8	4.8	105.0	133.3
550	550	0.044	0.04264	21.1	4.8	101.8	129.2

600	600	0.033		0.040825	19.6	4.9		95.2	120.9
650	650	0.030		0.039223	19.7	4.9		95.7	121.5
				Max (all axes)	28.3	4.9		134.3	170.6

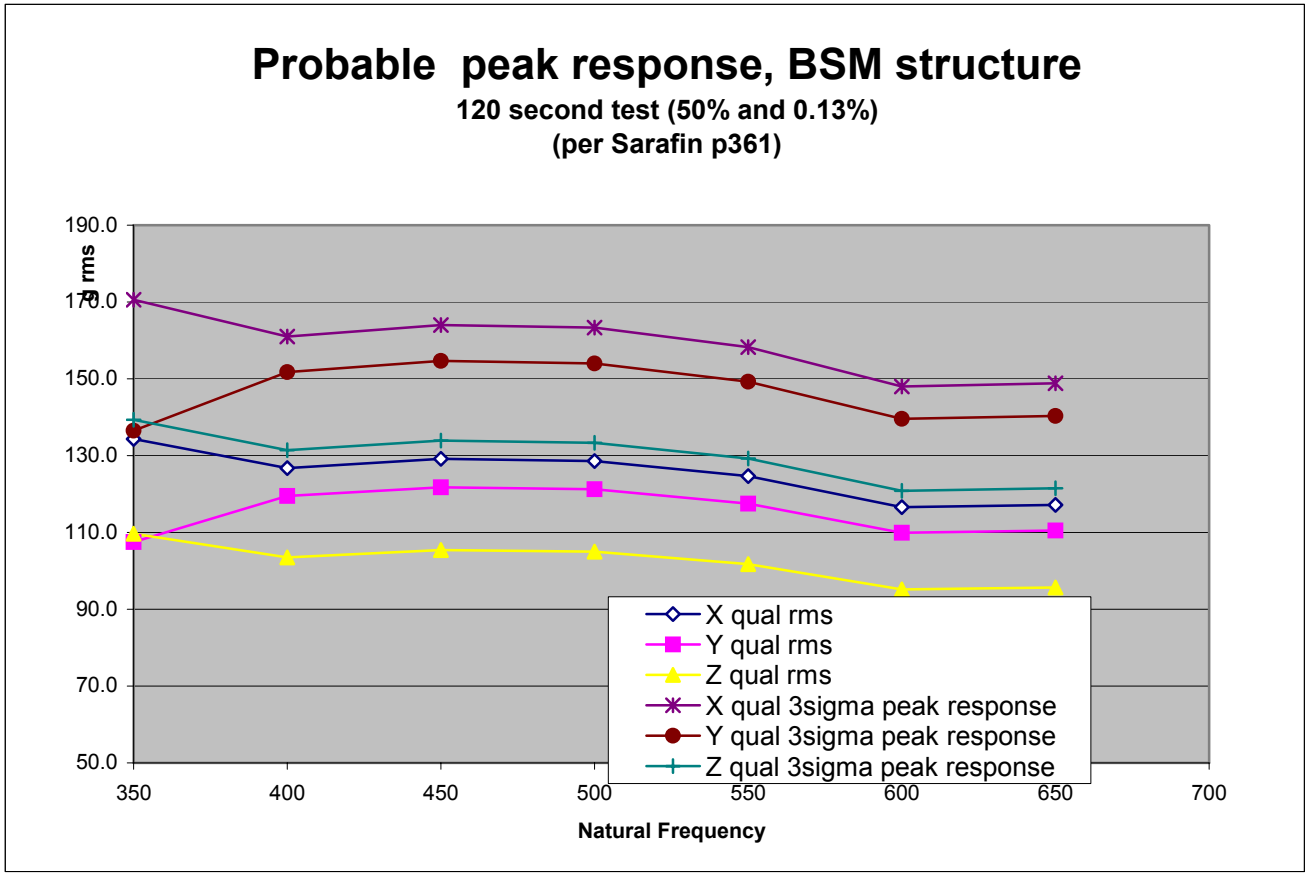

BSM margin - flex pivots & structural bolt					**calculated I.Pain 20.Feb.02**			**version 3.0**	
	Component	mass (incl contingency)	load limit of component (N)	required FoS	survival load (in g) for 2 pivots	margin on rms response	margin on 50% peak response		margin on 3-sigma peak response
WARM	C-Flex Chop axis flex pivot	21.0	25.4	1.0	246.6	8.70	1.84		1.45
	C-Flex Jiggle axis flex pivot	96.0	248.3	1.0	527.3	18.60	3.93		3.09
	LUCAS chop axis flex pivot	21.0	25.4	1.0	246.6	8.70	1.84		1.45
	LUCAS jiggle axis flex pivot	96.0	245.0	1.0	520.3	18.35	3.87		3.05
COLD	C-Flex Chop axis flex pivot	21.0	28.1	1.0	273.1	9.63	2.03		1.60
	C-Flex Jiggle axis flex pivot	96.0	275.0	1.0	584.0	20.60	4.35		3.42
	LUCAS chop axis flex pivot	21.0	26.9	1.0	260.9	9.20	1.94		1.53
	LUCAS jiggle axis flex pivot	96.0	259.2	1.0	550.4	19.42	4.10		3.23
WARM	structure bolt : yield (1 M4 only)	1112.0	3451.0	2.0	316.4	11.16	2.35		1.85
COLD	structure bolt yield (1 M4 only)	1112.0	3910.0	2.0	358.4	12.64	2.67		2.10

Buckling mode failure, scales with E					
	E warm	E cold	Ratio		
CuBe	121	134	1.11		
304 SS	190	201	1.06	(no data on 420 SS)	

Load limit on Structure interfaces TBC by MSSL (modified UNC bolt approximated by M4 bolt)

3 Discussion

This analysis does not cover

(a) flex pivots at their resonant frequency (approx >1000hz)
(b) flex pivots at resonant frequencies of rotating masses (approx 15 and 30 Hz), as these are not the driving design case

The load limits are as per the catalogue data for 429 grade stainless steel components.

The baseline and alternate flex pivots have a positive survival margin for qualification.

Document Ends

SPIRE BSM VIBRATION ANAYLSIS

Free And Forced Vibration Finite Element Analysis

FNC 5505/24072R Issue 1

Prepared for

U.K. Astronomy Technology Centre

FRAZER-NASH CONSULTANCY

DOCUMENT INFORMATION

Project : SPIRE BSM Vibration Anaylsis

Report Title : Free And Forced Vibration Finite Element Analysis

Client : U.K. Astronomy Technology Centre

Client Ref. : 024706

Classification :

Report No. : FNC 5505/24072R

Issue No. : 1

Compiled By : D C Reed
A J Vibert

Date : May 2002

Approved By : M W Anderson

DISTRIBUTION

Copy	Recipient	Organisation
1	I Pain	UK ATC
2	I Pain	UK ATC
3	I Pain	UK ATC
4	File	FNC

Copy No. 3

COPYRIGHT

The Copyright in this work is vested in Frazer-Nash Consultancy Limited. The document is issued in confidence solely for the purpose for which it is supplied. Reproduction in whole or in part or use for tendering or manufacturing purposes is prohibited except under an agreement with or with the written consent of Frazer-Nash Consultancy Limited and then only on the condition that this notice is included in any such reproduction.

Originating Office: FRAZER-NASH CONSULTANCY LIMITED
Stonebridge House, Dorking Business Park, Dorking, Surrey RH4 1HJ, UK
T: +44 (0)1306 885050 F: +44 (0)1306 886464 E: info@fnc.co.uk W: www.fnc.co.uk

SUMMARY

A dynamic finite element model of the SPIRE Beam Steering Mirror has been developed and analysed using the general purpose finite element code ABAQUS. A modal analysis has been performed that has identified that there are 19 modes in the frequency range up to 2000Hz. The lowest frequency modes are rotational modes of the mirror assembly about the jiggle and chop axes. The frequencies of these mirror modes are approximately 14Hz and 22Hz respectively. The first structural mode of the main casing and baseplate is a sideways rocking mode, which occurs at 392Hz.

Two types of forced response analysis were performed using the model. The first was a low frequency swept-sine analysis, and the second was a higher frequency random vibration response analysis.

The low frequency sine sweep predicted large levels of rotation of the chop and jiggle stages on the flex pivots, which would cause interaction between the chop magnet arm and the launch latch. To reduce the amplitude of this response, one or more of the following measures could be implemented:

- Better balancing of the chop and jiggle stages;
- Increasing the moment of inertia about the axis of rotation;
- Increasing the stiffness of the pivot springs;
- Fully locking the assembly during launch;
- Increasing the damping.

The frequencies of the first two fundamental modes of the main casing are close to the peak excitation plateau on the random response specification. Large levels of acceleration are seen on the structure at these frequencies. These modes are sideways and front-to-back rocking modes.

Stiffening the base of the BSM main casing would reduce the response to random vibration by shifting the main casing modes out of the peak excitation range. It may be advantageous to do this in such a way as to increase the separation between the modes, to reduce their coupled response.

© FNC 2002

CONTENTS

1. INTRODUCTION 5

2. DESCRIPTION OF THE STRUCTURE 6

3. FE MODEL GENERATION 7

3.1 GEOMETRY 7

3.2 MATERIALS 9

3.3 SPRING ELEMENTS 9

3.4 BOUNDARY CONDITIONS 11

3.5 APPLIED LOADS 11

4. FREE VIBRATION RESPONSE 13

5. SWEPT SINE FORCED RESPONSE 15

5.1 RESULTS PRESENTATION 15

5.2 DESCRIPTION OF RESULTS 15

5.3 CORRECTIVE MEASURES 15

6. RANDOM VIBRATION FORCED RESPONSE 17

6.1 RESULTS PRESENTATION 17

6.2 DESCRIPTION OF RESULTS 17

6.3 RMS CALCULATION 18

6.4 CORRECTIVE MEASURES 18

7. VERIFICATION PROCEDURE 19

7.1 OVERVIEW 19

7.2 INDEPENDENT CHECKS ON FIRST RESONANT FREQUENCIES 19

7.3 INDEPENDENT CHECKS ON MAGNITUDE OF FORCED RESPONSE 19

7.4 CONTROL OF MODEL VERSION NUMBERS 20

8. CONCLUSIONS 21

9. REFERENCES 23

FIGURES 24

APPENDIX A: DATA POINT POSITIONS 36

1. INTRODUCTION

The SPIRE Beam Steering Mirror (BSM) will undergo severe vibration loading when the European Space Agency (ESA) Herschel Space Observatory is launched using an Arianne V launch vehicle. Structural amplification by the structure of the SPIRE instrument means that there is a very challenging specification for the vibration qualification of the BSM.

The United Kingdom Astronomy Technology Centre (UKATC) has performed preliminary stress and vibration assessments that have taken the design to a state where it has passed the Detailed Design Review. There is however a need to perform a dynamic response analysis of the full assembly. UKATC has subcontracted Frazer-Nash Consultancy Limited to undertake the dynamic analysis of the assembly. The analyses include:

- Normal modes analysis of the BSM assembly,
- Swept sine dynamic response of the BSM assembly with excitation in three orthogonal axes (local to the optical bench axis system),
- Random response dynamic response of the BSM assembly with excitation in three orthogonal axes (local to the optical bench axis system).

The report describes the dynamic finite element model that has been generated and summarises the results from the analyses that have been performed.

© FNC 2002

2. DESCRIPTION OF THE STRUCTURE

The BSM comprises an aluminium mirror structure mounted in a gimbal frame arrangement. Rotational stiffness about the axes of rotation (chop and jiggle) is provided by flex-pivots. The outer ends of the jiggle axis flex-pivots are set into the main body of the BSM. Rotation of the mirror about each axis is controlled by magnets set into protruding arms, which are located between the coils of the motors. The motors are bolted to the main body of the BSM casing. Once energised, the motors will force the magnet beams to rotate about the appropriate axis against the stiffness of the respective pair of flex-pivots.

There is a thin cover plate over the front of the casing that is bolted to the casing at the four corners. The cover plate has a large aperture to allow optical access to the face of the mirror.

The main casing is bolted to a base plate that is in turn bolted to the optical bench of the SPIRE instrument.

In addition to the mirror assembly and motors, there are a number of additional discrete items. These items include:

- PCAL (calibration) unit, mounted behind the centre of the mirror
- Launch latch, a deployable end stop, mounted behind the farthest motor on the chop axis.
- Two connector units, providing electrical connection from the instrument to the motors and sensors.

The BSM will operate and be launched at a temperature of four degrees Kelvin.

© FNC 2002

3. FE MODEL GENERATION

This section describes the Finite Element model of the BSM assembly. The model was generated using FEMGV Version 6.1 (Reference 1), and analysed using the general purpose finite element code ABAQUS (STANDARD) Version 5.8 (Reference 2).

3.1 GEOMETRY

The model geometry was taken from drawings SPIRE-BSM-020-001 to SPIRE-BSM-020-012.

The model is constructed from point mass, beam, shell and solid elements. The FE model mesh is illustrated in Figures 1 to 3. Some simplifications to the BSM geometry have been made: for example, the hole in the cover plate has been modelled as rectangular rather then the complex rounded shape. These simplifications are not considered to significantly affect the results from the analyses.

The model has been defined in a co-ordinate system local to the main casing of the BSM. The orientation of this co-ordinate system is as shown in Figures 1 to 3. The x-axis is parallel to the chop axis; the y-axis is perpendicular to the mirror surface; and the z-axis is perpendicular to the optical bench. The nodal co-ordinates have then been converted into a global co-ordinate system, based on the axis system of the optical bench, as the model is read into ABAQUS. The local system is referred to using lower case (x, y, z) and the global system is referred to using upper case (X, Y, Z) in this report. The global co-ordinate system is illustrated in Figures 4 to 7. The global Y-direction is aligned with the negative local z-direction, and the global X-direction is at an angle of 17.94° to the local y-direction.

The main structural interface is primarily built from eight-noded thick shell elements, with 3-noded beam elements used for the stiffeners in the light-weight side wall sections at the rear of the main casing.

The base plate is primarily modelled with eight-noded thick shell elements with 20-noded brick elements used to represent the thicker areas and to ensure the correct geometric offset for the main casing.

The mirror has been modelled as a combination of shell elements representing the reflecting surface attached to a series of beam elements along the axis. It has also been necessary to create a small mass element away from the axis of rotation to provide the correct centre of gravity. Obtaining the correct centre of gravity of the mirror assembly relative to the chop axis is a key aspect of the model that drives the amplitude of the dynamic response in the chop mode.

The magnets for the chop motors have been modelled as mass elements on the ends of beam elements connected to the mirror axis beam.

The jiggle frame assembly is represented by a combination of 8-noded shells and 3-noded beams. The flex-pivots are represented by spring elements in all six degrees of freedom. The jiggle stage magnets are represented by shell elements with increased density. Point mass elements have also been added in order to approximate correctly

© FNC 2002

the position of the centre of gravity relative to the jiggle axis. This is important for the jiggle mode dynamic response.

The cover plate has been modelled as a series of eight-noded thick shell elements. The cover plate has been connected to the main casing via a series of springs at the four bolt locations. The springs represent the stiffnesses of the cover plate attachment bolts.

The main non-structural components (motors, PCAL unit, launch latch and electrical connectors) are simulated by rigid mass elements that are connected via multi-point constraints to appropriate nodes on the main casing.

The mass of other incidental items, including wiring and fixings, has been smeared uniformly over the casing structure by factoring the density of the casing material.

The moments of inertia and centre of gravity positions of the chop stage, jiggle stage and whole assembly are presented in Table 1 below.

Part	Mass (g)	Centre of gravity* (mm)			Moments of Inertia* (kg mm^2)		
		x	y	z	I_{xx}	I_{yy}	I_{zz}
Chop Stage	20.1	9.06	-0.304	0	2.64	14.9	12.5
Jiggle Stage	92.3	0.35	0.26	4.71	54.6	88.5	50.7
Whole Assembly	732	2.2	18.6	53.5	3950	3860	1120

Table 1: Centres of gravity and moments of inertia

*Note: the centres of gravity and moments of inertia are in the local (x, y, z) co-ordinate system. Distances are measured from the axes of rotation for the chop and jiggle stages, with the along-axis measurements taken from the mirror centre. For the whole assembly, the distance is measured from the front bolt hole centre on the baseplate underside.

The moments of inertia and centres of gravity in the model have been designed to match the values given by Reference 3. For the chop and jiggle stages, the CG locations match to within 1% except the for the chop stage x-direction, which does not affect the dynamic response of the primary mode. The chop and jiggle stage moments of inertia are within 6% of the specified values. The whole assembly CG position is within 1.5mm in each direction, and the moments of inertia are within 5% of the specified values.

The main casing is connected to the top face of the base plate by springs in the three translational directions at the nodes corresponding to the centre of the attachment bolts. The springs represent the stiffnesses of the attachment bolts. A spring in the direction perpendicular to the optical bench has been added at each corner of the contact areas. This prevents the contact areas overlapping each other. Ideally, the contact surfaces would be modelled explicitly, using gap elements for example.

© FNC 2002

However, this would introduce non-linearities into the model, which are not suitable for this type of linear mode-based dynamic analysis.

3.2 MATERIALS

The main components of the BSM are constructed from Aluminium alloy grade 6082. At 4 Kelvin, this has a Young's Modulus of 87 GPa. Poisson's ratio is assumed to remain constant with decreasing temperature, and is therefore taken to be 0.34. Thermal contraction is assumed to be negligible for the purposes of this analysis, therefore the density remains unchanged from its value at room temperature of 2.71×10^3 kg/m^3.

Note that the density of some parts of the model has been modified to approximate the various components that have not been explicitly included, such as the bolts and the wiring.

In some locations it has been necessary to have shell elements superimposed over one side of a brick element section in order to properly couple the rotational degrees of freedom. In these cases, the effective thickness of the section is artificially high, so the density of the brick elements is reduced to compensate. The main area where this has been necessary is on the baseplate. The density of the brick elements between the baseplate and the casing was reduced to 985 kg/m^3, since these elements are 5.5mm thick in the model but the amount of material they represent is only 2mm thick.

The chop stage is assumed to be rigid, therefore a very high Young's Modulus is used for its material. The first structural mode of the chop stage is anticipated to be a cantilever bending mode of the magnet arms. A hand calculation was performed which predicts this mode to occur at 4101 Hz, assuming all the mass to be concentrated at the end of the beam to give a lower bound. This is well above the maximum frequency considered, which justifies the assumption that the chop stage is effectively rigid.

The collars that represent the parts of the flex pivots attached to the main structure are also assumed to be rigid.

3.3 SPRING ELEMENTS

Linear spring elements have been used to represent the flex-pivots, the bolted connections between the cover plate and the casing, and between the casing and the base plate.

3.3.1 Flex Pivots

The stiffness of the springs used to represent the flex-pivots are summarised in Table 2, below:

© FNC 2002

	Chop Axis	Jiggle Axis
Axial Stiffness (N/mm)	1751	3152
Radial Stiffness – 2 axes (N/mm)	1369	2518
Torsional Stiffness (Nmm/radian)	23.3	185
Yaw Stiffness – 2 axes (Nmm/radian)	6×10^4	1×10^5

Table 2: Stiffness of Spring Elements Representing Flex-pivots

Note that there is no cross-coupling between the different directions of motion for the flex pivot springs. The values above are per pivot; the stiffness for each axis is double these. The radial stiffness values are taken as the average over the four angular directions quoted in the Lucas data book (Reference 4) – compression and tension of the flexures, at 0° and 45° to the plane of a flexure.

The yaw stiffness is estimated from the stiffness given in Reference 4 as follows.

The values given by Lucas are based on a measurement of force vs. deflection for a cantilever-type test, which will produce both bending and shear stress in the pivot. The force was applied at the centre of the unsupported half. The data book states that if the pivots are loaded in shear only, the stiffness will increase by a factor of 1.25.

The springs model the bending and shear stiffnesses independently, so they are effectively two springs in series when cantilever loading is applied. The radial stiffness is therefore 1.25× the quoted value, and the bending stiffness is 5× the quoted value, since:

$$\frac{1}{k_{bending}} = \frac{1}{k_{bending+shear}} - \frac{1}{k_{shear}}$$

$$= \frac{1}{k_{bending+shear}}\left(1 - \frac{1}{1.25}\right)$$

$$k_{bending} = 5 \times k_{bending+shear}$$

The bending stiffness is then converted into an equivalent torsional stiffness for the spring, using a moment arm d = 3.175mm:

$$k_{torsional} = d^2 \times k_{bending}$$

Warm (i.e. 20°C) stiffness values have been used, because no data were available for cold (4K) values in Reference 4. The error introduced by this approximation is likely to be within the manufacturing tolerance for the flex pivots, and is conservative since the pivots will be stiffer at the cold temperature. Stiffer pivots would give higher natural frequencies, which would have a lower magnitude of response.

3.3.2 Bolted Connections

The bolted connections have been represented by translational springs in three axes, with axial stiffnesses of 3.44×10^5 N/mm for the M2.5 bolts between the casing and front

baffle, and 6.6×10^5 N/mm for the M4 bolts between the baseplate and casing. These axial stiffnesses have also been used for the shear directions.

All springs have been specified in the local axis system of the main casing.

3.4 BOUNDARY CONDITIONS

The model of the BSM assembly is constrained at the interface with the optical bench. Nodes corresponding to the centre of the bolt hole of each of the thickened footprints are constrained in the two lateral directions (parallel to the plane of the optical bench).

All nodes on the bottom surface of the thickened footprints are constrained in the normal direction (perpendicular to the plane of the optical bench).

It has been identified that the degree of constraint at the boundary between the baseplate and the optical bench has a significant effect on the frequency of modes containing substantial amounts of bending of the baseplate. The baseplate would presumably be firmly bolted to the optical bench and a degree of compression would be expected at the interface. It is therefore unlikely that the footprint would peel away from the optical bench. Applying a nodal boundary constraint at every node on the interface plane is considered to be the most appropriate way to constrain the model in this location.

3.5 APPLIED LOADS

Base excitation loads have been applied to the boundary nodes for both sets of forced dynamic response analyses. The applied loads are specified in the global axis system of the optical bench. Loads are applied in each global axis individually, i.e. a separate analysis is performed for each excitation direction.

In the case of the swept sine analyses the base excitation has been specified as a combination of constant displacement in the frequency range 5-30 Hz and constant acceleration in the frequency range 30-100Hz. This has necessitated a two step analysis, splitting the frequency range into two sections.

The vibration loads have been extracted from the Analysis Specification (Reference 5) and are repeated below in Table 3:

Direction	5-30Hz Displacement (mm)	30-100Hz Acceleration (g)
X	11	40
Y	11	25
Z	11	25

Table 3: Excitation Levels for Swept Sine Analyses

In the case of the random response analyses the base excitation has been specified as an acceleration spectrum. The vibration loads have been extracted from the Analysis Specification (Reference 5) and are repeated below in Table 4:

© FNC 2002

Direction	Ramp Up	Plateau	Ramp Down
X	+6 dB/oct 20-100Hz	$0.2g^2$/Hz 100-300Hz	-6 dB/oct 300-2000Hz
Y	+6 dB/oct 20-100Hz	$0.7g^2$/Hz 100-200Hz $0.1g^2$/Hz 200-400Hz	-6 dB/oct 400-2000Hz
Z	+6 dB/oct 20-100Hz	$0.3g^2$/Hz 100-200Hz	-6 dB/oct 200-2000Hz

Table 4: Excitation Levels for Random Response Analyses

© FNC 2002

4. FREE VIBRATION RESPONSE

An eigenvalue extraction has been performed on the dynamic finite element model to determine the natural modes of vibration of the assembly. The assembly has nineteen modes in the frequency range up to 2000 Hz. The modal frequencies are listed in Table 5 below, together with a brief description of the corresponding mode shapes. In some of the higher frequency modes the motion is complex with many components taking part in the overall motion. In these cases the description highlights those areas that are moving the most. The descriptions at these higher frequencies may be somewhat subjective.

Mode	Frequency (Hz)	Description
1	13.6	Jiggle stage fundamental
2	21.4	Chop stage fundamental
3	392	Sideways rocking
4	398	Front-back rocking
5	791	Jiggle frame diagonal twist
6	925	Jiggle frame vertical motion & skew
7	1036	Jiggle magnet beam rocking + mirror sideways translation in phase
8	1087	Jiggle magnet beam rocking + mirror sideways translation in antiphase
9	1278	Jiggle magnets move side-side due to rotation of jiggle frame about front-back axis
10	1302	Front baffle bending about horizontal axis
11	1370	Front baffle twist about vertical axis + jiggle frame motion similar to mode 8
12	1510	Front baffle twist + whole assembly pistons vertically + jiggle frame vertical motion in antiphase
13	1557	Front baffle twist + jiggle frame rotation about the chop axis
14	1595	Front baffle twist + jiggle frame moves slightly side-side in phase
15	1682	Front baffle twist + jiggle frame moves slightly side-side in antiphase
16	1781	Jiggle magnet beam bending (magnets in phase) + jiggle frame panting (squeezing)
17	1937	Complex mode of front baffle
18	1960	Complex mode of front baffle
19	2066	Jiggle magnet beam bending (magnets in antiphase) + vertical motion of mirror & top pivot block in antiphase

Table 5: Natural Frequencies of BSM Assembly

© FNC 2002

In these descriptions, the vertical direction refers to the model z-axis, which is perpendicular to the optical bench. The sideways direction is in the model y-direction, which is aligned with the chop axis of rotation. The front-back direction is in the model x-direction, which is perpendicular to the mirror.

It has been identified that the degree of constraint at the boundary between the baseplate and the optical bench has a significant effect on the frequency of modes containing significant amounts of bending of the baseplate. The current analysis assumes that all nodes on the interface plane between the thickened footprint of the baseplate and the optical bench are constrained in the vertical direction, which is normal to the optical bench.

The mode shapes of the first four modes are illustrated in Figures 4 to 7.

Section 7.2 describes a hand calculation to verify the natural frequencies of the first two modes.

© FNC 2002

5. SWEPT SINE FORCED RESPONSE

5.1 RESULTS PRESENTATION

The results from four key data points for each of the X, Y and Z loading directions are presented in Figures 8 to 19. The units on these figures are in mm, s, and tonnes, which give forces in N (and therefore torque in Nmm). The load directions are aligned with the optical bench co-ordinates, which should not be confused with the x, y and z local model co-ordinates. The results are in the local co-ordinates.

Note that the curves are labelled as follows: s8_6_10608, for example, refers to the force in spring number 8, which restrains local degree of freedom 6 (element number 10608). The designation of response points (P), relative displacements (E) spring forces/torques (S) and reaction forces (R) are summarised in Appendix A. The degrees of freedom 1 to 3 refer to translations in the x, y, and z directions. The degrees of freedom 4 to 6 refer to rotations about the x, y, and z axes.

5.2 DESCRIPTION OF RESULTS

In the swept sine load cases, the main driver for the response is the motion of the gimbal frame. This is not surprising, since the jiggle and chop natural frequencies are within the frequency range of the load specification. All other modes are well outside this frequency range, so they would not be expected to contribute significantly to the response.

The excitation of the gimbal frame does not transmit significant motion to the rest of the BSM structure, nor does it significantly affect the reaction forces at the base plate boundary conditions. The reaction forces in this frequency range are close to the rigid body response; i.e., they are simply proportional to the applied acceleration.

The peak deflection of the jiggle magnets in the local y-direction (i.e. their intended direction of motion) is 6.5mm (Figure 8), due to the X-axis loading. The corresponding deflection for the chop magnets is 11.8mm (Figure 12), due to the Y-axis loading. These represent angular rotations of ±12° about the jiggle axis and ±38° about the chop axis.

Deflections of more than a few degrees are likely to cause problems for the BSM. The analysis indicates that interaction between the chop magnet arm and the launch latch end-stop will occur. According to the launch latch specification (Reference 6), it should limit rotation of the chop axis to less than 0.573 degrees, which equates to a chop magnet displacement of 0.18mm. However, this contact is not modelled, as agreed with UKATC (Reference 7). The large rotations indicated by this analysis would also cause the magnet arms to interfere with the motors, since the clearance between the arms and the motors is only 0.5mm.

5.3 CORRECTIVE MEASURES

A key aspect of the model that strongly influences the magnitude of the dynamic response of the mode of the mirror assembly as it rotates about the chop axis is the offset of the centre of gravity of the mirror assembly away from the axis of rotation.

© FNC 2002

The centre of gravity is quite close to the axis of rotation, but it is that offset that provides the excitation for that mode. Similarly, the offset of the centre of gravity of the jiggle stage assembly (including the chop stage) from the jiggle axis strongly influences the dynamic response of its fundamental mode.

Corrective measures to reduce the deflection magnitudes could include a tighter tolerance on the out of balance on the chop and jiggle assemblies. This would bring the centre of gravity of the jiggle and chop stages closer to their axes of rotation and reduce the driving force on these modes. UKATC should also consider fully locking both axes of rotation during launch.

The full set of results for 22 acceleration data points, 11 springs, 6 relative deflections and 3 reaction forces are presented in Annex 1 to Annex 3. A list of the data points is provided in Appendix A.

© FNC 2002

6. RANDOM VIBRATION FORCED RESPONSE

6.1 RESULTS PRESENTATION

Figure 20 illustrates the PSD curves for the data point where the highest acceleration occurs. This is at the data point furthest from the base plate. The peak value is at 8.89×10^{9} mm^2s^{-4} per Hz, which equates to $92.4g^2$ per Hz.

Figure 21 shows the acceleration PSD curves for the top chop motor. The peak acceleration here is $66.0g^2$ per Hz. This is the most severe of the four motor positions.

Figure 22 shows the acceleration PSD curves for the point at the centre of the mirror.

Figure 23 shows the displacement PSD curves (in mm^2 per Hz) for the relative motion between the top chop magnet and the corresponding motor, for comparison with the swept sine results. The largest displacement is at the first frequency point (20Hz), therefore the displacement is likely to be larger at frequencies lower than those analysed. However, the load specification does not include frequencies below 20Hz. The maximum value is 5.34×10^{-6} mm^2 per Hz.

Figure 24 shows the PSD of the reaction loads in the footprint in the middle of the BSM at the front edge. The units of this PSD are N^2 per Hz, and the peak value is 9894 N^2 per Hz.

Acceleration results are total acceleration, i.e. the base motion is included.

Acceleration and reaction force results are in the global X, Y, Z co-ordinate system. Relative displacement and spring force/torque results are in the local x, y, z co-ordinate system.

The units on the acceleration plots are in units of mm^2s^{-4} per Hz. To obtain the value of acceleration in g^2 per Hz, the PSD value is divided by 9.62×10^{7}.

The full set of results for all the data points requested is presented in Annex 4 to Annex 6.

6.2 DESCRIPTION OF RESULTS

In the random vibration forced response load cases, the gimbal frame fundamental modes are much less important than they are in the swept sine load cases. This is because the natural frequency of the jiggle axis mode (13.6Hz) is outside the frequency range considered and the magnitude of the of the base motion at the frequency of the chop rotation mode (21.4Hz) is 13.4dB lower than the peak excitation, due to the 6dB per octave roll off below 100Hz.

The third and fourth modes are therefore generally the most significant, since they are in the most severe part of the load frequency spectrum, at 392Hz and 398Hz. These modes are sideways and front-back rocking modes respectively. For all the data points considered, the highest acceleration occurs around the frequency of these two modes.

© FNC 2002

For most of the data points considered, the highest results occur under X-direction loading (nearly perpendicular to the mirror). This is probably because the Y-direction loading is less likely to excite the third and fourth modes, and the Z-direction loading is of lower magnitude. The results presented are therefore all for the X-direction load case.

There are five springs in the direction normal to the optical bench for each contact region between the base plate and the main structure. These represent a single bolted connection. In order to work out the axial force in the bolt, the individual spring force PSDs are square-rooted, summed and then squared to give a combined force. This provides an upper bound by assuming perfect correlation between the spring forces.

6.3 RMS CALCULATION

For the point of highest total acceleration (Figure 20, top jiggle flex pivot point), the following analysis was performed.

The acceleration PSD was integrated between the half-power points either side of the peak at 398Hz. This integral was then square-rooted to give the RMS acceleration due to this peak, which works out to be 50.5g. The total RMS acceleration for this point is 55.0g, calculated by integrating the PSD from 20Hz to 2000Hz. The majority of the acceleration experienced by the top jiggle pivot point is therefore due to the resonance at the 3rd and 4th modes.

6.4 CORRECTIVE MEASURES

The first two casing modes occur primarily through bending of the bottom section of the casing. Stiffening this section would increase the natural frequencies of these modes, which would lower the peak response because the vibration load rolls off with increasing frequency.

The first two casing modes are also very close together; therefore considerable coupling would occur between them. This coupling increases the response in the nearby frequency range, which is undesirable. The peak response could be lowered by stiffening the baseplate in such a way as to increase the separation between the modes.

© FNC 2002

7. VERIFICATION PROCEDURE

7.1 OVERVIEW

This project has been executed in accordance with the Frazer-Nash Consultancy Quality Management System (Reference 8) and FNC standard quality procedures (Reference 9). A quality statement (Reference 10) has been prepared that summaries the specific quality procedures that will be used to control the project. All staff that work on the project are required to comply with the quality statement. The FNC Quality Management System and the associated procedures comply with the requirements of ISO 9001.

The finite element model has been verified in accordance with FNC modelling procedures. The following checks have been undertaken:

- Technical audit and discussion of methodology in advance of model generation.
- Detailed independent checks on geometry, element selection, physical and material properties, boundary conditions and loads.
- Review of selected results.
- Analytical hand checks on modal frequencies of the first two modes.
- Analytical hand checks on the magnitude of response of the first two modes for the swept sine analysis.
- Review of report and final technical audit.

Records of technical audits, detail checks on the finite element model and review of the report are contained in the project and technical files.

7.2 INDEPENDENT CHECKS ON FIRST RESONANT FREQUENCIES

Hand calculations have been performed on the natural frequencies of the first two modes of the assembly. The modes in question are the rotational modes of the mirror assembly about the chop and jiggle axes. These modes can be approximated by an equivalent rotational inertia on the corresponding torsional spring.

The frequencies of the first two modes were calculated to be:

- Rotation about jiggle axis: 14Hz
- Rotation about chop axis: 21Hz

The frequencies correlate well with those obtained from the finite element model of the assembly. This is as to be expected, given that there is a large frequency separation between these modes and the first mode of the casing. Had the gimbal modes been close to the main structural resonances of the assembly, one would expect there to be a greater degree of coupling and hence the modal frequency of the compound system would have varied from the uncoupled mode calculated above.

7.3 INDEPENDENT CHECKS ON MAGNITUDE OF FORCED RESPONSE

Hand calculations have also been done to check the magnitude of the response for the first two modes due to the excitation at their respective natural frequencies. The static

© FNC 2002

deflection was first calculated for the peak acceleration level, based on the moment exerted by the off-centre mass on the torsional spring. The direction of loading which gave the largest deflection was chosen in each case – these were the X and Y (load) directions for jiggle and chop modes. Modal damping of 2% is assumed throughout the analysis, which gives a dynamic response factor of 25 at resonance. The peak response for the jiggle and chop modes at their natural frequencies is calculated to be:

- Jiggle axis: 12° rotation → 6.4mm peak deflection of the jiggle magnets,
- Chop axis: 37° rotation → 11.8mm peak deflection of the chop magnets.

These compare very well to the results from the FE model (6.5mm and 11.8mm deflections for the jiggle and chop magnets respectively). The swept sine FE model therefore behaves as expected.

7.4 CONTROL OF MODEL VERSION NUMBERS

A number of variants of the dynamic model have been generated as part of the development process. The filenames of the models reported in this document are:

FEMGEN Model:	BSMN.G61
ABAQUS Normal Modes:	bsmn_run12.inp, bsmn_run13.inp
ABAQUS Swept Sine X:	bsmn_ssx_13.inp
ABAQUS Swept Sine Y:	bsmn_ssy_13.inp
ABAQUS Swept Sine Z:	bsmn_ssz_13.inp
ABAQUS Random Response X:	bsmn_rrx_12.inp, bsmn_rrx_13.inp
ABAQUS Random Response Y:	bsmn_rry_12.inp, bsmn_rry_13.inp
ABAQUS Random Response Z:	bsmn_rrz_12.inp, bsmn_rrz_13.inp

© FNC 2002

8. CONCLUSIONS

A dynamic finite element model of the SPIRE Beam Steering Mirror has been generated and analysed using the general purpose finite element code ABAQUS (STANDARD) Version 5.8. A series of dynamic analyses have been performed including:

- Modal Analysis (Normal Modes)
- Swept Sine (in three orthogonal directions)
- Random Response (in three orthogonal directions)

The modal analysis has shown there to be 19 modes in the frequency range up to 2000 Hz, of which the lowest frequency modes are rotational modes of the mirror assembly on the flex pivots about the jiggle and chop axes. The frequencies of these modes are 13.6Hz and 21.4Hz. These frequencies correlate well with previous analyses by UKATC and hand calculations performed by FNC.

The first mode of the main casing occurs at approximately 392Hz. It has been identified that the degree of constraint at the boundary between the baseplate and the optical bench has a significant effect on the frequency of modes containing substantial amounts of bending of the baseplate. The current analysis assumes that all nodes on the interface plane between the thickened footprint of the baseplate and the optical bench are constrained in the direction normal to the optical bench. This results in only a small amount of bending in the baseplate, but there is still a significant amount of bending in the bottom plate of the main casing.

The swept sine analyses reveal there to be potential problems due to the large magnitude of the gimbal frame rotation in both axes (modes 1 and 2). The launch latch would, in the real device, limit the rotation in the chop axis to a much lower value, therefore significant interaction with the end-stop would occur. The size of the motor air gaps would also limit the rotation to a much smaller value than is seen in the model. The magnitude of response about the two axes is corroborated by the hand calculations performed in Section 7.

The magnitude of the response could be reduced by:

- Better balancing of the chop and jiggle stages;
- Increasing the moment of inertia about the axis of rotation;
- Increasing the stiffness of the pivot springs;
- Fully locking the assembly during launch;
- Increasing the damping.

The first of these suggestions is thought to be easier to implement than the other four, within the current BSM design.

The random response analyses show there to be large acceleration levels at the frequencies of the third and fourth modes of the system (sideways and front-back rocking). These modal frequencies are close to the frequencies of the peak excitation levels of the system. The highest acceleration seen in the model occurs at the top of the BSM, and has an RMS value of 55.0g for the whole frequency range of 20-2000Hz.

© FNC 2002

To reduce the overall random vibration response, the BSM could be stiffened so that the third and fourth modes occur at higher frequencies, outside the high plateau in the excitation spectrum. It may be advantageous to do this in such a way as to increase the separation between the modes, to reduce their coupled response.

© FNC 2002

9. REFERENCES

1 FEMGV User Manual
Version 6.1-02
FEMSYS Engineering Software, August 1999

2 ABAQUS/Standard User Manual
Version 5.8
Hibbitt, Karlsson & Sorensen Inc., 1998

3 Email from Ian Pain on 15/02/2002, 'BSM mass and inertia properties'
I Pain
SPIRE-ATC-NOT-0012.

4 'Flex-Free Pivot Frictionless Bearing' data book
Lucas Aerospace

5 SPIRE BSM Vibration Response Analysis Specification
I Pain
ATC Report SPI-BSM-DOC-0008, Issue 1, June 00

6 Email from Ian Pain on 13/03/2002, containing launch latch data
Bruce Swinyard
DCR/ECR number HR-SP-ATC-002, March 2002

7 Notes from SPIRE BSM vibration meeting on 15/01/02
A J Vibert

8 Quality Assurance: Quality Manual
M Harris
FNC Report FNC/7516R, Issue 9, January 2002

9 Quality Assurance: Handbook of Quality Procedures
M Harris
FNC Report FNC 8100R, Issue 9, January 2002

10 Quality Statement
A J Vibert
FNC 5505/23610V, Issue 1, January 2002

© FNC 2002

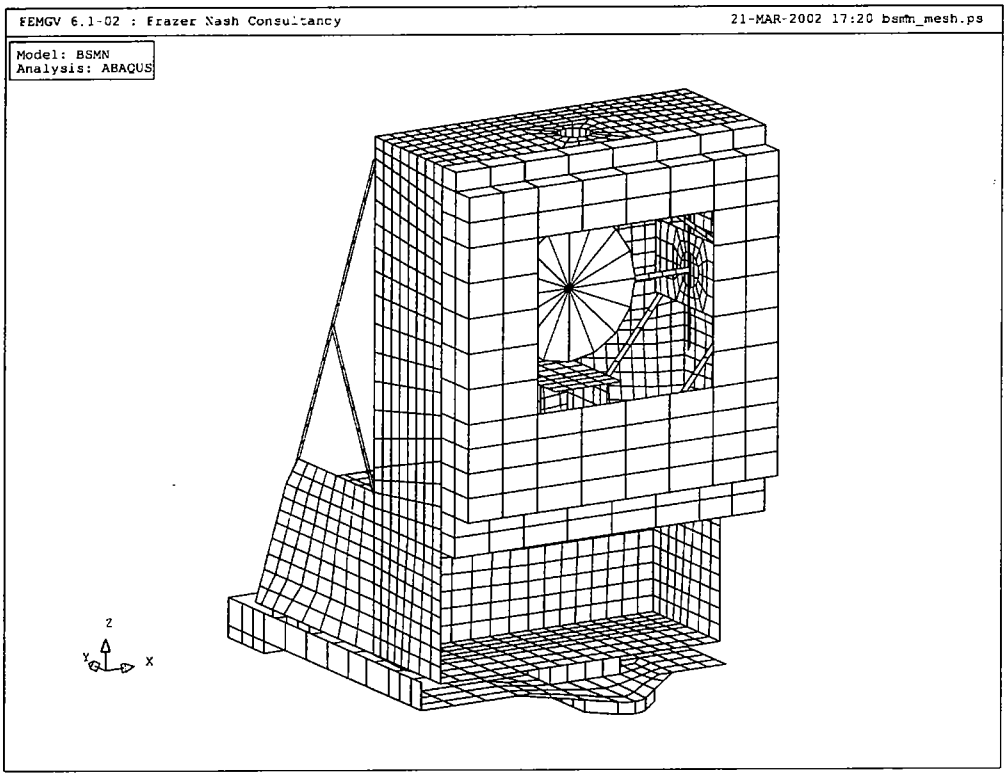

Figure 1 – Complete FE Model Mesh

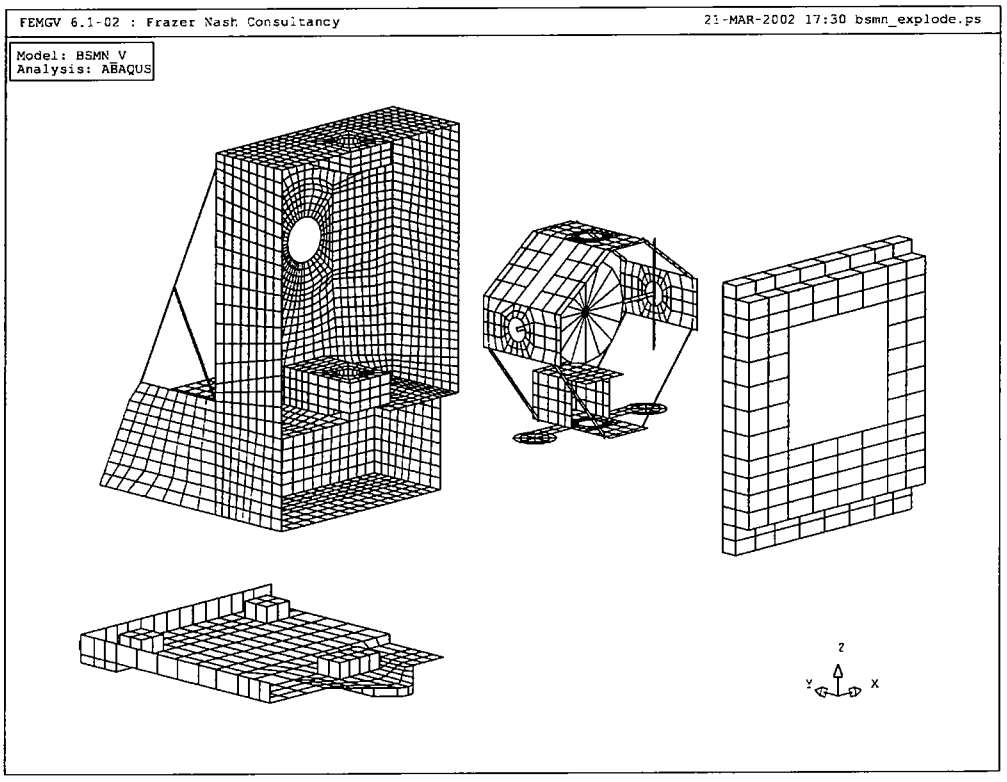

Figure 2 – Exploded View of FE Model Mesh

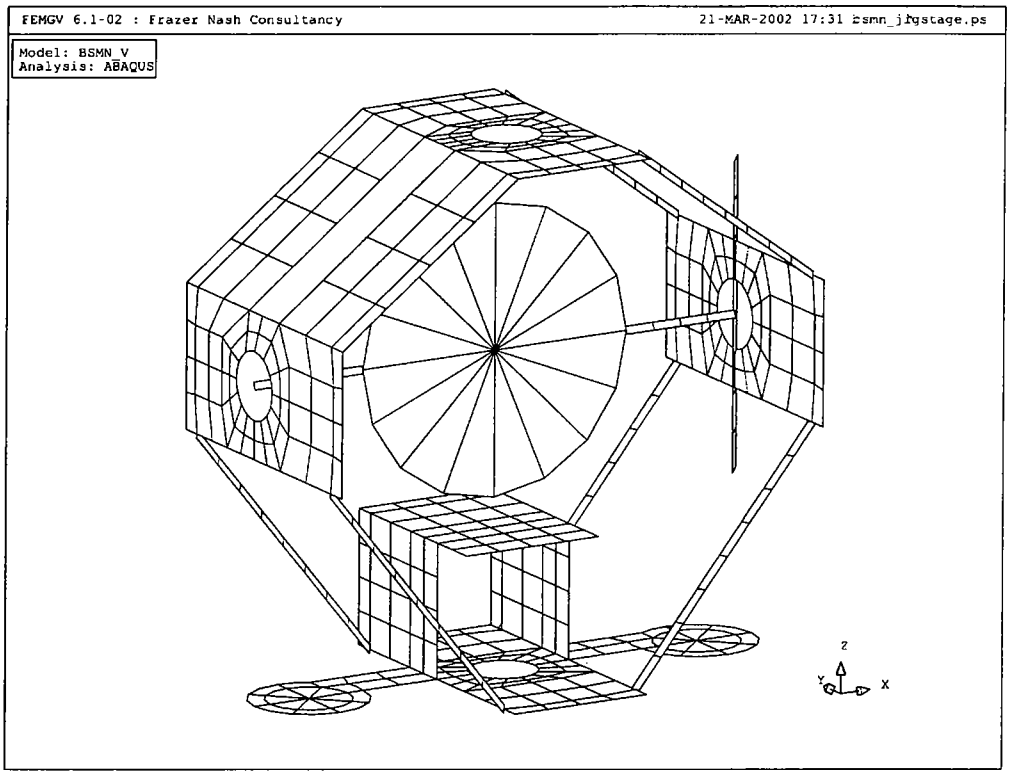

Figure 3 – View of Jiggle & Chop Stage Mesh

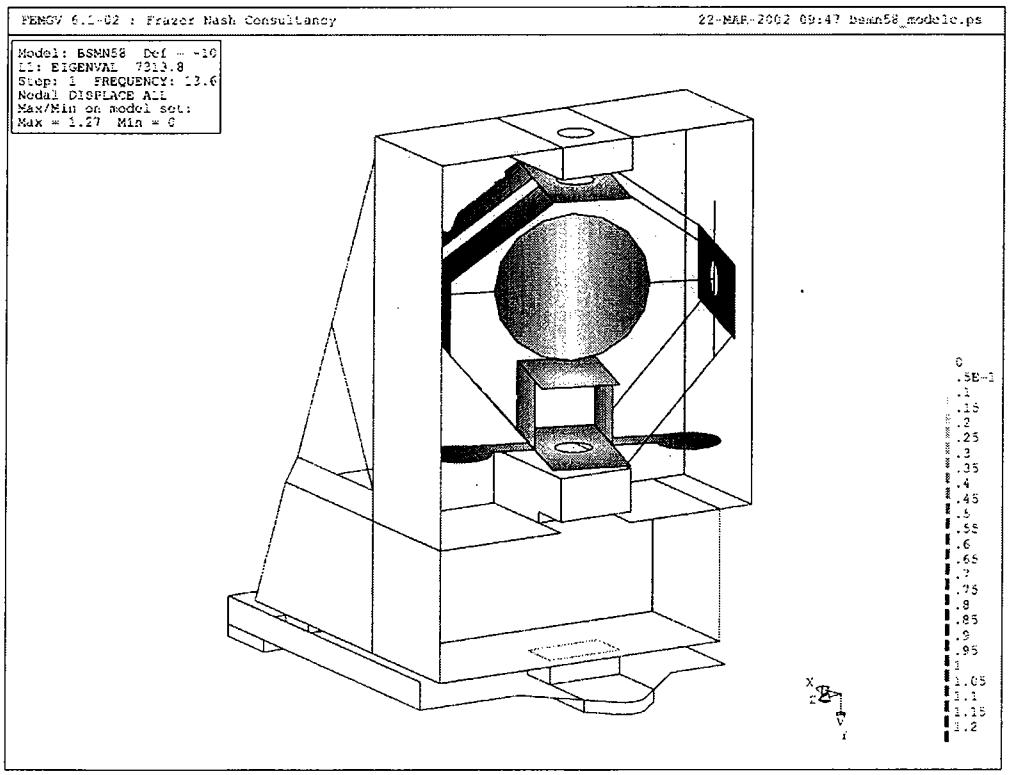

Figure 4 –Shape of First Vibration Mode (Jiggle Stage Fundamental)

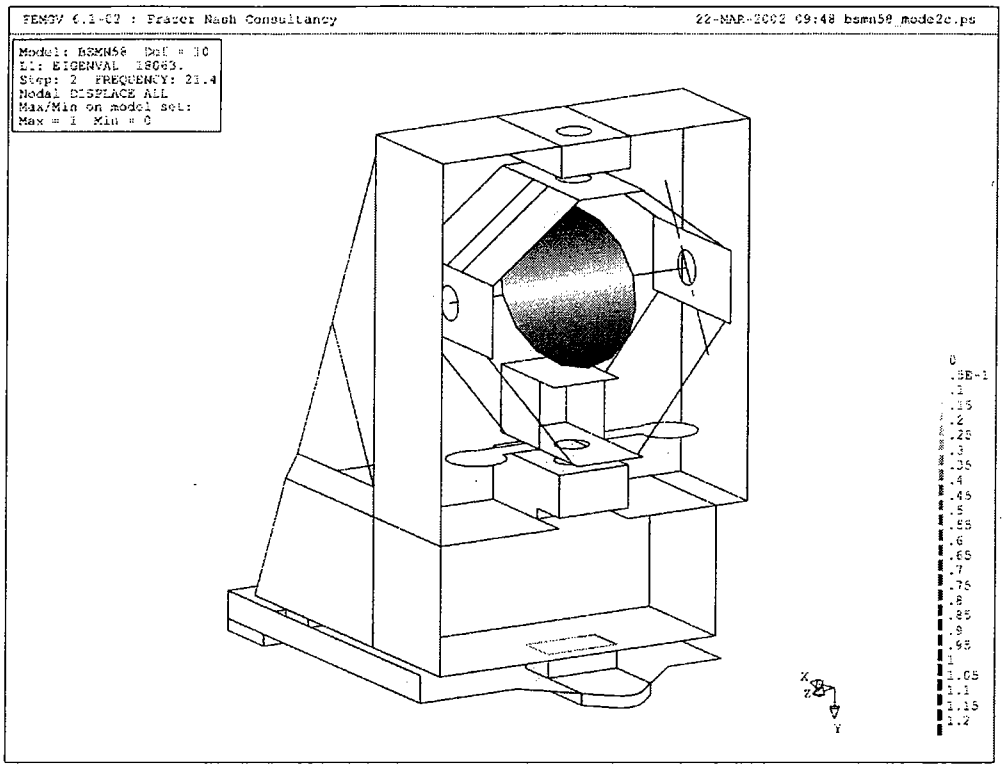

Figure 5 – Shape of Second Vibration Mode (Chop Stage Fundamental)

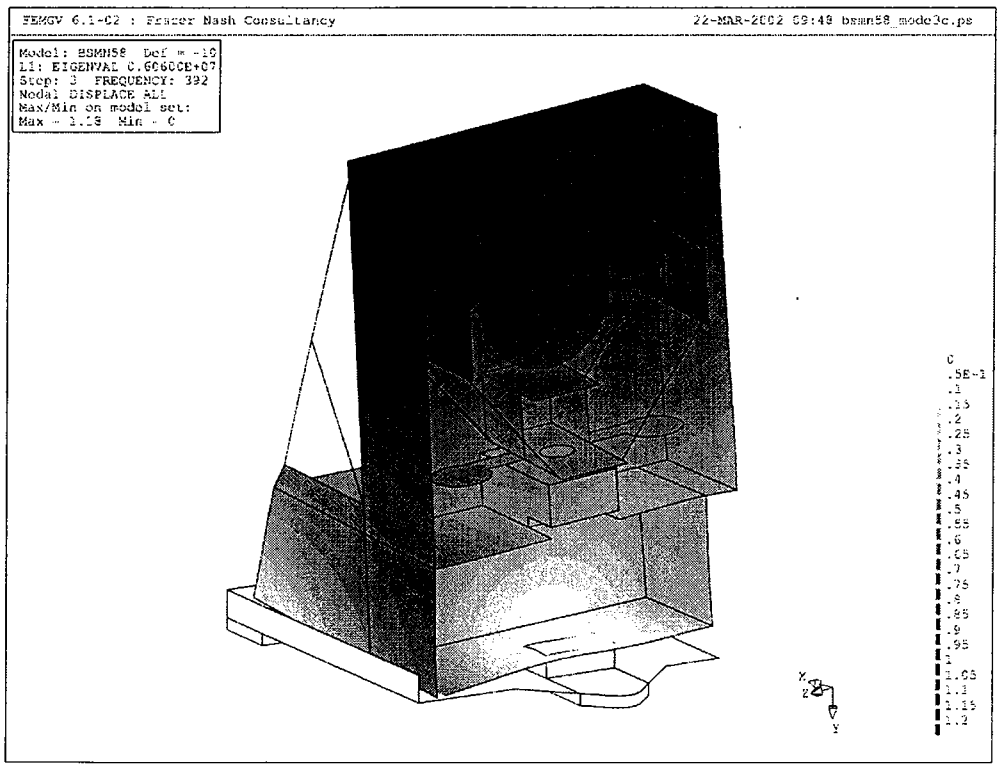

Figure 6 - Shape of Third Vibration Mode (Sideways Rocking)

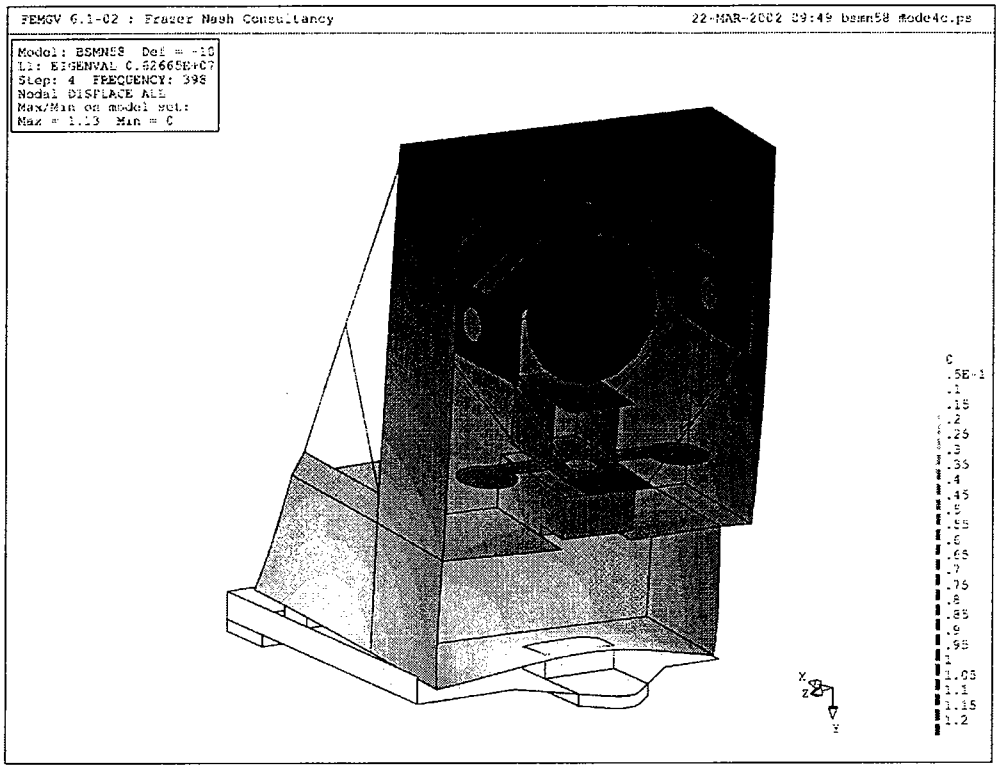

Figure 7 – Shape of Fourth Vibration Mode (Front-Back Rocking)

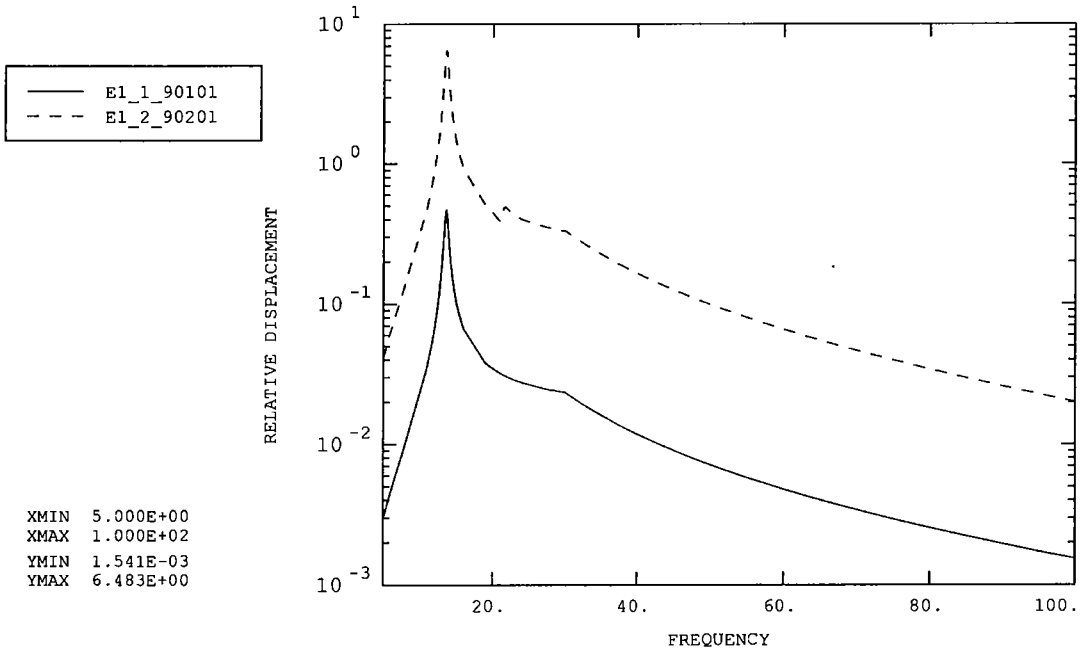

——— Lateral magnet sway, - - - - Front-back magnet motion (mm)

Figure 8 – X-direction swept sine load: top chop magnet relative to motor

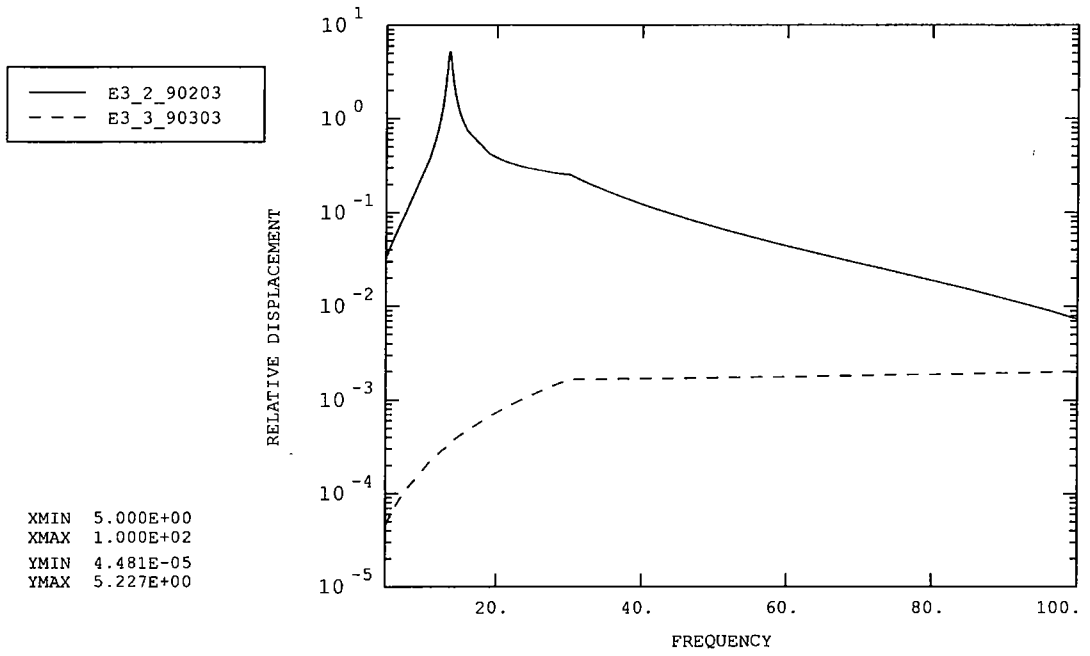

——— Front-back magnet motion, - - - - Lateral magnet sway (mm)

Figure 9 – X-direction swept sine load: right-hand jiggle magnet relative to motor

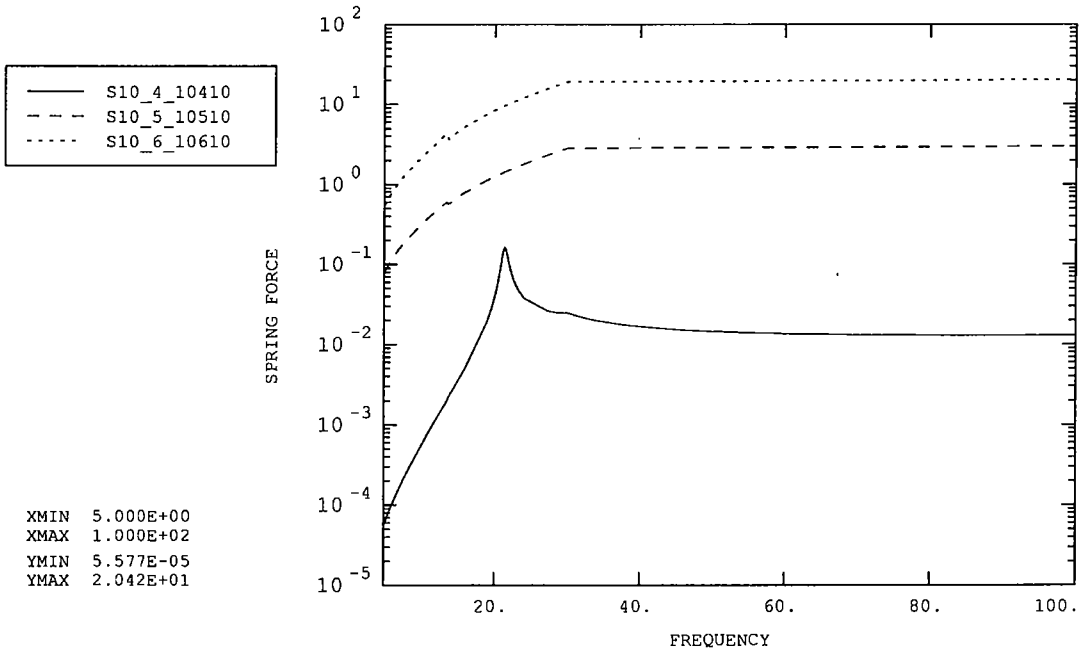

——— Flex pivot torque, - - - - & · · · · Yaw rotation torque (Nmm)

Figure 10 – X-direction swept sine load: chop flex pivot spring torque (s10_4_10410)

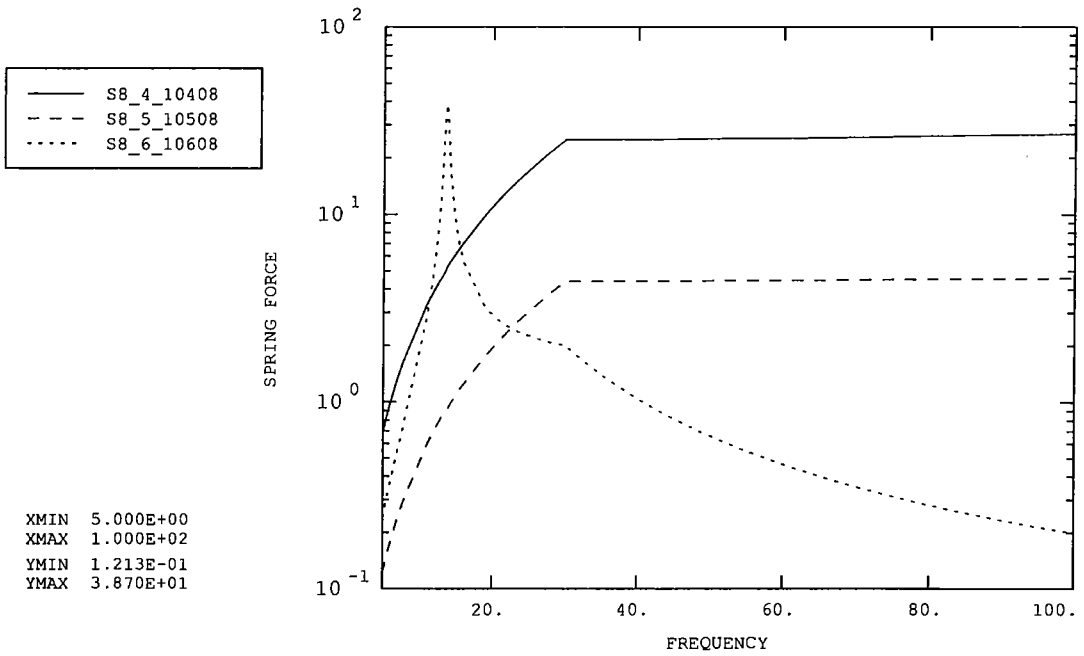

···· Flex pivot torque, ——— & - - - - Yaw rotation torque (Nmm)

Figure 11 – X-direction swept sine load: jiggle flex pivot spring torque (s8_6_10608)

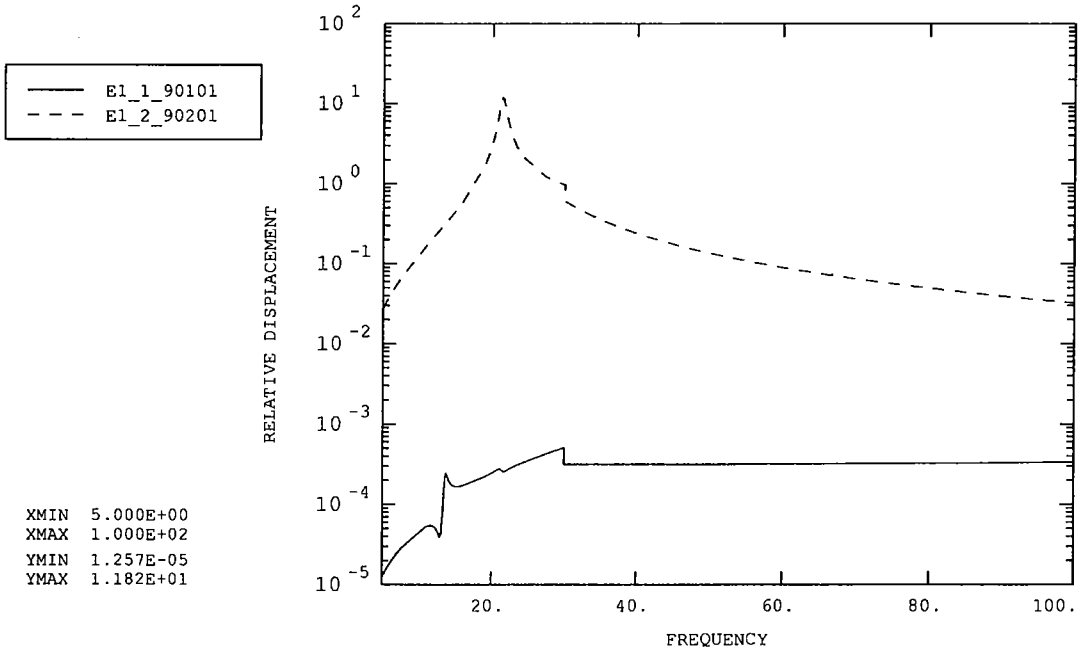

——— Lateral magnet sway, - - - - Front-back magnet motion (mm)

Figure 12 – Y-direction swept sine load: top chop magnet relative to motor

© FNC 2002

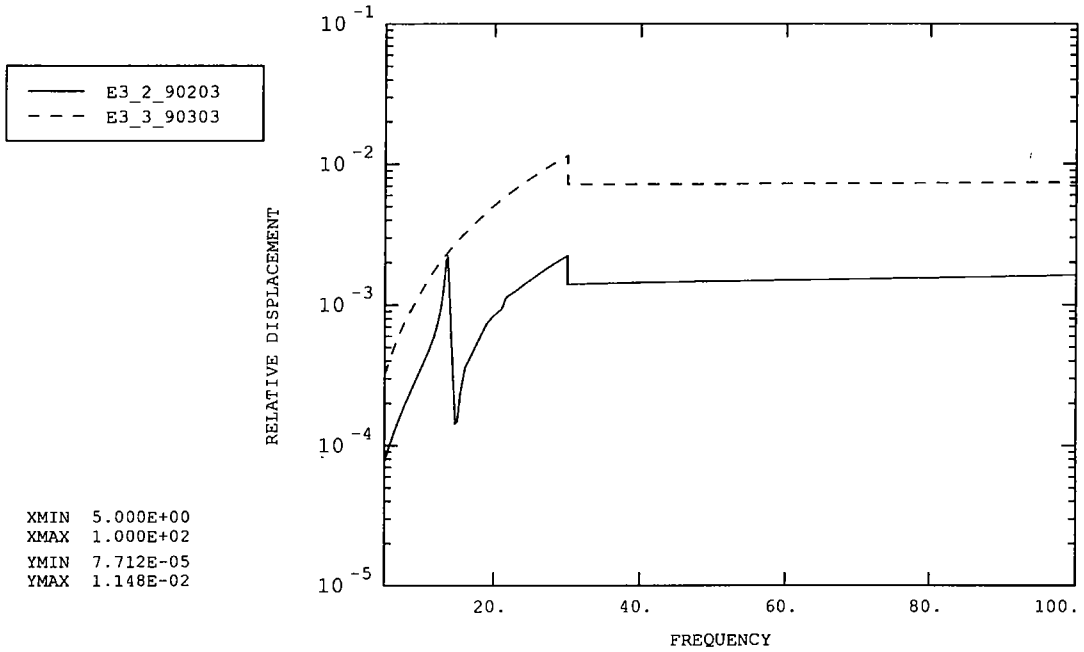

——— Front-back magnet motion, - - - - Lateral magnet sway (mm)

Figure 13 – Y-direction swept sine load: right-hand jiggle magnet relative to motor

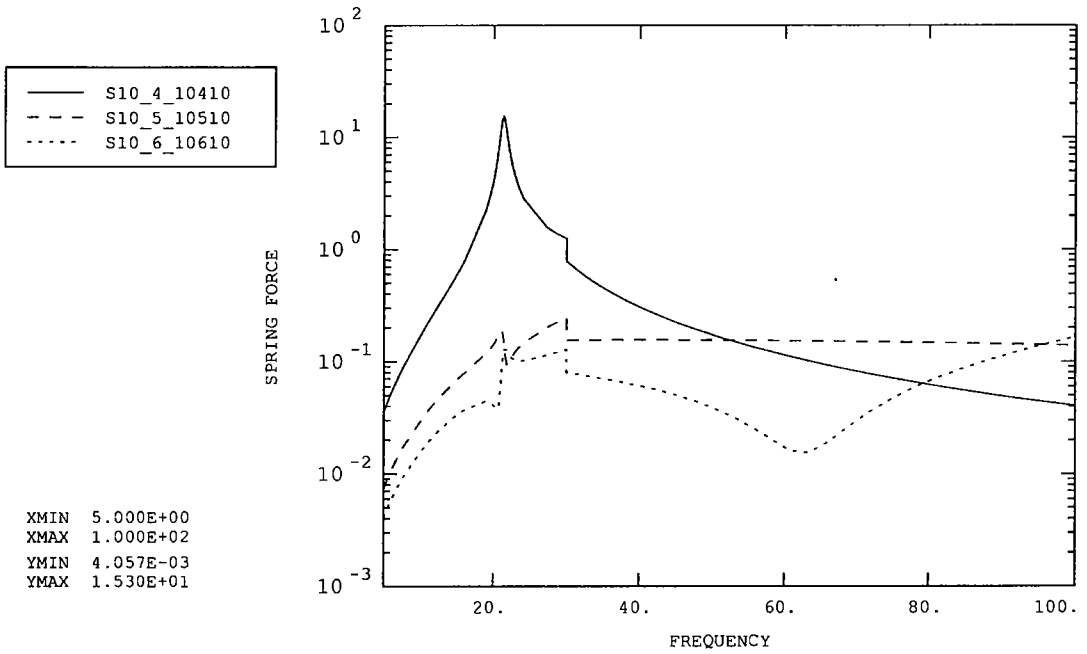

——— Flex pivot torque, - - - - & · · · · Yaw rotation torque (Nmm)

Figure 14 – Y-direction swept sine load: chop flex pivot spring torque (s10_4_10410)

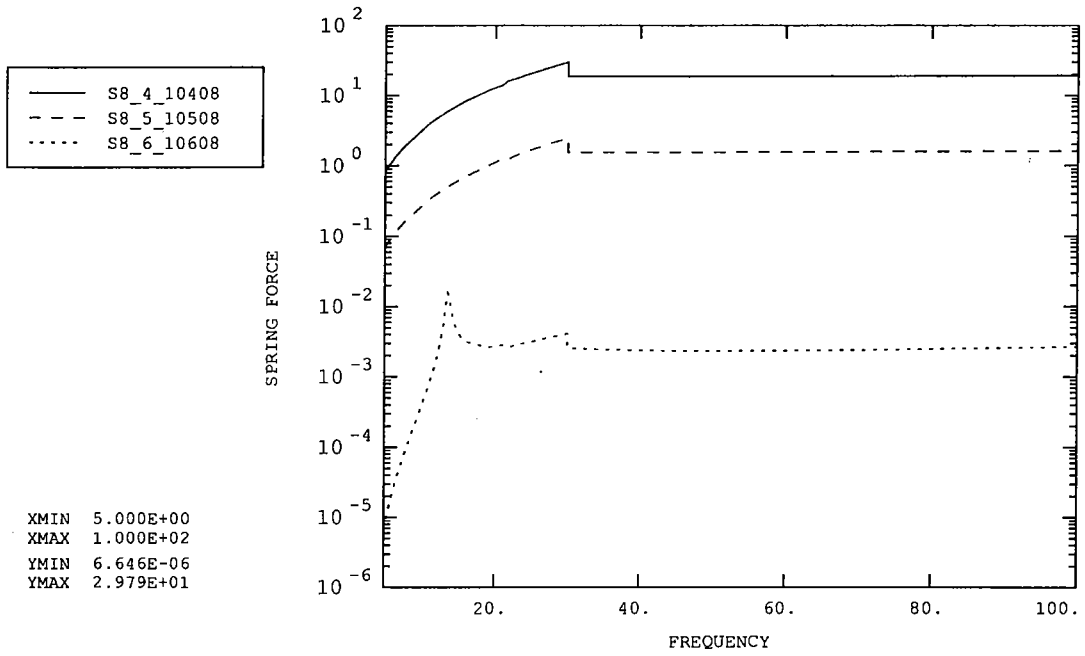

···· Flex pivot torque, ——— & - - - - Yaw rotation torque (Nmm)

Figure 15 – Y-direction swept sine load: jiggle flex pivot spring torque (s8_6_10608)

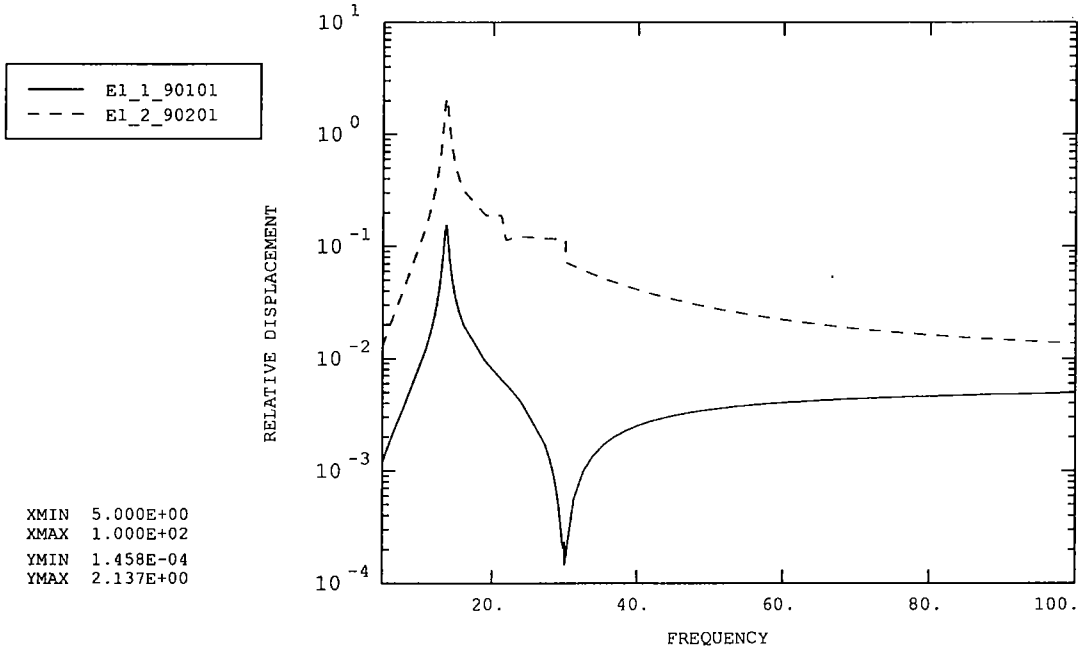

——— Lateral magnet sway, - - - - Front-back magnet motion (mm)

Figure 16 – Z-direction swept sine load: top chop magnet relative to motor

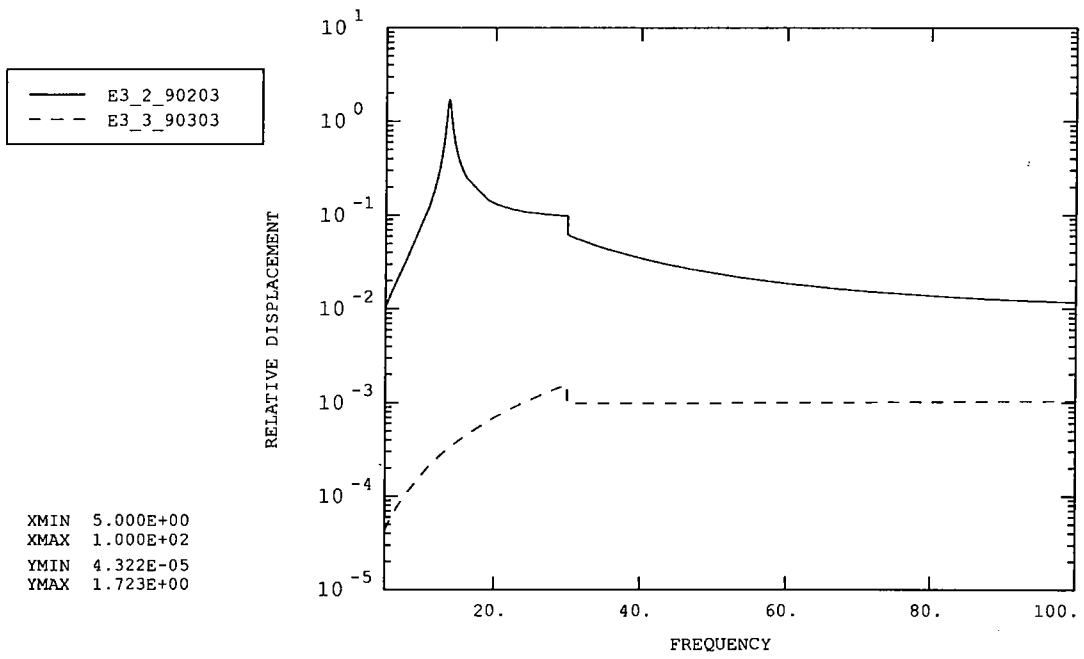

——— Front-back magnet motion, - - - - Lateral magnet sway (mm)

Figure 17 – Z-direction swept sine load: right-hand jiggle magnet relative to motor

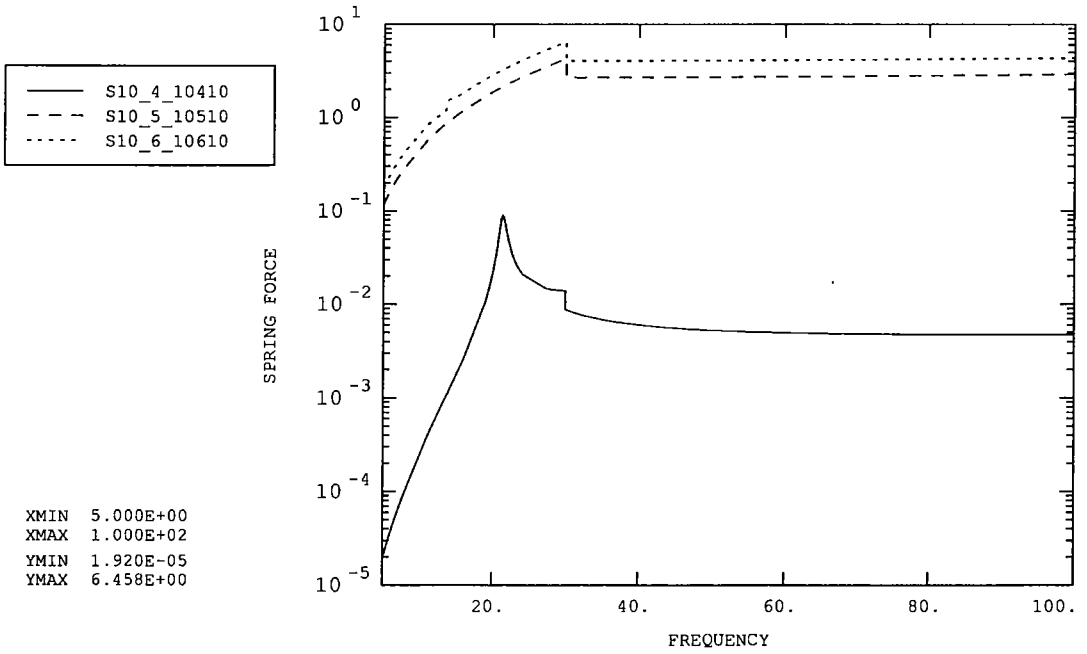

——— Flex pivot torque, - - - - & · · · · Yaw rotation torque (Nmm)

Figure 18 – Z-direction swept sine load: chop flex pivot spring torque (s10_4_10410)

© FNC 2002

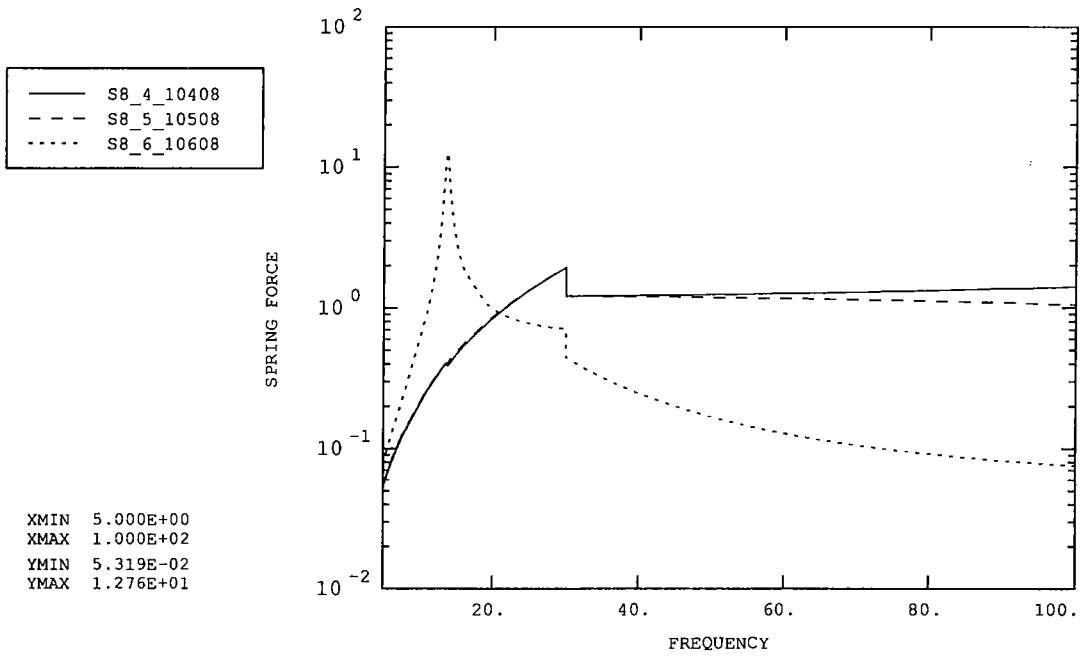

···· Flex pivot torque, ——— & - - - - Yaw rotation torque (Nmm)

Figure 19 – Z-direction swept sine load: jiggle flex pivot spring torque (s8_6_10608)

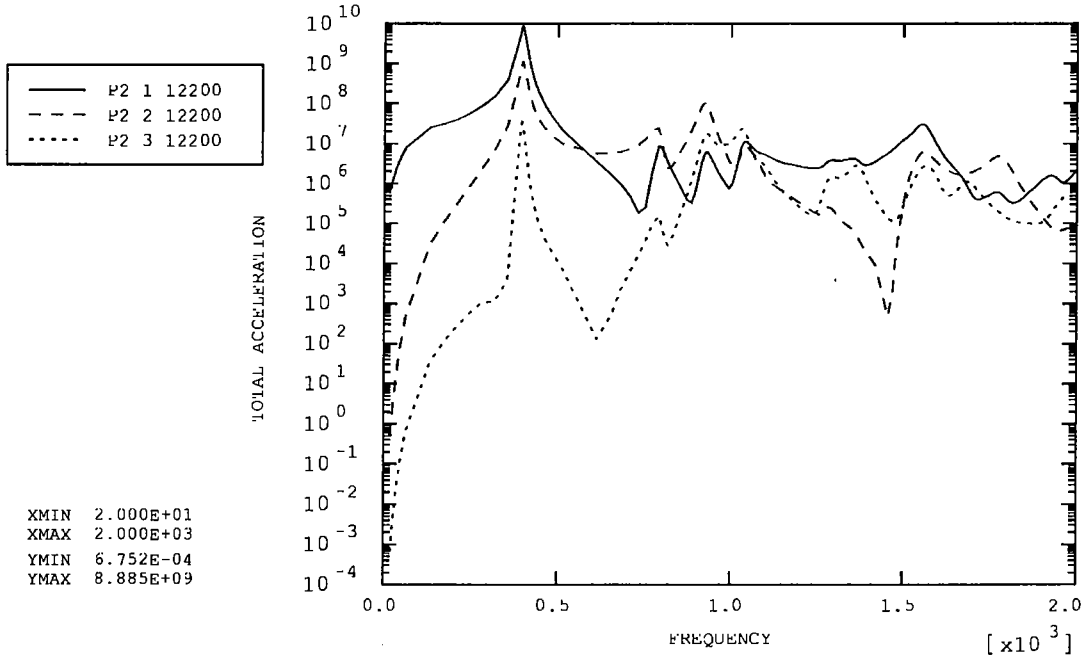

——— X, - - - - Y, ···· Z acceleration (mm^2/s^4 per Hz)

Figure 20 – X-direction random vibration: top jiggle flex pivot acceleration PSD

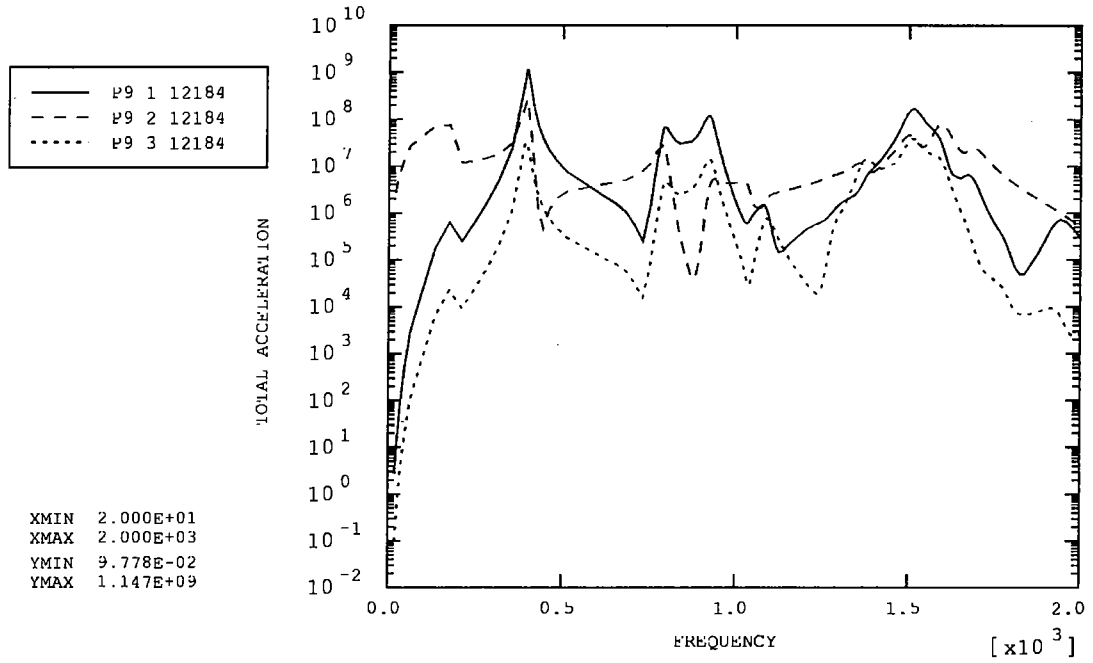

——— X, - - - - Y, · · · · Z acceleration (mm^2/s^4 per Hz)

Figure 21 – X-direction random vibration: top chop motor acceleration PSD

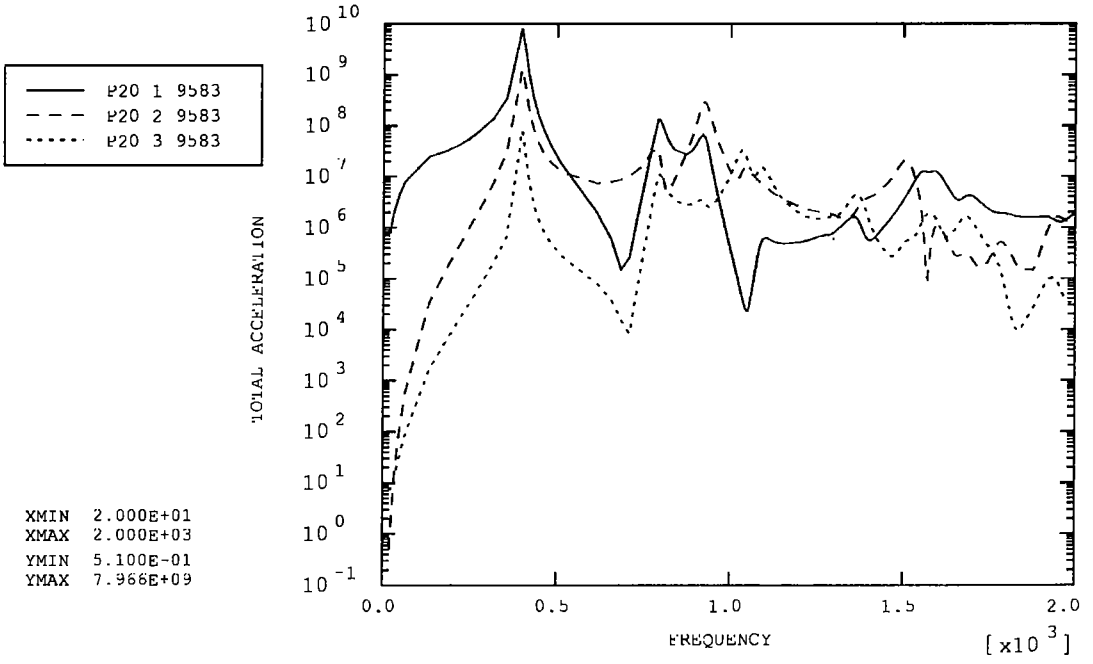

——— X, - - - - Y, · · · · Z acceleration (mm^2/s^4 per Hz)

Figure 22 – X-direction random vibration: mirror centre acceleration PSD

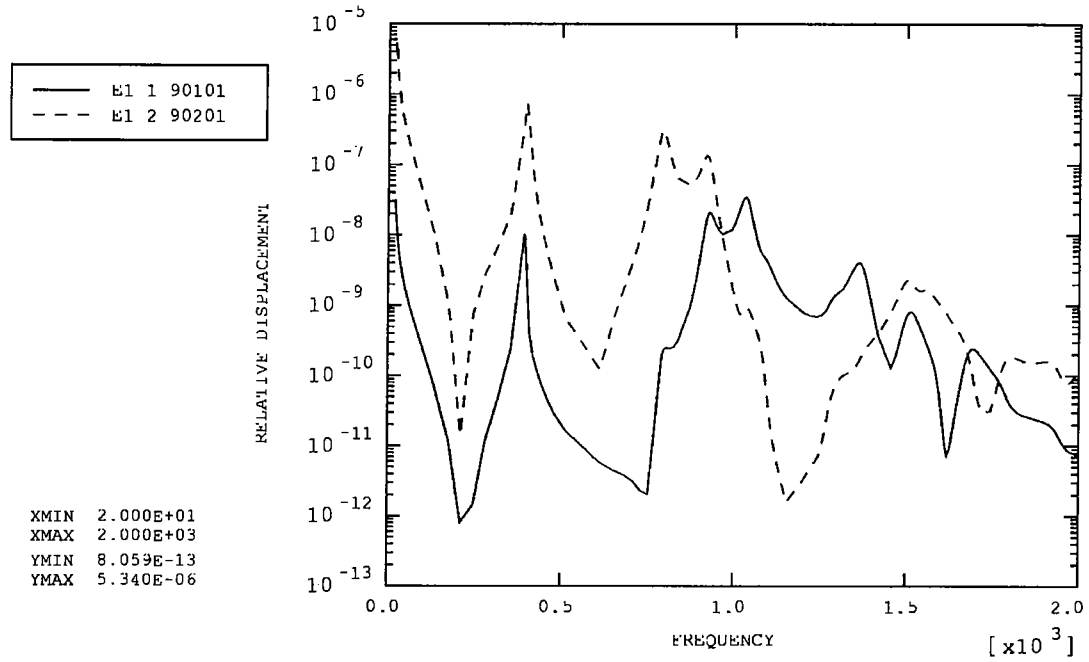

——— Lateral magnet sway, - - - - Front-back magnet motion (mm^2 per Hz)

Figure 23 – X-direction random vibration: top chop magnet displacement relative to motor

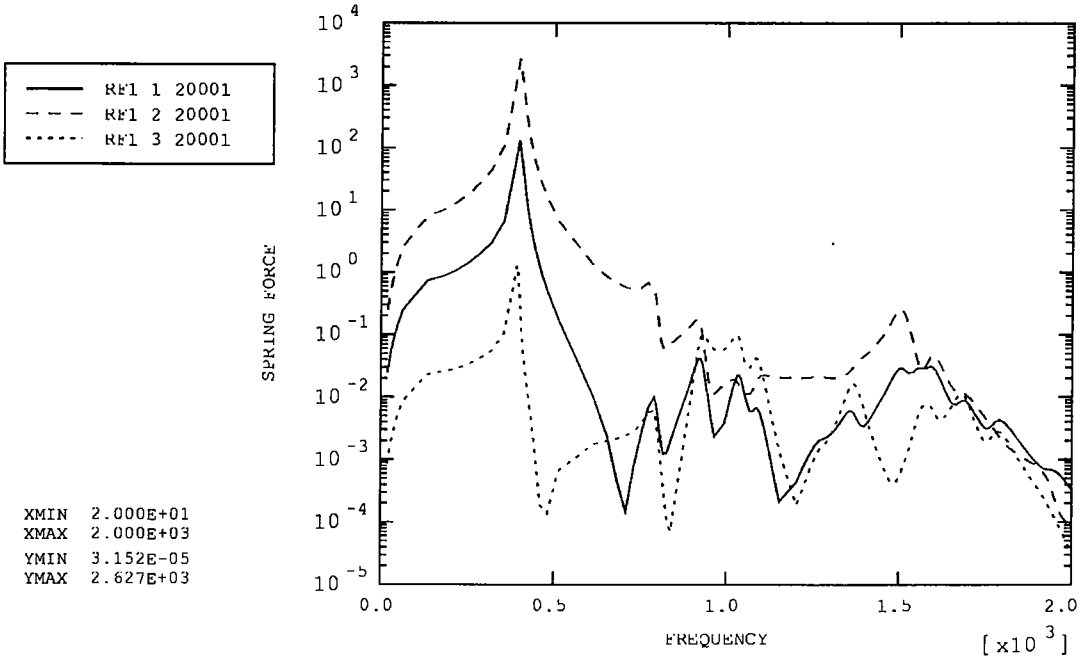

——— X, - - - - Y, · · · · Z reaction force (N^2 per Hz)

Figure 24 – X-direction random vibration: reaction force at front middle footprint

APPENDIX A: DATA POINT POSITIONS

P	Acceleration data points	Node number
1	Jiggle axis pivot (top) – frame	12182
2	Jiggle axis pivot (top) – jiggle stage	12200
3	Jiggle axis pivot (bottom) – frame	12183
4	Jiggle axis pivot (bottom) – jiggle stage	12192
5	Chop axis pivot (right side) – jiggle stage	12189
6	Chop axis pivot (right side) – chop stage	114
7	Chop axis pivot (left side) – jiggle stage	12188
8	Chop axis pivot (left side) – chop stage	105
9	Chop motor (top)	12184
10	Chop motor (bottom)	12185
11	Jiggle motor (right side)	12186
12	Jiggle motor (left side)	12187
13	PCAL CG	12193
14	PCAL extension to mirror centre	12199
15	Launch latch 'A' CG	12196
16	Launch latch 'A' extension to magnet centre	12197
17	Connector (top)	12194
18	Chop magnet (top)	115
19	Chop magnet (bottom)	122
20	Mirror Centre	9583
21	Jiggle magnet (right)	9276
22	Jiggle magnet (left)	9264

E	Displacement between...	Node number
1	Chop magnet vs. motor (top)	90001
2	Chop magnet vs. motor (bottom)	90002
3	Jiggle magnet vs. motor (right)	90003
4	Jiggle magnet vs. motor (left)	90004
5	Mirror centre vs. PCAL extension	90005
6	Chop magnet (top) vs. launch latch 'A'	90006

© FNC 2002

S	Position of spring elements	Node 1	Element
1	Front baffle (top left)	9702	10n01, n=1,2,3
2	Front baffle (top right)	9739	10n02, n=1,2,3
3	Front baffle (bottom left)	9629	10n03, n=1,2,3
4	Front baffle (bottom right)	9594	10n04, n=1,2,3
5	Base (front middle)	3894	10n05, n=1,2,3
6	Base (back left)	3414	10n06, n=1,2,3
7	Base (back right)	3622	10n07, n=1,2,3
8	Jiggle pivot (top)	12200	10n08, n=1 to 6
9	Jiggle pivot (bottom)	12192	10n09, n=1 to 6
10	Chop pivot (left)	12188	10n10, n=1 to 6
11	Chop pivot (right)	12189	10n11, n=1 to 6

RF	Reaction Forces	Node number
1	Reaction Force (front middle)	10587
2	Reaction Force (back left)	10722
3	Reaction Force (back right)	10671

© FNC 2002

SPIRE Beam Steering Mirror PFM Test Report

Document Prepared By:	David McNeill		
Document Approved By:	Gary Rae / Colin Cunningham	Signature and Date:	
Document Approved By:	Gillian Wright	Signature and Date:	
Document Released By:	Philip Parr-Burman	Signature and Date:	

SPIRE BSM VIBRATION ANALYSIS

Annex 1 - Swept Sine X-Direction

FNC 5505/24072R Issue 1

Prepared for

U.K. Astronomy Technology Centre

DOCUMENT INFORMATION

Project : SPIRE BSM Vibration Analysis

Report Title : Annex 1 - Swept Sine X-Direction

Client : U.K. Astronomy Technology Centre

Client Ref. : 024706

Classification :

Report No. : FNC 5505/24072R

Issue No. : 1 **Compiled By :** D C Reed

Date : May 2002 A J Vibert

Approved By : M W Anderson

DISTRIBUTION

Copy	Recipient	Organisation
1	I Pain	UK ATC
2	I Pain	UK ATC
3	I Pain	UK ATC
4	File	FNC

Copy No. 2

COPYRIGHT

The Copyright in this work is vested in Frazer-Nash Consultancy Limited. The document is issued in confidence solely for the purpose for which it is supplied. Reproduction in whole or in part or use for tendering or manufacturing purposes is prohibited except under an agreement with or with the written consent of Frazer-Nash Consultancy Limited and then only on the condition that this notice is included in any such reproduction.

Originating Office: FRAZER-NASH CONSULTANCY LIMITED
Stonebridge House, Dorking Business Park, Dorking, Surrey RH4 1HJ, UK
T: +44 (0)1306 885050 F: +44 (0)1306 886464 E: info@fnc.co.uk W: www.fnc.co.uk

DATA POINT POSITIONS

Note:

- The labels on the plots are as follows: e.g. P9_1_12184 refers to acceleration data point P9, degree of freedom 1 (node number 12184).
- Degrees of freedom 1, 2 and 3 refer to motion in the x, y and z directions (or X, Y and Z directions), while degrees of freedom 4, 5 and 6 refer to rotations about the x, y and z axes (or X, Y and Z axes).
- Acceleration is total acceleration (i.e. includes base motion)
- Accelerations and reaction forces are given in the global X, Y, Z co-ordinates
- Relative displacements and spring forces/torques are given in the local model x, y, z co-ordinates.
- 'Left' and 'right' directions are defined from a point of view looking towards the mirror surface, with the top of the casing furthest from the baseplate.

Fig.	P	Acceleration data points	Node number
1	1	Jiggle axis pivot (top) – frame	12182
2	2	Jiggle axis pivot (top) – jiggle stage	12200
3	3	Jiggle axis pivot (bottom) – frame	12183
4	4	Jiggle axis pivot (bottom) – jiggle stage	12192
5	5	Chop axis pivot (right side) – jiggle stage	12189
6	6	Chop axis pivot (right side) – chop stage	114
7	7	Chop axis pivot (left side) – jiggle stage	12188
8	8	Chop axis pivot (left side) – chop stage	105
9	9	Chop motor (top)	12184
10	10	Chop motor (bottom)	12185
11	11	Jiggle motor (right side)	12186
12	12	Jiggle motor (left side)	12187
13	13	PCAL CG	12193
14	14	PCAL extension to mirror centre	12199
15	15	Launch latch 'A' CG	12196
16	16	Launch latch 'A' extension to magnet centre	12197
17	17	Connector (top)	12194
18	18	Chop magnet (top)	115
19	19	Chop magnet (bottom)	122
20	20	Mirror Centre	9583
21	21	Jiggle magnet (right)	9276
22	22	Jiggle magnet (left)	9264

© FNC 2002

Fig.	E	Displacement between...	Element
23	1	Chop magnet vs. motor (top)	90n01, n=1, 2
24	2	Chop magnet vs. motor (bottom)	90n02, n=1, 2
25	3	Jiggle magnet vs. motor (right)	90n03, n=2, 3
26	4	Jiggle magnet vs. motor (left)	90n04, n=2, 3
27	5	Mirror centre vs. PCAL extension	90n05, n=1, 2, 3
28	6	Chop magnet (top) vs. launch latch 'A'	90206

Fig.	S	Position of spring elements	Node 1	Element
29	1	Front baffle (top left)	9702	10n01, n=1,2,3
30	2	Front baffle (top right)	9739	10n02, n=1,2,3
31	3	Front baffle (bottom left)	9629	10n03, n=1,2,3
32	4	Front baffle (bottom right)	9594	10n04, n=1,2,3
33	5	Base (front middle)*	3894	10n05, n=1,2,3
34	6	Base (back left)*	3414	10n06, n=1,2,3
35	7	Base (back right)*	3622	10n07, n=1,2,3
36,37	8	Jiggle pivot (top)	12200	10n08, n=1 to 6
38,39	9	Jiggle pivot (bottom)	12192	10n09, n=1 to 6
40,41	10	Chop pivot (left)	12188	10n10, n=1 to 6
42,43	11	Chop pivot (right)	12189	10n11, n=1 to 6

Fig.	RF	Reaction Forces	Node number
44	1	Reaction Force (front middle)	10587
45	2	Reaction Force (back left)	10722
46	3	Reaction Force (back right)	10671

* The baseplate-casing connections are each modelled using a single spring in the local x and y directions, and five springs in the local z direction. The forces from these five springs are added together to calculate the total connective force. The curve labels for the z direction degrees of freedom have the prefix 'B'.

© FNC 2002

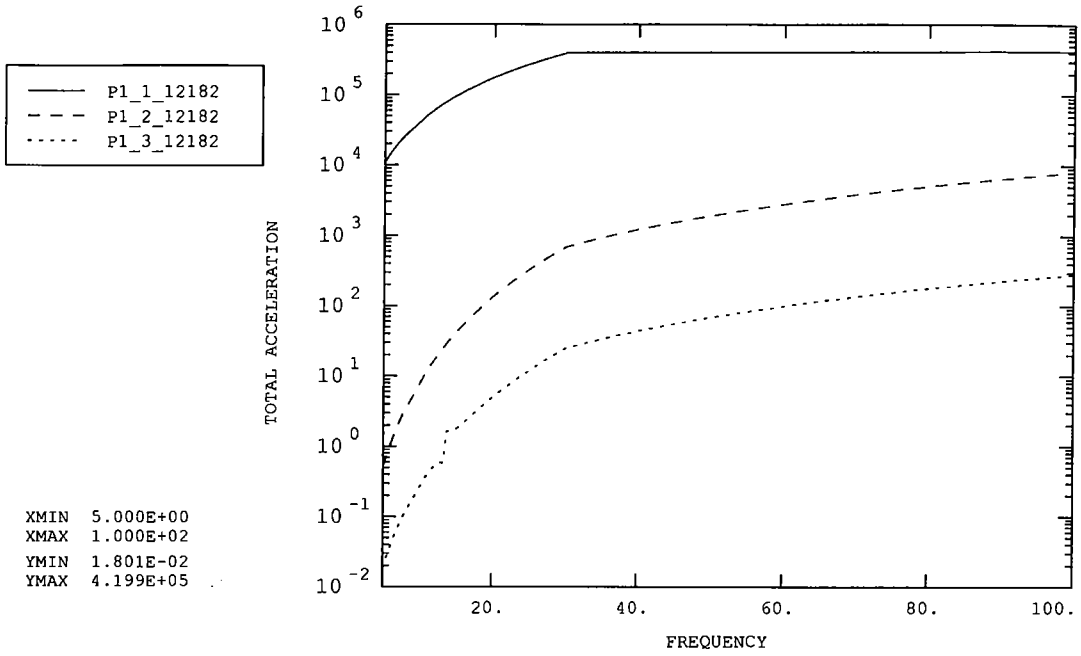

Figure 1: Jiggle axis pivot (top) – frame

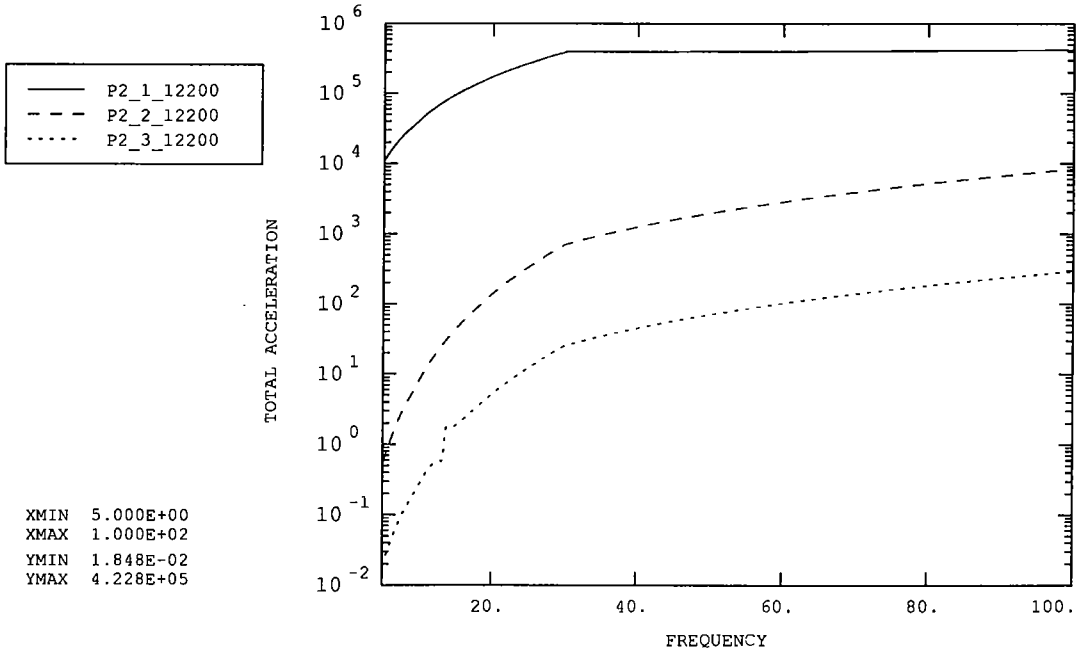

Figure 2: Jiggle axis pivot (top) – jiggle stage

© FNC 2002

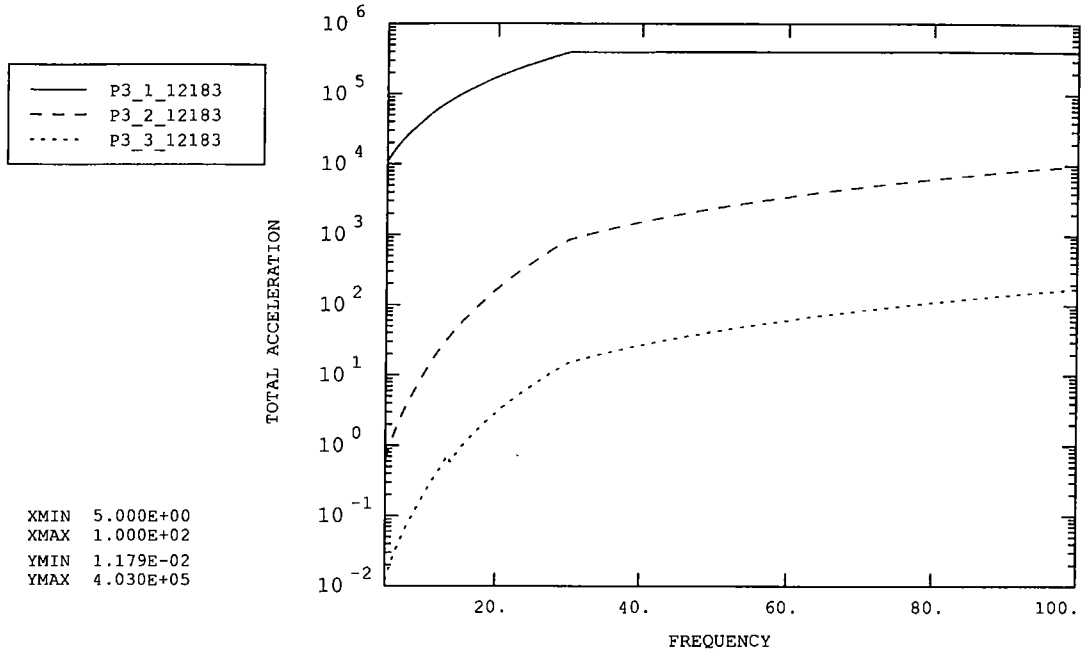

Figure 3: Jiggle axis pivot (bottom) – frame

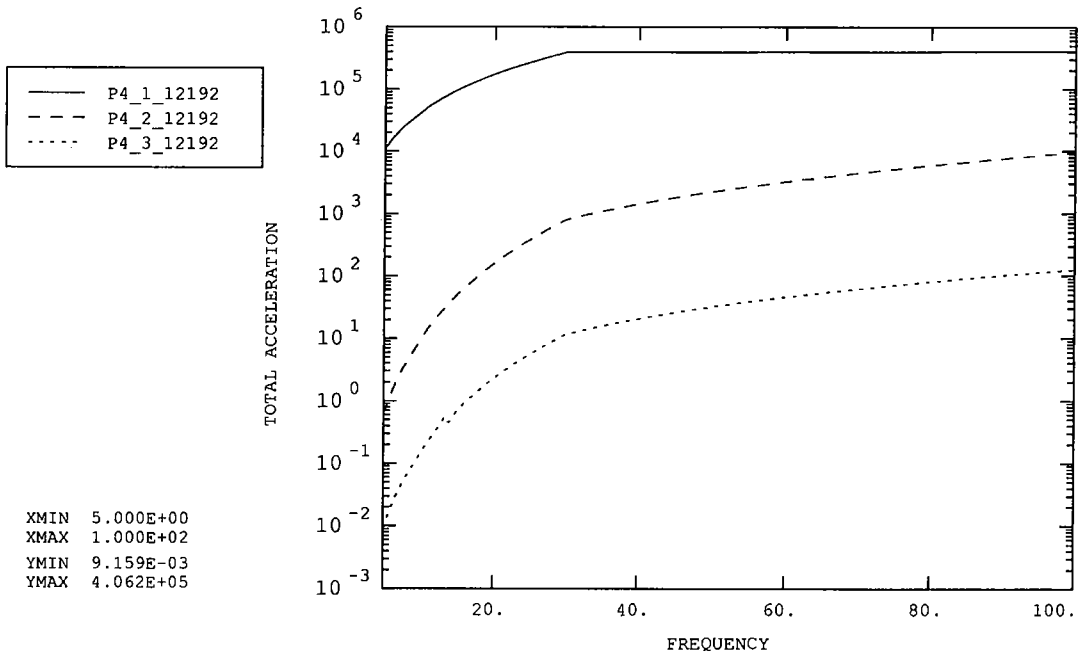

Figure 4: Jiggle axis pivot (bottom) – jiggle stage

© FNC 2002

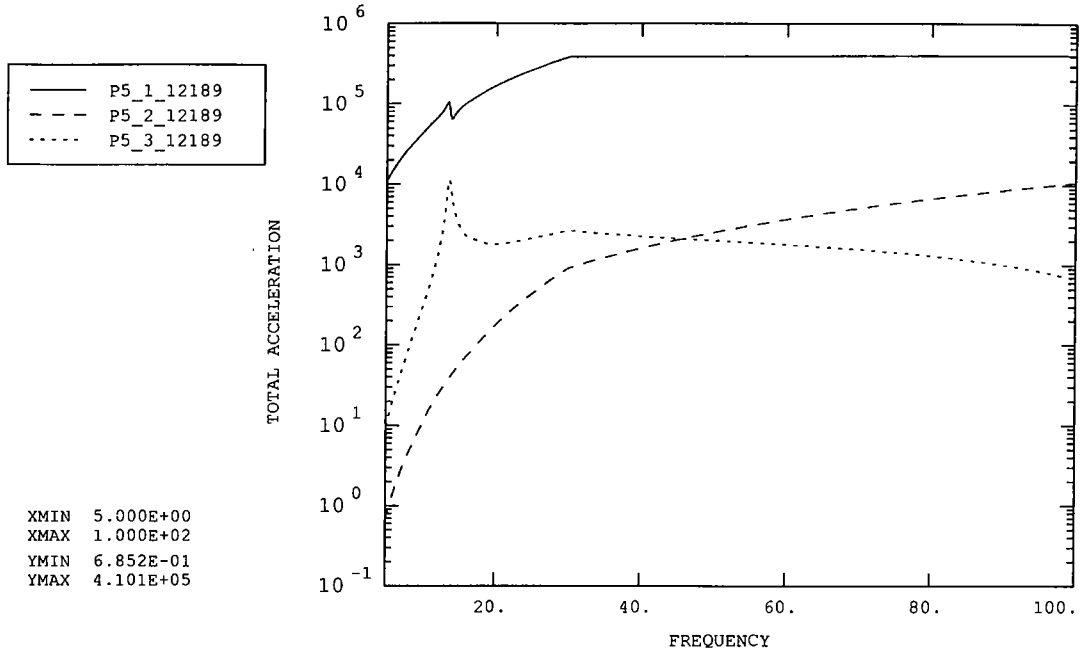

Figure 5: Chop axis pivot (right side) – jiggle stage

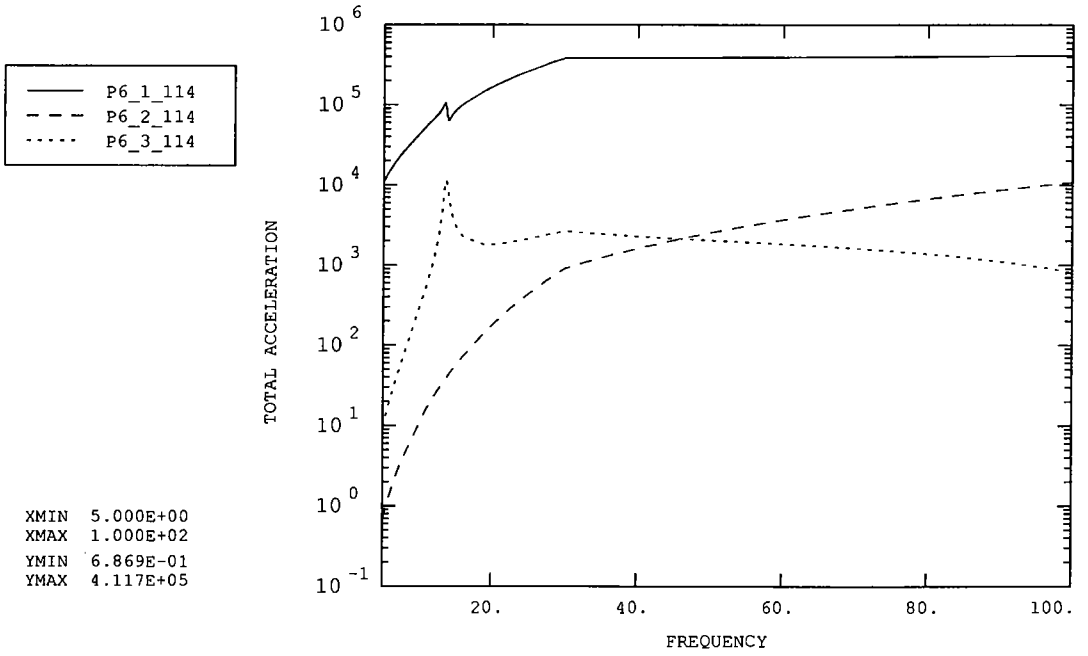

Figure 6: Chop axis pivot (right side) – chop stage

© FNC 2002

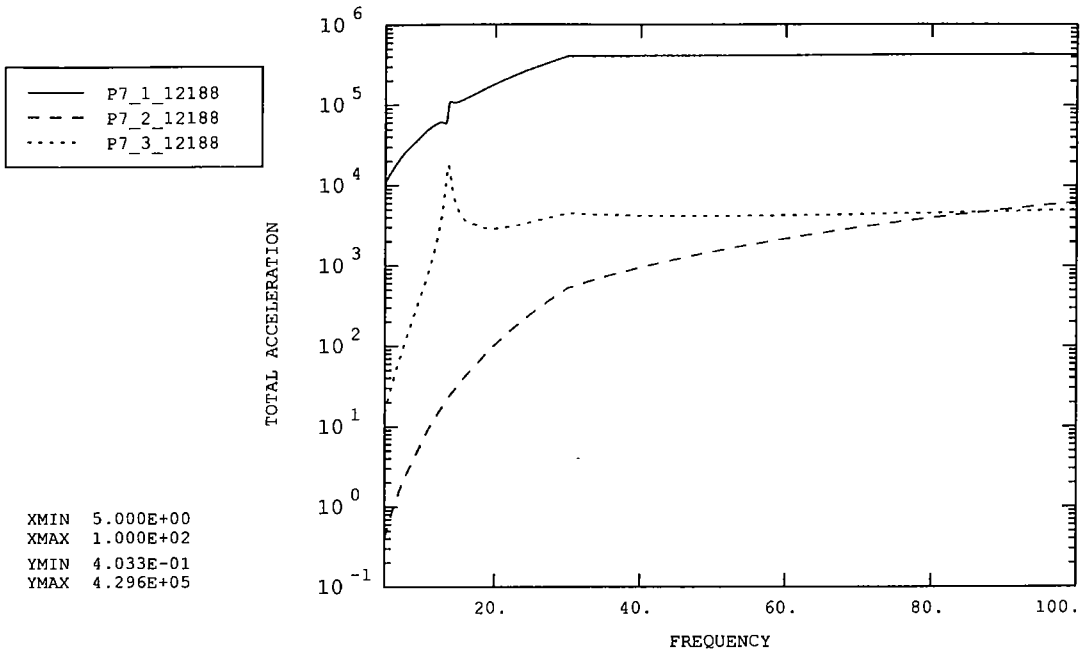

Figure 7: Chop axis pivot (left side) – jiggle stage

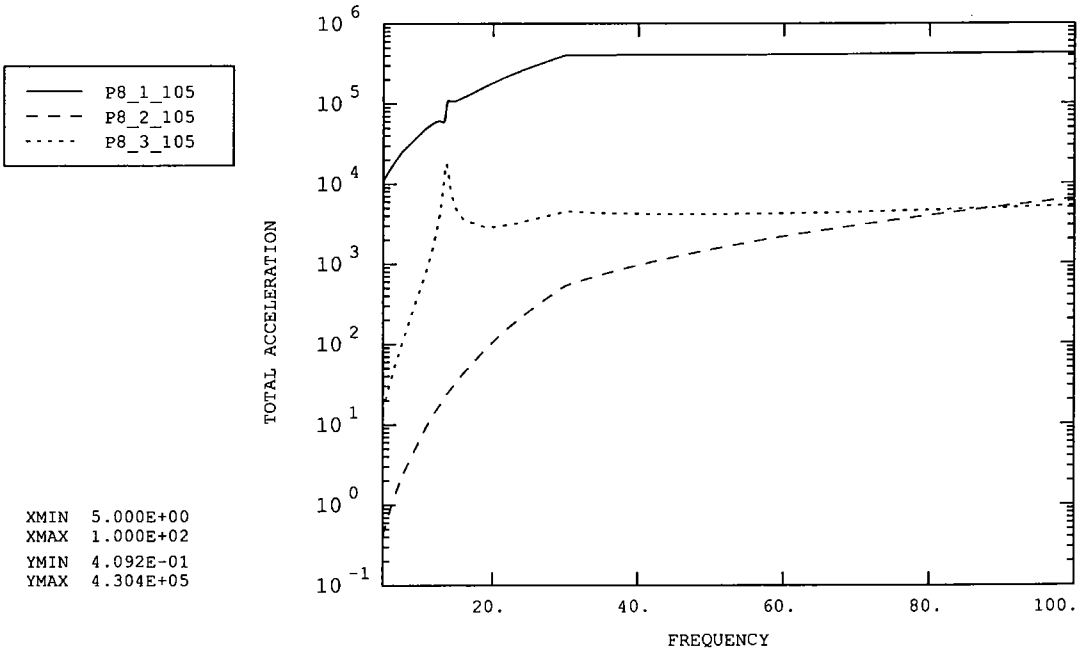

Figure 8: Chop axis pivot (left side) – chop stage

© FNC 2002

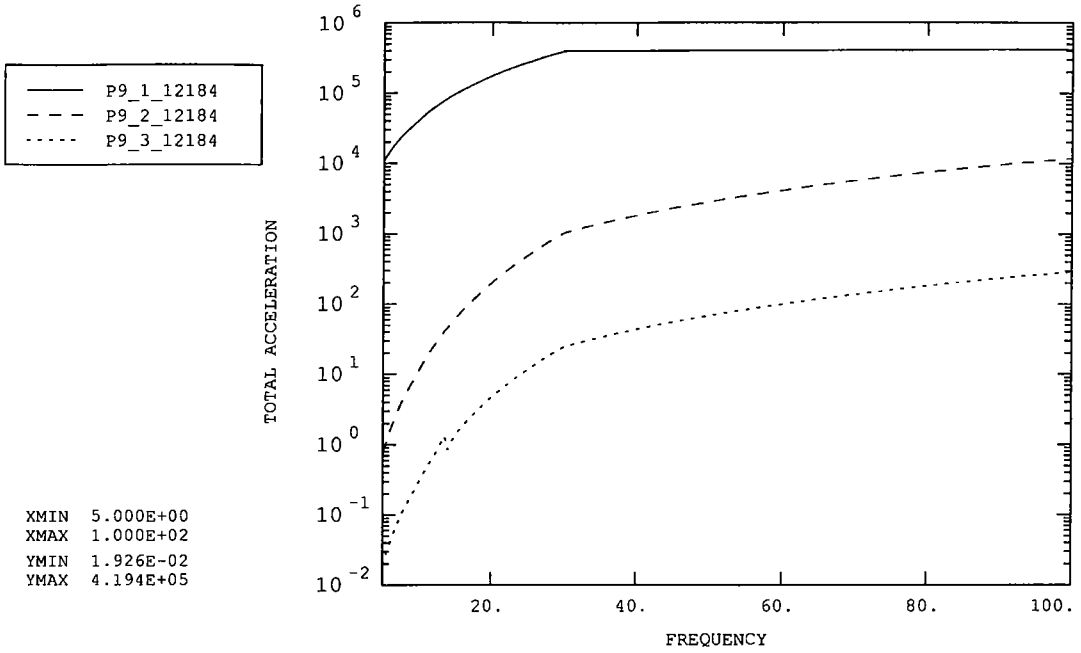

Figure 9: Chop motor (top)

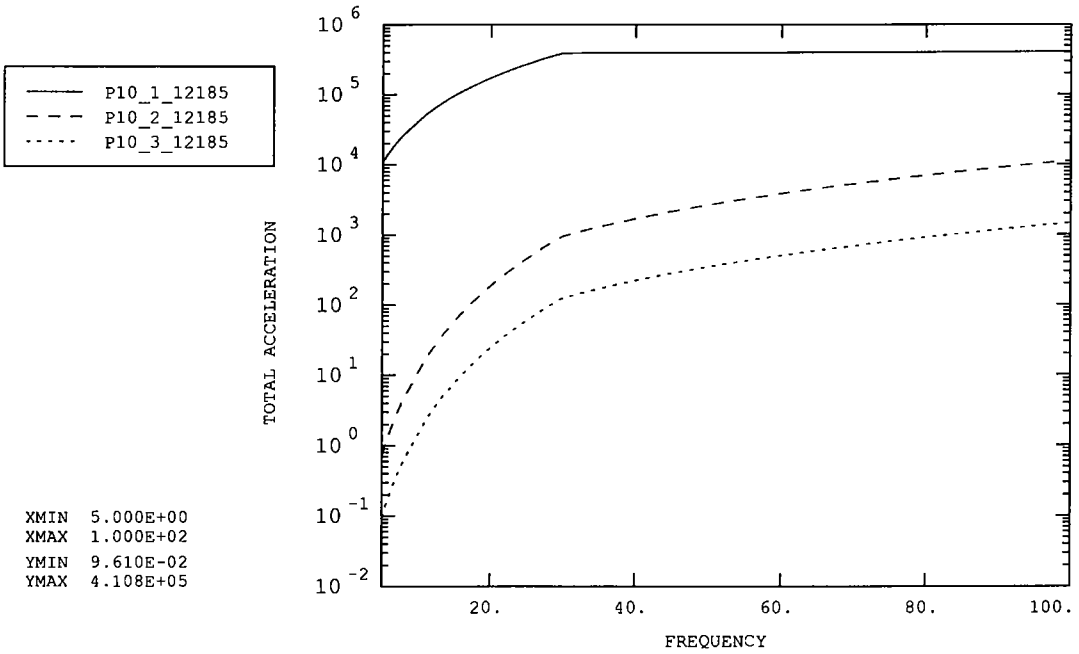

Figure 10: Chop motor (bottom)

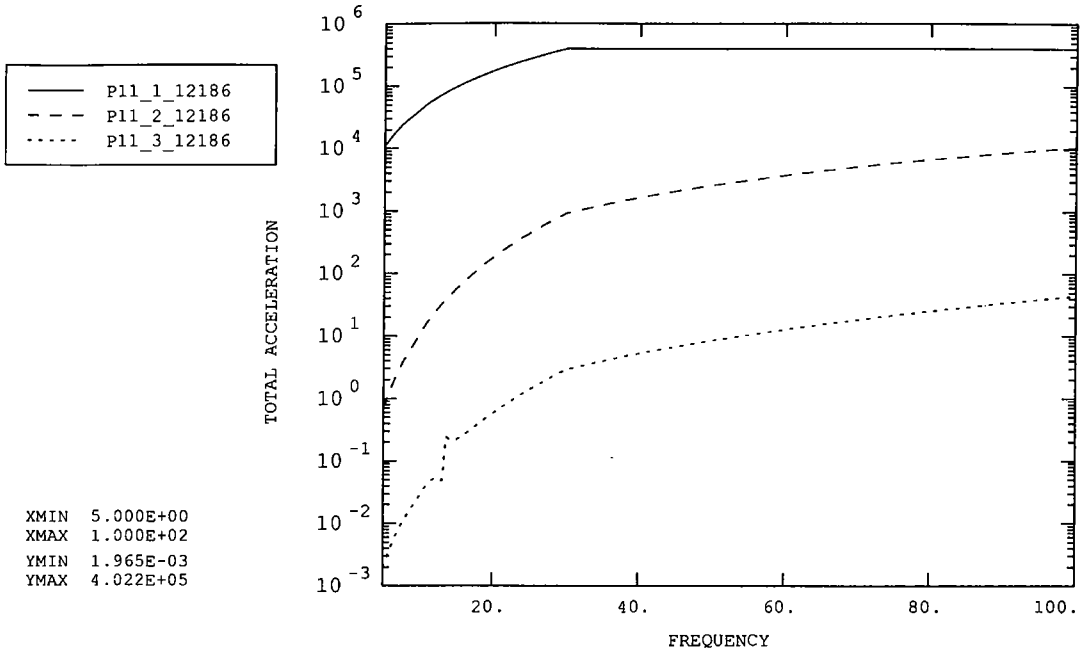

Figure 11: Jiggle motor (right side)

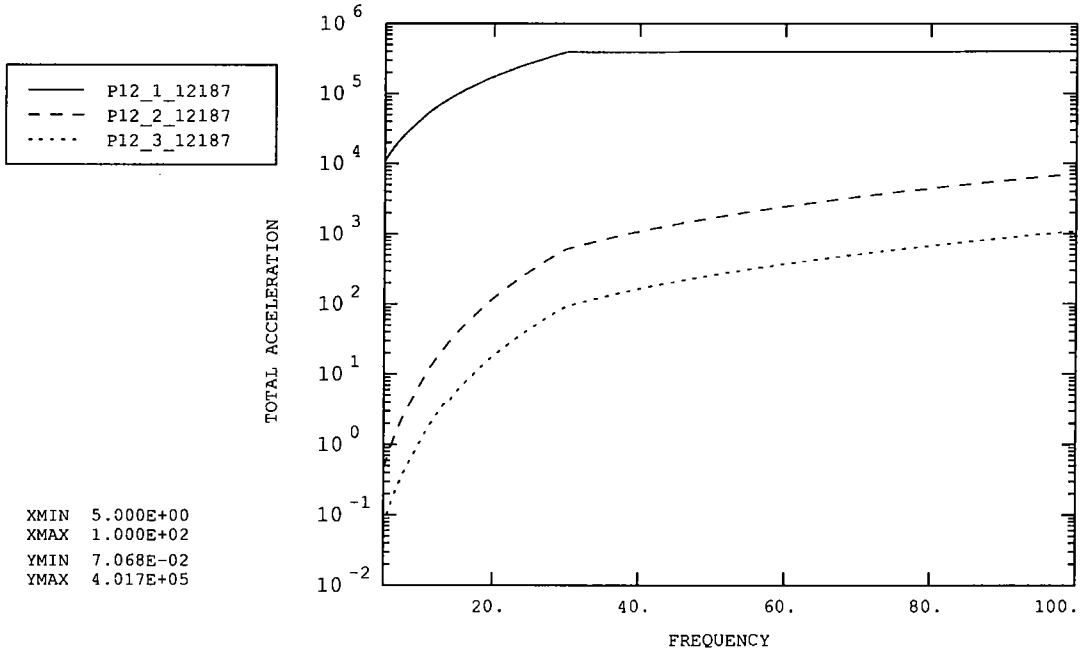

Figure 12: Jiggle motor (left side)

© FNC 2002

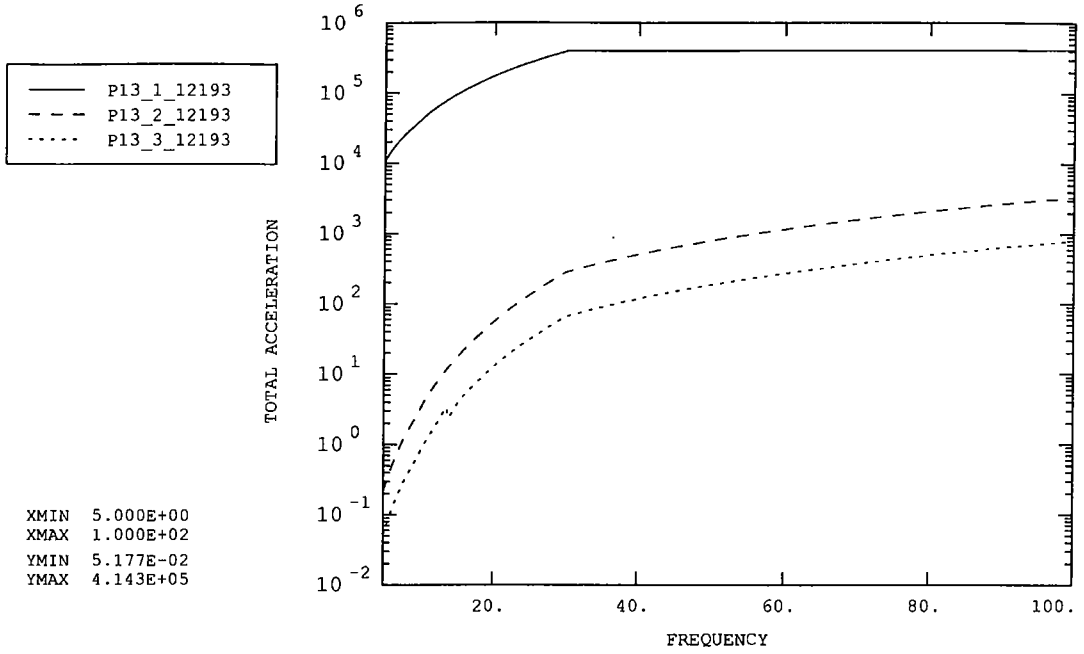

Figure 13: PCAL CG

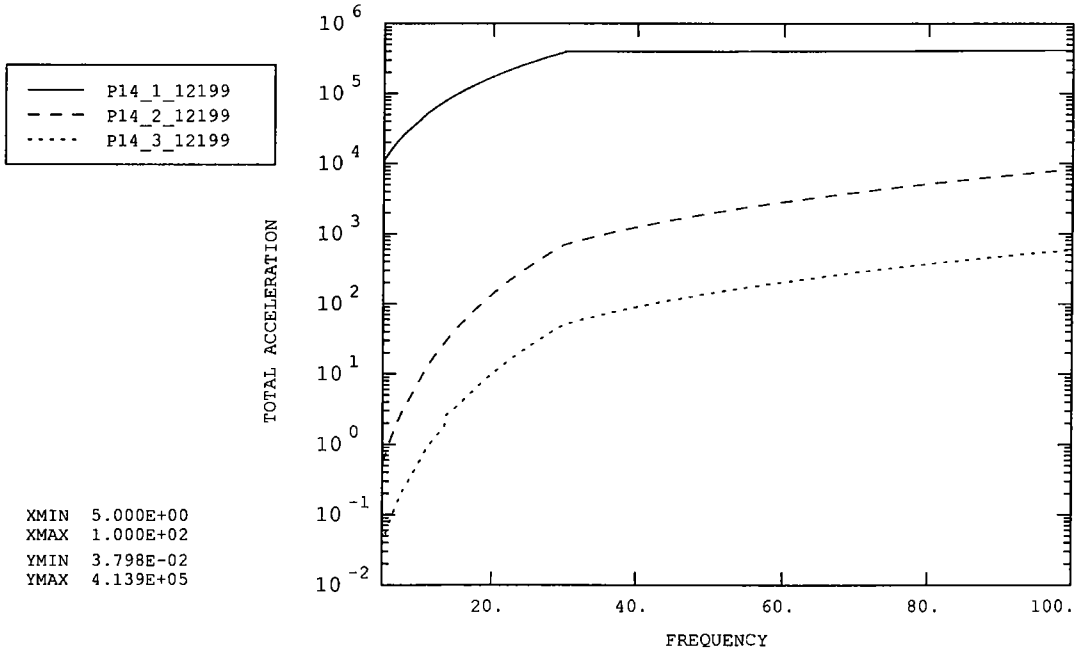

Figure 14: PCAL extension to mirror centre

© FNC 2002

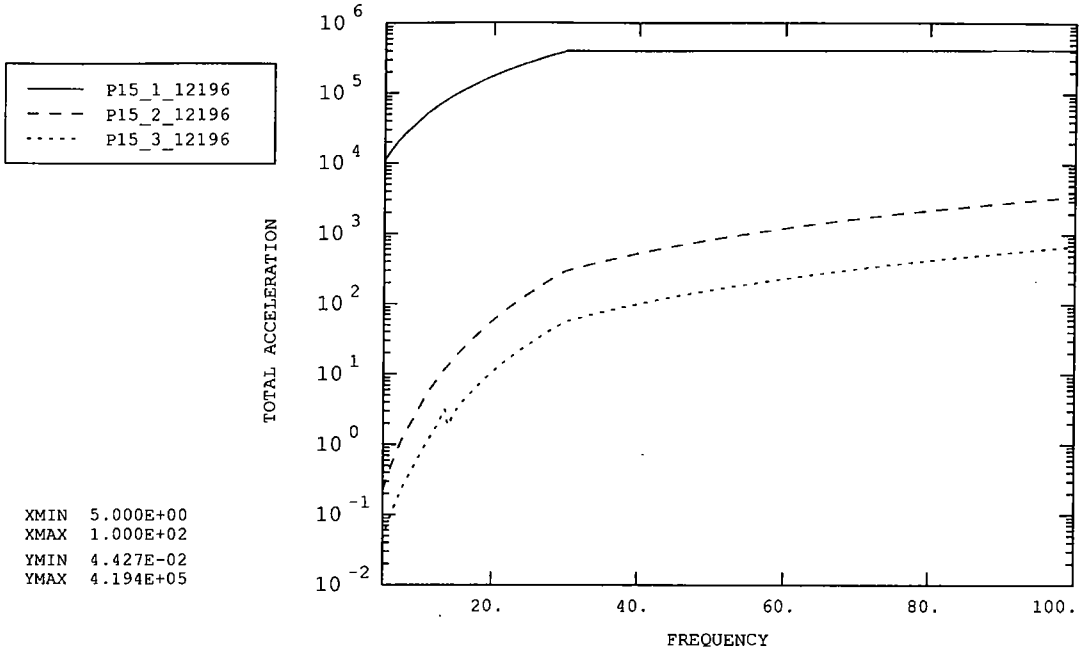

Figure 15: Launch latch 'A' CG

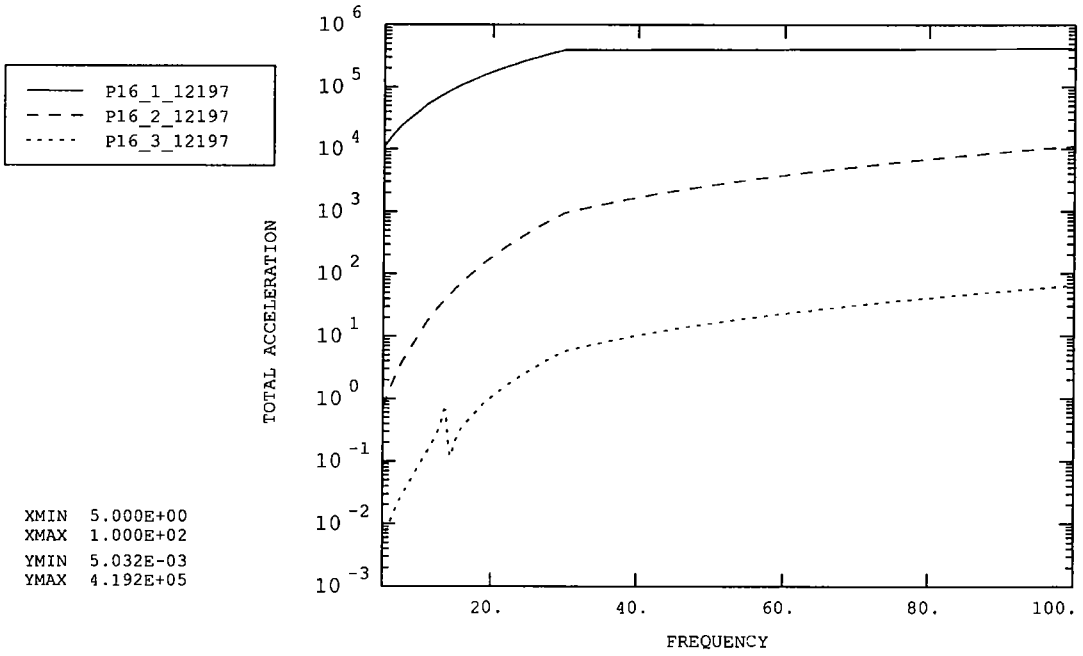

Figure 16: Launch latch 'A' extension to magnet centre

© FNC 2002

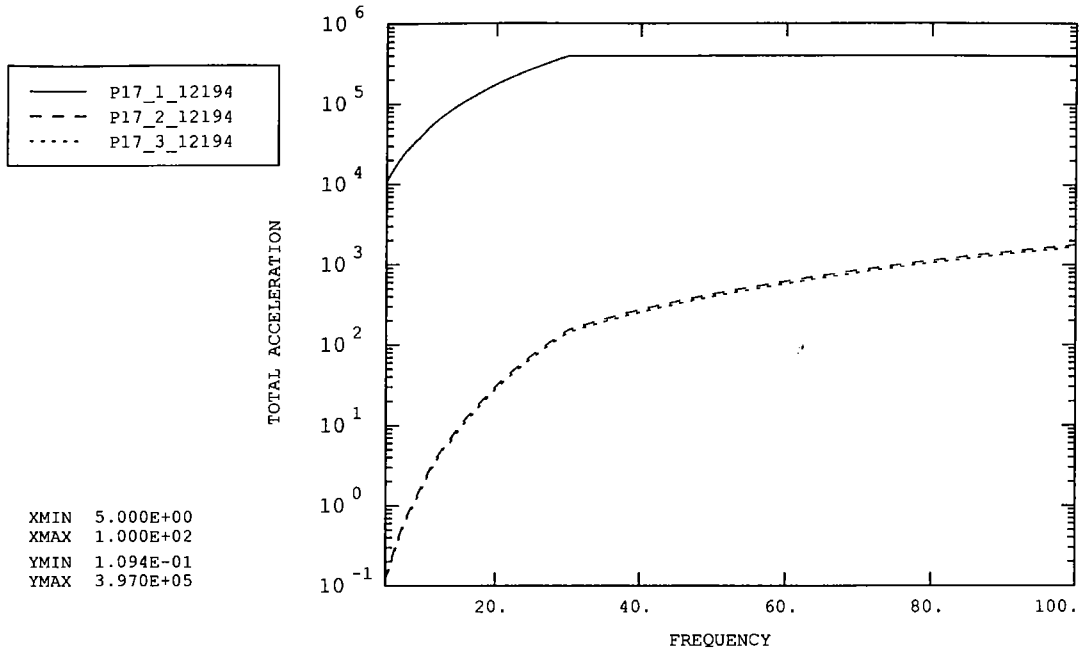

Figure 17: Connector (top)

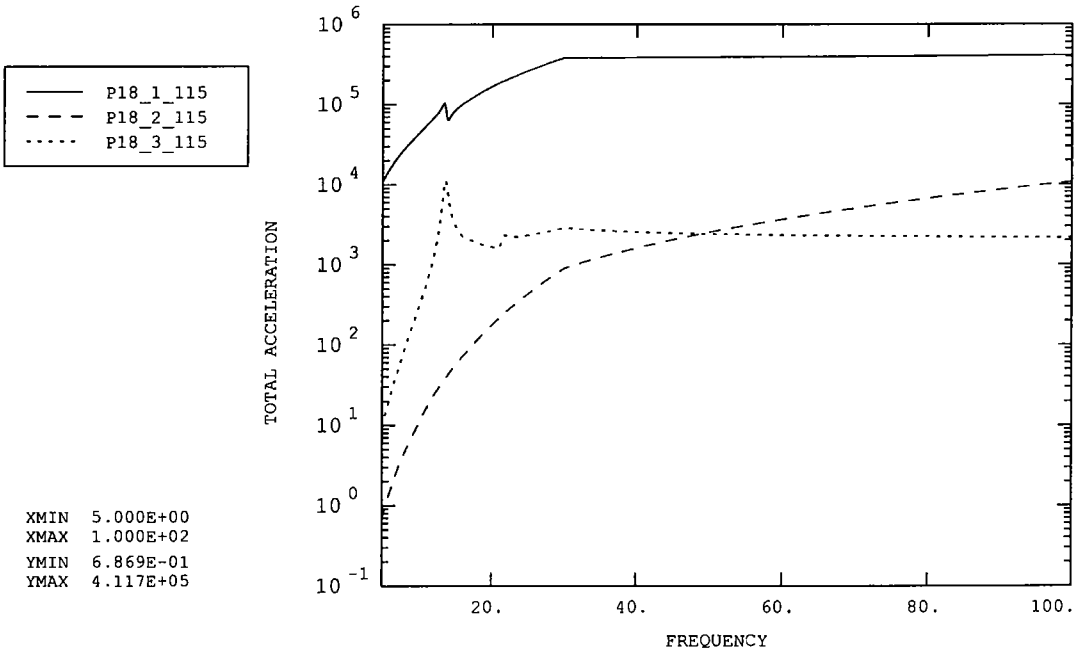

Figure 18: Chop magnet (top)

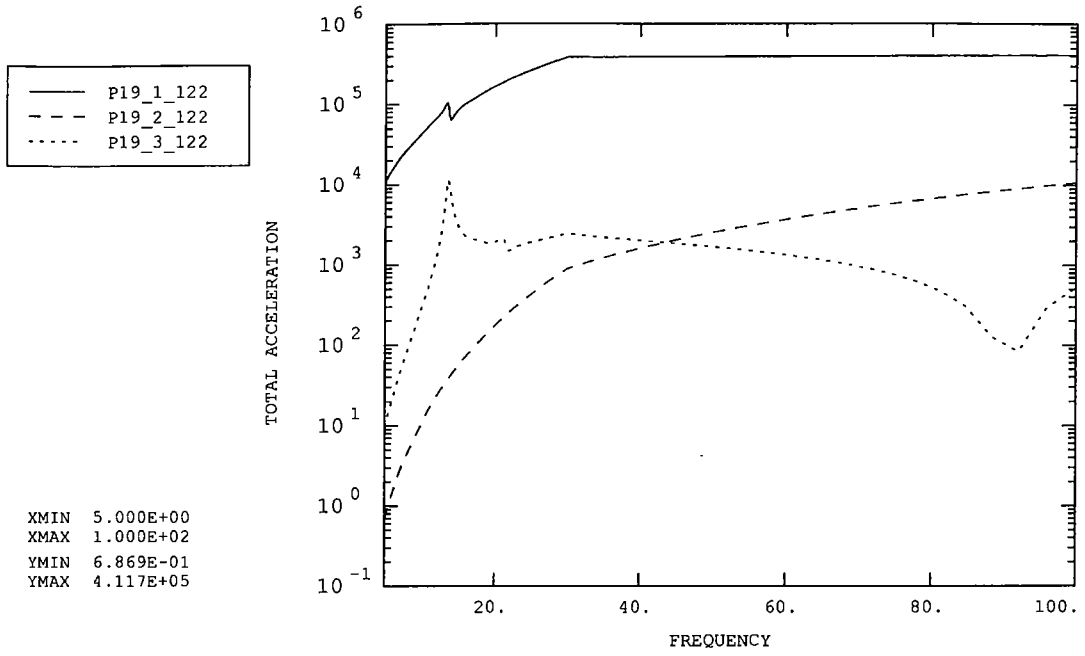

Figure 19: Chop magnet (bottom)

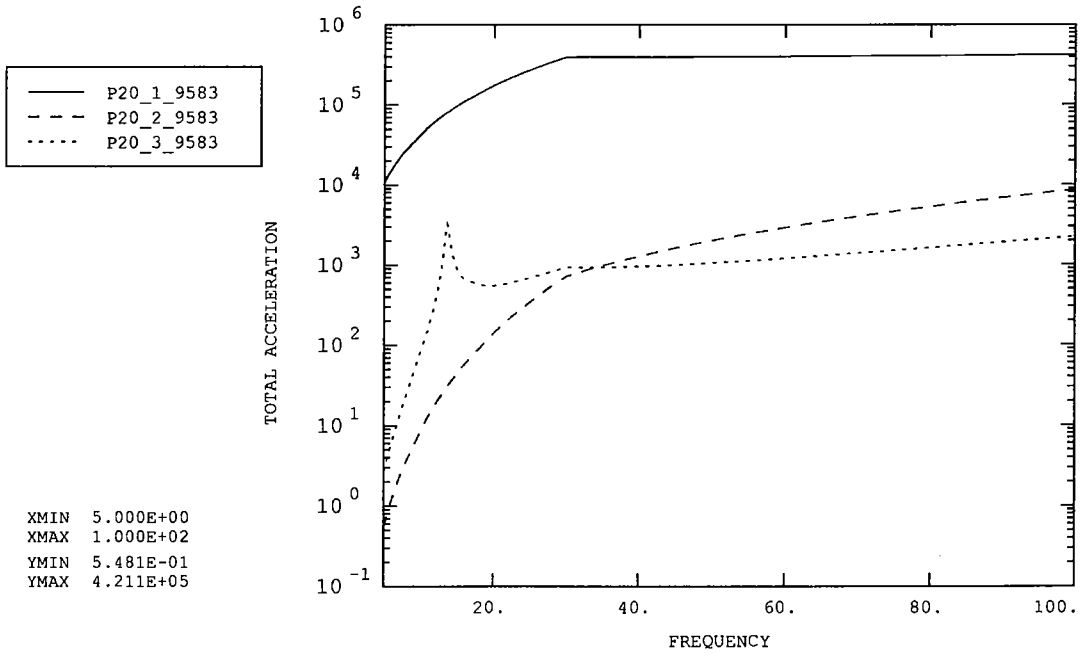

Figure 20: Mirror Centre

© FNC 2002

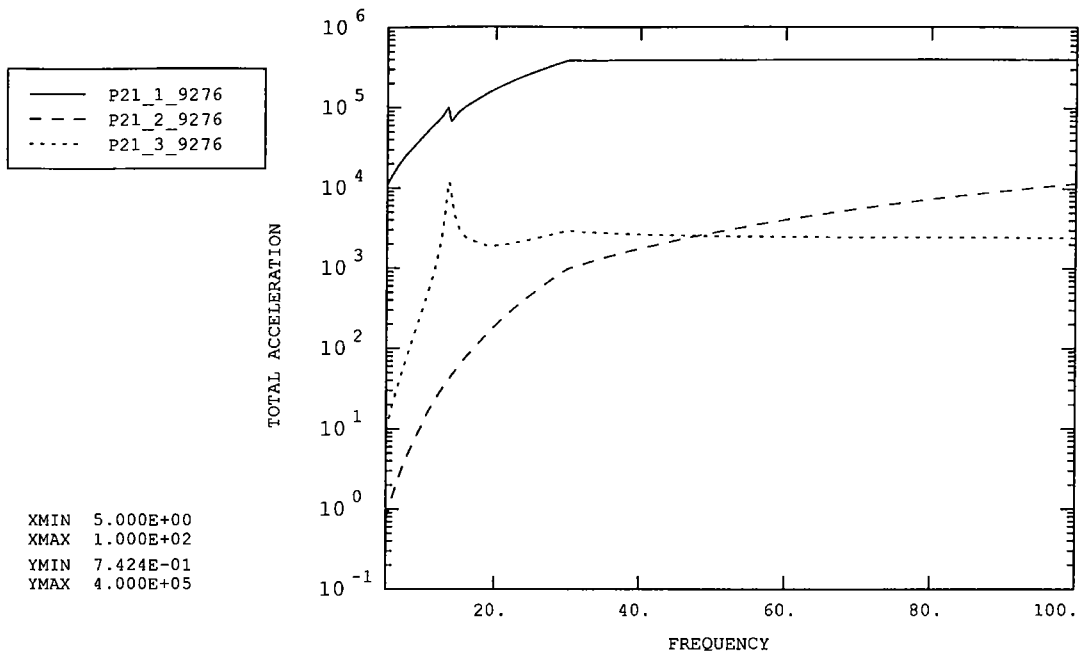

Figure 21: Jiggle magnet (right)

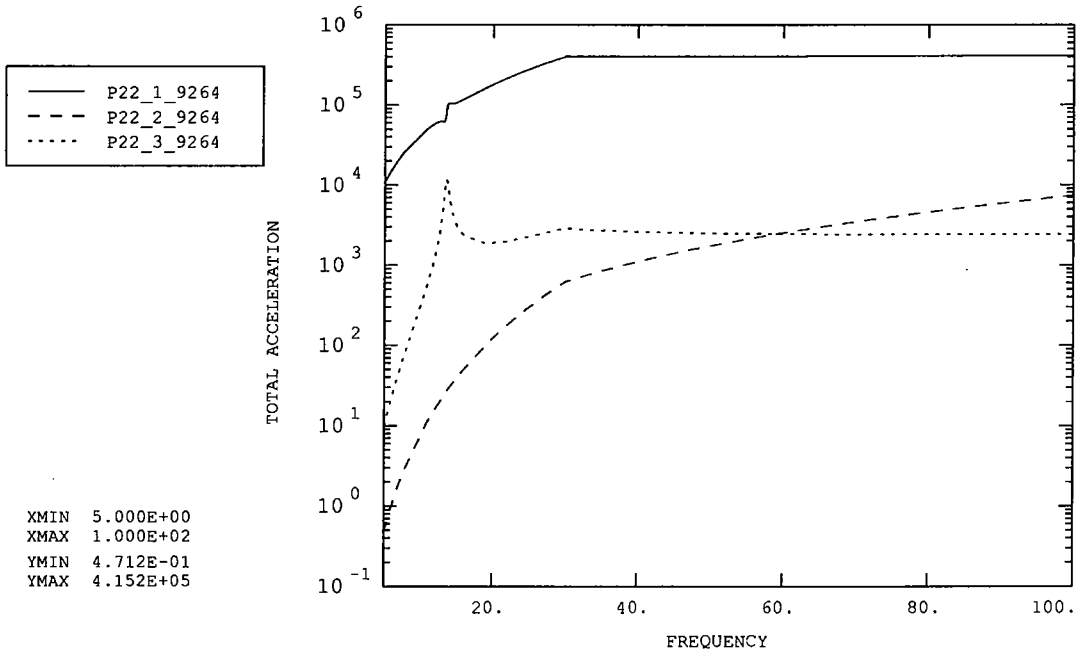

Figure 22: Jiggle magnet (left)

© FNC 2002

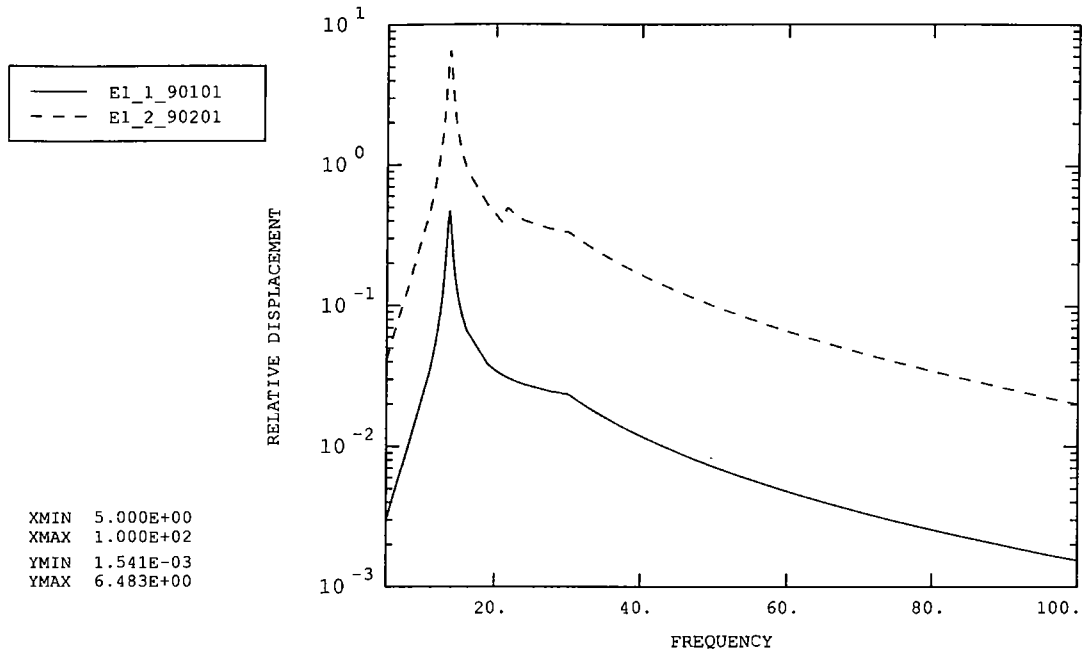

Figure 23: Chop magnet vs. motor (top)

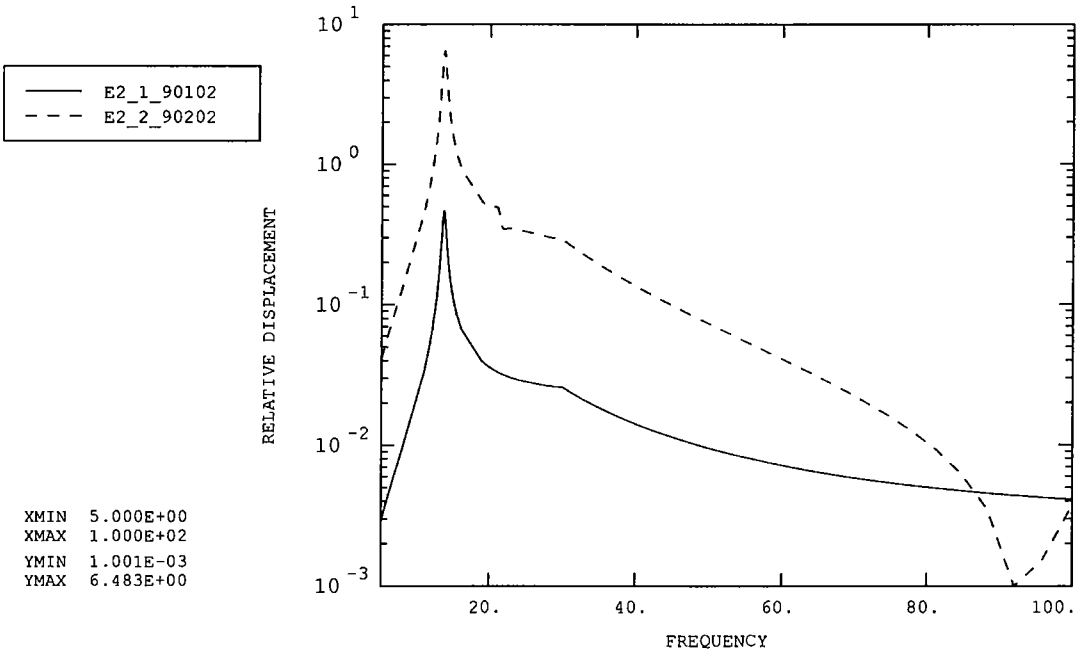

Figure 24: Chop magnet vs. motor (bottom)

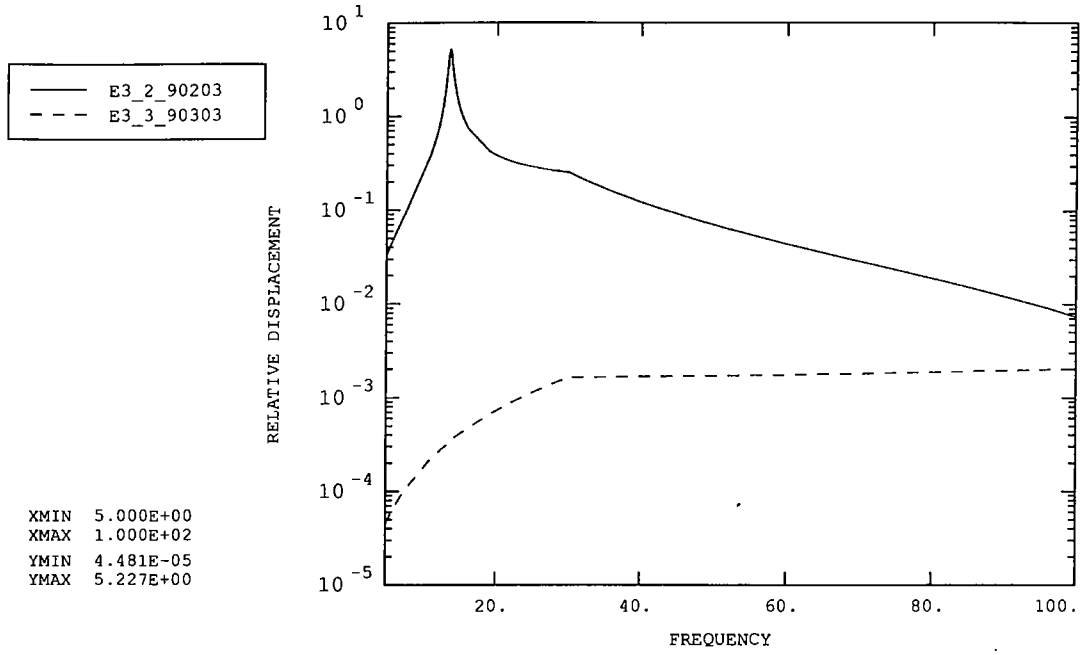

Figure 25: Jiggle magnet vs. motor (right)

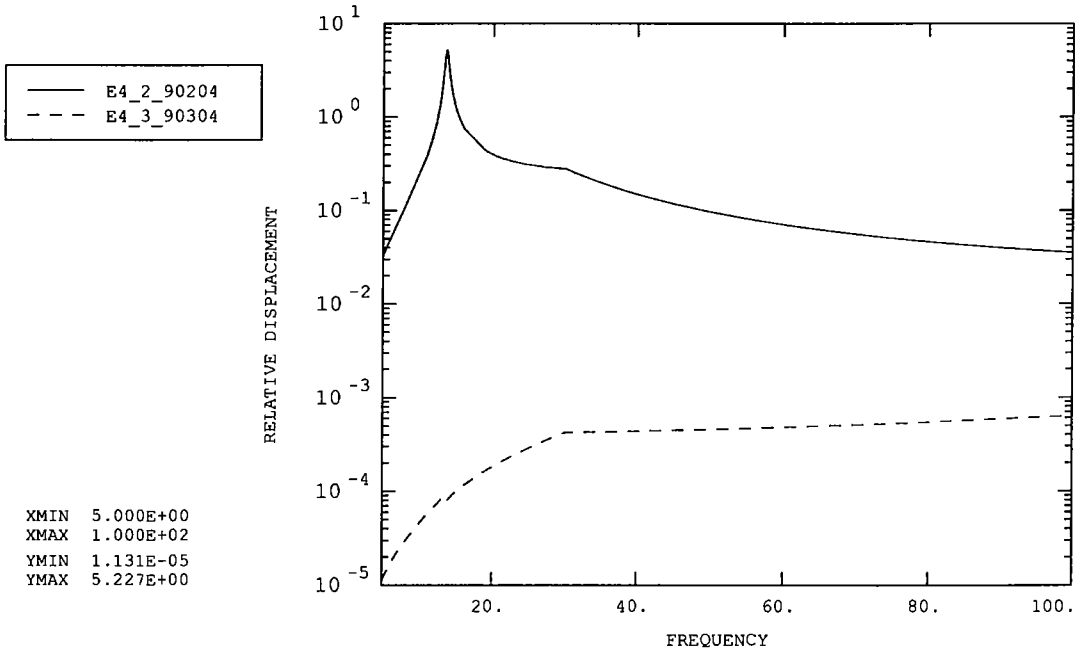

Figure 26: Jiggle magnet vs. motor (left)

© FNC 2002

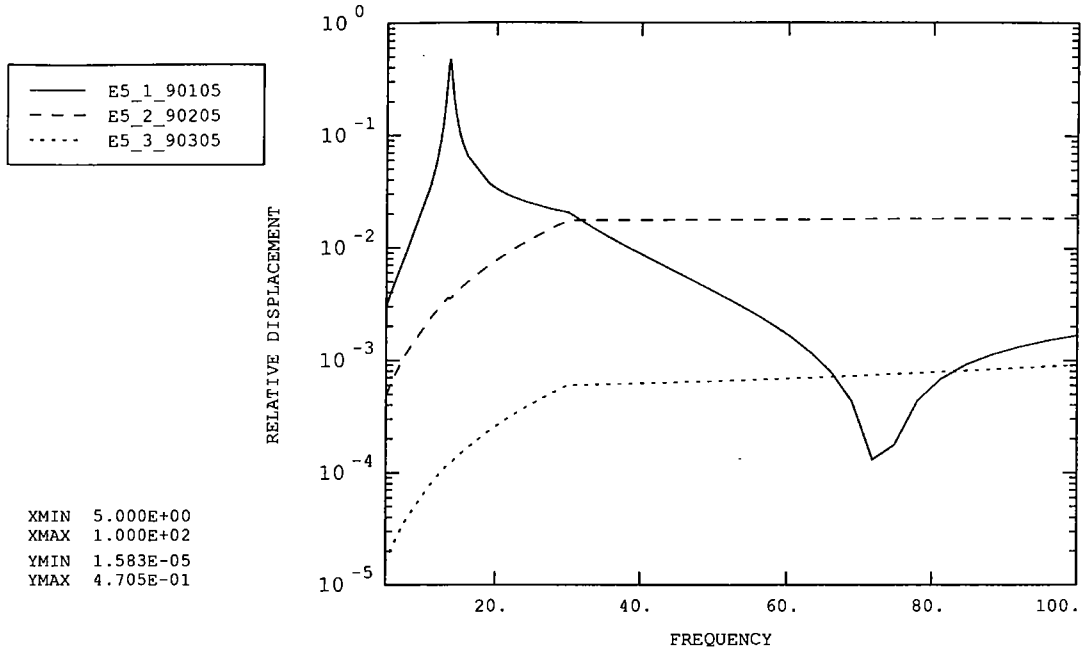

Figure 27: Mirror centre vs. PCAL extension

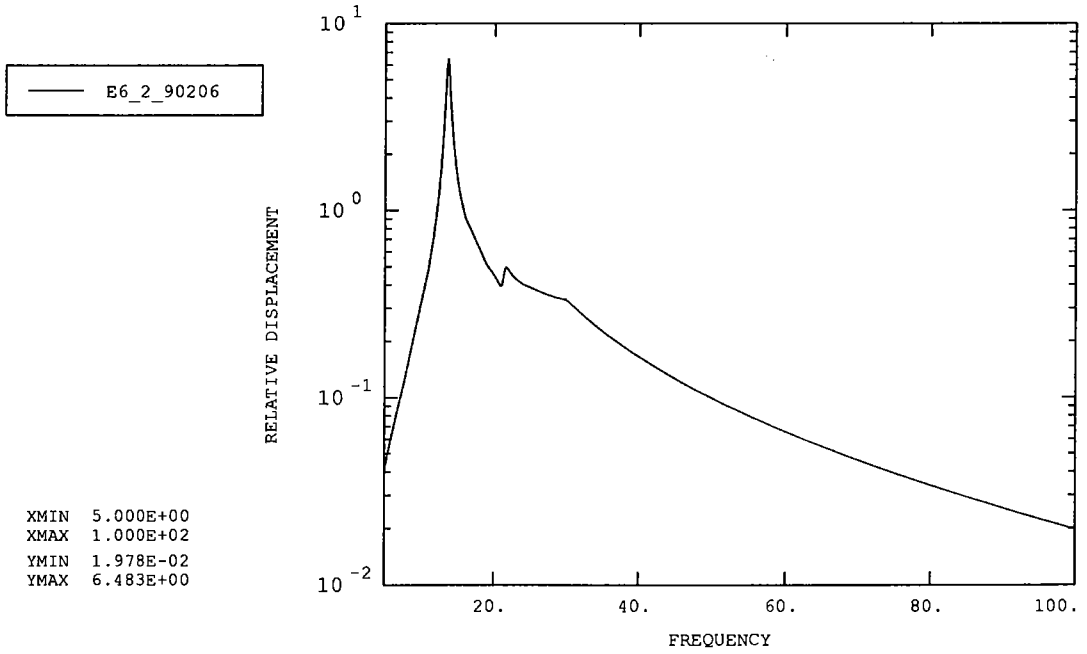

Figure 28: Chop magnet (top) vs. launch latch 'A'

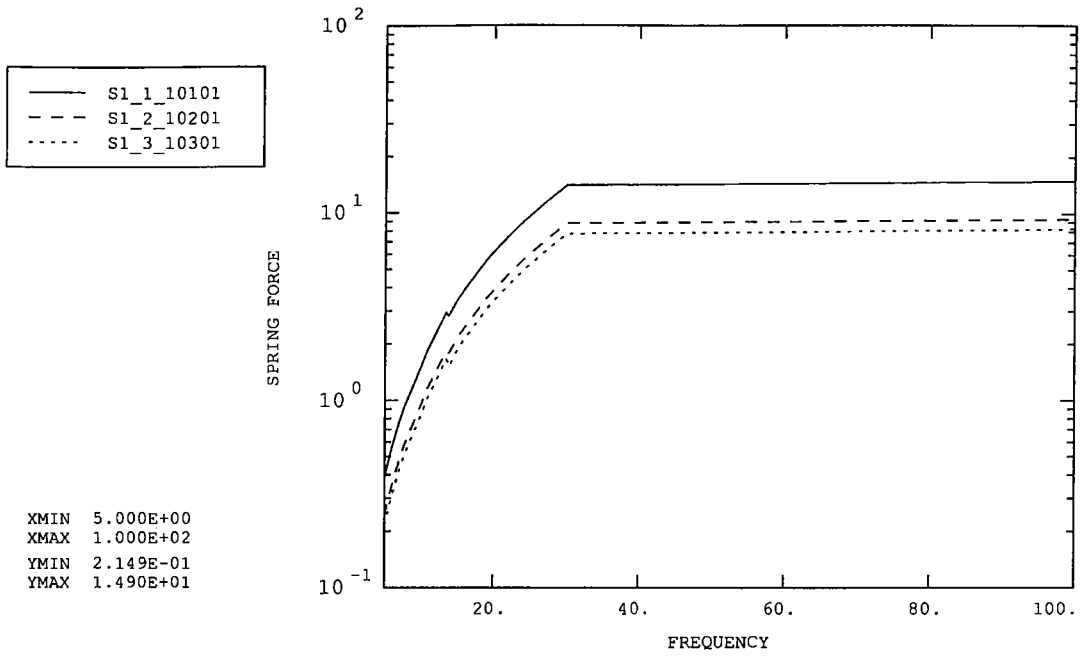

Figure 29: Front baffle (top left)

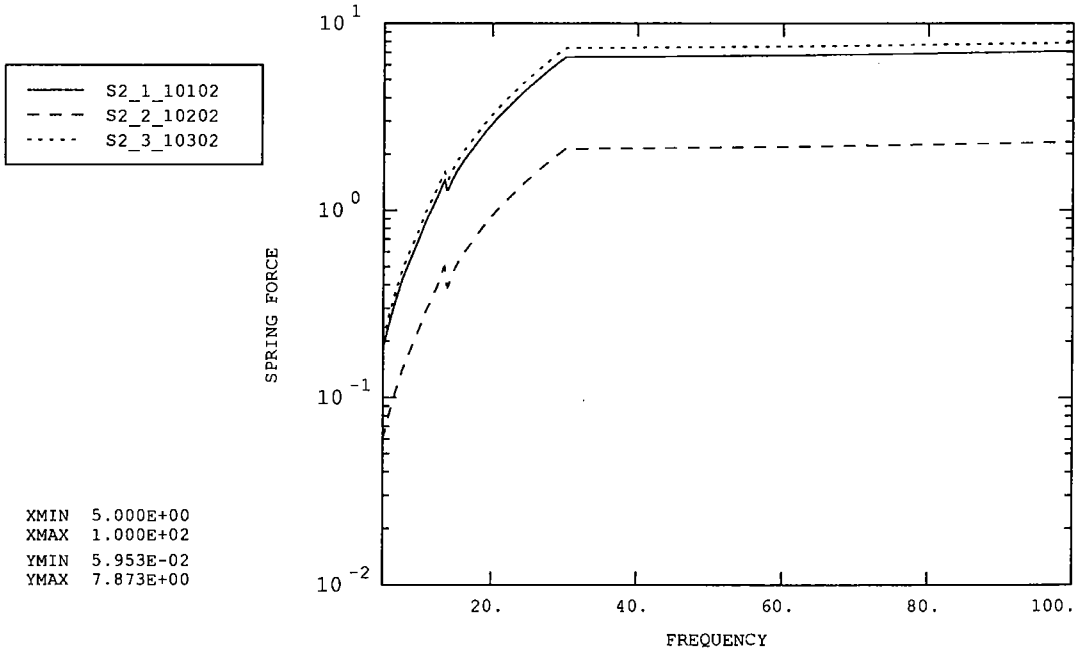

Figure 30: Front baffle (top right)

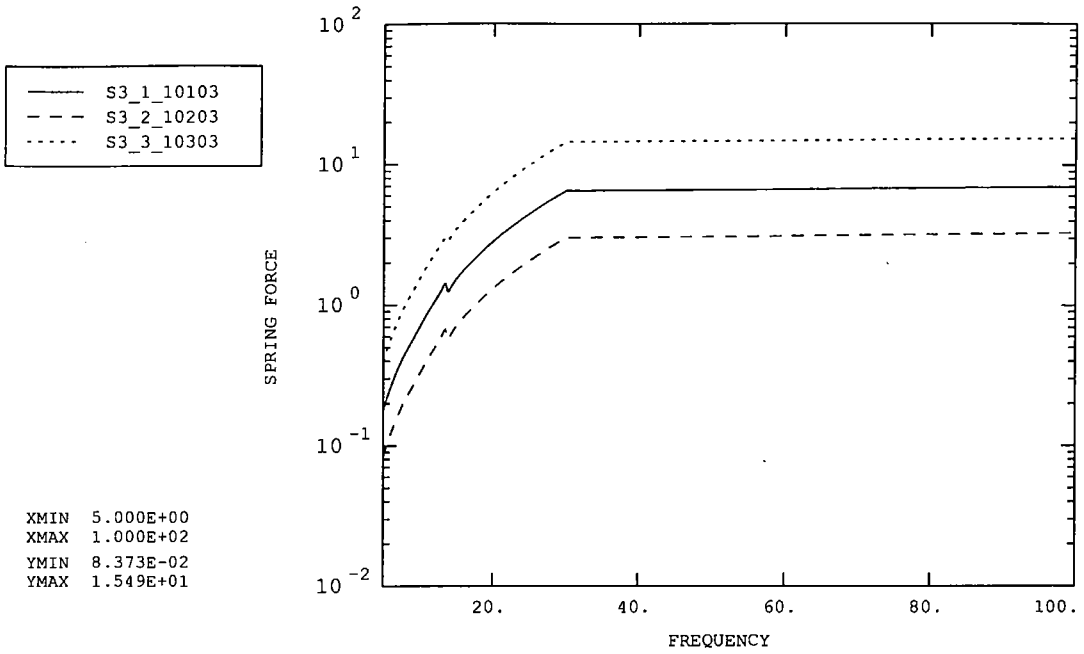

Figure 31: Front baffle (bottom left)

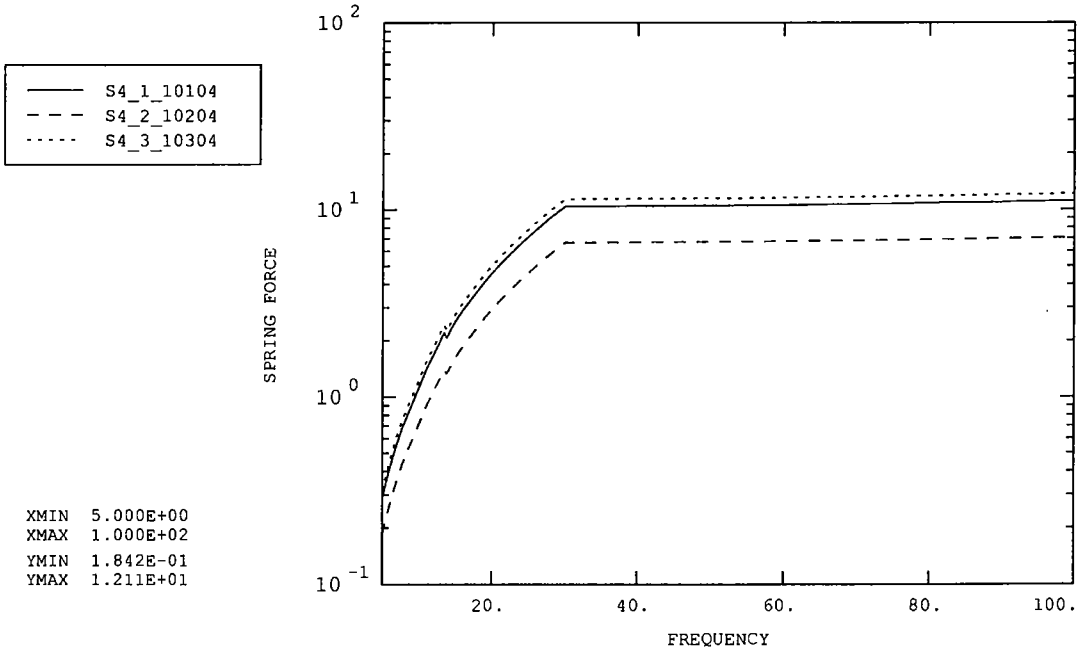

Figure 32: Front baffle (bottom right)

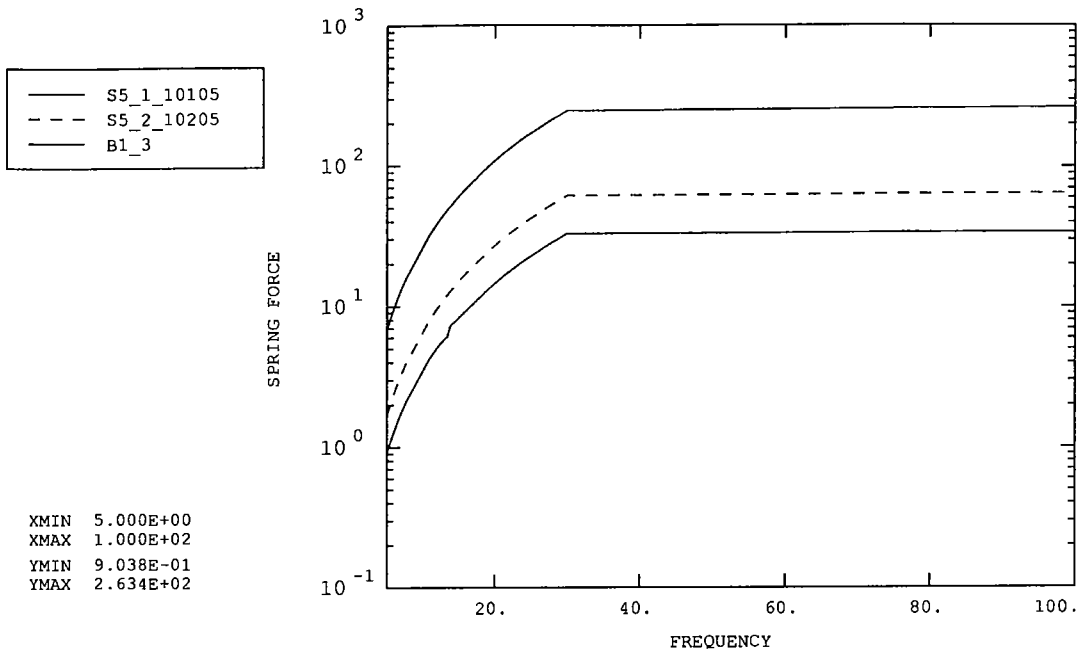

Figure 33: Base (front middle)

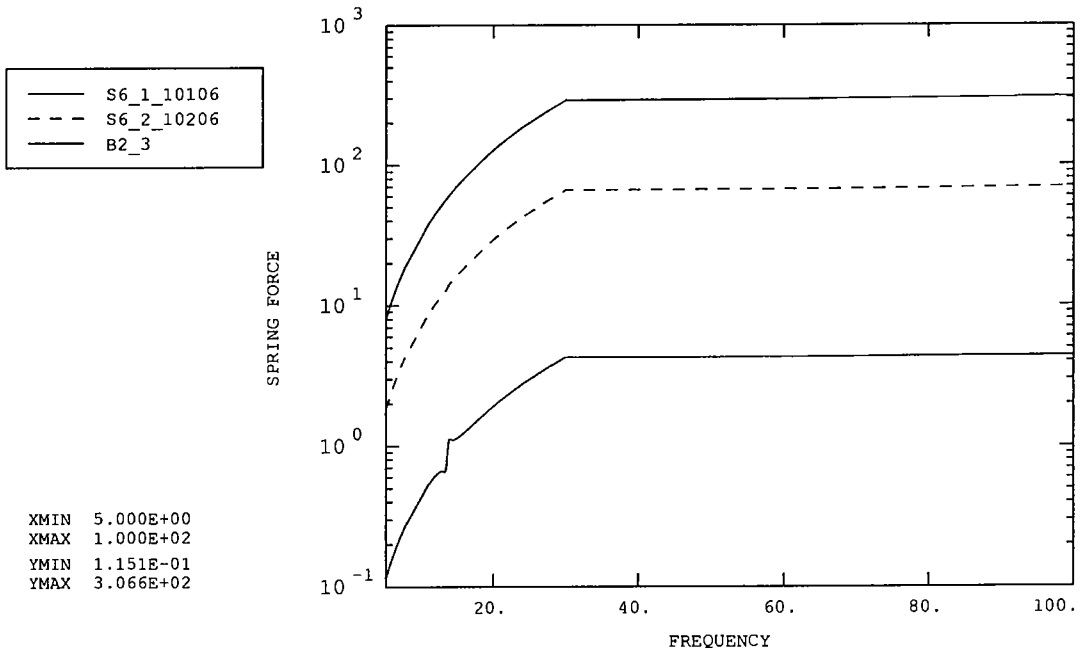

Figure 34: Base (back left)

© FNC 2002

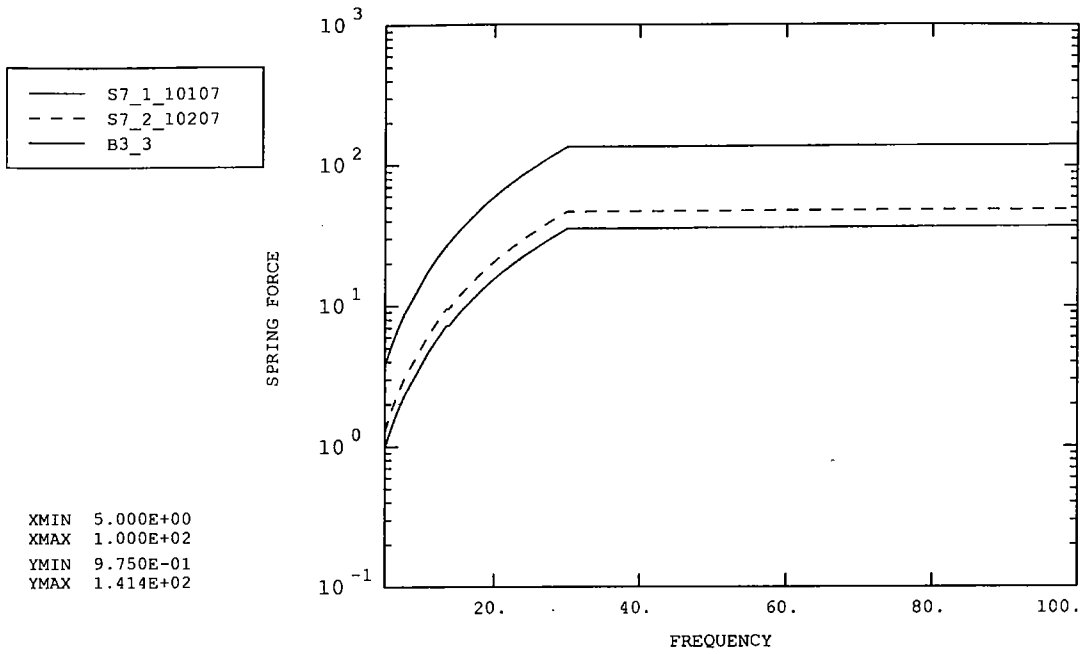

Figure 35: Base (back right)

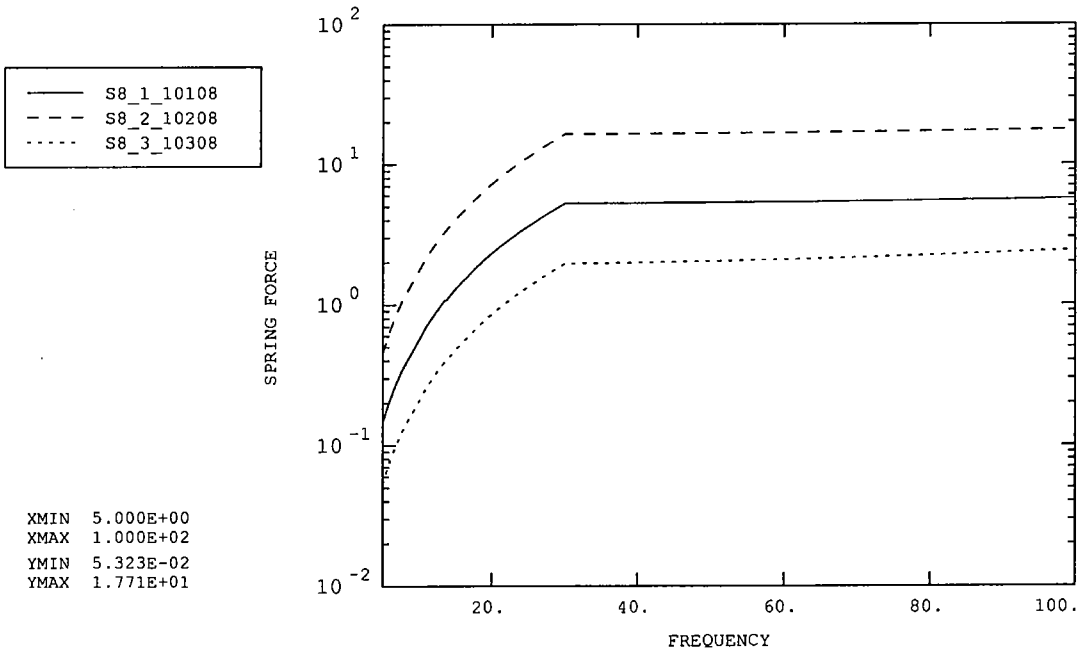

Figure 36: Jiggle pivot (top)

© FNC 2002

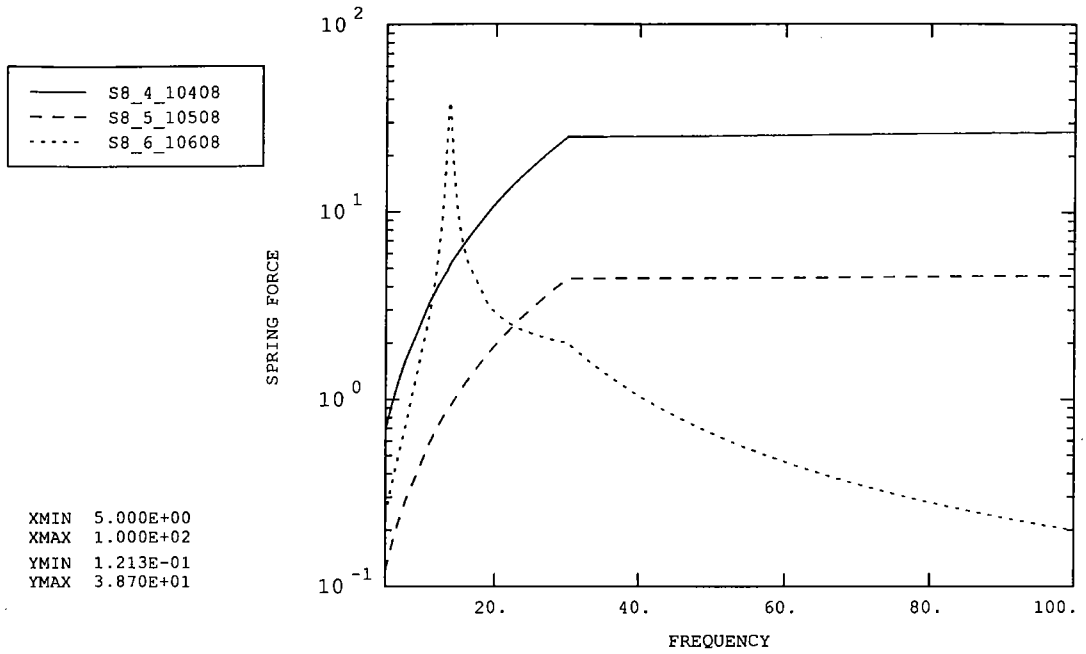

Figure 37: Jiggle pivot (top)

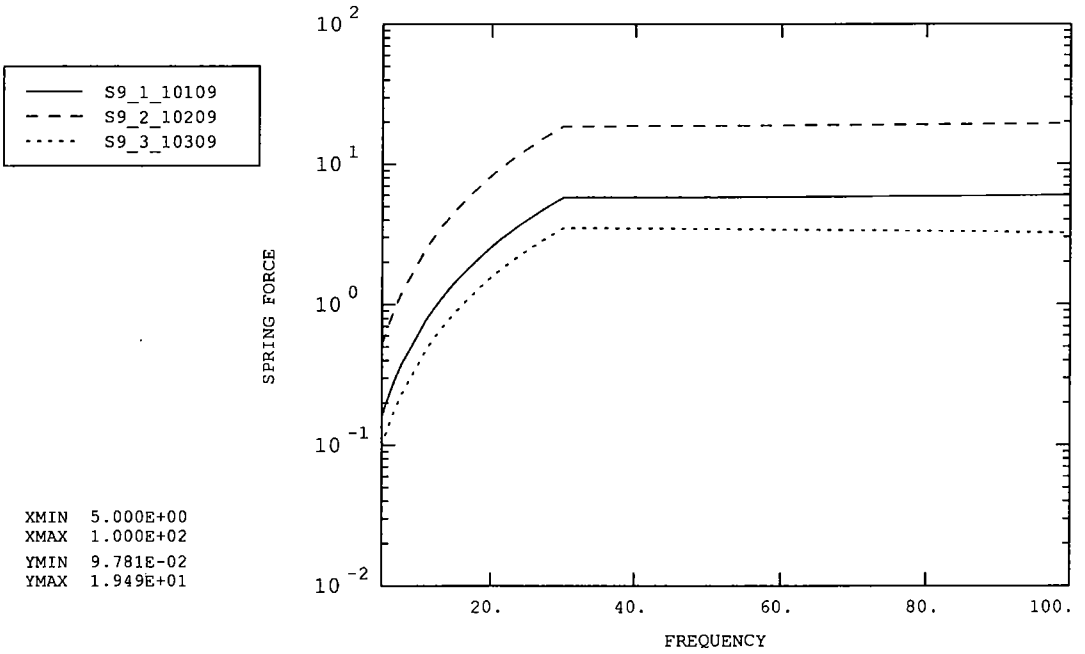

Figure 38: Jiggle pivot (bottom)

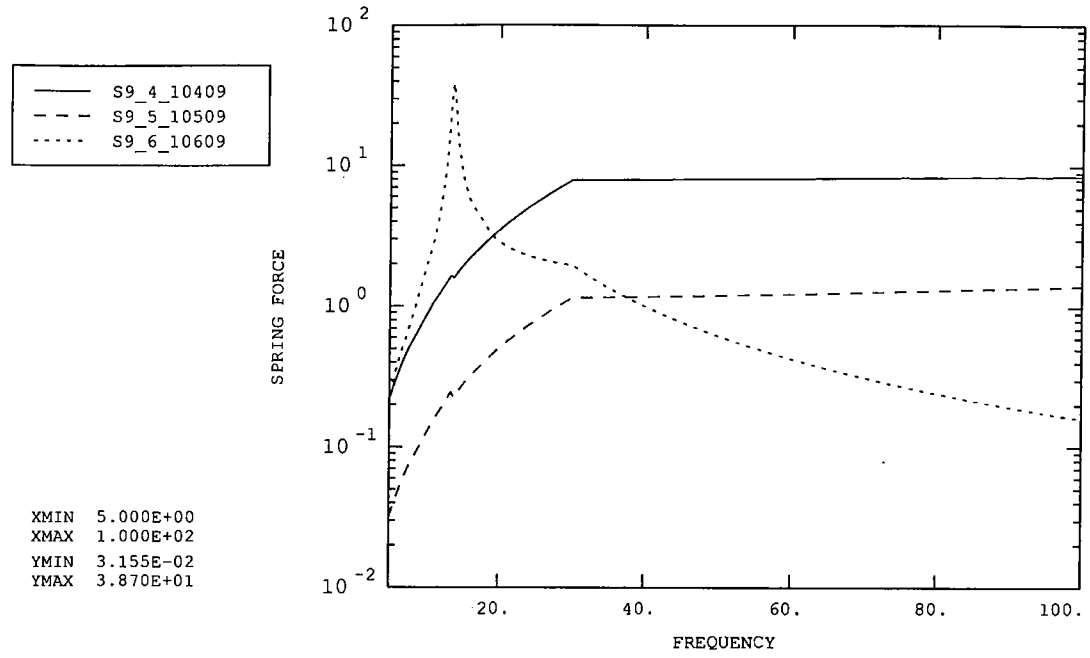

Figure 39: Jiggle pivot (bottom)

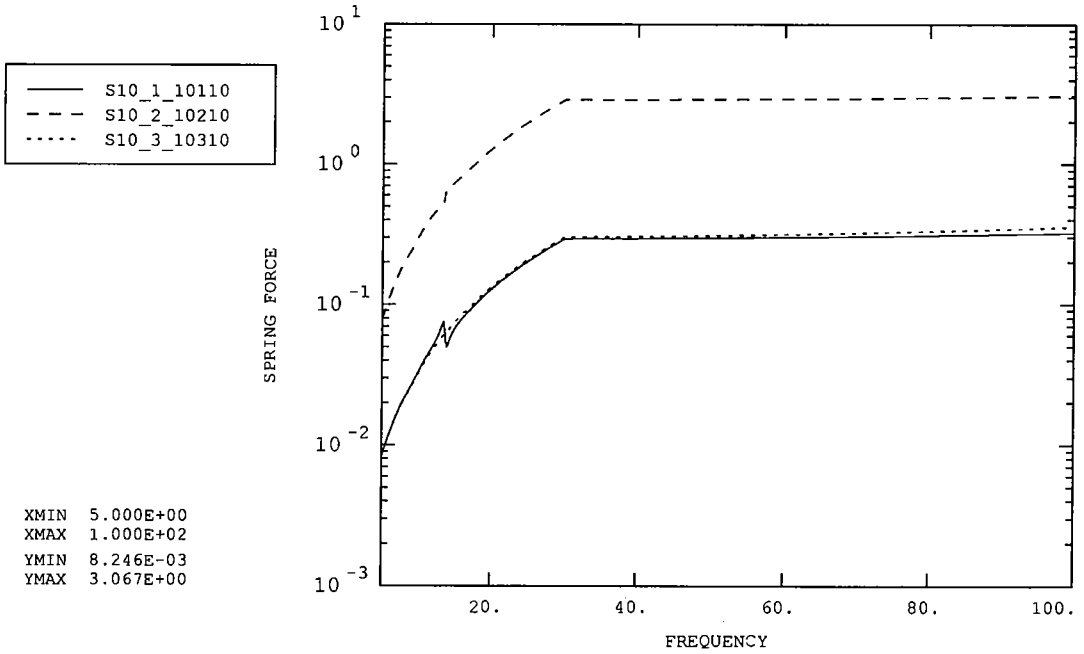

Figure 40: Chop pivot (left)

© FNC 2002

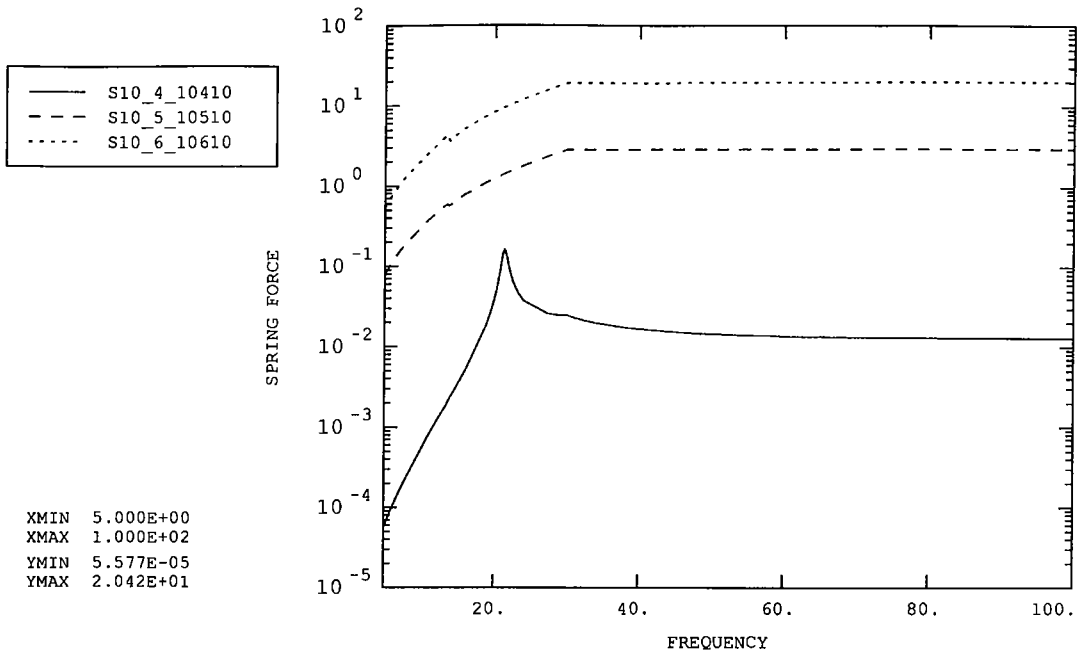

Figure 41: Chop pivot (left)

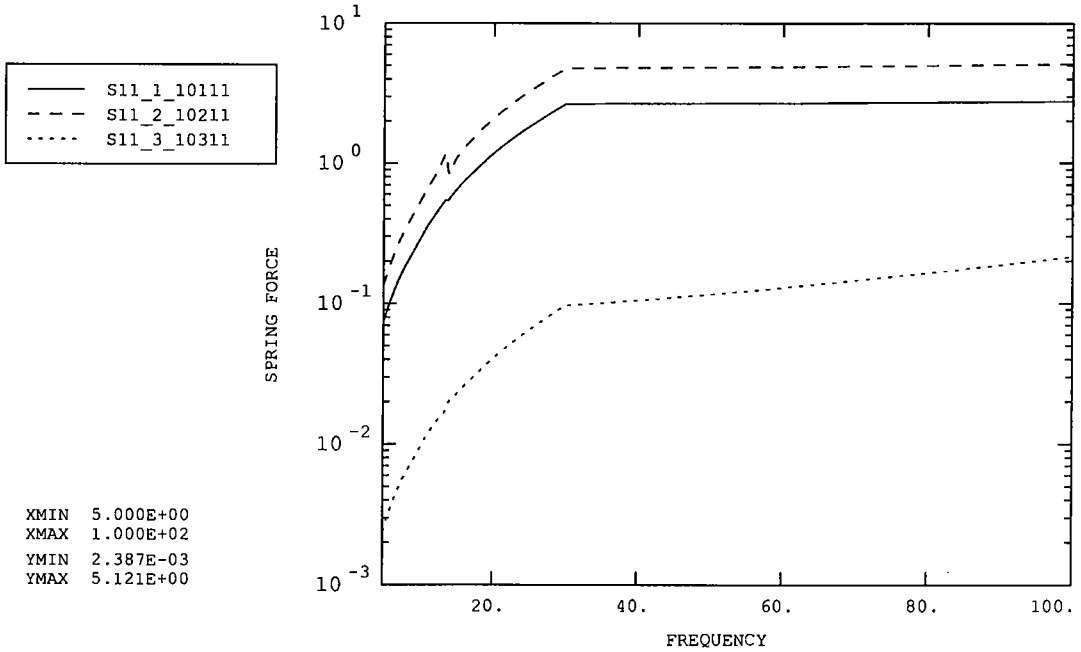

Figure 42: Chop pivot (right)

© FNC 2002

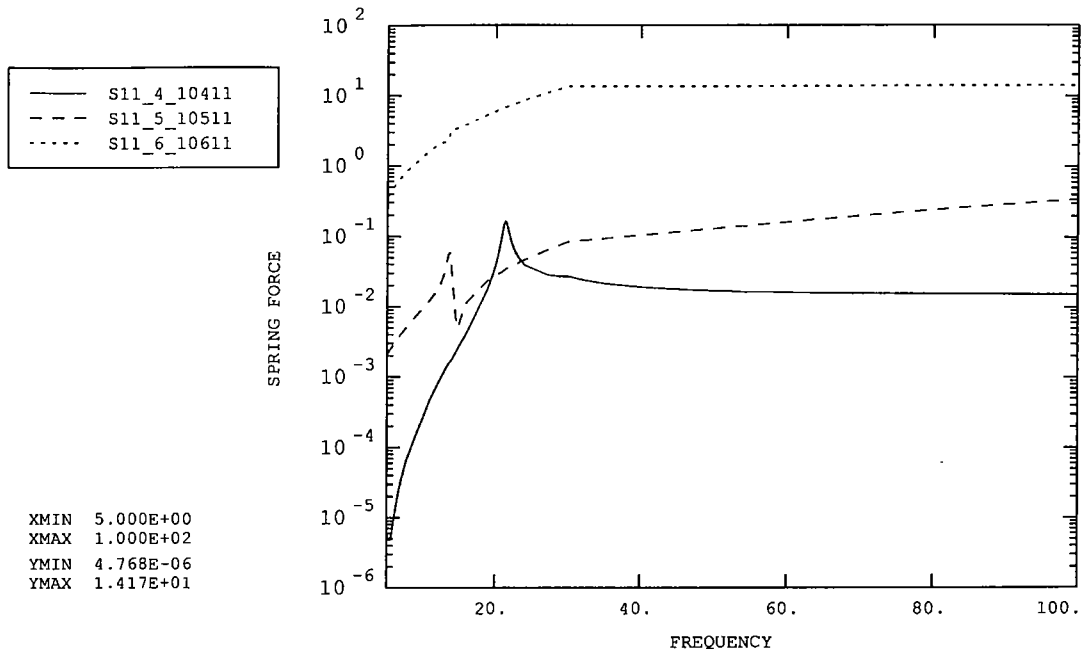

Figure 43: Chop pivot (right)

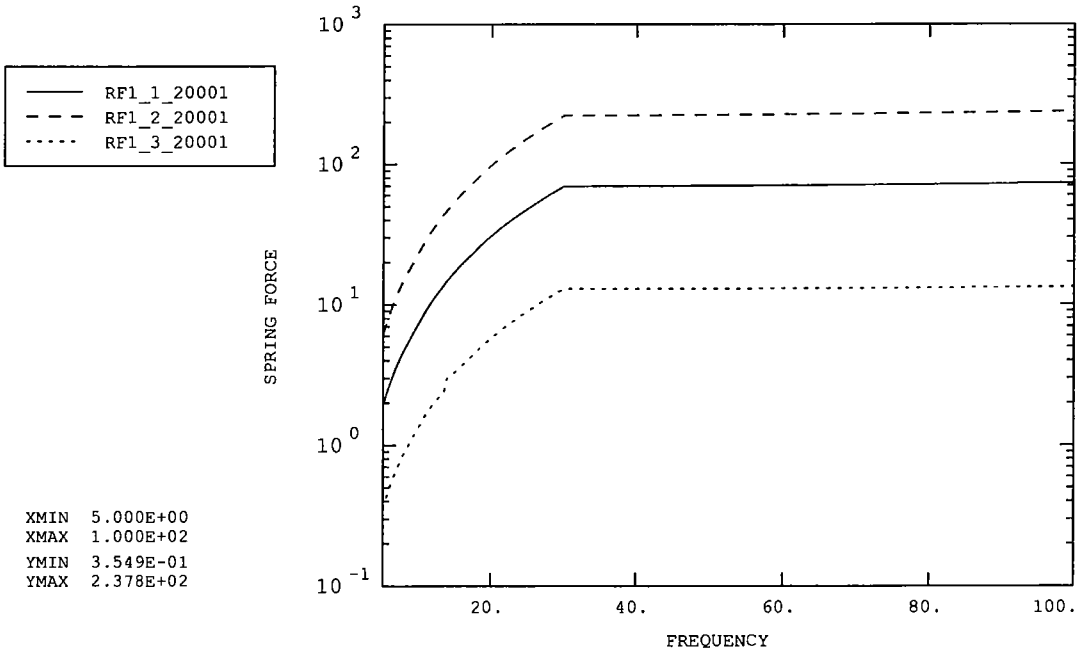

Figure 44: Reaction Force (front middle)

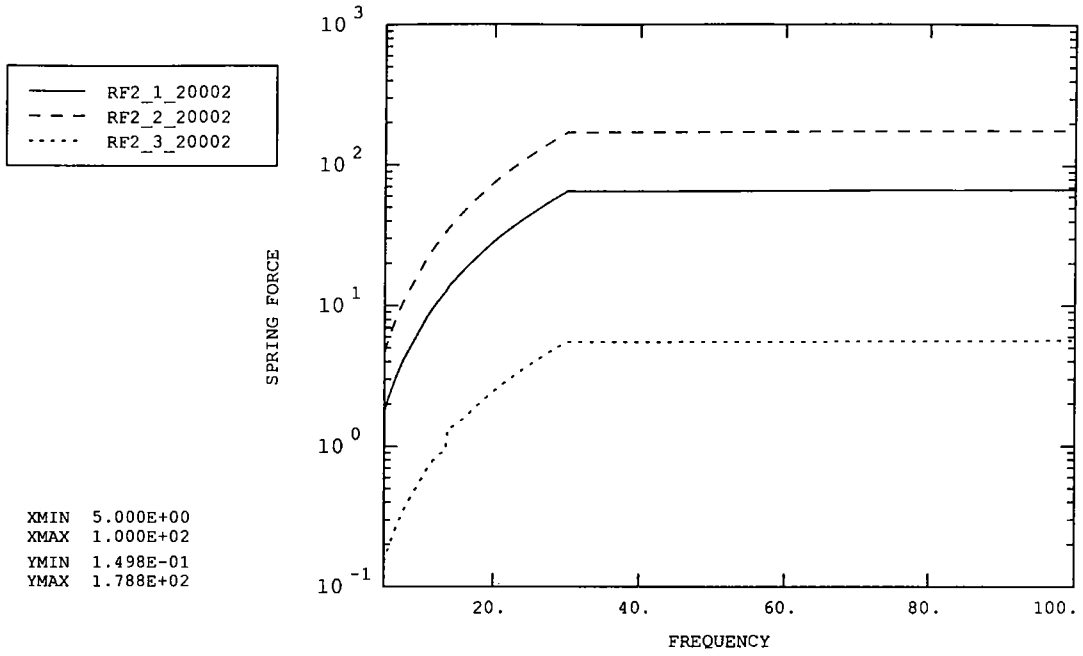

Figure 45: Reaction Force (back left)

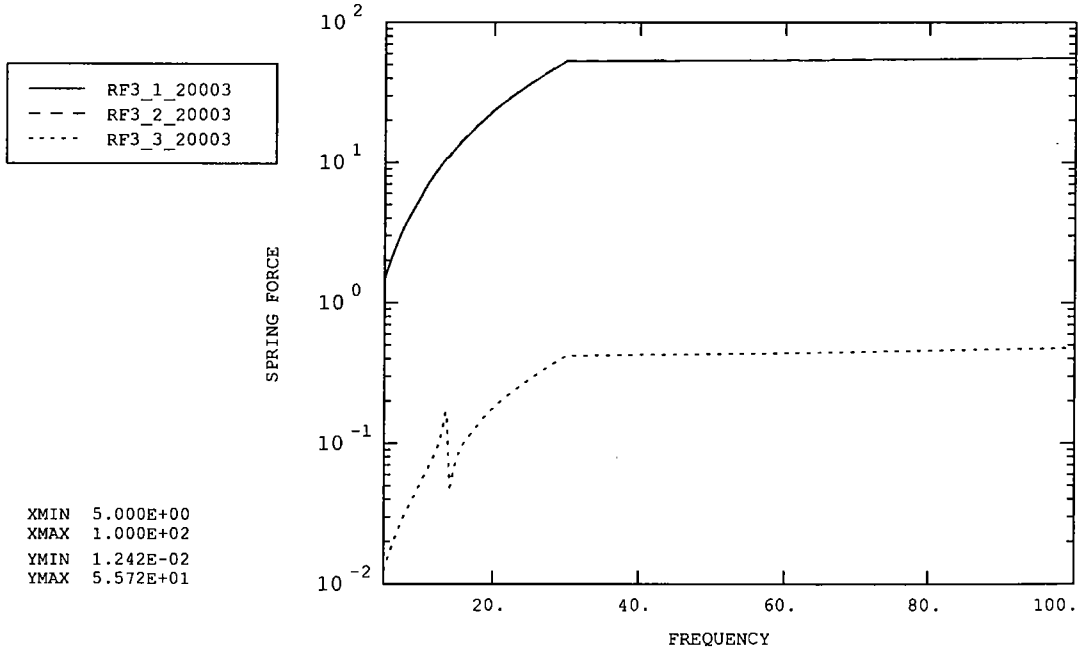

Figure 46: Reaction Force (back right)

© FNC 2002

SPIRE BSM VIBRATION ANALYSIS

Annex 2 - Swept Sine Y-Direction

FNC 5505/24072R Issue 1

Prepared for

U.K. Astronomy Technology Centre

DOCUMENT INFORMATION

Project : SPIRE BSM Vibration Analysis

Report Title : Annex 2 - Swept Sine Y-Direction

Client : U.K. Astronomy Technology Centre

Client Ref. : 024706

Classification :

Report No. : FNC 5505/24072R

Issue No. : 1

Compiled By : D C Reed
A J Vibert

Date : May 2002

Approved By : M W Anderson

DISTRIBUTION

Copy	Recipient	Organisation
1	I Pain	UK ATC
2	I Pain	UK ATC
3	I Pain	UK ATC
4	File	FNC

Copy No. ____

COPYRIGHT

The Copyright in this work is vested in Frazer-Nash Consultancy Limited. The document is issued in confidence solely for the purpose for which it is supplied. Reproduction in whole or in part or use for tendering or manufacturing purposes is prohibited except under an agreement with or with the written consent of Frazer-Nash Consultancy Limited and then only on the condition that this notice is included in any such reproduction.

Originating Office: FRAZER-NASH CONSULTANCY LIMITED
Stonebridge House, Dorking Business Park, Dorking, Surrey RH4 1HJ, UK
T: +44 (0)1306 885050 F: +44 (0)1306 886464 E: info@fnc.co.uk W: www.fnc.co.uk

DATA POINT POSITIONS

Note:

- The labels on the plots are as follows: e.g. P9_1_12184 refers to acceleration data point P9, degree of freedom 1 (node number 12184).
- Degrees of freedom 1, 2 and 3 refer to motion in the x, y and z directions (or X, Y and Z directions), while degrees of freedom 4, 5 and 6 refer to rotations about the x, y and z axes (or X, Y and Z axes).
- Acceleration is total acceleration (i.e. includes base motion)
- Accelerations and reaction forces are given in the global X, Y, Z co-ordinates
- Relative displacements and spring forces/torques are given in the local model x, y, z co-ordinates.
- 'Left' and 'right' directions are defined from a point of view looking towards the mirror surface, with the top of the casing furthest from the baseplate.

Fig.	P	Acceleration data points	Node number
1	1	Jiggle axis pivot (top) – frame	12182
2	2	Jiggle axis pivot (top) – jiggle stage	12200
3	3	Jiggle axis pivot (bottom) – frame	12183
4	4	Jiggle axis pivot (bottom) – jiggle stage	12192
5	5	Chop axis pivot (right side) – jiggle stage	12189
6	6	Chop axis pivot (right side) – chop stage	114
7	7	Chop axis pivot (left side) – jiggle stage	12188
8	8	Chop axis pivot (left side) – chop stage	105
9	9	Chop motor (top)	12184
10	10	Chop motor (bottom)	12185
11	11	Jiggle motor (right side)	12186
12	12	Jiggle motor (left side)	12187
13	13	PCAL CG	12193
14	14	PCAL extension to mirror centre	12199
15	15	Launch latch 'A' CG	12196
16	16	Launch latch 'A' extension to magnet centre	12197
17	17	Connector (top)	12194
18	18	Chop magnet (top)	115
19	19	Chop magnet (bottom)	122
20	20	Mirror Centre	9583
21	21	Jiggle magnet (right)	9276
22	22	Jiggle magnet (left)	9264

© FNC 2002

Fig.	E	Displacement between...	Element
23	1	Chop magnet vs. motor (top)	90n01, n=1, 2
24	2	Chop magnet vs. motor (bottom)	90n02, n=1, 2
25	3	Jiggle magnet vs. motor (right)	90n03, n=2, 3
26	4	Jiggle magnet vs. motor (left)	90n04, n=2, 3
27	5	Mirror centre vs. PCAL extension	90n05, n=1, 2, 3
28	6	Chop magnet (top) vs. launch latch 'A'	90206

Fig.	S	Position of spring elements	Node 1	Element
29	1	Front baffle (top left)	9702	10n01, n=1,2,3
30	2	Front baffle (top right)	9739	10n02, n=1,2,3
31	3	Front baffle (bottom left)	9629	10n03, n=1,2,3
32	4	Front baffle (bottom right)	9594	10n04, n=1,2,3
33	5	Base (front middle)*	3894	10n05, n=1,2,3
34	6	Base (back left)*	3414	10n06, n=1,2,3
35	7	Base (back right)*	3622	10n07, n=1,2,3
36,37	8	Jiggle pivot (top)	12200	10n08, n=1 to 6
38,39	9	Jiggle pivot (bottom)	12192	10n09, n=1 to 6
40,41	10	Chop pivot (left)	12188	10n10, n=1 to 6
42,43	11	Chop pivot (right)	12189	10n11, n=1 to 6

Fig.	RF	Reaction Forces	Node number
44	1	Reaction Force (front middle)	10587
45	2	Reaction Force (back left)	10722
46	3	Reaction Force (back right)	10671

* The baseplate-casing connections are each modelled using a single spring in the local x and y directions, and five springs in the local z direction. The forces from these five springs are added together to calculate the total connective force. The curve labels for the z direction degrees of freedom have the prefix 'B'.

© FNC 2002

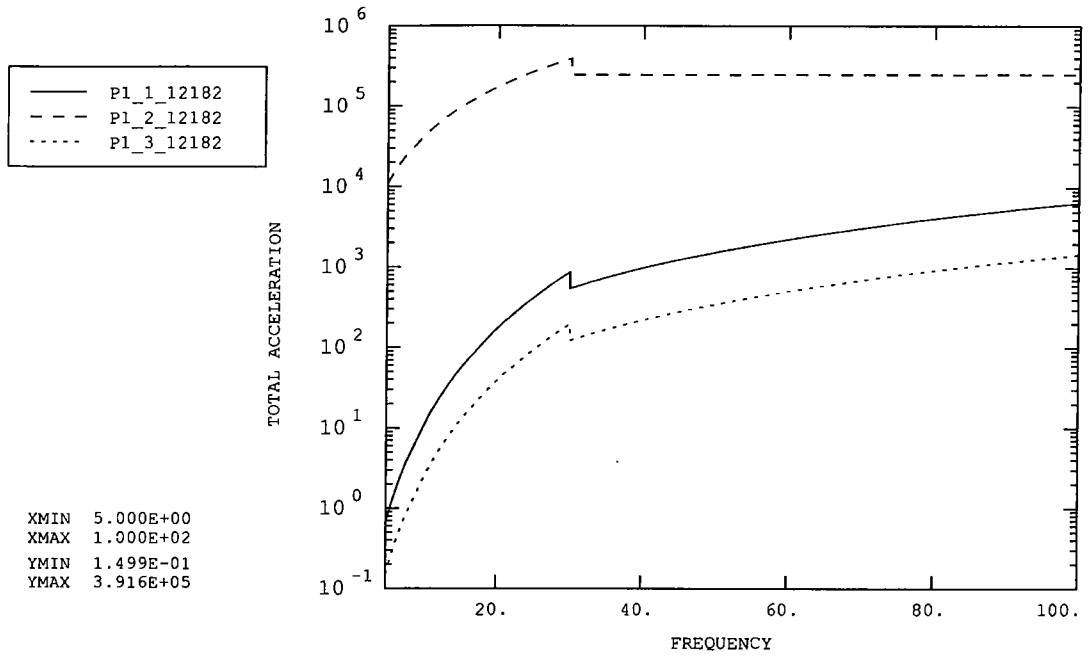

Figure 1: Jiggle axis pivot (top) – frame

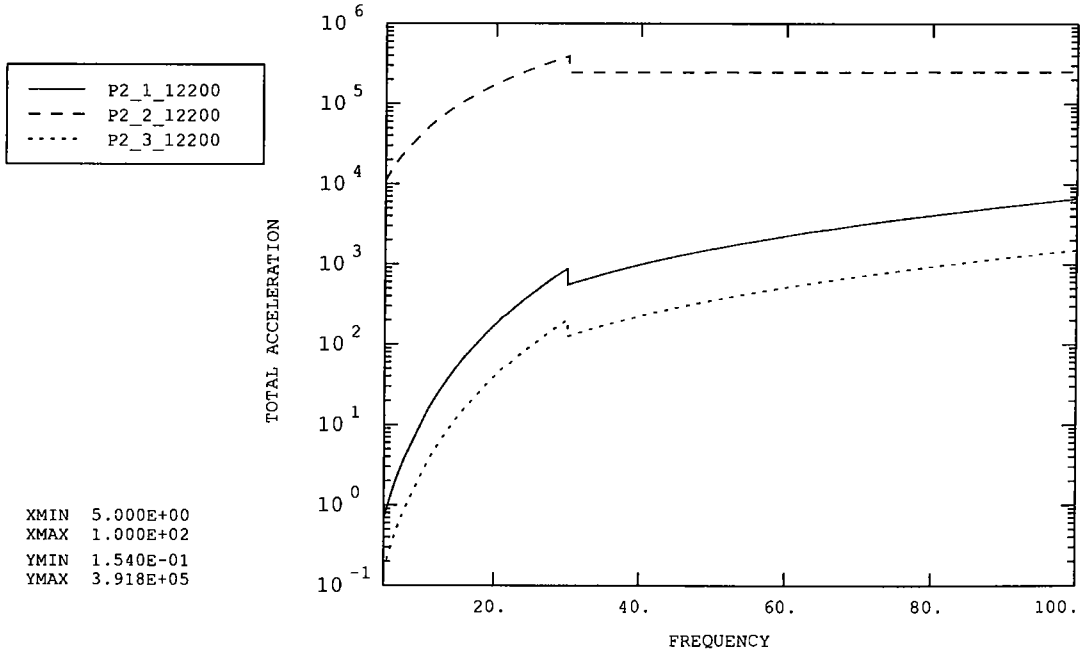

Figure 2: Jiggle axis pivot (top) – jiggle stage

© FNC 2002

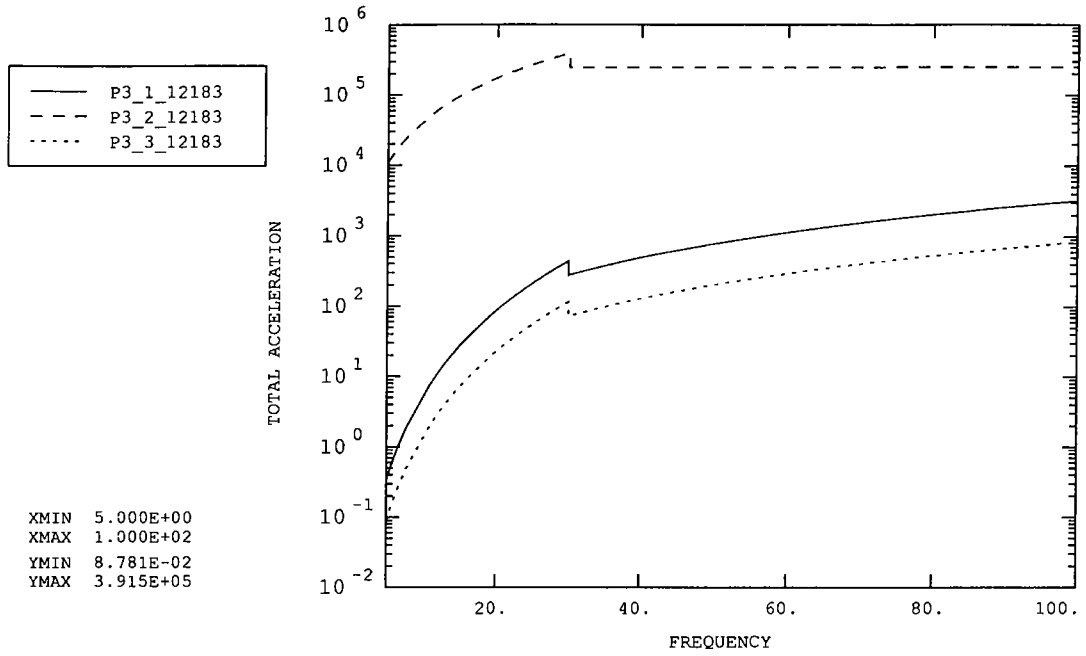

Figure 3: Jiggle axis pivot (bottom) – frame

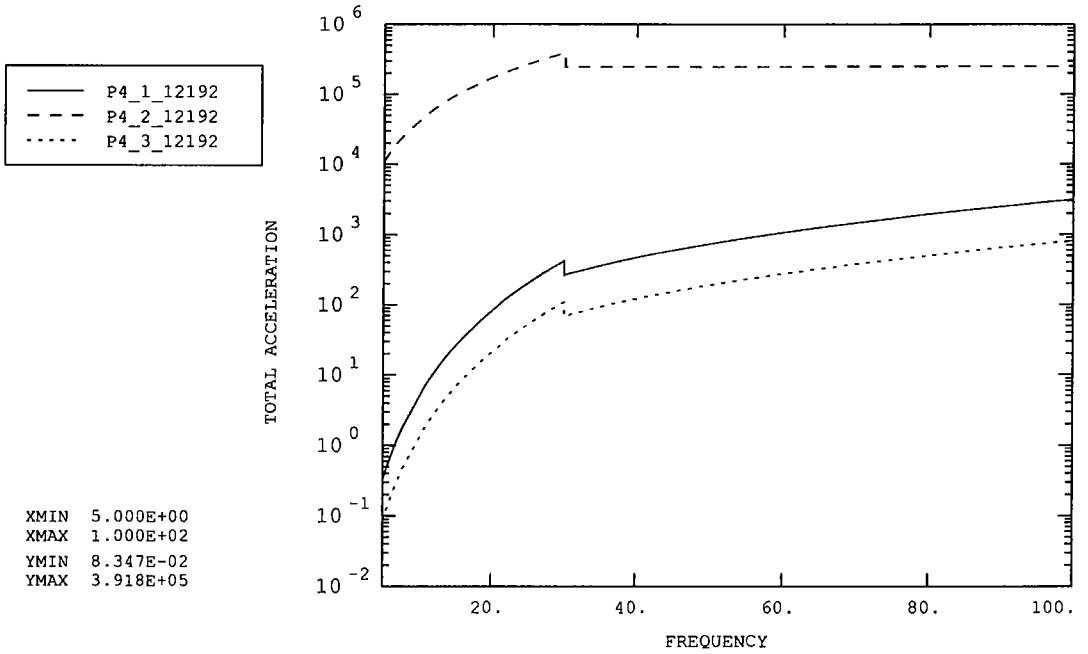

Figure 4: Jiggle axis pivot (bottom) – jiggle stage

© FNC 2002

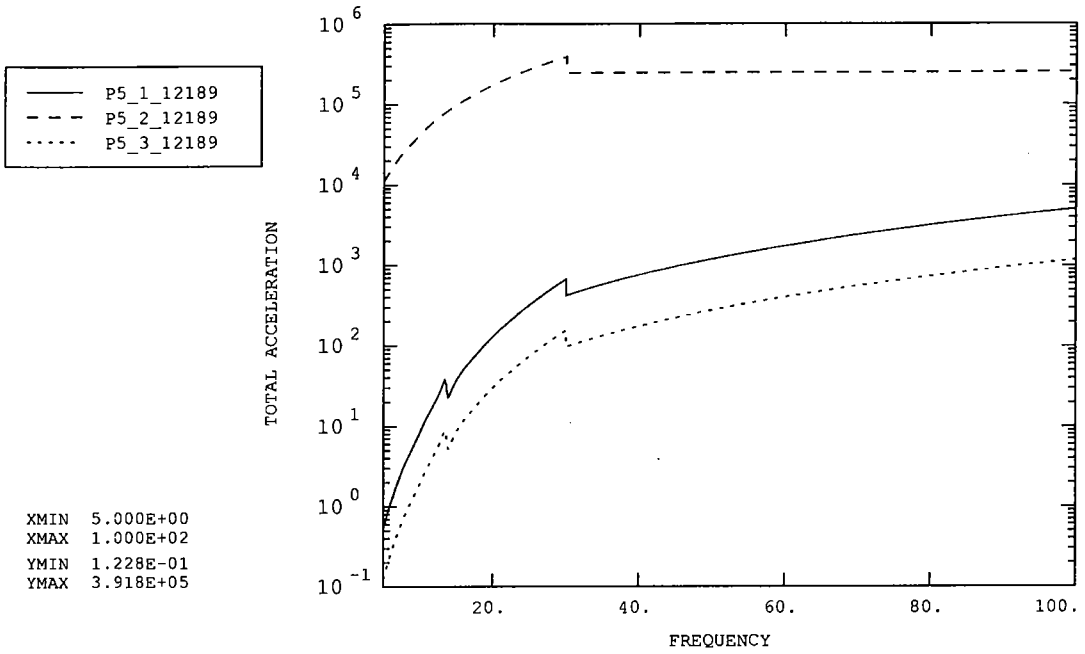

Figure 5: Chop axis pivot (right side) – jiggle stage

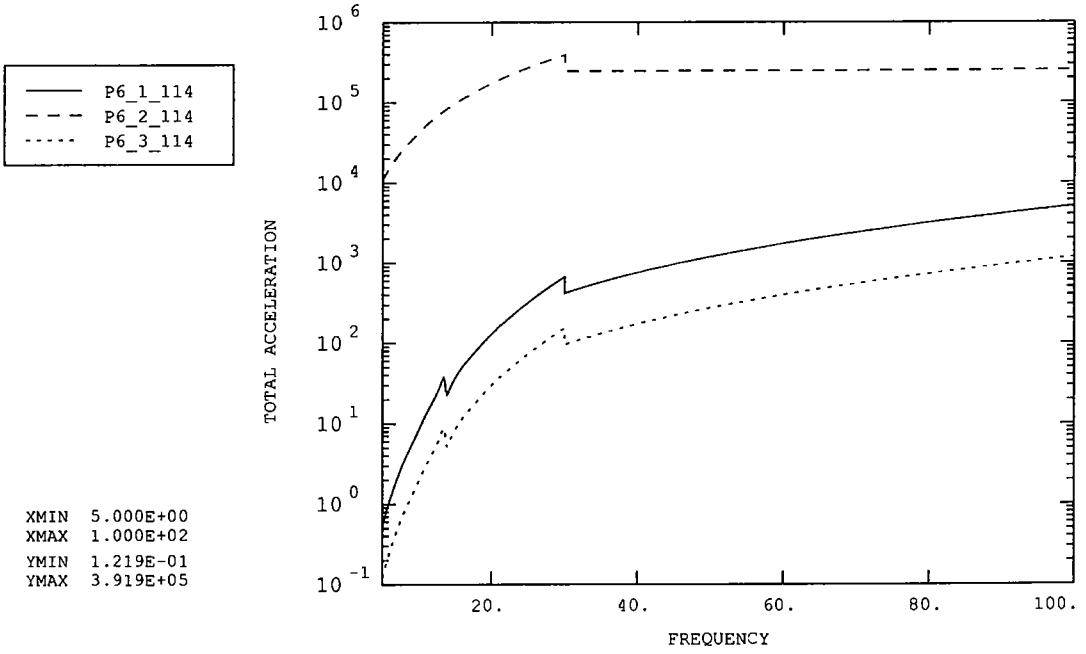

Figure 6: Chop axis pivot (right side) – chop stage

© FNC 2002

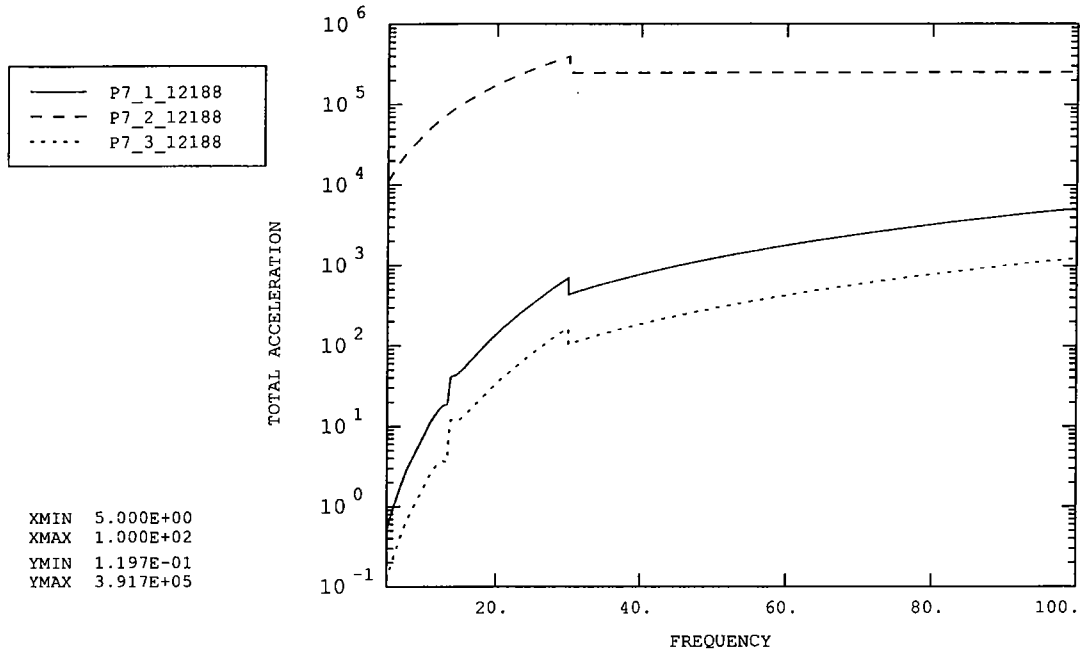

Figure 7: Chop axis pivot (left side) – jiggle stage

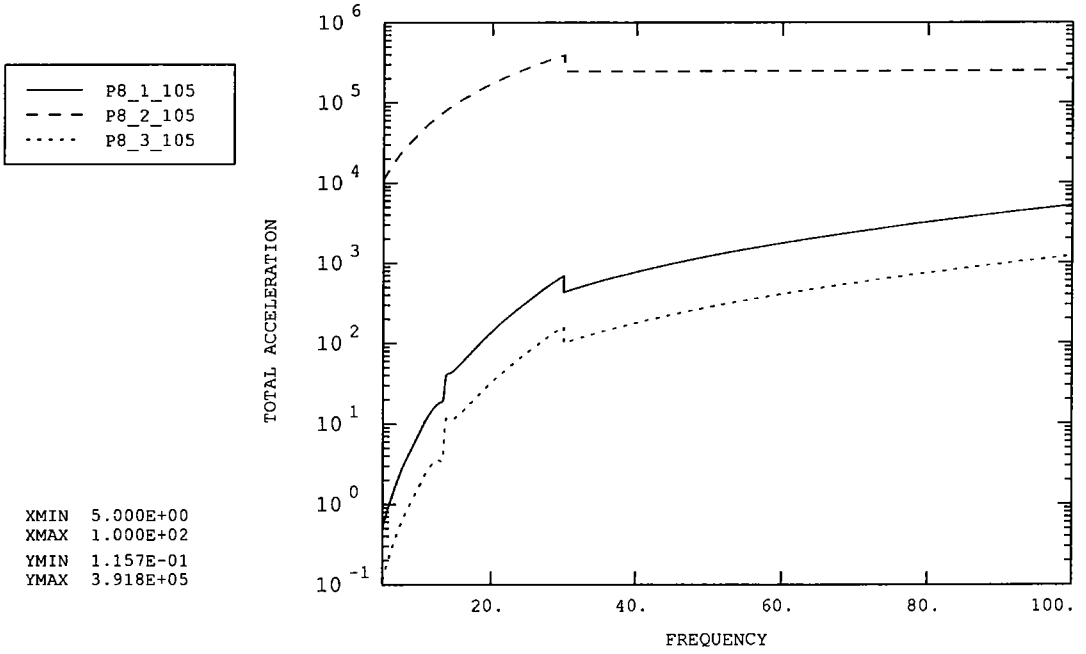

Figure 8: Chop axis pivot (left side) – chop stage

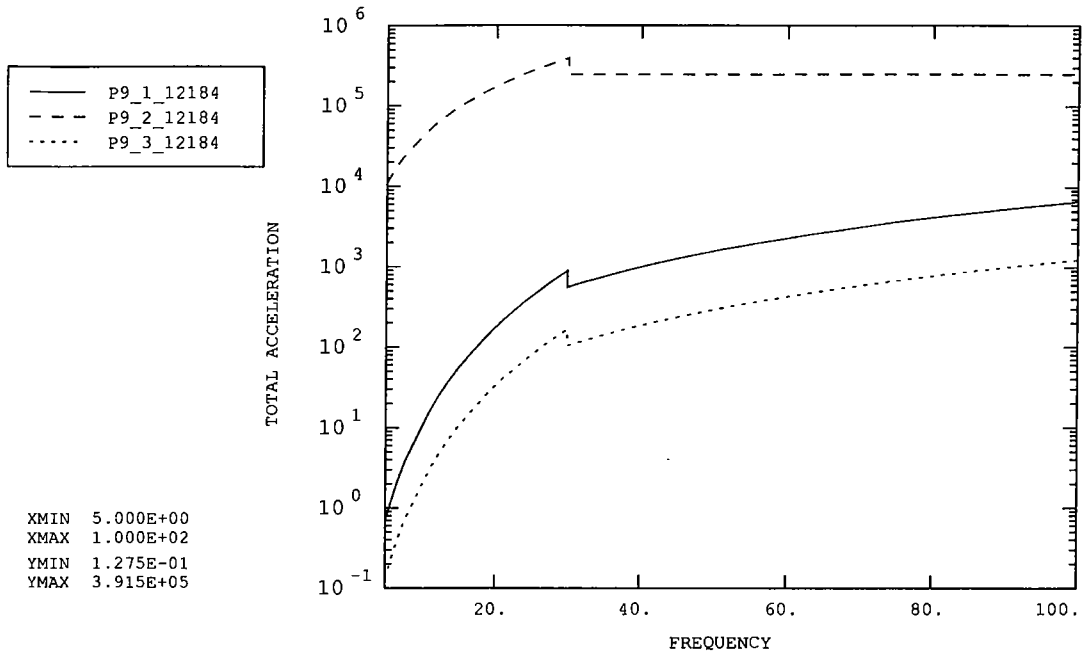

Figure 9: Chop motor (top)

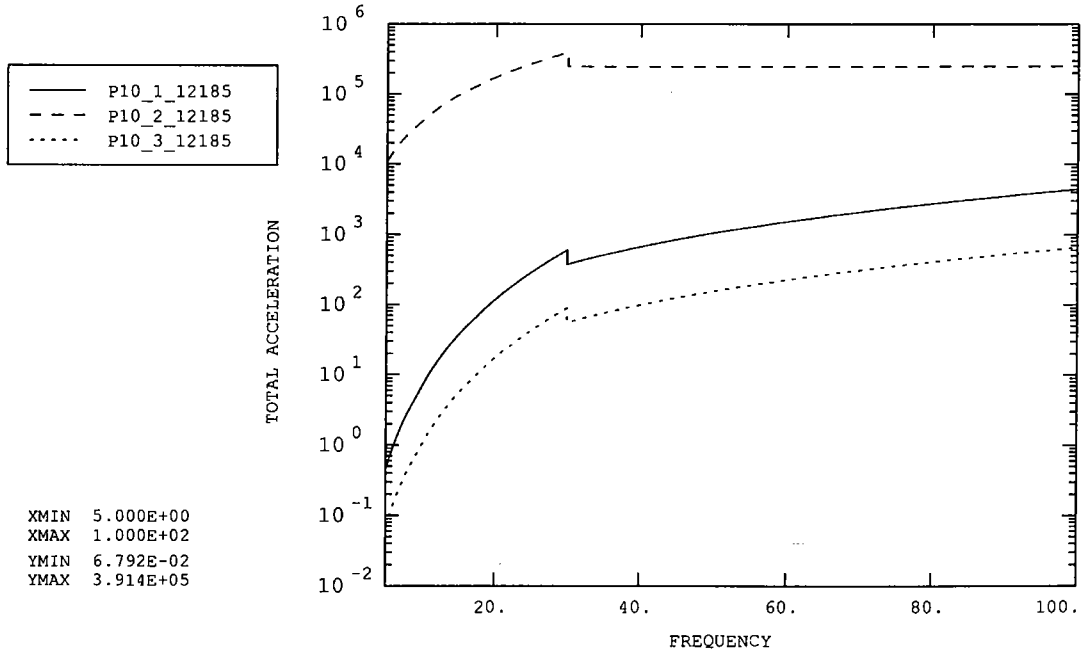

Figure 10: Chop motor (bottom)

© FNC 2002

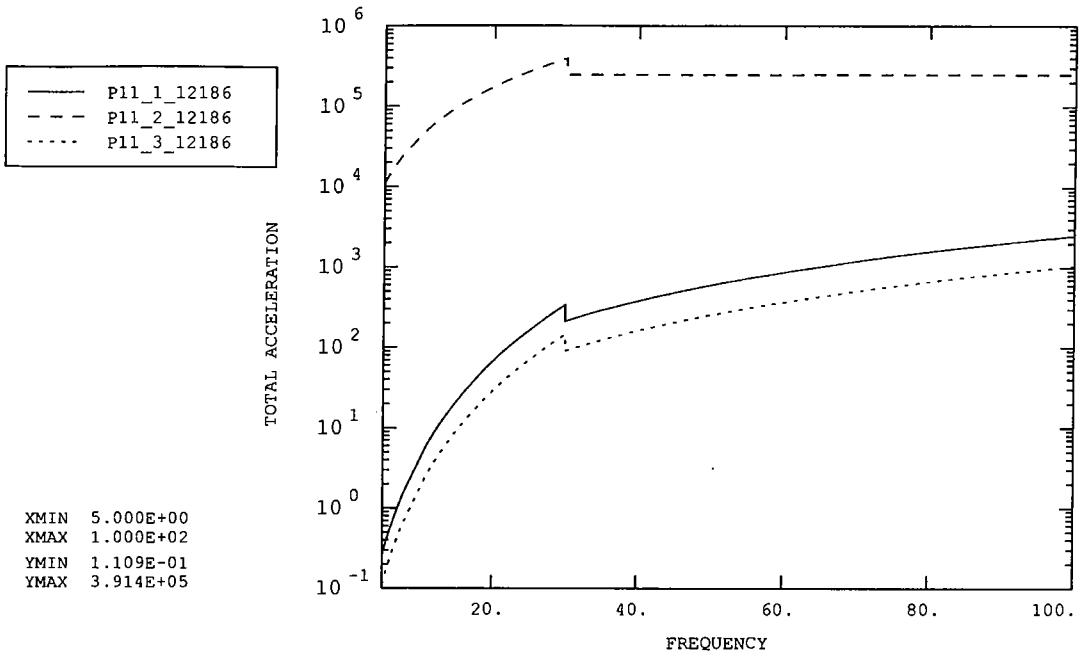

Figure 11: Jiggle motor (right side)

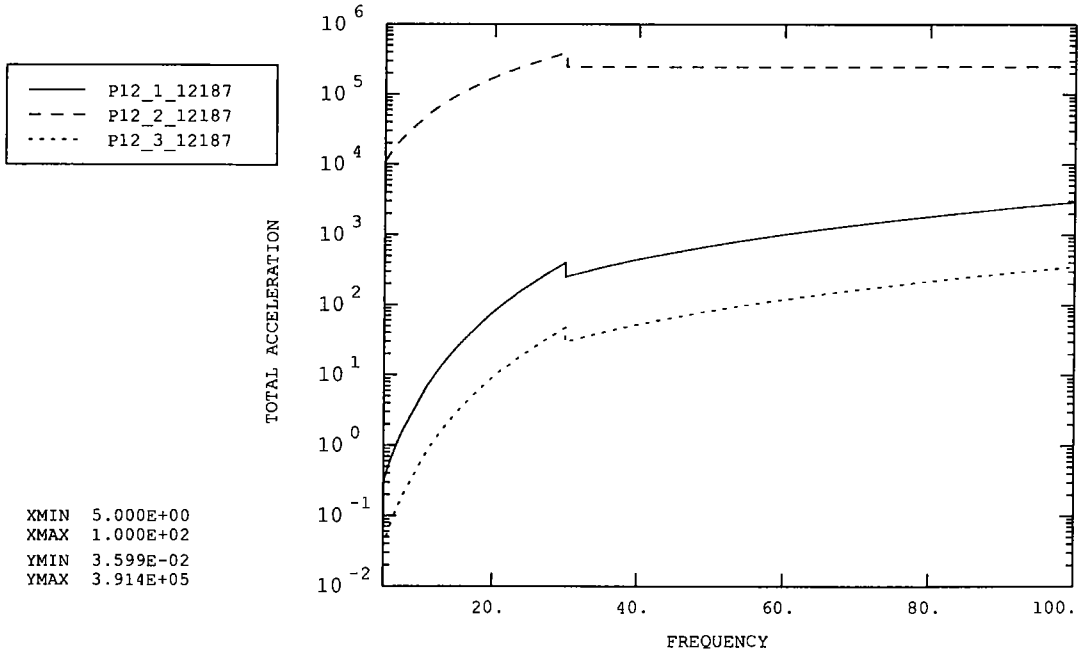

Figure 12: Jiggle motor (left side)

© FNC 2002

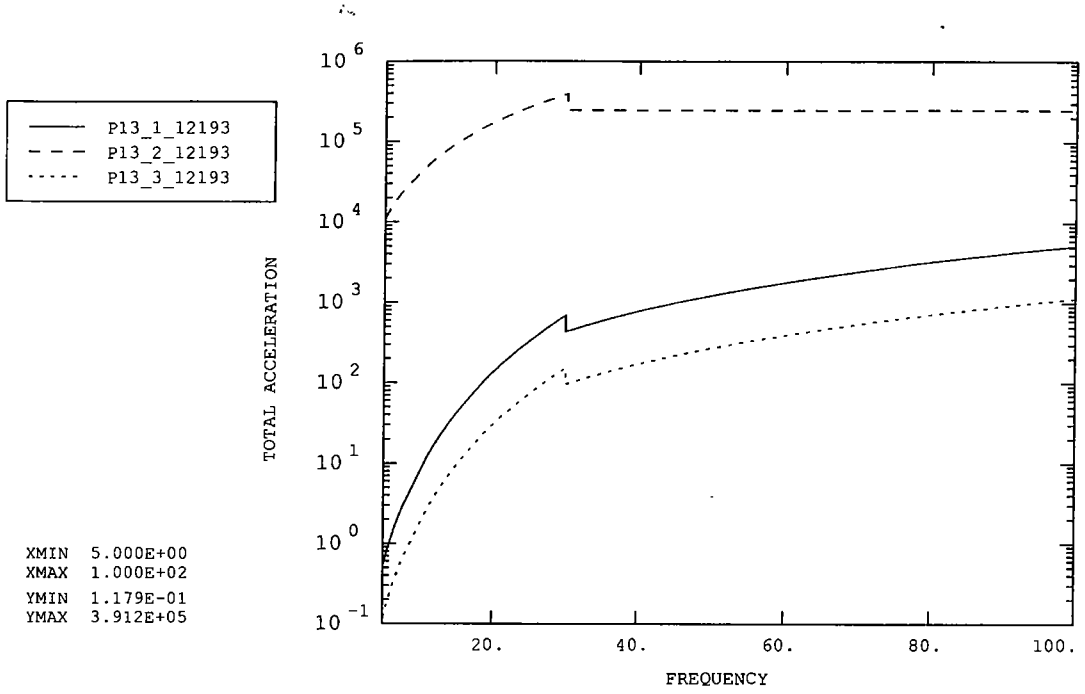

Figure 13: PCAL CG

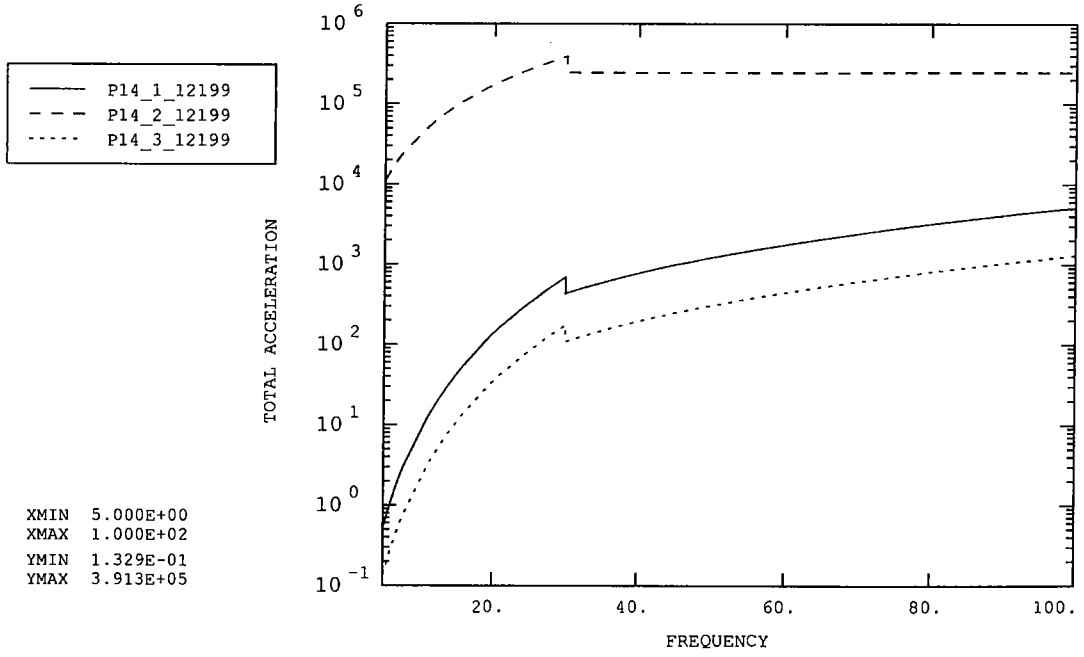

Figure 14: PCAL extension to mirror centre

© FNC 2002

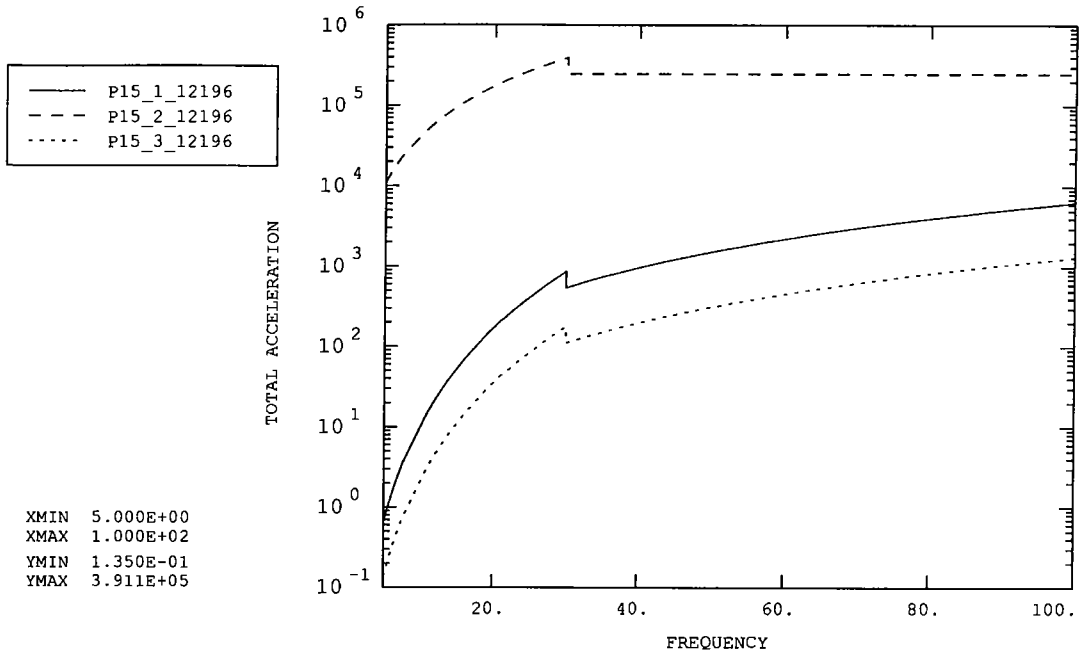

Figure 15: Launch latch 'A' CG

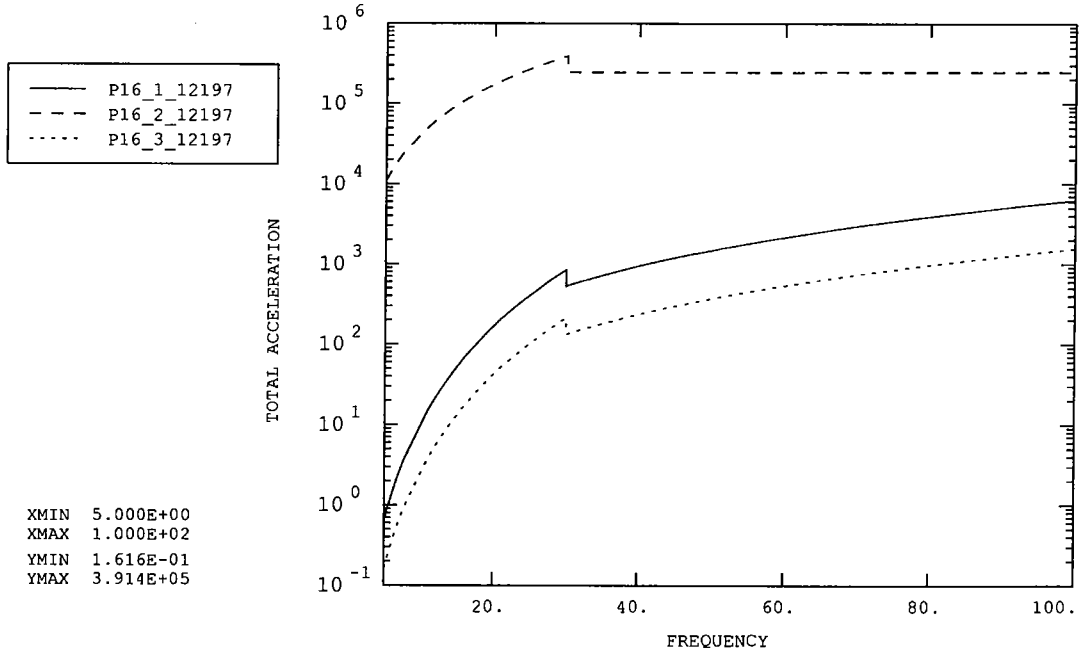

Figure 16: Launch latch 'A' extension to magnet centre

© FNC 2002

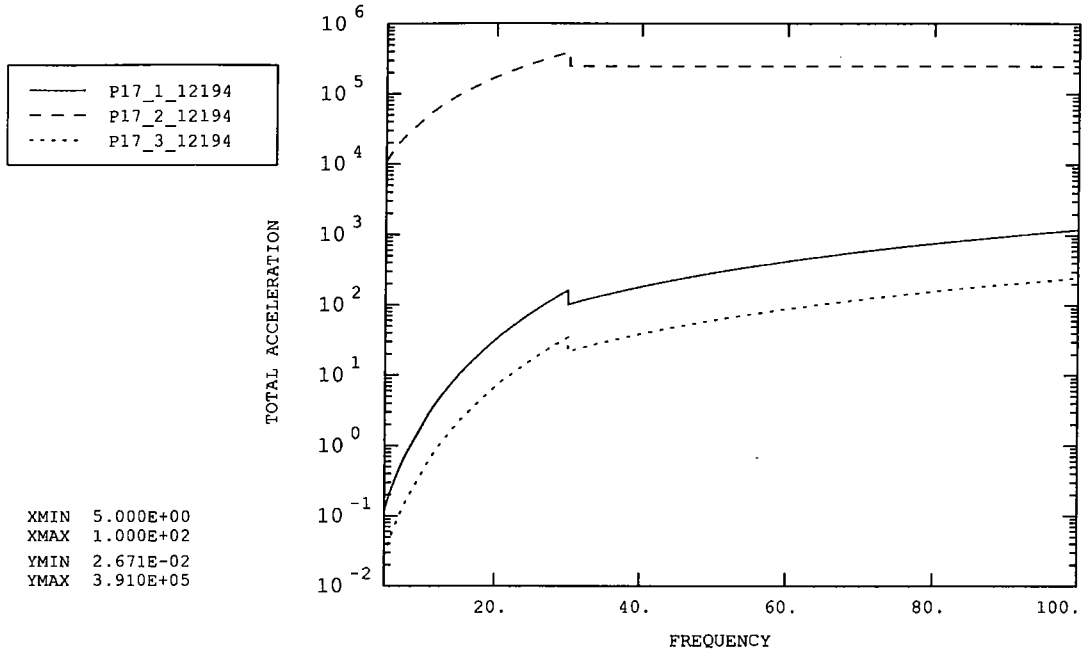

Figure 17: Connector (top)

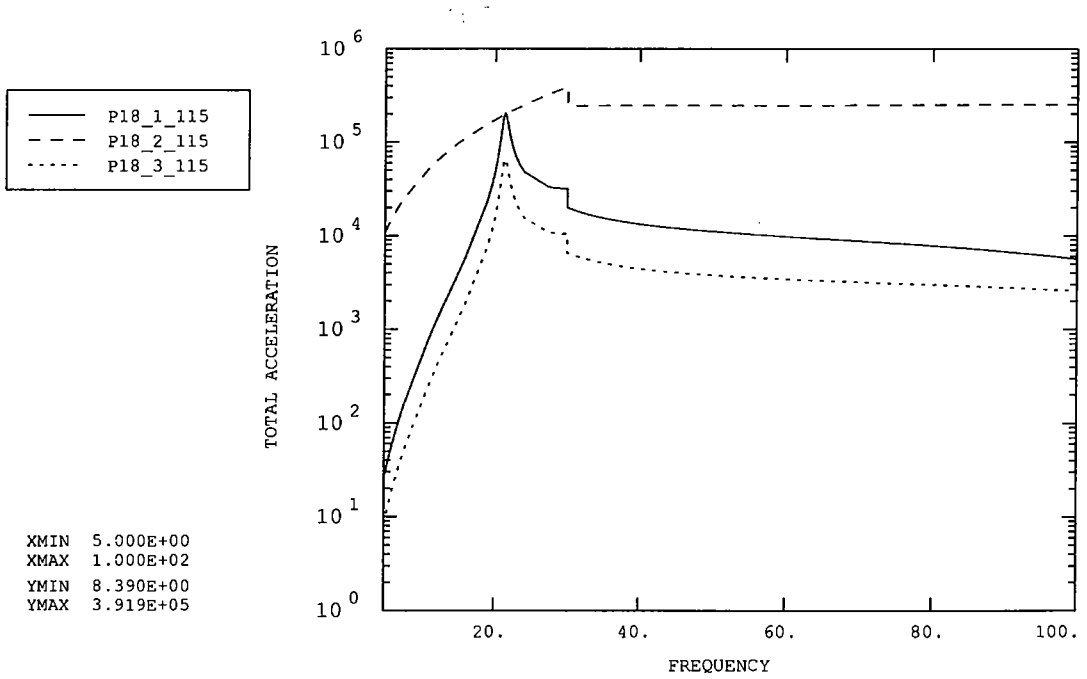

Figure 18: Chop magnet (top)

© FNC 2002

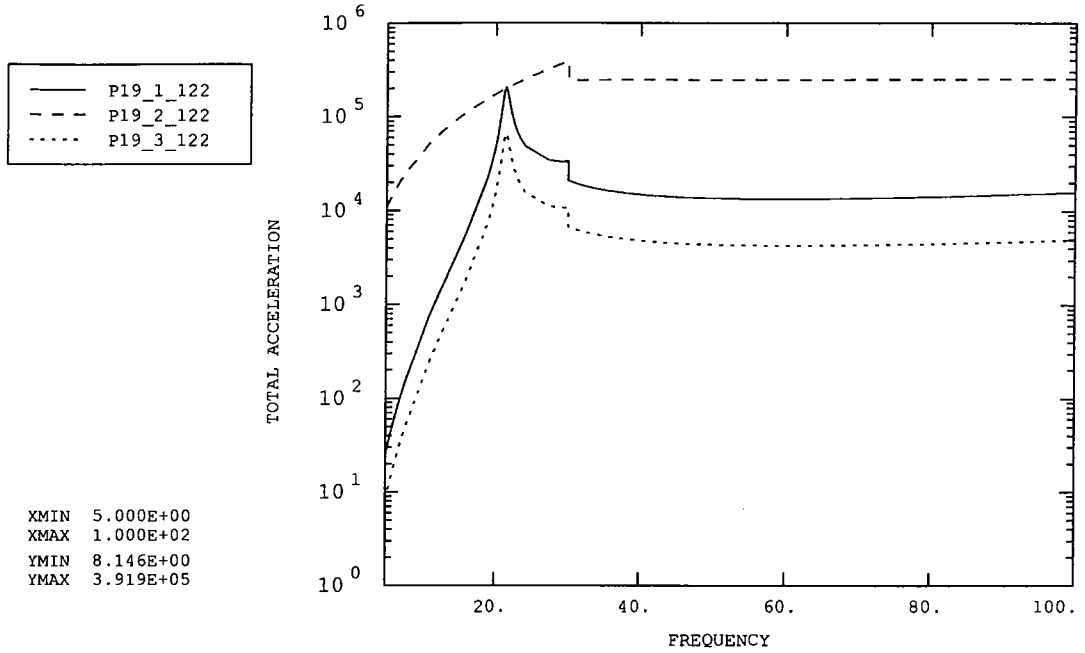

Figure 19: Chop magnet (bottom)

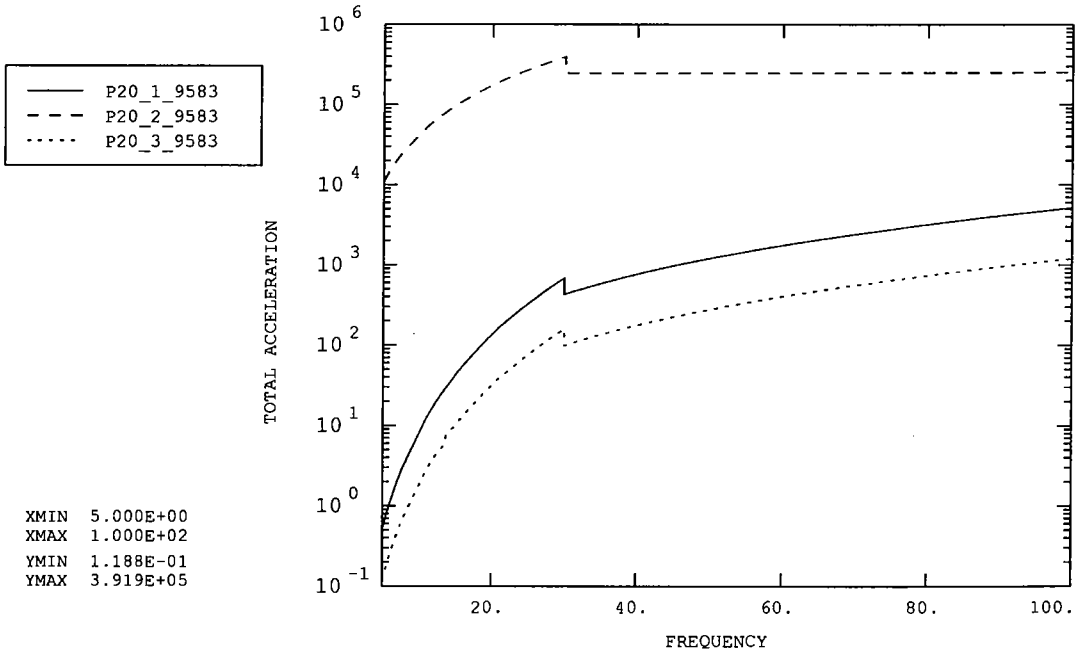

Figure 20: Mirror Centre

© FNC 2002

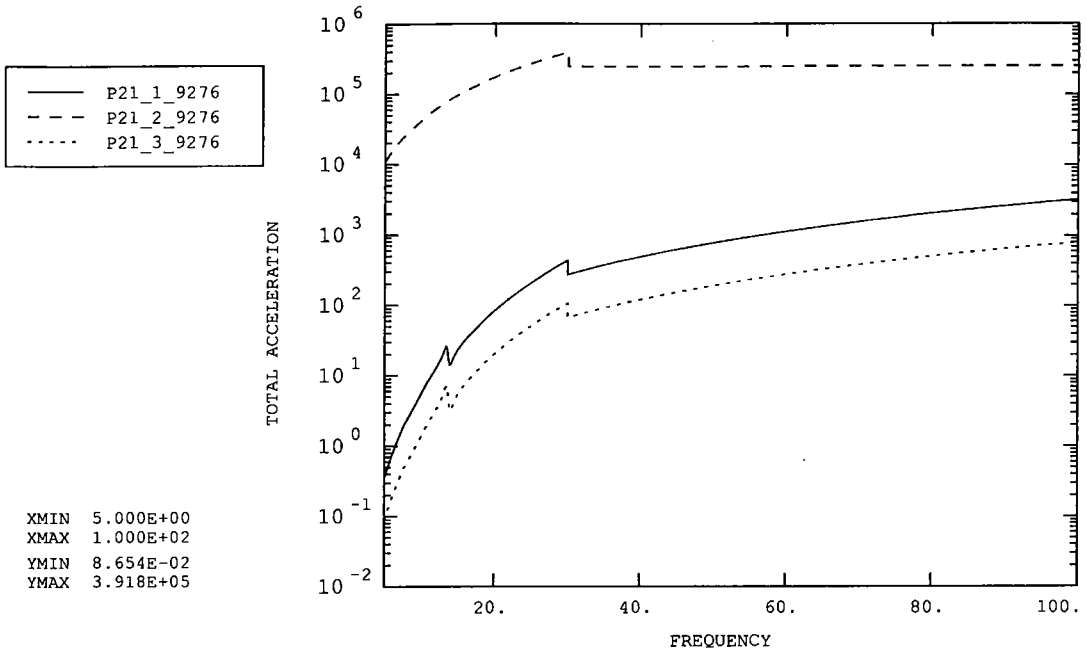

Figure 21: Jiggle magnet (right)

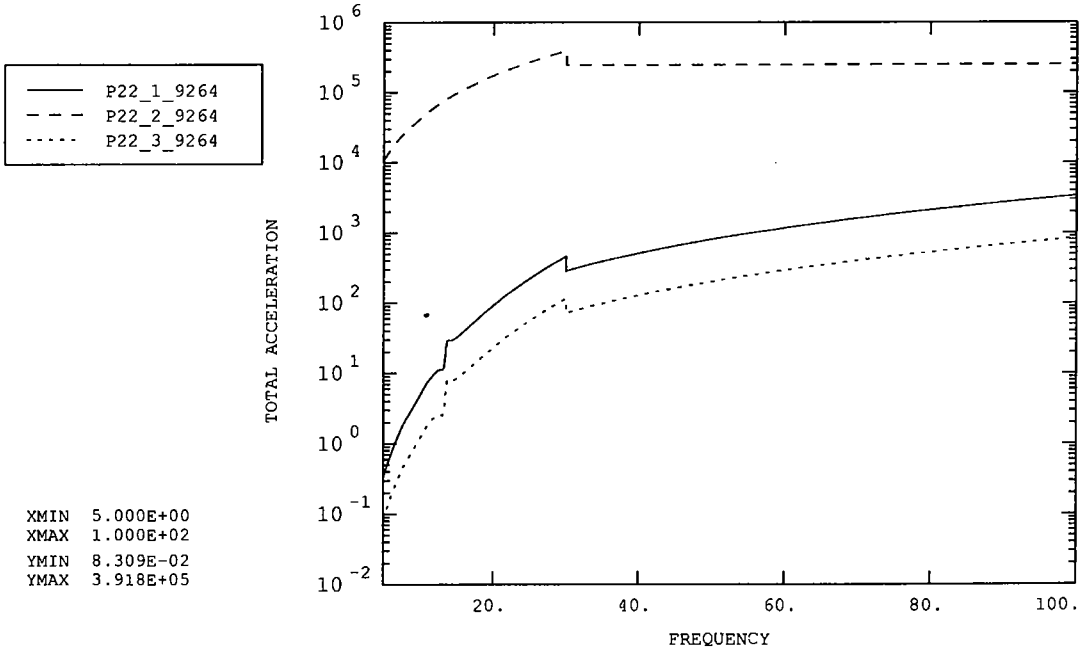

Figure 22: Jiggle magnet (left)

© FNC 2002

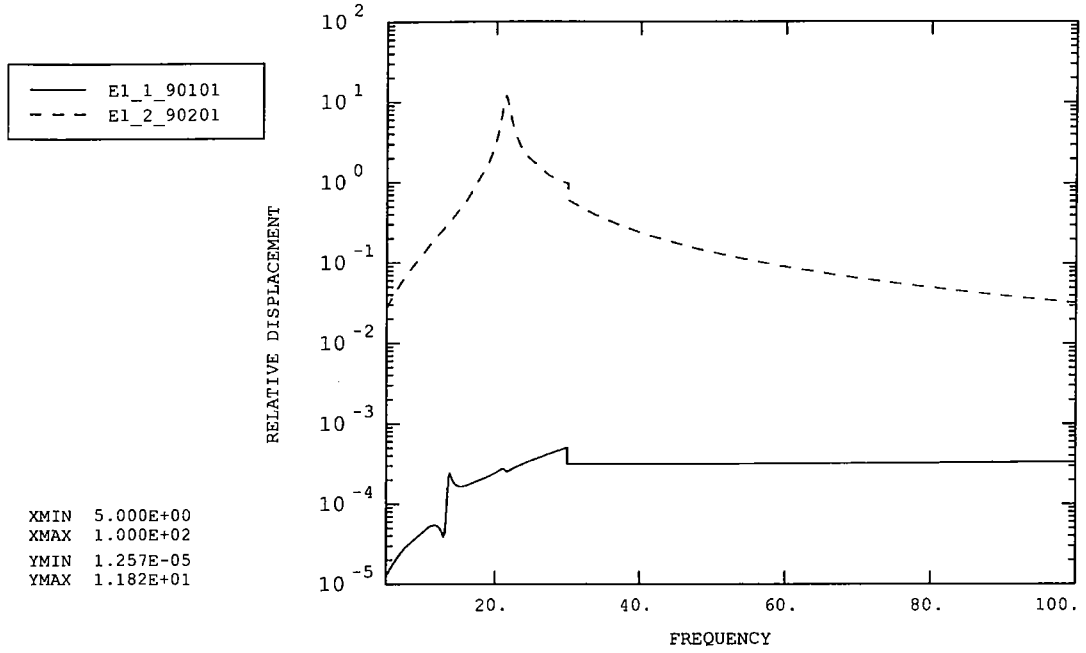

Figure 23: Chop magnet vs. motor (top)

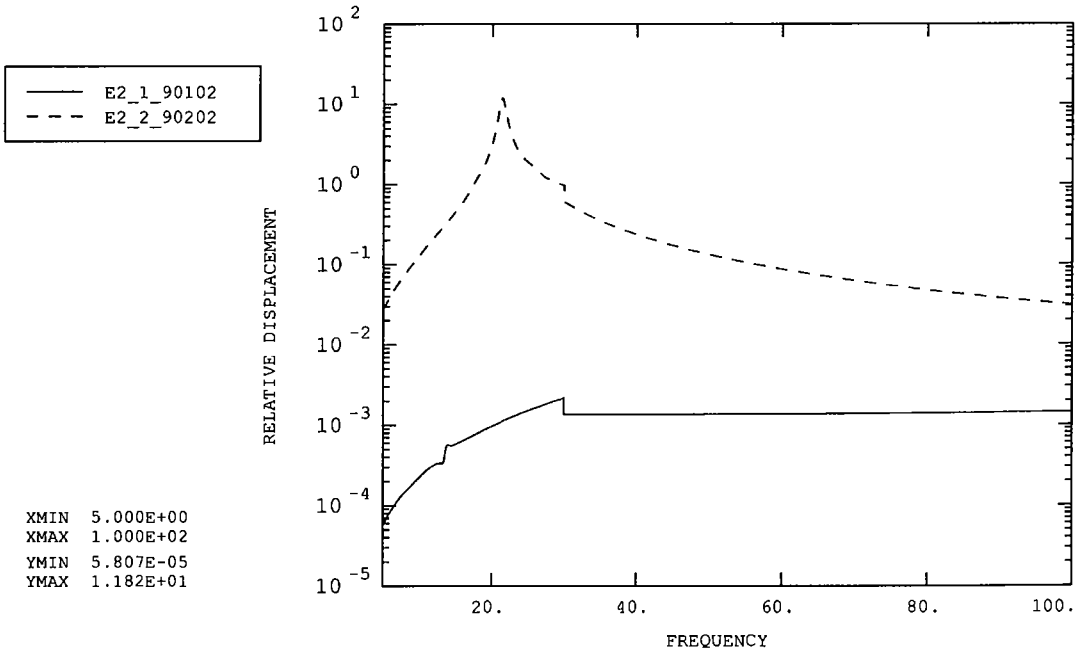

Figure 24: Chop magnet vs. motor (bottom)

© FNC 2002

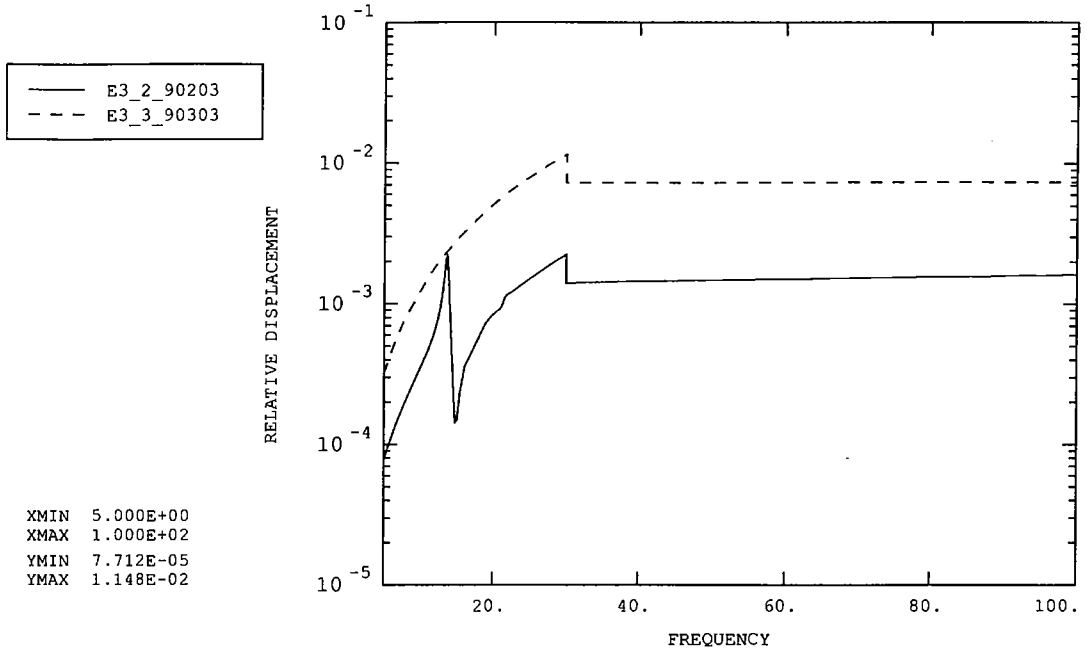

Figure 25: Jiggle magnet vs. motor (right)

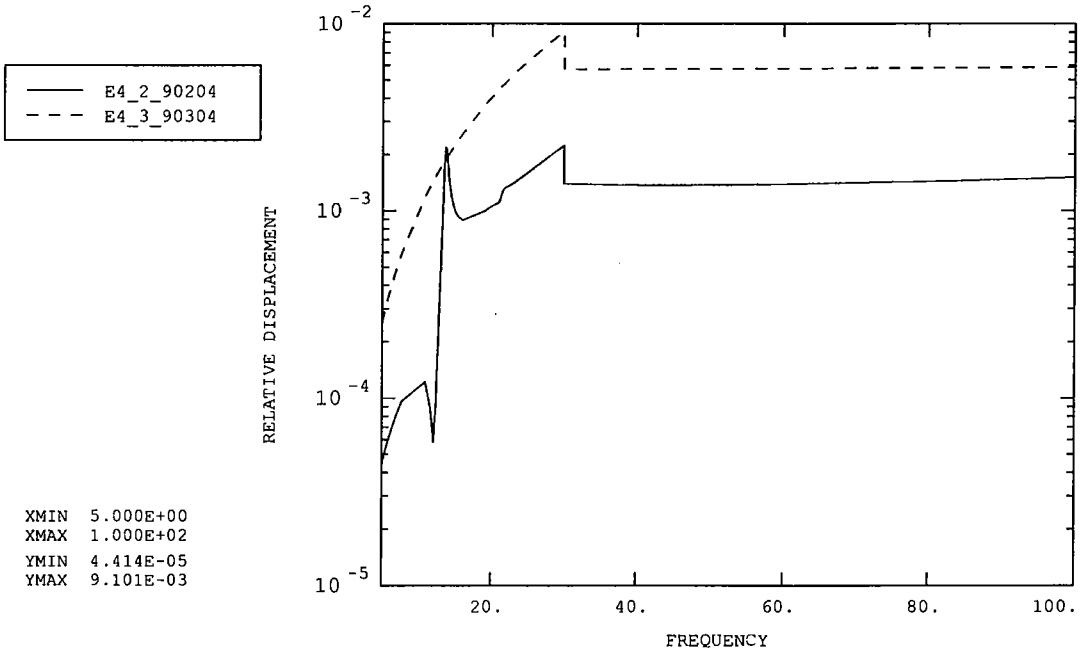

Figure 26: Jiggle magnet vs. motor (left)

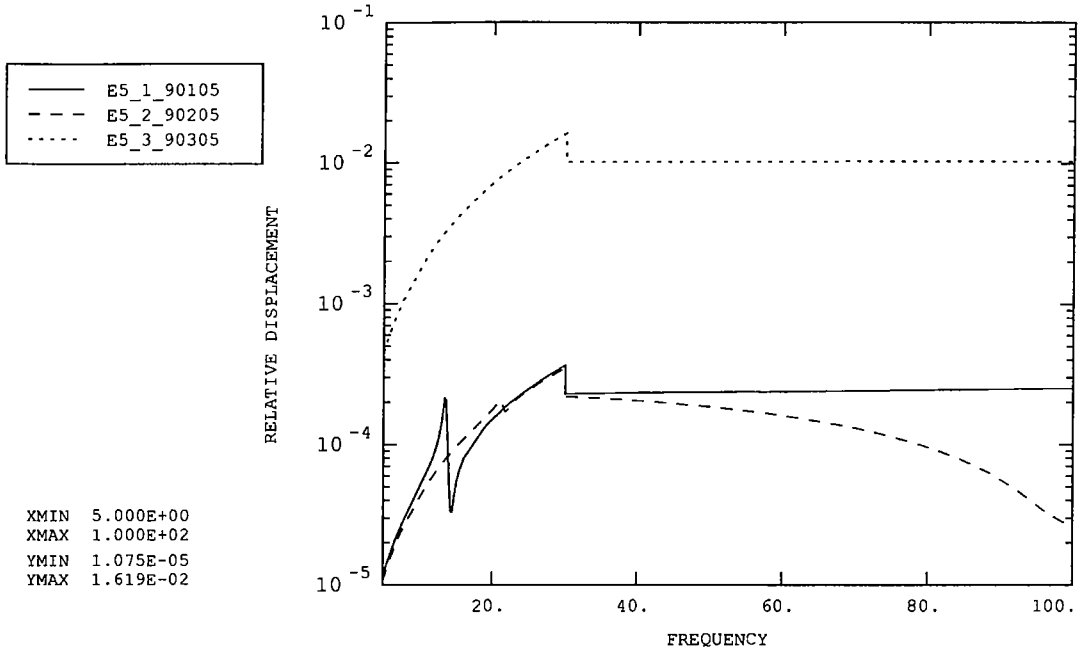

Figure 27: Mirror centre vs. PCAL extension

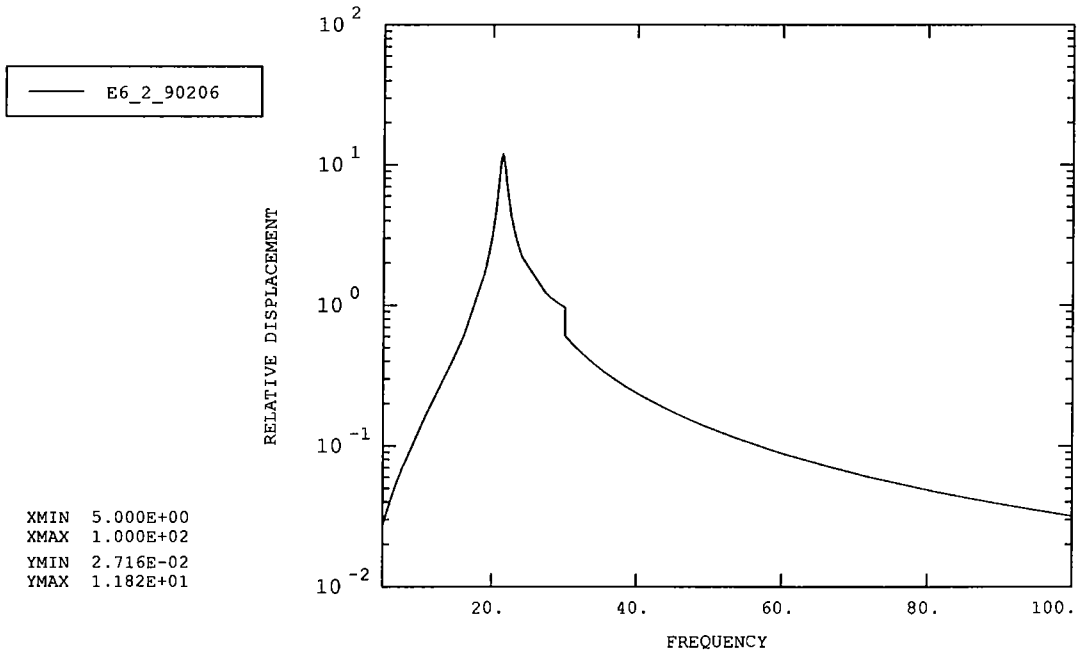

Figure 28: Chop magnet (top) vs. launch latch 'A'

© FNC 2002

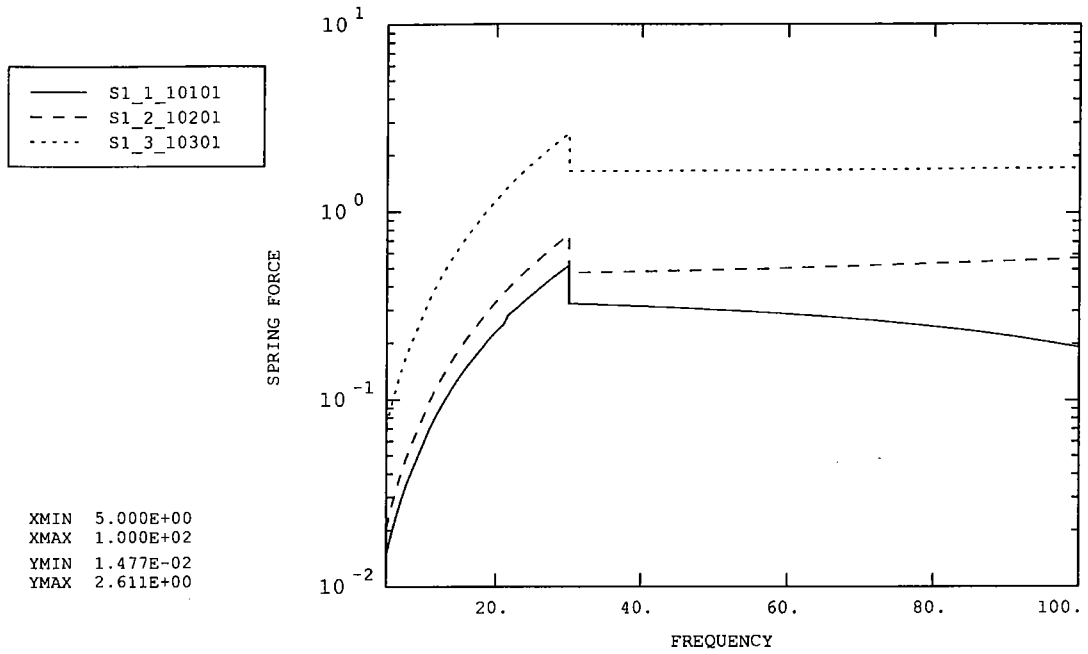

Figure 29: Front baffle (top left)

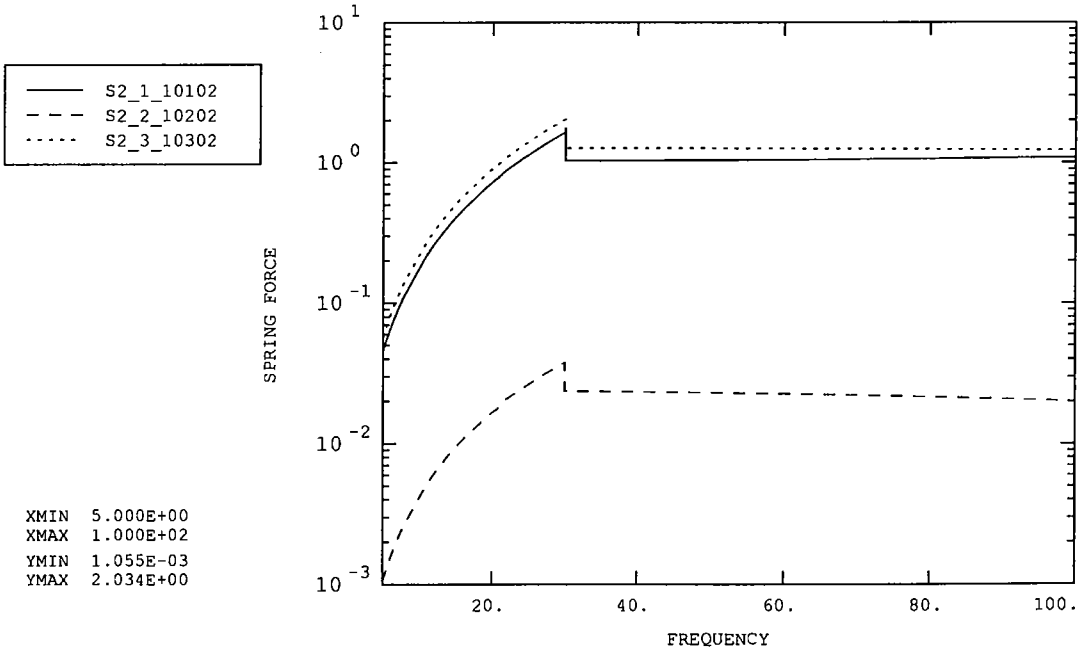

Figure 30: Front baffle (top right)

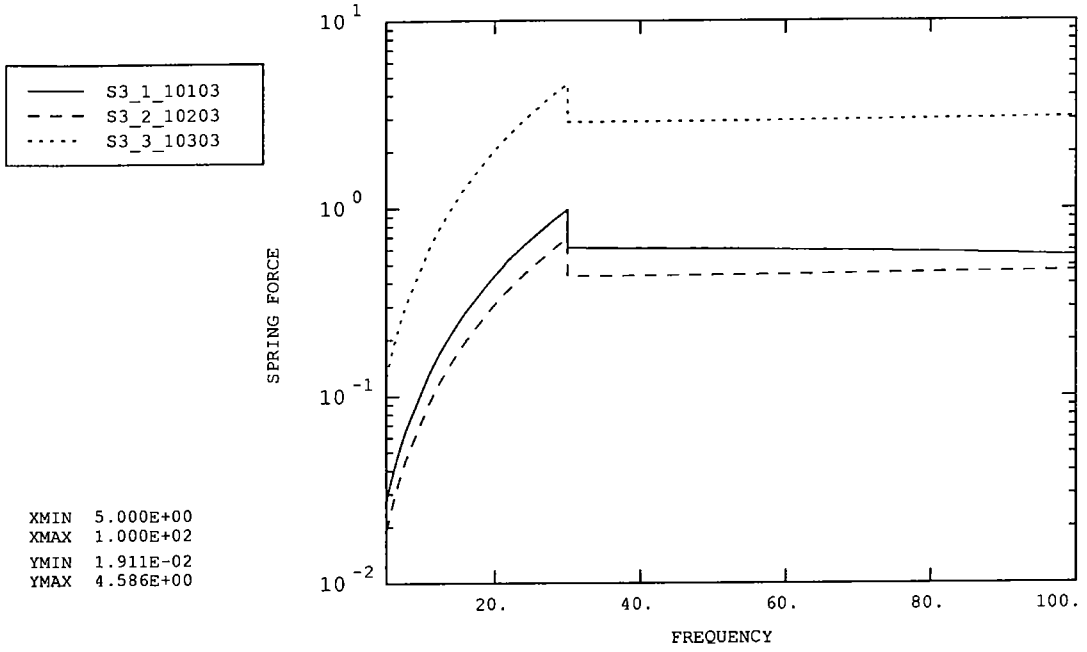

Figure 31: Front baffle (bottom left)

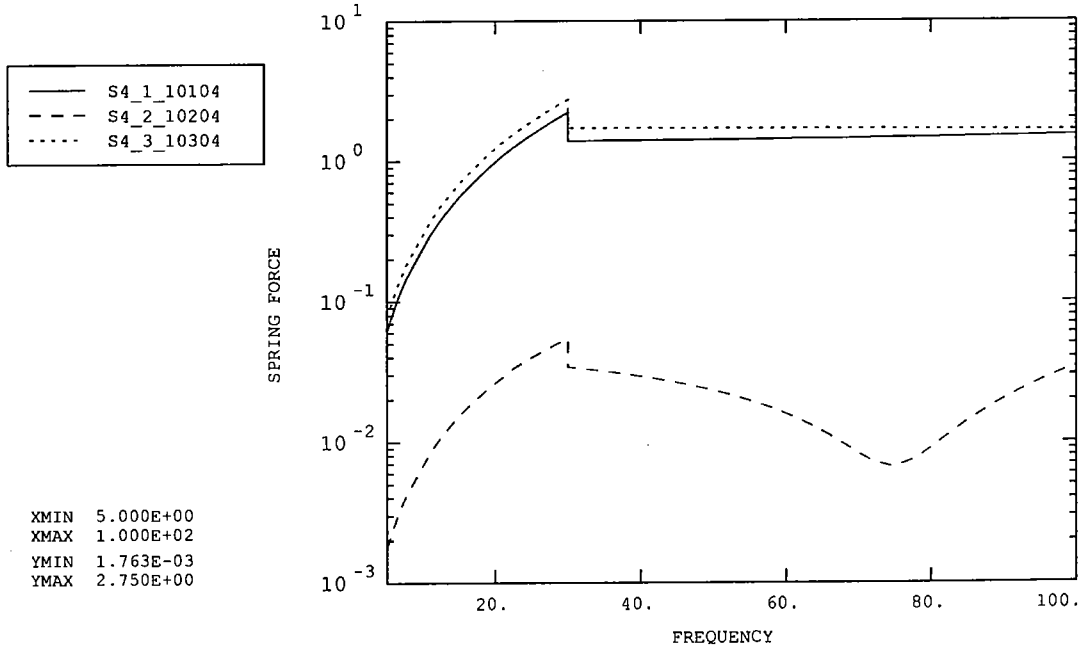

Figure 32: Front baffle (bottom right)

© FNC 2002

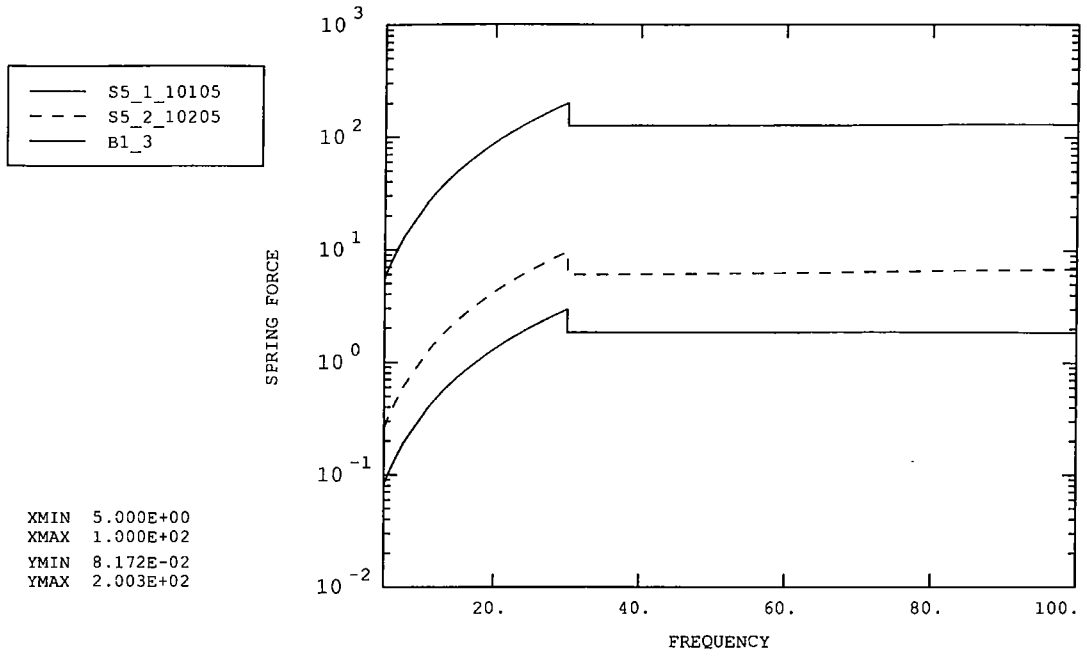

Figure 33: Base (front middle)

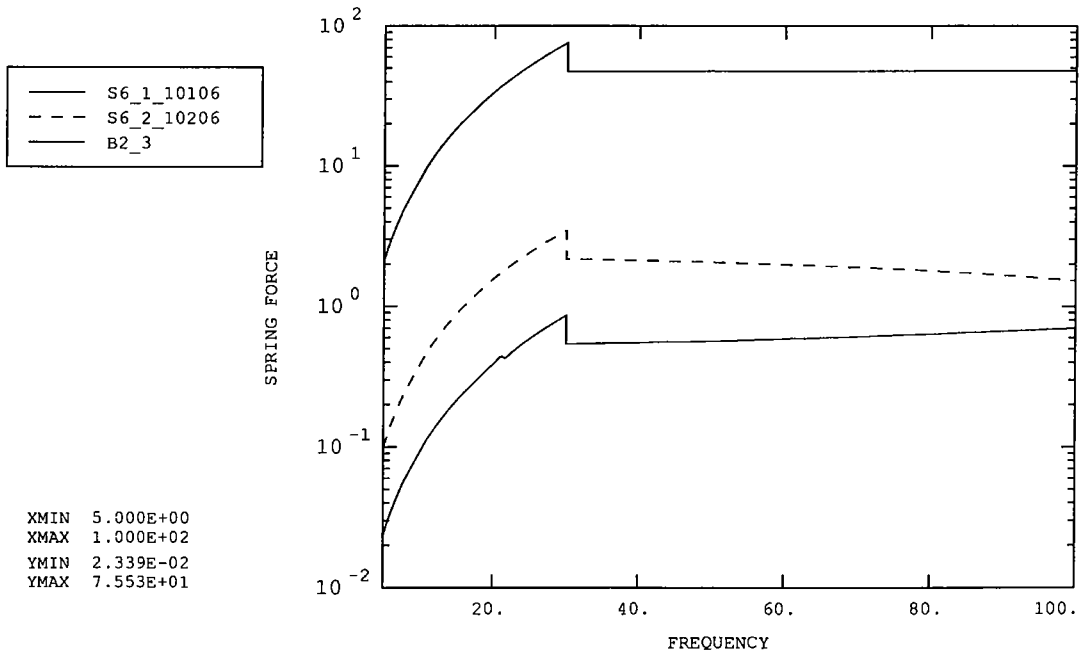

Figure 34: Base (back left)

© FNC 2002

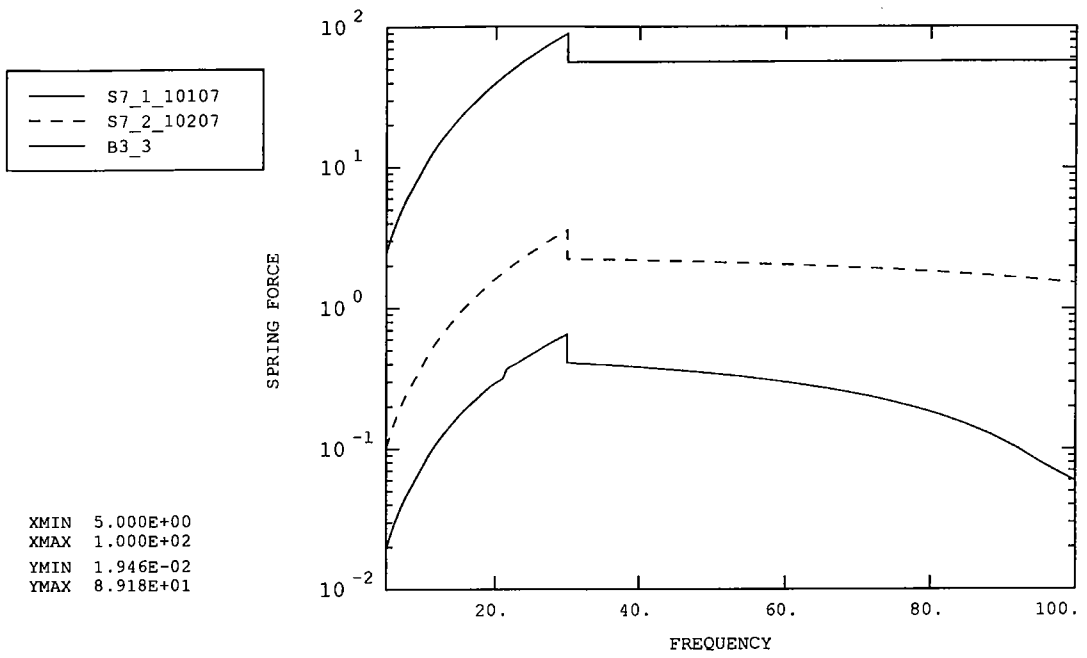

Figure 35: Base (back right)

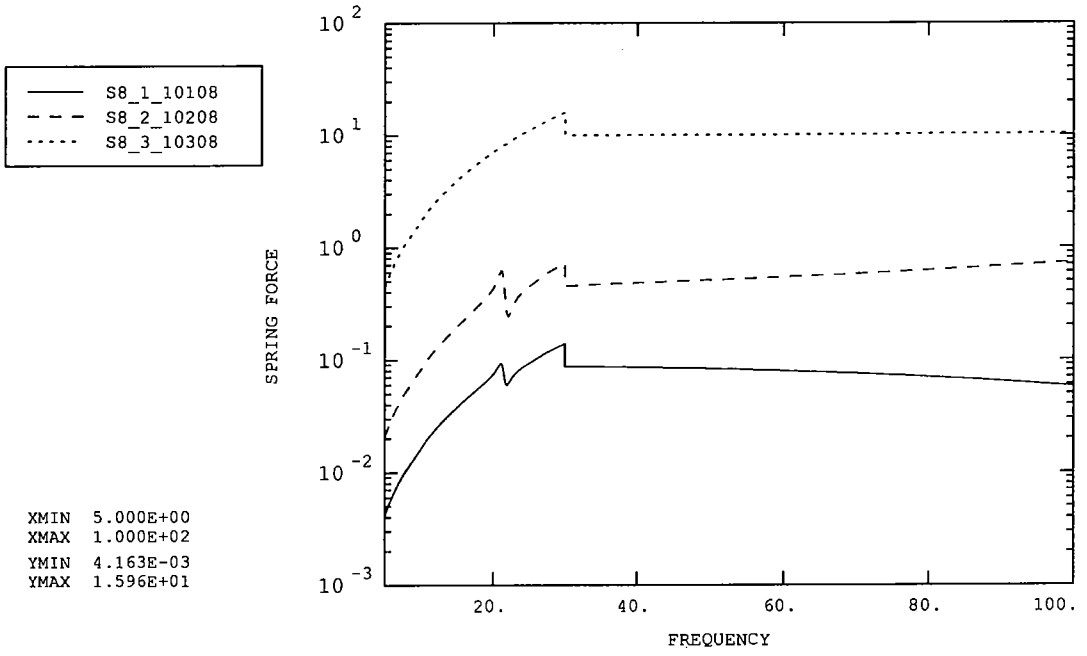

Figure 36: Jiggle pivot (top)

© FNC 2002

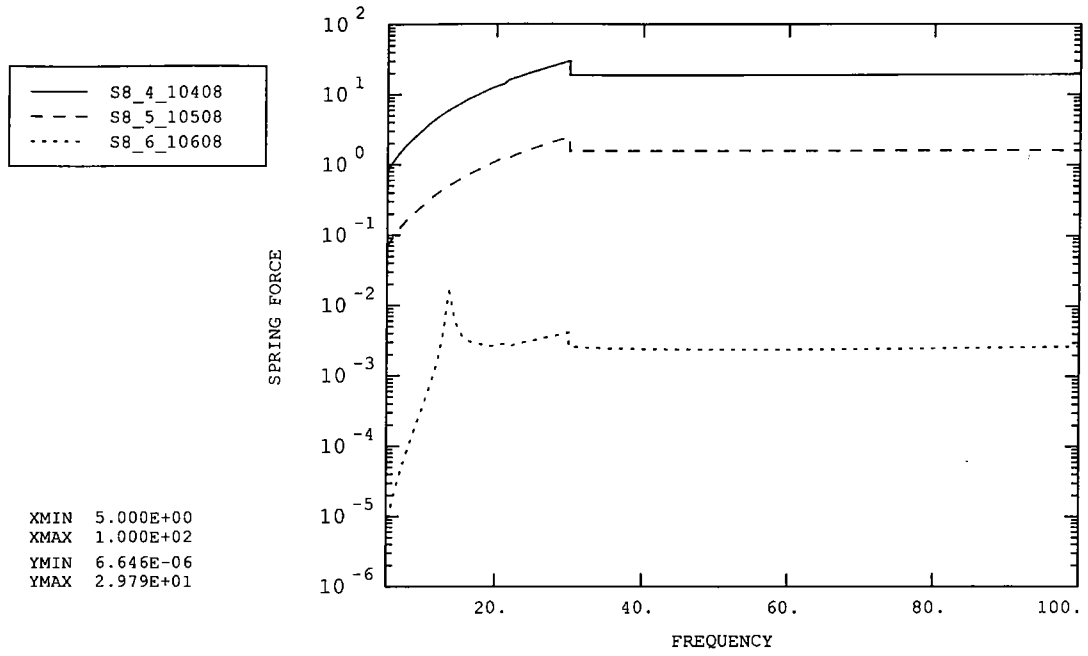

Figure 37: Jiggle pivot (top)

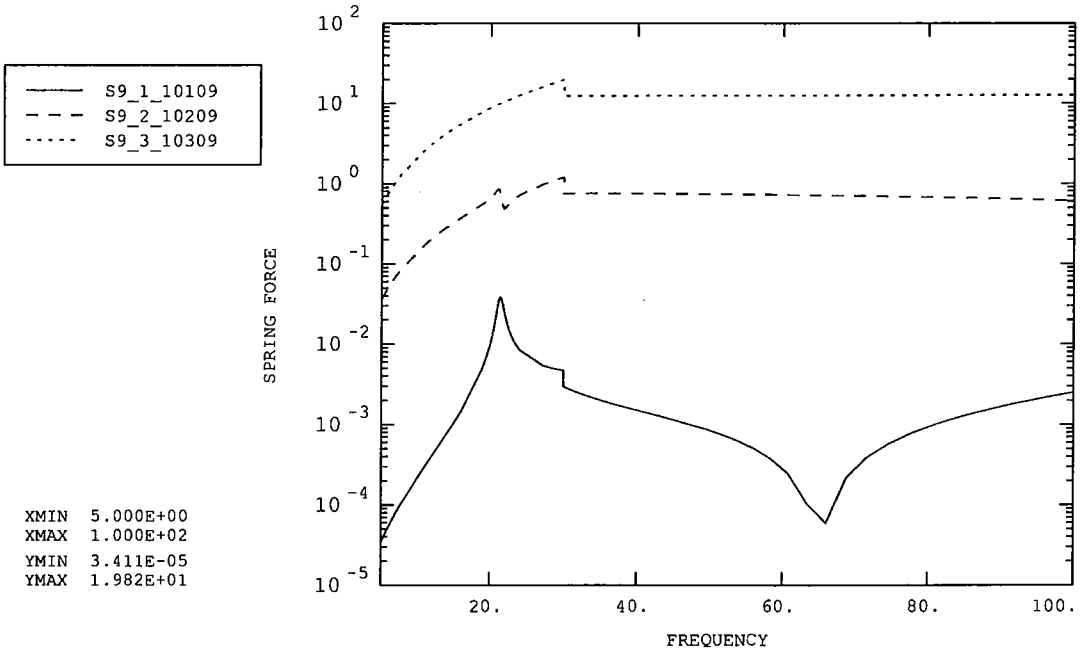

Figure 38: Jiggle pivot (bottom)

© FNC 2002

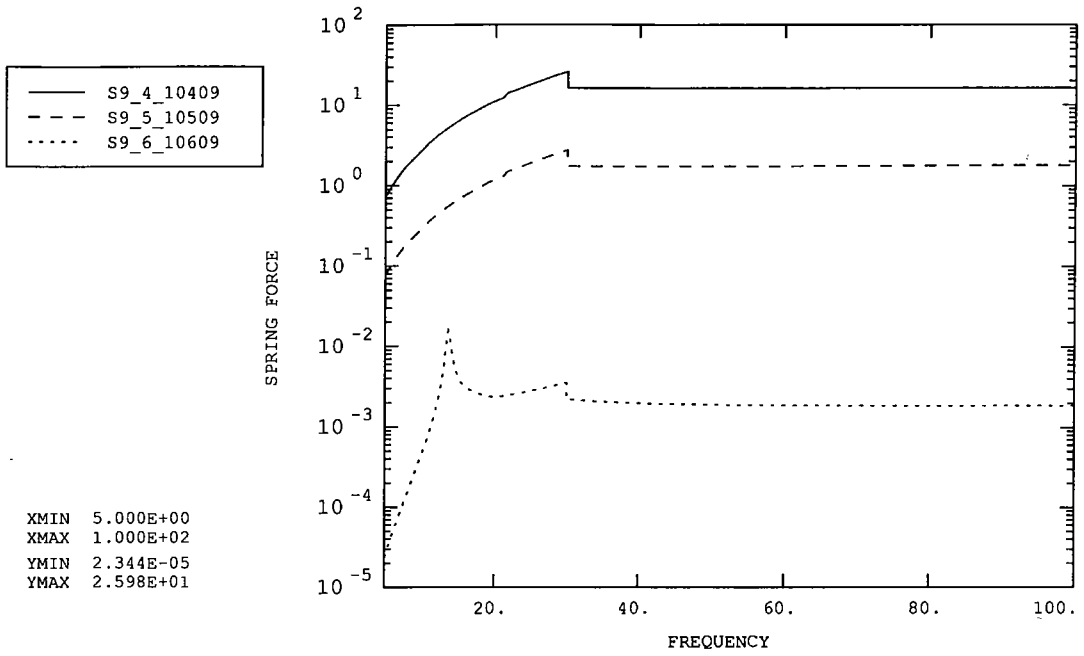

Figure 39: Jiggle pivot (bottom)

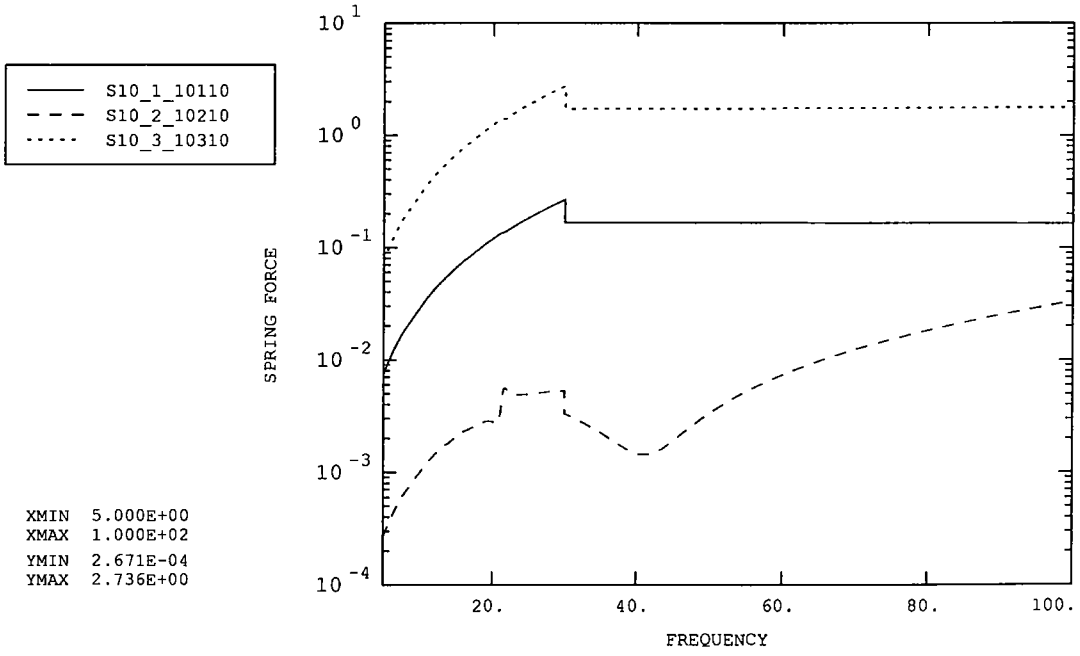

Figure 40: Chop pivot (left)

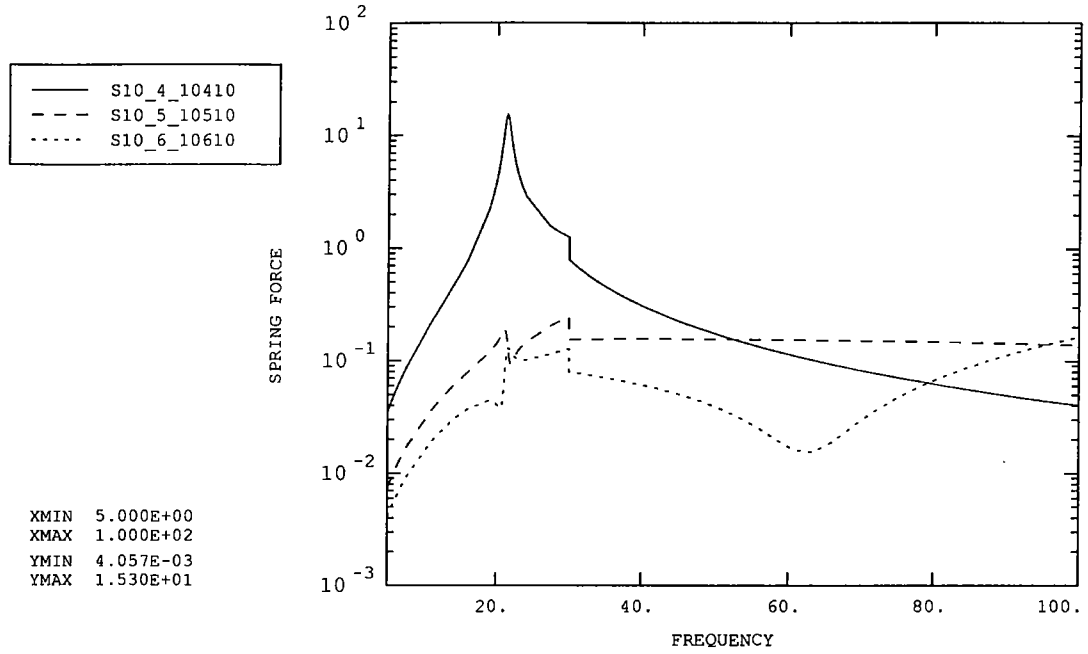

Figure 41: Chop pivot (left)

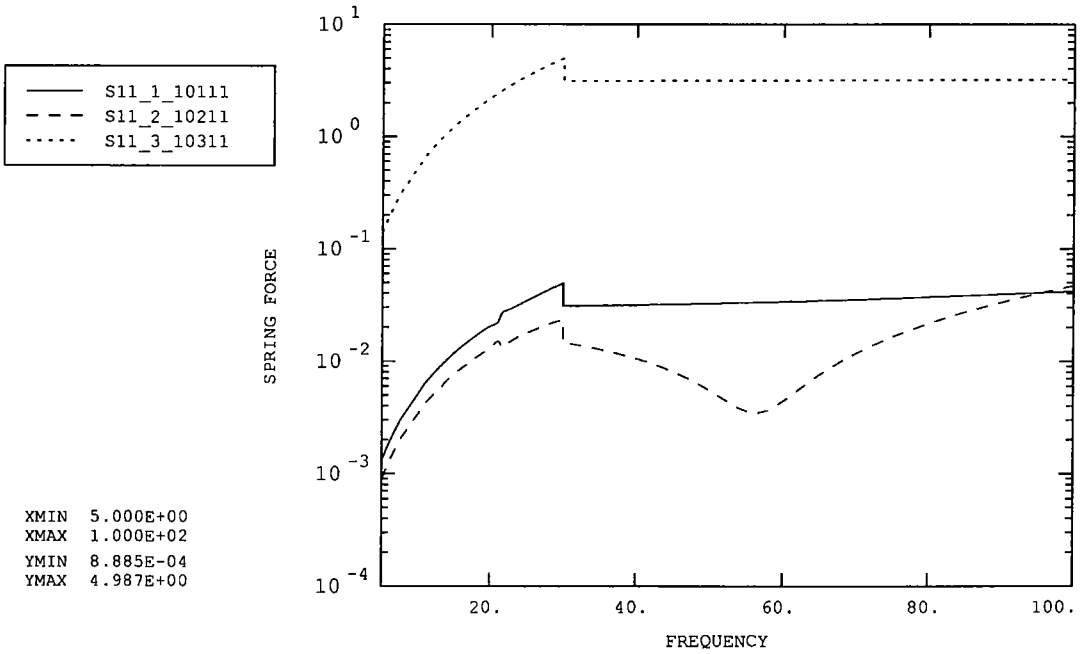

Figure 42: Chop pivot (right)

© FNC 2002

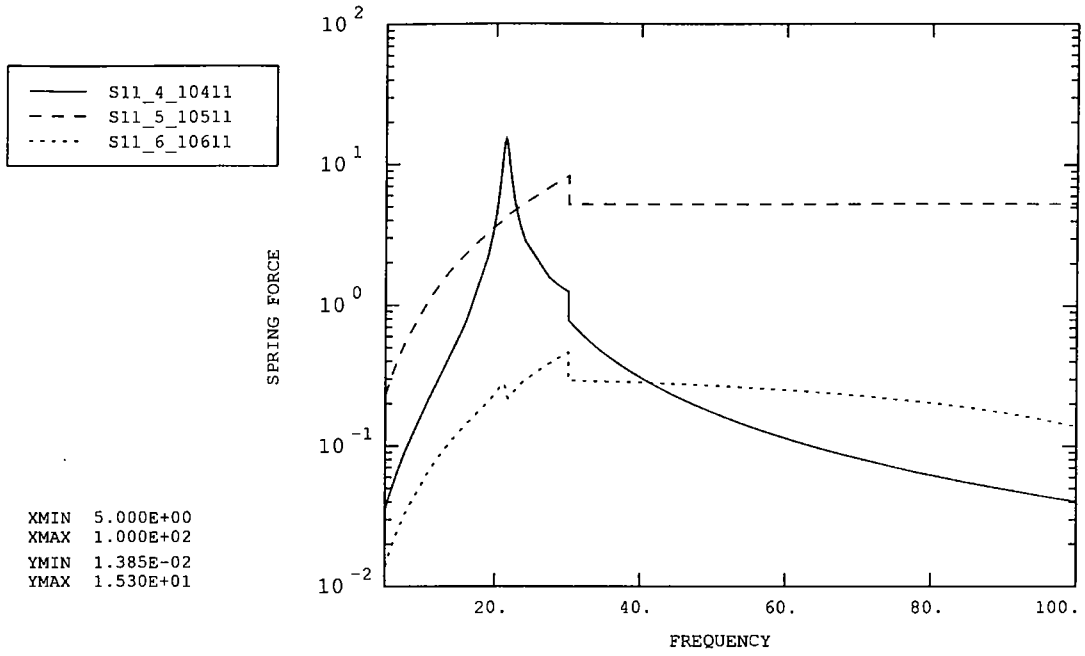

Figure 43: Chop pivot (right)

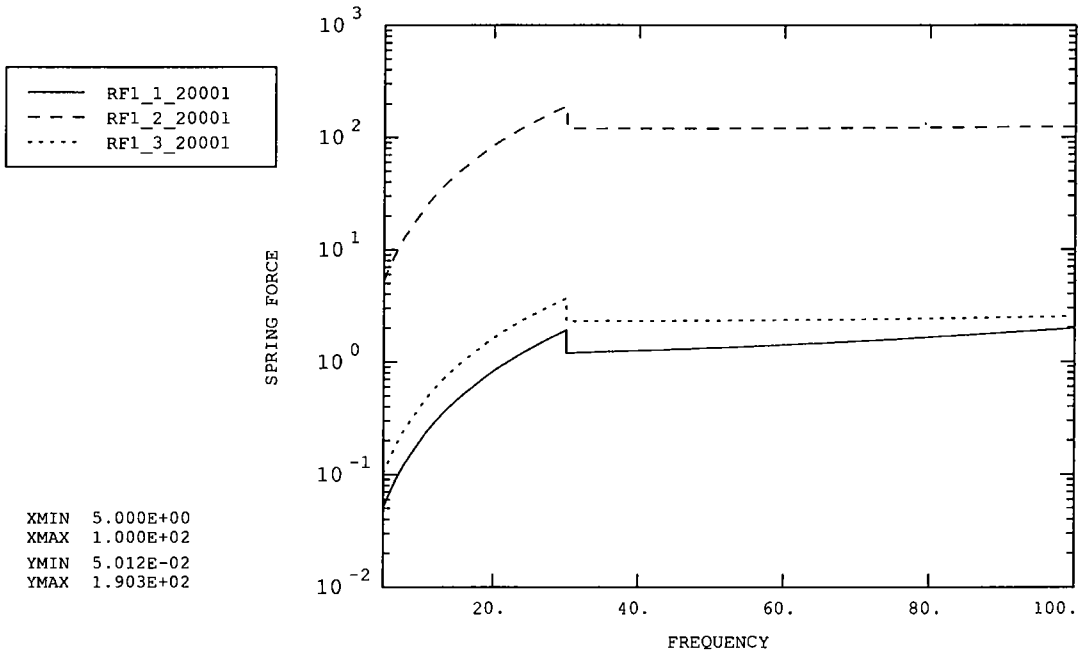

Figure 44: Reaction Force (front middle)

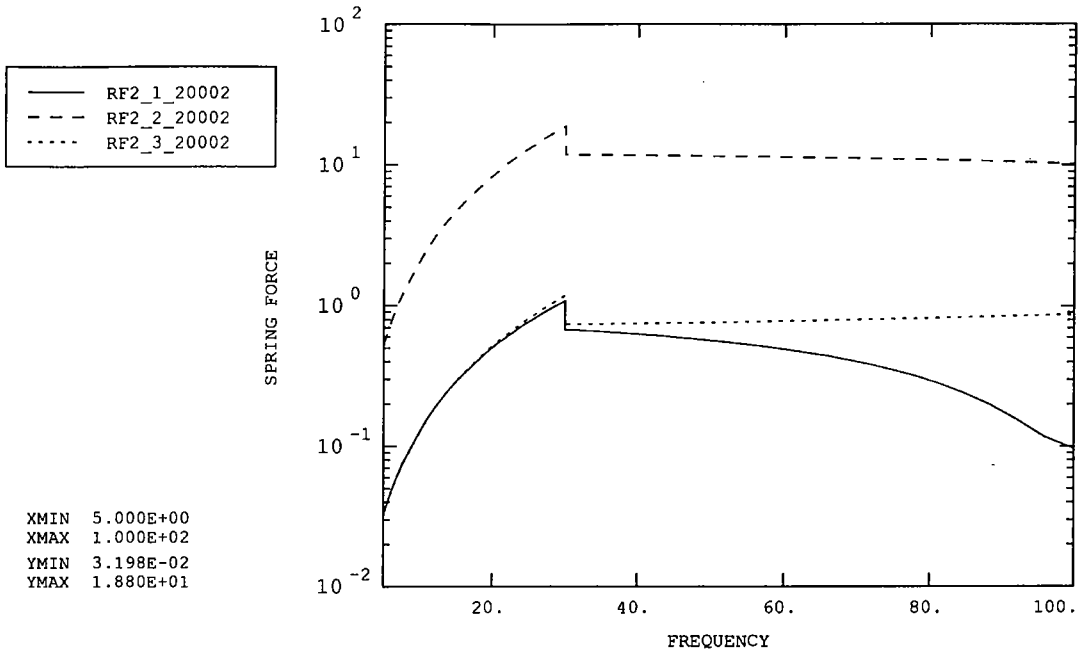

Figure 45: Reaction Force (back left)

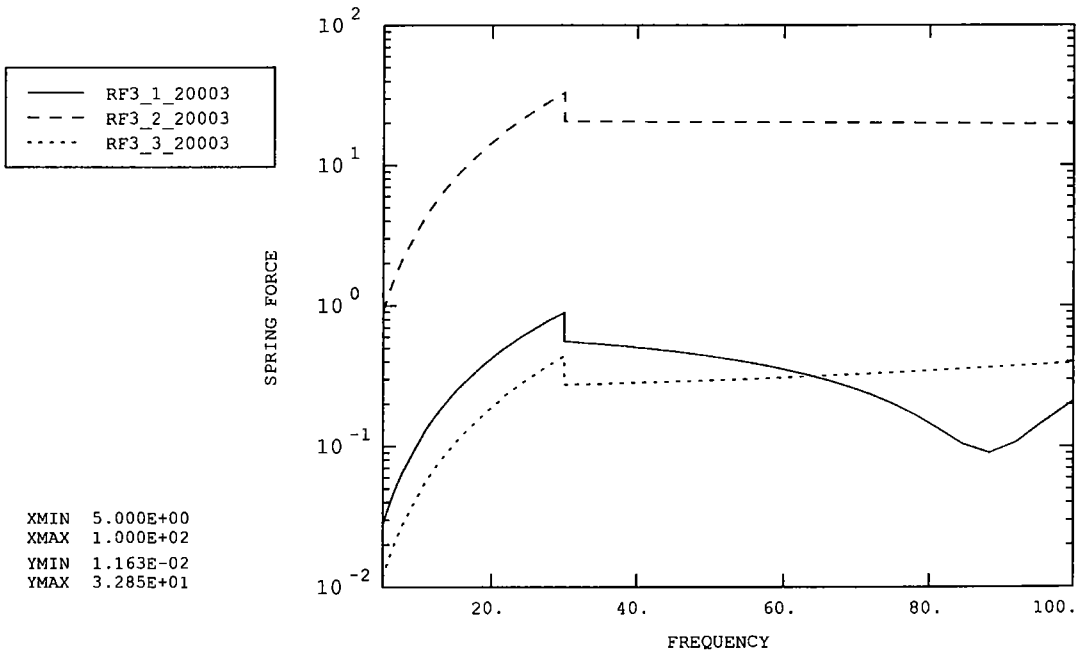

Figure 46: Reaction Force (back right)

© FNC 2002

SPIRE BSM VIBRATION ANALYSIS

Annex 3 - Swept Sine Z-Direction

FNC 5505/24072R Issue 1

Prepared for

U.K. Astronomy Technology Centre

DOCUMENT INFORMATION

Project : SPIRE BSM Vibration Analysis

Report Title : Annex 3 - Swept Sine Z-Direction

Client : U.K. Astronomy Technology Centre

Client Ref. : 024706

Classification :

Report No. : FNC 5505/24072R

Issue No. : 1

Compiled By : D C Reed
A J Vibert

Date : May 2002

Approved By : M W Anderson

DISTRIBUTION

Copy	Recipient	Organisation
1	I Pain	UK ATC
2	I Pain	UK ATC
3	I Pain	UK ATC
4	File	FNC

Copy No. ____

COPYRIGHT

The Copyright in this work is vested in Frazer-Nash Consultancy Limited. The document is issued in confidence solely for the purpose for which it is supplied. Reproduction in whole or in part or use for tendering or manufacturing purposes is prohibited except under an agreement with or with the written consent of Frazer-Nash Consultancy Limited and then only on the condition that this notice is included in any such reproduction.

Originating Office: FRAZER-NASH CONSULTANCY LIMITED
Stonebridge House, Dorking Business Park, Dorking, Surrey RH4 1HJ, UK
T: +44 (0)1306 885050 F: +44 (0)1306 886464 E: info@fnc.co.uk W: www.fnc.co.uk

DATA POINT POSITIONS

Note:

- The labels on the plots are as follows: e.g. P9_1_12184 refers to acceleration data point P9, degree of freedom 1 (node number 12184).
- Degrees of freedom 1, 2 and 3 refer to motion in the x, y and z directions (or X, Y and Z directions), while degrees of freedom 4, 5 and 6 refer to rotations about the x, y and z axes (or X, Y and Z axes).
- Acceleration is total acceleration (i.e. includes base motion)
- Accelerations and reaction forces are given in the global X, Y, Z co-ordinates
- Relative displacements and spring forces/torques are given in the local model x, y, z co-ordinates.
- 'Left' and 'right' directions are defined from a point of view looking towards the mirror surface, with the top of the casing furthest from the baseplate.

Fig.	P	Acceleration data points	Node number
1	1	Jiggle axis pivot (top) – frame	12182
2	2	Jiggle axis pivot (top) – jiggle stage	12200
3	3	Jiggle axis pivot (bottom) – frame	12183
4	4	Jiggle axis pivot (bottom) – jiggle stage	12192
5	5	Chop axis pivot (right side) – jiggle stage	12189
6	6	Chop axis pivot (right side) – chop stage	114
7	7	Chop axis pivot (left side) – jiggle stage	12188
8	8	Chop axis pivot (left side) – chop stage	105
9	9	Chop motor (top)	12184
10	10	Chop motor (bottom)	12185
11	11	Jiggle motor (right side)	12186
12	12	Jiggle motor (left side)	12187
13	13	PCAL CG	12193
14	14	PCAL extension to mirror centre	12199
15	15	Launch latch 'A' CG	12196
16	16	Launch latch 'A' extension to magnet centre	12197
17	17	Connector (top)	12194
18	18	Chop magnet (top)	115
19	19	Chop magnet (bottom)	122
20	20	Mirror Centre	9583
21	21	Jiggle magnet (right)	9276
22	22	Jiggle magnet (left)	9264

© FNC 2002

Fig.	E	Displacement between...	Element
23	1	Chop magnet vs. motor (top)	90n01, n=1, 2
24	2	Chop magnet vs. motor (bottom)	90n02, n=1, 2
25	3	Jiggle magnet vs. motor (right)	90n03, n=2, 3
26	4	Jiggle magnet vs. motor (left)	90n04, n=2, 3
27	5	Mirror centre vs. PCAL extension	90n05, n=1, 2, 3
28	6	Chop magnet (top) vs. launch latch 'A'	90206

Fig.	S	Position of spring elements	Node 1	Element
29	1	Front baffle (top left)	9702	10n01, n=1,2,3
30	2	Front baffle (top right)	9739	10n02, n=1,2,3
31	3	Front baffle (bottom left)	9629	10n03, n=1,2,3
32	4	Front baffle (bottom right)	9594	10n04, n=1,2,3
33	5	Base (front middle)*	3894	10n05, n=1,2,3
34	6	Base (back left)*	3414	10n06, n=1,2,3
35	7	Base (back right)*	3622	10n07, n=1,2,3
36,37	8	Jiggle pivot (top)	12200	10n08, n=1 to 6
38,39	9	Jiggle pivot (bottom)	12192	10n09, n=1 to 6
40,41	10	Chop pivot (left)	12188	10n10, n=1 to 6
42,43	11	Chop pivot (right)	12189	10n11, n=1 to 6

Fig.	RF	Reaction Forces	Node number
44	1	Reaction Force (front middle)	10587
45	2	Reaction Force (back left)	10722
46	3	Reaction Force (back right)	10671

* The baseplate-casing connections are each modelled using a single spring in the local x and y directions, and five springs in the local z direction. The forces from these five springs are added together to calculate the total connective force. The curve labels for the z direction degrees of freedom have the prefix 'B'.

© FNC 2002

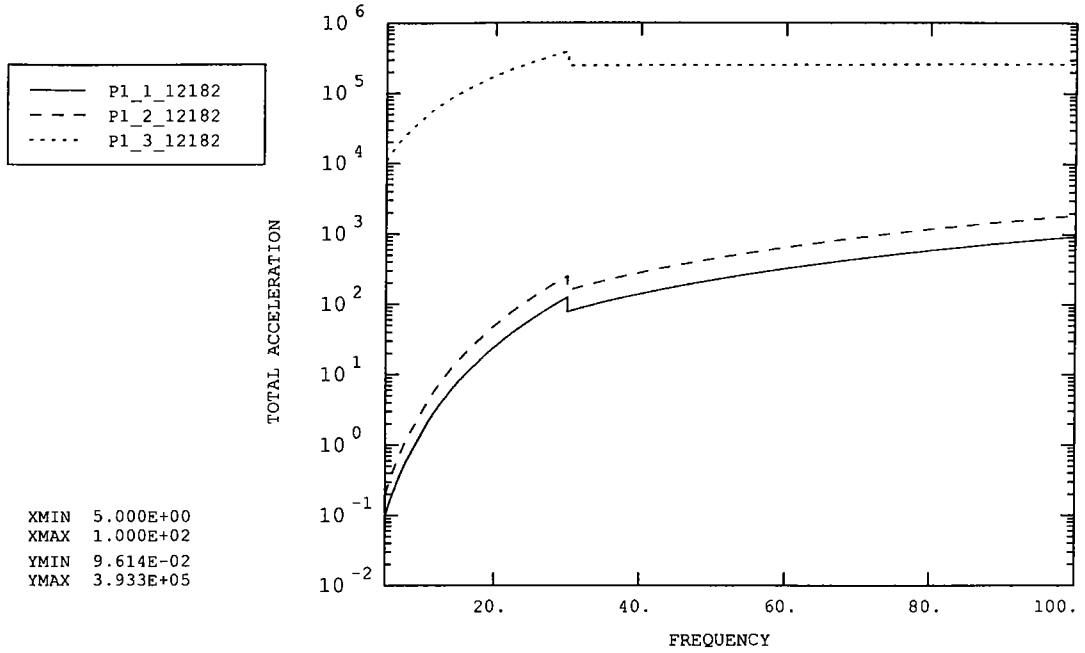

Figure 1: Jiggle axis pivot (top) – frame

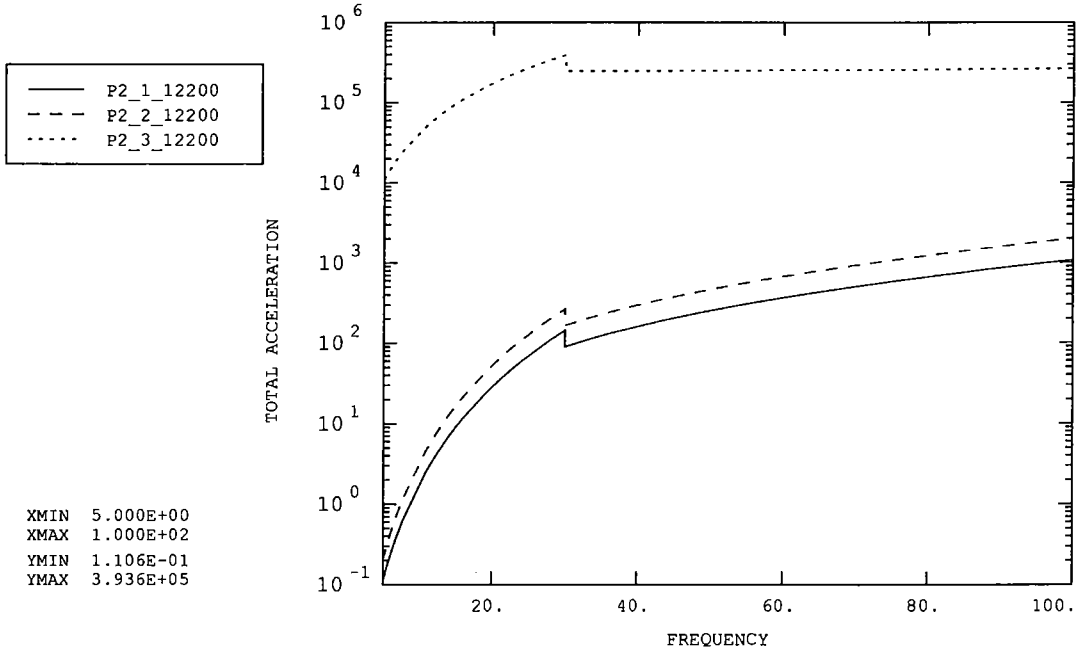

Figure 2: Jiggle axis pivot (top) – jiggle stage

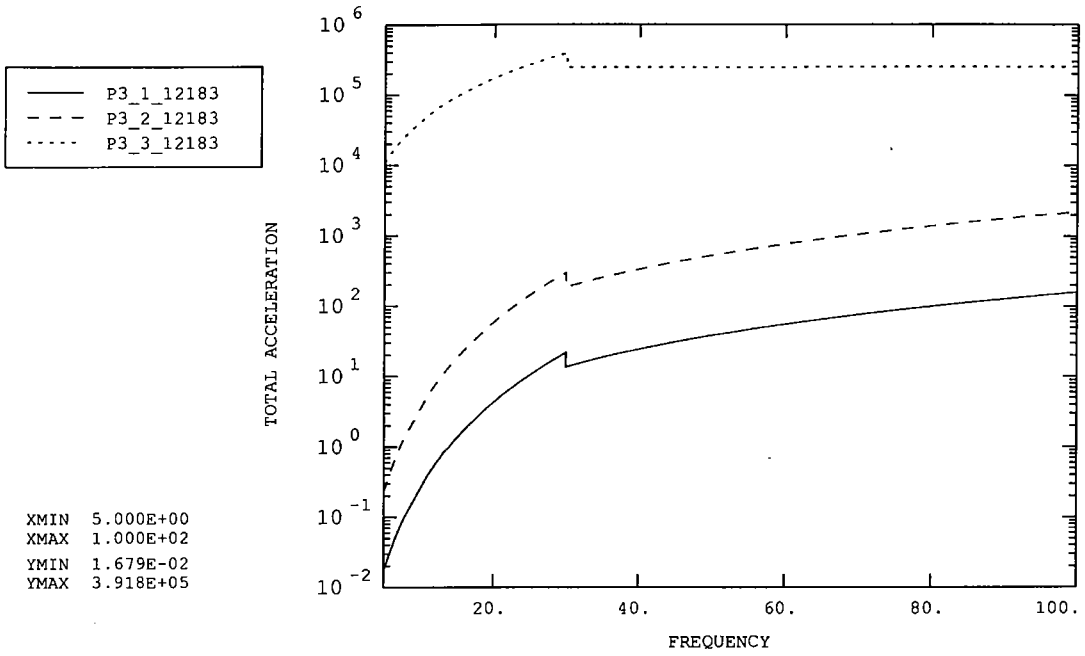

Figure 3: Jiggle axis pivot (bottom) – frame

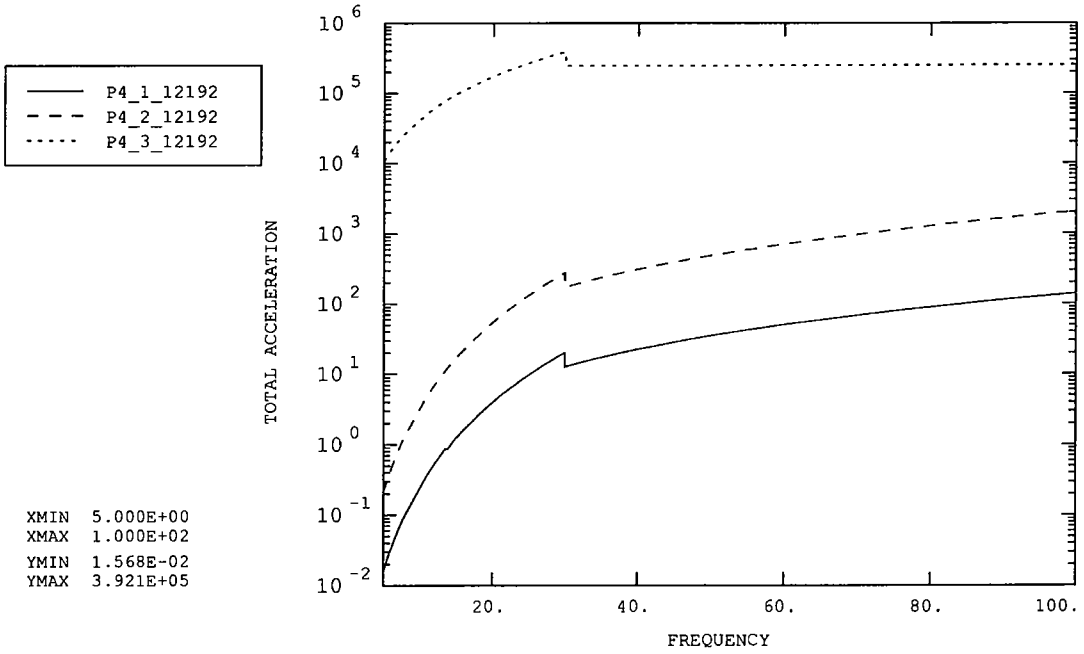

Figure 4: Jiggle axis pivot (bottom) – jiggle stage

© FNC 2002

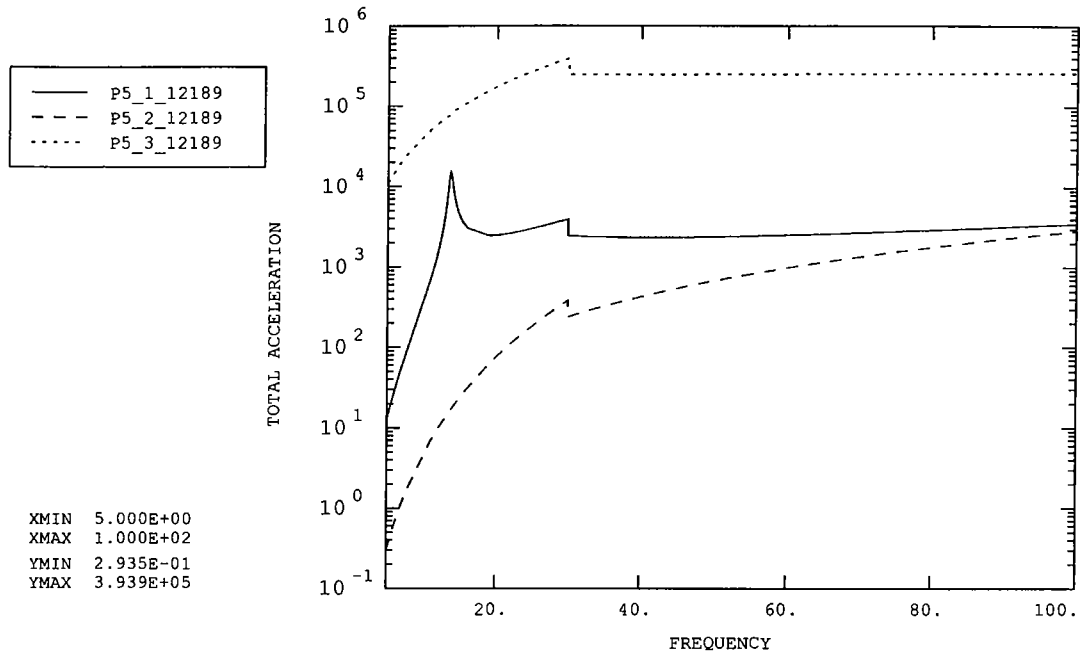

Figure 5: Chop axis pivot (right side) – jiggle stage

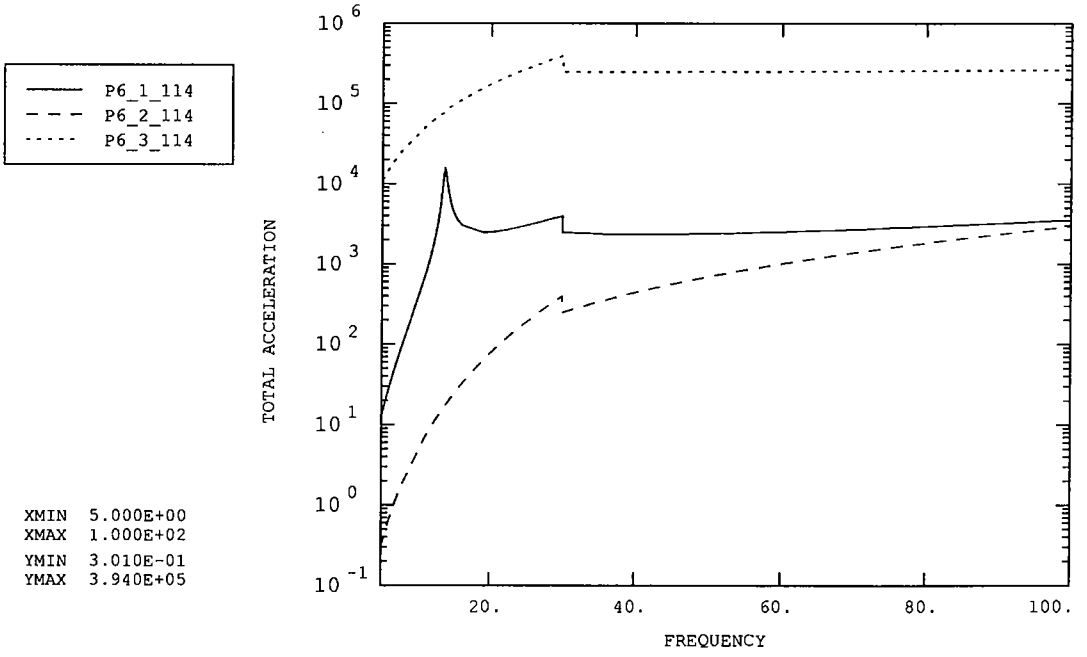

Figure 6: Chop axis pivot (right side) – chop stage

© FNC 2002

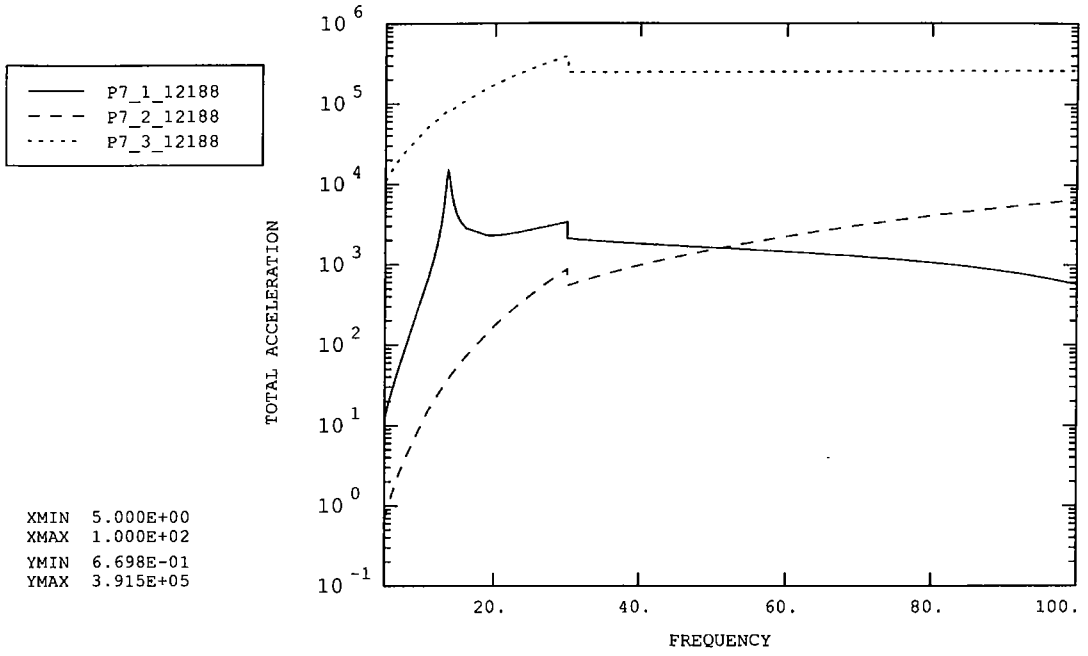

Figure 7: Chop axis pivot (left side) – jiggle stage

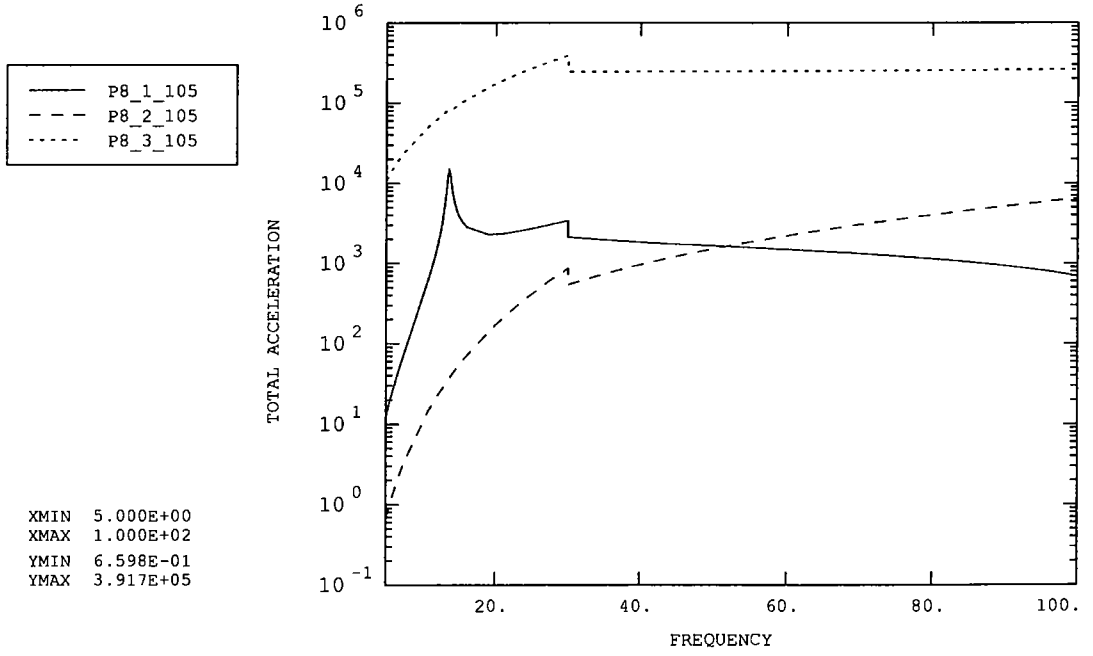

Figure 8: Chop axis pivot (left side) – chop stage

© FNC 2002

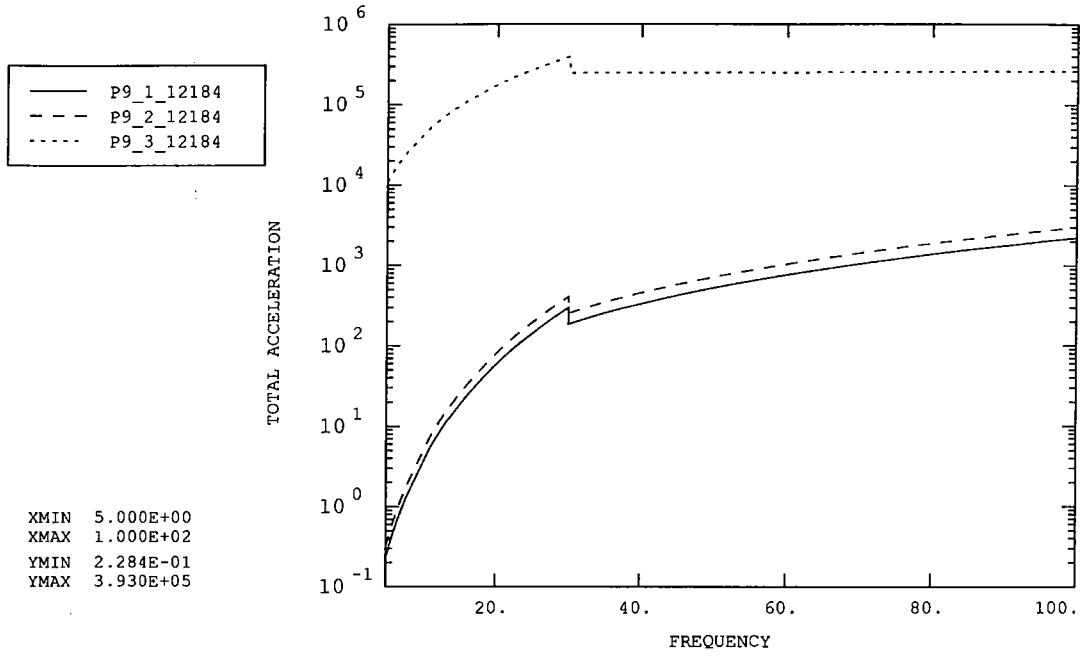

Figure 9: Chop motor (top)

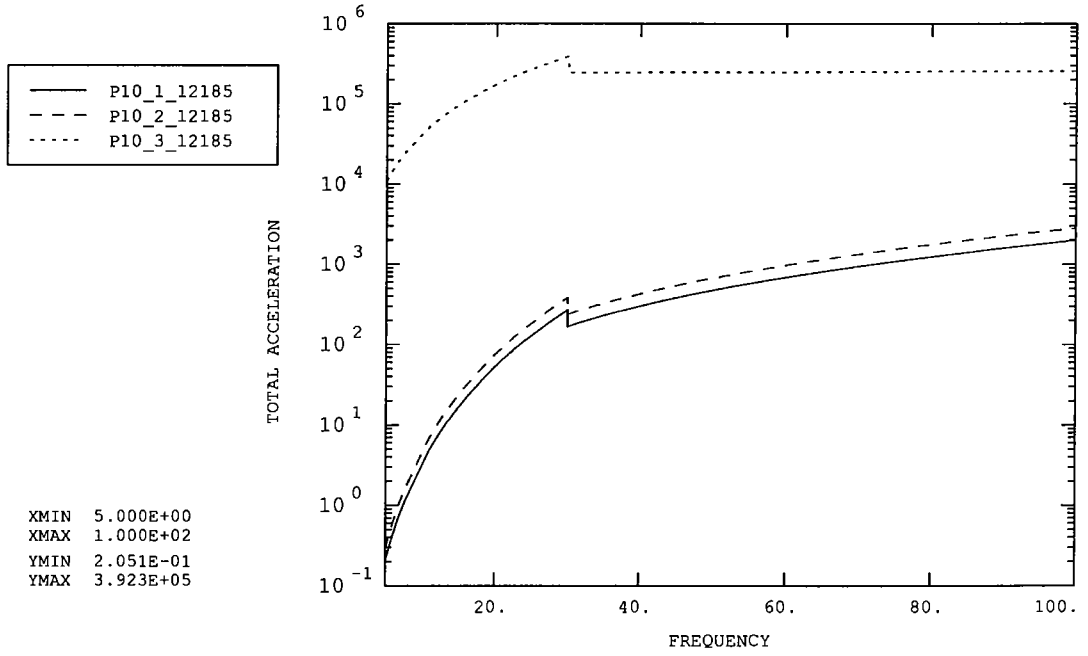

Figure 10: Chop motor (bottom)

© FNC 2002

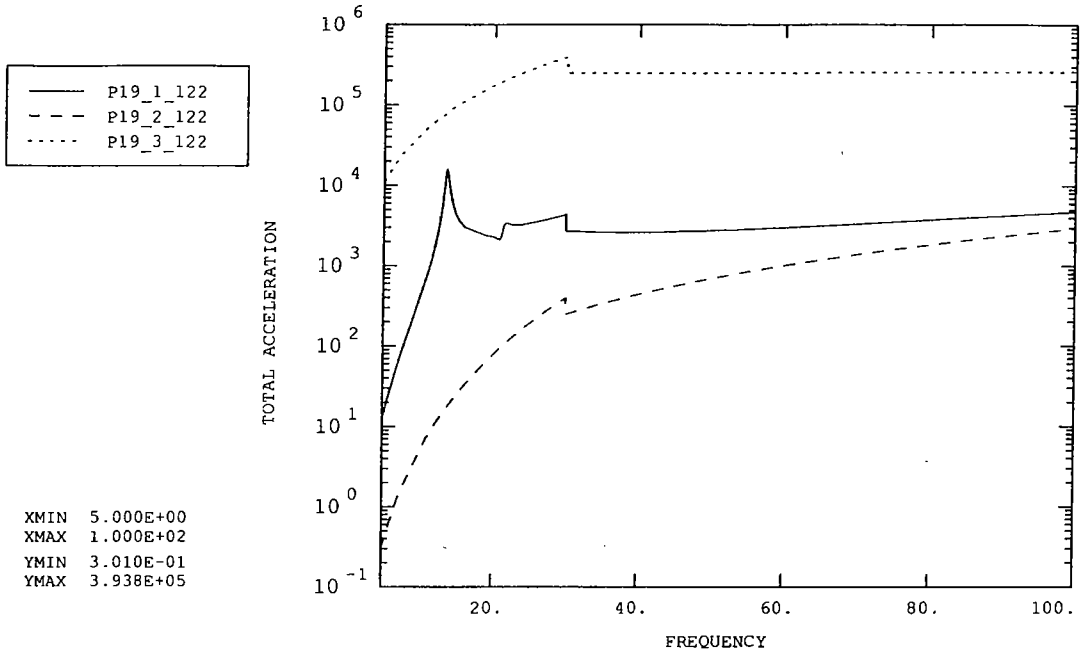

Figure 19: Chop magnet (bottom)

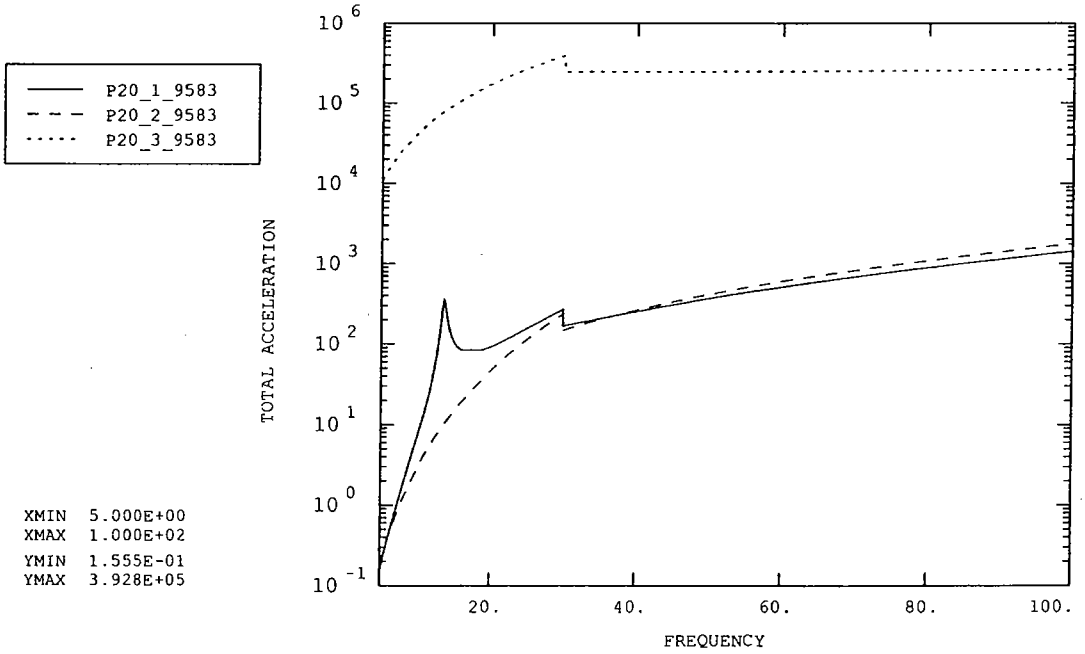

Figure 20: Mirror Centre

© FNC 2002

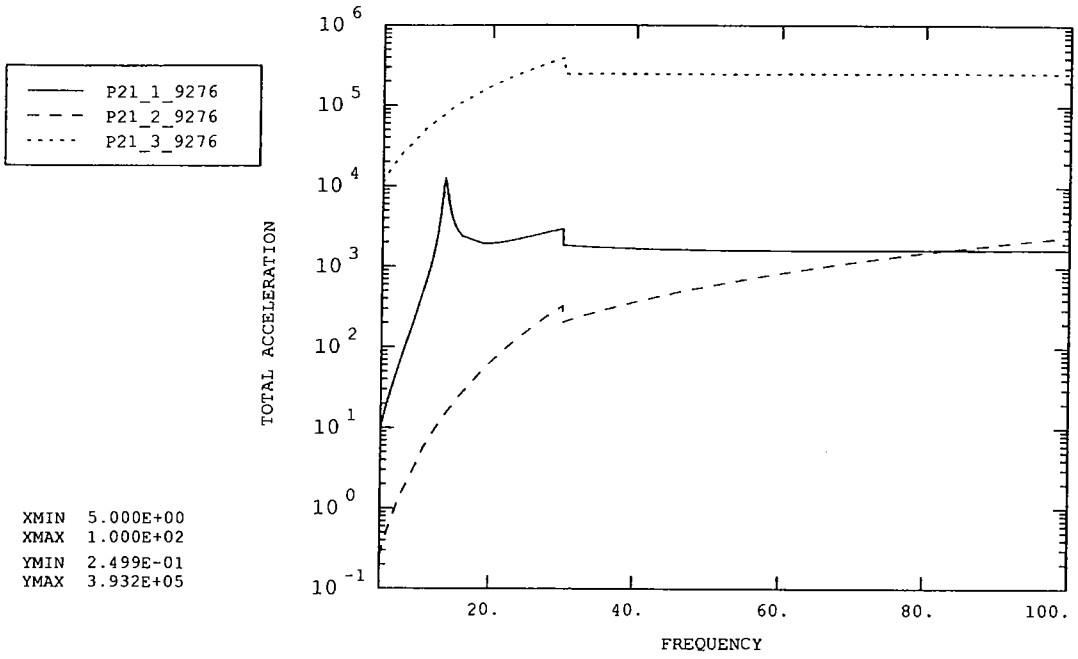

Figure 21: Jiggle magnet (right)

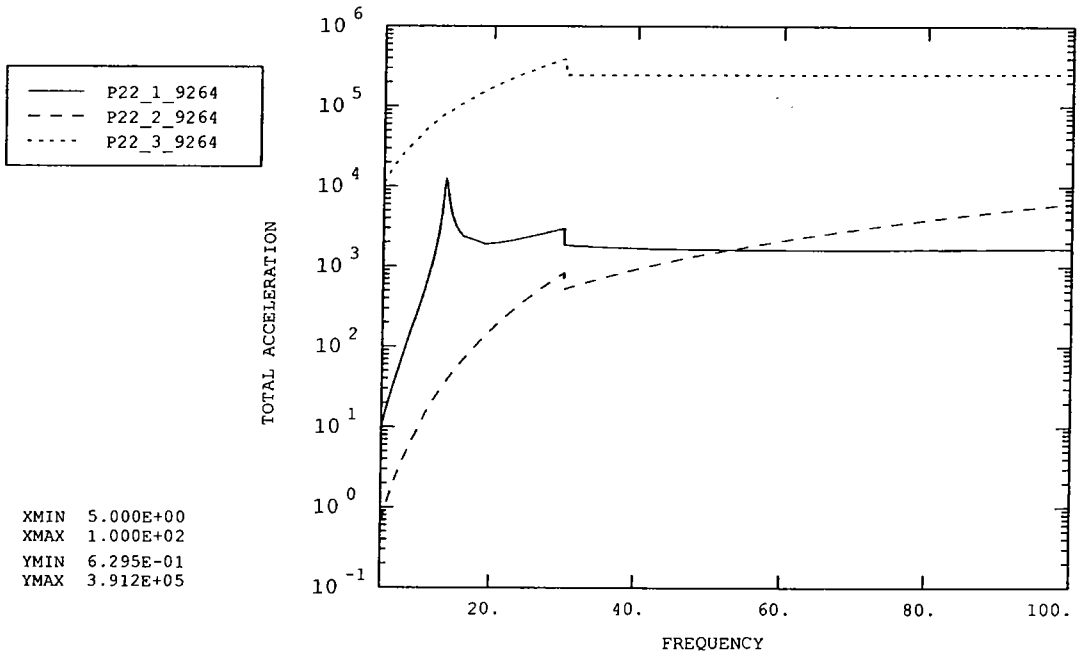

Figure 22: Jiggle magnet (left)

© FNC 2002

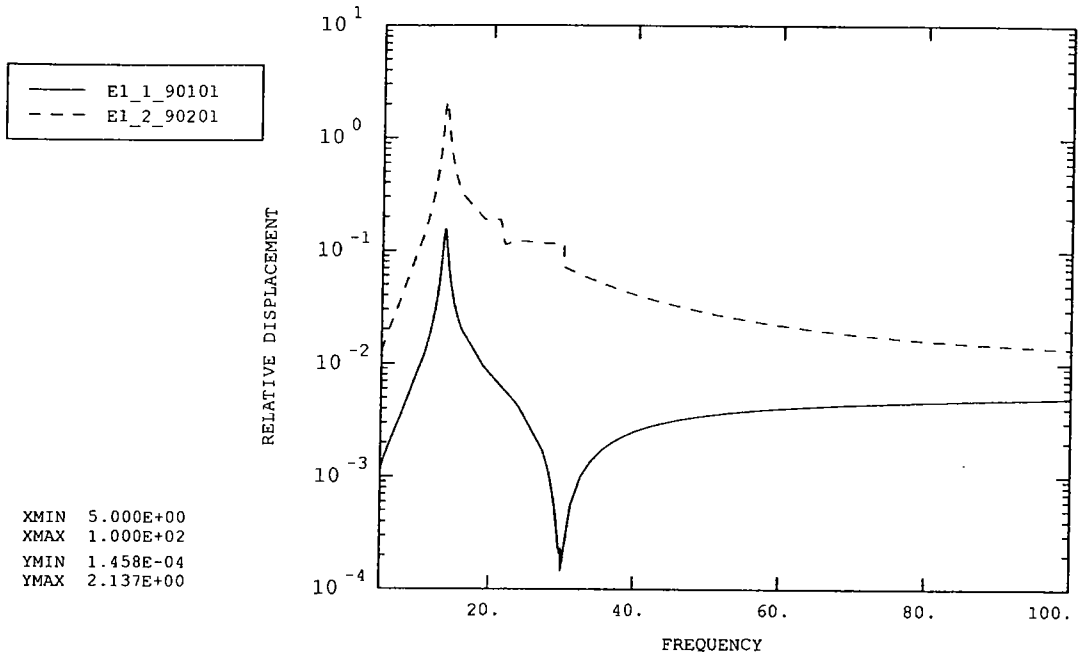

Figure 23: Chop magnet vs. motor (top)

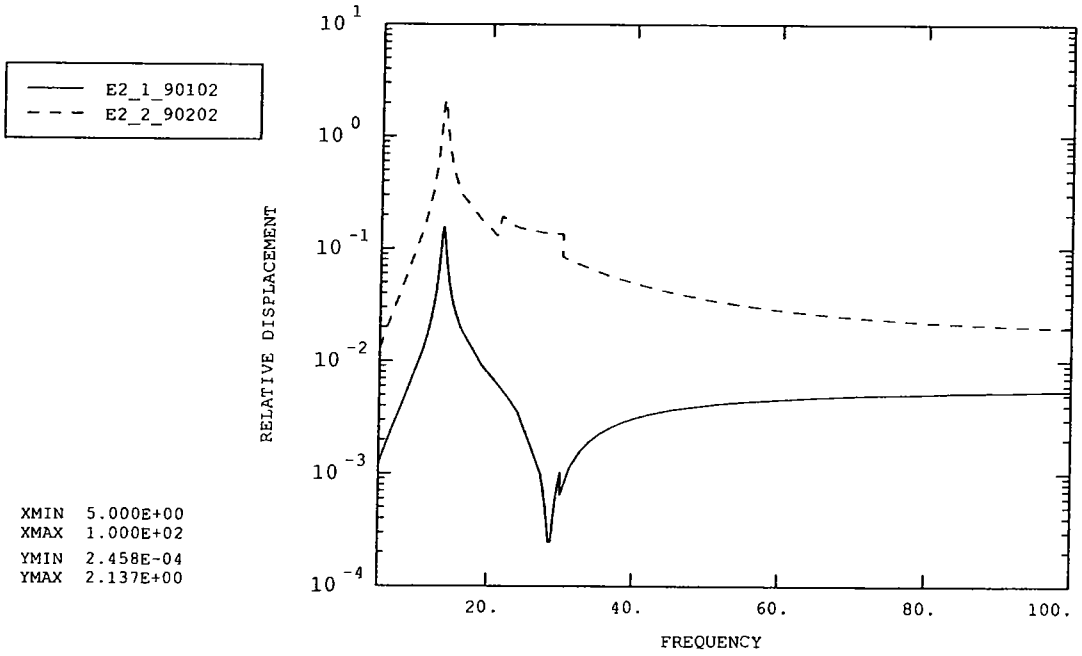

Figure 24: Chop magnet vs. motor (bottom)

© FNC 2002

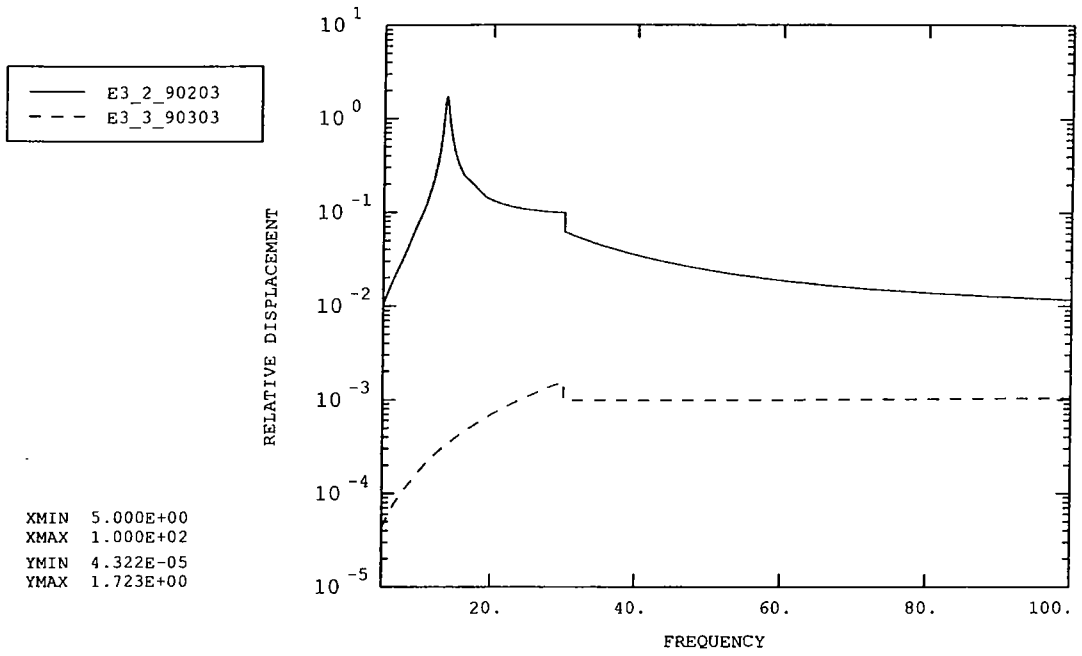

Figure 25: Jiggle magnet vs. motor (right)

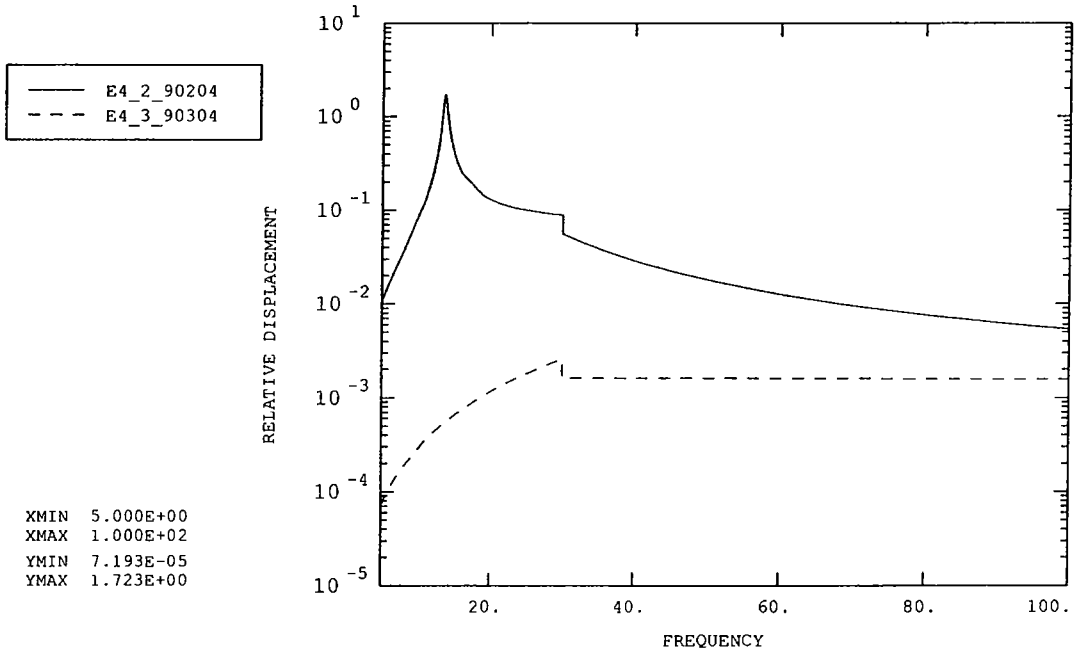

Figure 26: Jiggle magnet vs. motor (left)

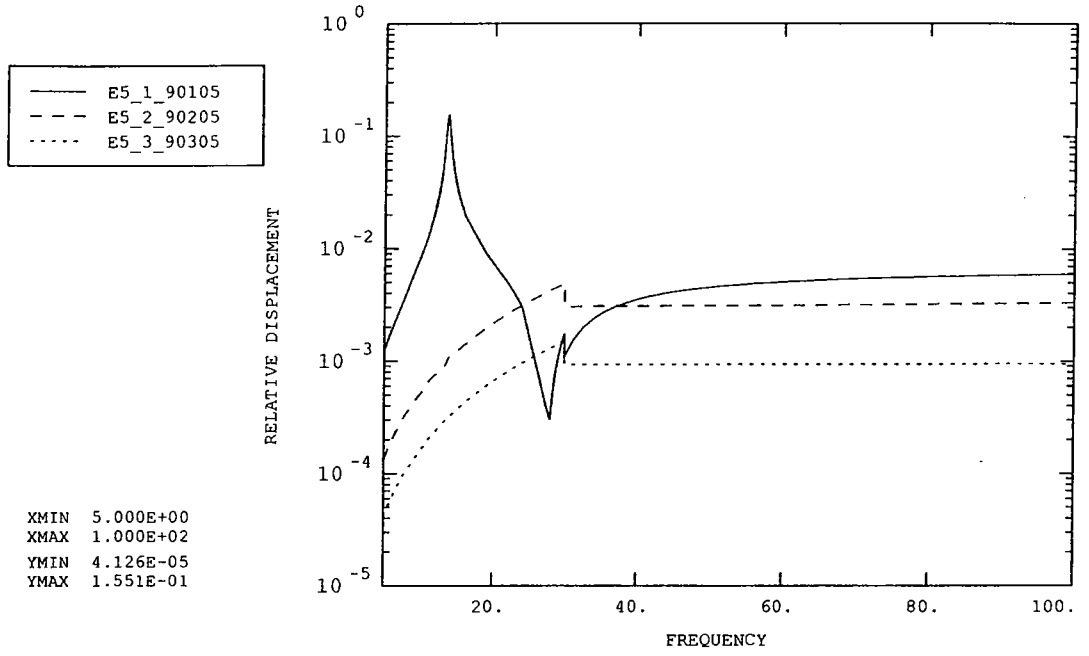

Figure 27: Mirror centre vs. PCAL extension

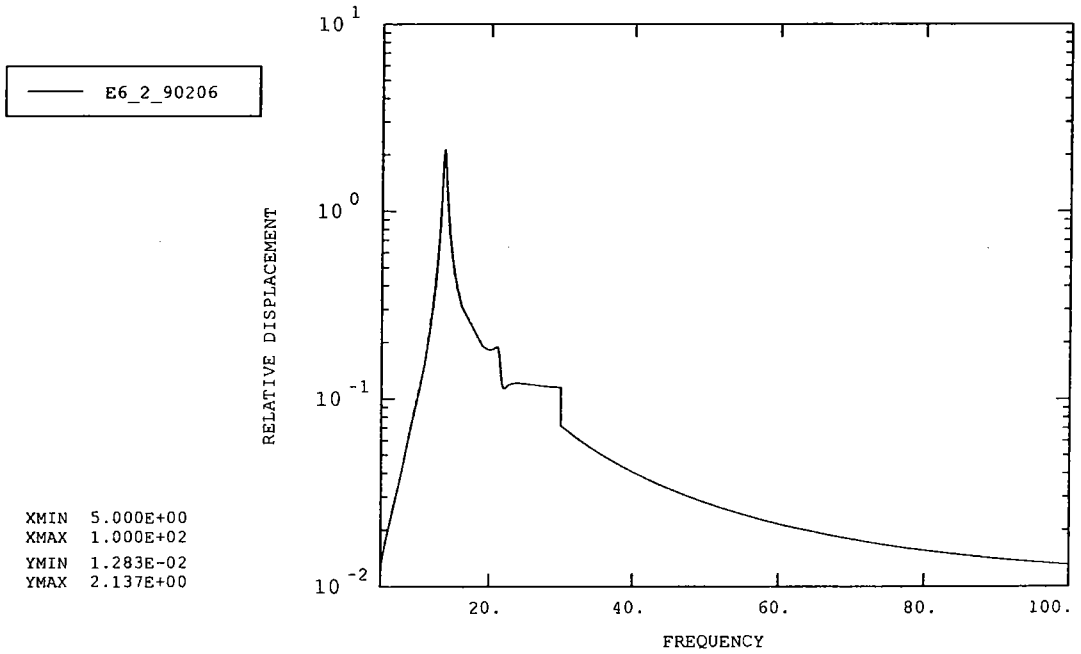

Figure 28: Chop magnet (top) vs. launch latch 'A'

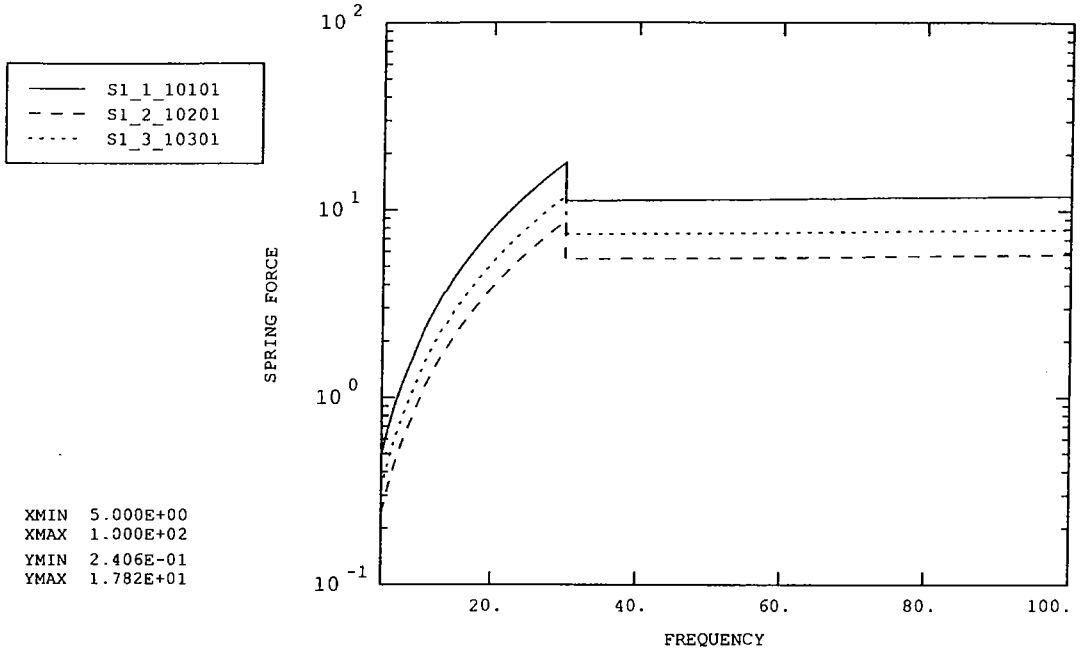

Figure 29: Front baffle (top left)

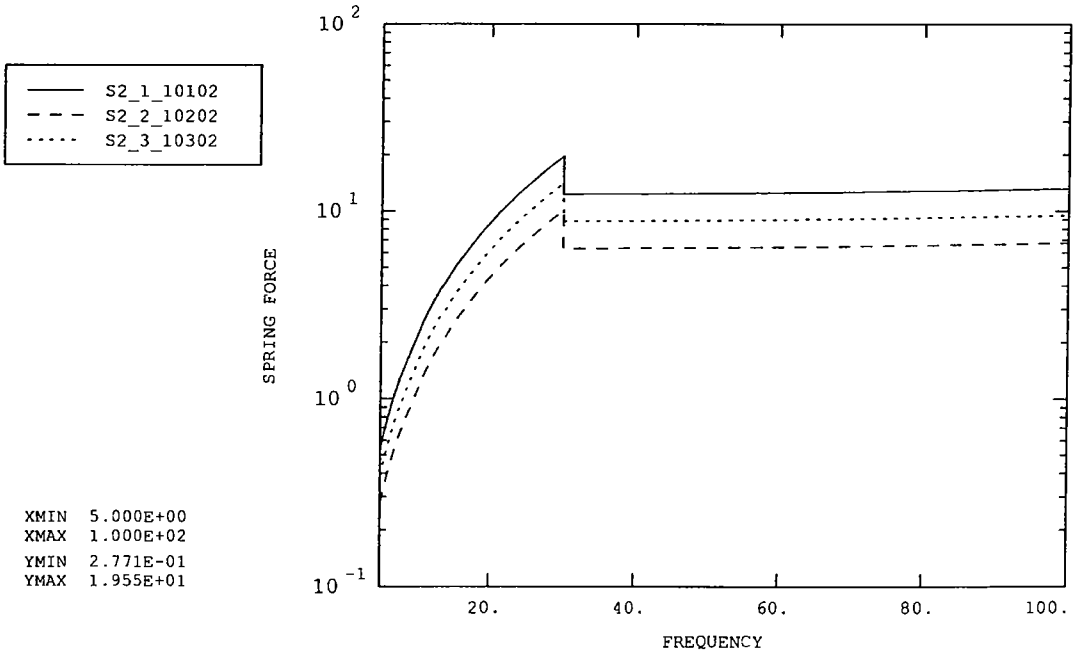

Figure 30: Front baffle (top right)

© FNC 2002

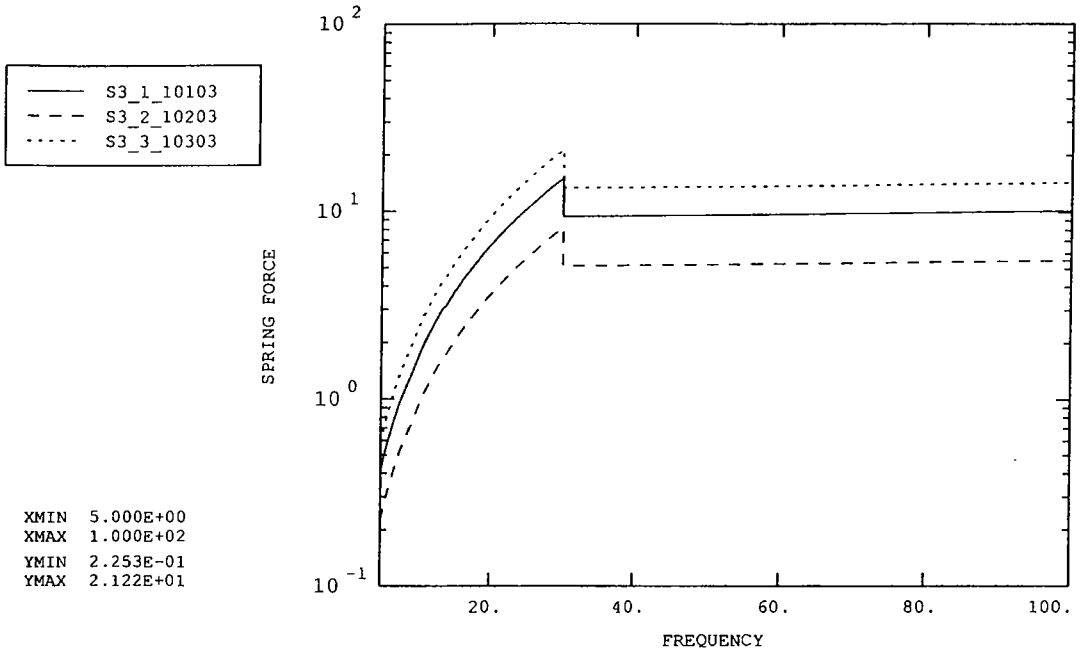

Figure 31: Front baffle (bottom left)

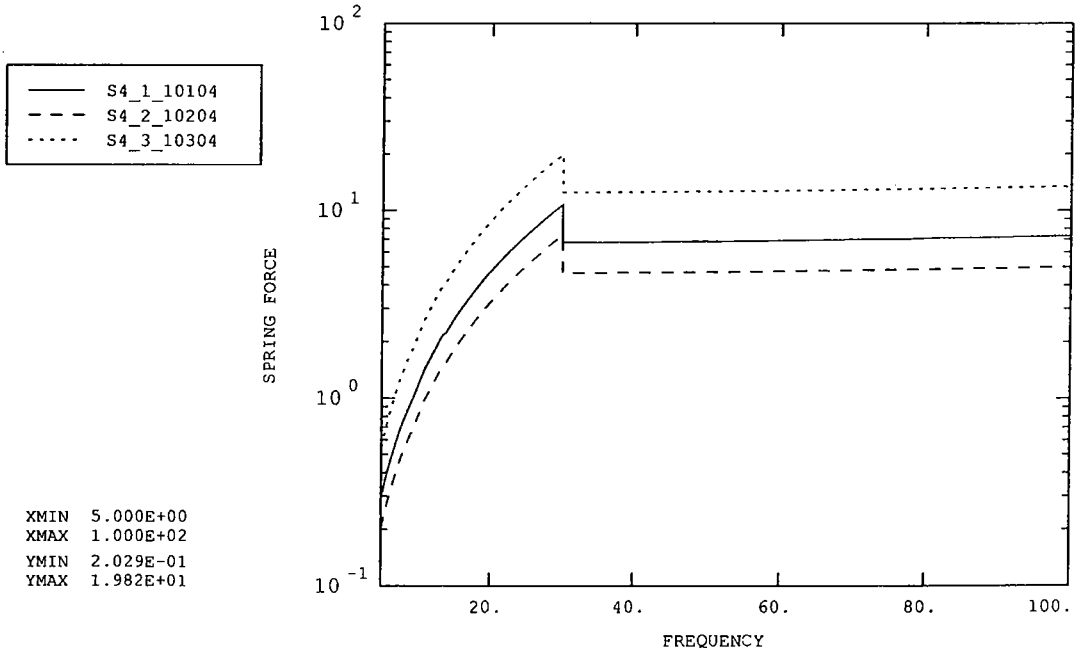

Figure 32: Front baffle (bottom right)

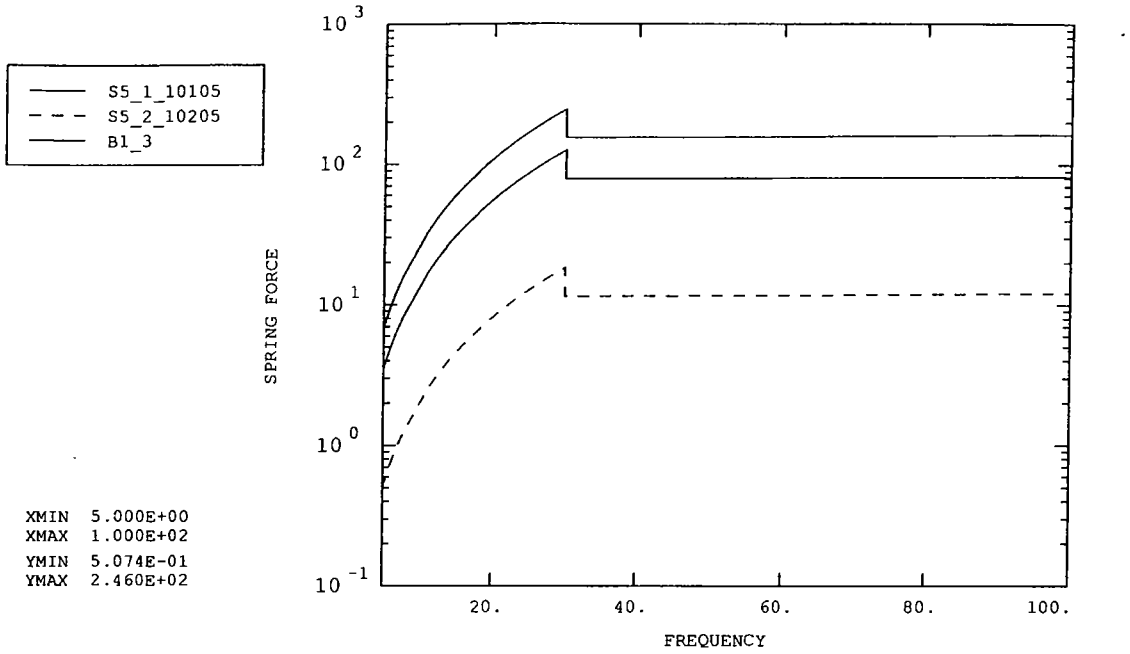

Figure 33: Base (front middle)

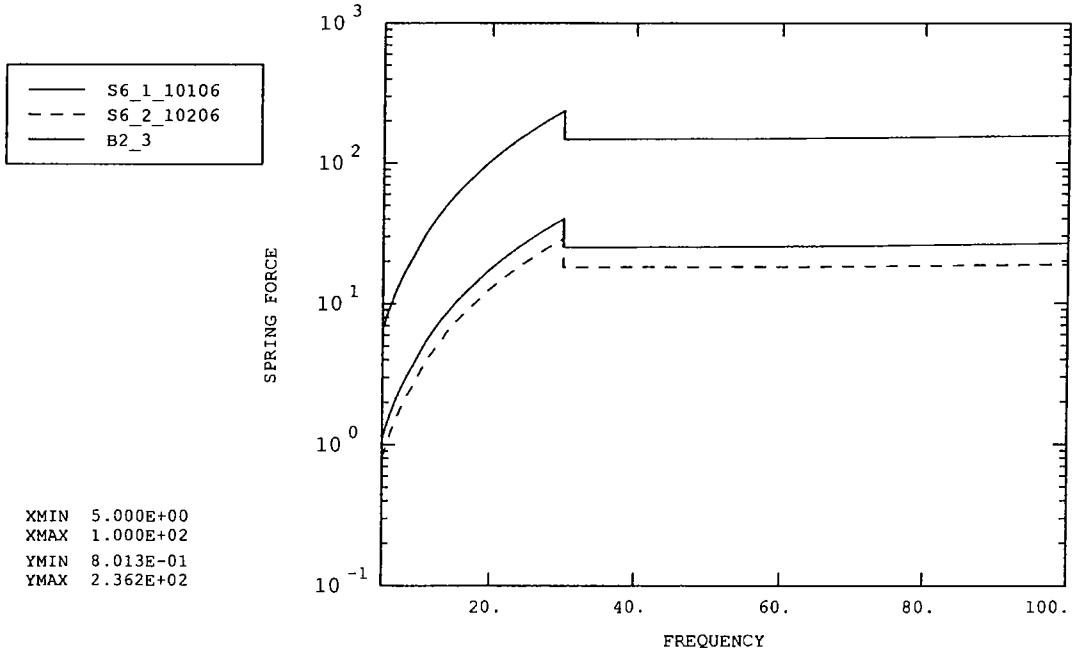

Figure 34: Base (back left)

© FNC 2002

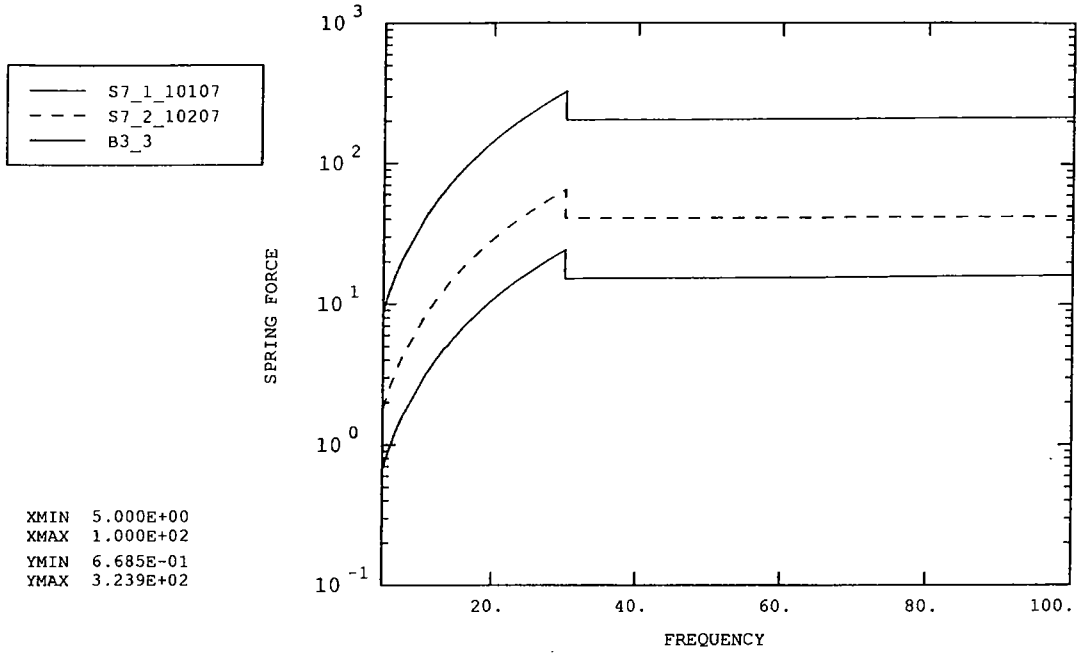

Figure 35: Base (back right)

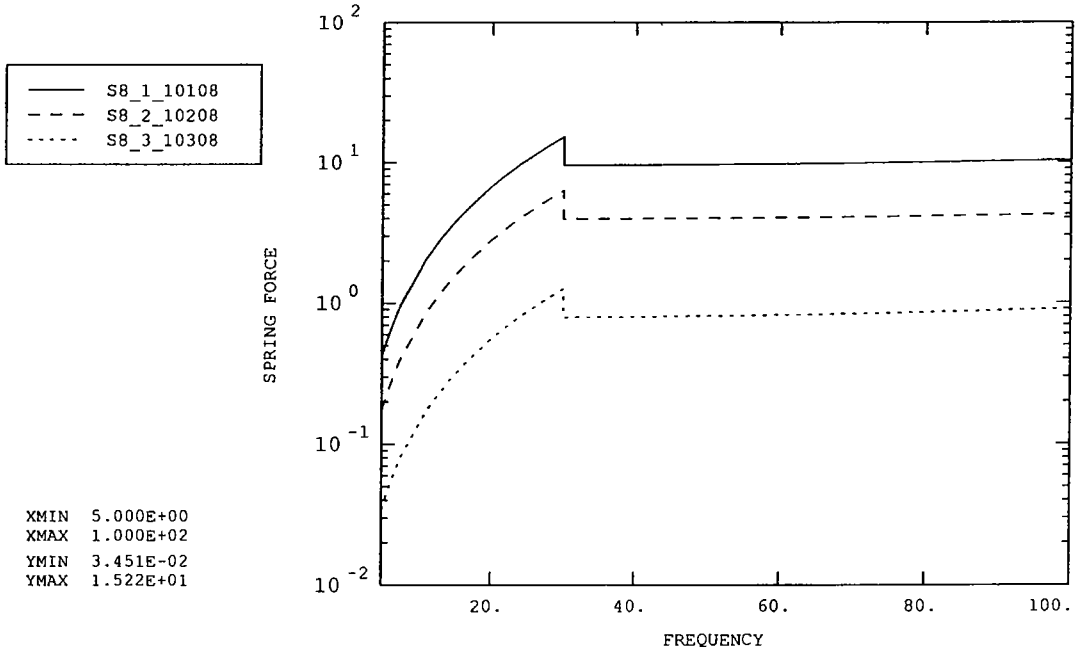

Figure 36: Jiggle pivot (top)

© FNC 2002

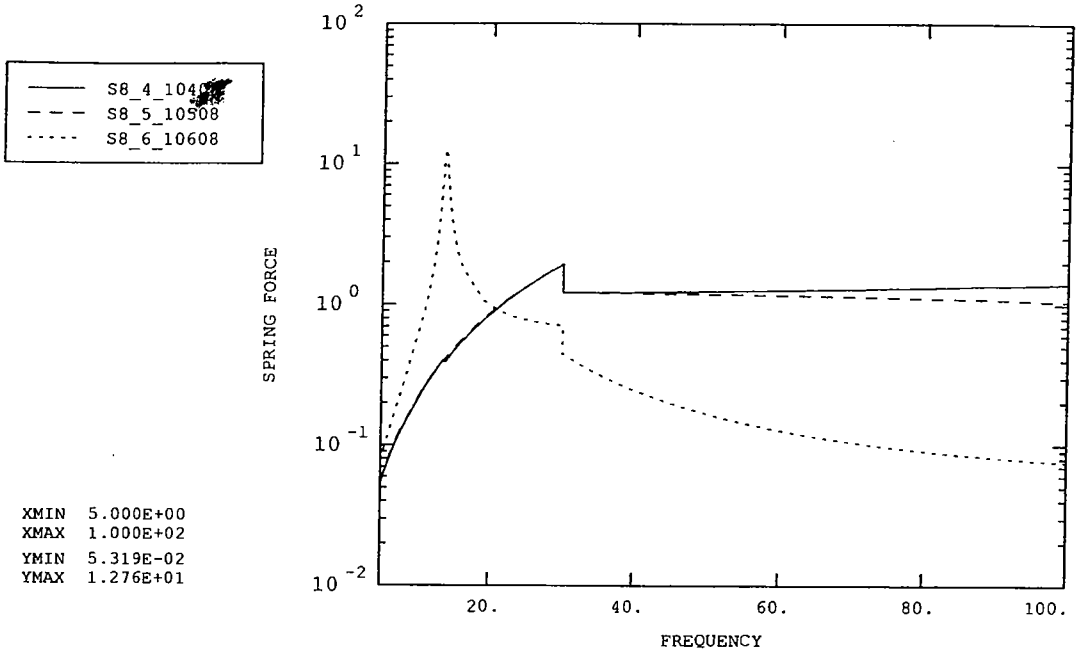

Figure 37: Jiggle pivot (top)

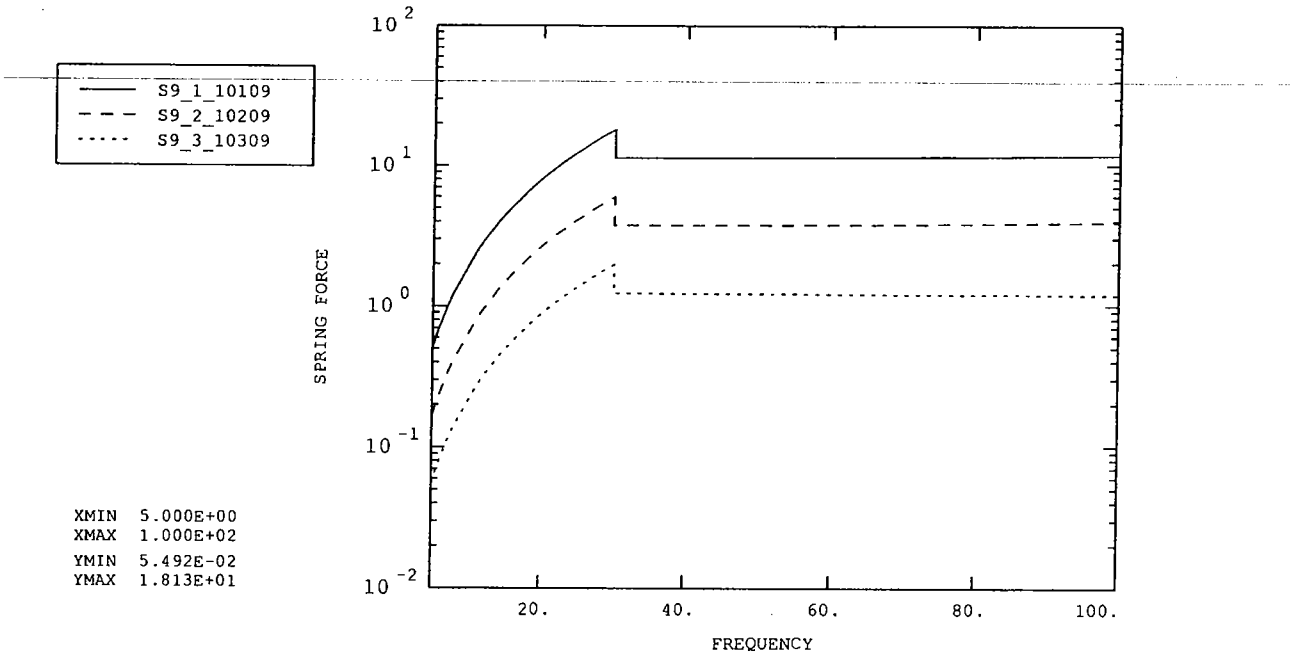

Figure 38: Jiggle pivot (bottom)

© FNC 2002

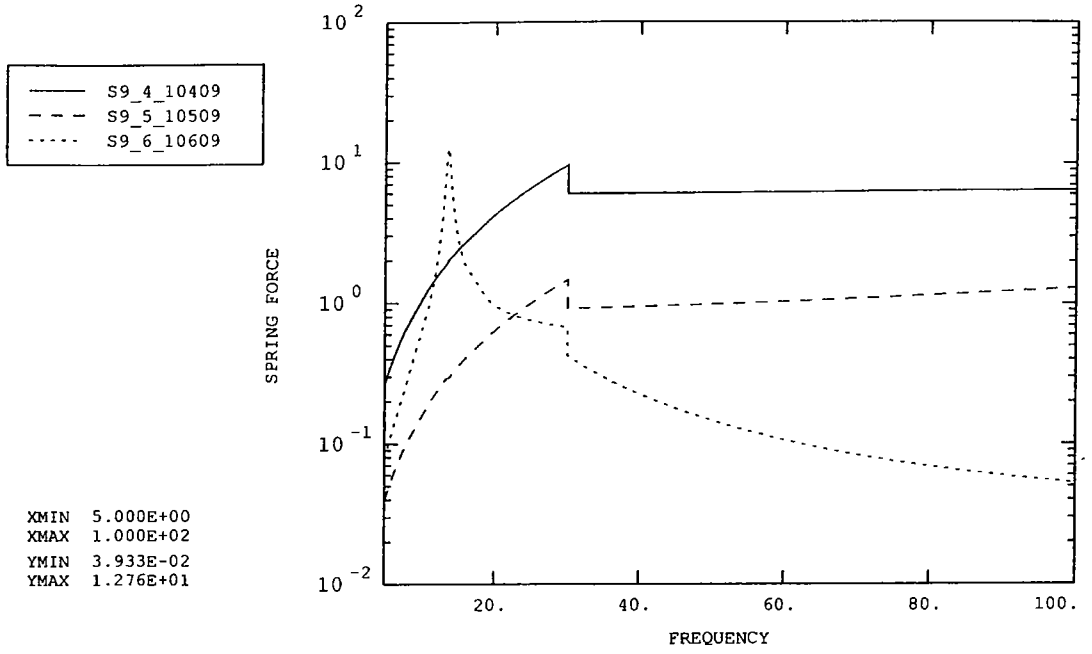

Figure 39: Jiggle pivot (bottom)

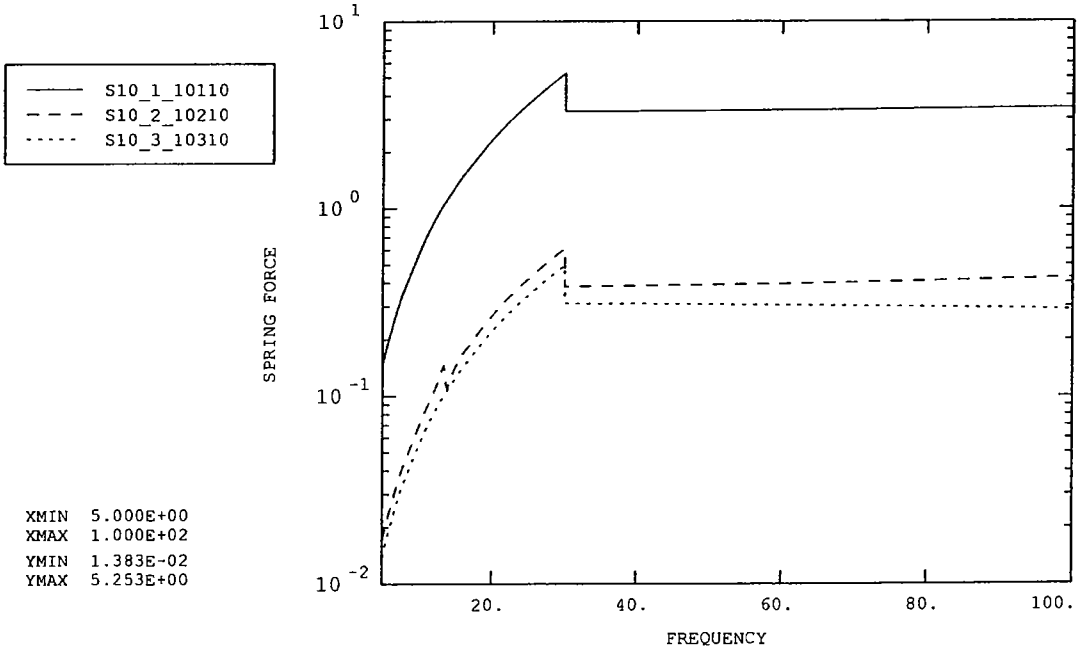

Figure 40: Chop pivot (left)

© FNC 2002

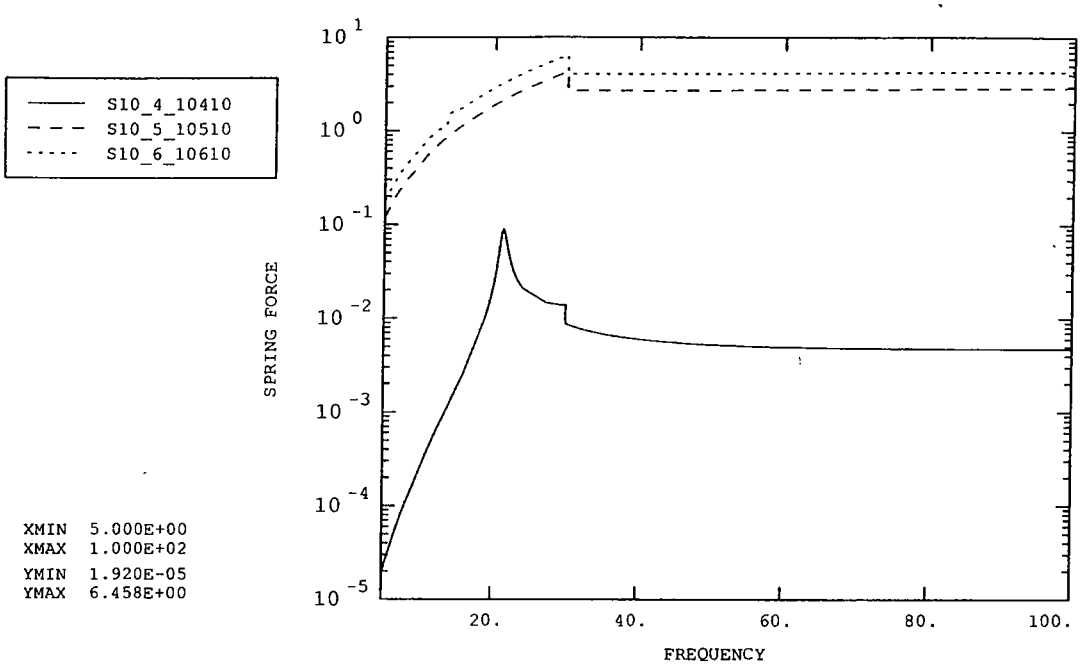

Figure 41: Chop pivot (left)

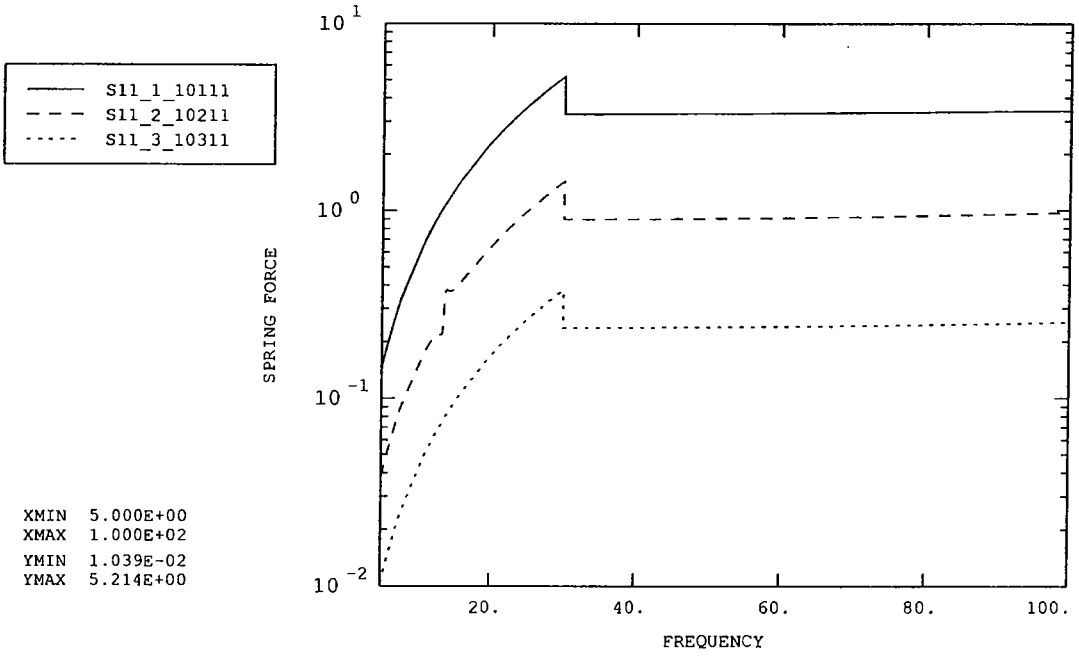

Figure 42: Chop pivot (right)

© FNC 2002

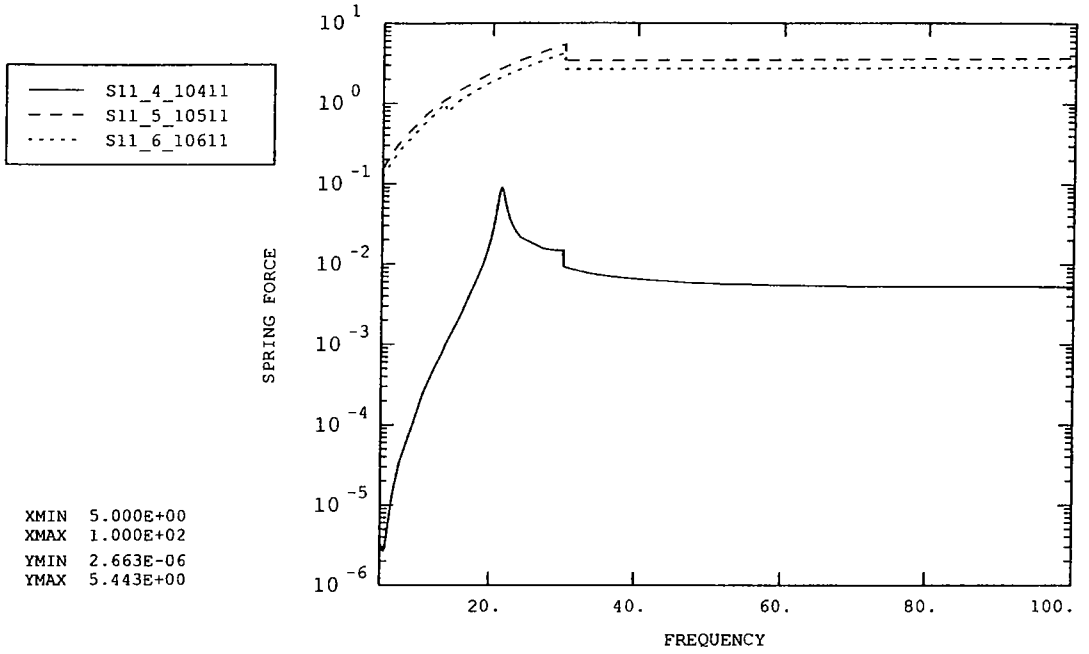

Figure 43: Chop pivot (right)

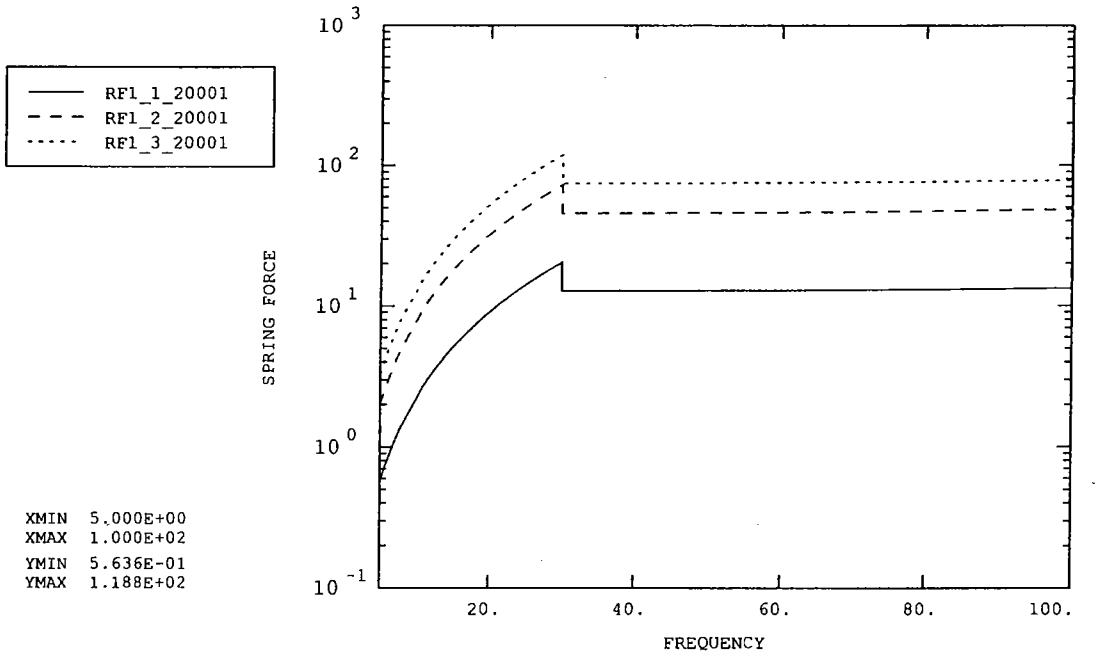

Figure 44: Reaction Force (front middle)

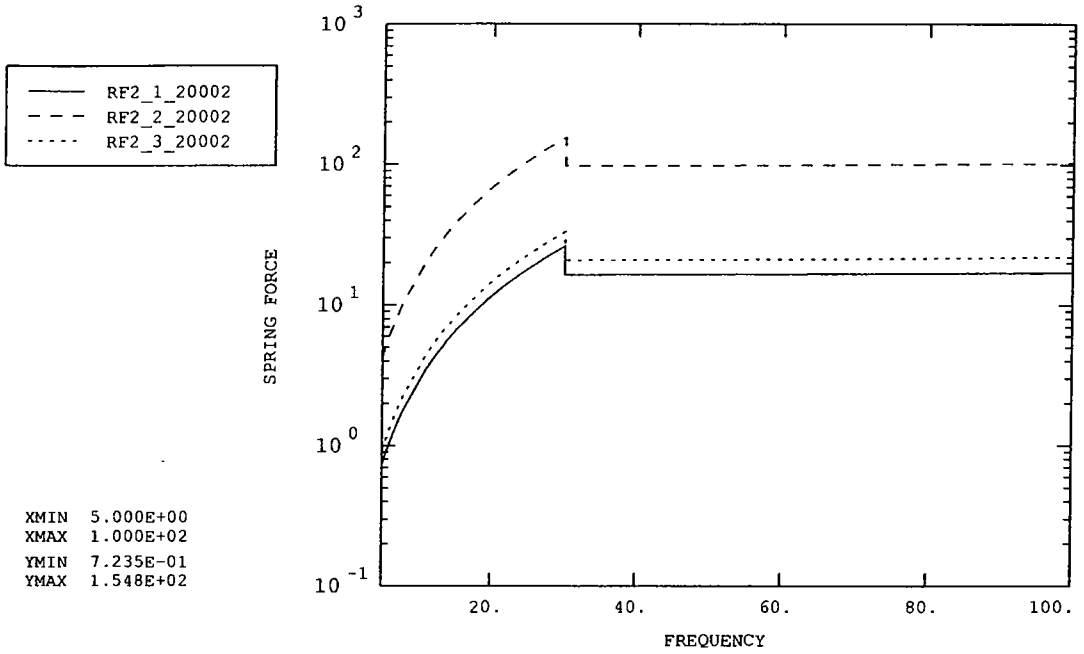

Figure 45: Reaction Force (back left)

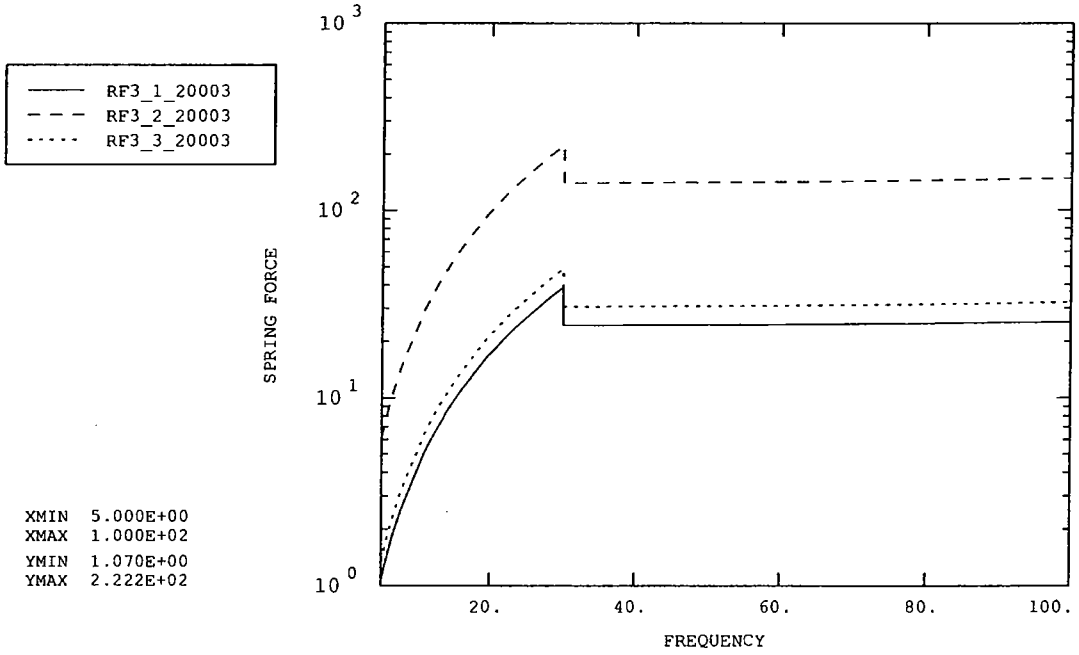

Figure 46: Reaction Force (back right)

© FNC 2002

SPIRE BSM VIBRATION ANALYSIS

Annex 4 - Random Response X-Direction

FNC 5505/24072R Issue 1

Prepared for

U.K. Astronomy Technology Centre

DOCUMENT INFORMATION

Project : SPIRE BSM Vibration Analysis

Report Title : Annex 4 - Random Response X-Direction

Client : U.K. Astronomy Technology Centre

Client Ref. : 024706

Classification :

Report No. : FNC 5505/24072R

Issue No. : 1

Date : May 2002

Compiled By : D C Reed
A J Vibert

Approved By : M W Anderson

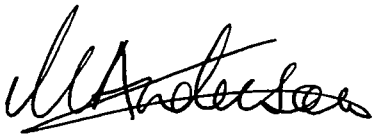

DISTRIBUTION

Copy	Recipient	Organisation
1	I Pain	UK ATC
2	I Pain	UK ATC
3	I Pain	UK ATC
4	File	FNC

Copy No. ____

COPYRIGHT

The Copyright in this work is vested in Frazer-Nash Consultancy Limited. The document is issued in confidence solely for the purpose for which it is supplied. Reproduction in whole or in part or use for tendering or manufacturing purposes is prohibited except under an agreement with or with the written consent of Frazer-Nash Consultancy Limited and then only on the condition that this notice is included in any such reproduction.

Originating Office: FRAZER-NASH CONSULTANCY LIMITED
Stonebridge House, Dorking Business Park, Dorking, Surrey RH4 1HJ, UK
T: +44 (0)1306 885050 F: +44 (0)1306 886464 E: info@fnc.co.uk W: www.fnc.co.uk

DATA POINT POSITIONS

Note:

- The labels on the plots are as follows: e.g. P9_1_12184 refers to acceleration data point P9, degree of freedom 1 (node number 12184).
- Degrees of freedom 1, 2 and 3 refer to motion in the x, y and z directions (or X, Y and Z directions), while degrees of freedom 4, 5 and 6 refer to rotations about the x, y and z axes (or X, Y and Z axes).
- Acceleration is total acceleration (i.e. includes base motion)
- Accelerations and reaction forces are given in the global X, Y, Z co-ordinates
- Relative displacements and spring forces/torques are given in the local model x, y, z co-ordinates.
- 'Left' and 'right' directions are defined from a point of view looking towards the mirror surface, with the top of the casing furthest from the baseplate.

Fig.	P	Acceleration data points	Node number
1	1	Jiggle axis pivot (top) – frame	12182
2	2	Jiggle axis pivot (top) – jiggle stage	12200
3	3	Jiggle axis pivot (bottom) – frame	12183
4	4	Jiggle axis pivot (bottom) – jiggle stage	12192
5	5	Chop axis pivot (right side) – jiggle stage	12189
6	6	Chop axis pivot (right side) – chop stage	114
7	7	Chop axis pivot (left side) – jiggle stage	12188
8	8	Chop axis pivot (left side) – chop stage	105
9	9	Chop motor (top)	12184
10	10	Chop motor (bottom)	12185
11	11	Jiggle motor (right side)	12186
12	12	Jiggle motor (left side)	12187
13	13	PCAL CG	12193
14	14	PCAL extension to mirror centre	12199
15	15	Launch latch 'A' CG	12196
16	16	Launch latch 'A' extension to magnet centre	12197
17	17	Connector (top)	12194
18	18	Chop magnet (top)	115
19	19	Chop magnet (bottom)	122
20	20	Mirror Centre	9583
21	21	Jiggle magnet (right)	9276
22	22	Jiggle magnet (left)	9264

© FNC 2002

Fig.	E	Displacement between...	Element
23	1	Chop magnet vs. motor (top)	90n01, n=1, 2
24	2	Chop magnet vs. motor (bottom)	90n02, n=1, 2
25	3	Jiggle magnet vs. motor (right)	90n03, n=2, 3
26	4	Jiggle magnet vs. motor (left)	90n04, n=2, 3
27	5	Mirror centre vs. PCAL extension	90n05, n=1, 2, 3
28	6	Chop magnet (top) vs. launch latch 'A'	90206

Fig.	S	Position of spring elements	Node 1	Element
29	1	Front baffle (top left)	9702	10n01, n=1,2,3
30	2	Front baffle (top right)	9739	10n02, n=1,2,3
31	3	Front baffle (bottom left)	9629	10n03, n=1,2,3
32	4	Front baffle (bottom right)	9594	10n04, n=1,2,3
33	5	Base (front middle)*	3894	10n05, n=1,2,3
34	6	Base (back left)*	3414	10n06, n=1,2,3
35	7	Base (back right)*	3622	10n07, n=1,2,3
36,37	8	Jiggle pivot (top)	12200	10n08, n=1 to 6
38,39	9	Jiggle pivot (bottom)	12192	10n09, n=1 to 6
40,41	10	Chop pivot (left)	12188	10n10, n=1 to 6
42,43	11	Chop pivot (right)	12189	10n11, n=1 to 6

Fig.	RF	Reaction Forces	Node number
44	1	Reaction Force (front middle)	10587
45	2	Reaction Force (back left)	10722
46	3	Reaction Force (back right)	10671

* The baseplate-casing connections are each modelled using a single spring in the local x and y directions, and five springs in the local z direction. The forces from these five springs are added together to calculate the total connective force. The curve labels for the z direction degrees of freedom have the prefix 'B'.

© FNC 2002

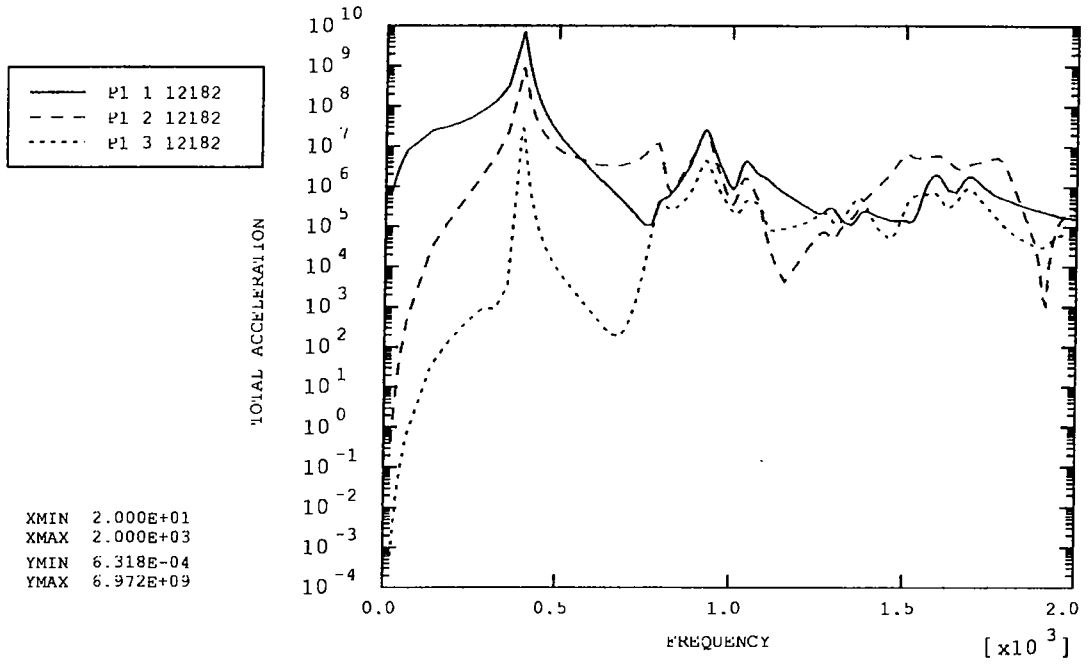

Figure 1: Jiggle axis pivot (top) – frame

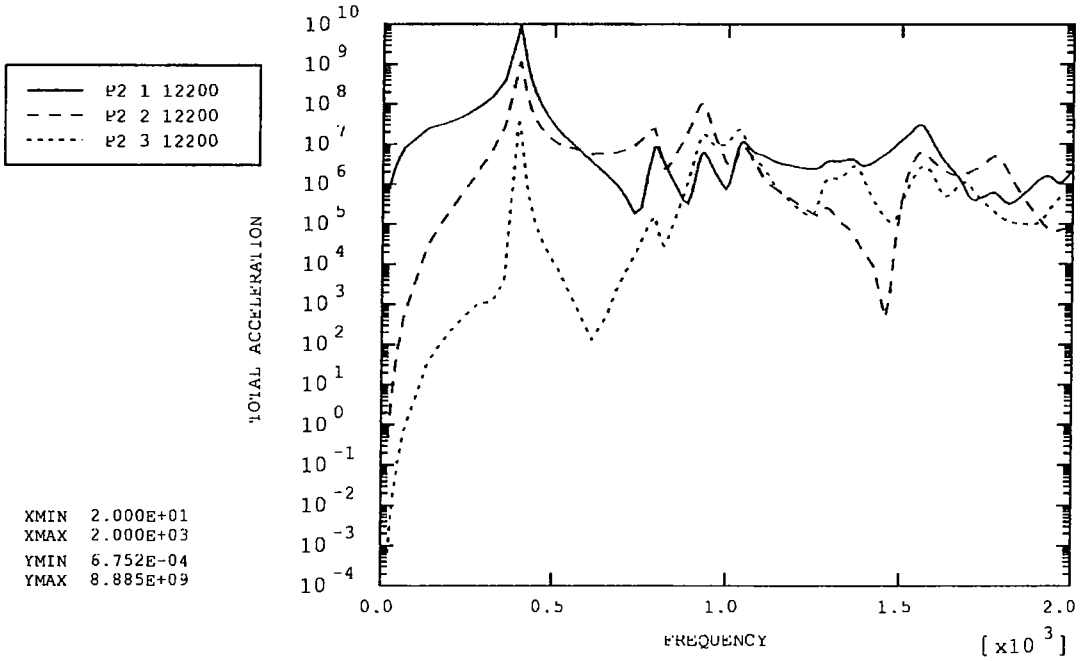

Figure 2: Jiggle axis pivot (top) – jiggle stage

© FNC 2002

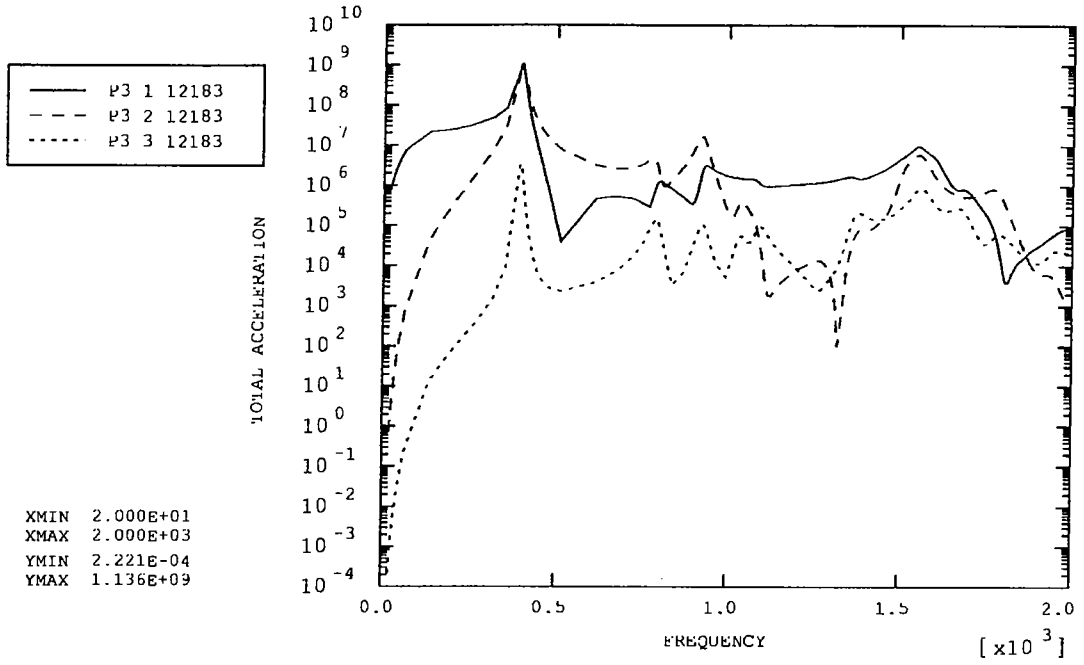

Figure 3: Jiggle axis pivot (bottom) – frame

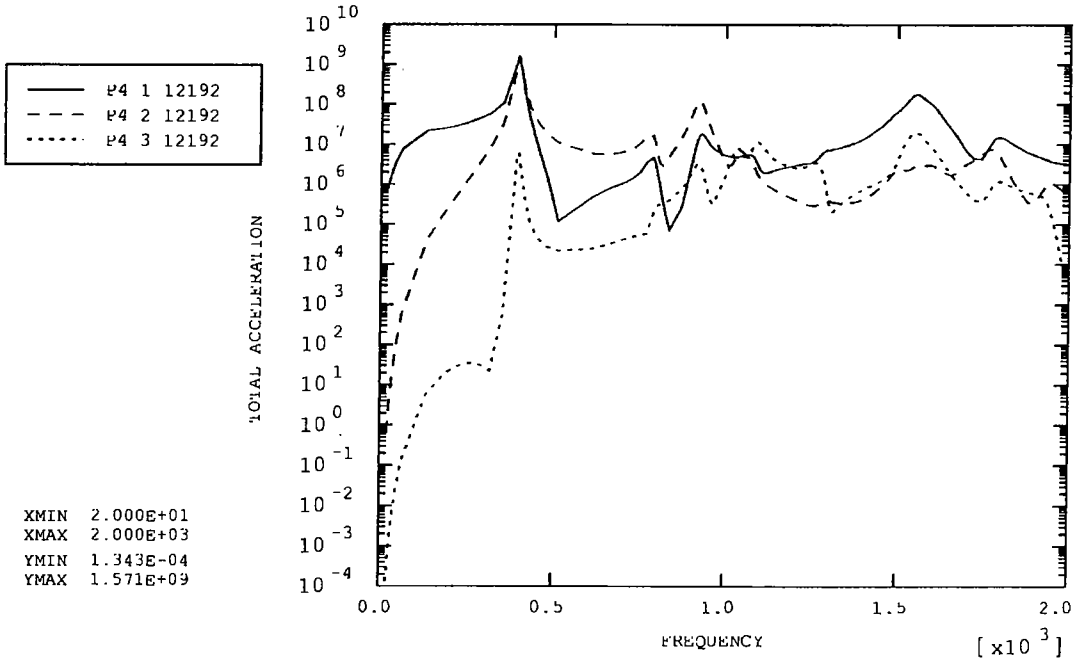

Figure 4: Jiggle axis pivot (bottom) – jiggle stage

© FNC 2002

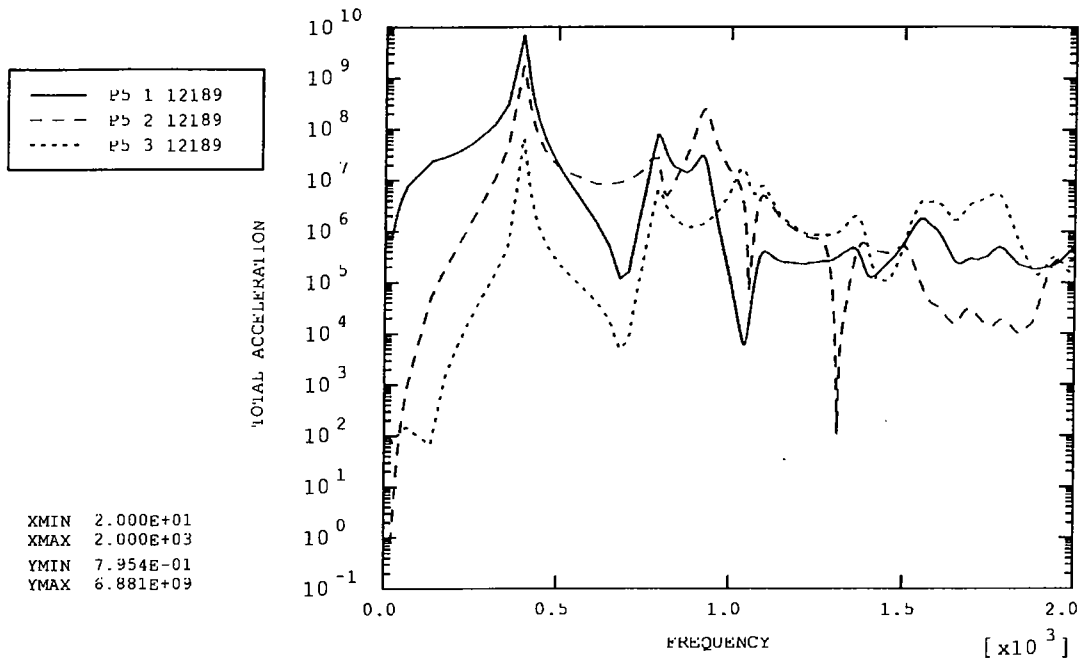

Figure 5: Chop axis pivot (right side) – jiggle stage

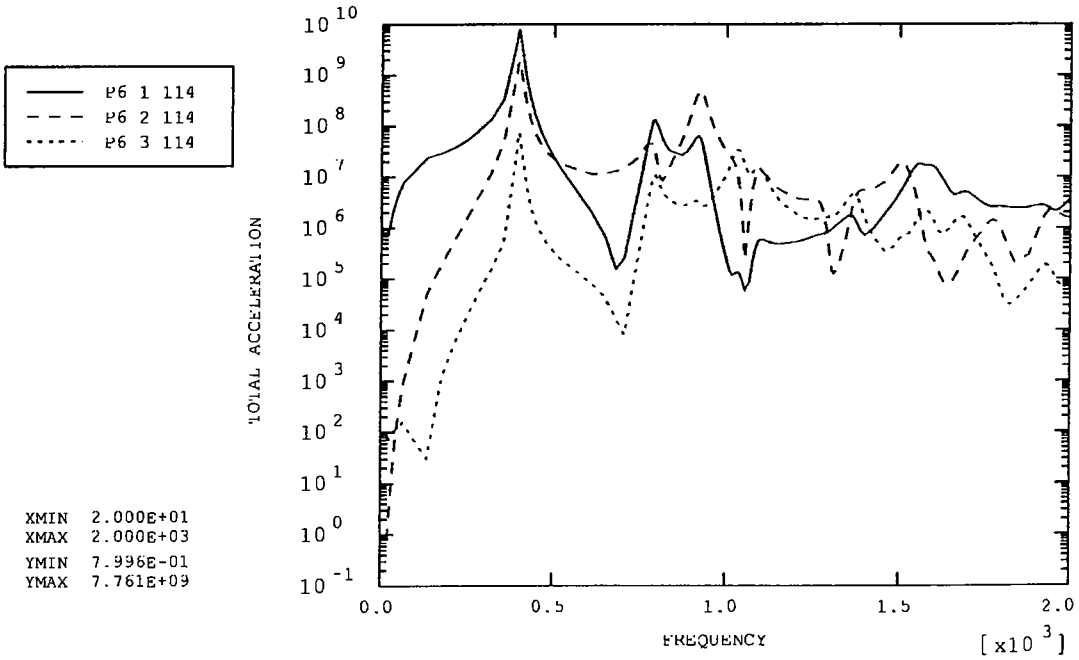

Figure 6: Chop axis pivot (right side) – chop stage

© FNC 2002

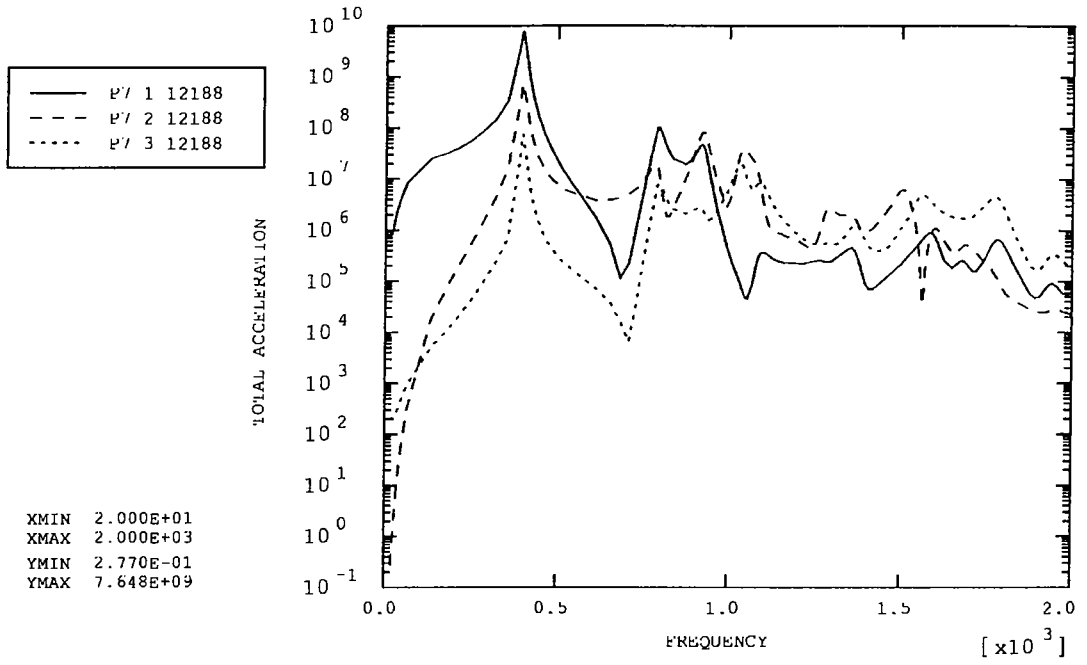

Figure 7: Chop axis pivot (left side) – jiggle stage

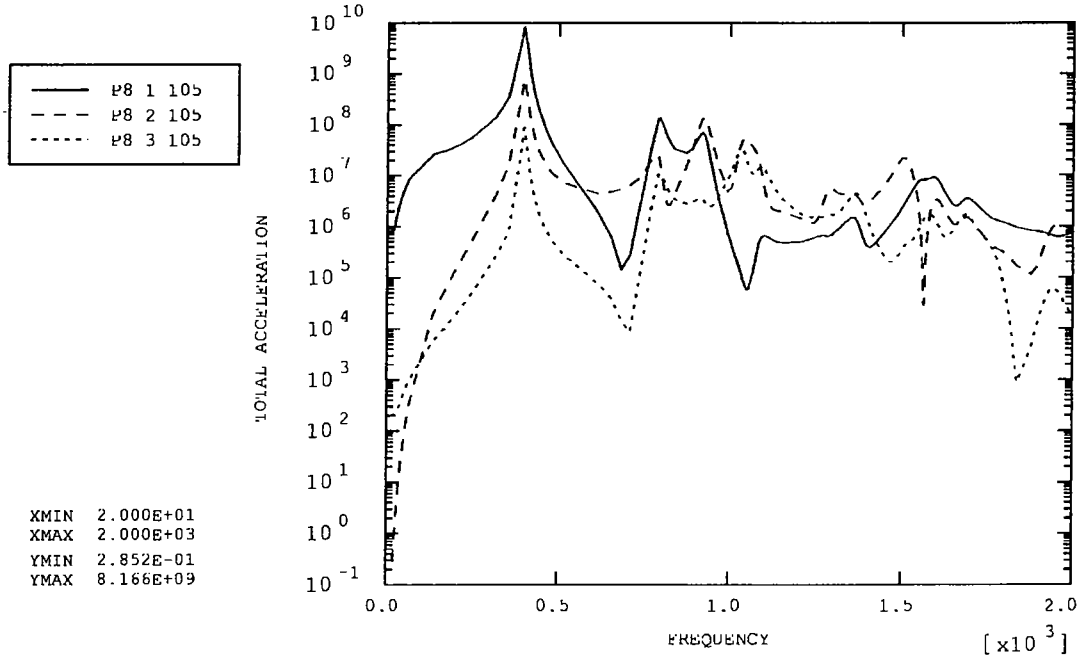

Figure 8: Chop axis pivot (left side) – chop stage

© FNC 2002

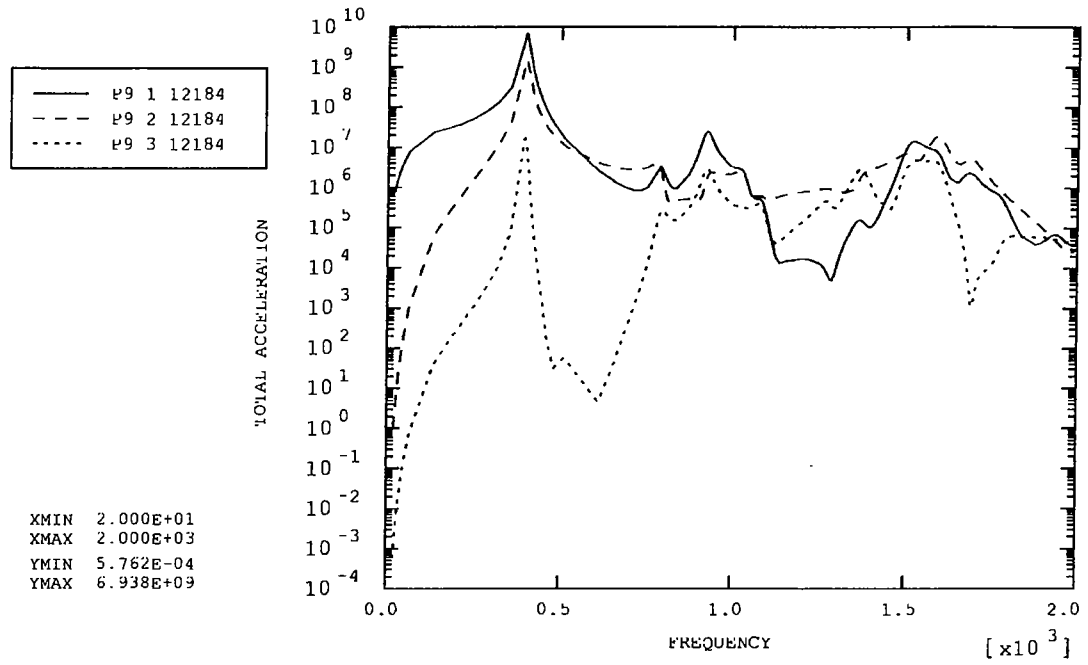

Figure 9: Chop motor (top)

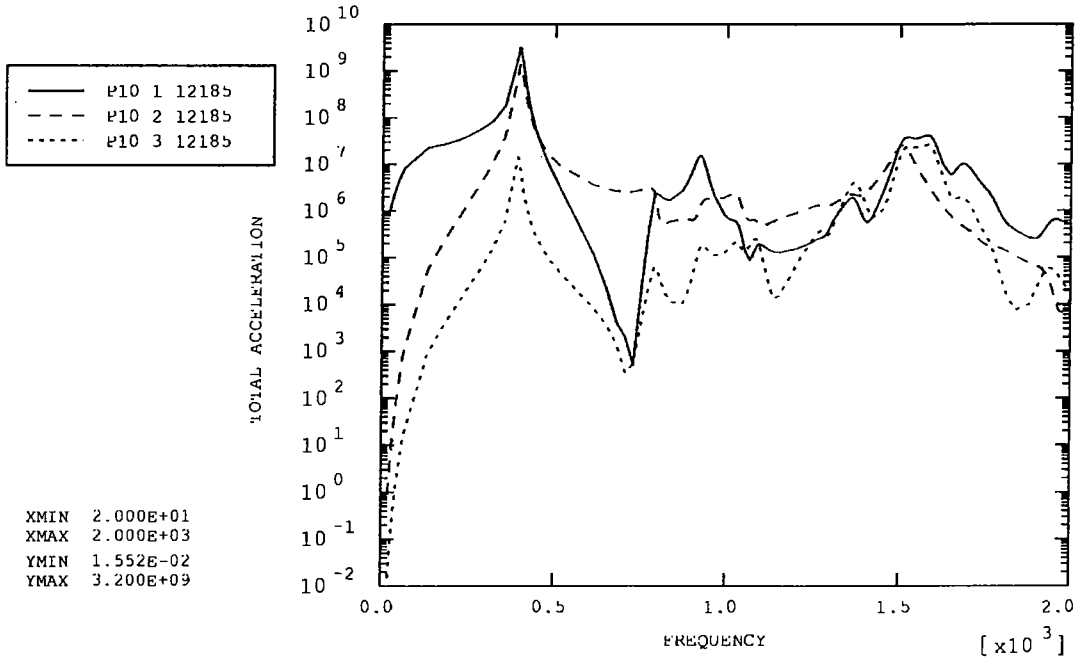

Figure 10: Chop motor (bottom)

© FNC 2002

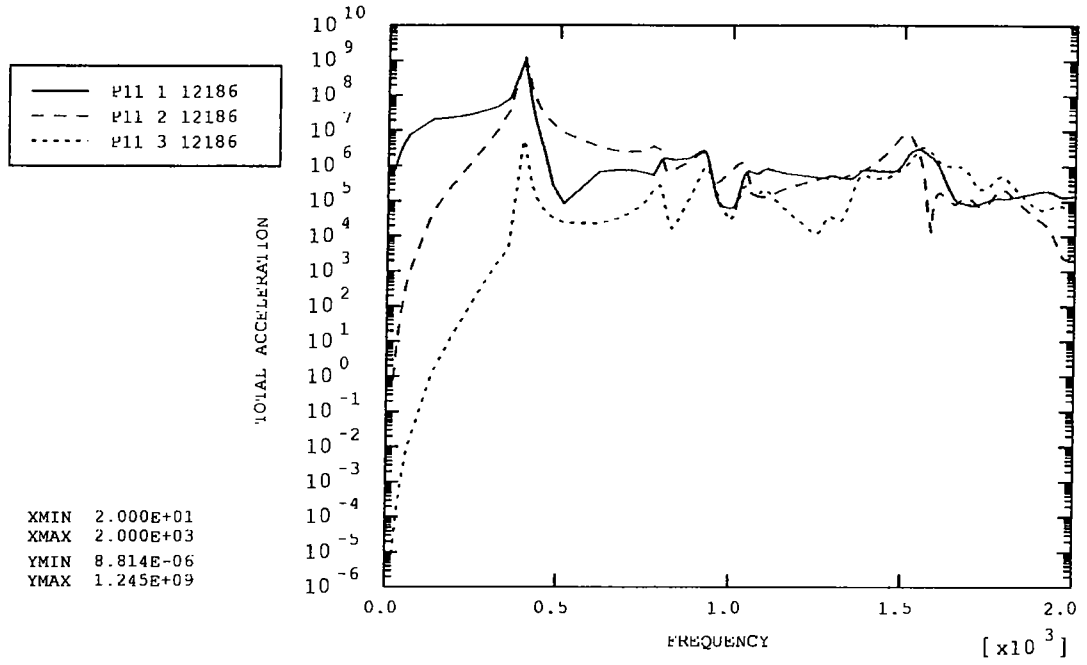

Figure 11: Jiggle motor (right side)

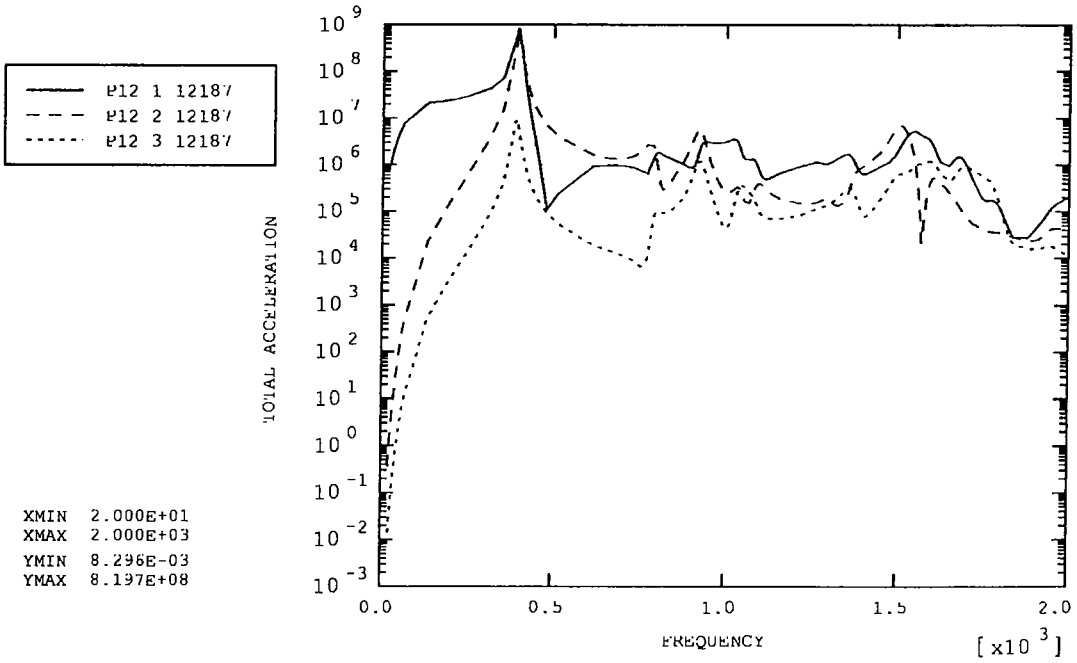

Figure 12: Jiggle motor (left side)

© FNC 2002

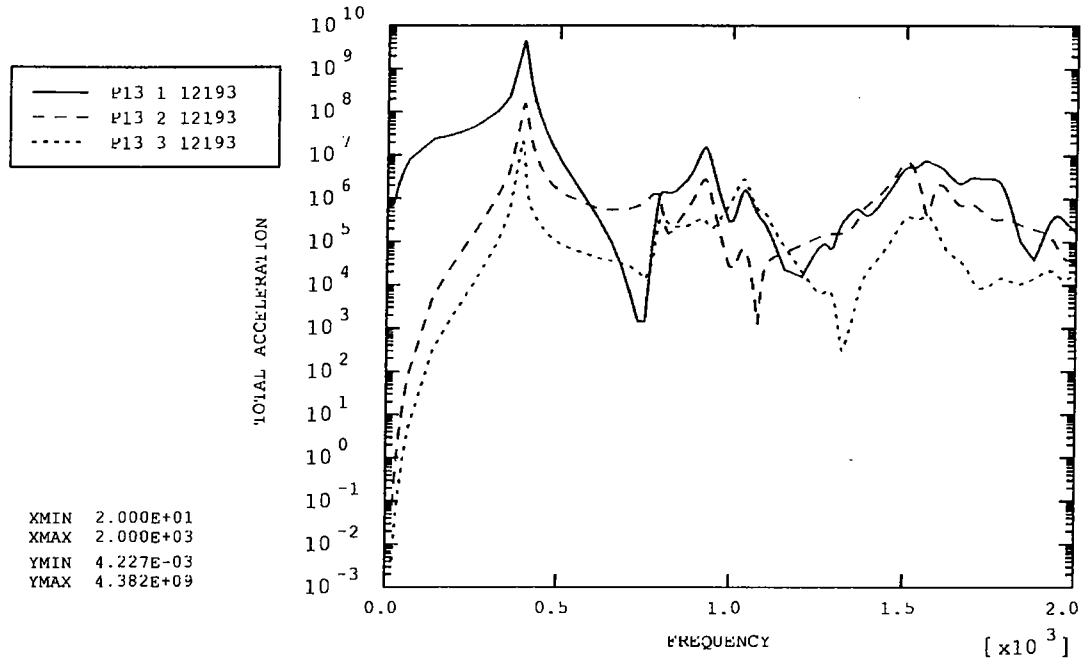

Figure 13: PCAL CG

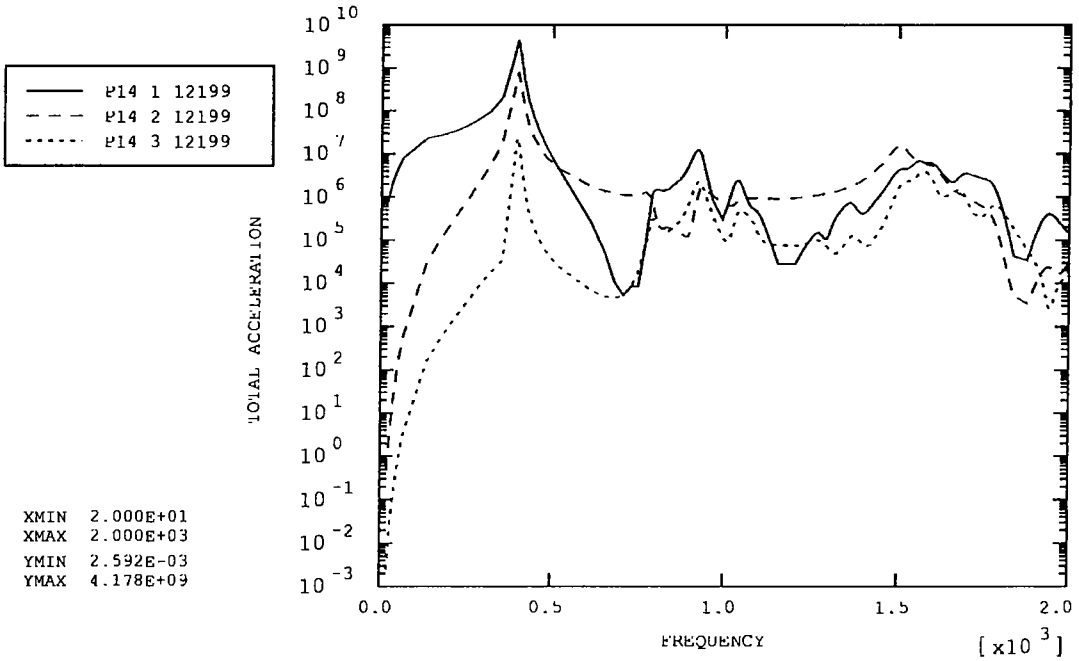

Figure 14: PCAL extension to mirror centre

© FNC 2002

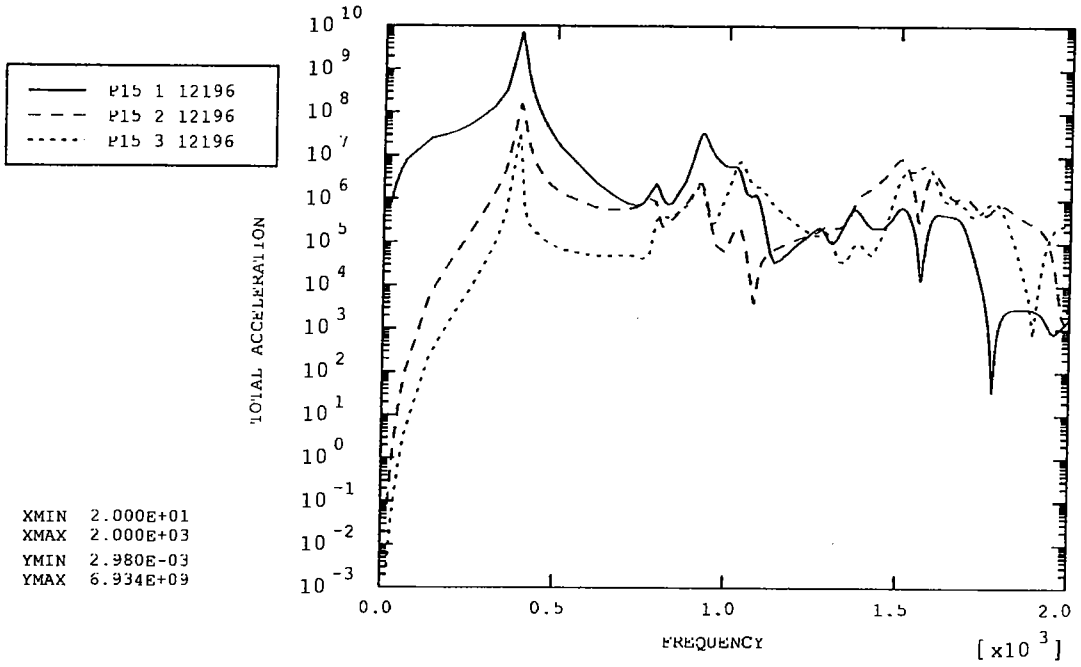

Figure 15: Launch latch 'A' CG

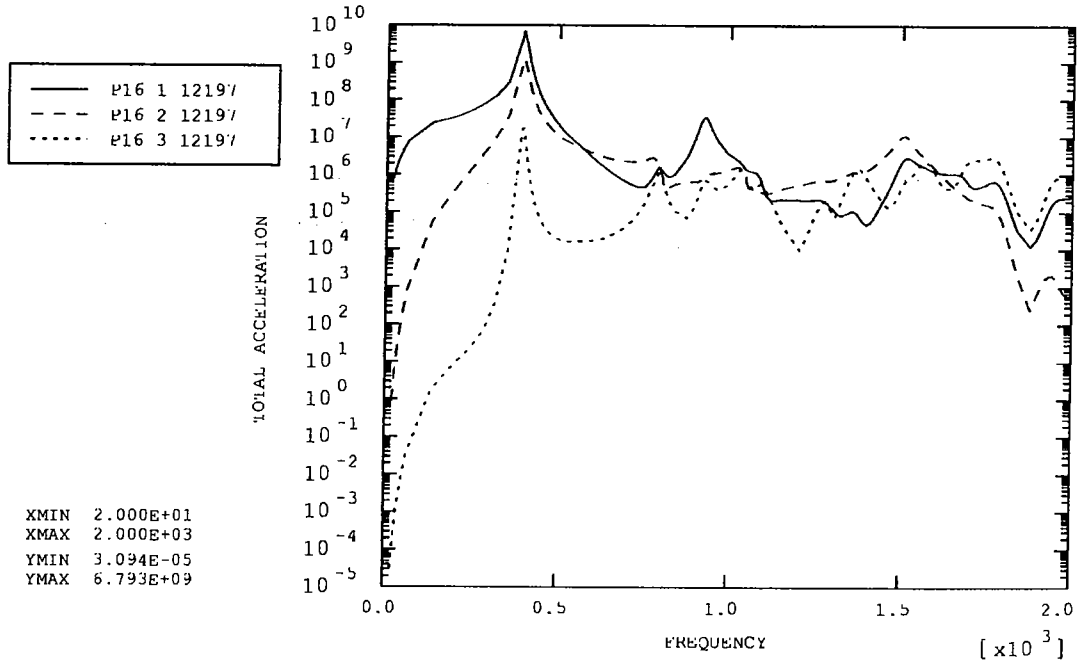

Figure 16: Launch latch 'A' extension to magnet centre

© FNC 2002

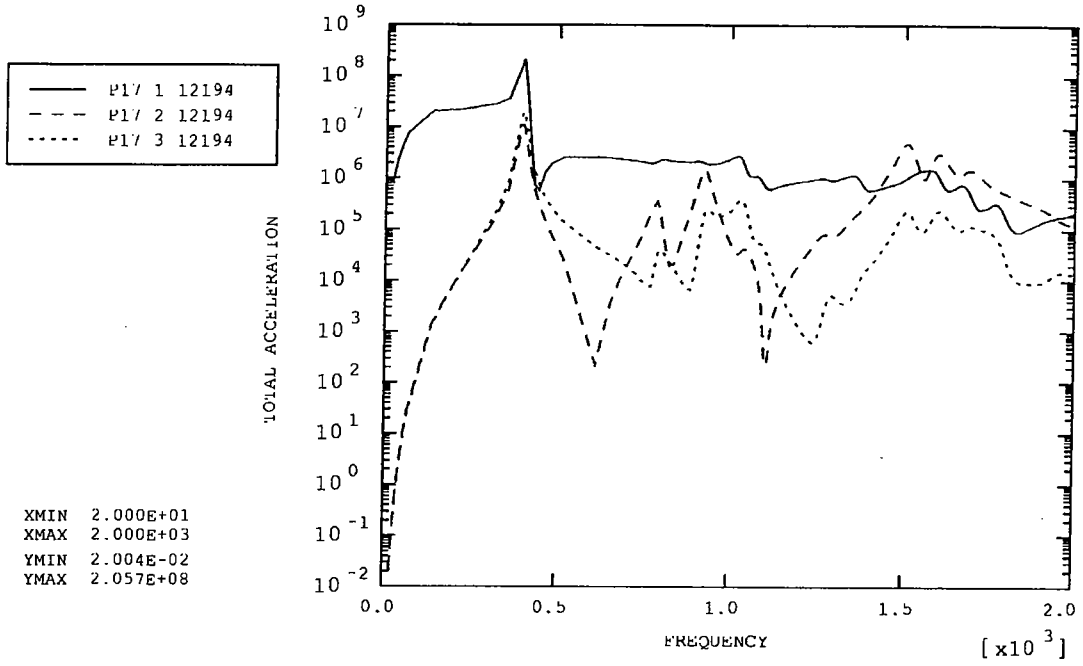

Figure 17: Connector (top)

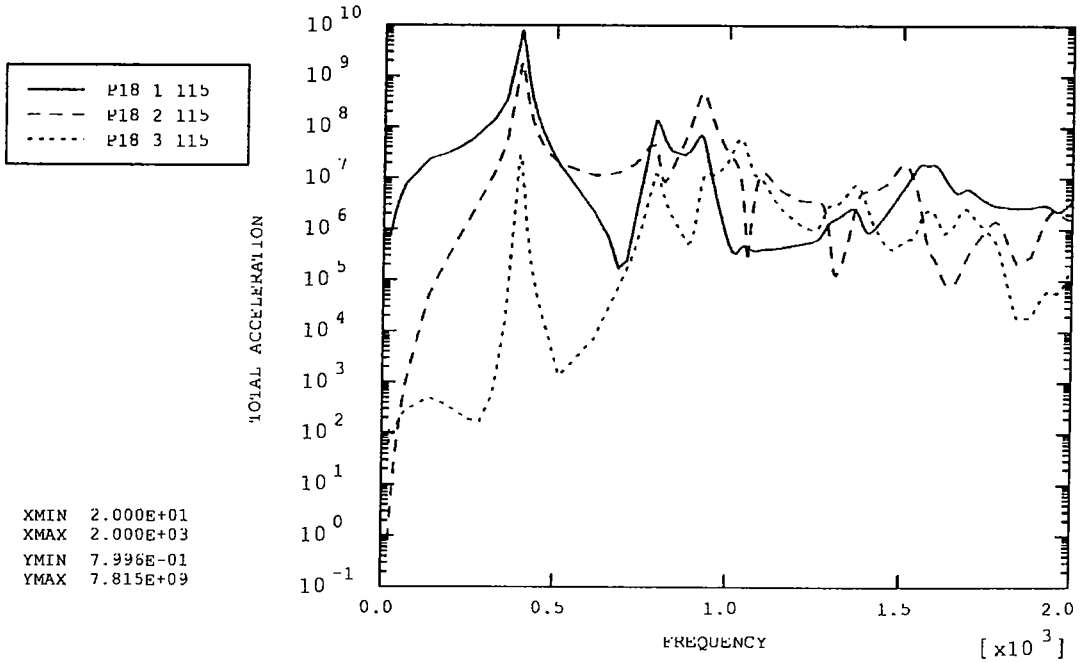

Figure 18: Chop magnet (top)

© FNC 2002

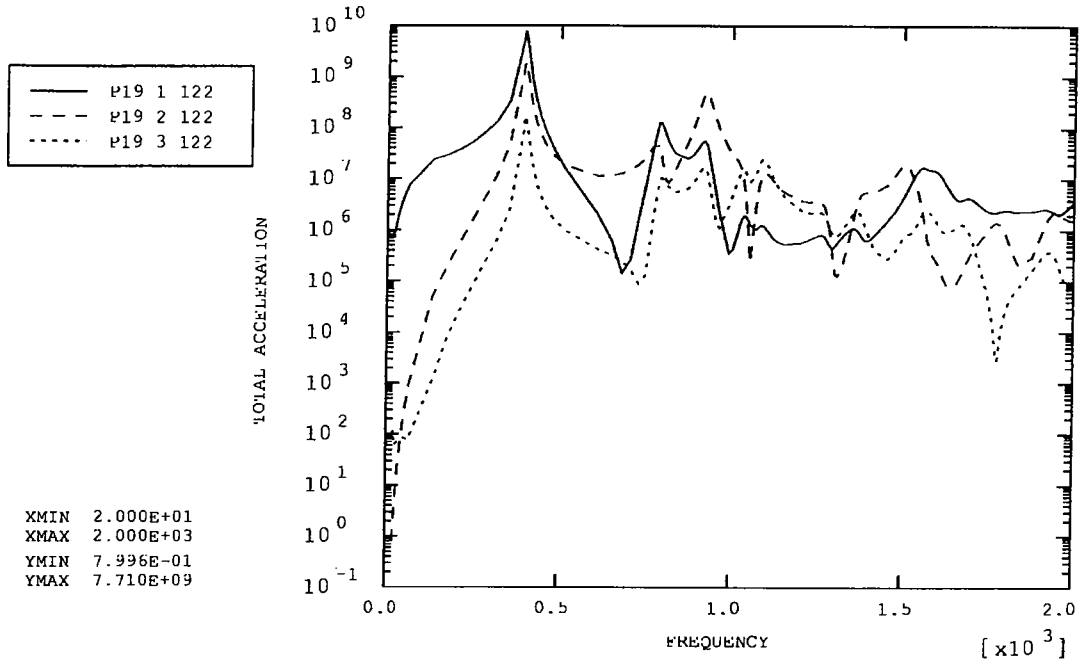

Figure 19: Chop magnet (bottom)

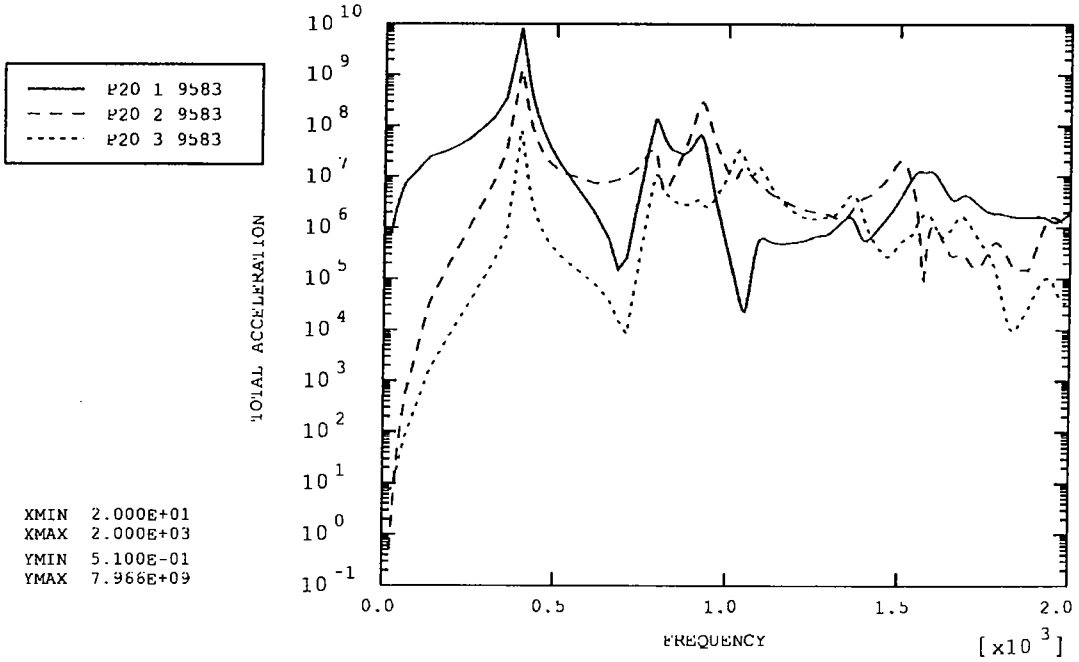

Figure 20: Mirror Centre

© FNC 2002

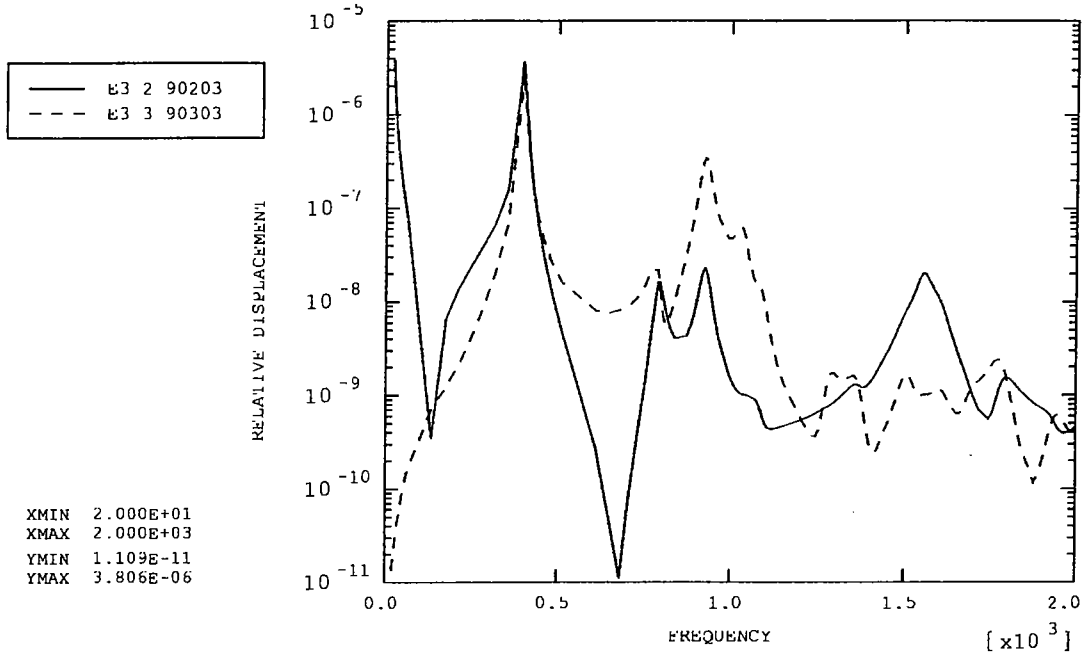

Figure 25: Jiggle magnet vs. motor (right)

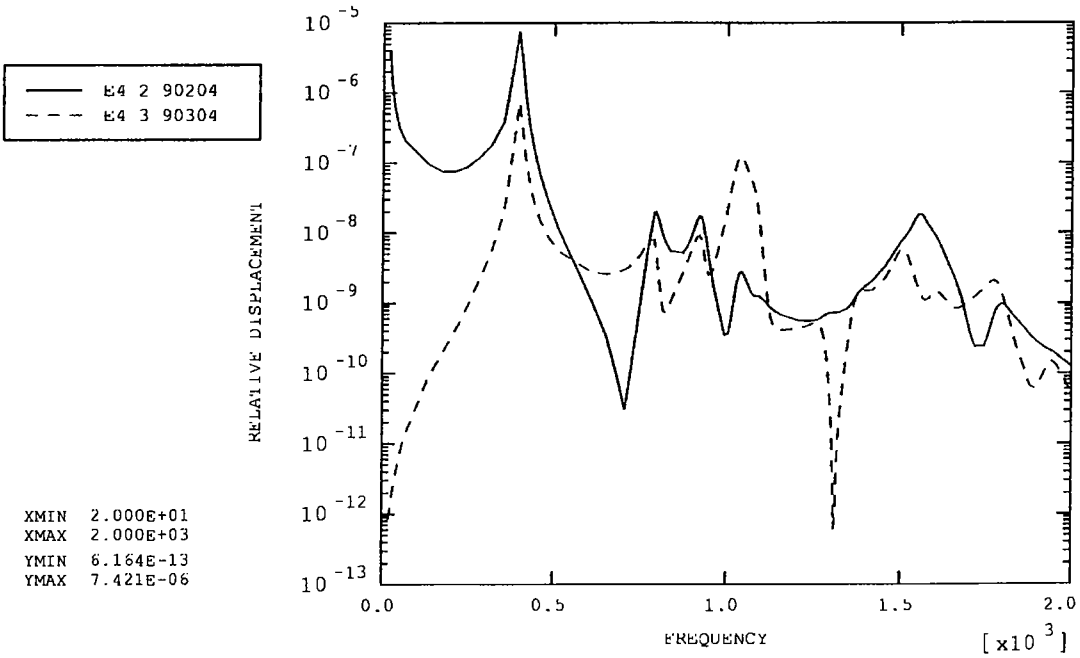

Figure 26: Jiggle magnet vs. motor (left)

© FNC 2002

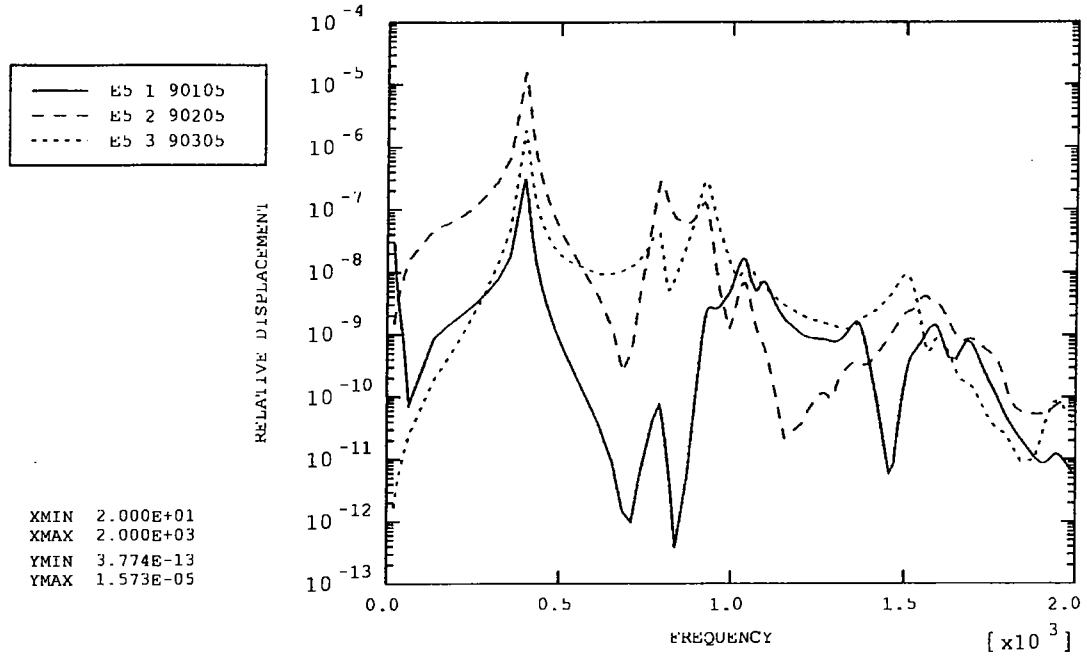

Figure 27: Mirror centre vs. PCAL extension

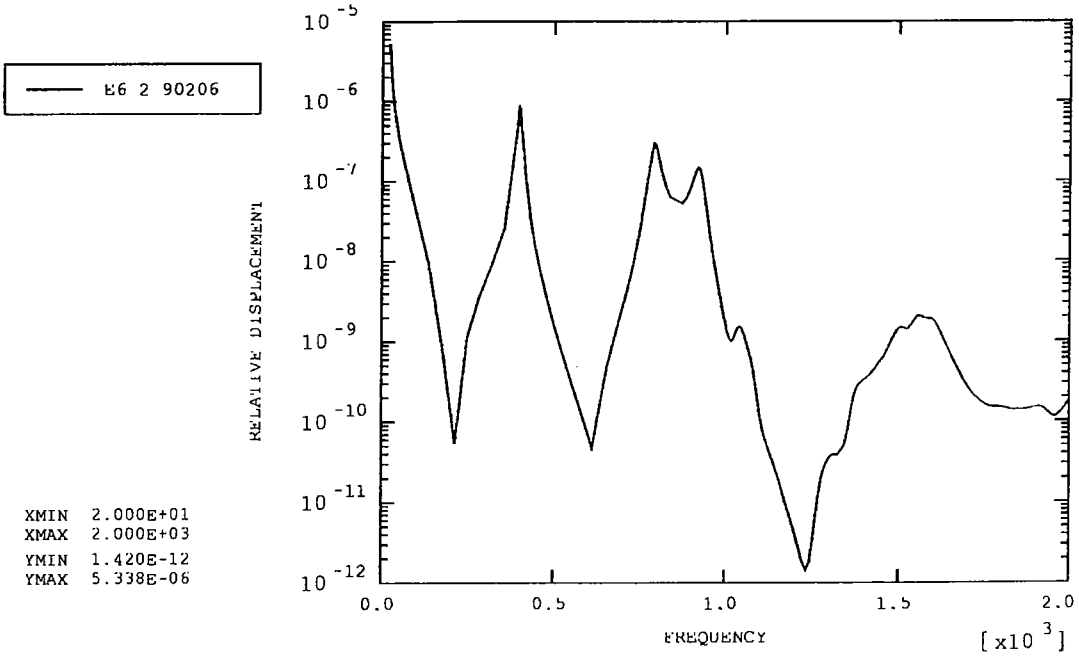

Figure 28: Chop magnet (top) vs. launch latch 'A'

© FNC 2002

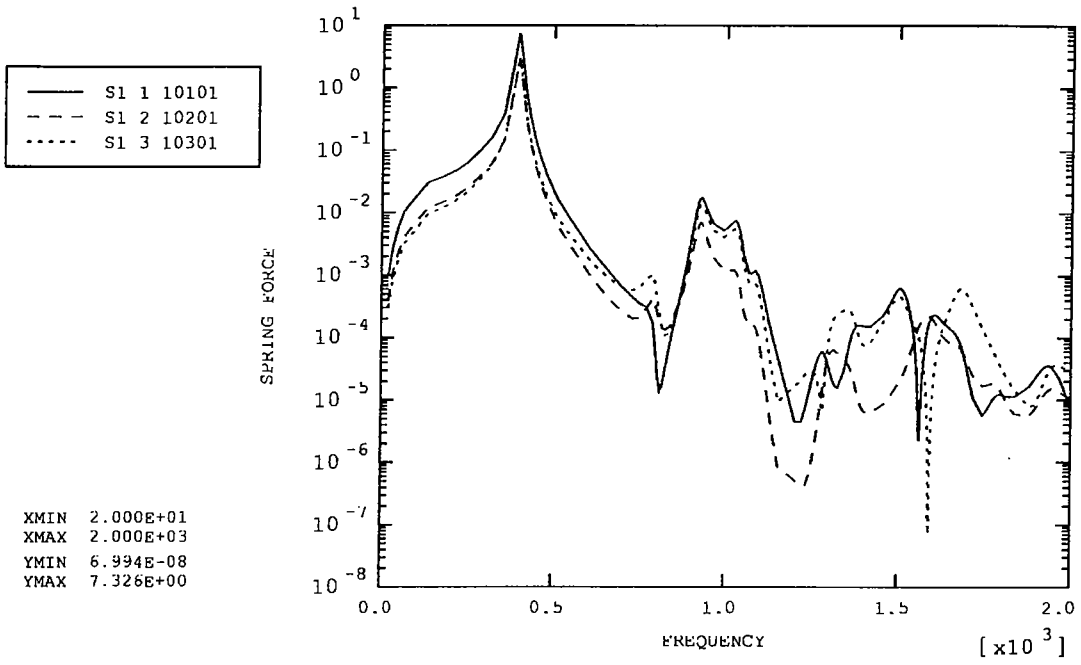

Figure 29: Front baffle (top left)

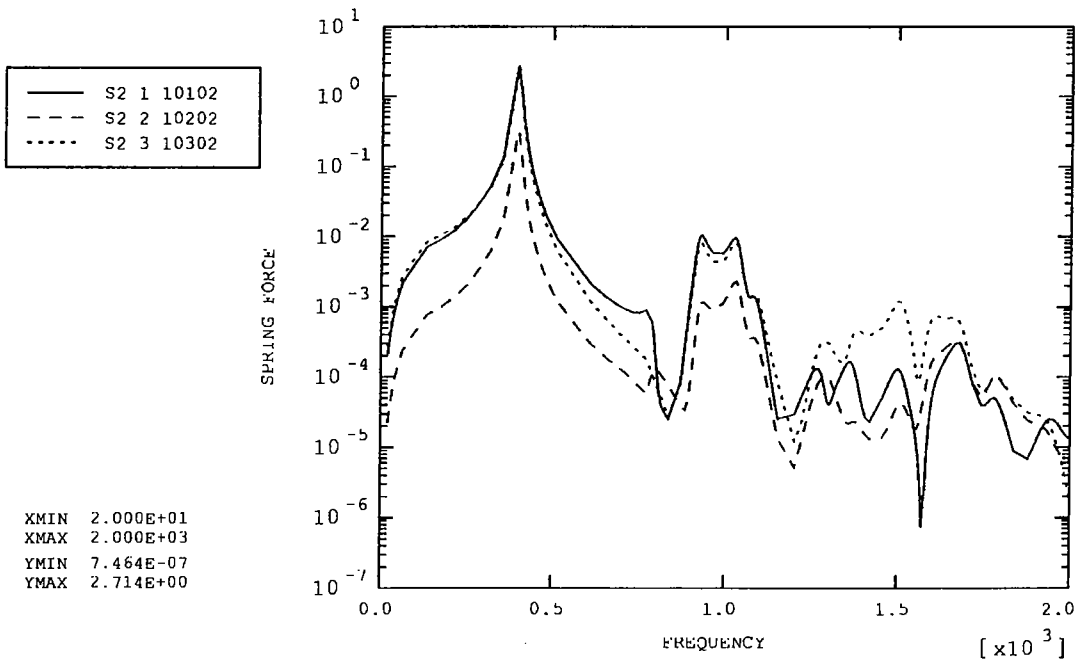

Figure 30: Front baffle (top right)

© FNC 2002

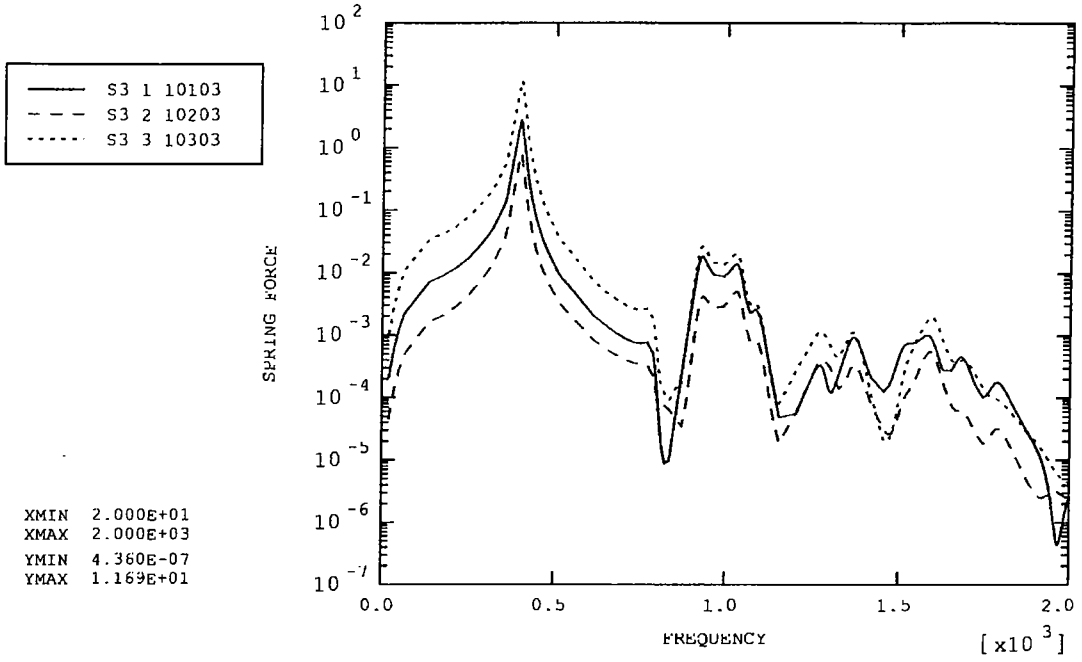

Figure 31: Front baffle (bottom left)

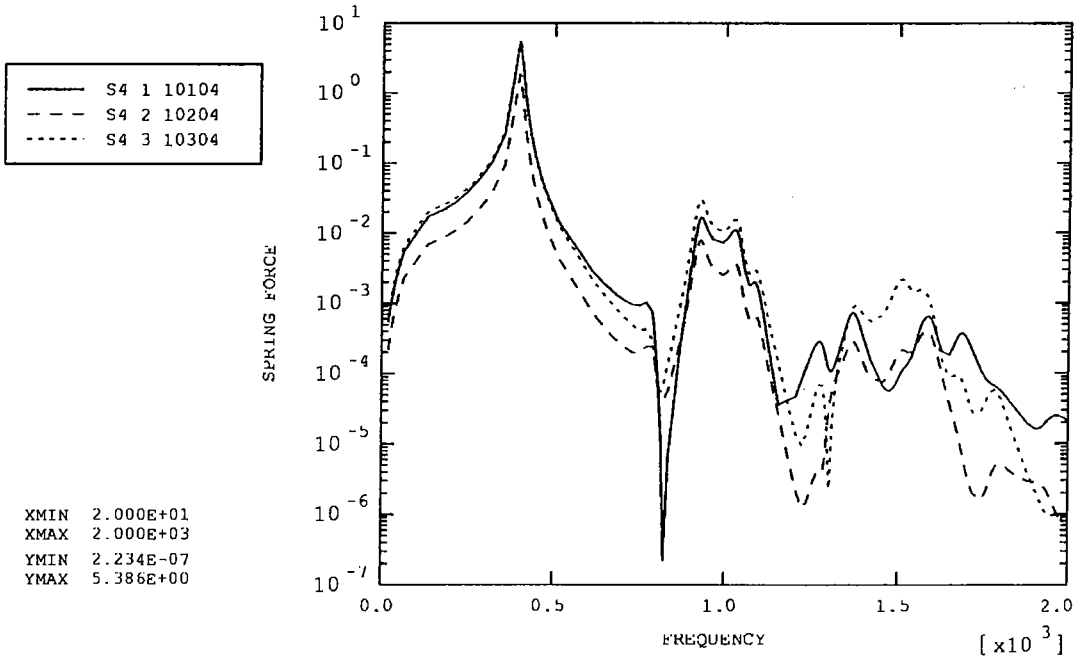

Figure 32: Front baffle (bottom right)

© FNC 2002

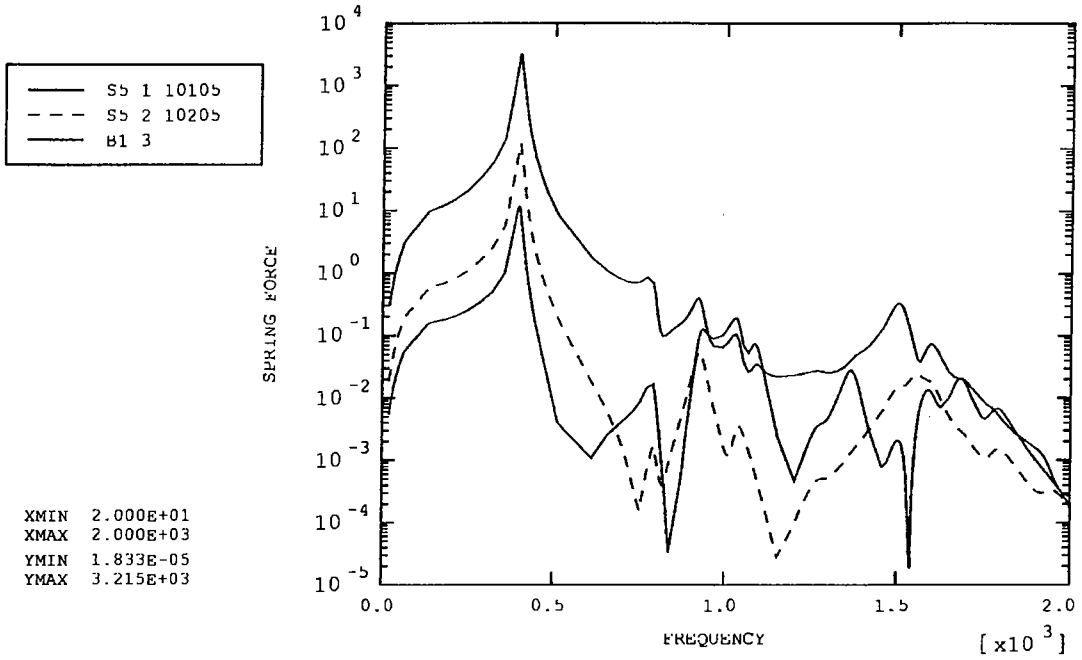

Figure 33: Base (front middle)

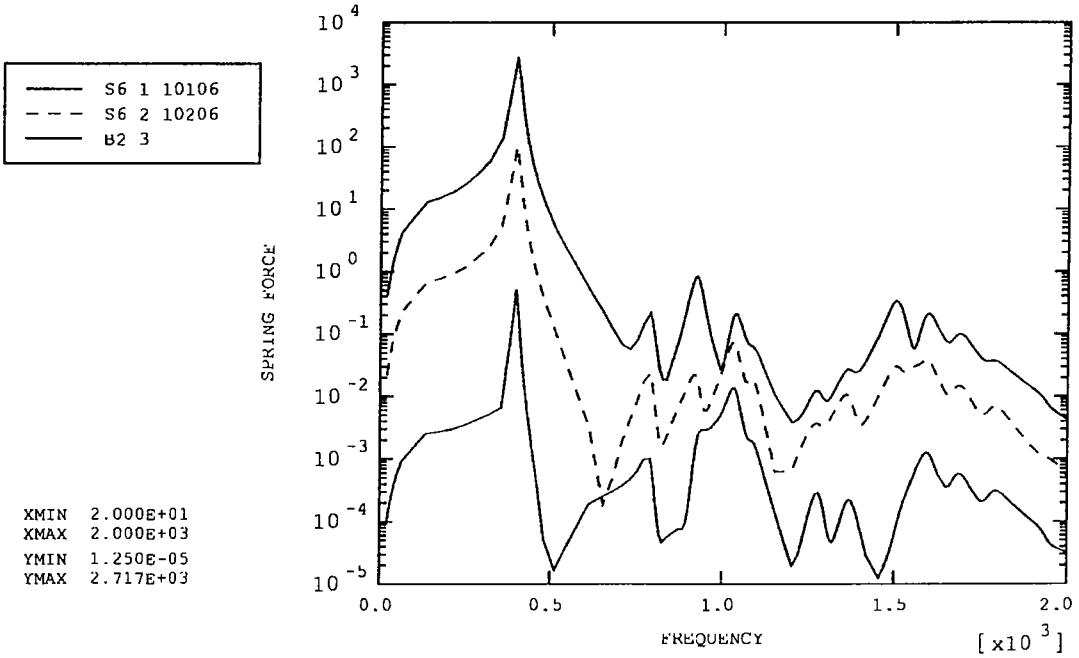

Figure 34: Base (back left)

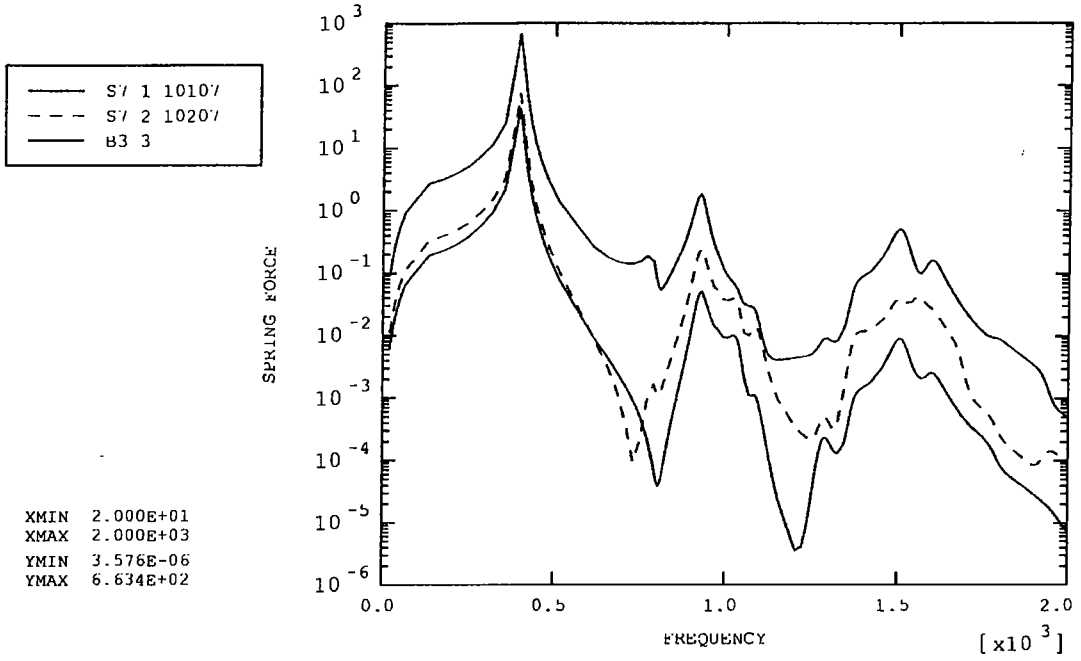

Figure 35: Base (back right)

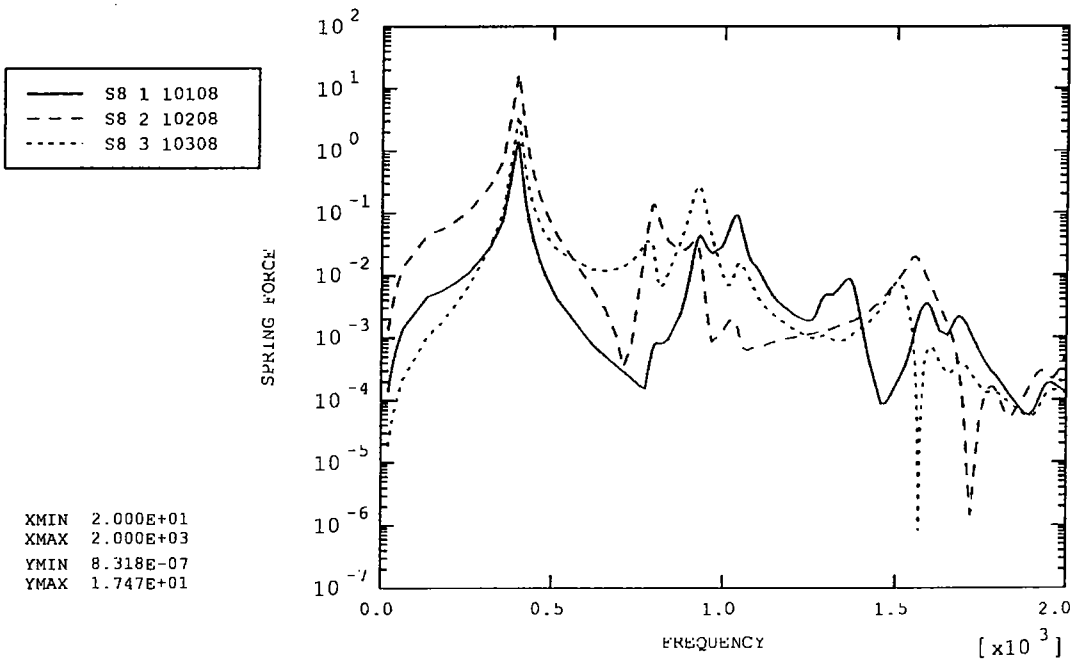

Figure 36: Jiggle pivot (top)

© FNC 2002

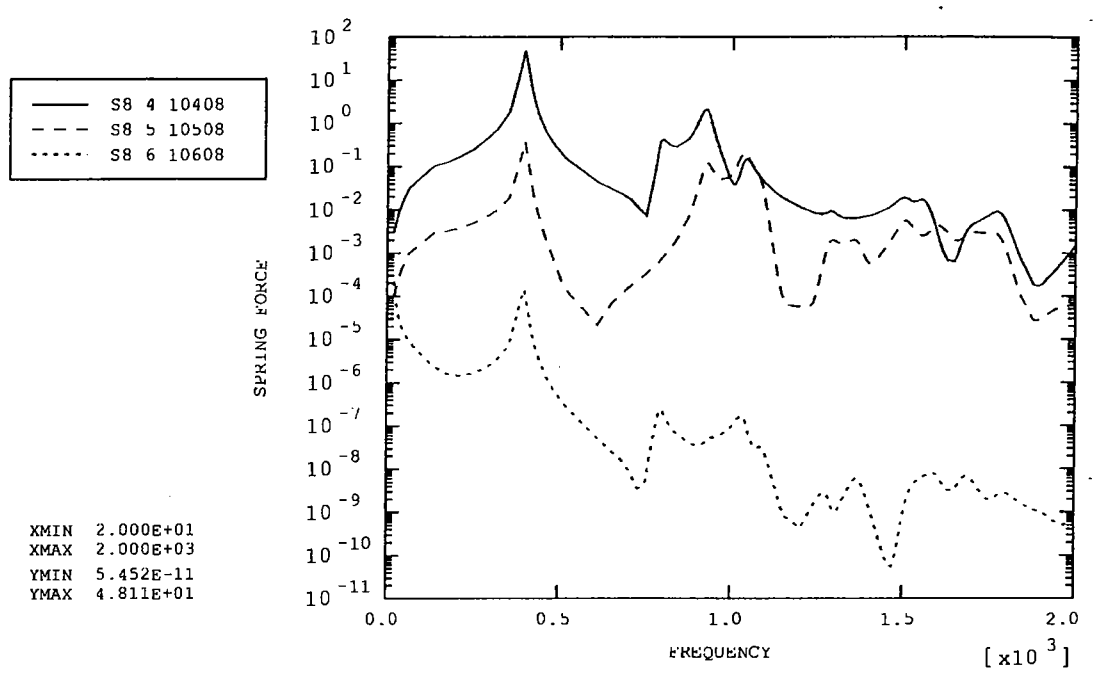

Figure 37: Jiggle pivot (top)

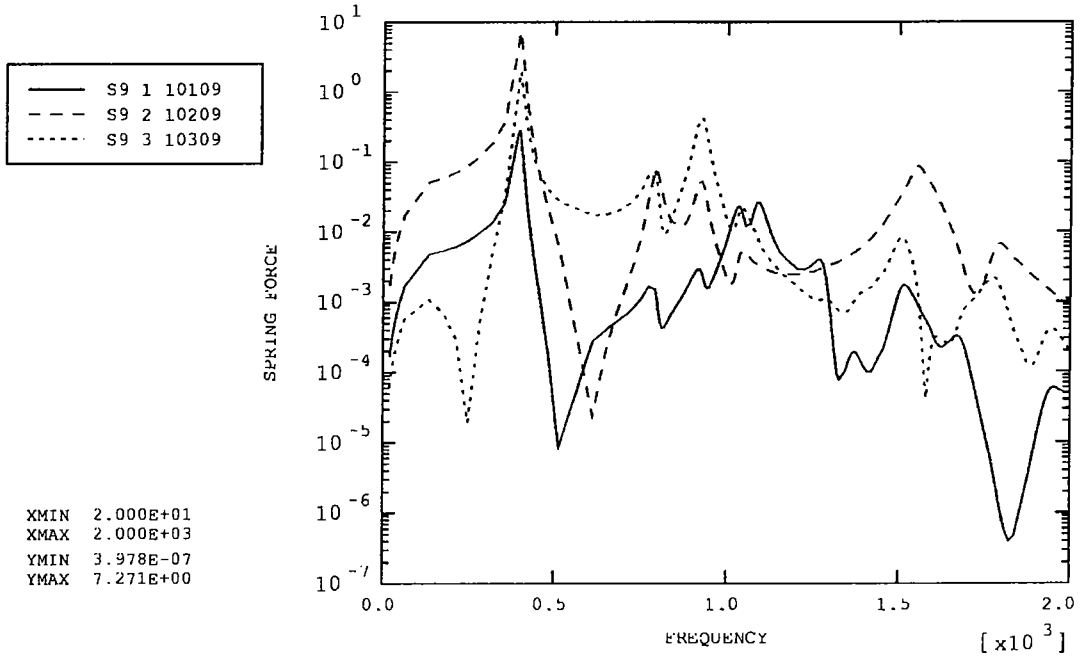

Figure 38: Jiggle pivot (bottom)

© FNC 2002

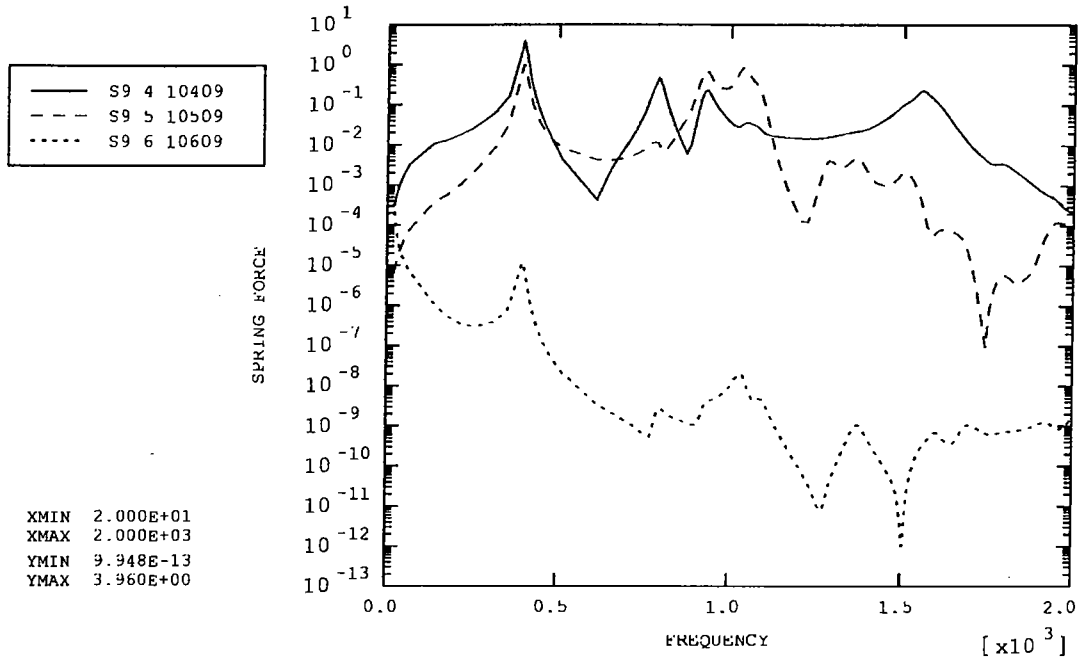

Figure 39: Jiggle pivot (bottom)

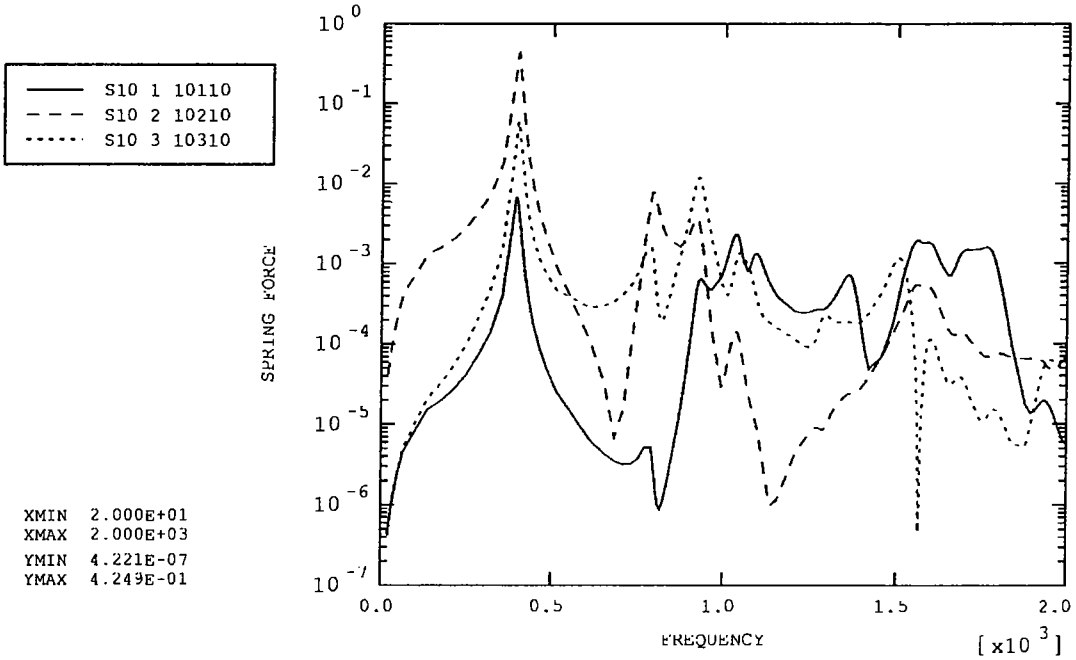

Figure 40: Chop pivot (left)

© FNC 2002

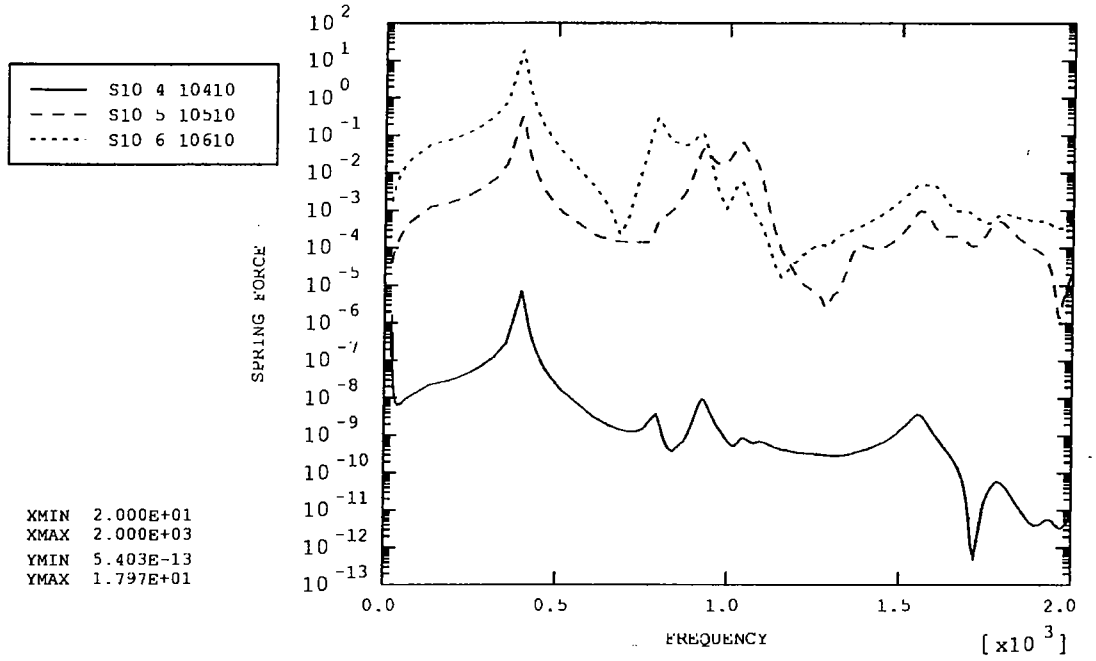

Figure 41: Chop pivot (left)

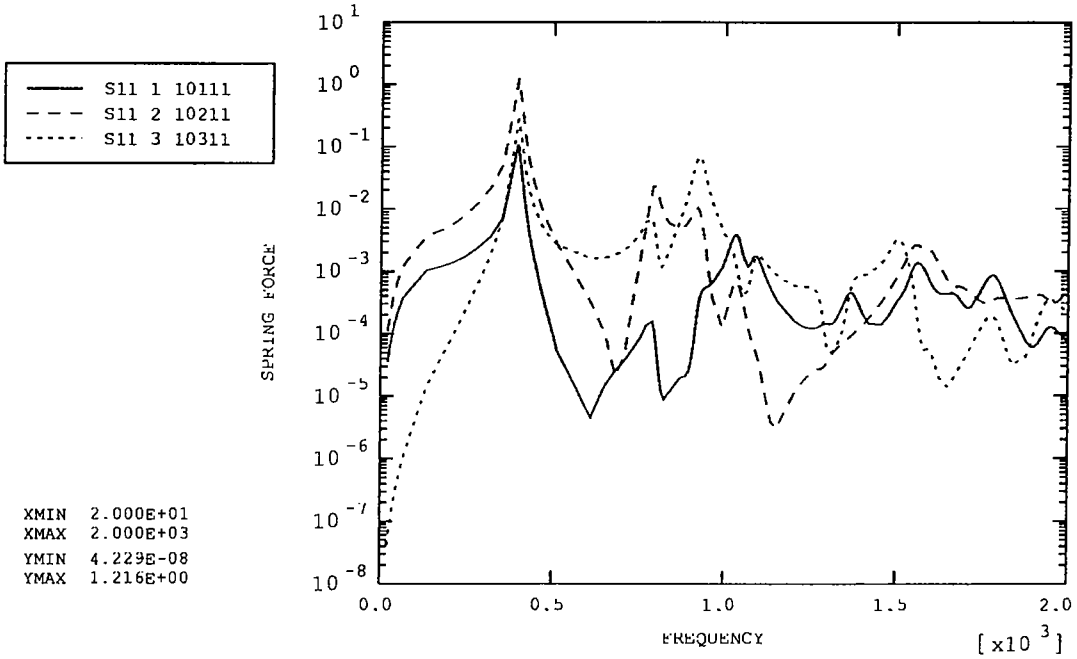

Figure 42: Chop pivot (right)

© FNC 2002

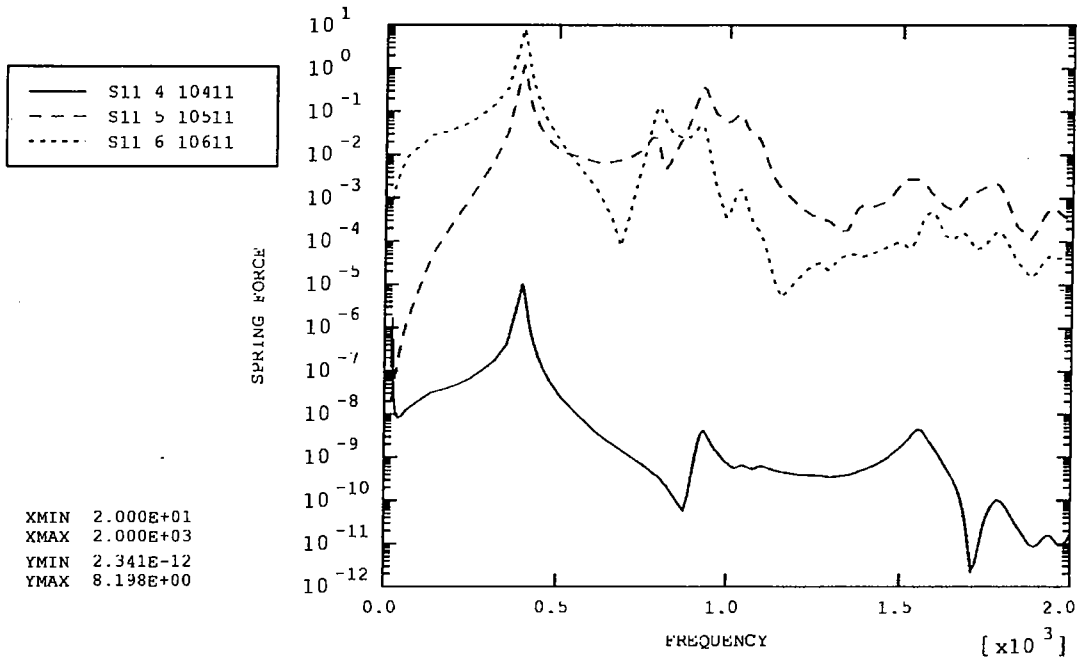

Figure 43: Chop pivot (right)

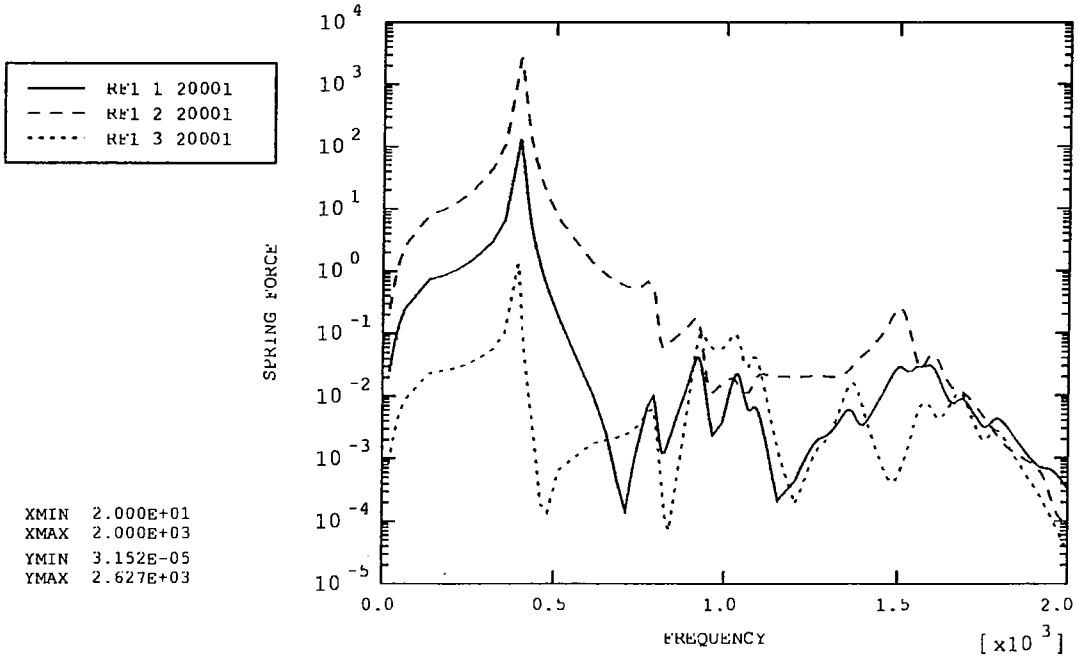

Figure 44: Reaction Force (front middle)

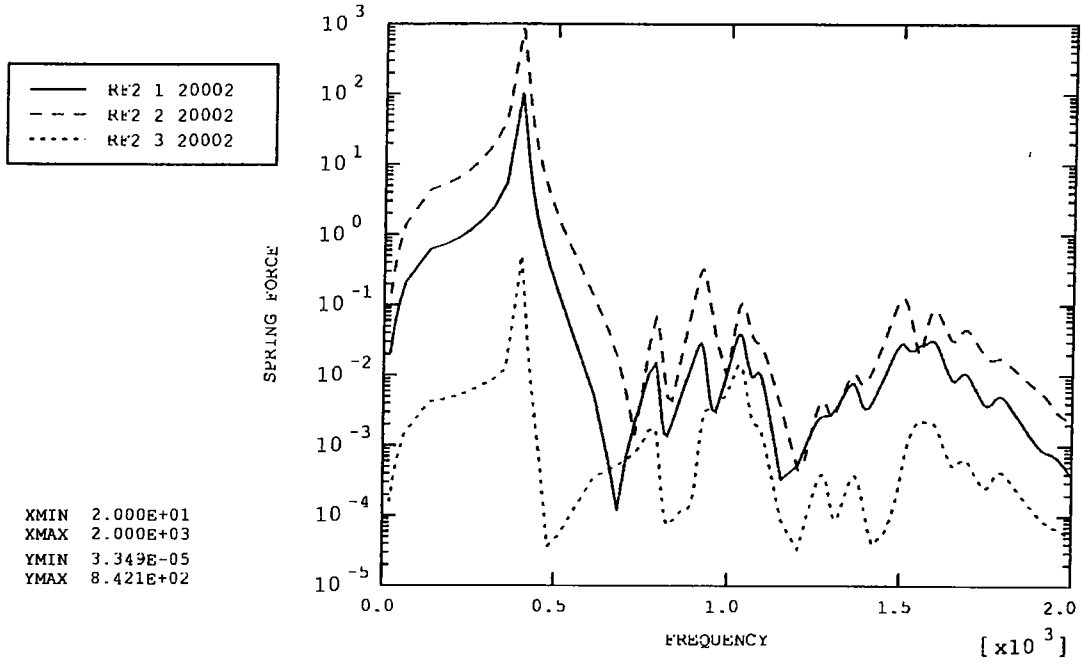

Figure 45: Reaction Force (back left)

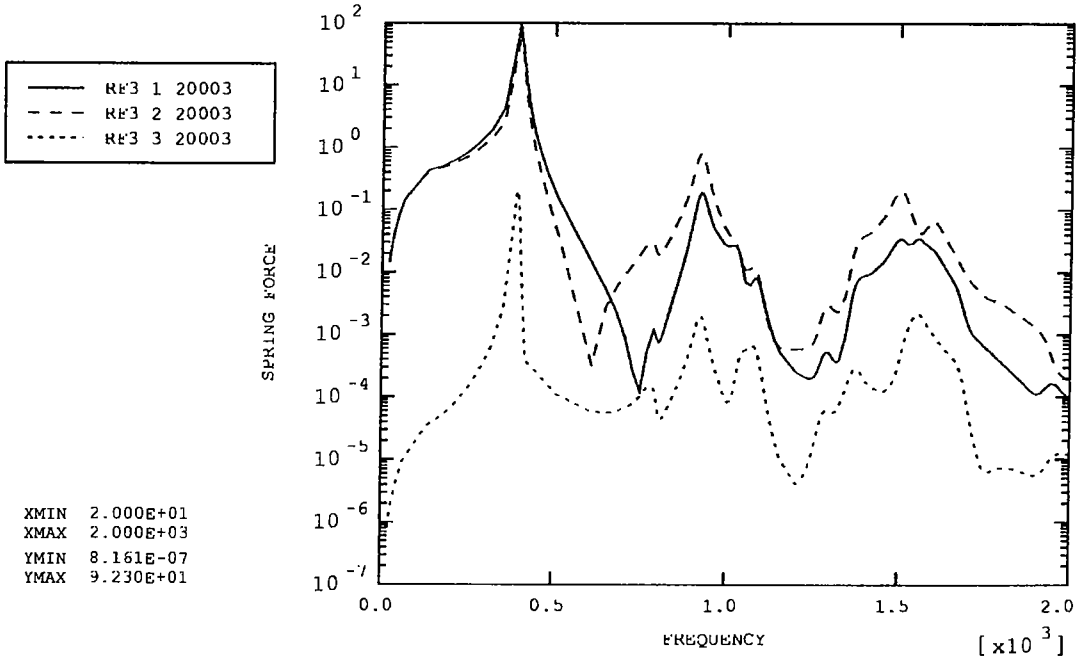

Figure 46: Reaction Force (back right)

© FNC 2002

SPIRE BSM VIBRATION ANALYSIS

Annex 5 - Random Response Y-Direction

FNC 5505/24072R Issue 1

Prepared for

U.K. Astronomy Technology Centre

FRAZER-NASH CONSULTANCY

DOCUMENT INFORMATION

Project : SPIRE BSM Vibration Analysis

Report Title : Annex 5 - Random Response Y-Direction

Client : U.K. Astronomy Technology Centre

Client Ref. : 024706

Classification :

Report No. : FNC 5505/24072R

Issue No. : 1

Date : May 2002

Compiled By : D C Reed
A J Vibert

Approved By : M W Anderson

DISTRIBUTION

Copy	Recipient	Organisation
1	I Pain	UK ATC
2	I Pain	UK ATC
3	I Pain	UK ATC
4	File	FNC

Copy No. ____

COPYRIGHT

The Copyright in this work is vested in Frazer-Nash Consultancy Limited. The document is issued in confidence solely for the purpose for which it is supplied. Reproduction in whole or in part or use for tendering or manufacturing purposes is prohibited except under an agreement with or with the written consent of Frazer-Nash Consultancy Limited and then only on the condition that this notice is included in any such reproduction.

Originating Office: FRAZER-NASH CONSULTANCY LIMITED
Stonebridge House, Dorking Business Park, Dorking, Surrey RH4 1HJ, UK
T: +44 (0)1306 885050 F: +44 (0)1306 886464 E: info@fnc.co.uk W: www.fnc.co.uk

DATA POINT POSITIONS

Note:

- The labels on the plots are as follows: e.g. P9_1_12184 refers to acceleration data point P9, degree of freedom 1 (node number 12184).
- Degrees of freedom 1, 2 and 3 refer to motion in the x, y and z directions (or X, Y and Z directions), while degrees of freedom 4, 5 and 6 refer to rotations about the x, y and z axes (or X, Y and Z axes).
- Acceleration is total acceleration (i.e. includes base motion)
- Accelerations and reaction forces are given in the global X, Y, Z co-ordinates
- Relative displacements and spring forces/torques are given in the local model x, y, z co-ordinates.
- 'Left' and 'right' directions are defined from a point of view looking towards the mirror surface, with the top of the casing furthest from the baseplate.

Fig.	P	Acceleration data points	Node number
1	1	Jiggle axis pivot (top) – frame	12182
2	2	Jiggle axis pivot (top) – jiggle stage	12200
3	3	Jiggle axis pivot (bottom) – frame	12183
4	4	Jiggle axis pivot (bottom) – jiggle stage	12192
5	5	Chop axis pivot (right side) – jiggle stage	12189
6	6	Chop axis pivot (right side) – chop stage	114
7	7	Chop axis pivot (left side) – jiggle stage	12188
8	8	Chop axis pivot (left side) – chop stage	105
9	9	Chop motor (top)	12184
10	10	Chop motor (bottom)	12185
11	11	Jiggle motor (right side)	12186
12	12	Jiggle motor (left side)	12187
13	13	PCAL CG	12193
14	14	PCAL extension to mirror centre	12199
15	15	Launch latch 'A' CG	12196
16	16	Launch latch 'A' extension to magnet centre	12197
17	17	Connector (top)	12194
18	18	Chop magnet (top)	115
19	19	Chop magnet (bottom)	122
20	20	Mirror Centre	9583
21	21	Jiggle magnet (right)	9276
22	22	Jiggle magnet (left)	9264

© FNC 2002

Fig.	E	Displacement between...	Element
23	1	Chop magnet vs. motor (top)	90n01, n=1, 2
24	2	Chop magnet vs. motor (bottom)	90n02, n=1, 2
25	3	Jiggle magnet vs. motor (right)	90n03, n=2, 3
26	4	Jiggle magnet vs. motor (left)	90n04, n=2, 3
27	5	Mirror centre vs. PCAL extension	90n05, n=1, 2, 3
28	6	Chop magnet (top) vs. launch latch 'A'	90206

Fig.	S	Position of spring elements	Node 1	Element
29	1	Front baffle (top left)	9702	10n01, n=1,2,3
30	2	Front baffle (top right)	9739	10n02, n=1,2,3
31	3	Front baffle (bottom left)	9629	10n03, n=1,2,3
32	4	Front baffle (bottom right)	9594	10n04, n=1,2,3
33	5	Base (front middle)*	3894	10n05, n=1,2,3
34	6	Base (back left)*	3414	10n06, n=1,2,3
35	7	Base (back right)*	3622	10n07, n=1,2,3
36,37	8	Jiggle pivot (top)	12200	10n08, n=1 to 6
38,39	9	Jiggle pivot (bottom)	12192	10n09, n=1 to 6
40,41	10	Chop pivot (left)	12188	10n10, n=1 to 6
42,43	11	Chop pivot (right)	12189	10n11, n=1 to 6

Fig.	RF	Reaction Forces	Node number
44	1	Reaction Force (front middle)	10587
45	2	Reaction Force (back left)	10722
46	3	Reaction Force (back right)	10671

* The baseplate-casing connections are each modelled using a single spring in the local x and y directions, and five springs in the local z direction. The forces from these five springs are added together to calculate the total connective force. The curve labels for the z direction degrees of freedom have the prefix 'B'.

© FNC 2002

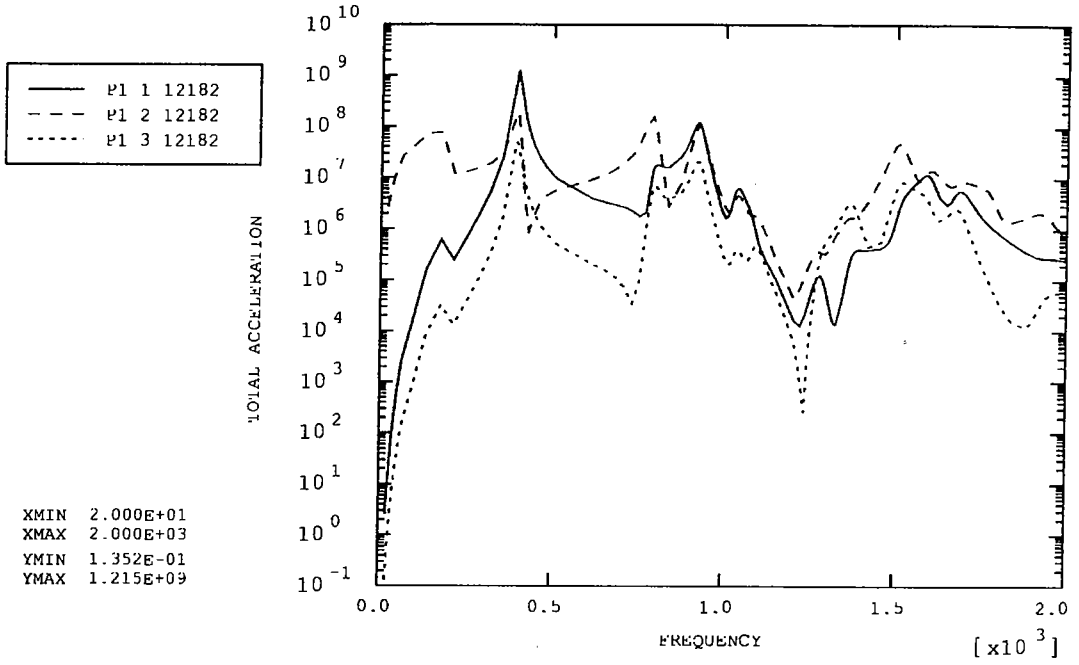

Figure 1: Jiggle axis pivot (top) – frame

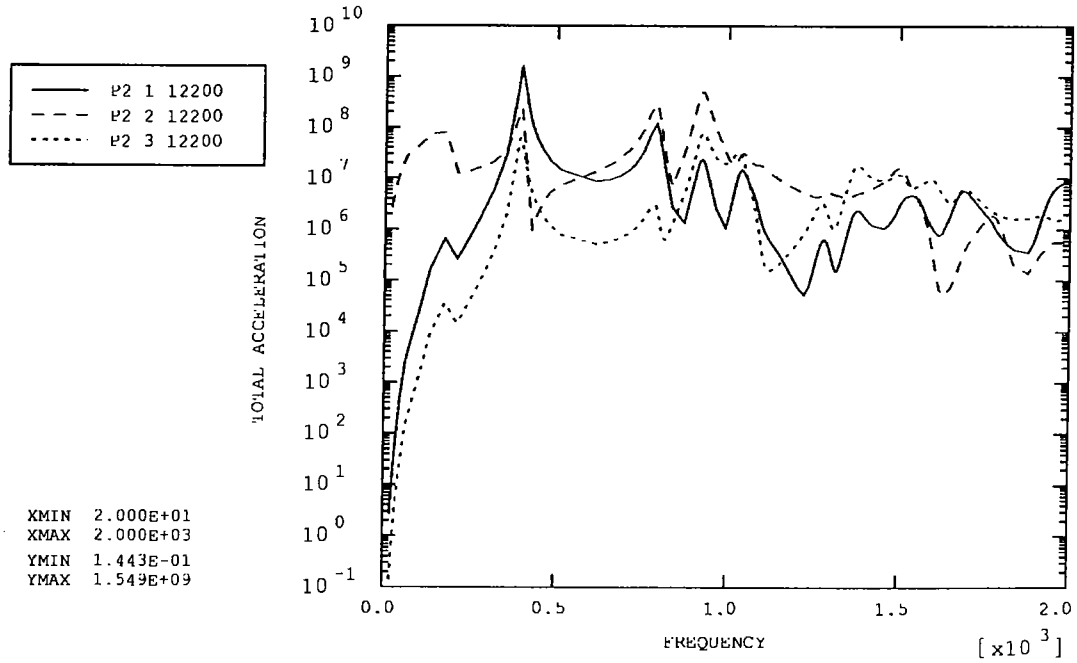

Figure 2: Jiggle axis pivot (top) – jiggle stage

© FNC 2002

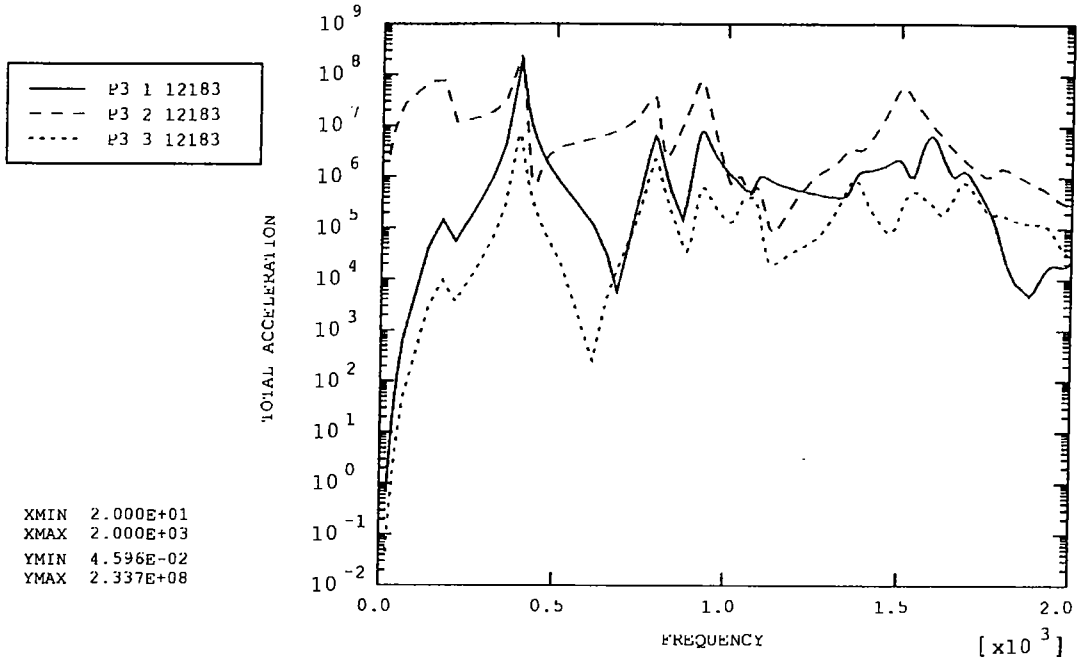

Figure 3: Jiggle axis pivot (bottom) – frame

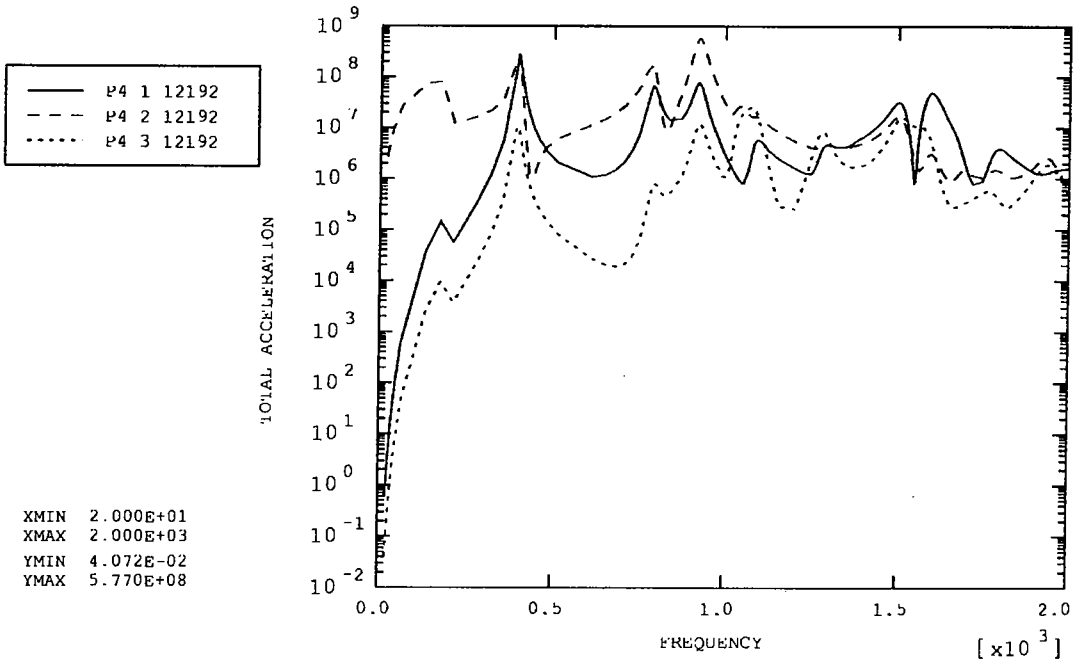

Figure 4: Jiggle axis pivot (bottom) – jiggle stage

© FNC 2002

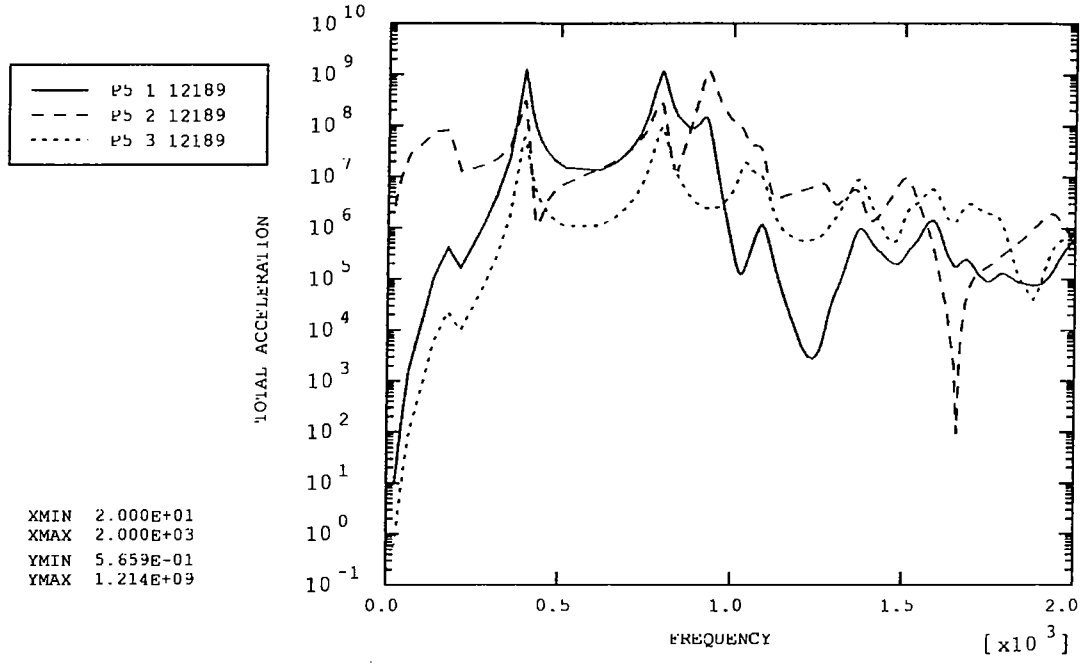

Figure 5: Chop axis pivot (right side) – jiggle stage

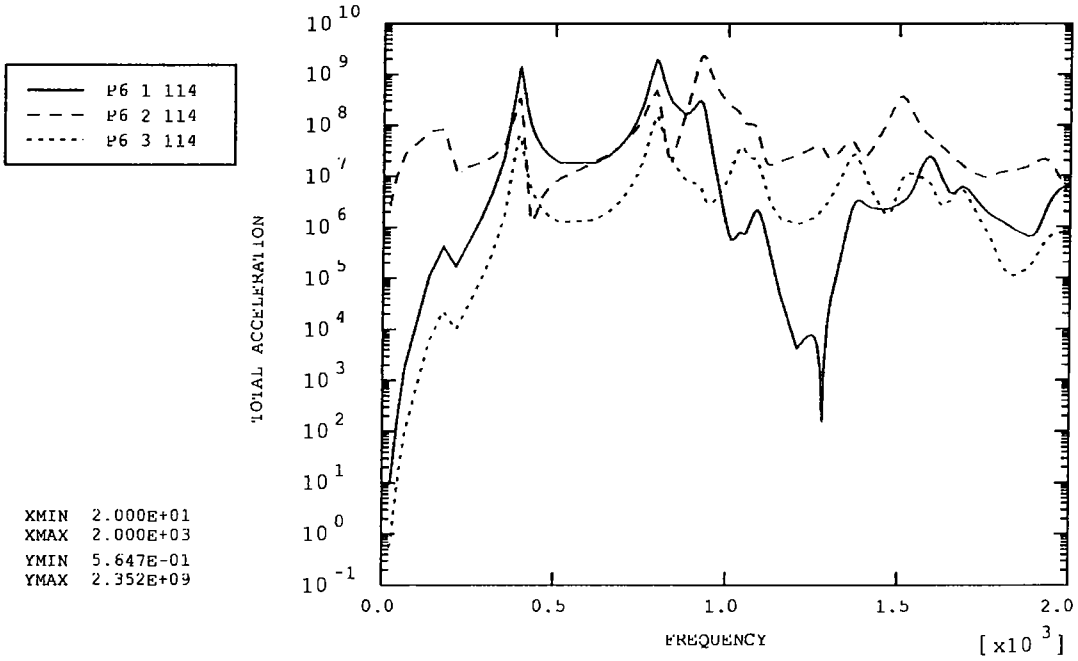

Figure 6: Chop axis pivot (right side) – chop stage

© FNC 2002

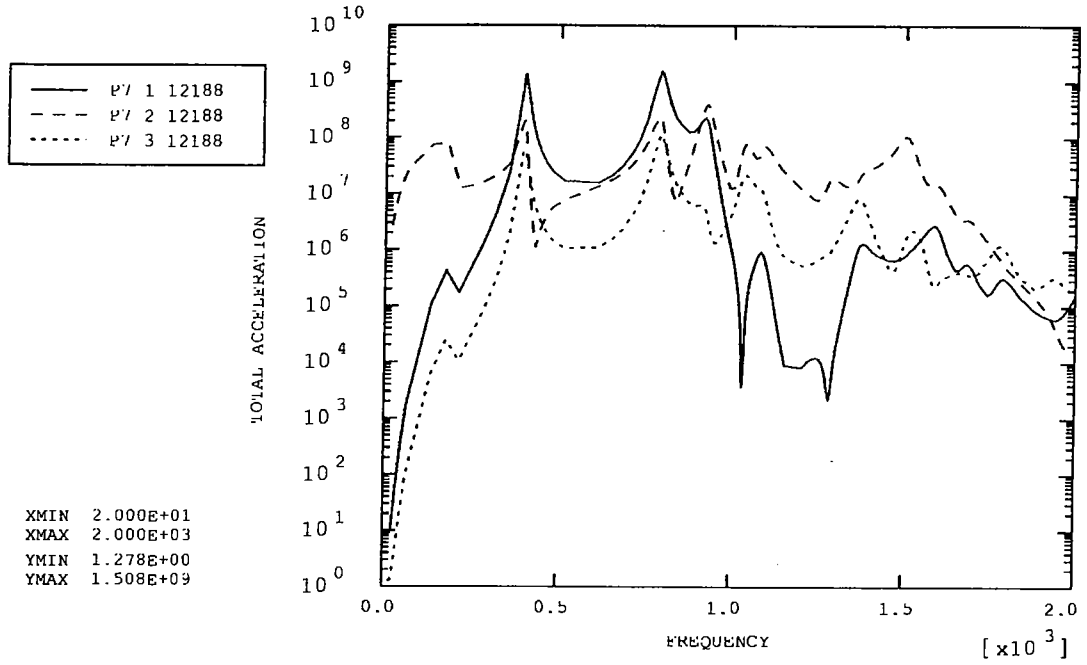

Figure 7: Chop axis pivot (left side) – jiggle stage

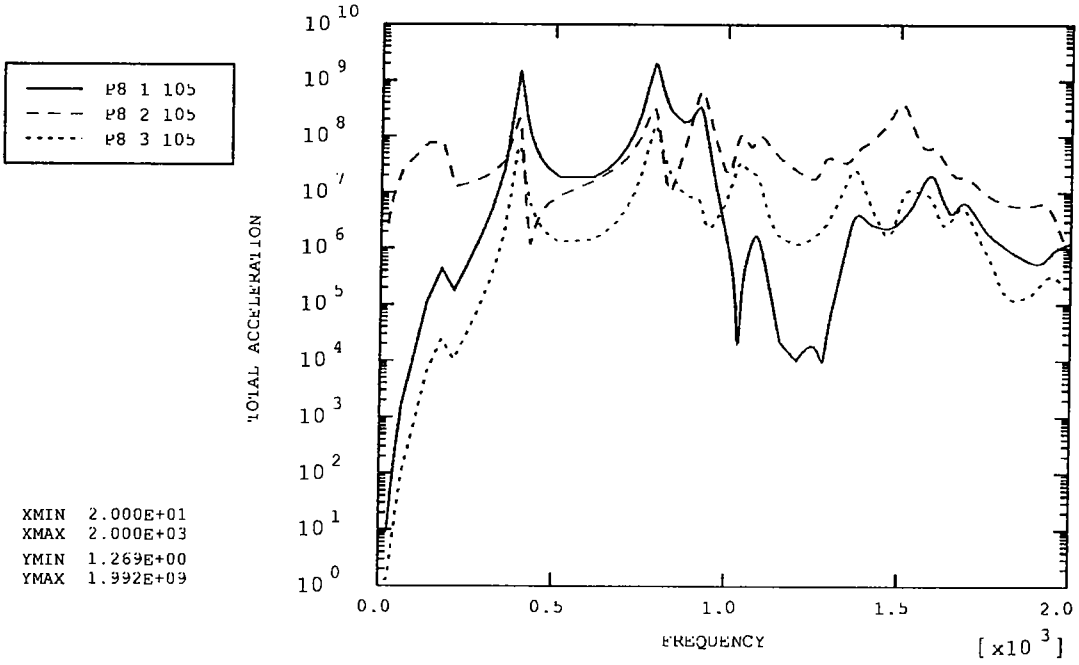

Figure 8: Chop axis pivot (left side) – chop stage

© FNC 2002

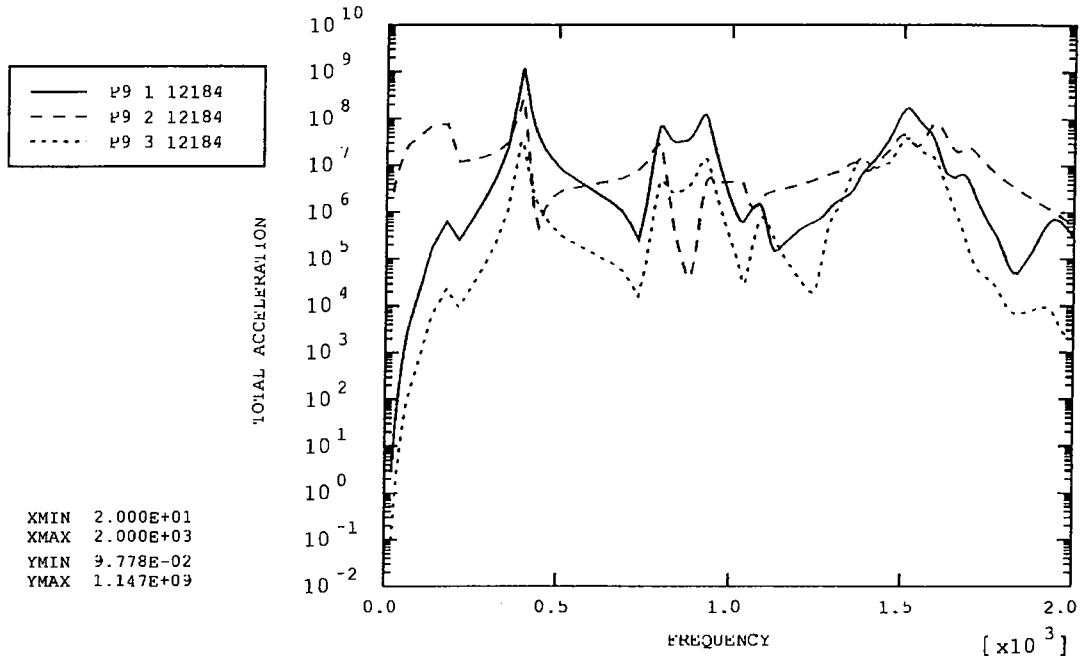

Figure 9: Chop motor (top)

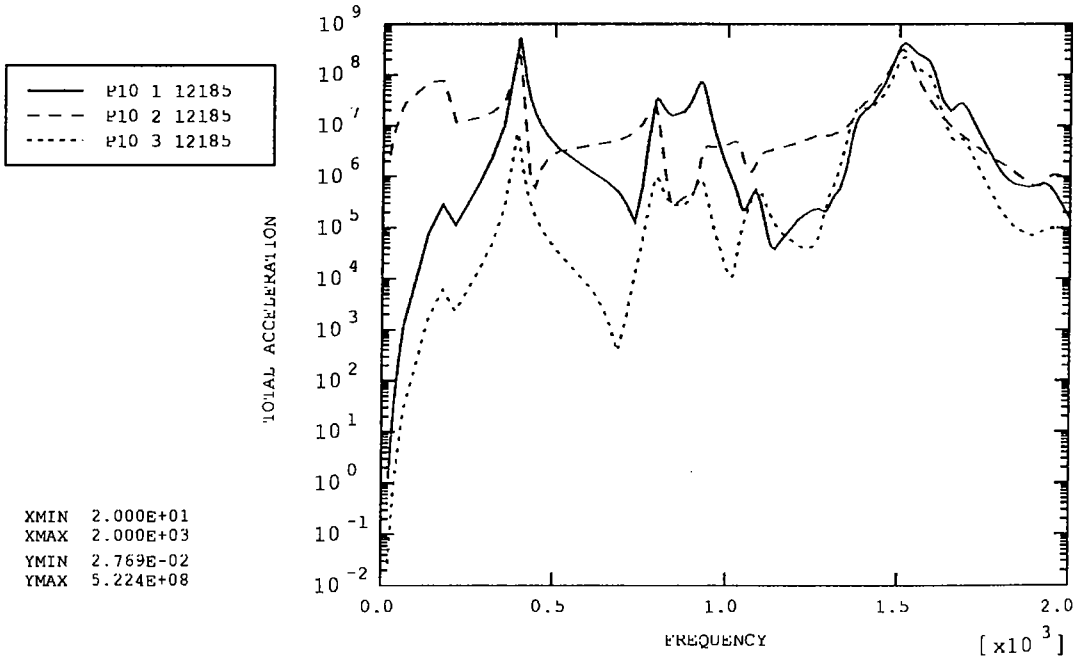

Figure 10: Chop motor (bottom)

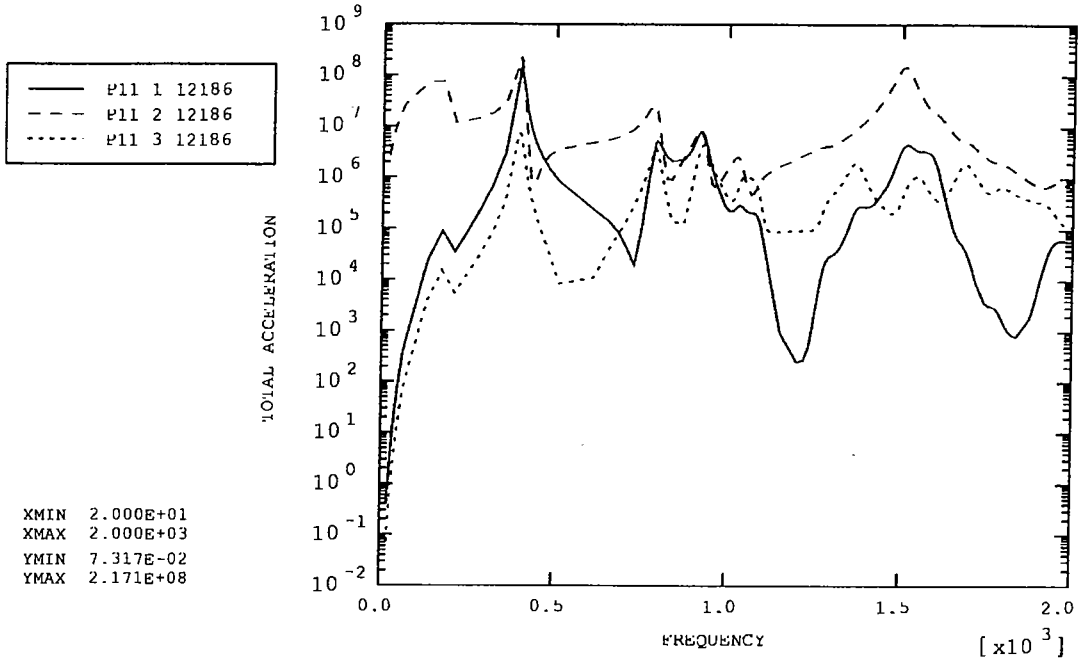

Figure 11: Jiggle motor (right side)

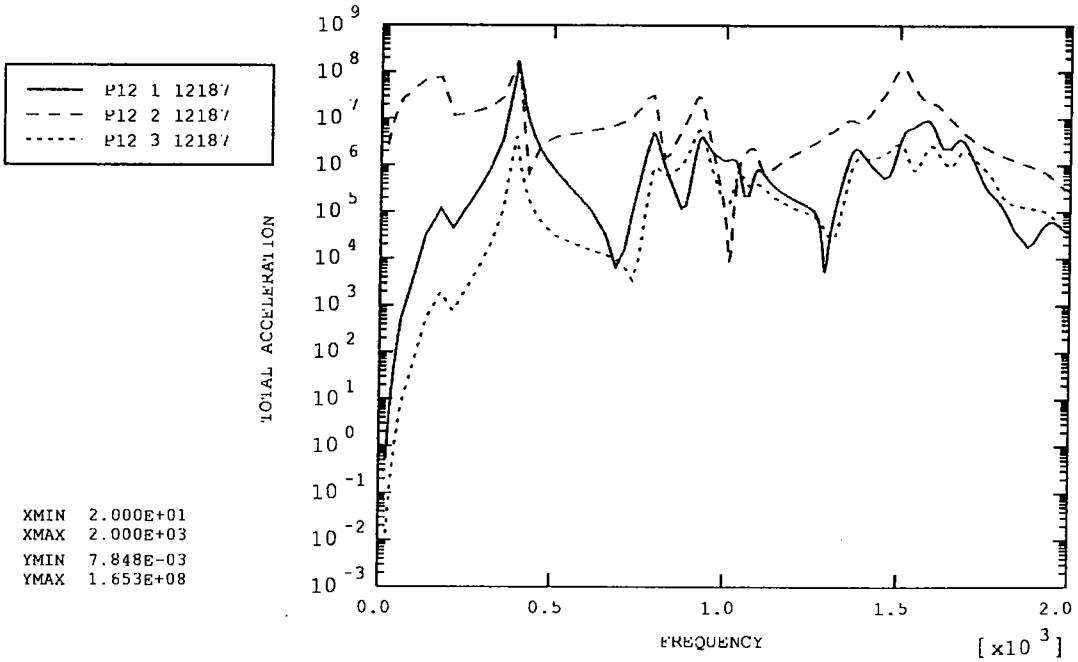

Figure 12: Jiggle motor (left side)

© FNC 2002

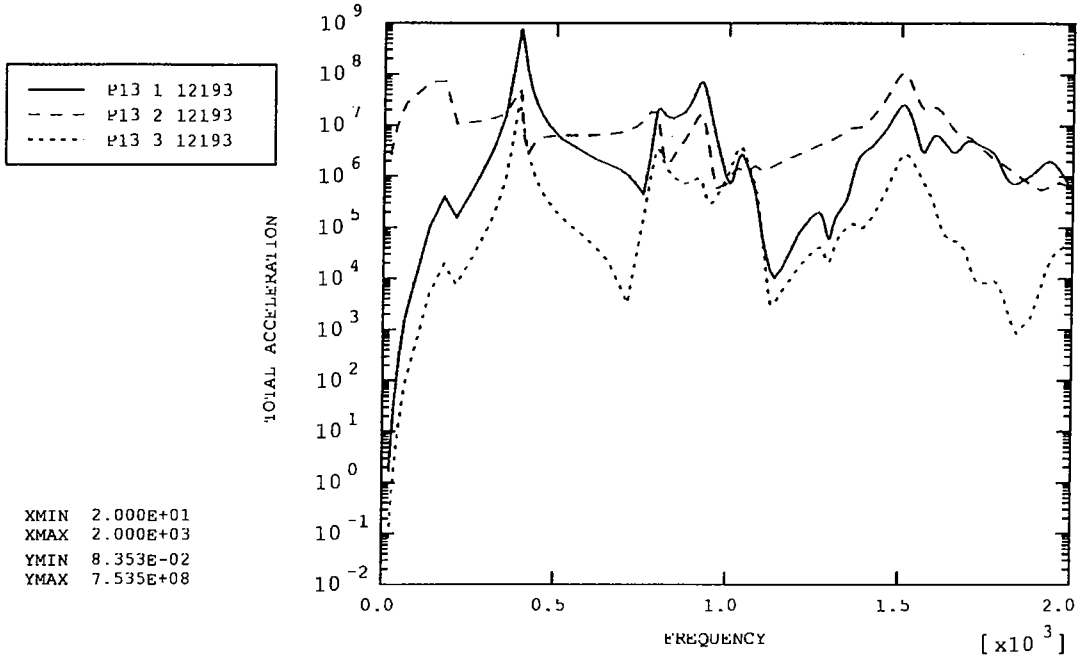

Figure 13: PCAL CG

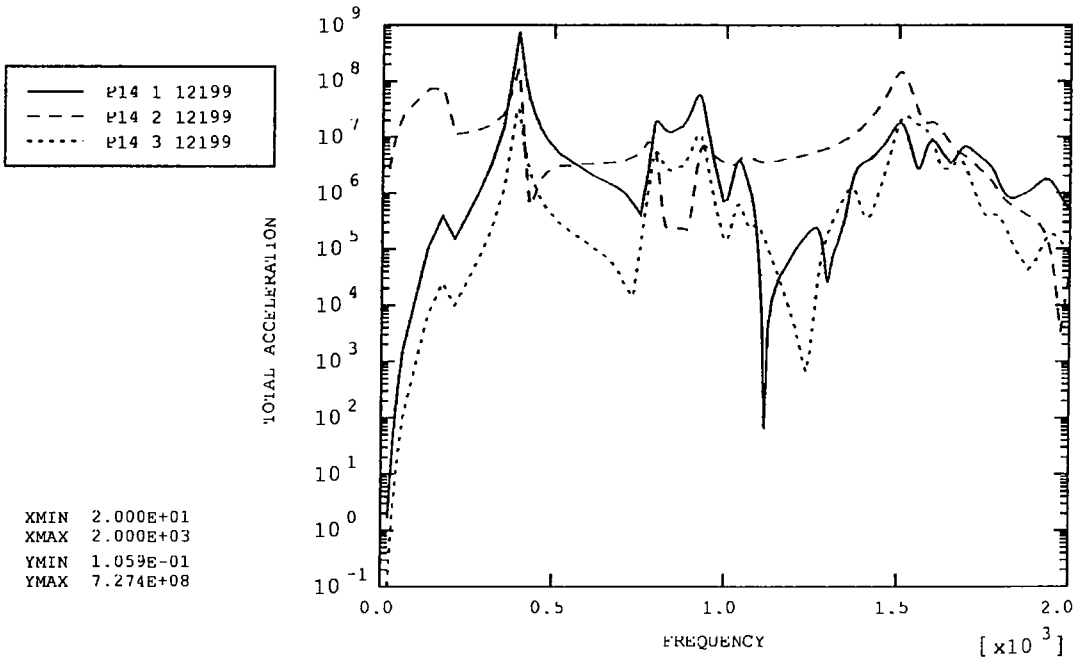

Figure 14: PCAL extension to mirror centre

© FNC 2002

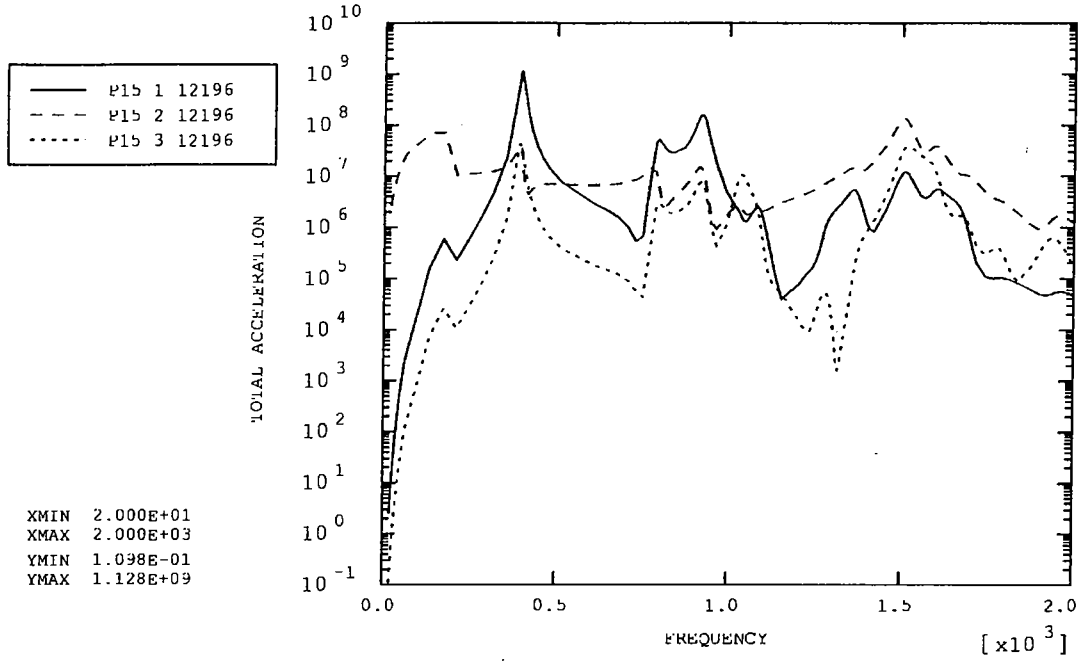

Figure 15: Launch latch 'A' CG

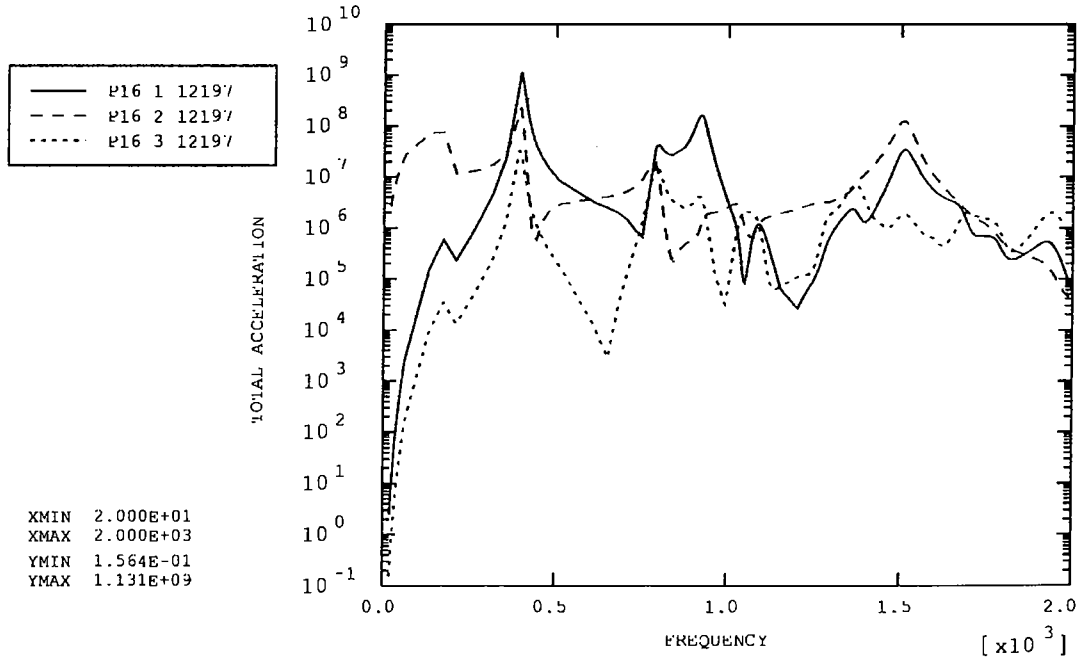

Figure 16: Launch latch 'A' extension to magnet centre

© FNC 2002

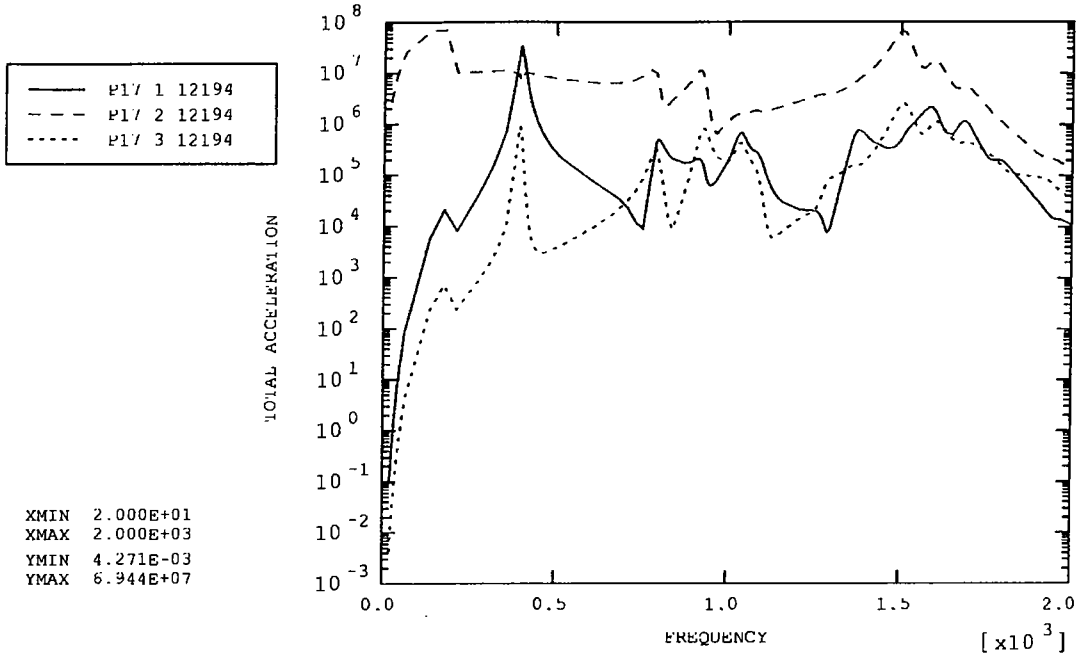

Figure 17: Connector (top)

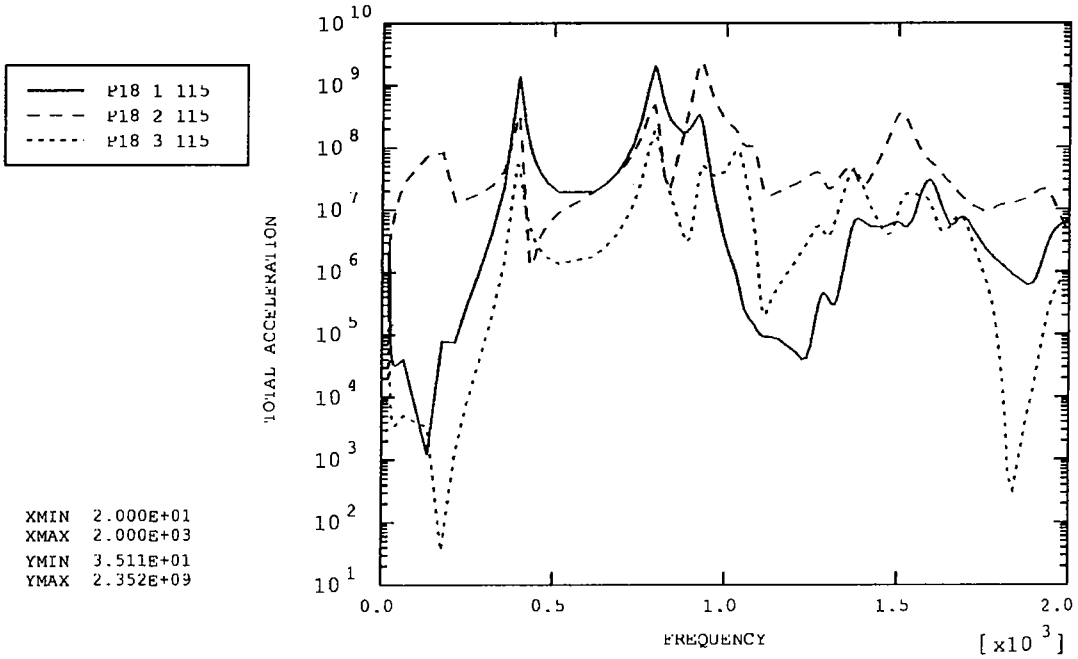

Figure 18: Chop magnet (top)

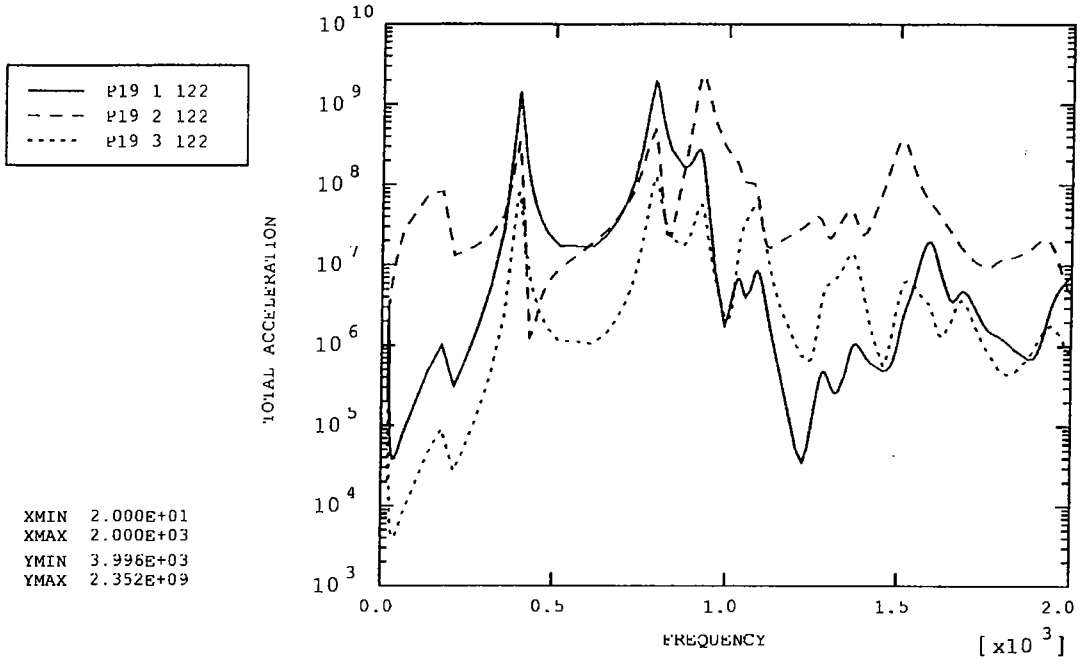

Figure 19: Chop magnet (bottom)

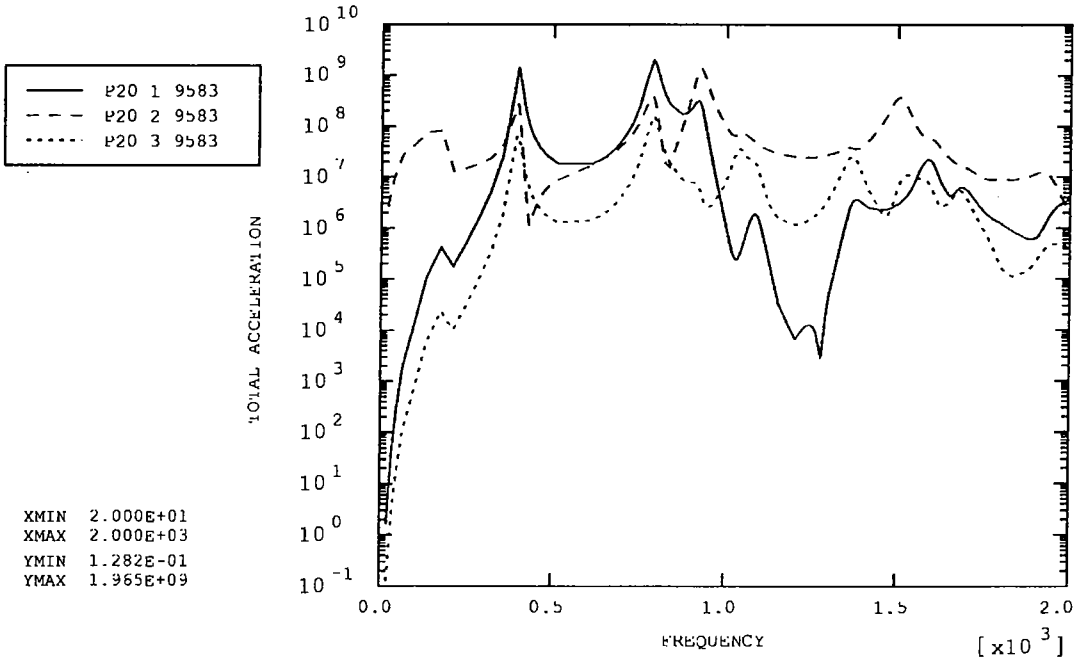

Figure 20: Mirror Centre

© FNC 2002

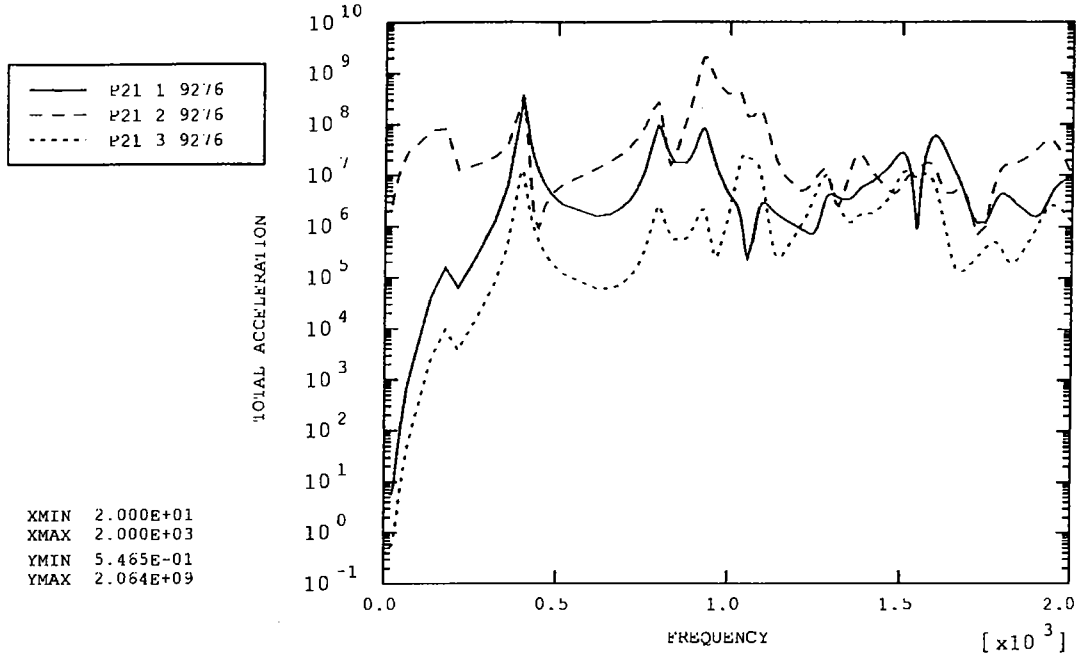

Figure 21: Jiggle magnet (right)

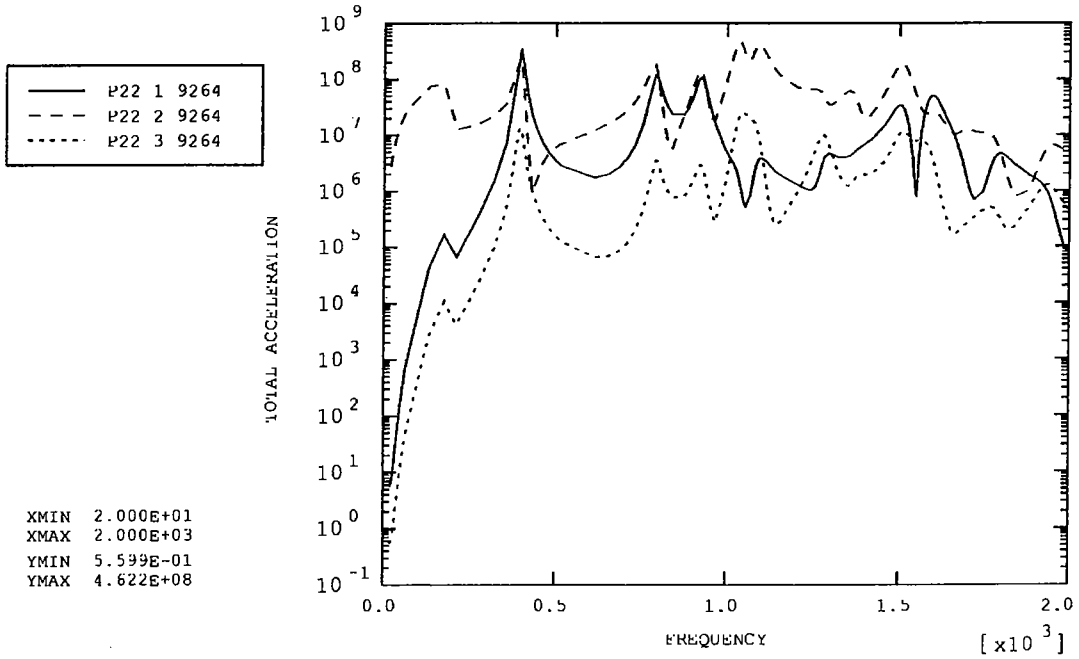

Figure 22: Jiggle magnet (left)

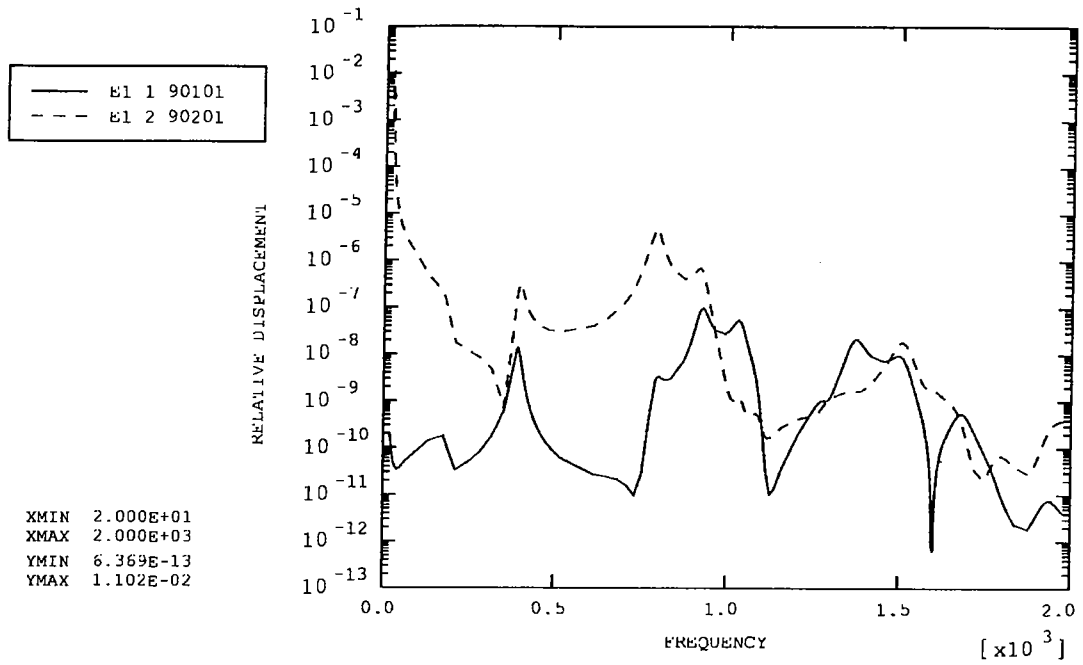

Figure 23: Chop magnet vs. motor (top)

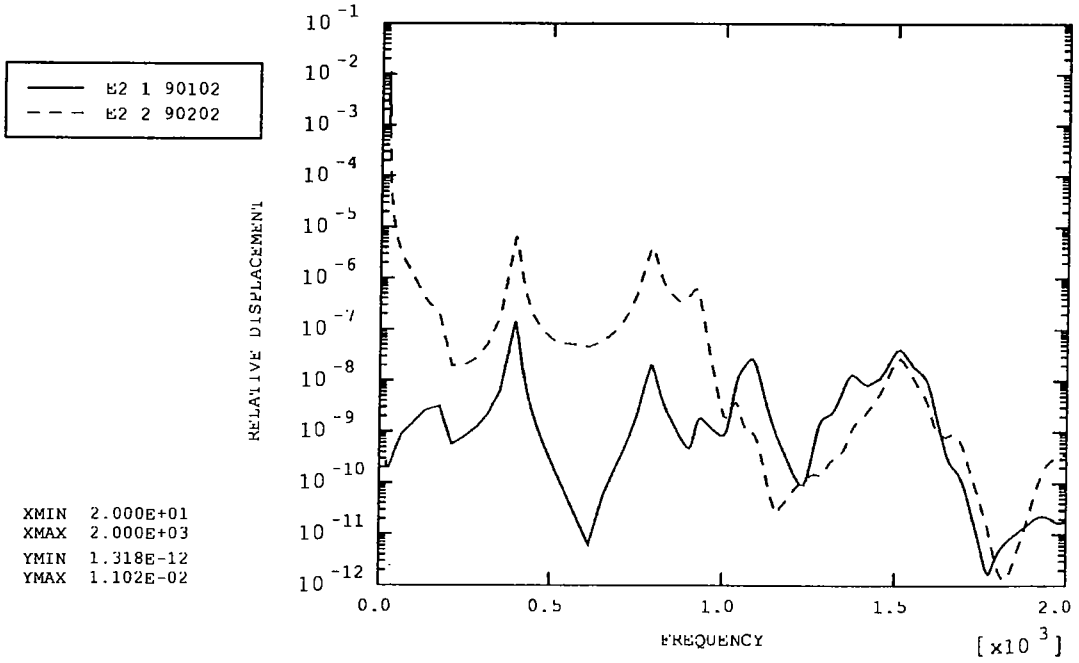

Figure 24: Chop magnet vs. motor (bottom)

© FNC 2002

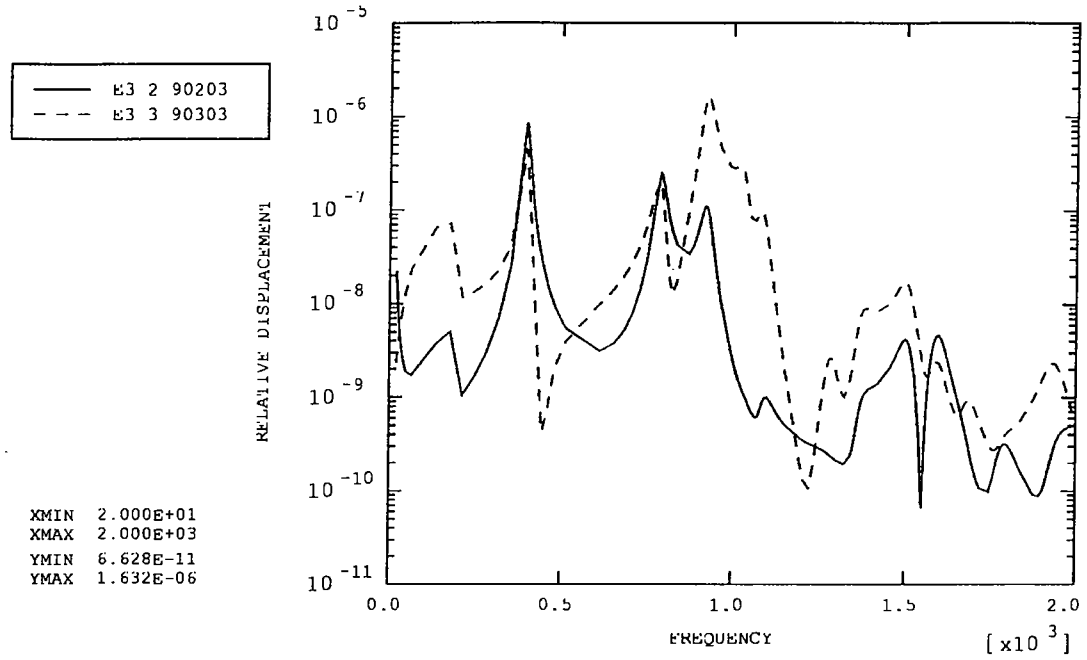

Figure 25: Jiggle magnet vs. motor (right)

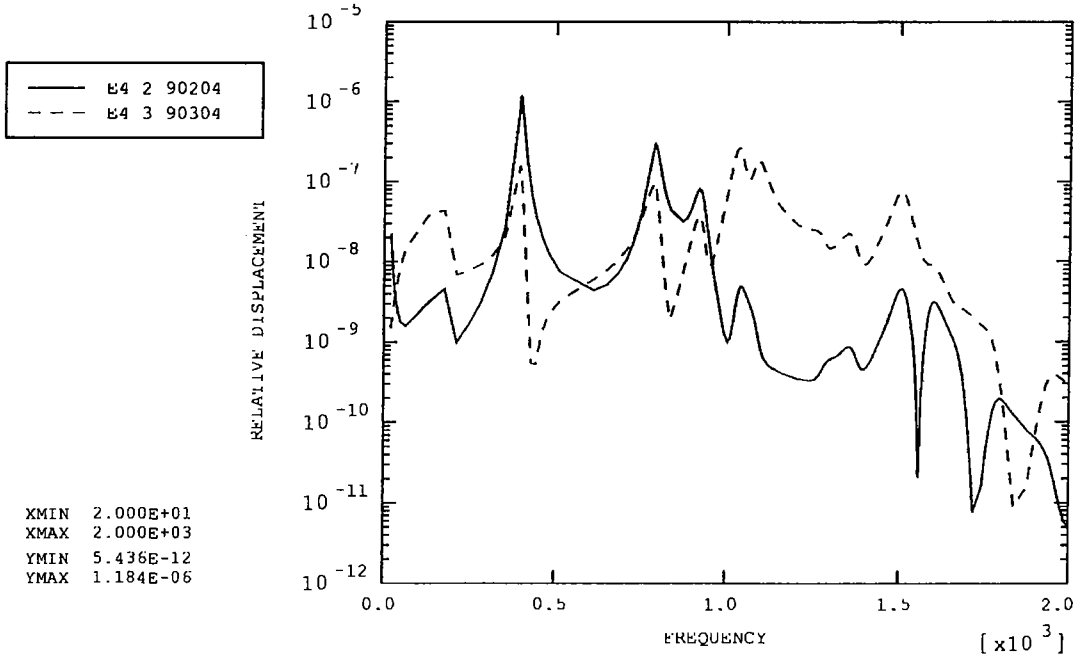

Figure 26: Jiggle magnet vs. motor (left)

© FNC 2002

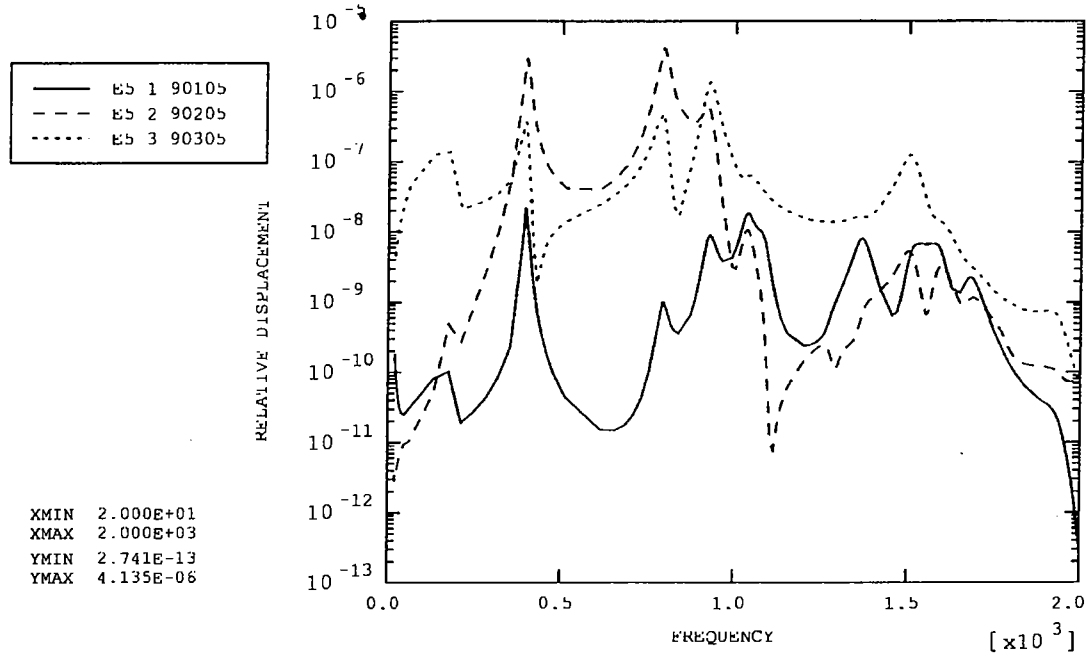

Figure 27: Mirror centre vs. PCAL extension

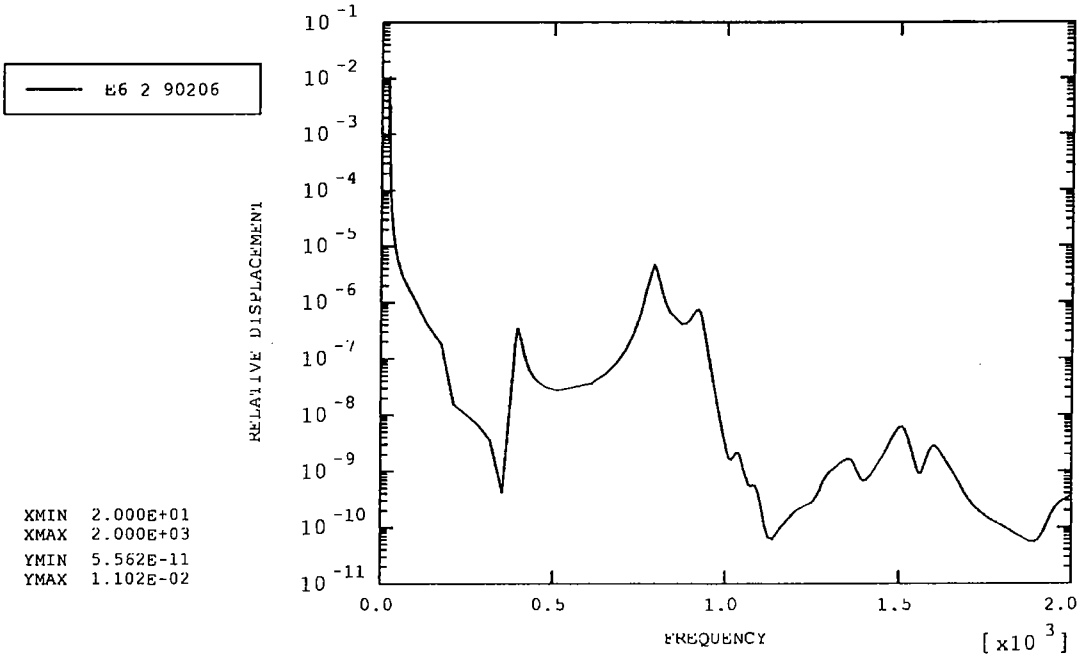

Figure 28: Chop magnet (top) vs. launch latch 'A'

© FNC 2002

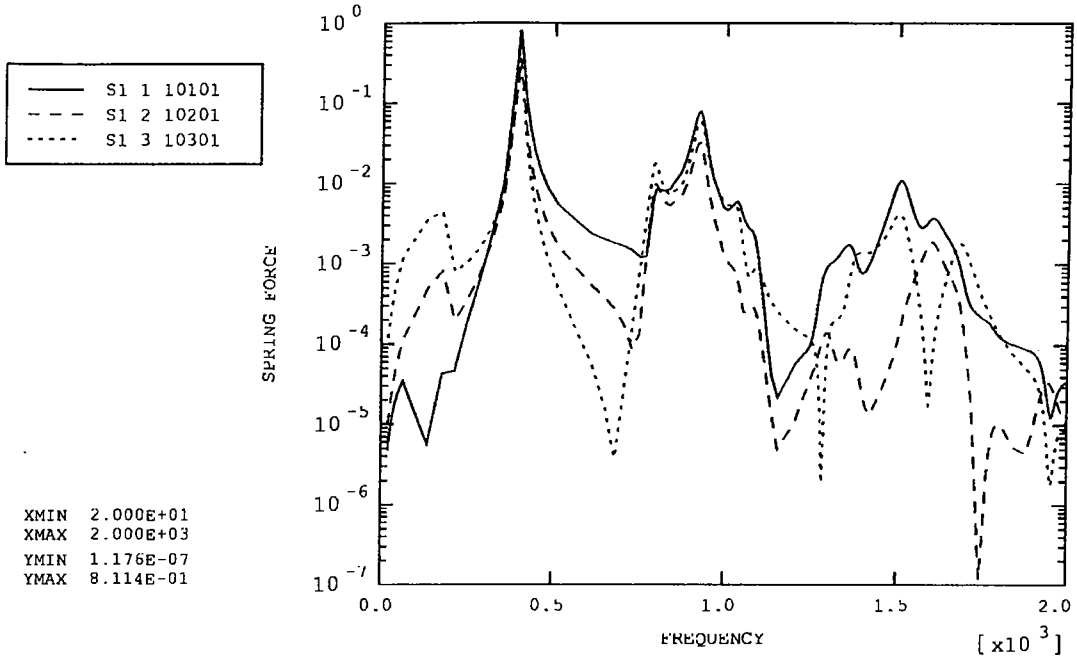

Figure 29: Front baffle (top left)

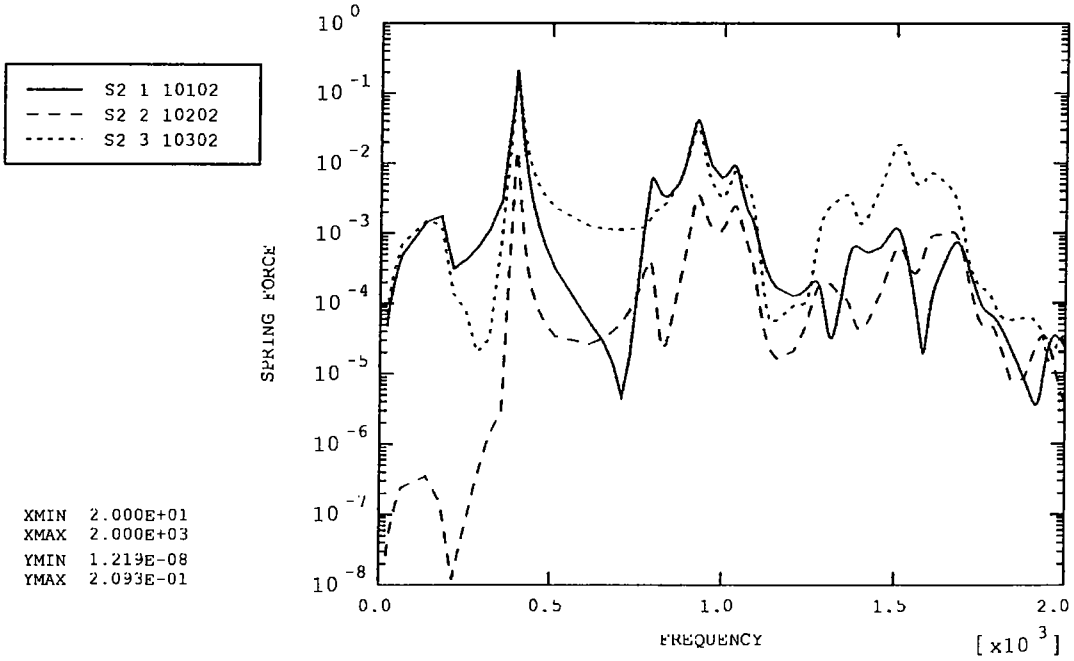

Figure 30: Front baffle (top right)

© FNC 2002

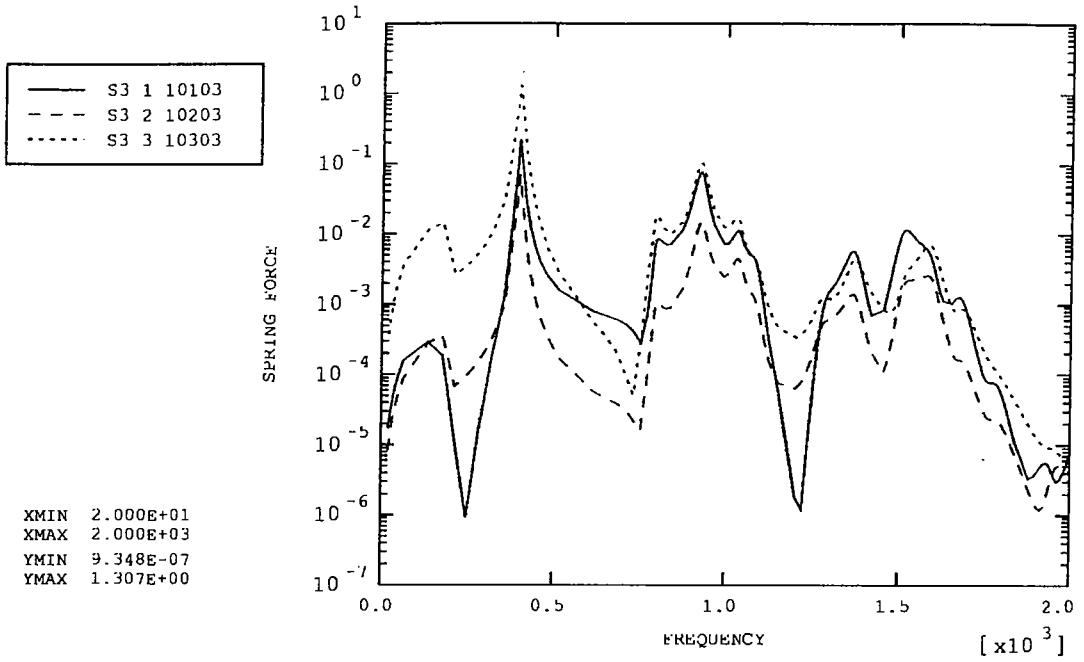

Figure 31: Front baffle (bottom left)

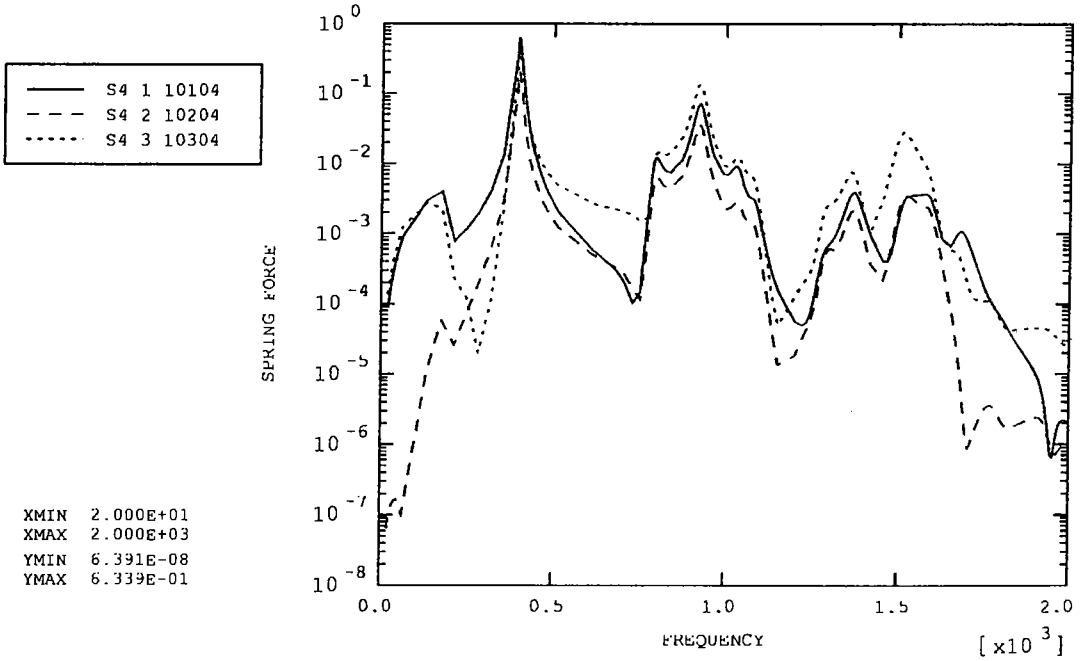

Figure 32: Front baffle (bottom right)

© FNC 2002

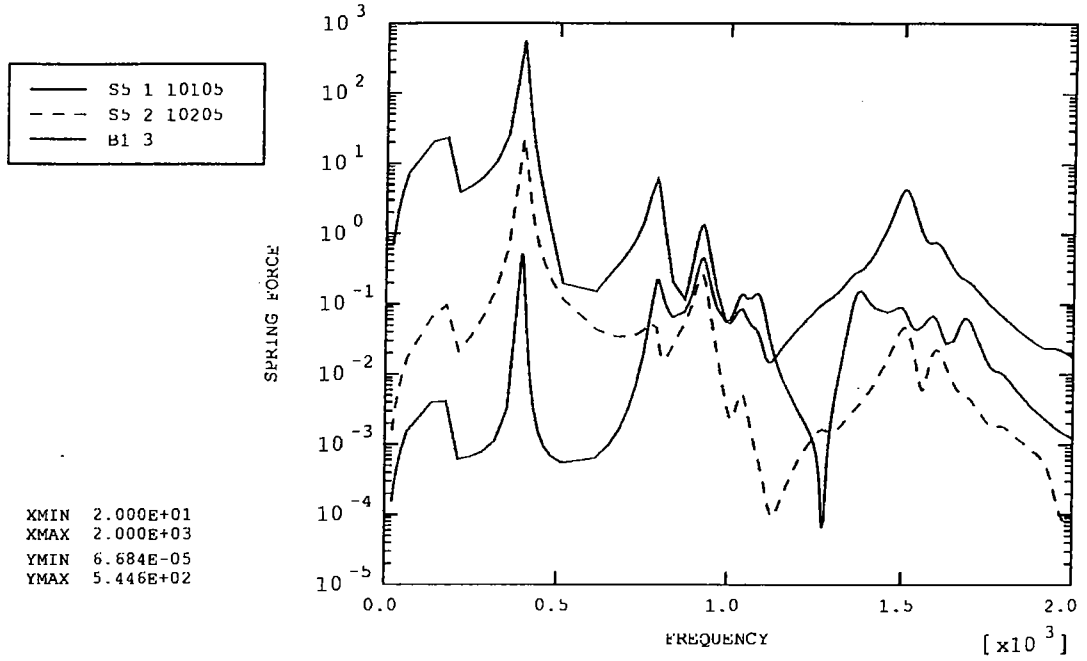

Figure 33: Base (front middle)

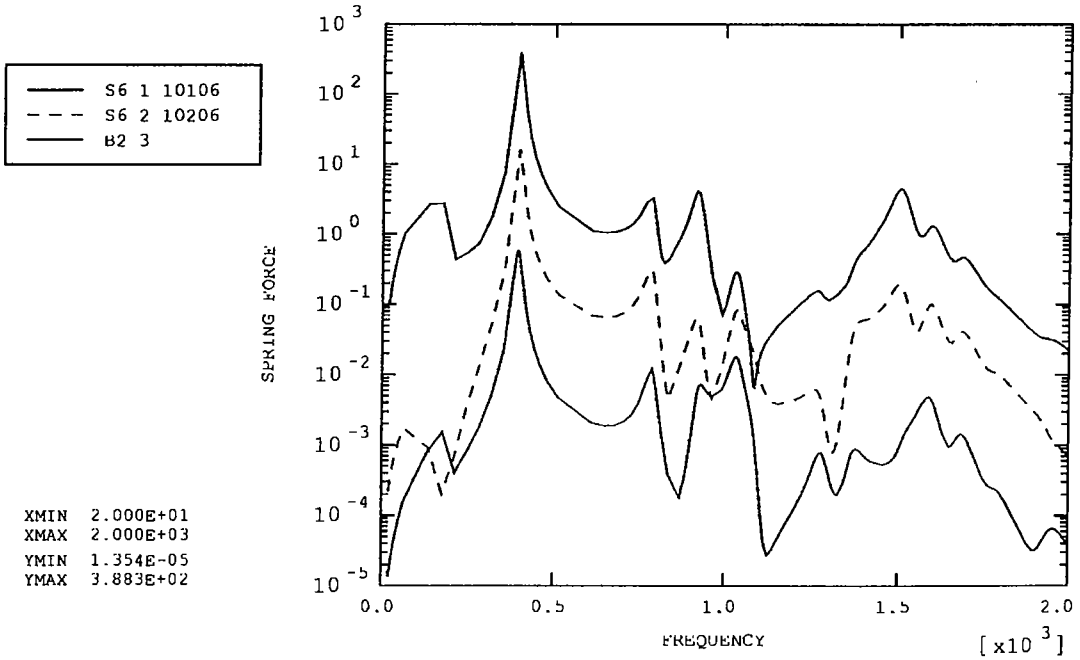

Figure 34: Base (back left)

© FNC 2002

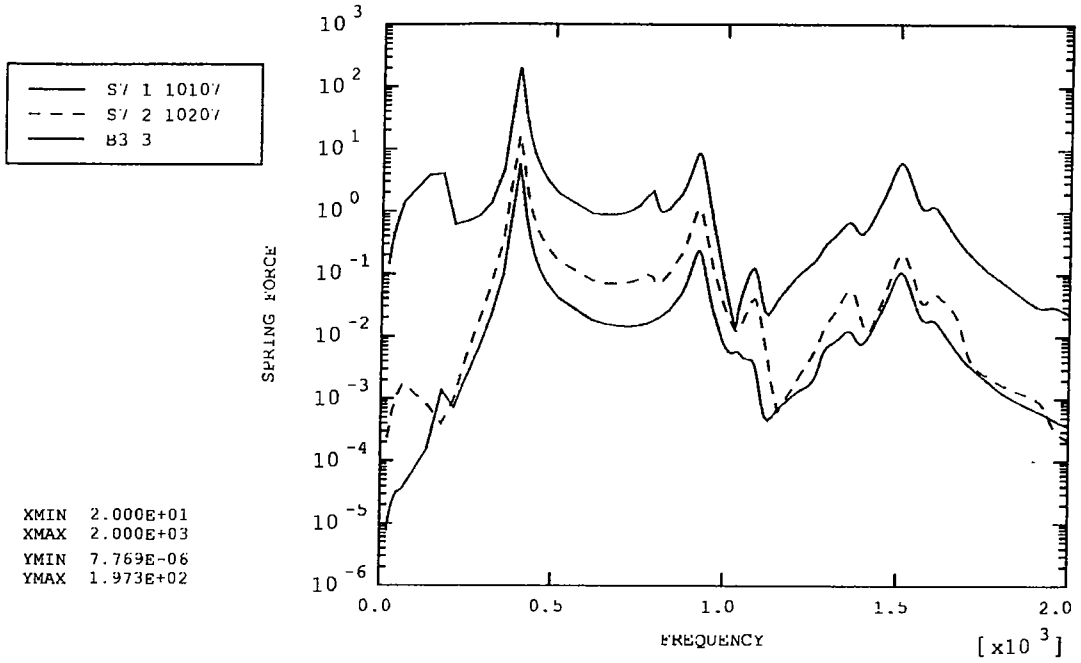

Figure 35: Base (back right)

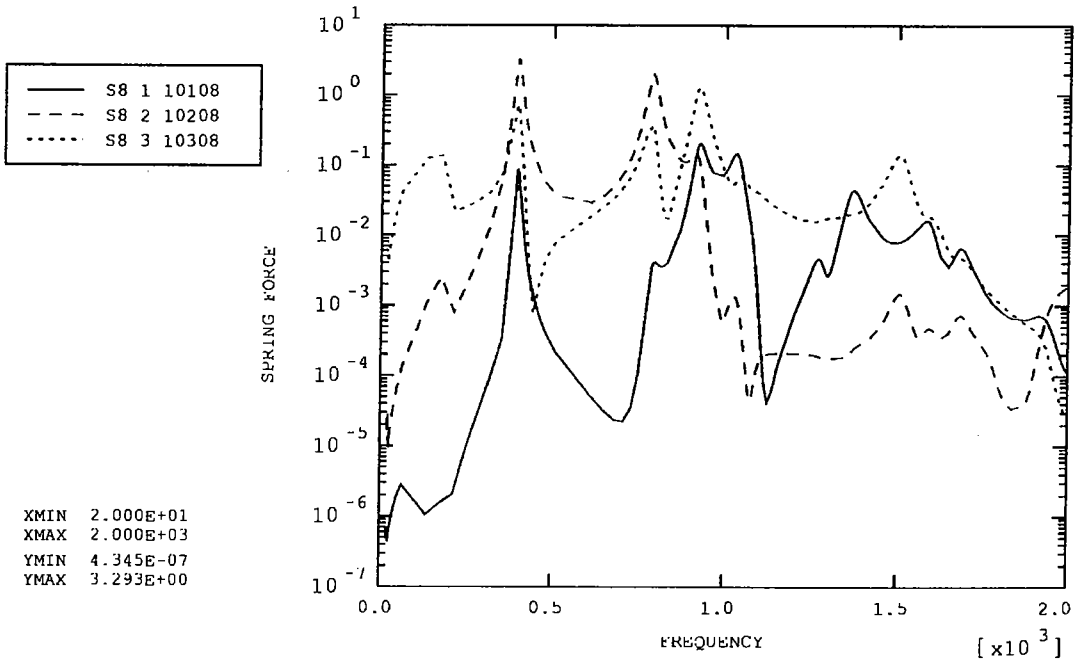

Figure 36: Jiggle pivot (top)

© FNC 2002

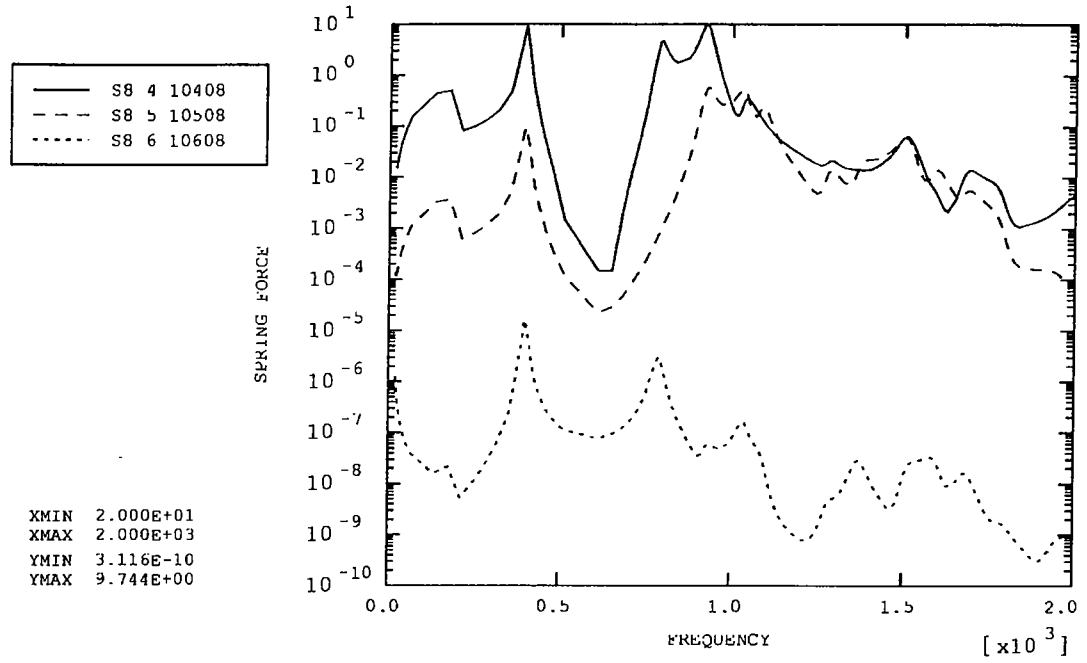

Figure 37: Jiggle pivot (top)

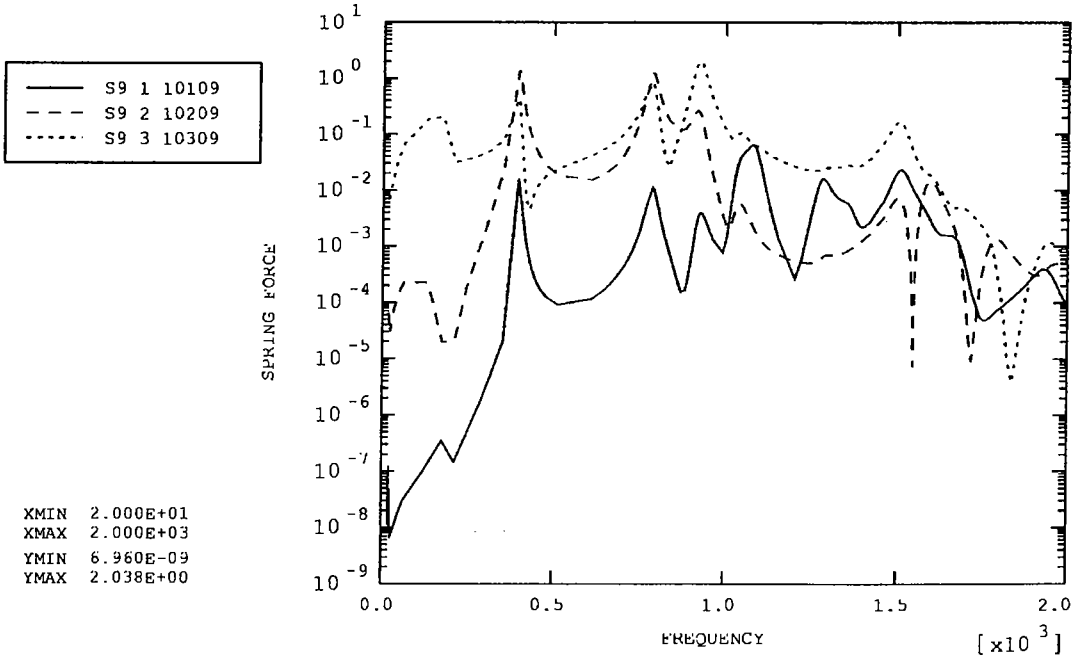

Figure 38: Jiggle pivot (bottom)

© FNC 2002

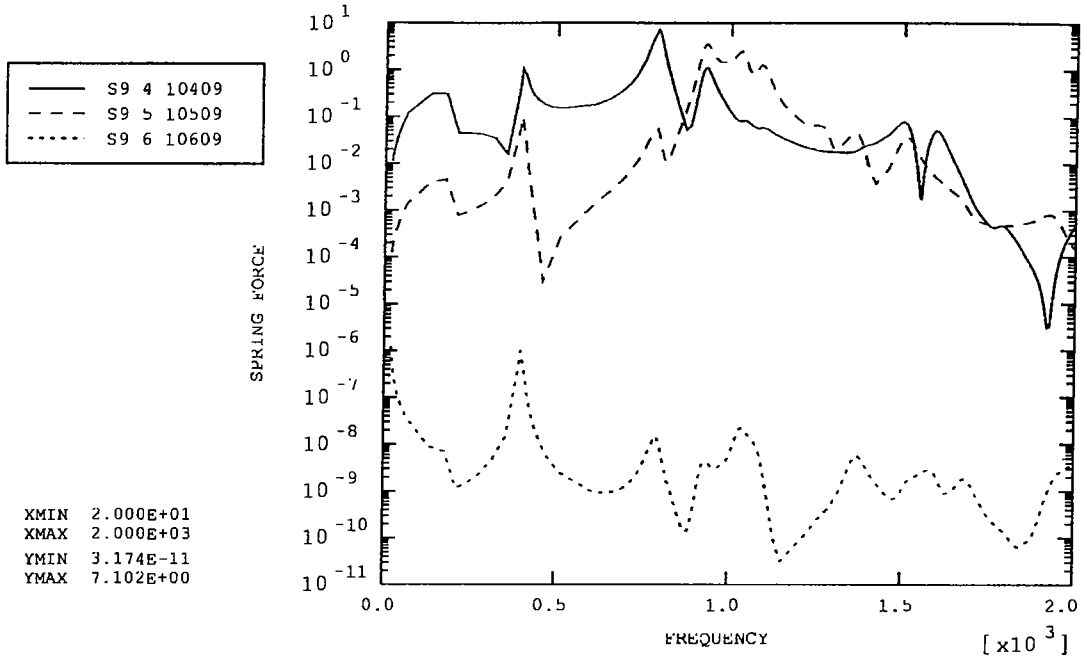

Figure 39: Jiggle pivot (bottom)

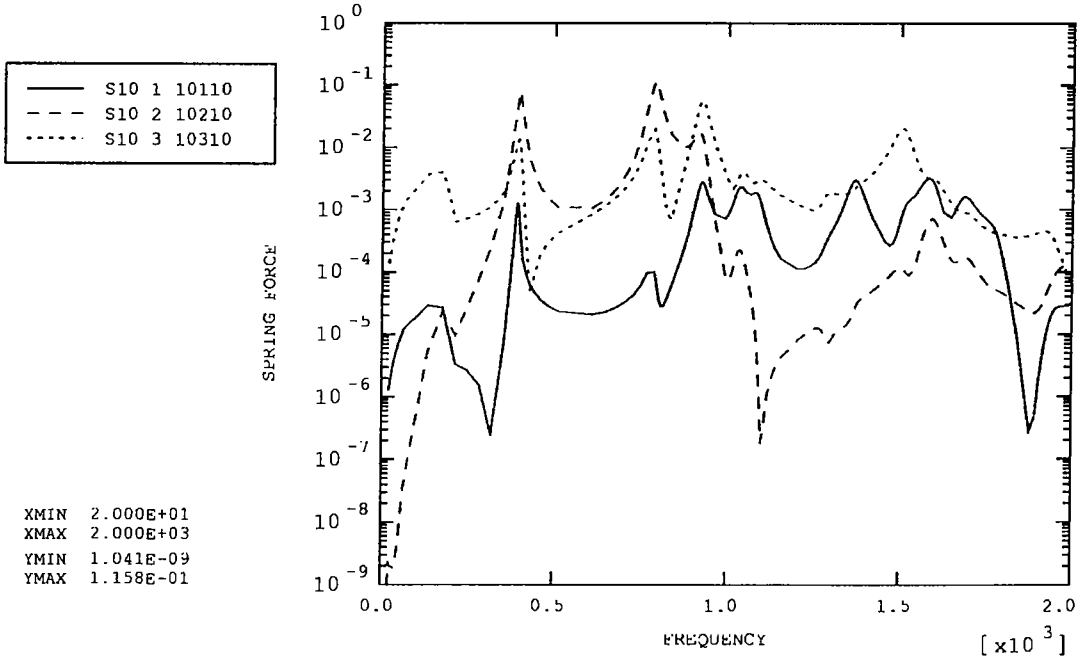

Figure 40: Chop pivot (left)

© FNC 2002

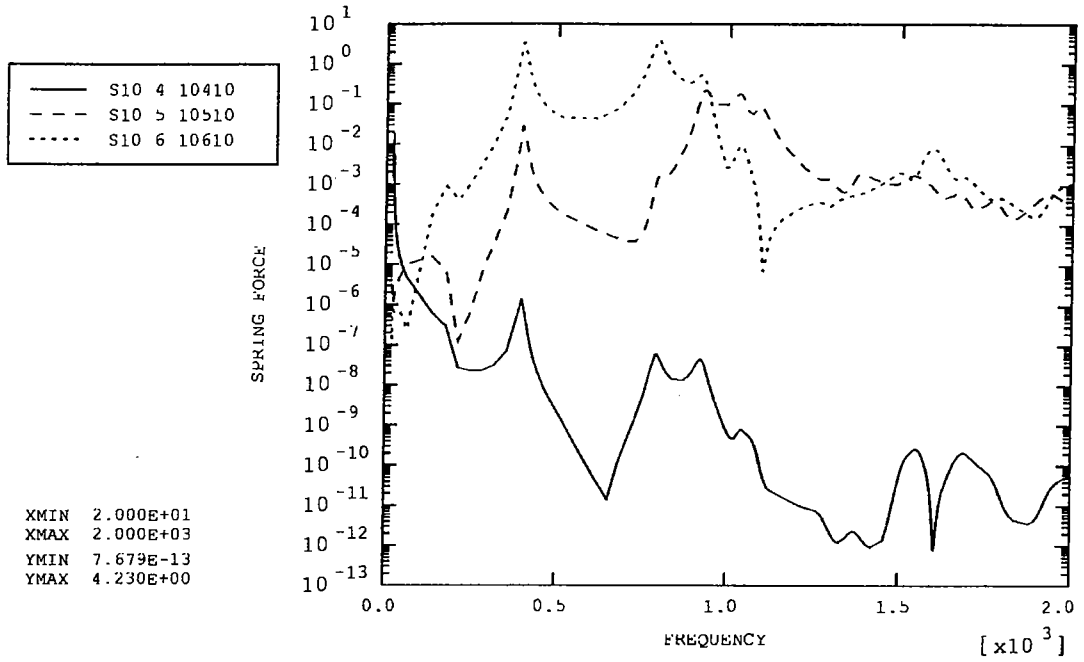

Figure 41: Chop pivot (left)

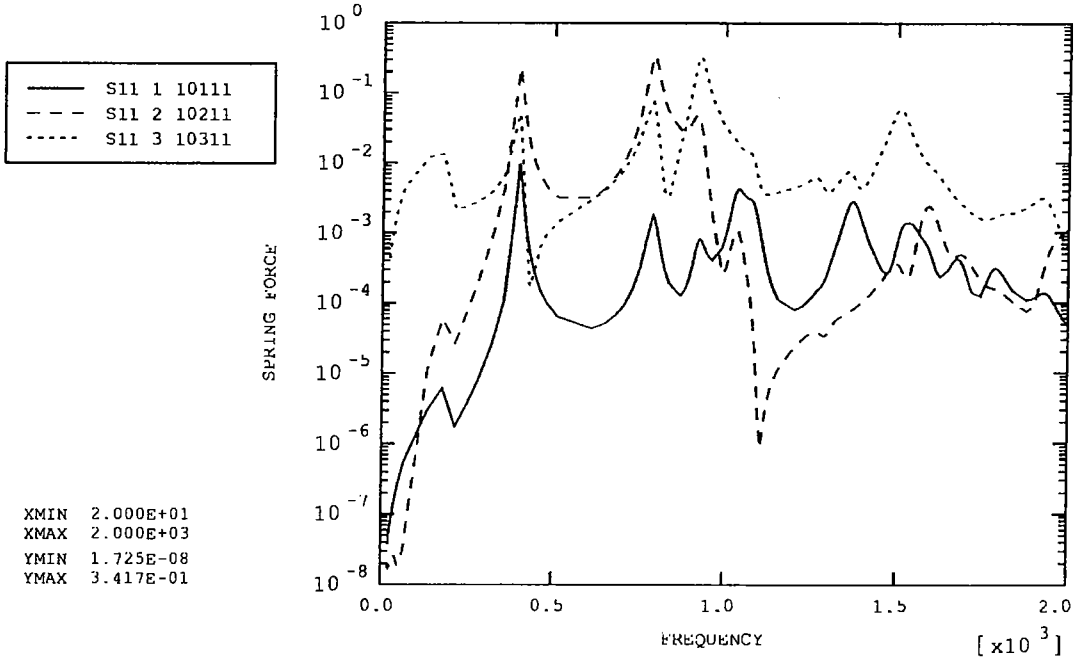

Figure 42: Chop pivot (right)

© FNC 2002

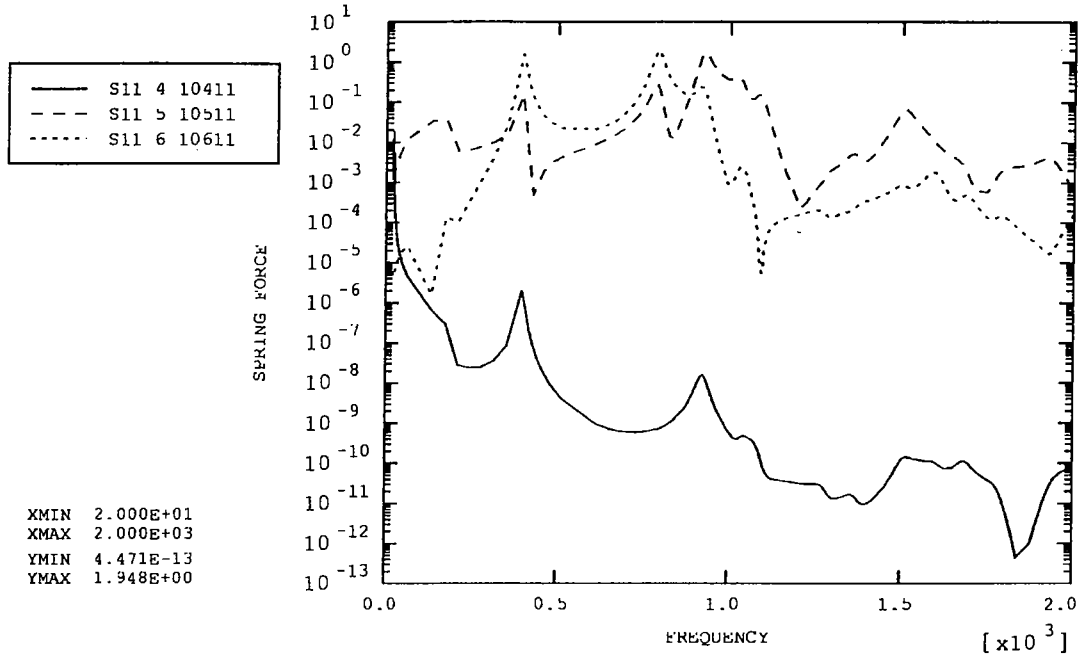

Figure 43: Chop pivot (right)

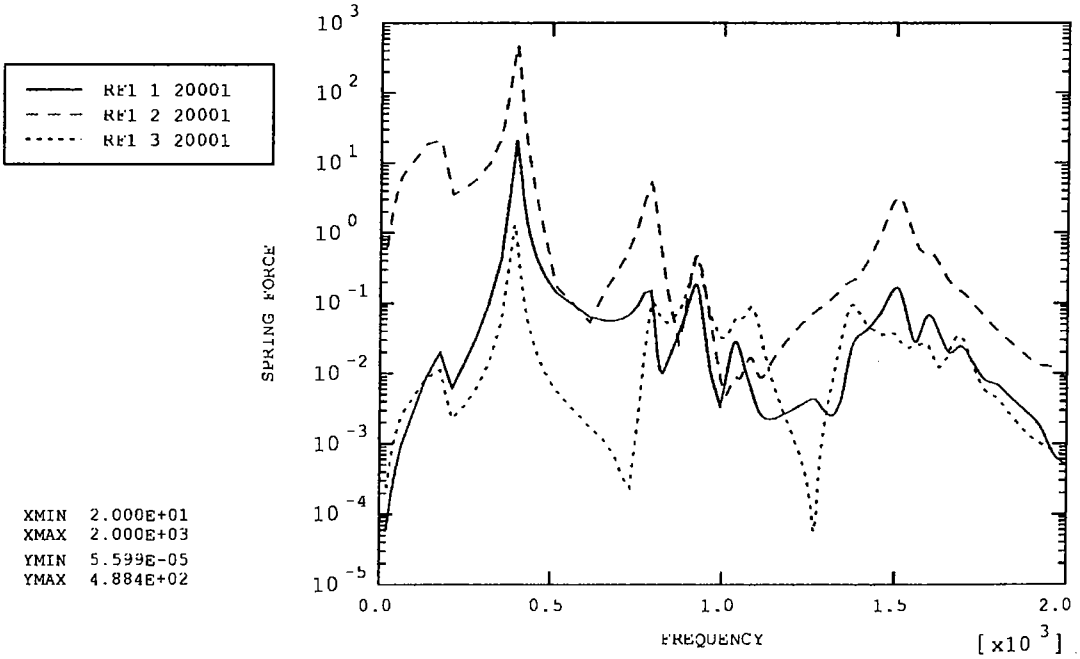

Figure 44: Reaction Force (front middle)

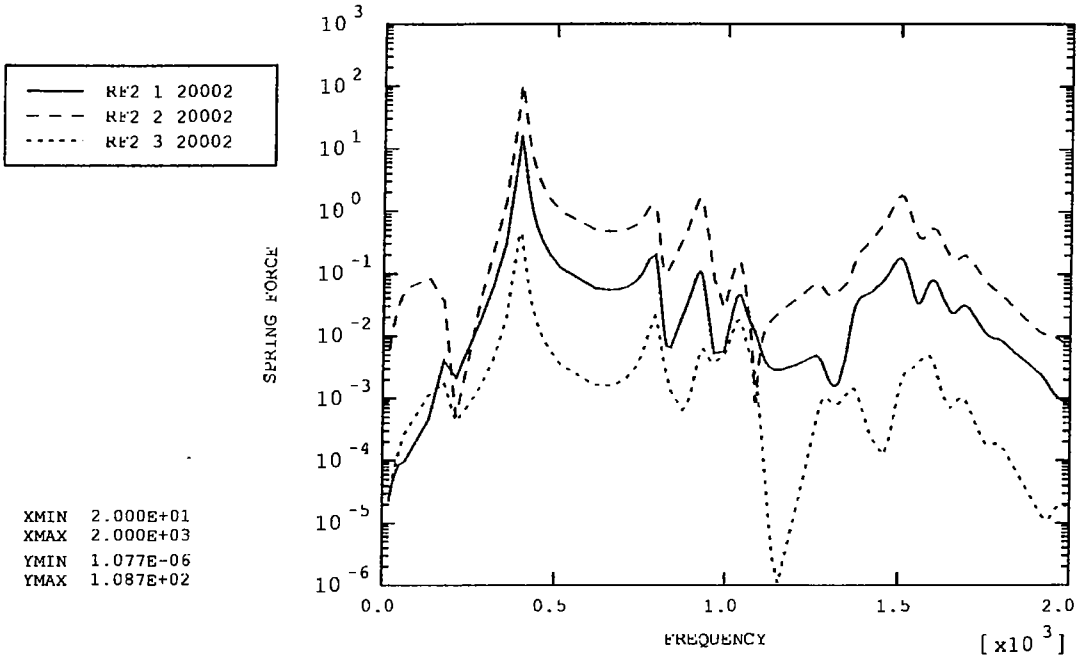

Figure 45: Reaction Force (back left)

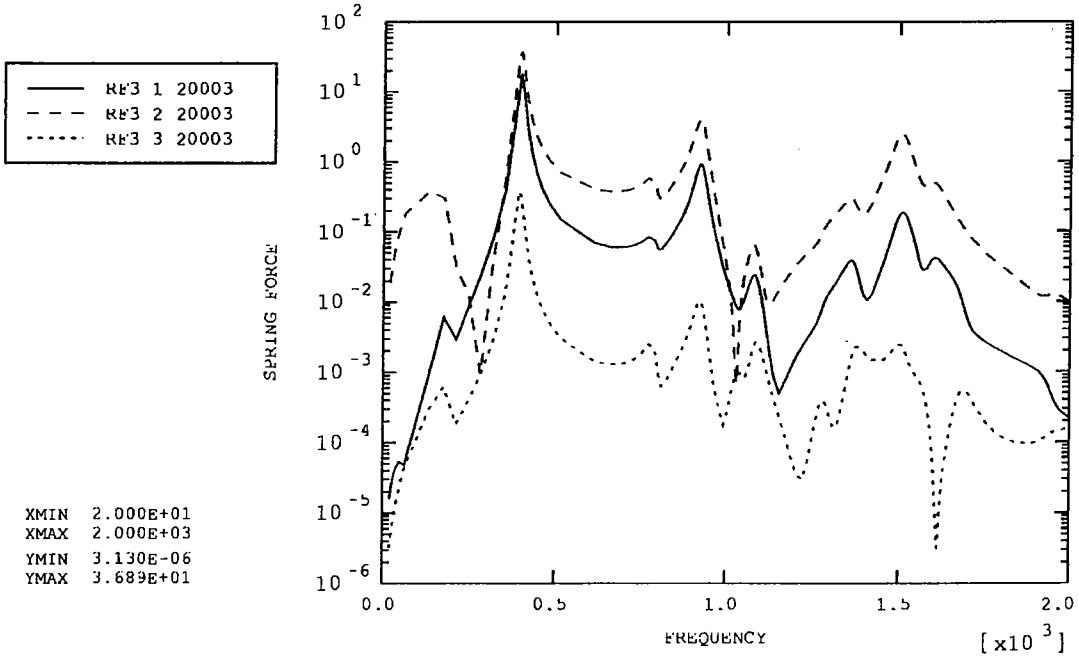

Figure 46: Reaction Force (back right)

© FNC 2002

SPIRE BSM VIBRATION ANALYSIS

Annex 6 - Random Response Z-Direction

FNC 5505/24072R Issue 1

Prepared for

U.K. Astronomy Technology Centre

DOCUMENT INFORMATION

Project : SPIRE BSM Vibration Analysis

Report Title : Annex 6 - Random Response Z-Direction

Client : U.K. Astronomy Technology Centre

Client Ref. : 024706

Classification :

Report No. : FNC 5505/24072R

Issue No. : 1

Compiled By : D C Reed
A J Vibert

Date : May 2002

Approved By : M W Anderson

DISTRIBUTION

Copy	Recipient	Organisation
1	I Pain	UK ATC
2	I Pain	UK ATC
3	I Pain	UK ATC
4	File	FNC

Copy No. ____

COPYRIGHT

The Copyright in this work is vested in Frazer-Nash Consultancy Limited. The document is issued in confidence solely for the purpose for which it is supplied. Reproduction in whole or in part or use for tendering or manufacturing purposes is prohibited except under an agreement with or with the written consent of Frazer-Nash Consultancy Limited and then only on the condition that this notice is included in any such reproduction.

Originating Office: FRAZER-NASH CONSULTANCY LIMITED
Stonebridge House, Dorking Business Park, Dorking, Surrey RH4 1HJ, UK
T: +44 (0)1306 885050 F: +44 (0)1306 886464 E: info@fnc.co.uk W: www.fnc.co.uk

DATA POINT POSITIONS

Note:

- The labels on the plots are as follows: e.g. P9_1_12184 refers to acceleration data point P9, degree of freedom 1 (node number 12184).
- Degrees of freedom 1, 2 and 3 refer to motion in the x, y and z directions (or X, Y and Z directions), while degrees of freedom 4, 5 and 6 refer to rotations about the x, y and z axes (or X, Y and Z axes).
- Acceleration is total acceleration (i.e. includes base motion)
- Accelerations and reaction forces are given in the global X, Y, Z co-ordinates
- Relative displacements and spring forces/torques are given in the local model x, y, z co-ordinates.
- 'Left' and 'right' directions are defined from a point of view looking towards the mirror surface, with the top of the casing furthest from the baseplate.

Fig.	P	Acceleration data points	Node number
1	1	Jiggle axis pivot (top) – frame	12182
2	2	Jiggle axis pivot (top) – jiggle stage	12200
3	3	Jiggle axis pivot (bottom) – frame	12183
4	4	Jiggle axis pivot (bottom) – jiggle stage	12192
5	5	Chop axis pivot (right side) – jiggle stage	12189
6	6	Chop axis pivot (right side) – chop stage	114
7	7	Chop axis pivot (left side) – jiggle stage	12188
8	8	Chop axis pivot (left side) – chop stage	105
9	9	Chop motor (top)	12184
10	10	Chop motor (bottom)	12185
11	11	Jiggle motor (right side)	12186
12	12	Jiggle motor (left side)	12187
13	13	PCAL CG	12193
14	14	PCAL extension to mirror centre	12199
15	15	Launch latch 'A' CG	12196
16	16	Launch latch 'A' extension to magnet centre	12197
17	17	Connector (top)	12194
18	18	Chop magnet (top)	115
19	19	Chop magnet (bottom)	122
20	20	Mirror Centre	9583
21	21	Jiggle magnet (right)	9276
22	22	Jiggle magnet (left)	9264

© FNC 2002

Fig.	E	Displacement between...	Element
23	1	Chop magnet vs. motor (top)	90n01, n=1, 2
24	2	Chop magnet vs. motor (bottom)	90n02, n=1, 2
25	3	Jiggle magnet vs. motor (right)	90n03, n=2, 3
26	4	Jiggle magnet vs. motor (left)	90n04, n=2, 3
27	5	Mirror centre vs. PCAL extension	90n05, n=1, 2, 3
28	6	Chop magnet (top) vs. launch latch 'A'	90206

Fig.	S	Position of spring elements	Node 1	Element
29	1	Front baffle (top left)	9702	10n01, n=1,2,3
30	2	Front baffle (top right)	9739	10n02, n=1,2,3
31	3	Front baffle (bottom left)	9629	10n03, n=1,2,3
32	4	Front baffle (bottom right)	9594	10n04, n=1,2,3
33	5	Base (front middle)*	3894	10n05, n=1,2,3
34	6	Base (back left)*	3414	10n06, n=1,2,3
35	7	Base (back right)*	3622	10n07, n=1,2,3
36,37	8	Jiggle pivot (top)	12200	10n08, n=1 to 6
38,39	9	Jiggle pivot (bottom)	12192	10n09, n=1 to 6
40,41	10	Chop pivot (left)	12188	10n10, n=1 to 6
42,43	11	Chop pivot (right)	12189	10n11, n=1 to 6

Fig.	RF	Reaction Forces	Node number
44	1	Reaction Force (front middle)	10587
45	2	Reaction Force (back left)	10722
46	3	Reaction Force (back right)	10671

* The baseplate-casing connections are each modelled using a single spring in the local x and y directions, and five springs in the local z direction. The forces from these five springs are added together to calculate the total connective force. The curve labels for the z direction degrees of freedom have the prefix 'B'.

© FNC 2002

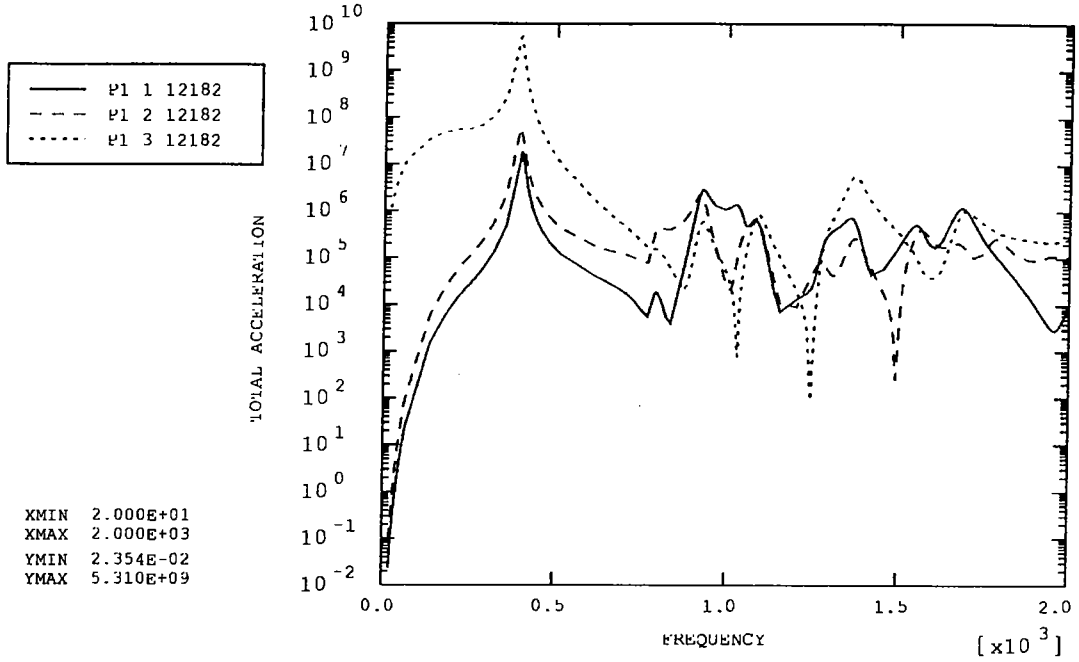

Figure 1: Jiggle axis pivot (top) – frame

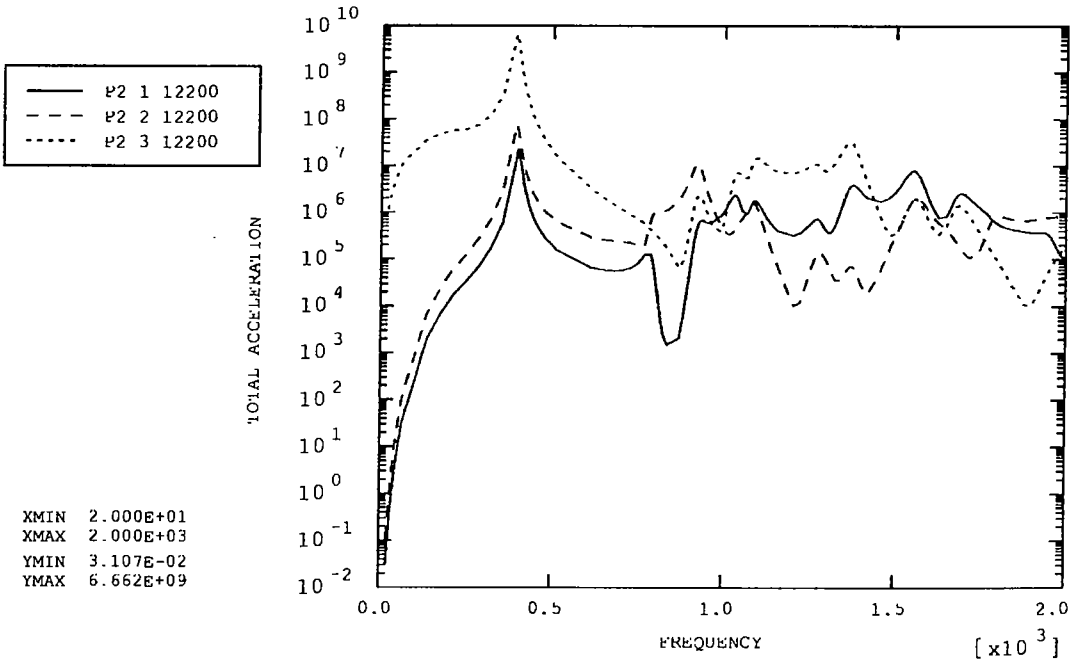

Figure 2: Jiggle axis pivot (top) – jiggle stage

© FNC 2002

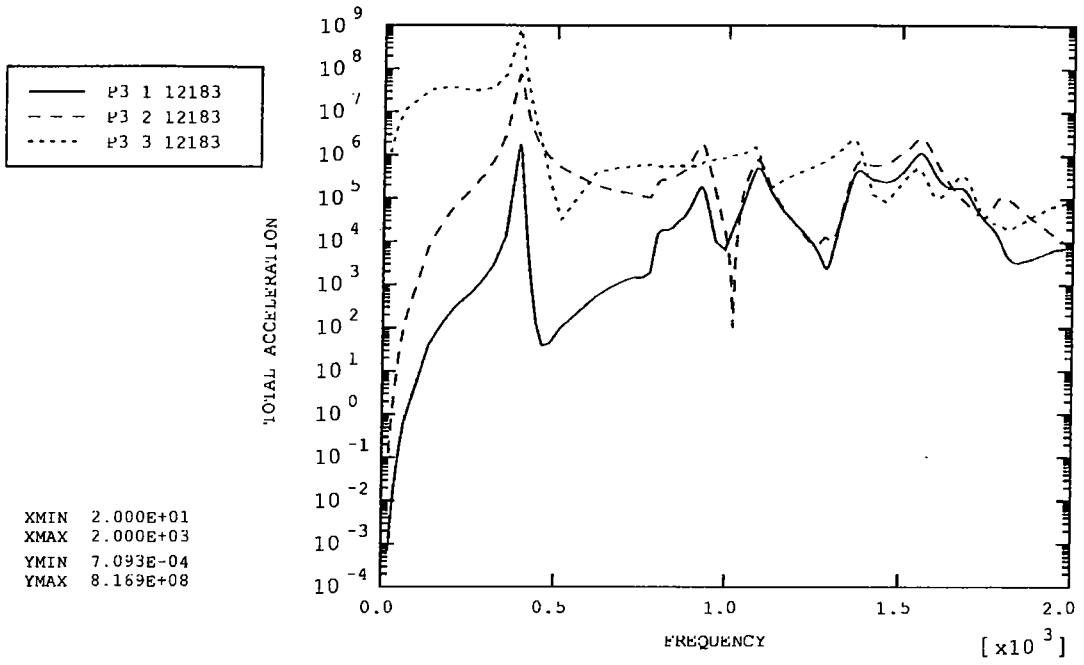

Figure 3: Jiggle axis pivot (bottom) – frame

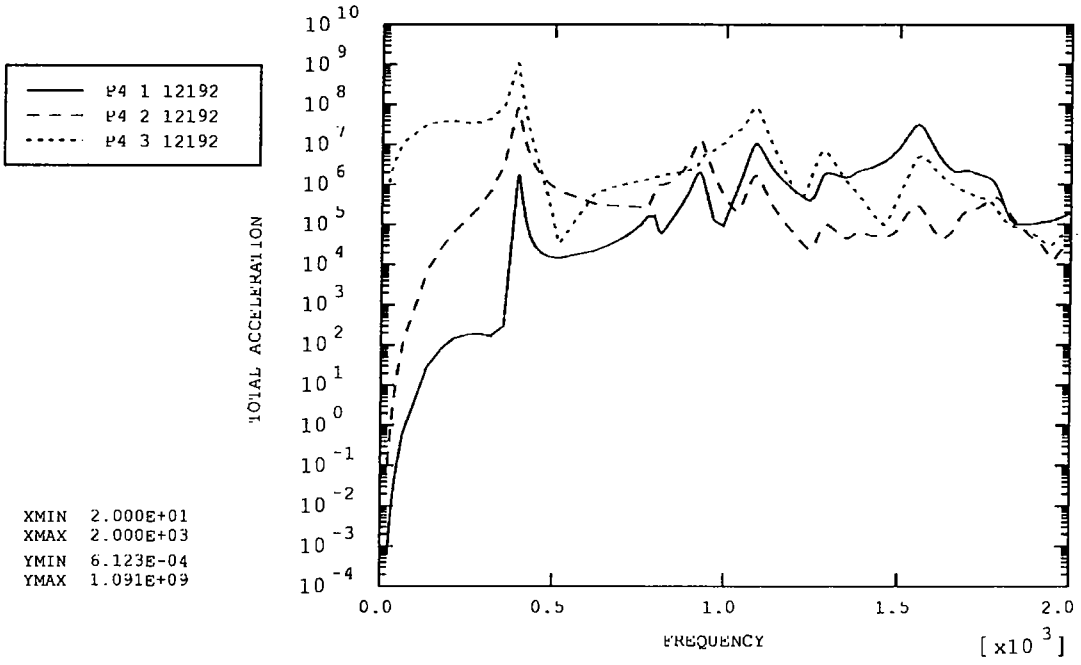

Figure 4: Jiggle axis pivot (bottom) – jiggle stage

© FNC 2002

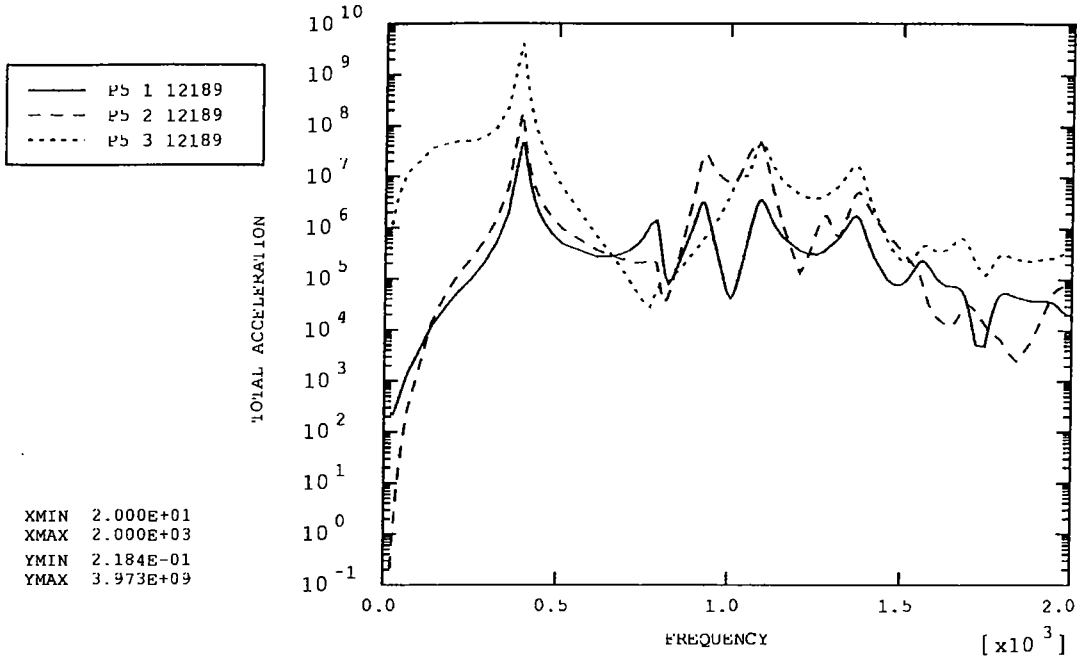

Figure 5: Chop axis pivot (right side) – jiggle stage

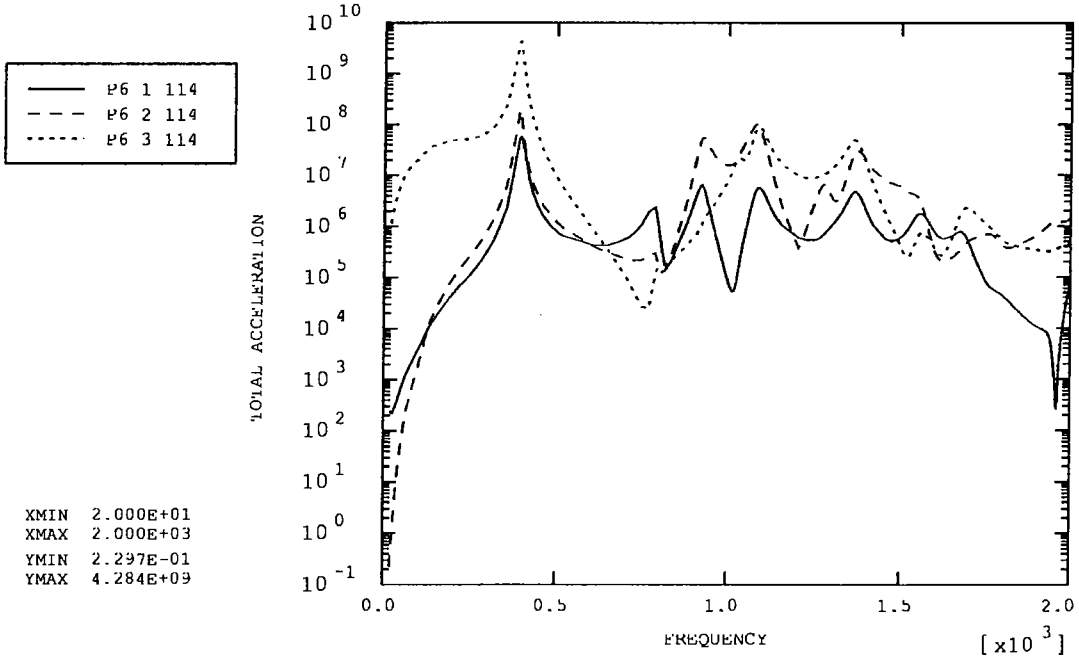

Figure 6: Chop axis pivot (right side) – chop stage

© FNC 2002

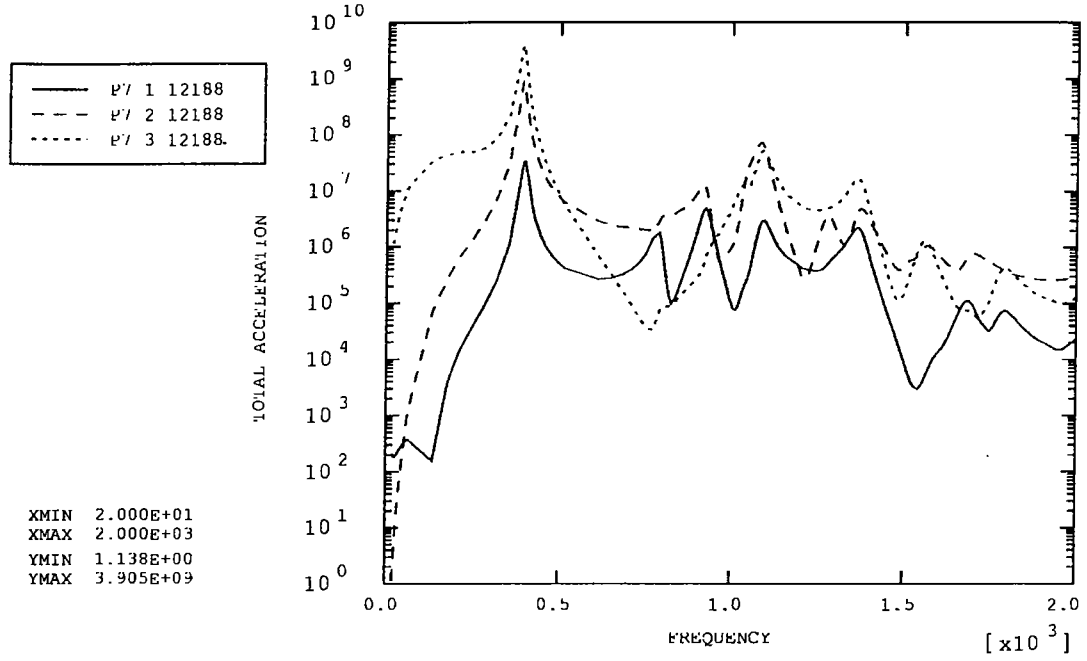

Figure 7: Chop axis pivot (left side) – jiggle stage

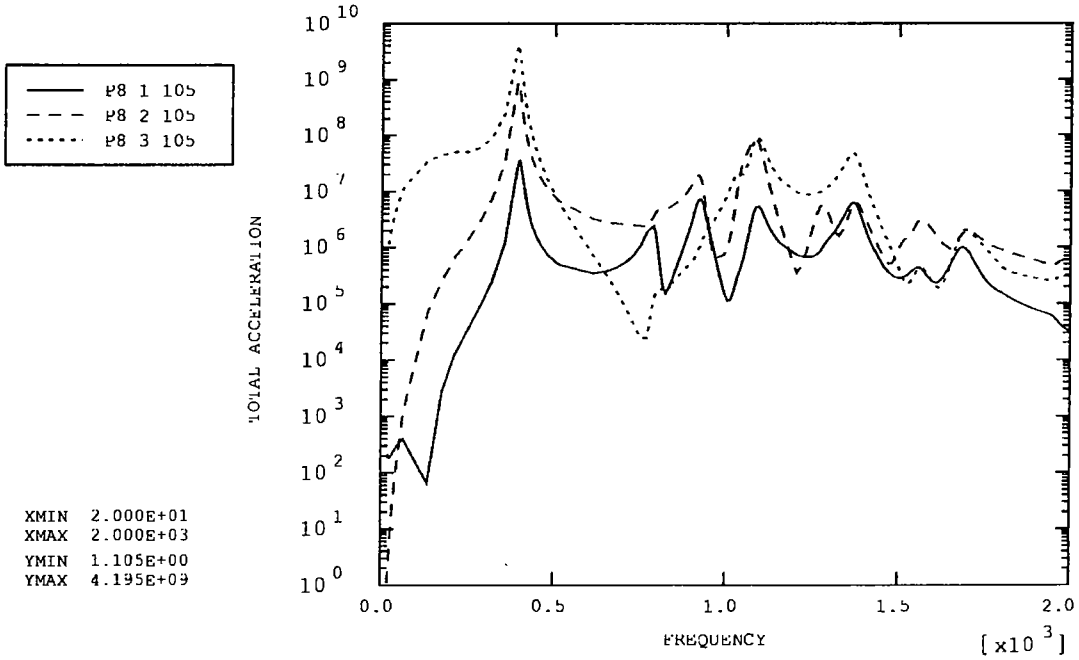

Figure 8: Chop axis pivot (left side) – chop stage

© FNC 2002

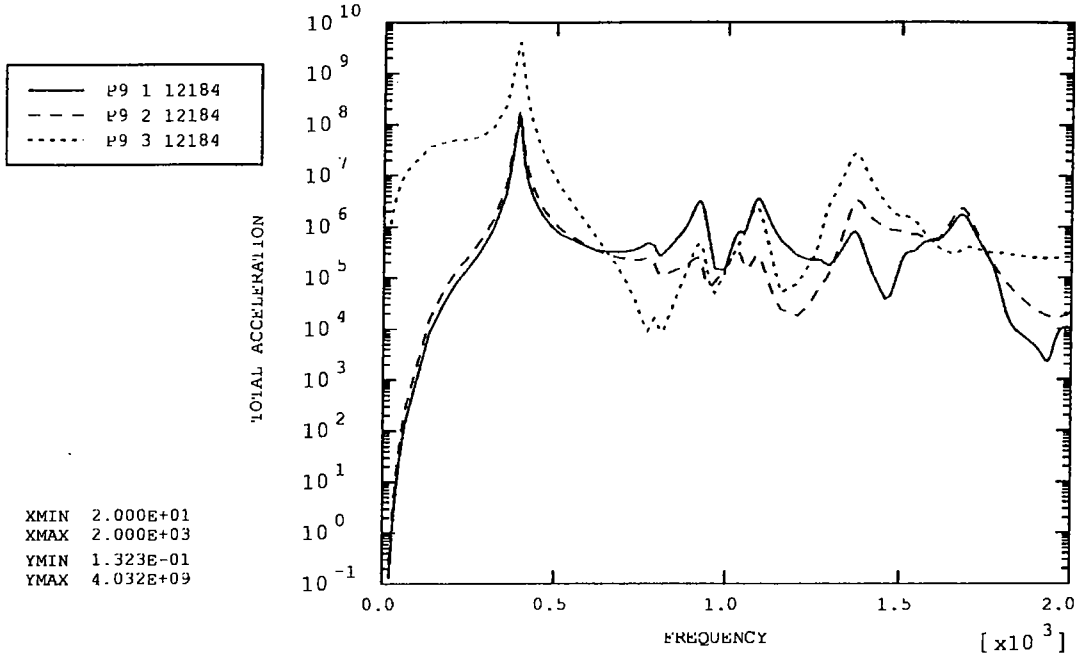

Figure 9: Chop motor (top)

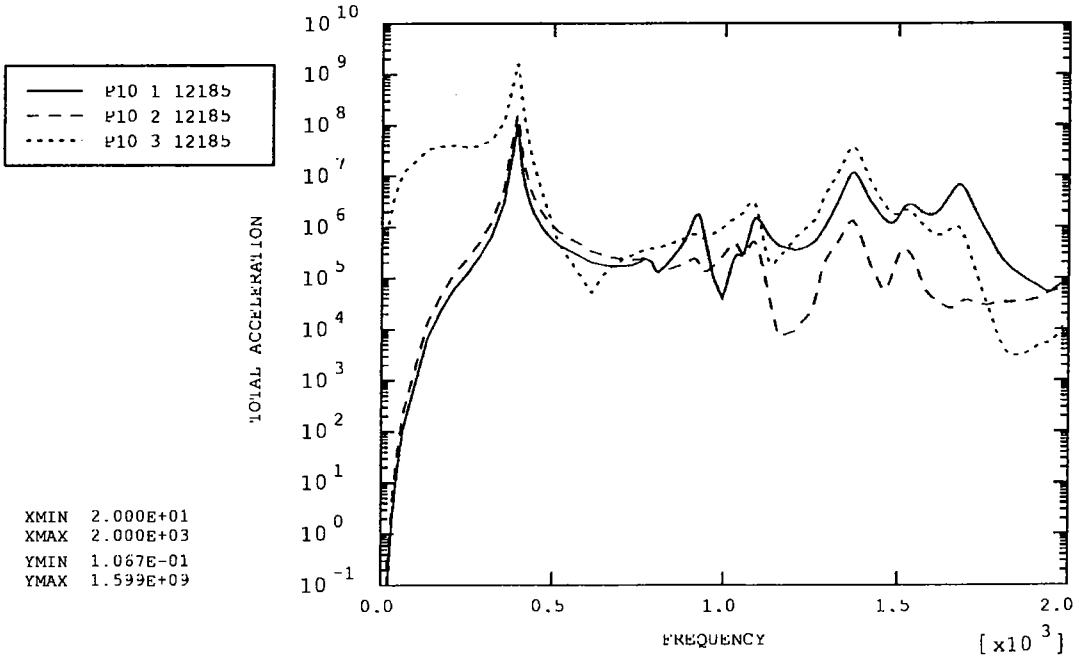

Figure 10: Chop motor (bottom)

© FNC 2002

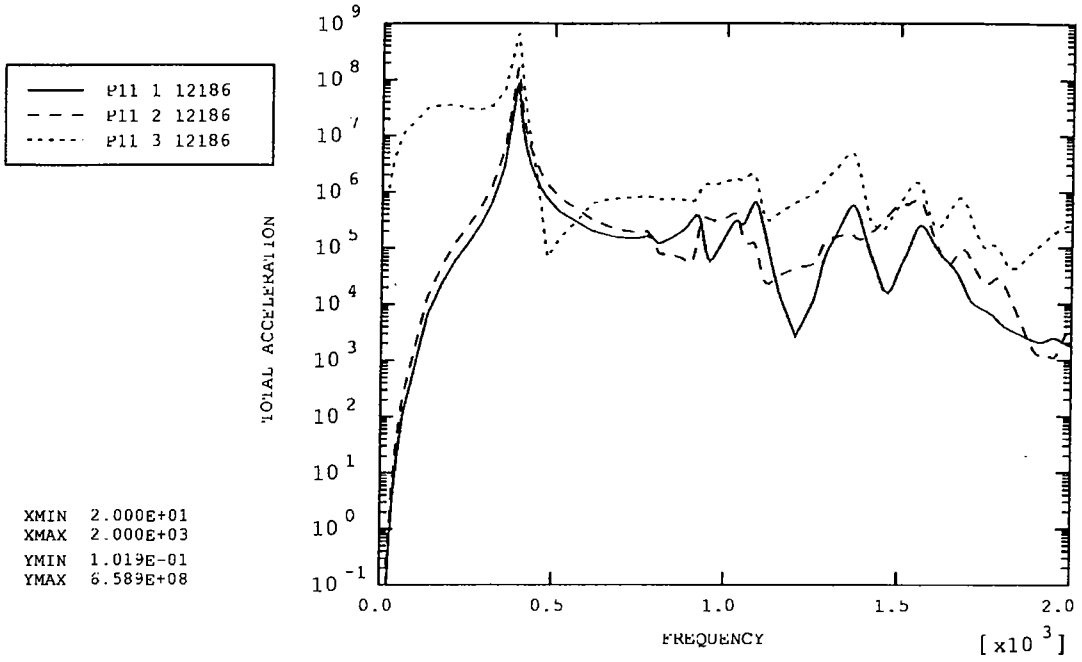

Figure 11: Jiggle motor (right side)

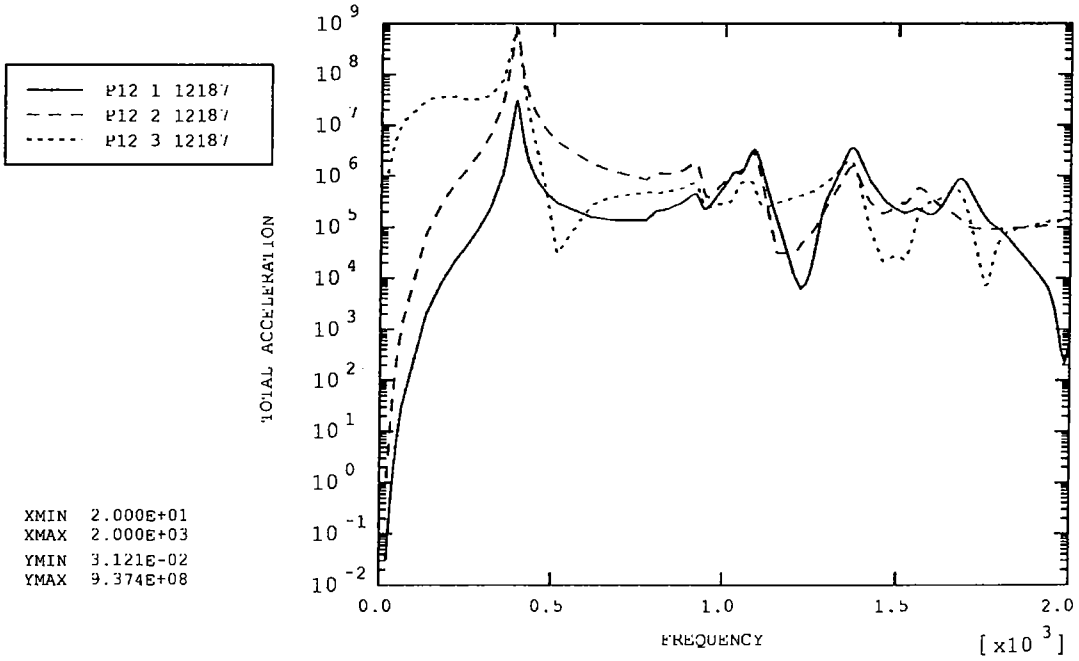

Figure 12: Jiggle motor (left side)

© FNC 2002

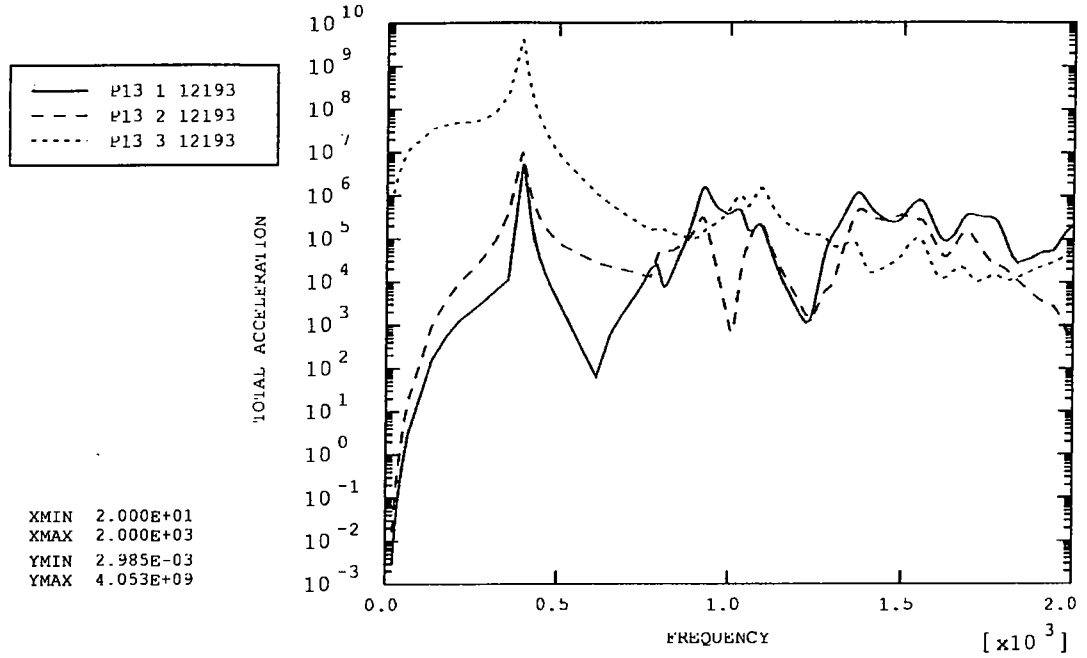

Figure 13: PCAL CG

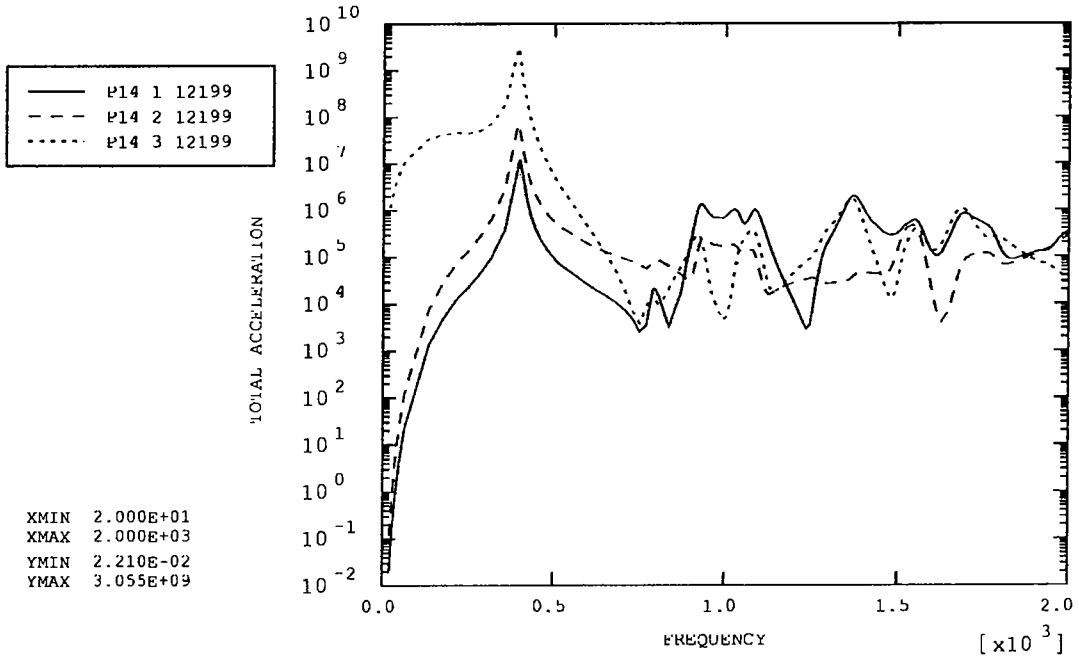

Figure 14: PCAL extension to mirror centre

© FNC 2002

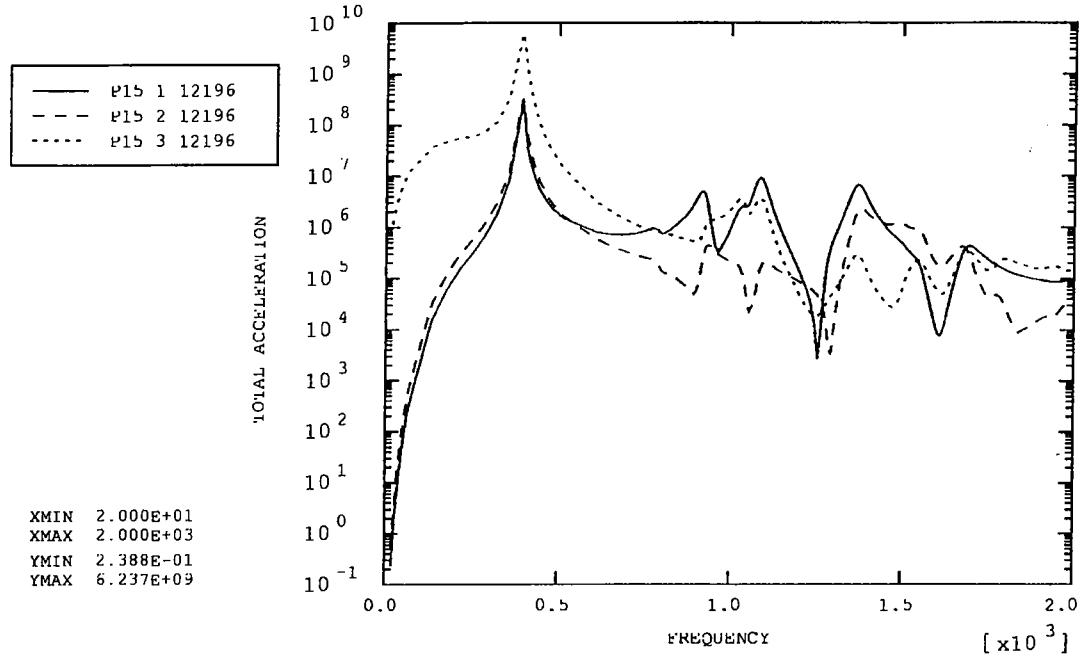

Figure 15: Launch latch 'A' CG

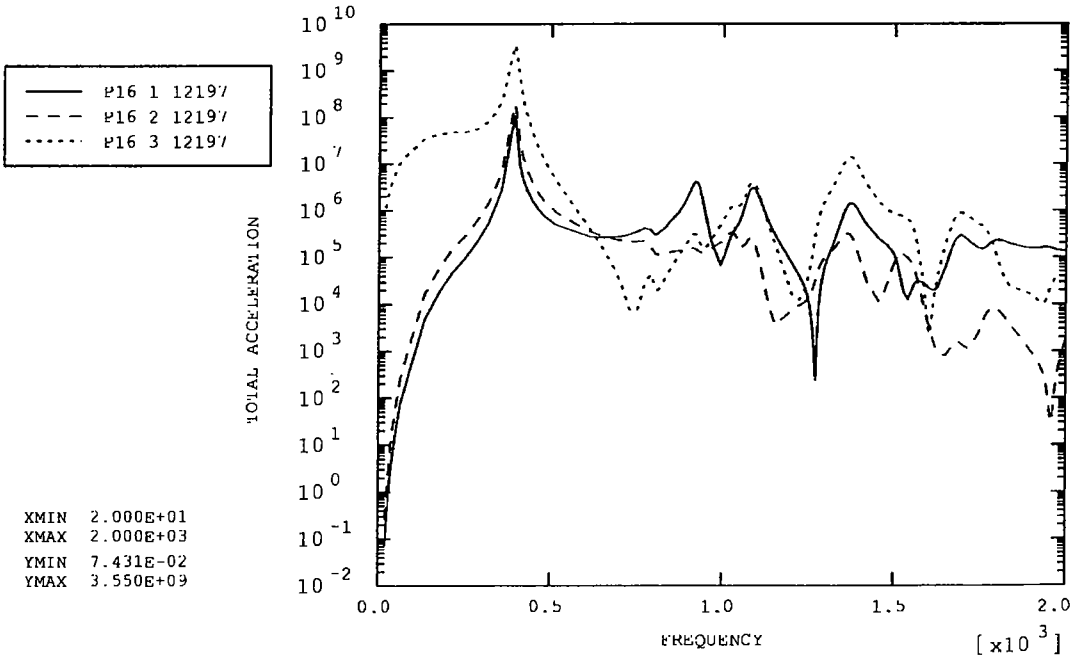

Figure 16: Launch latch 'A' extension to magnet centre

© FNC 2002

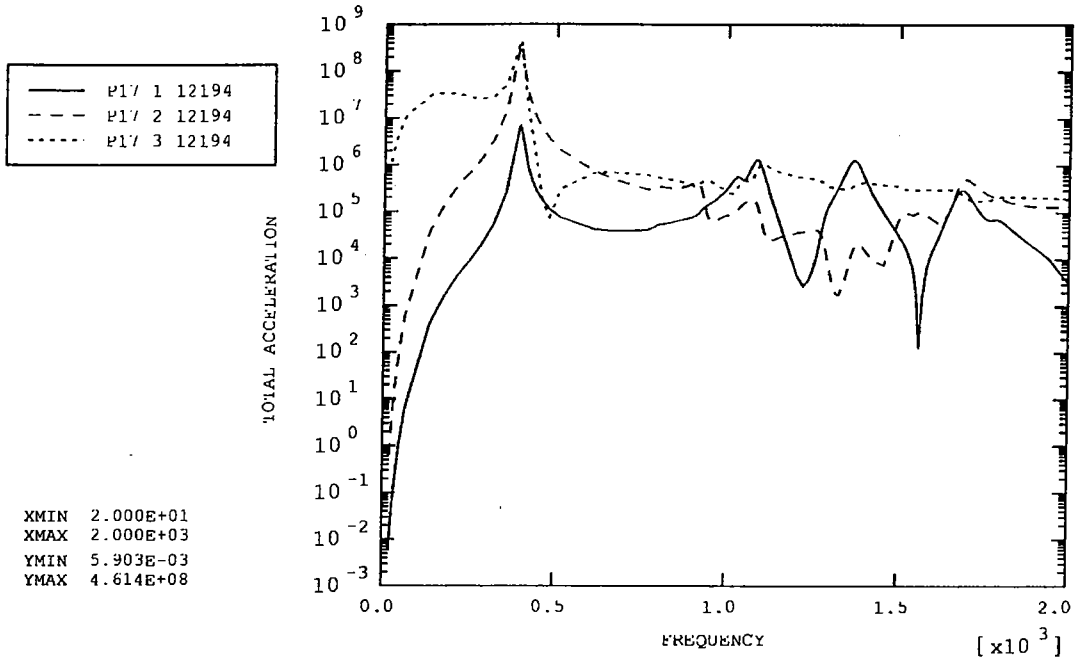

Figure 17: Connector (top)

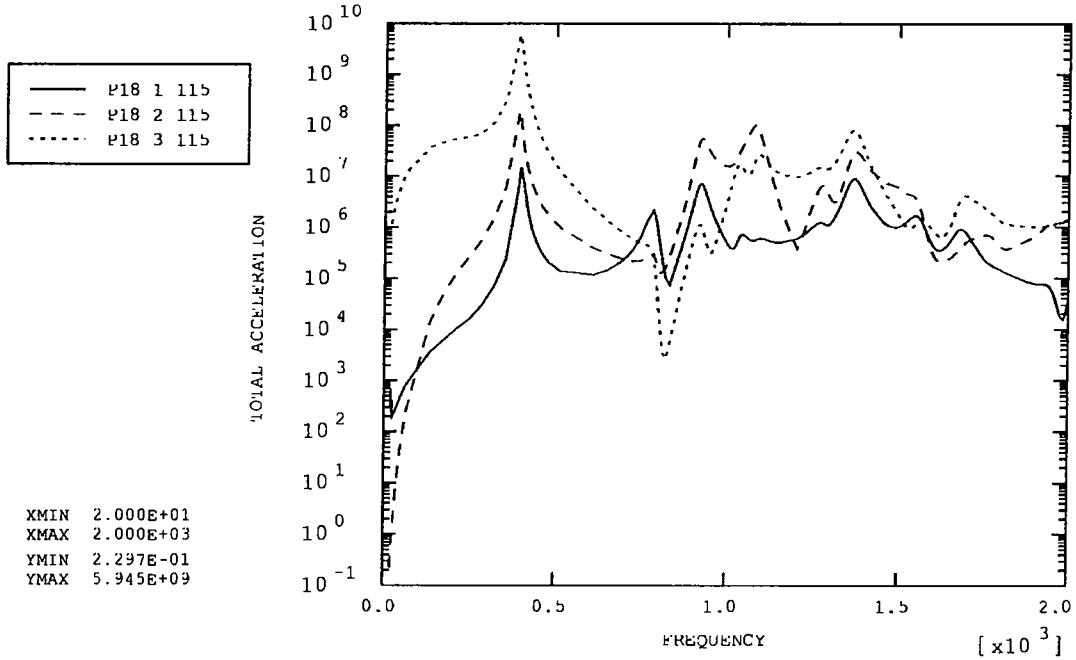

Figure 18: Chop magnet (top)

© FNC 2002

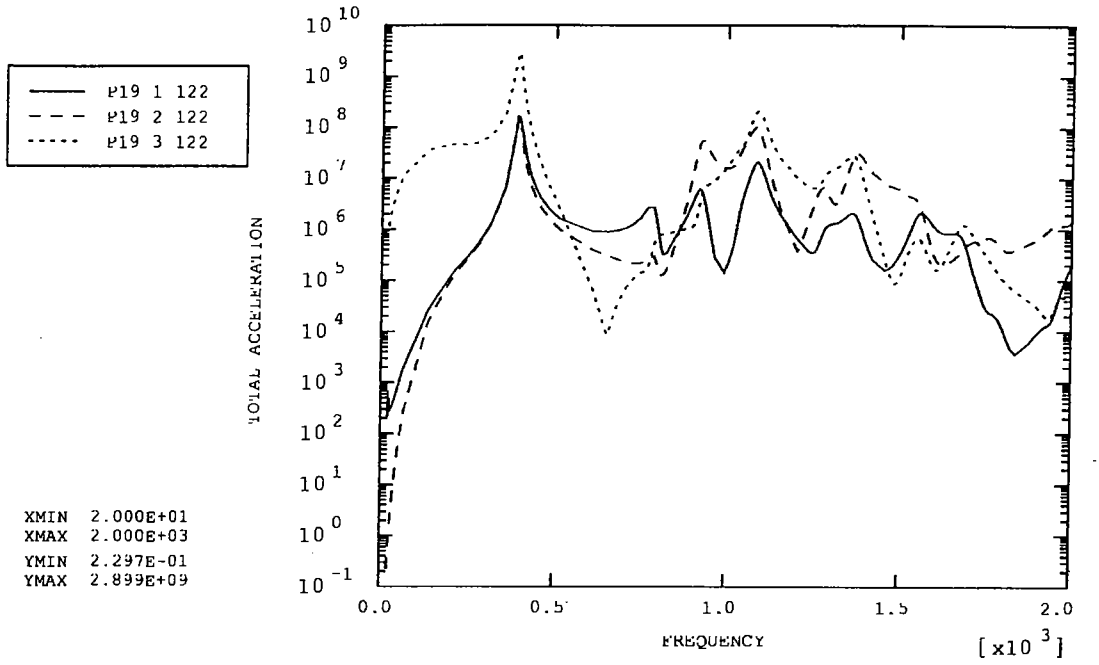

Figure 19: Chop magnet (bottom)

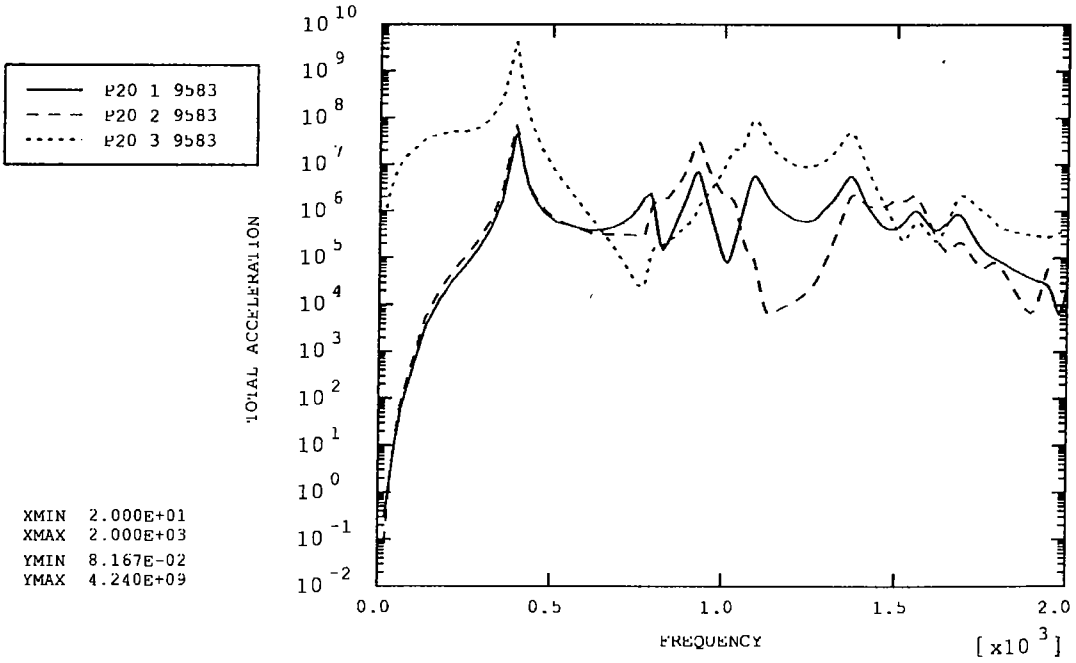

Figure 20: Mirror Centre

© FNC 2002

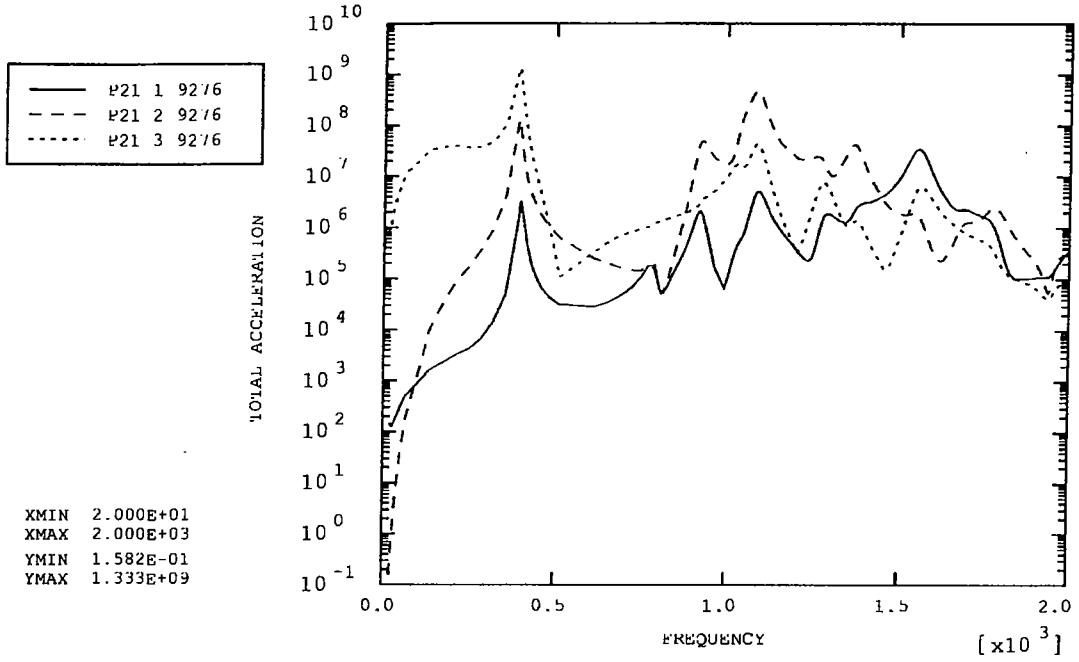

Figure 21: Jiggle magnet (right)

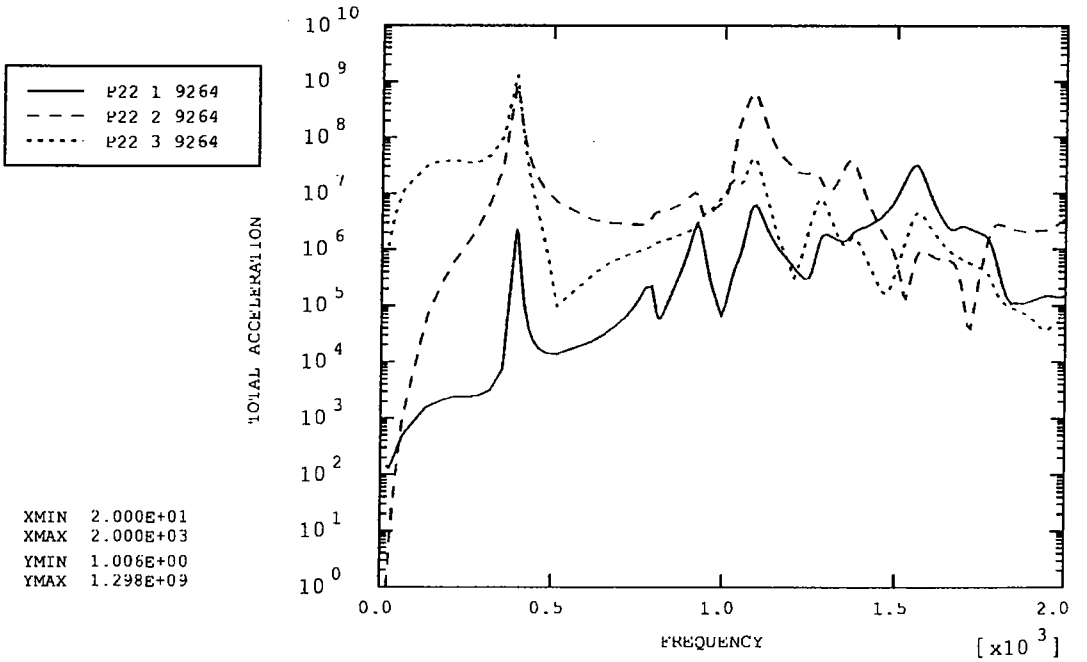

Figure 22: Jiggle magnet (left)

© FNC 2002

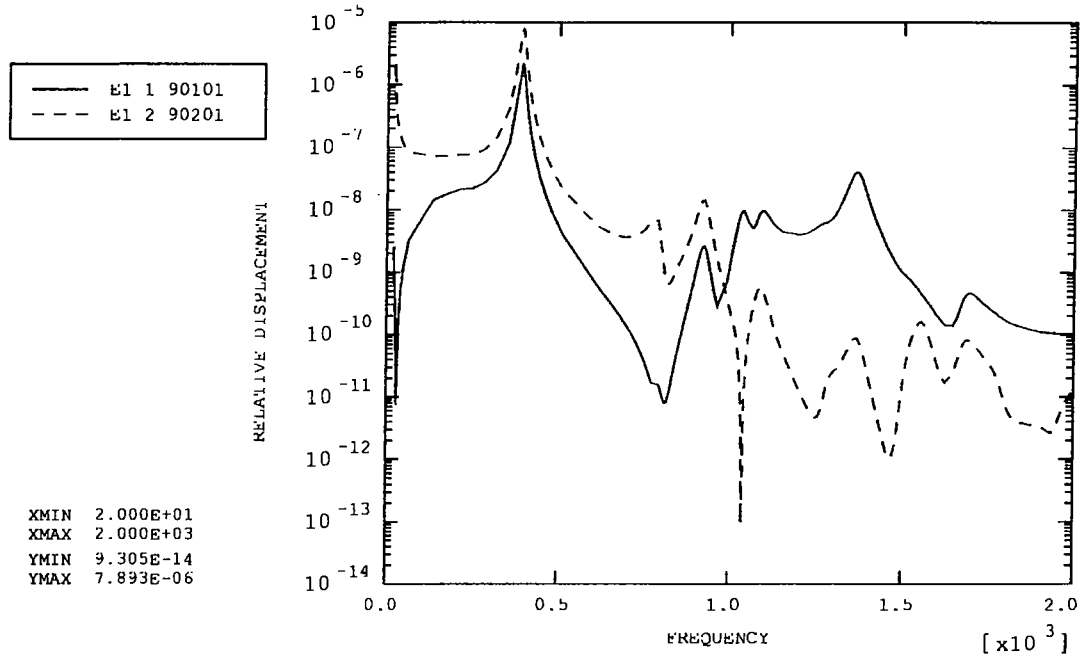

Figure 23: Chop magnet vs. motor (top)

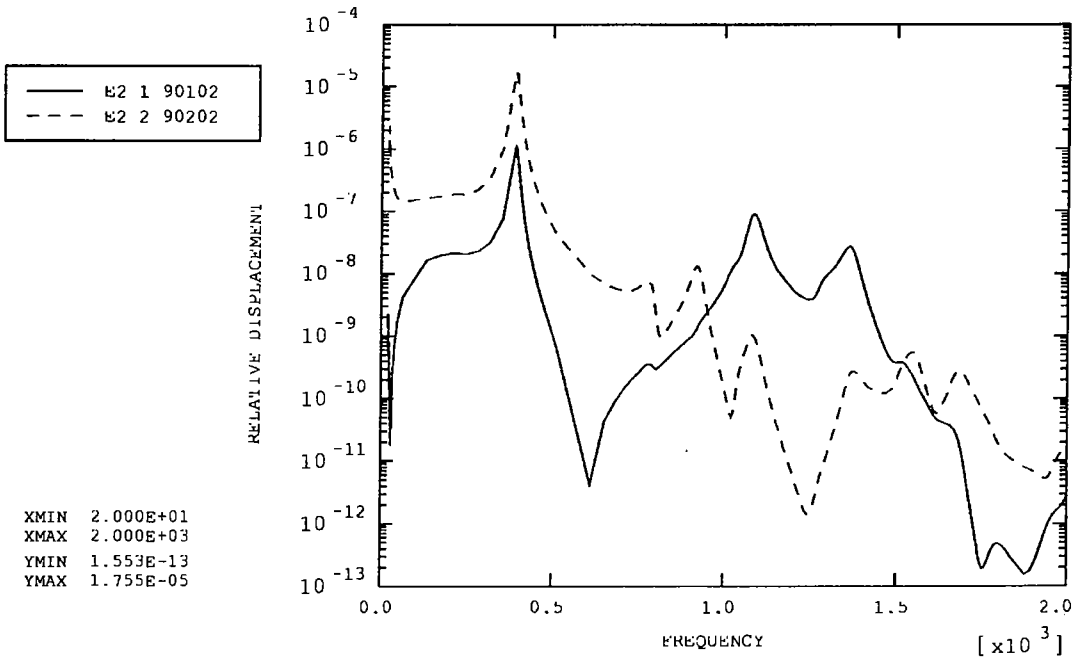

Figure 24: Chop magnet vs. motor (bottom)

© FNC 2002

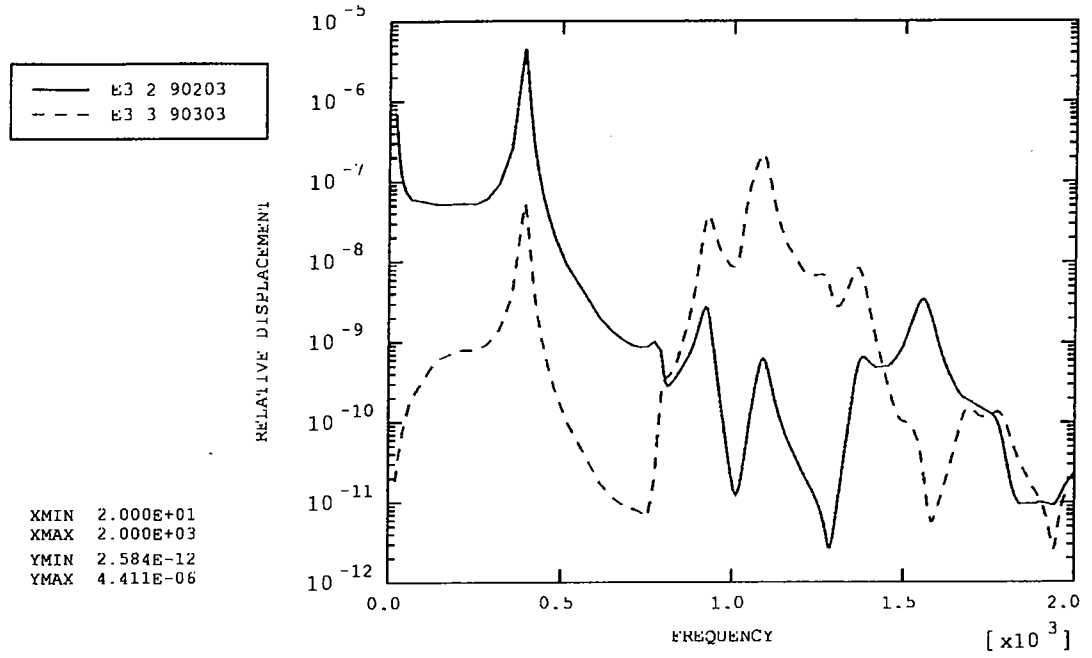

Figure 25: Jiggle magnet vs. motor (right)

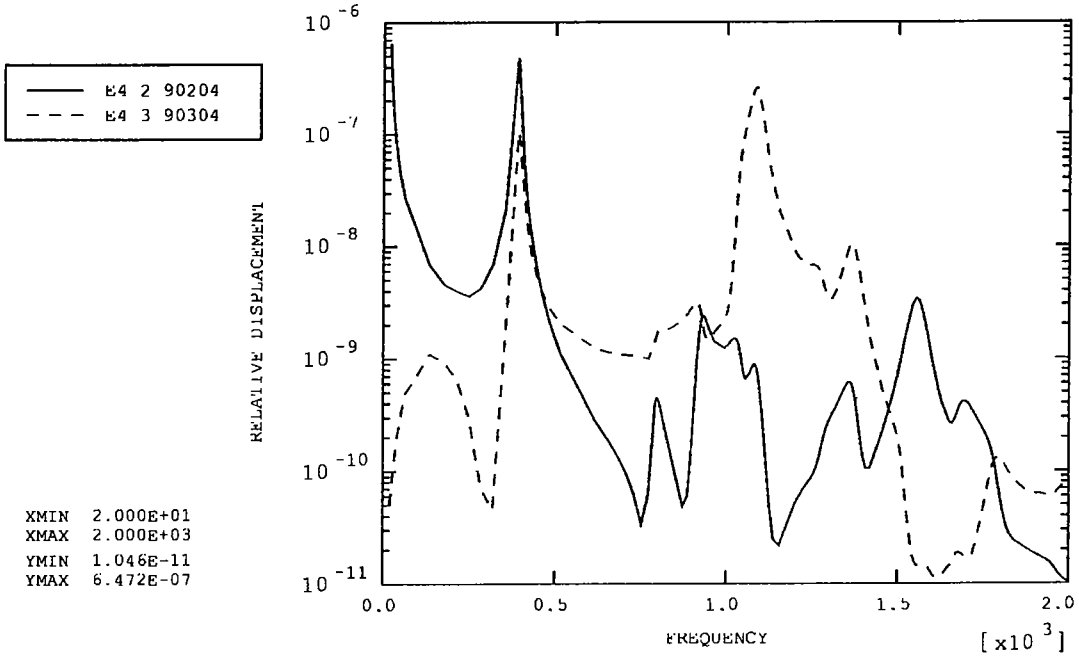

Figure 26: Jiggle magnet vs. motor (left)

© FNC 2002

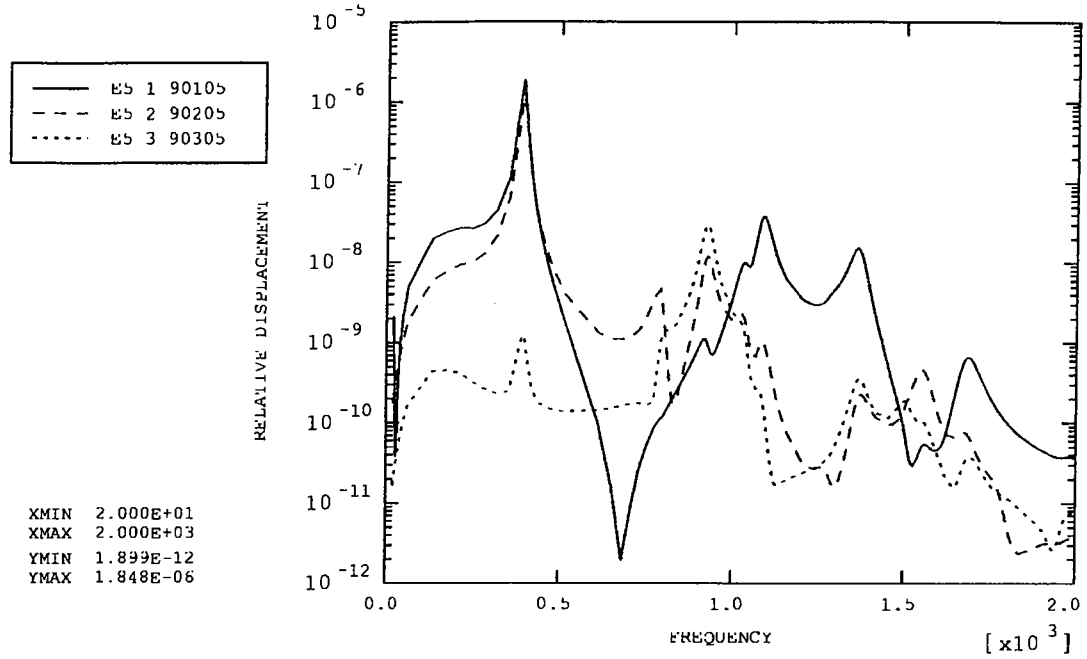

Figure 27: Mirror centre vs. PCAL extension

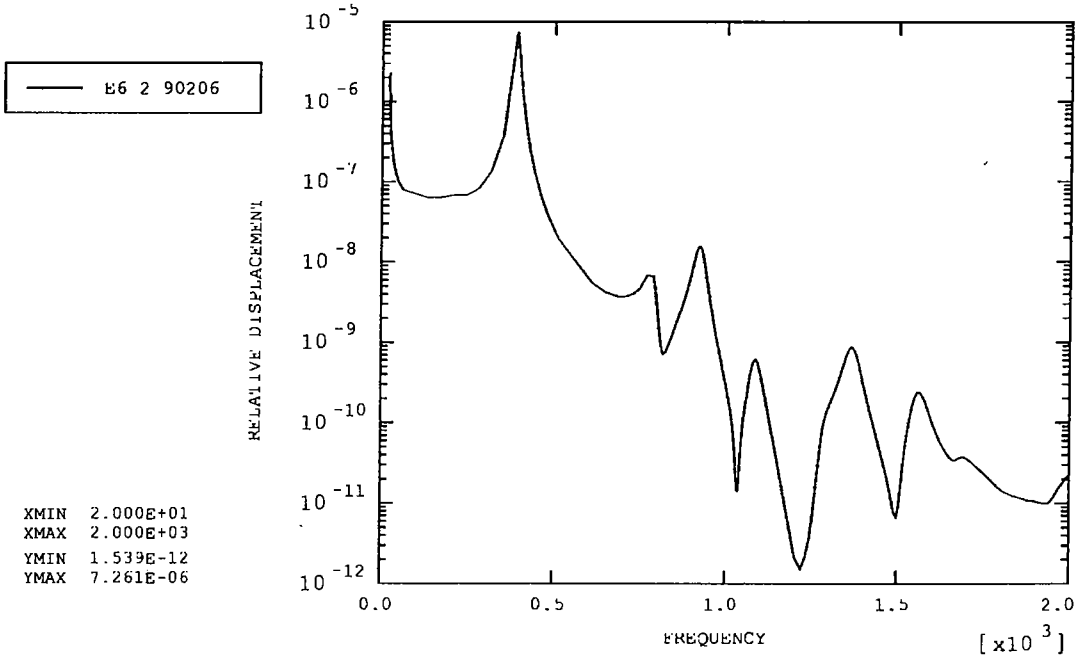

Figure 28: Chop magnet (top) vs. launch latch 'A'

© FNC 2002

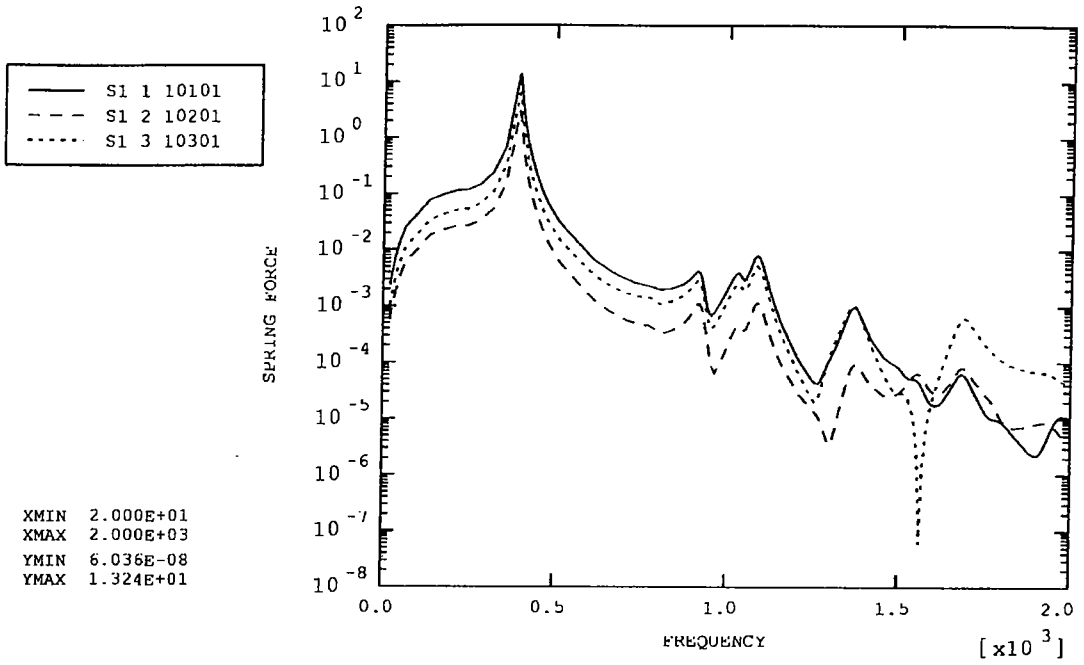

Figure 29: Front baffle (top left)

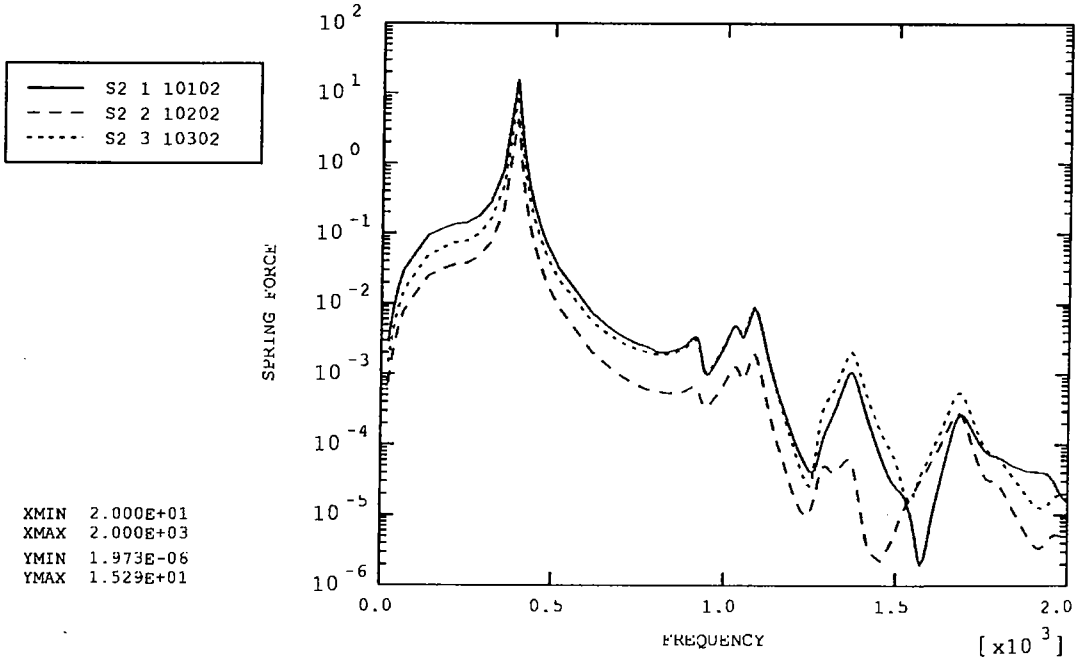

Figure 30: Front baffle (top right)

© FNC 2002

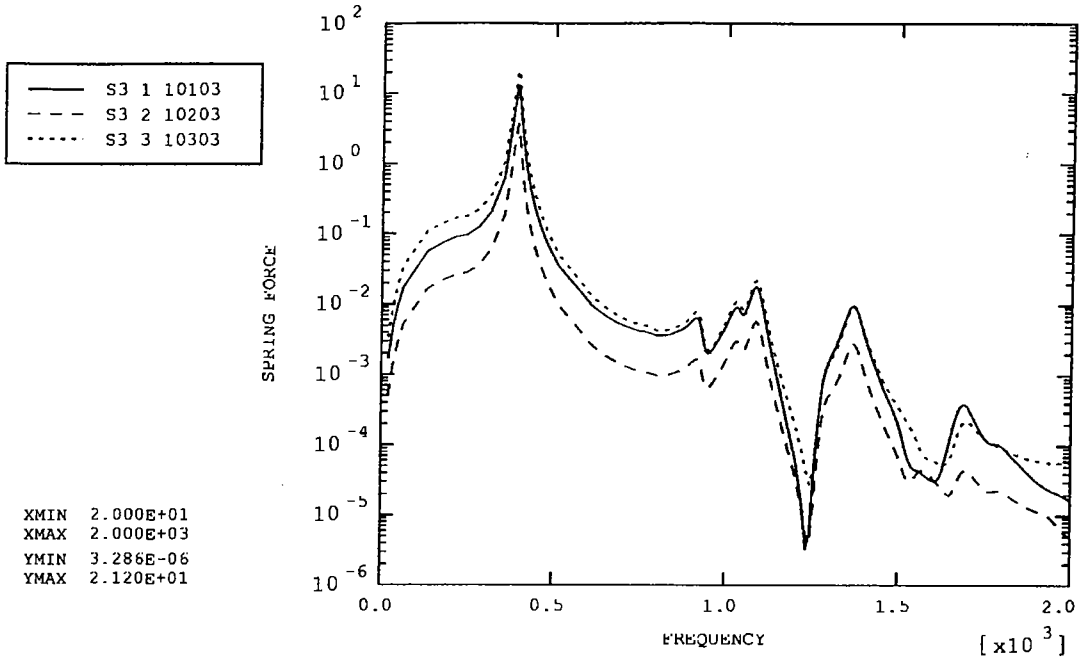

Figure 31: Front baffle (bottom left)

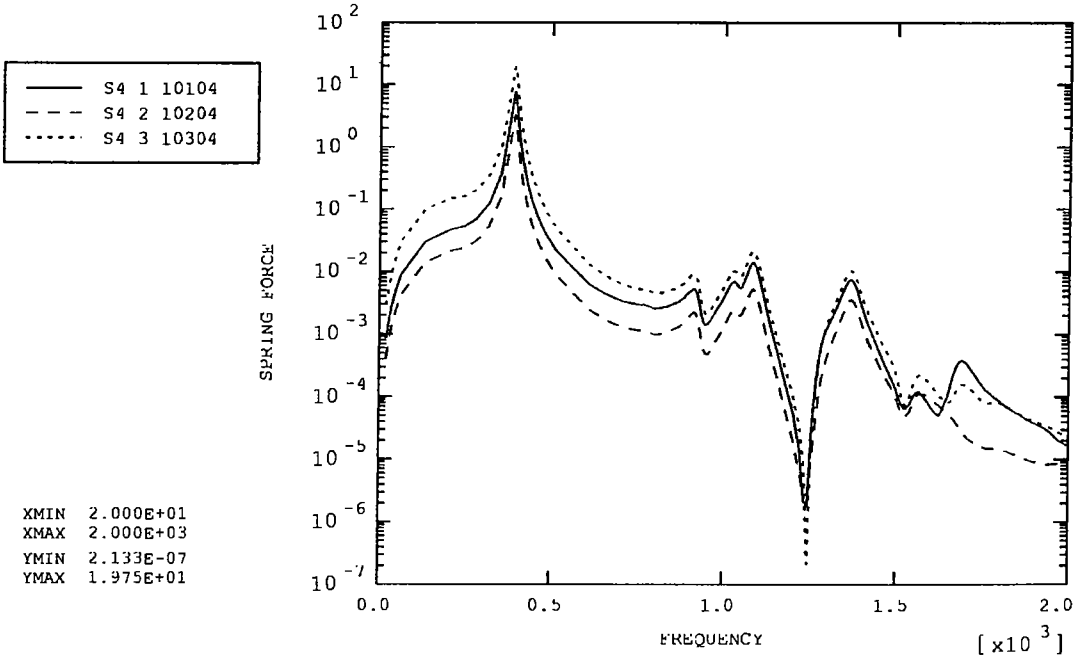

Figure 32: Front baffle (bottom right)

© FNC 2002

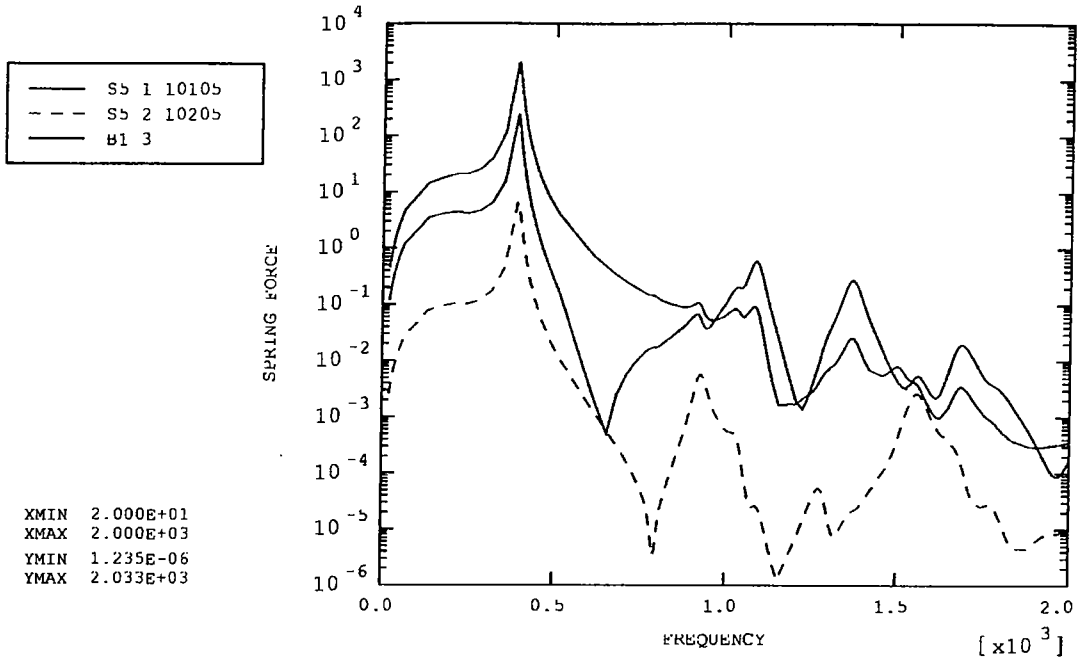

Figure 33: Base (front middle)

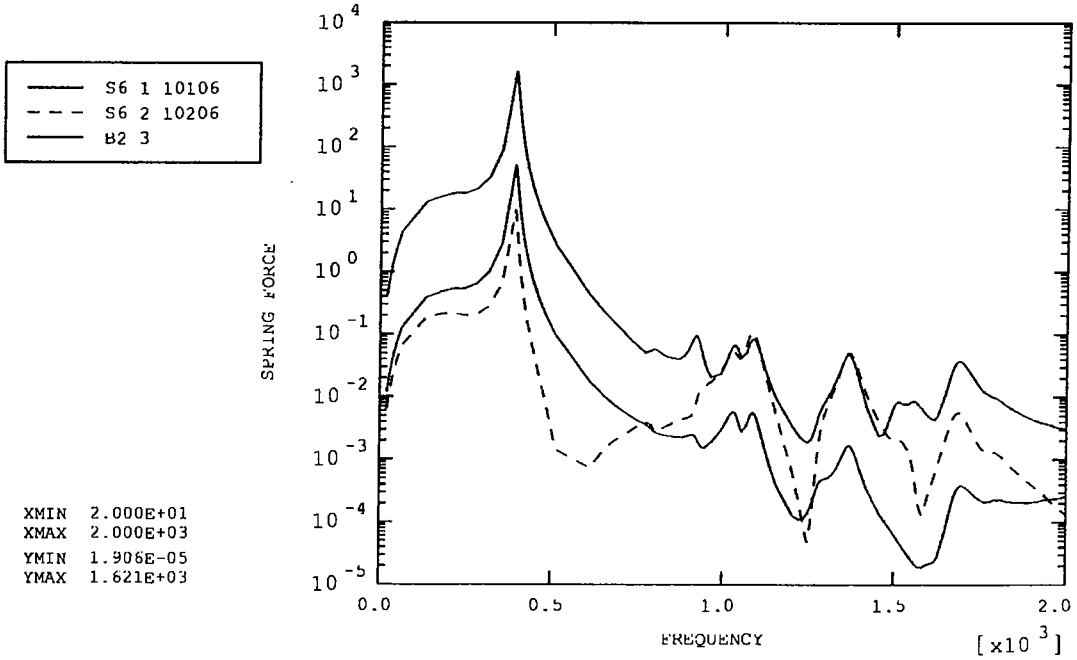

Figure 34: Base (back left)

© FNC 2002

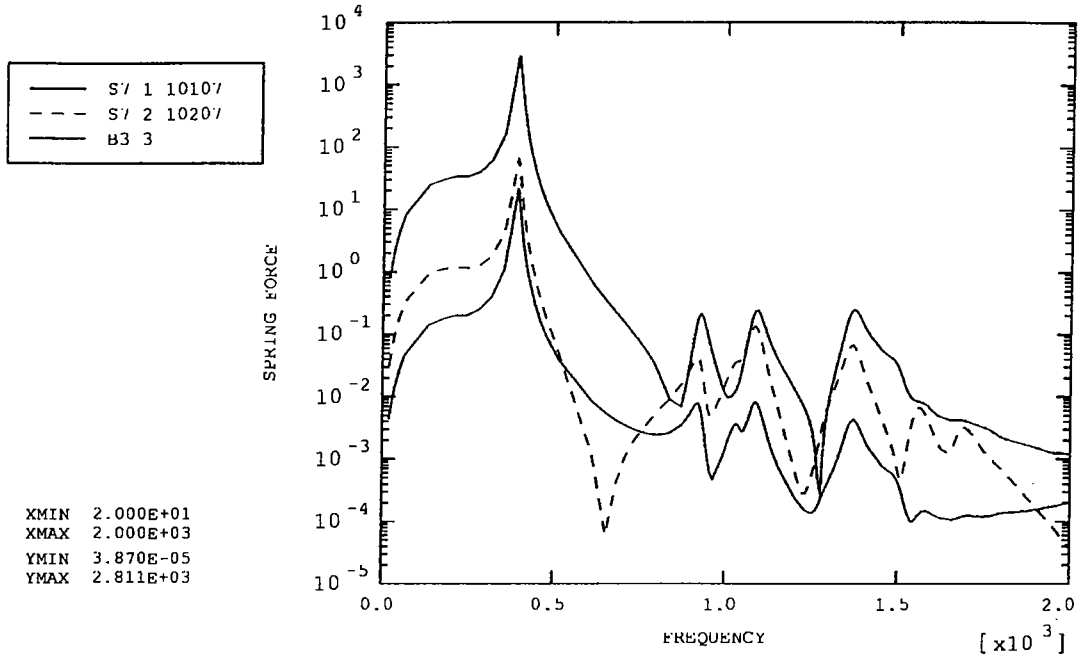

Figure 35: Base (back right)

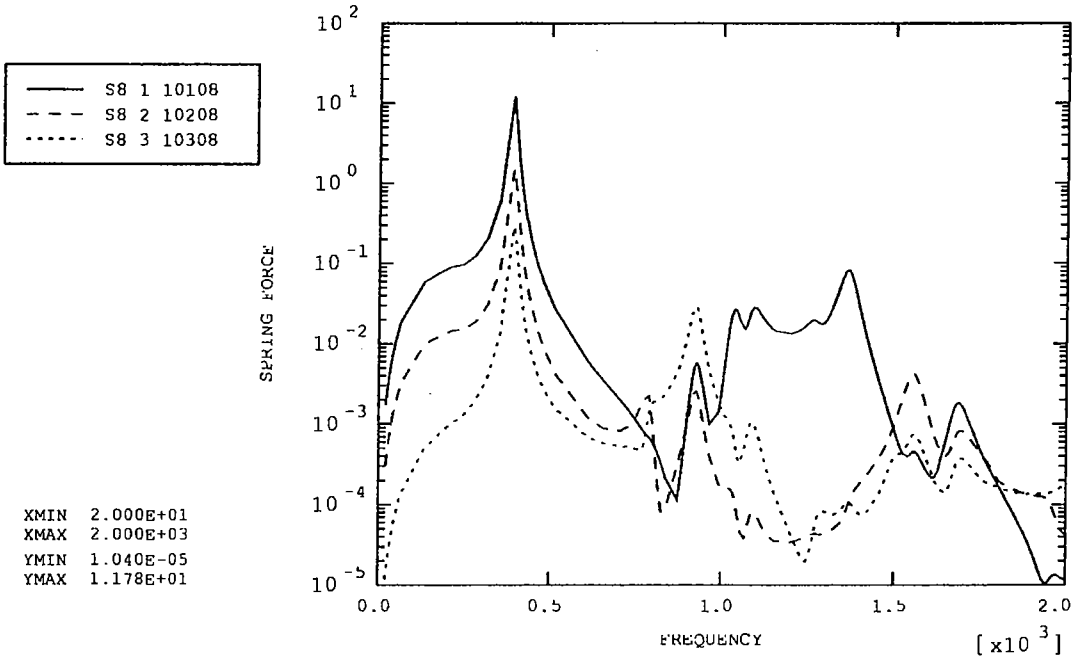

Figure 36: Jiggle pivot (top)

© FNC 2002

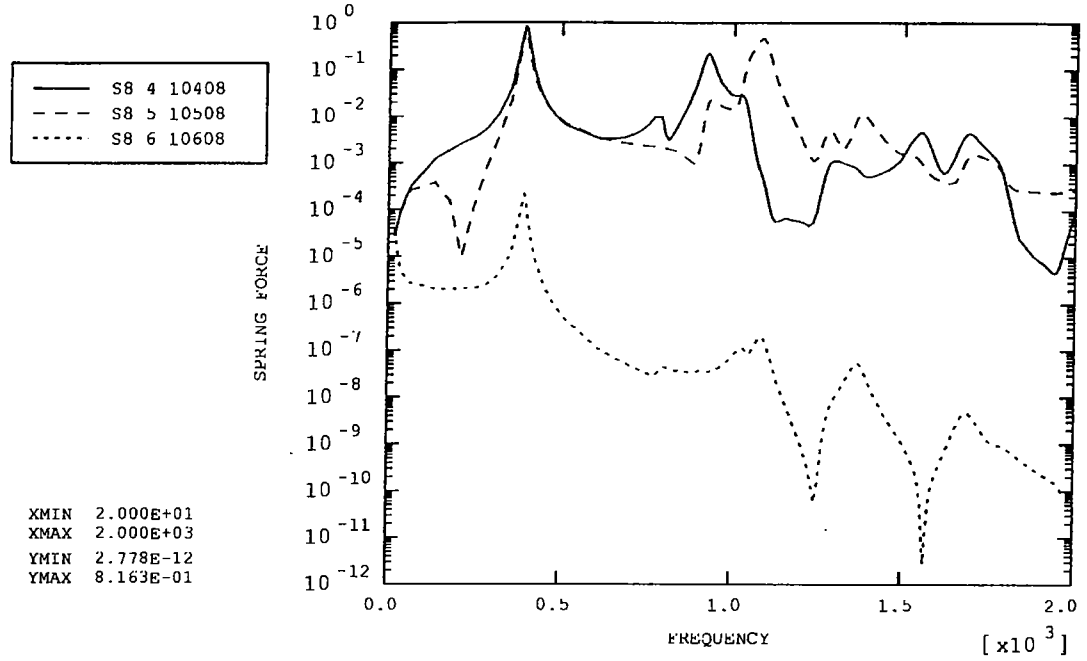

Figure 37: Jiggle pivot (top)

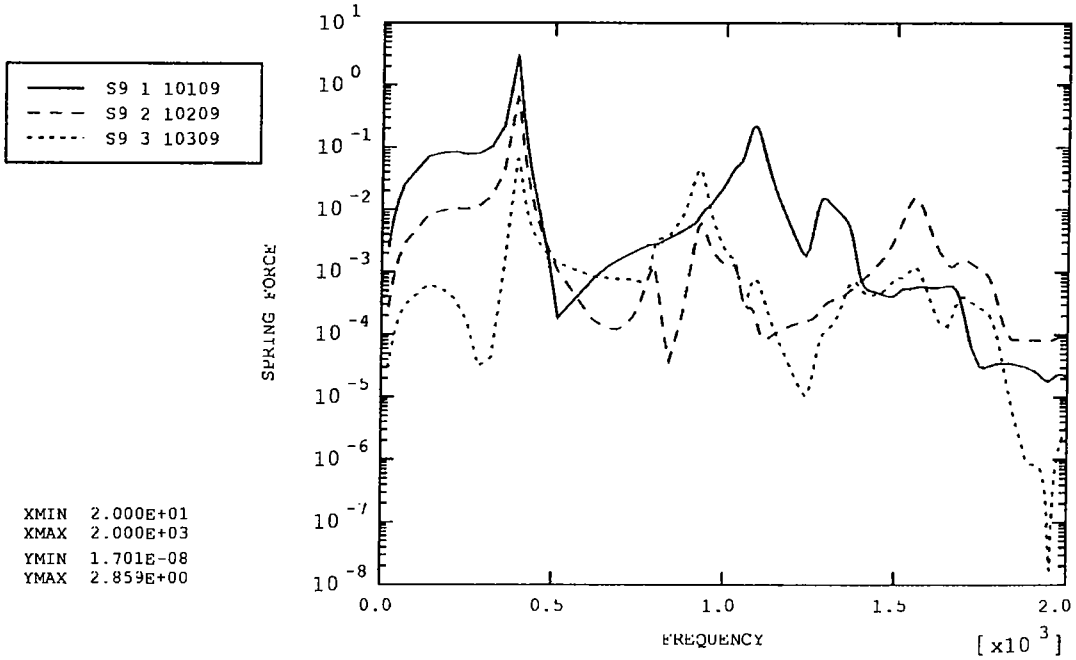

Figure 38: Jiggle pivot (bottom)

© FNC 2002

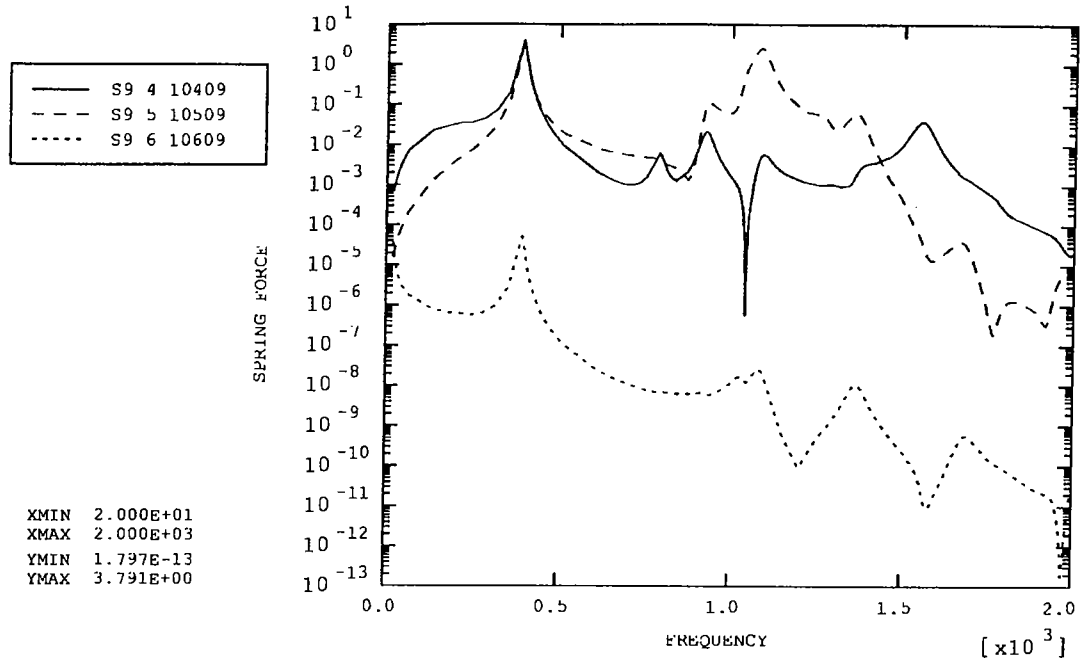

Figure 39: Jiggle pivot (bottom)

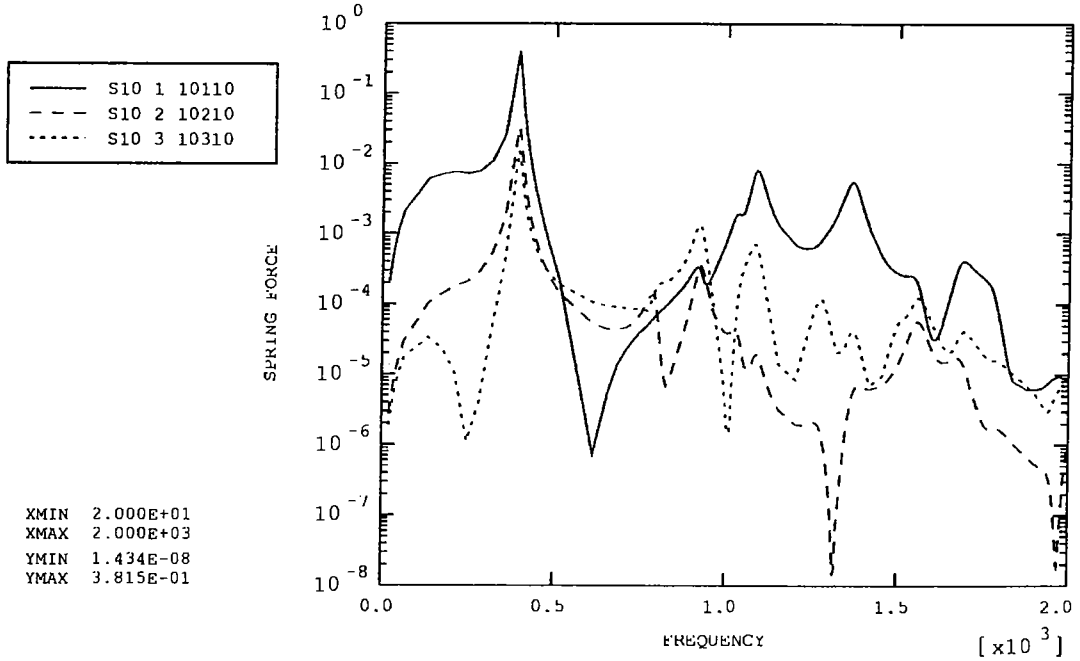

Figure 40: Chop pivot (left)

© FNC 2002

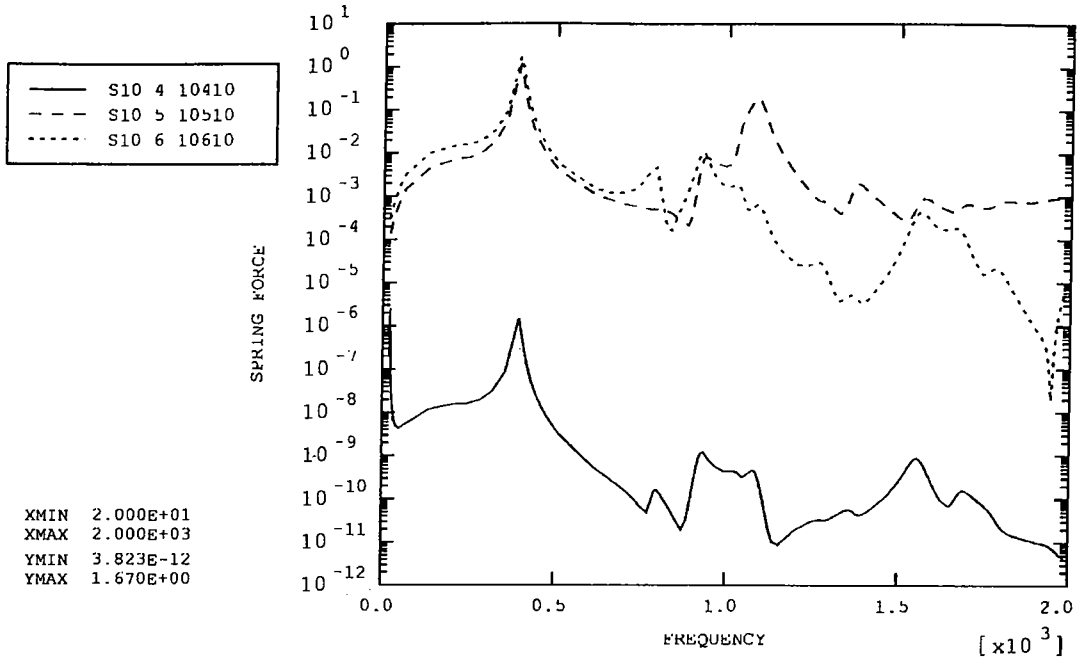

Figure 41: Chop pivot (left)

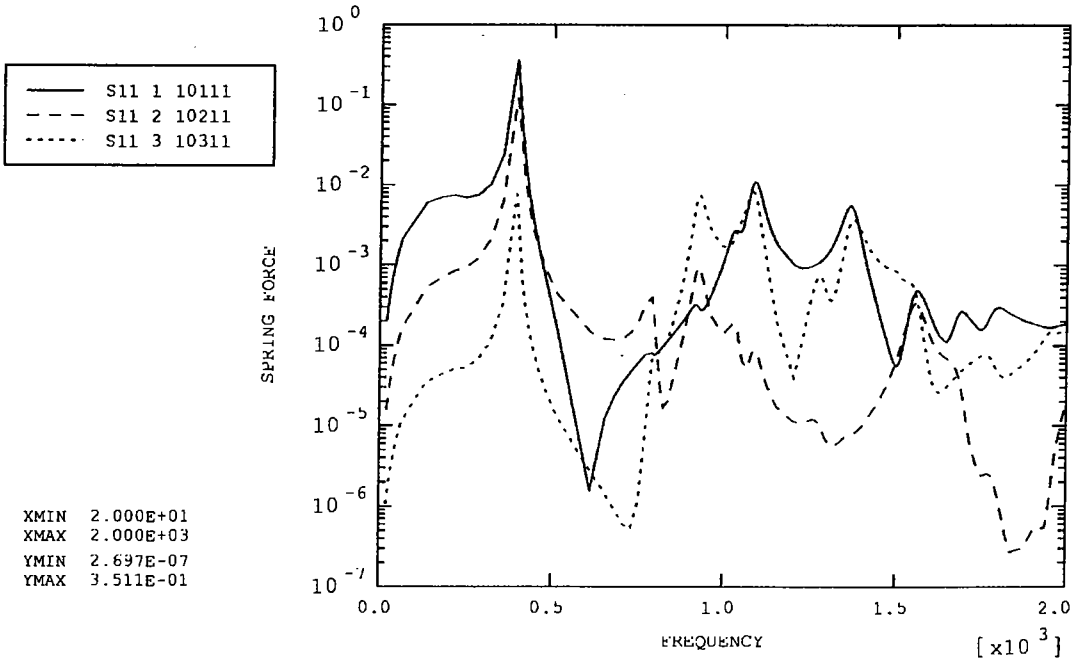

Figure 42: Chop pivot (right)

© FNC 2002

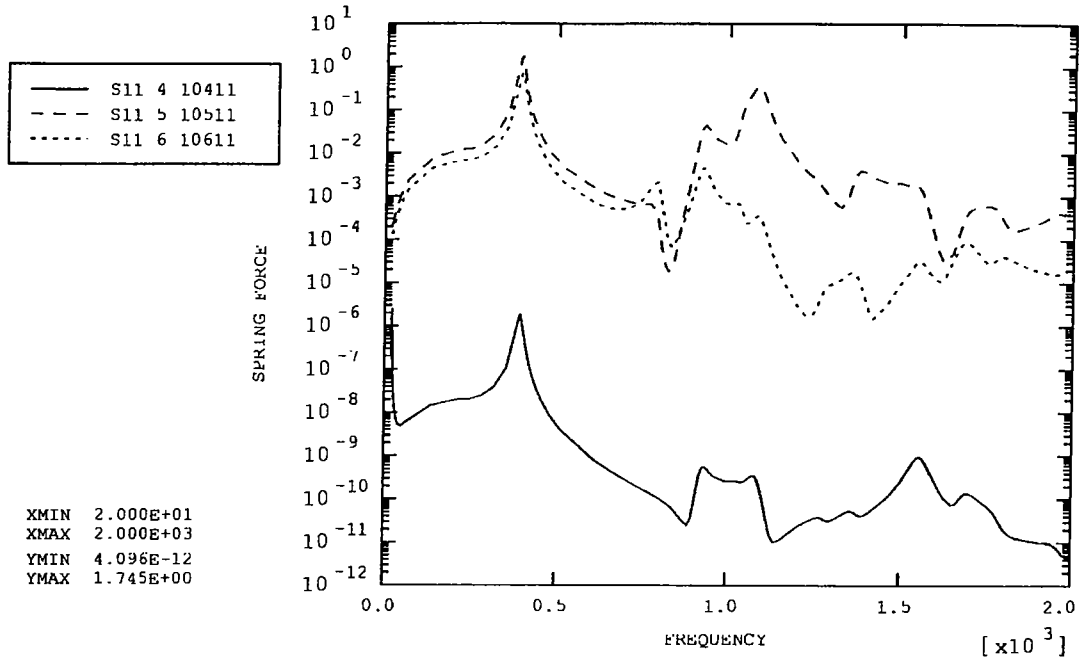

Figure 43: Chop pivot (right)

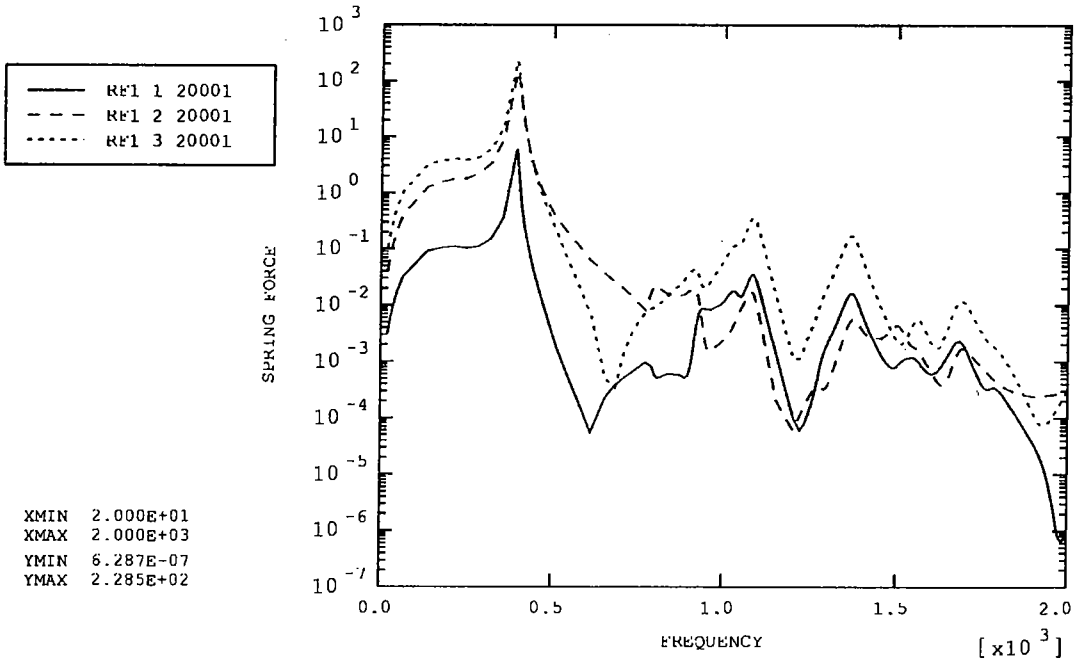

Figure 44: Reaction Force (front middle)

© FNC 2002

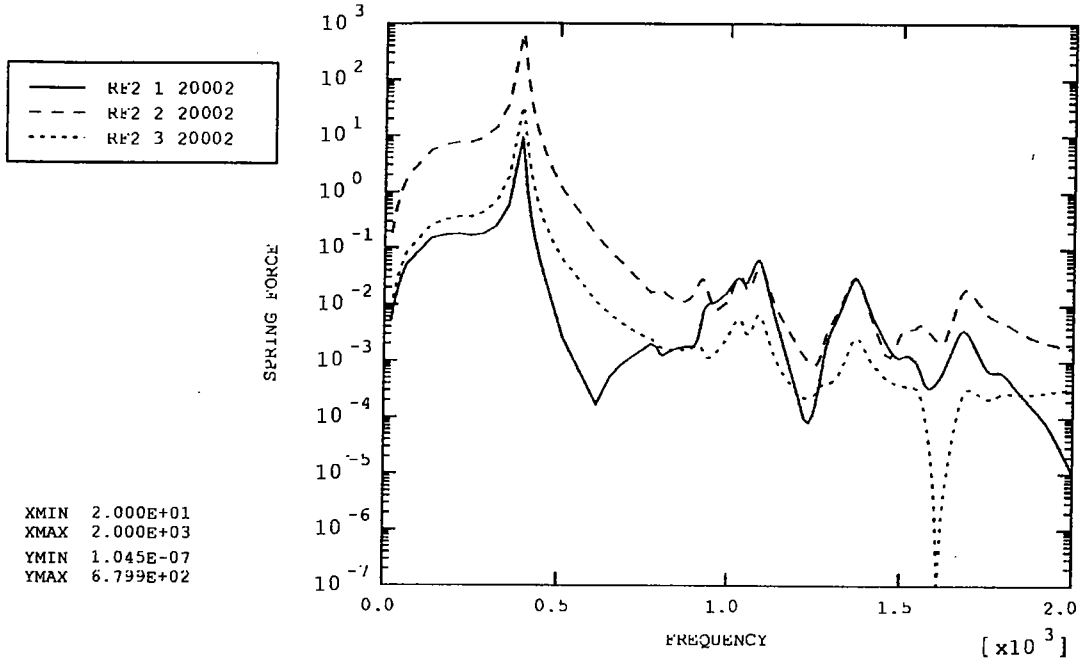

Figure 45: Reaction Force (back left)

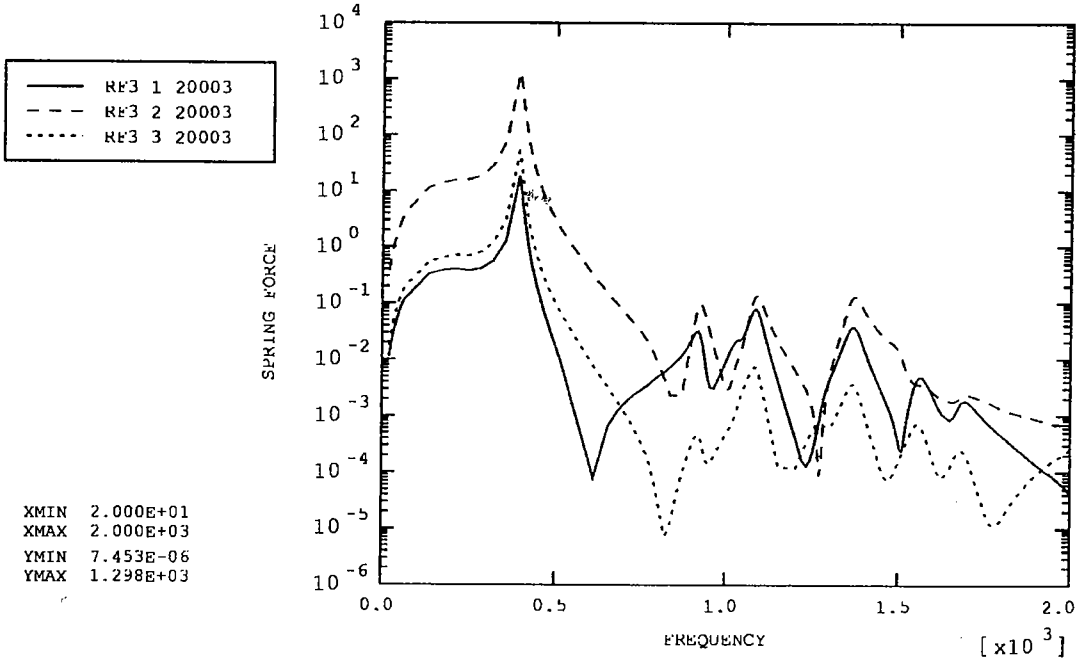

Figure 46: Reaction Force (back right)

© FNC 2002

Appendix 6
v1.0
Thermal Calculations

Contents

CALCULATION: THERMAL EQUILIBRIUM OF MOTOR COILS, MATERIALS G10 VS ALUMINIUM 2

1.1 DISCUSSION 2
1.2 VARIABLES: 2

2 MIRROR TEMPERATURE ESTIMATE 6

2.1 BLOCK DIAGRAM 6
2.2 CALCULATION 7
2.3 RESULTS 8
2.4 CHECK ON LIMITING HEAT PATH 9

3 CERNOX 1030 THERMOMETER DATA SHEET 11

Figures

1.1 Discussion 2
Figure 2: Pure radiative cooliunng 3
Figure 3: Predicted temperatures, motor mount components 5
Figure 4: thermal block diagram 6
Figure 5 mirror temperature sensitivity 8

Calculation: thermal equilibrium of motor coils, materials G10 vs Aluminium

1.1 Discussion

The motor coils operate at an average power of 1mW per motor, 0.5mW per coil. These are cooled via a conductive path through the motor core, potted joint to aluminium housing, bolted joint to BSM structure and thus to the optical bench and/or thermal strap.

1.2 Variables:

data			Source	
Stephan-Boltzman	5.67E-08			
Motor area	5.18E-04	m^2		
Motor emissivity	8.00E-01	%		
Aluminium thermal integral (AL 6082)	14	W/mK	RAL	6-4.2K
Stycast 1266	1.00E-01	W/mK	Cornell	3-4K
vespel sp-1	0.0125	W/m	RAL	6-4.2K
mild steel (use for motor cores)	6.1111	W/mK		6-4.2K
joints :				
al-al	6.00E+01	W/m^2K	RAL	
al-au-al	7.50E+02	W/m^2K	RAL	
stainless-stainless	1.00E+02	W/m^2K	RAL	
inconel-al	4.00E+02	W/m^2K	approx	
Al-eccobon-inconel	4.00E+02	W/m^2K	approx	

Motor Dissipation (W)	0-1.5	mW
Surface area (coils)	0.0005208	m^2
BSM structure temperature (worst case)	6.0	K

Coil surface area based on dimensions (mm)		
L	B	W
15.5	12	6.2

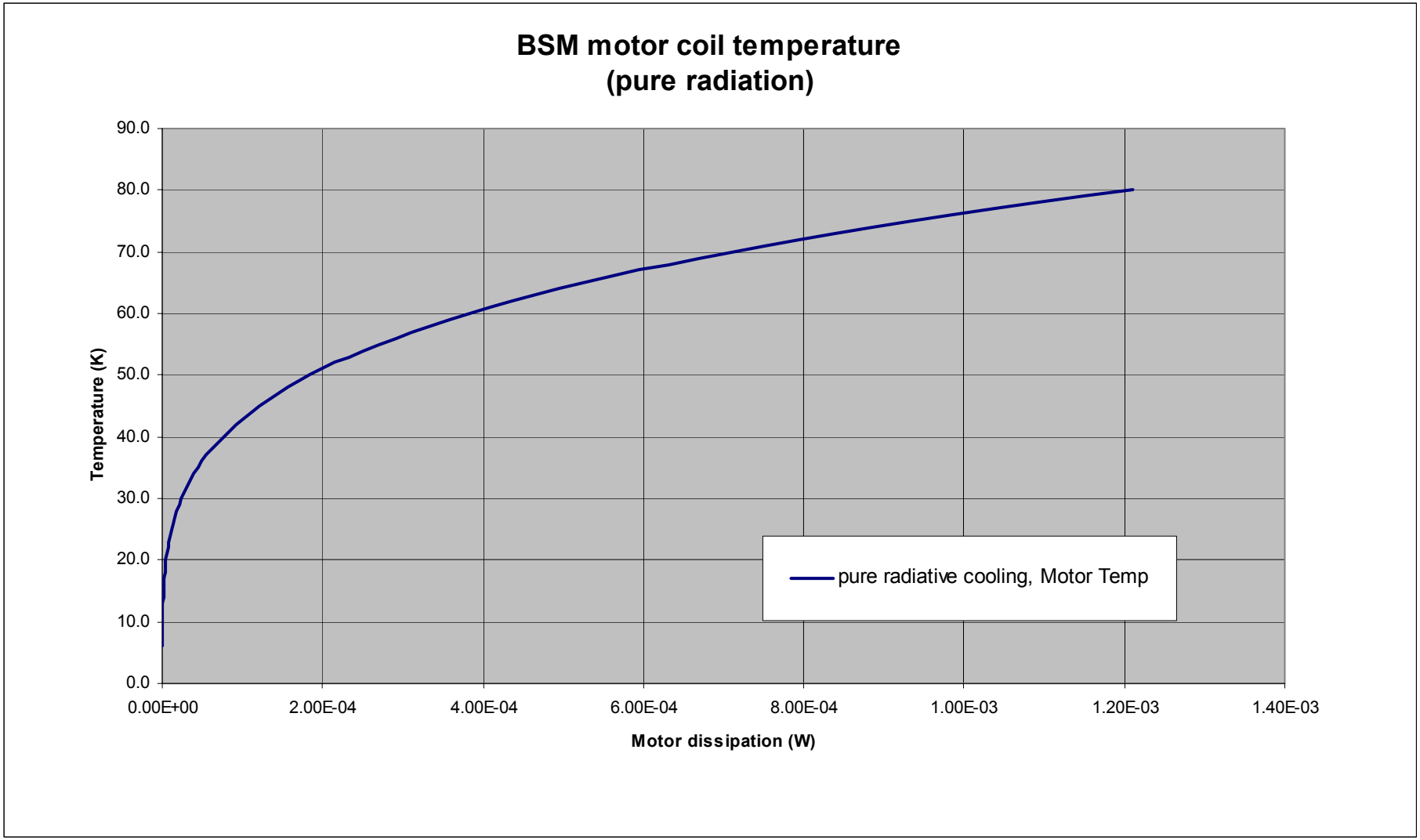

Figure 1: Pure radiative cooliunng

The figure above indicates that at 1mW the motors would reach temperatures of ~76K. In the case with conductive cooling, however, the situation is much improved.

For example, at a 1.0 K temperature differential, driven by a load of ~33 nanoW, the cooling path 'choke point' provides approximately:17mW of cooling path

Conductive cooling via Aluminium		
c(at temp, valid 4-80K)	Wm	134.1697
Area of Aluminium (min restriction)	m^2	3.78E-05
length (to inner coil)	m	0.0097
length (to outer coil)	m	0.0199
Q = A.c/L	inner	0.5228
	outer	0.2549
limit on conduction - joint		0.0173
limit on conduction - potting (0.5mm Stycast)		0.0187
Heat conduction capability (away from inner coil)		0.0169
Heat conduction capability (away from outer coil)		0.0162
margin on heat flow away from inner coil (W)		0.0168
margin on heat flow away from outer coil (W)		0.0168

To study this further, a balanced heat flow situation is considered, looking at the temperature rise required to 'drive' 0.5mW of power through the heat path.

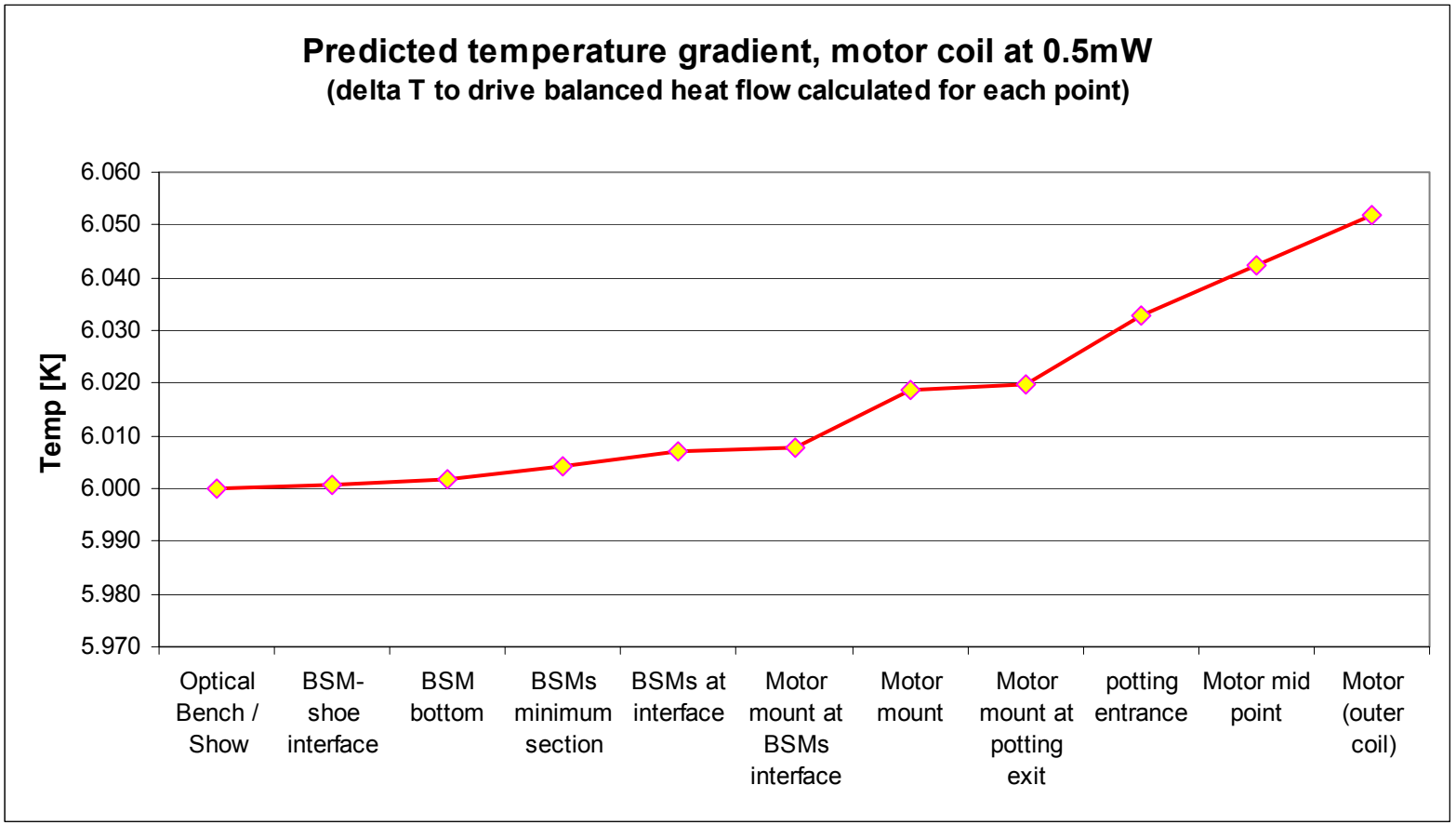

Figure 2: Predicted temperatures, motor mount components

2 Mirror temperature estimate

2.1 Block Diagram

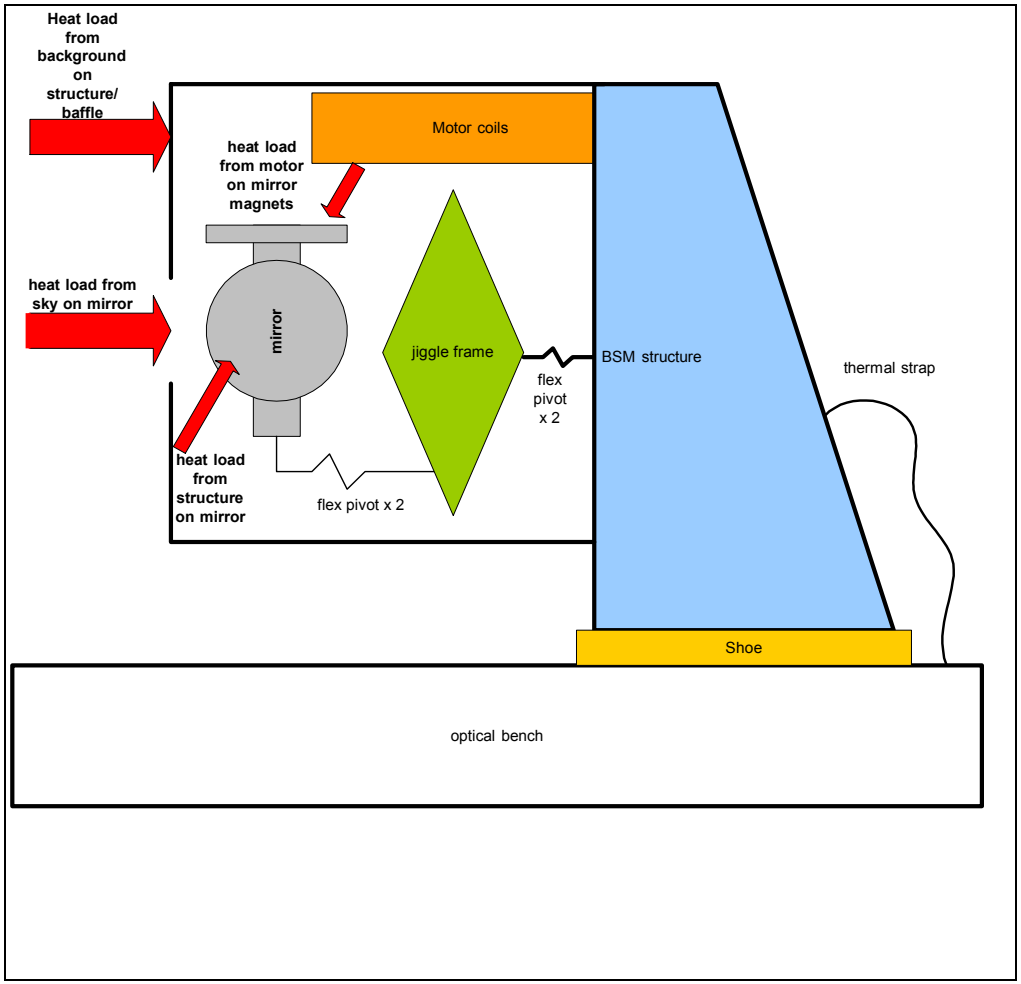

Figure 3: thermal block diagram

2.2 Calculation

Ac	8.30E-04	m^2	Chop axis area sees sky
Am	3.00E-04	m^2	Chop axis area sees motor
Ap	4.48E-07	m^2	csa pivots
Cp	0.6	W/ m^2	conduction pivots (stainless steel)
Lp	6.53E-03	m	length pivots (approx)
Tj	5	K	bsm structure & jiggle frame temp
Ts	4-150	K	Temperature of sky
Tm	4-180	K	temperature of motors

Steady state:

Q sky + Q motor = Q flex pivot (ignoring re-radiation by mirror)

$Ac.\sigma.(Ts^4 - Tc^4) + Am\ \sigma.(Tm^4 - Tc^4) = Ap.cp/Lp\ (Tc - Tj)$

$(Ac-Am)Tc^4 \quad +(Ap.Cp/Lp.\ \sigma).Tc = (Ap.cp/Lp.\ \sigma).Tj + Ac.Ts^4 \quad +Am.Tm^4$

Solve for Tc, results below

2.3 Results

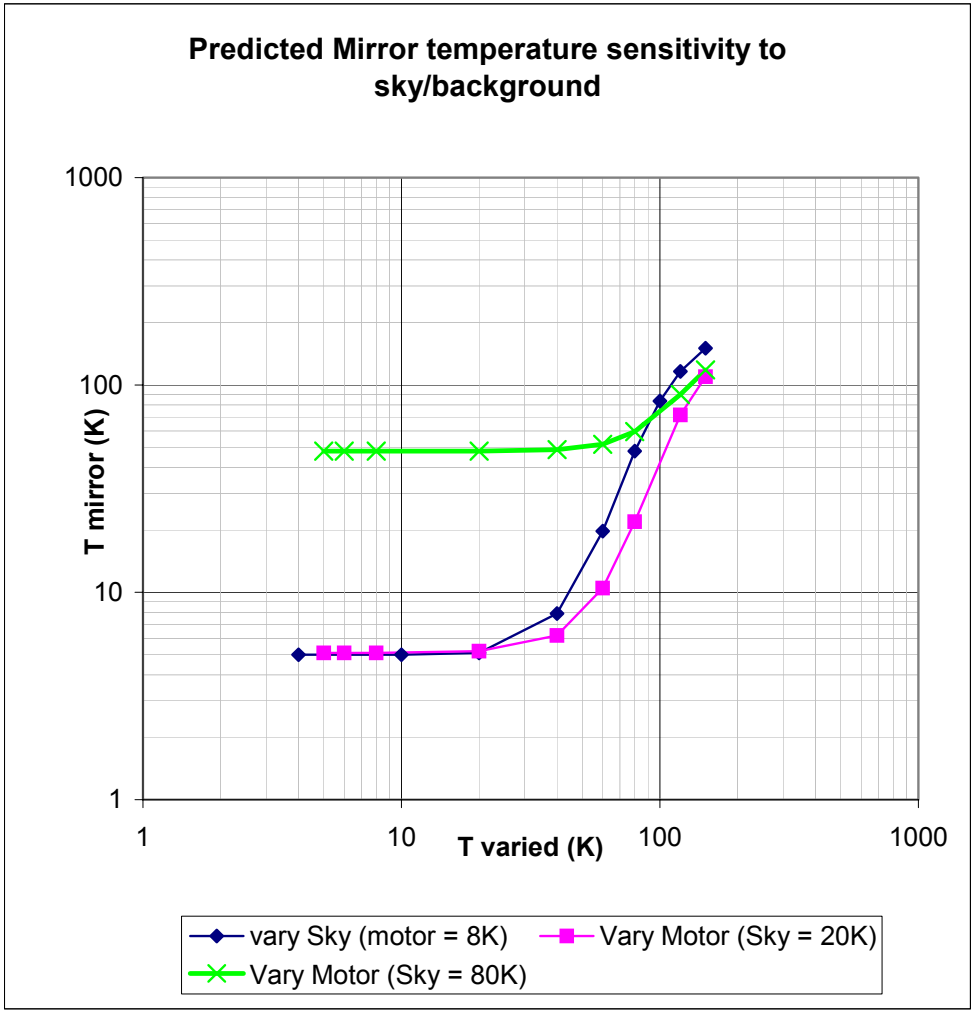

Figure 4 mirror temperature sensitivity

2.4 Check on limiting heat path

Note the above assumes the Stainless Steel flex pivots are the limit on the heat path. This can be confirmed by crude calculation, below.

Allowing a 0.1 deg K differential across each section or interface, the chop axis pivot clearly has the lowest conducted heat.

Component	Conduction (4-6k)	conductance (W/m^2K)	Contact Area	min CSA	Length	max Conducted heat (W)	Delta-T	Notes
Optical Bench							0.1	
Bench-Shoe interface		7.50E+02	4.10E-04			3.08E-02	0.1	Al-Au-Al
Shoe minimum section	33.600			4.00E-04	0.008	1.68E+00	0.1	Al 6082
shoe-BSMs interface		7.50E+02	4.00E-04			3.00E-02	0.1	Al-Au-Al
BSMs minimum section	33.600			3.37E-04	0.093	1.22E-01	0.1	Al 6082
BSMs-flex pivot capture sleeve		6.00E+01	1.30E-04			7.80E-04	0.1	al-al. surface area of top pivot half factored by .75 to allow for joint conduction
Flex pivot capture sleeve x2	33.600			2.14E-02	0.006	2.40E+02	0.1	Al 6082
Flex pivot capture sleeve- flex pivot x2		4.00E+02	1.37E-04			5.48E-03	0.1	Al-eccobon-inconel
Jiggle flex pivot minimum section x2	0.600			3.00E-06	0.008	4.50E-04	0.1	Inconel (or stainless)
Jiggle flex pivot - jiggle frame		4.00E+02	1.00E-02			4.00E-01	0.1	inconel-al
Jiggle frame minimum section	33.600			2.00E-05	0.040	1.68E-02	0.1	Al 6082
Jiggle frame - capture sleeve x2		6.00E+01	1.00E-02			6.00E-02	0.1	al-al
capture sleeve - chop flex pivot x2		4.00E+02	1.00E-02			4.00E-01	0.1	Al-eccobon-inconel
chop flex pivot min section x2	0.600			2.00E-06	0.008	3.00E-04	0.1	Inconel (or stainless)
chop flex pivot - chop stage		4.00E+02	1.00E-02			4.00E-01	0.1	inconel-al
Chop stage (mirror) min section	33.600			2.00E-05	0.025	2.69E-02	0.1	Al 6061

Data:

Aluminium thermal integral (AL 6082)	33.6 6-4.2K		W/m	RAL doc gives ~14 W/mK	ATC has 85 for Al 6063
inconel (use stainless steel)	0.6 6-4.2K		W/m	RAL & ATC agree	
vespel sp-1	0.0125 6-4.2K		W/m	RAL	
joints :					
al-al		6.00E+01	W/m^2K		
al-au-al		7.50E+02	W/m^2K		
stainless-stainless		1.00E+02	W/m^2K		
inconel-al		4.00E+02	W/m^2K	guess	
Al-eccobon-inconel		4.00E+02	W/m^2K	guess	

3 Cernox 1030 Thermometer data sheet

See

http://www.lakeshore.com/temperature/cernox.pdf

This page intentionally left blank

Document Ends.

Appendix 7:
Controls Analysis
v1.0

Table of Contents

7 Controls Analysis 1

7.1 BSM Control System Analysis 1
7.1.1 SCOPE 1
7.1.2 LINEAR ANALYSIS 1
7.1.3 NON-LINEAR SIMULATION 4

Table of Figures

Figure 1 Chop Axis Closed-Loop Bode Diagram *3*
Figure 2 Chop Axis Nichols Chart *4*
Figure 3 Chop Axis Step Response (non-linear simulation) *5*
Figure 4 Chop Axis Motor Power Dissipation (at 4 deg.K) *6*

7 Controls Analysis

7.1 BSM Control System Analysis

7.1.1 SCOPE

This analysis describes the control system for the SPIRE Beam Steering Mirror (BSM).
The BSM is a two-axis device, using flex-joint supports to give a negligible friction control of the axes, allowing high accuracy positioning.
The description concentrates on the Chop axis, as the Jiggle axis has exactly the same control scheme, with parameters changed to suit the larger inertia and flex-joint spring rate. However some Jiggle modelling results are included.

7.1.2 LINEAR ANALYSIS

As the lowest BSM structural resonance has been estimated at around 800 Hz by FE modelling, The BSM axes can be modelled for the purposes of control as a simple spring-mass-damper system, using the flex-joint spring rate.

The mechanism can be represented by the second-order system

$$G(s) = \frac{\omega_n^{\,2}}{s^2 + 2*d*\omega_n*s + \omega_n^{\,2}}$$

where the system natural frequency

$$\omega_n = \sqrt{\frac{Ks}{J}}$$

with Ks = flex joint spring rate, 0.047 Nm/rad Chop and 0.37 Nm/rad Jiggle
J = axis inertia. 1.7e-6 Kgm^2 Chop and 45.0e-6 Kgm^2 Jiggle
d = flex joint damping 2.3e-5 Nm/rad/sec

The Chop step specification requires a sinusoidal step profile to be achieved in less than 20mS. With a design target of 15 mS, a nominal system risetime of about 5mS is required to closely follow the externally generated profile.

A second order linear system has a 2% settling time of 4 time constants, or $\frac{4}{d*\omega_n}$. With d = 0.707, this becomes $\approx \frac{5.7}{\omega_n}$. This requires a bandwidth of approximately 200 Hz to meet the design target.

A linear frequency-domain model was constructed to evaluate a standard nested velocity and position loop control system.
All linear elements in the mechanism, motor power amplifier and position sensor were included in the model. An acceleration loop was included to limit the system acceleration, as the slew rate of the electronic power amplifier may produce instability for large step demands.

The following control parameters were used. Note that the position loop integrator is of the form (1 +s*t) / s .

Parameter	Description
position sensor gain	100
position loop gain	21.9
position loop integrator time constant	0.013
rate loop feedback gain	2.66
Acceleration loop feedback gain	0.5e-3

Figure 1 Chop Axis Closed-Loop Bode Diagram

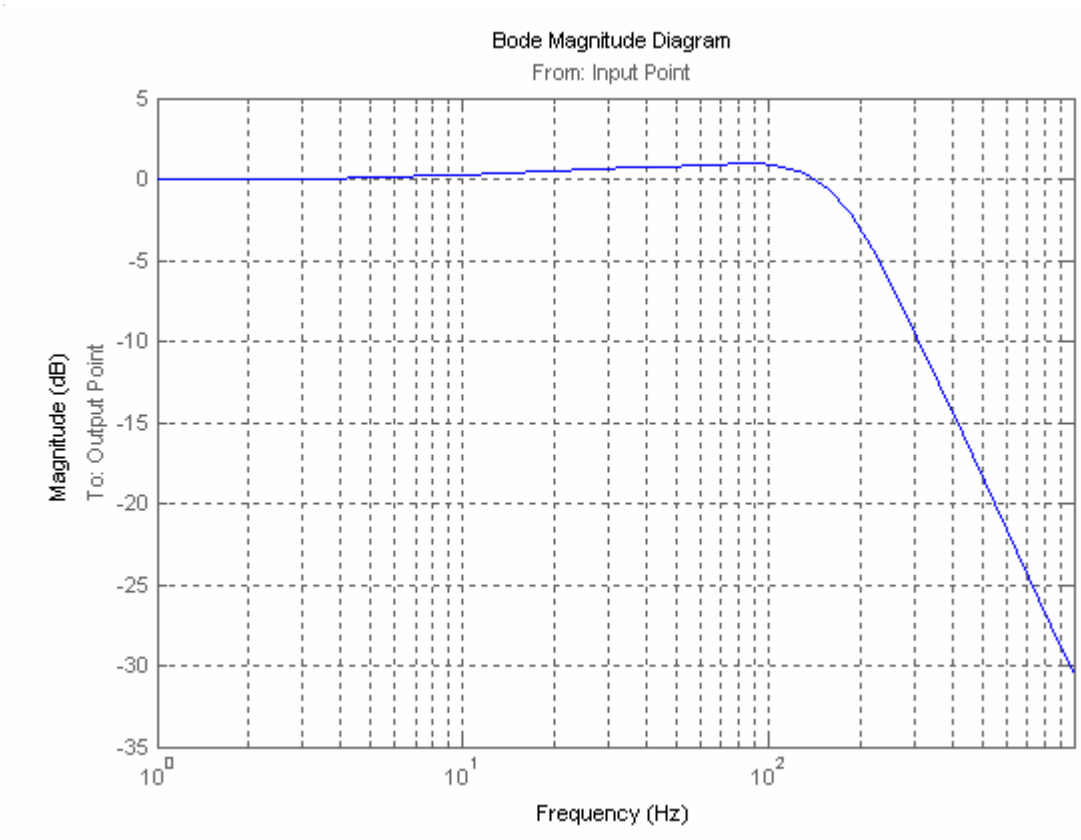

It can be seen from the above closed-loop Bode plot that the –3dB bandwidth is approximately 200 Hz.

The loop stability can be evaluated using the Nichols chart, which plots open-loop response with overlaid closed-loop contours.

Figure 2 Chop Axis Nichols Chart

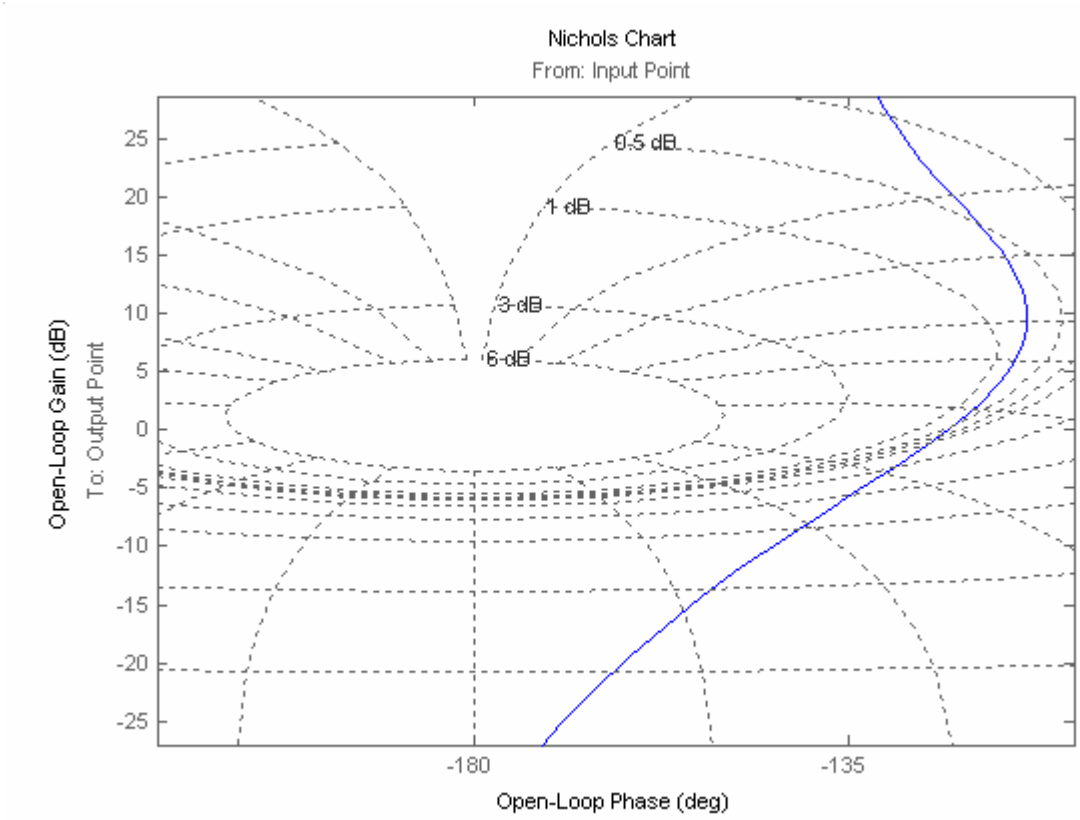

The gain margin is 33dB and the phase margin is approximately 57 degrees.

7.1.3 NON-LINEAR SIMULATION

Though the foregoing analysis gives a good guide to general performance, there are a number of significant non-linearities present in the system, particularly the voltage limits of the power amplifier. More significantly, the control system will be implemented entirely in software, apart from the power amplifier and the position sensor preamplification. Standard linear analysis cannot handle the sampling effects and quantisation in a simple manner.
There is also the assumption in the above modelling that rate and acceleration signals were available for feedback, however the system uses only a magnotorestive position sensor. Therefore the required signals need to be estimated from the existing information. A standard method of achieving this is using a state observer, which employs a basic model of the system, and uses feedback from the available system signals to correct any errors in these estimates due to, for example, incorrect estimates of system parameters such as inertia and spring rate. This method also copes with variations in parameters such as the spring rate. However, the calculations can only be done accurately by a processor and associated software.

For these reasons, a detailed time domain non-linear simulation of the BSM axes control system has been created using matlab-Simulink, an industry standard tool.
This model is described in detail in the SPIRE BSM Design Description document, however, some results are presented here for convenience.

The following figure shows the demanded sinusoidal position step demand (blue) for the Chop axis, and the system response (green).

Figure 3 Chop Axis Step Response (non-linear simulation)

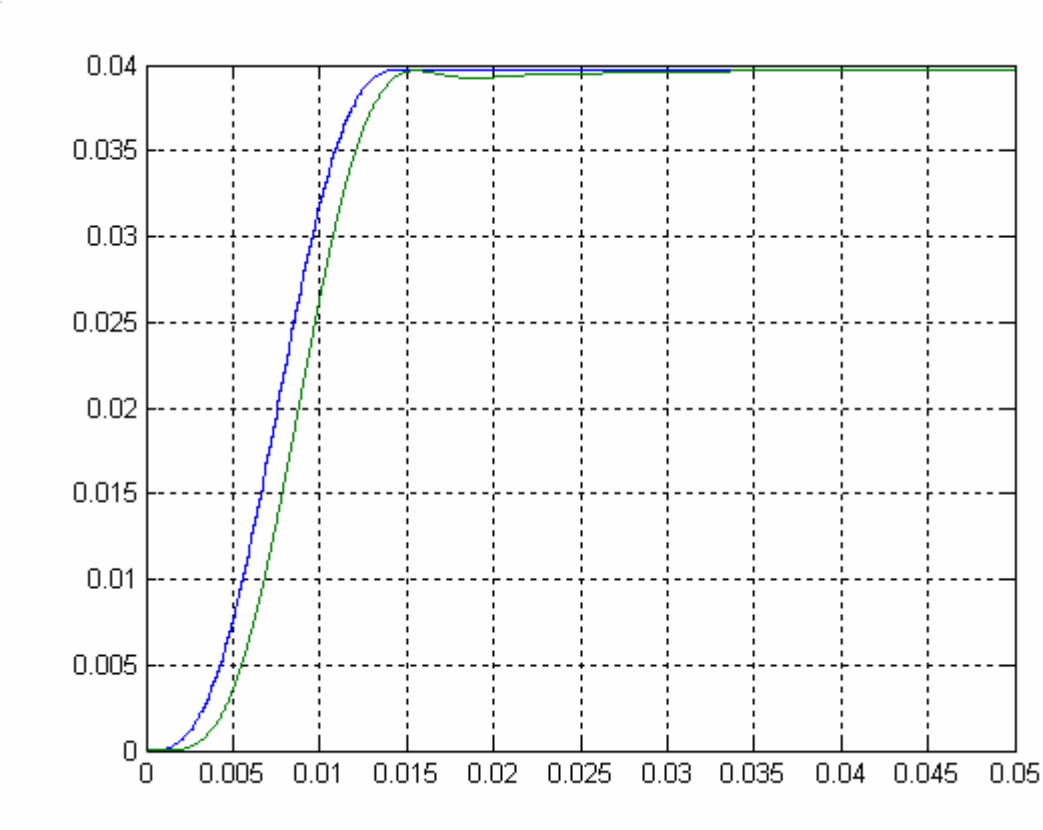

Note that the simulated performance meets the original design target step response of 15 mS.

Finally, as power dissipation is an important parameter to be minised for the BSM, as it is in a cryogenic environment, the non-linear simulation enables the calaculation of dynamic power dissipation. It is interesting to note from the following figure that the peak motor power required to slew the axis is approximately the same as that required to hold the axis at a fixed angle.
Indeed over time, the dominant power dissipation requirement for the BSM mechanism is that required to hold the axes against the flex joint spring forces – this is the trade-off for almost zero friction during axis rotation.

Figure 4 Chop Axis Motor Power Dissipation (at 4 deg.K)

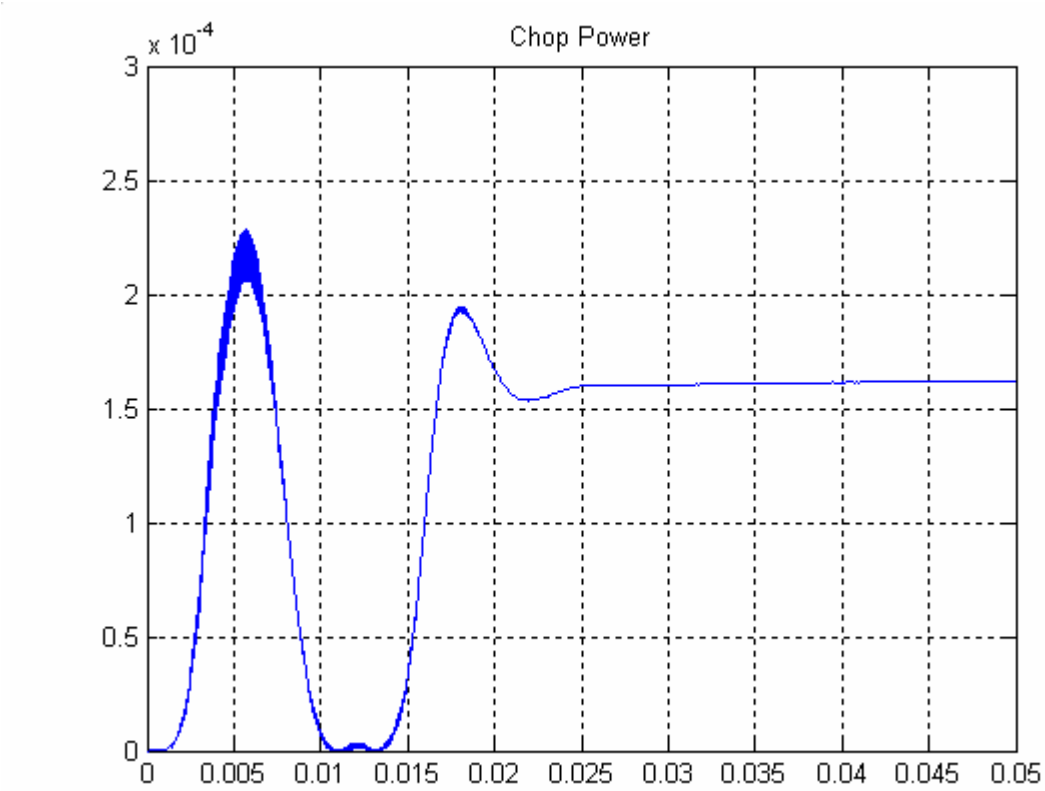

Document Ends

Appendix 9: v1.0
Single Axis Prototype Test Report

Table of Contents

9 Single Axis Prototype Warm Tests ____ 1
9.1 BSM Control System: Position Sensor Output Noise ____ 2
9.2 BSM Electronics: Motor Torque Constant ____ 8
9.3 SPIRE: Current Source Test ____ 11
9.4 Preliminary Cross-talk test ____ 12
9.5 Single Axis proto-type Cold tests ____ 13
9.6 Two- Axis proto-type ____ 16

Table of Figures

Figure 1 Single Axis Prototype ... 2
Figure 2 Noise in the Sensor and Preamplifier Electronics ... 4
Figure 3 100kHz Spectrum Bandwidth ... 5
Figure 4 Ungrounded low frequency spectrum (500Hz bandwidth ... 6
Figure 5 Grounded Low Frequency Spectrum (500Hz) ... 7
Figure 6 Tilt Measurement Apparatus Configuration ... 8
Figure 7 Torque Analysis Graph ... 10
Figure 8 Current Load Source Voltage vs Time ... 12
Figure 9 Power Dissipation (AC input) ... 15
Figure 10 Sensor Output vs Motor Input ... 15
Figure 11 Sensor Output vs Motor Input ... 16
Figure 12 Two-axis Prototype ... 17

As described in the development plan, single and two axis prototypes are being constructed and tested prior to the DM, in order to validate the design of the BSM and identify as early as possible any critical areas, or issues where further development work is needed. For example meeting the requirements for the positional stability and power consumption with the design presented here requires specific performance from the position sensors and the motor torque. The validity of many of these design assumptions can be tested to first order with warm tests of the simple single axis prototype, followed by cold tests and without the need for space rated components. The results of these tests and their conclusions are described in the following sections. The two-axis prototype, which is currently under construction, will be tested in a more rigorous fashion.

9 Single Axis Prototype Warm Tests

The single axis prototype BSM was machined to the design drawing so that it had approximately the correct mass. Since the prototype did not have a polished test spot on the surface, a glass mirror was mounted on it for the motor torque measurements. The motor was one of the PACs prototypes assembled in the BSM two coils/one-magnet configuration. A Dspace program constructed in the Simulink programming environment - which emulated the final controlling software (and hardware) - was used to control the motor and monitor the feedback. A PC based ADC provided the interface between the Dspace software and BSM hardware. A photograph of the single axis prototype is shown in figure 1.

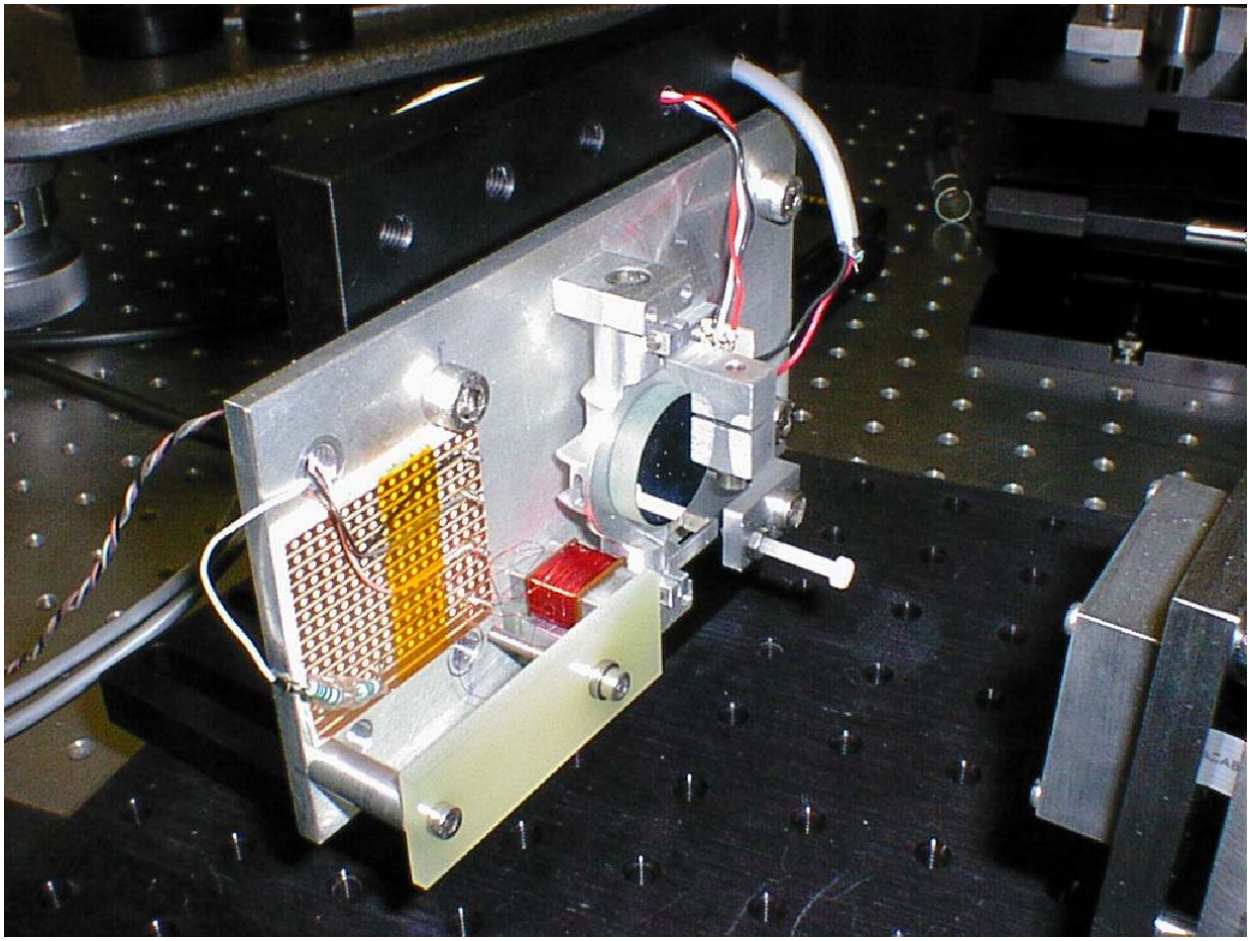

Figure 1 Single Axis Prototype

9.1 BSM Control System: Position Sensor Output Noise

9.1.1 INTRODUCTION

The specification requires a maximum position error of 0.34%rms (including motor drift). Allowing 25% of this error to be electrical noise in the position sensor electronics means that the noise limit is 0.085 % of the output of the preamplifier when the mirror is at an end-stop, measured at approximately 11.2V magnitude (see page 13). This gives a maximum noise output of 9.5 mV. Since the BSM design is based on use of the ISOPHOT chopper position sensors, this ought to be the case - however the details of the performance of the position sensors were poorly documented and the SPIRE requirements differ in that they are far more demanding. We therefore carried out the following test of the position sensor output noise.

In order to investigate sightline noise in the single-axis BSM prototype, the output from the position sensor and its preamplifier was captured using a Tektronix TDS 224 digital oscilloscope, but without closing the BSM control loop. Therefore the noise measured was due to the sensor and its associated electronics (current source and preamplifier) only. The measured noise was then analysed in the frequency domain using the FFT function on a Hewlett Packard 3562A Dynamic Signal Analyser. If the noise had a flat spectrum, it would be sensible to anti-alias filter it to remove any high frequency element that would be folded down into the control loop bandwidth by the subsequent 10 kHz sampling process.

9.1.2 RESULTS

Figure 2 shows the output from the preamplifier, with the motor depowered. The amplitude of the noise is approximately 10mV.

Figure 3 shows the frequency spectrum of the sensor and preamplifier over a 100KHz bandwidth. Implementing a high frequency filter into the electronics can easily eliminate the large peaks at and after 50kHz. Figures 4 and 5 show the spectra for low frequency bandwidth. Figure 5 demonstrates that by even crudely shielding the preamplifier - in this case a very thin metal shield was used - will reduce extraneous noise significantly.

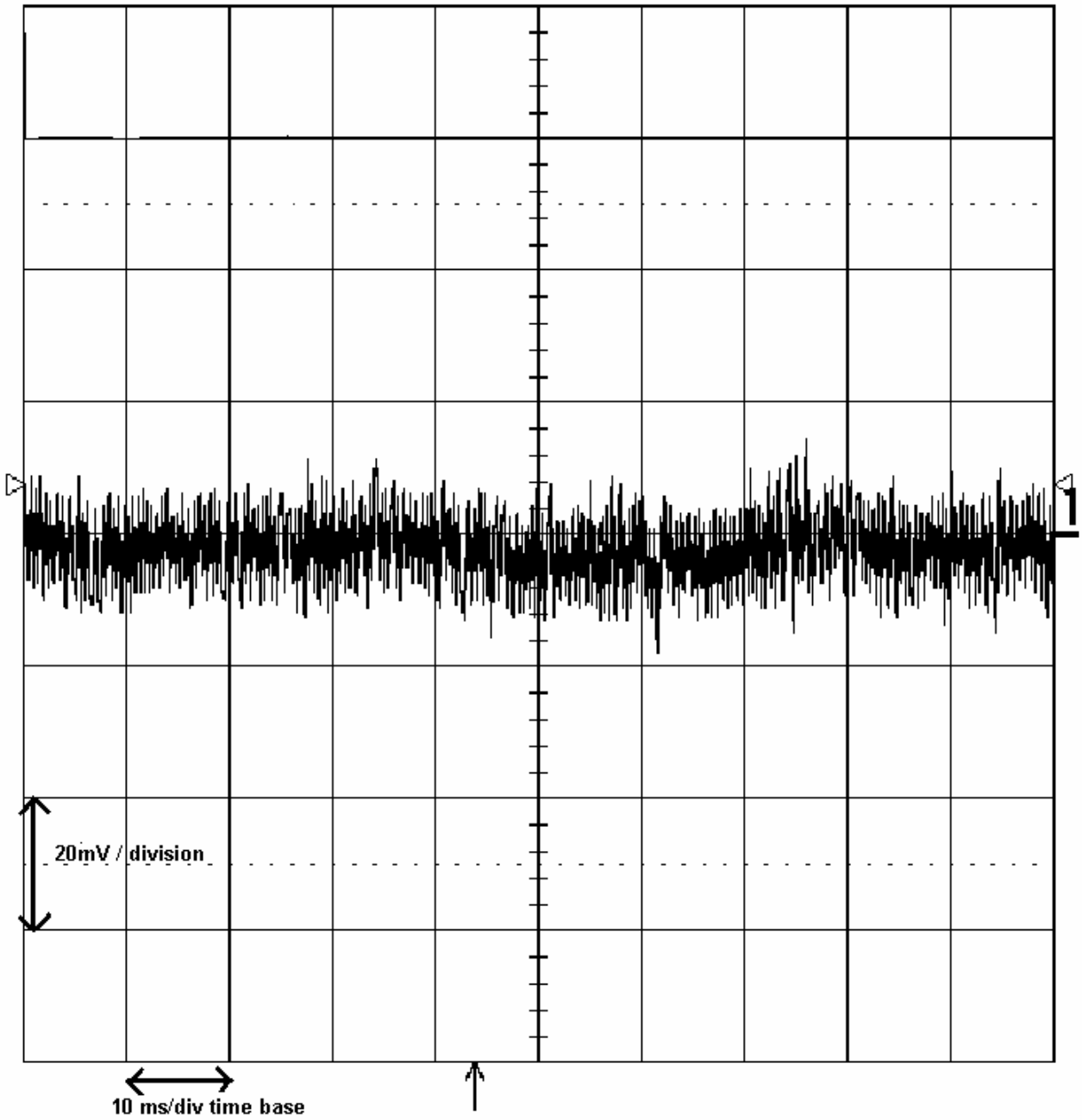

Figure 2 Noise in the Sensor and Preamplifier Electronics

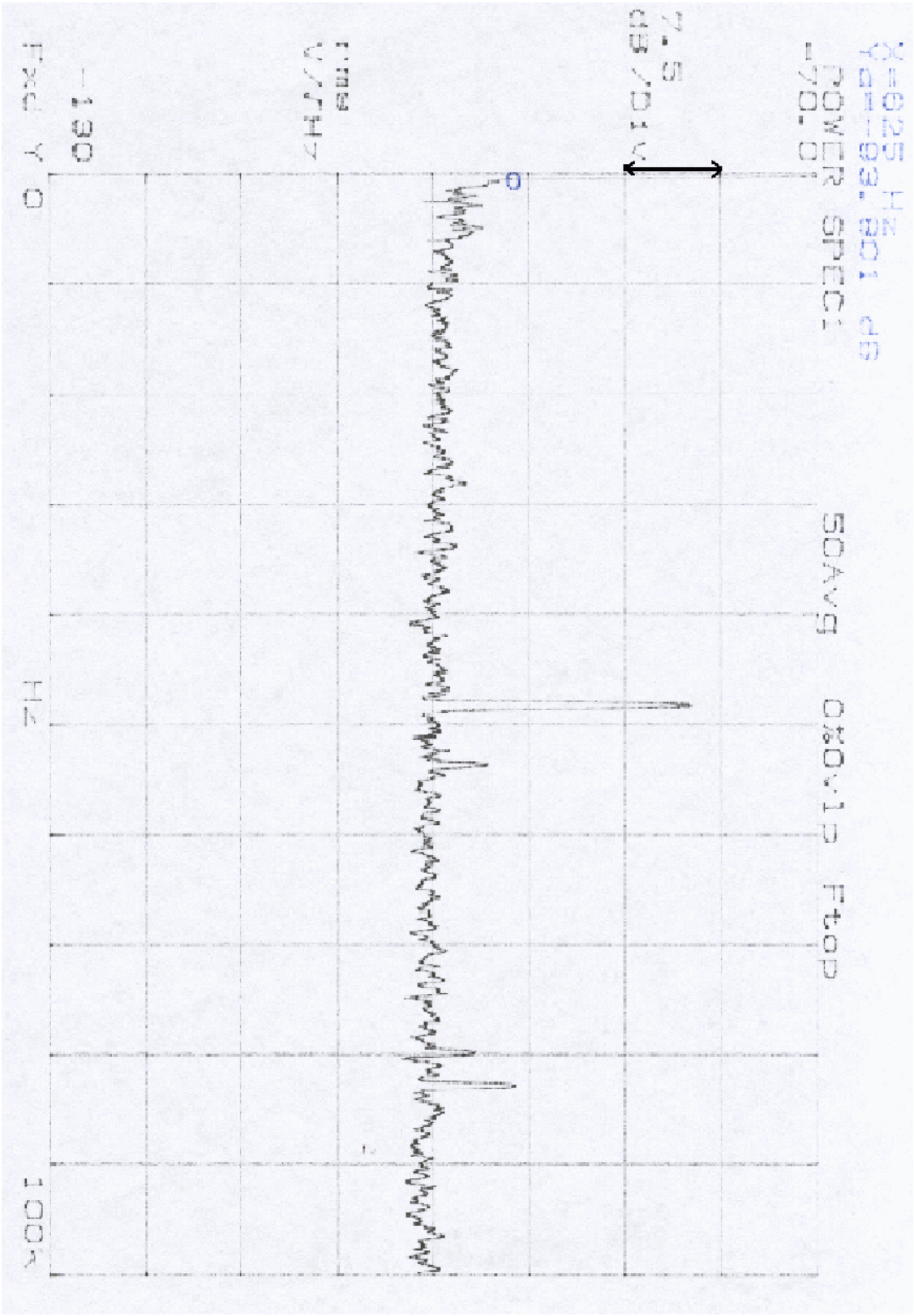

Figure 3 100kHz Spectrum Bandwidth

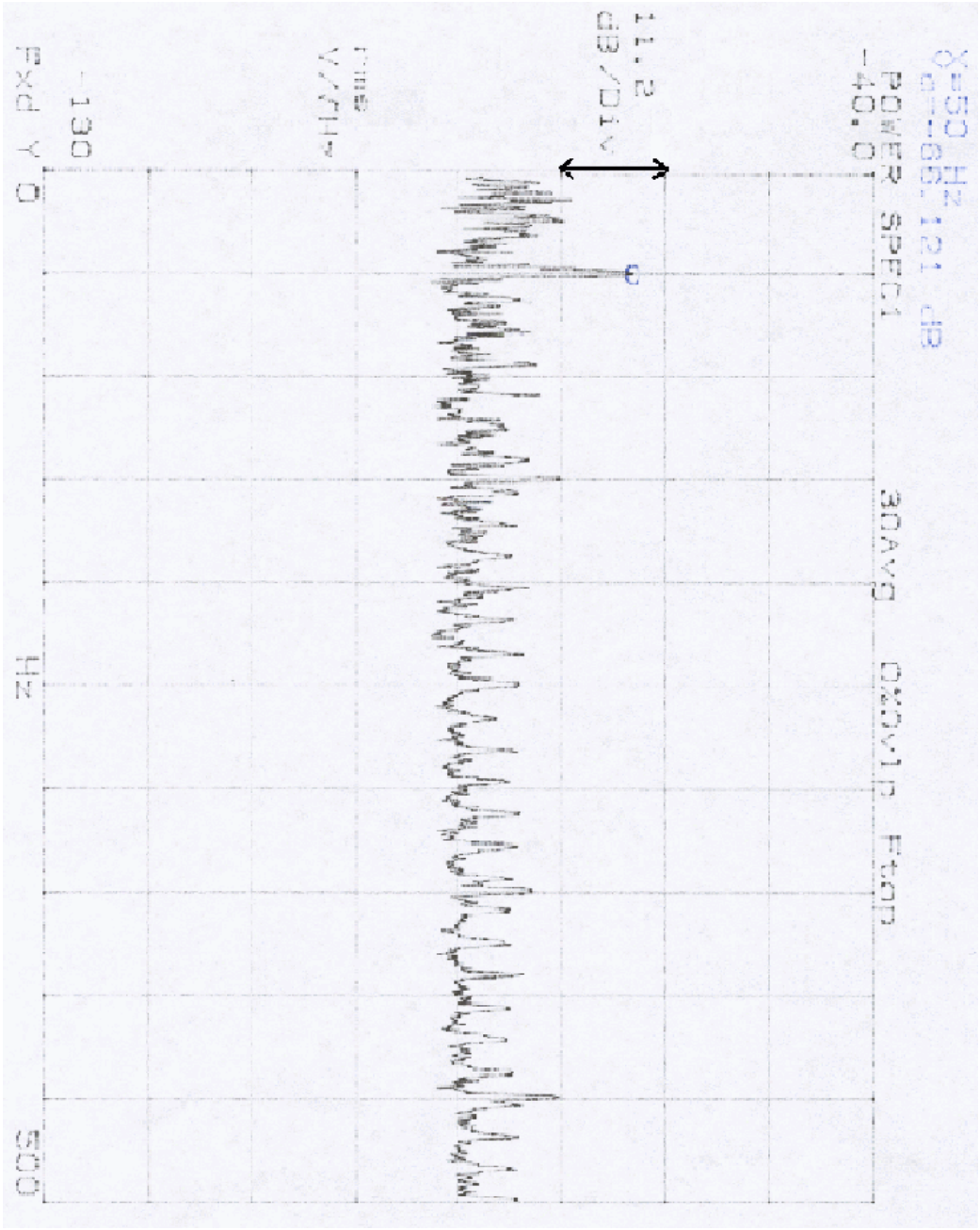

Figure 4 Ungrounded low frequency spectrum (500Hz bandwidth

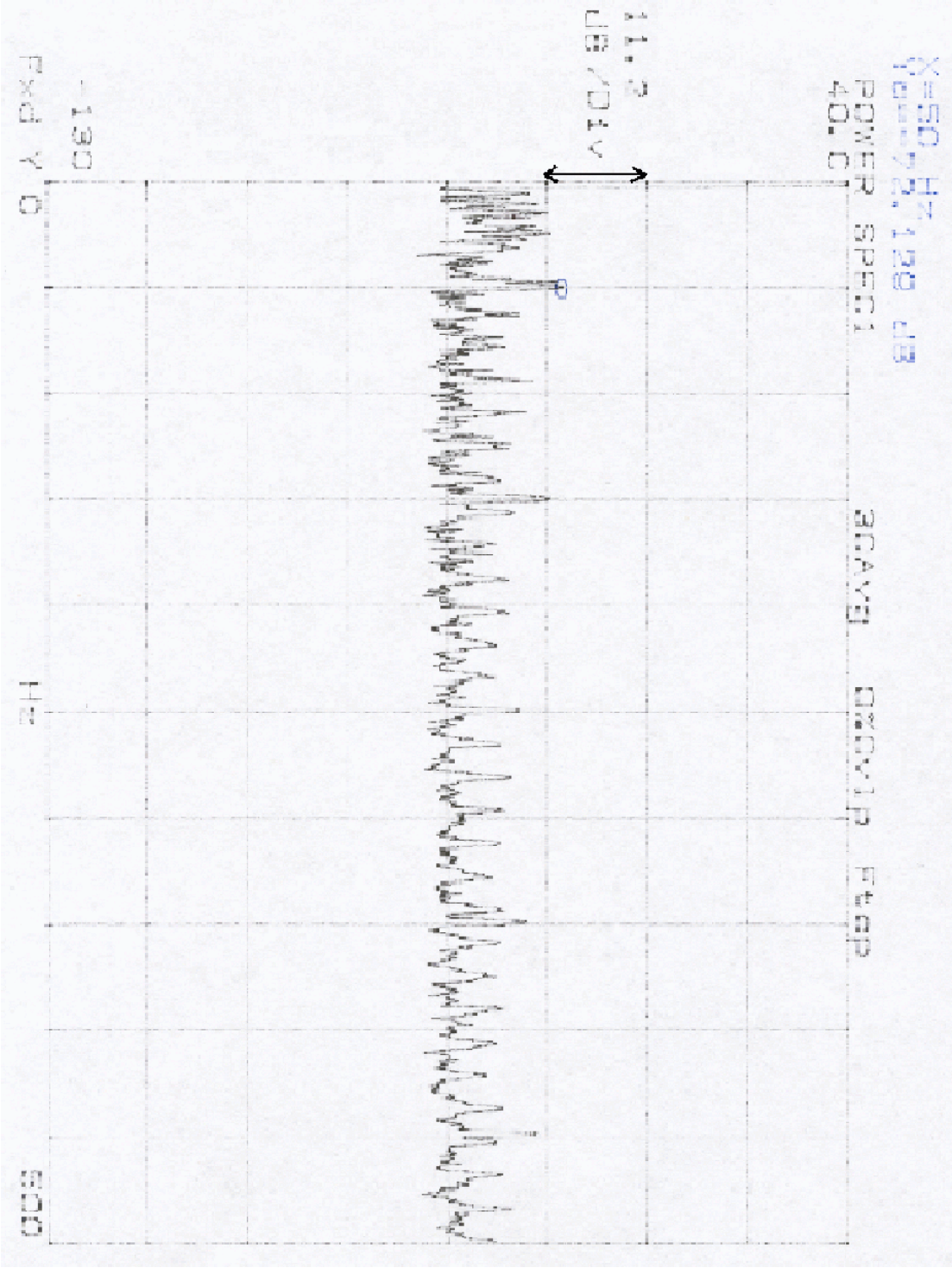

Figure 5 Grounded Low Frequency Spectrum (500Hz)

9.1.3 CONCLUSION

These tests demonstrate that the noise output of the sensor and preamplifier can be easily brought within the required parameters by implementing a high frequency filter into the sensor electronics and by ensuring that they are properly electromagnetically shielded from external interference.

9.2 BSM Electronics: Motor Torque Constant

9.2.1 INTRODUCTION

The motors used for the BSM are constructed from parts used in the MPIA-designed PACS system. Though the MPIA motors were designed in a thorough manner, UKATC has neither the expertise nor necessary magnetic modelling software to follow a similar process to produce a space-qualified motor. It was in any case desirable to build on the extensive MPIA experience in this area and have some commonality of design between PACS and SPIRE.

Based on simple calculations, it was concluded that two coils and one magnet (from the PACS three-coil two-magnet design) would give the required torques for our BSM system. Therefore the motor 'design' task is limited to simply verifying this conclusion, by testing.

In order to establish the motor torque constant, the single-axis prototype was tested with various applied voltages, and the subsequent angular movement measured using the 'C.D.L.' Tilt Measurement Apparatus (TMA). Figure 6 demonstrates the set-up and configuration of the TMA.

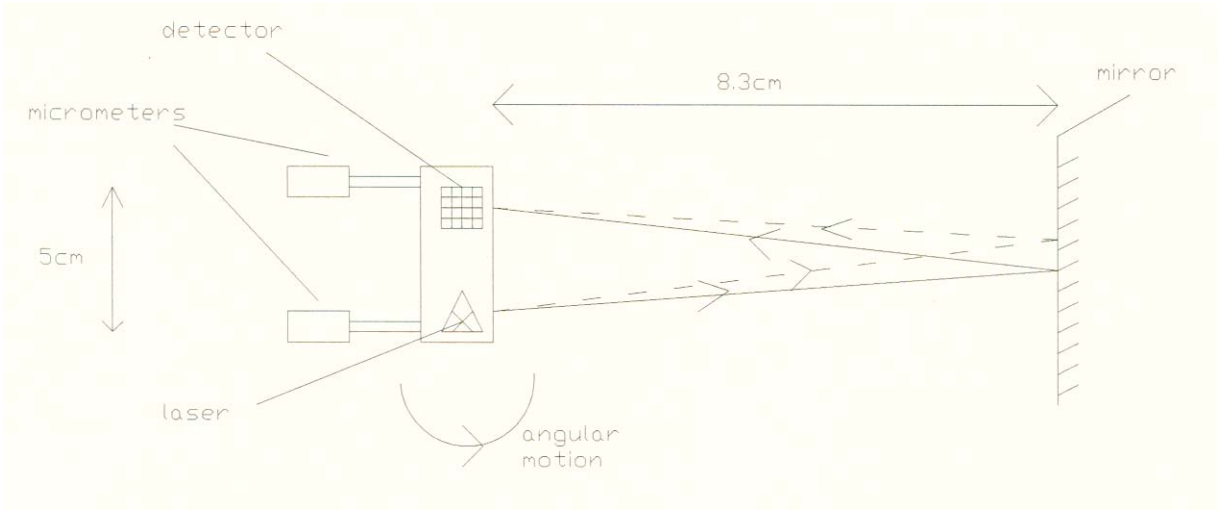

Figure 6 Tilt Measurement Apparatus Configuration

As the axis was restrained by the flex pivot mountings, which have a known spring constant, the angular movement could be converted to an equivalent force and the motor torque constant derived.

9.2.2 RESULTS

Firstly, the TMA was calibrated using a simple laser reflection against a fixed scale, as shown in figure 6.

The following results were obtained:

Mirror distance to TMA = 8.30E-02 m

Beam Movement	TMA o/p	angle	Scale Factor rad/pixel
1.00E-04	262	2.00E-03	7.63E-06
2.00E-04	525	4.00E-03	7.62E-06
3.00E-04	787	6.00E-03	7.62E-06
4.00E-04	1045	8.00E-03	7.66E-06
5.00E-04	1316	1.00E-02	7.60E-06

Average Scale factor = 7.63E-06 Rad/pixel

The following test data was obtained by applying a range of voltages to the motor, and using the following measurements and catalogue data:

Resistance of coils + series resistor	=	1720	ohm
Flex pivot scale factor (2 off)	=	6.40E-02	N-m/Rad
Mirror distance to TMA	=	8.30E-02	m
Micrometer-to-pivot distance	=	5.00E-02	m
Magnet distance from centre of rotation	=	1.70E-02	m

		TMA				
Volts	Current	o/p	angle	Torque	Kt Nm/A	Kf N/A
5	0.002906977	655	5.00E-03	3.20E-04	0.109972917	6.47E+00
4	0.002325581	522	3.98E-03	2.55E-04	0.109553173	6.44E+00
3	0.001744186	390	2.97E-03	1.90E-04	0.109133429	6.42E+00
2	0.001162791	259	1.98E-03	1.26E-04	0.108713685	6.39E+00
1	0.000581395	130	9.91E-04	6.34E-05	0.109133429	6.42E+00
-1	-0.000581395	-132	-1.01E-03	-6.44E-05	0.110812405	6.52E+00
-2	-0.001162791	-265	-2.02E-03	-1.29E-04	0.111232149	6.54E+00
-3	-0.001744186	-398	-3.04E-03	-1.94E-04	0.111372064	6.55E+00
-4	-0.002325581	-532	-4.06E-03	-2.60E-04	0.111651893	6.57E+00
-5	-0.002906977	-662	-5.05E-03	-3.23E-04	0.1111482	6.54E+00

		Kt Nm/A		Kf N/A	
AVERAGE VALUES	=	0.110272334	+/- 0.011	6.486607909	+/- 0.649

(Error originates from 10% error in flex-pivot scale factor, which is the dominating error in test data. The above data is below presented as a graph.)

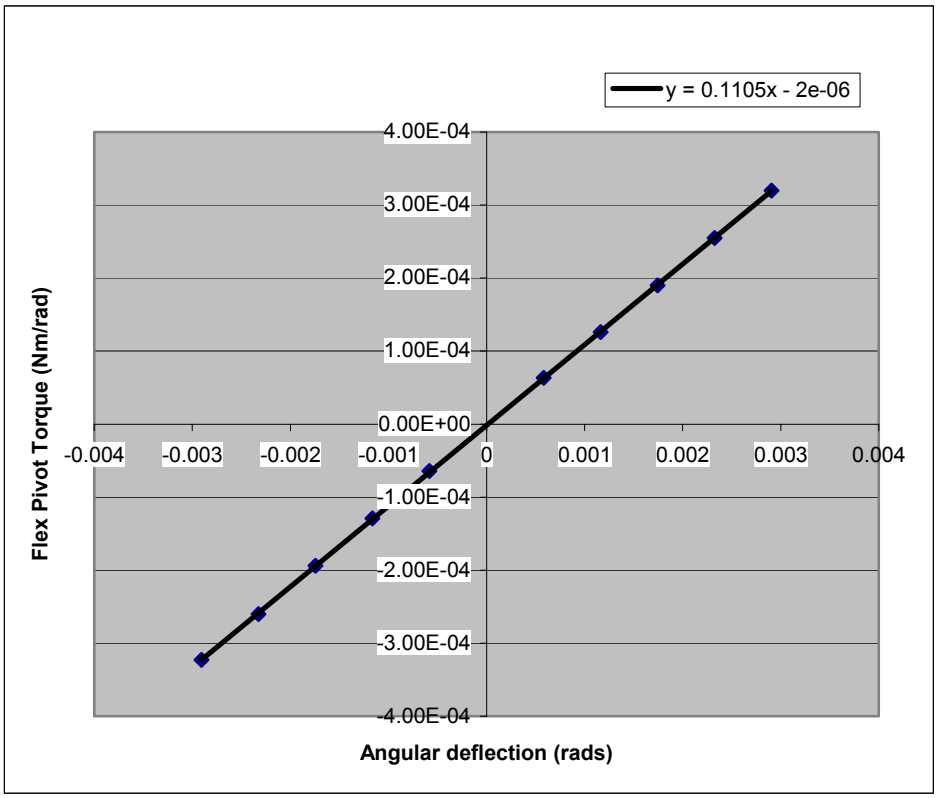

Figure 7 Torque Analysis Graph

9.2.3 CONCLUSION

The tests indicate that an average motor torque constant of 0.11 Nm/A can be obtained for the BSM Chop axis motor. As can be seen from figure 7, the flex-pivot torque varies linearly with the angular deflection of the mirror.
By extrapolation, Figure 7 predicts that at the maximum required angular deflection (+/- 0.042 rad) the motor torque will produce an acceleration sufficient to meet the Angle Step Time requirements. The motor torque will also be enough to meet the required settling times.

9.3 SPIRE: Current Source Test

9.3.1 INTRODUCTION

Current source stability directly impacts the long-term stability of the BSM mirror. In order to verify the current source stability with time the ISOPHOT current source design (which is used on the SPIRE BSM) was built with 1% resistors and a 0.1% 333 ohm load and was tested by measuring the load voltage over time using an H-P 3478A multimeter.
Voltage supplies were maintained at +/- 15.1V.

9.3.2. RESULTS

Time – min.	Load Voltage	% variation from start
0	0.34180	0
0.5	0.34418	0.696314
1	0.34472	0.854301
1.5	0.34499	0.933294
2	0.34513	0.974254
2.5	0.34522	1.000585
3	0.34528	1.018139
3.5	0.34532	1.029842
4	0.34535	1.038619
4.5	0.34537	1.04447
5	0.34538	1.047396
5.5	0.34539	1.050322
6	0.34541	1.056173
6.5	0.34542	1.059099
7	0.34543	1.062025
7.5	0.34544	1.06495
8	0.34544	1.06495
8.5	0.34546	1.070802
9	0.34547	1.073727
10	0.34548	1.076653
11	0.34549	1.079579
12	0.34550	1.082504
13	0.34550	1.082504
14	0.34550	1.082504
15	0.34550	1.082504
16	0.34550	1.082504
17	0.34546	1.070802
18	0.34545	1.067876
19	0.34548	1.076653
20	0.34549	1.079579

The results are also plotted in the following graph:

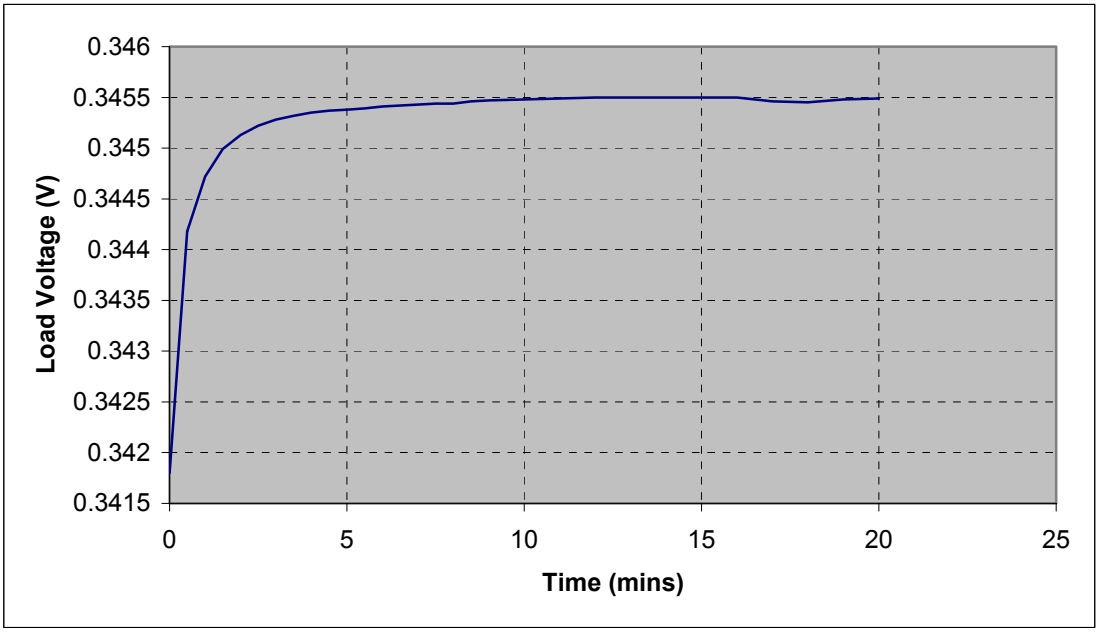

Figure 8 Current Load Source Voltage vs Time

9.3.3 CONCLUSION

It is clear (assuming that there is negligible variation in the 0.1% precision resistor) that the source current - after an initial warm-up period - settles to a value that is constant to about 30 PPM. The current source stability will therefore be a negligible component of the position stability requirement, which corresponds to about 0.16% over 4 hours.

9.4 Preliminary Cross-talk test

9.4.1 INTRODUCTION

An instruction to move the BSM to a given position will consist of two independent orthogonal steps. Given the proximity of motor coils and position sensors it is important that there is no significant cross talk between the motor coils of one axis and the position sensor of the other. If the sensor from one axis was able to detect magnetic field fluctuations caused by motion in the other axis the controlling hardware/software would try to compensate for what it would see as a position error thus reducing position accuracy.

In order to verify that cross talk would be unlikely in the two-axis prototype the sensor output with the motor on was compared to that with the motor off. If there was no distinct change in the results then it would seem unlikely that cross talk would occur.

The experiment was as follows;

1) Position sensor was held in its correct position and it was verified that there was an output when the motor was powered.

2) Removed the sensor and held it in the position of the Jiggle axis sensor. Here no signal was picked up at the output of the sensor amplifier, whilst the chop motor was running. The output from the sensor was the same as when power is removed from the motor, i.e. noise in the sensor circuit only (see figure 2).

3) Moved the sensor close to the motor and still no output was obtained hence there should be no cross talk between the position sensors of the two axes.

4) Replaced the position sensor and found that the sensor had to be very close to the mirror before an output was obtained

9.4.2 CONCLUSION

The results of this experiment strongly suggest that there should be no cross talk between the two axes, therefor positional accuracy will not be jeopardised. This will be confirmed with more precise tests on the two-axis prototype.

9.5 Single Axis proto-type Cold tests

9.5.1 INTRODUCTION

In order to test the performance of the BSM at the operating temperature of 4K the single axis prototype described above was fixed inside the cryostat and was cooled in two stages, firstly to 77K using liquid Nitrogen and then to 4K using liquid Helium. As the mirror cooled significantly slower then the base-plate it was concluded that the flex pivots are poor heat conductors - in order for the mirror to cool at a reasonable rate an aluminium shield had to be place over it.

The primary motives for cooling the single axis prototype were;

a) to check whether the power dissipation in the motor coils were within the required parameters (approximately 2mW)
b) measure the resistance of the motor coils at operating temperature
c) to look for changes in the BSM's performance when cooled for potential faults

Power Dissipation Tests

Using a Phillips PM5135 Function Generator, an AC voltage wave - sinusoidal, frequency 2Hz - of varying amplitude was used as the input to the motor. An ammeter was placed in series with the input signal so that the rms current could be measured, and thus the total power dissipated in the drive circuit could be calculated. The output from the sensor was viewed on a Tektronix TDS 224 oscilloscope.

To find the resistance of the coils at 5K and at room temperature the coils were probed with a FLUKE multimeter. It was found that the resistance dropped from 330Ω at room temperature to 60Ω at 5.2K.

9.5.2 POWER DISSIPATION RESULTS

Test results at 5.2K

Voltage (V)	Current (A)	Total Power (W)	Sensor offset (V)	sensor fdbk (pk-pk) (V)
0.5	2.75E-03	9.72E-04	-4.6	6.4
1	5.80E-03	4.10E-03	-3.6	12.6
1.5	8.90E-03	9.44E-03	0	16.4
2	1.14E-02	1.61E-02	0	18.8
2.5	1.41E-02	2.49E-02	0	22.4
3	1.73E-02	3.67E-02	0	22.4
3.5	1.97E-02	4.88E-02	0	23.2
4	2.14E-02	6.05E-02	0	23.2
4.5	2.46E-02	7.83E-02	0	23.2
5	2.75E-02	9.72E-02	0	23.2

Test results at 295K

Voltage (V)	Current (A)	Total Power (W)	Sensor offset (V)	sensor fdbk (pk-pk) (V)
0.5	5.70E-04	2.02E-04	-7.60E-01	7.60E-01
1	1.55E-03	1.10E-03	-7.60E-01	1.4
1.5	2.00E-03	2.12E-03	-7.60E-01	2.9
2	2.63E-03	3.72E-03	-7.60E-01	3.8
2.5	3.35E-03	5.92E-03	-7.60E-01	5
3	3.92E-03	8.32E-03	-7.60E-01	6
3.5	4.70E-03	1.16E-02	-7.60E-01	7.2
4	5.21E-03	1.47E-02	-7.60E-01	8.2
4.5	5.80E-03	1.85E-02	-7.60E-01	9
5	6.60E-03	2.33E-02	-7.60E-01	9.8

These results were then plotted on a graph:

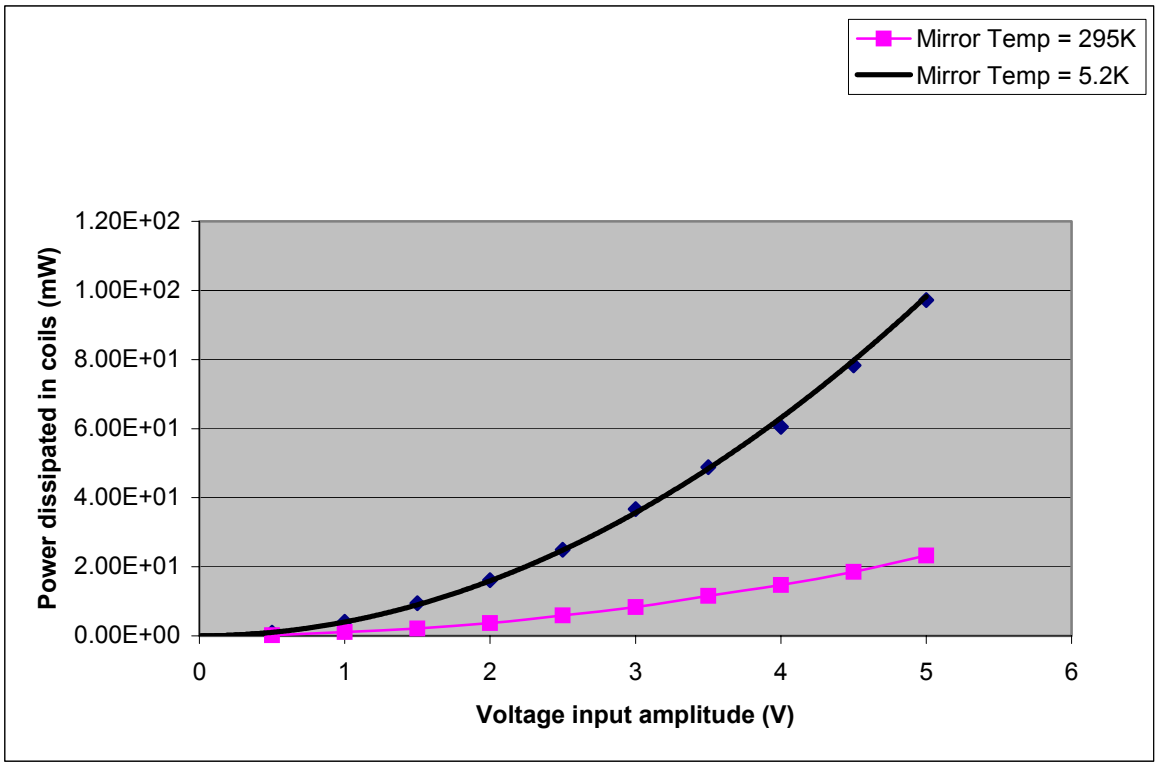

Figure 9 Power Dissipation (AC input)

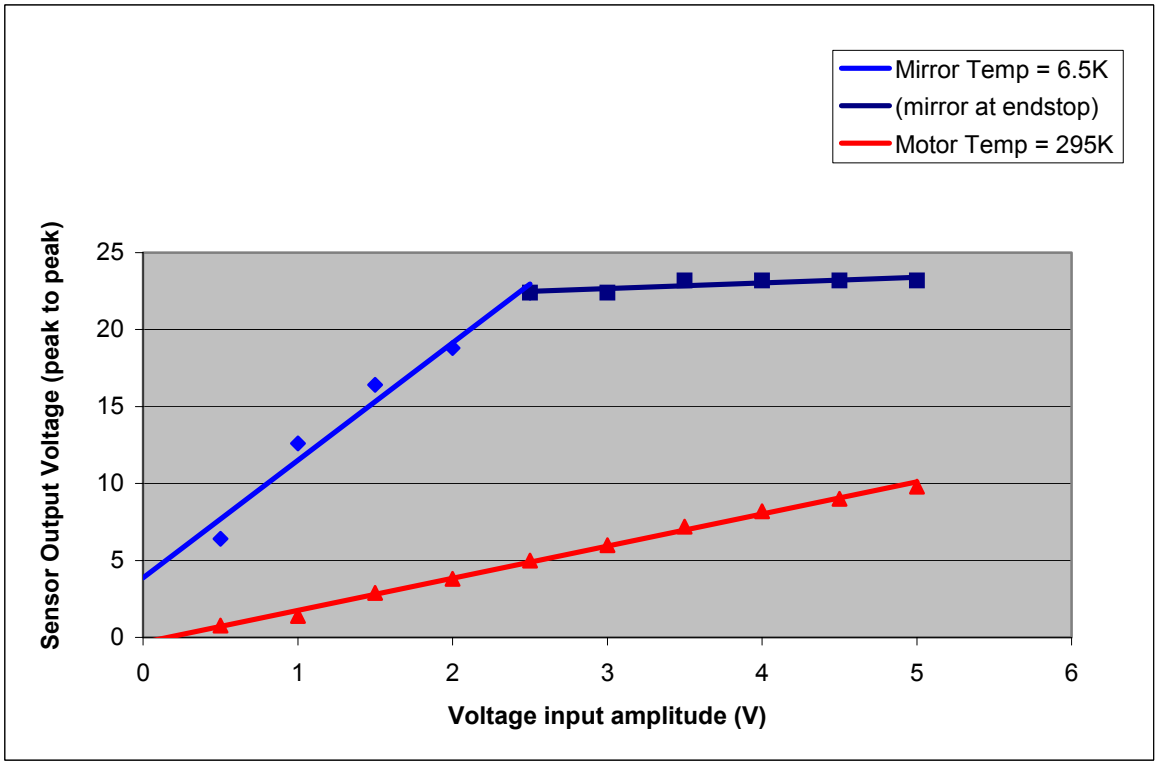

Figure 10 Sensor Output vs Motor Input

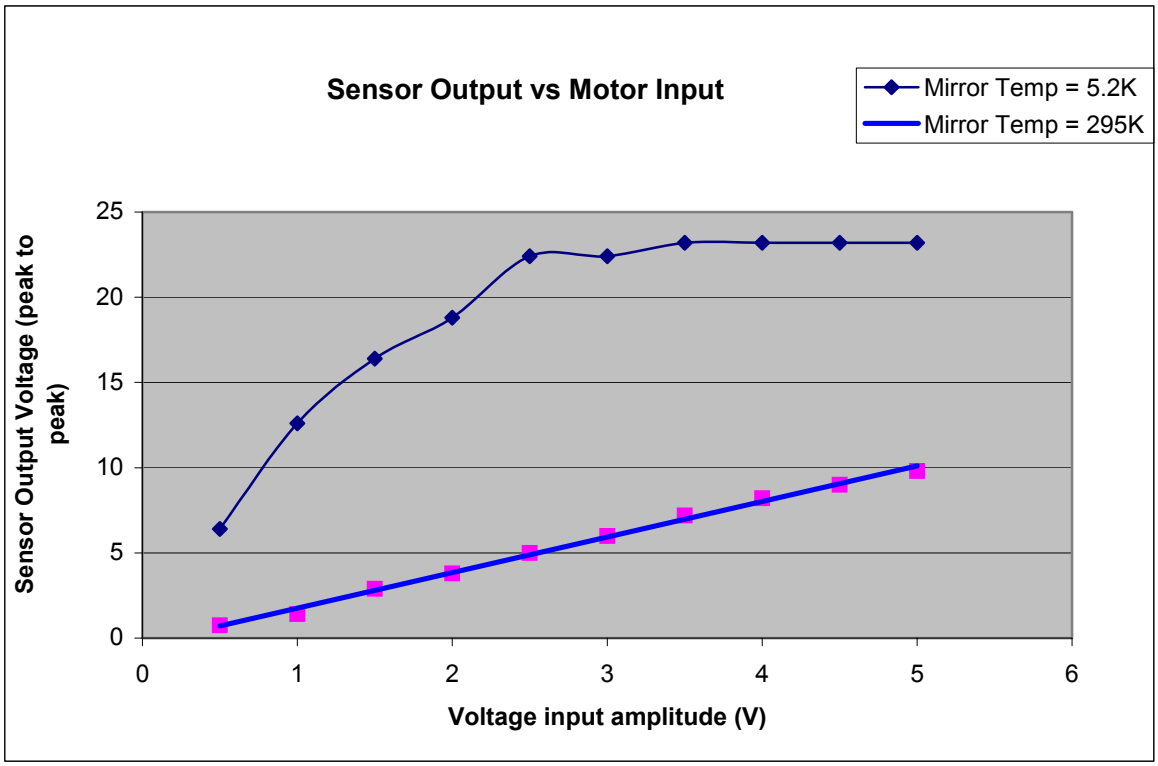

Figure 11 Sensor Output vs Motor Input

9.5.2 POWER DISSIPATION CONCLUSION

Far more power is dissipated when the motor is cold. This is because as the temperature decreases the resistance of the coils will decrease, so if the input voltage is kept constant as the temperature drops the current (and therefore the power dissipated) through the coils will increase. Figure 10 shows the sensor output levels at about 2.5V suggesting the motor has reached its endstop. It also indicates that a current of around 22mA will be sufficient to drive the motor to an end-stop.
There are two reasons why the measured power dissipation in these tests was far greater then the 2.5mW requirement. The first is that the single-axis prototype motor coils were constructed out of copper, which is not superconductive at 5K. It is hoped that aluminium, which has a far lower resistance when cold, will be used in future test (and the flight) models. A coil resistance of 5 Ω (combined with a reduced input voltage) would be sufficient to bring the dissipation down to the specification requirement. An input voltage of 0.11V would generate the 25mA current required to move the motor to an endstop. A second reason is that in these tests a 2Hz continuous sine wave was used as the motor input signal whereas a DC input would have been a better representation (in practice the mirror would not be continuously moving). It is possible that this may have also significantly effected the results.
More cold tests are required (and are planned) to verify these conclusions.

9.6 Two- Axis proto-type

The two-axis prototype is, at the time of writing, nearing completion. More varied and rigorous tests are planned for the two-axis model, including a repeat of all the tests described here on the Jiggle axis. Figure 11 shows the Two-Axis Prototype at its current status.

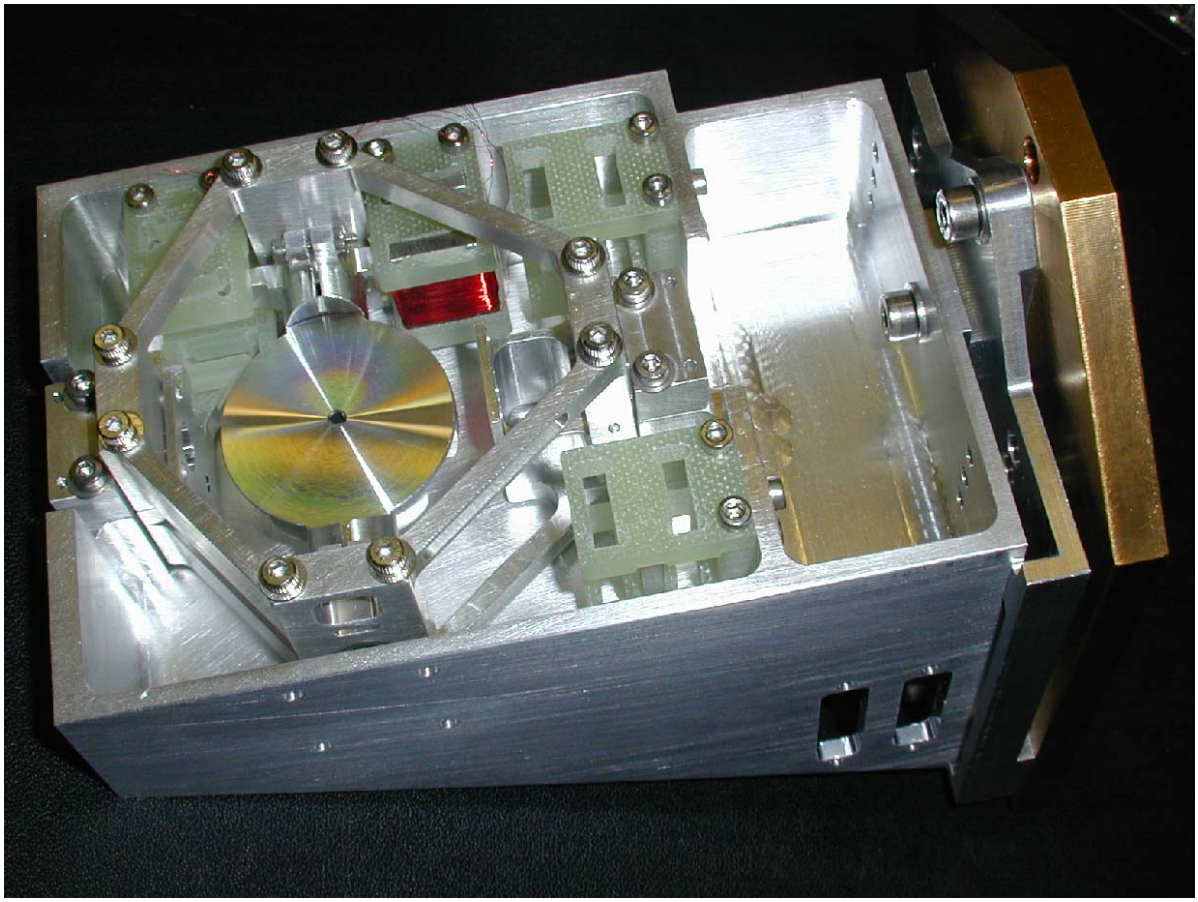

Figure 12 Two-axis Prototype

This page intentionally left blank

Document Ends